Assessment of ceramic materials for thermally insulated reciprocating engines

Manton, S. M.

Award date:
1986

Awarding institution:
University of Bath

ASSESSMENT OF CERAMIC MATERIALS FOR THERMALLY INSULATED RECIPROCATING ENGINES

submitted by:
S. M. Manton for the Degree of Ph. D.
of the University of Bath
1986

ProQuest LLC
789 East Eisenhower Parkway
P.O. Box 1346
Ann Arbor, MI 48106-1346

SUMMARY

There is a continuing demand for improvements in both the emission levels and operating efficiency of all internal combustion engines. The diesel engine is able to make improvements in both of these areas through the use of thermal insulation. In addition a low heat rejection engine should be capable of using lower cetane fuels and exhibiting reduced noise levels than its uninsulated equivalent. The refractory nature of many ceramics make them ideal candidate materials for thermal insulators.

This thesis includes a theoretical study of the temperatures and stresses likely to be encountered by ceramic engine components. Both ceramic monoliths and zirconia coatings have been examined, under both steady state and transient loadings. The finite element code ANSYS was used for some of this steady state work. In addition a program was written specifically for the analysis of disc shaped components. This program was used to examine the propagation of stress waves through ceramics in response to a transient thermal load. Further work examined the residual stresses introduced into zirconia coatings during the process of plasma spraying.

An experimental programme was initiated to explore the ability of ceramic coated or capped components to withstand the thermal and mechanical stress cycling of the diesel engine. A rig was built to simulate the in cylinder conditions of a diesel engine without the process of combustion. Ceramic components can be tested to distruction within this environment without damaging the test rig.

ACKNOWLEDGEMENTS

I would like to gratefully acknowledge the help of the following people:

Professor F.J. Wallace for his supervision and understanding, as well as patience with my unique spelling.

Mr W. Alexander for technical advice and assistance, especially with the instrumentation.

Mr K. Pepler and the rest of the workshop personnel for their excellent machining.

Mr D. Rushton for building the rig and performing other miracles.

CONTENTS

CHAPTER FOUR: ANALYSIS OF DISC SHAPED COMPONENTS

CHAPTER FIVE: FINITE ELEMENT WORK

CHAPTER SIX: RESIDUAL STRESSES IN ZIRCONIA COATINGS

CHAPTER SEVEN: INSULATION TEST RIG

CHAPTER EIGHT: CONCLUSIONS AND SUGGESTIONS FOR FURTHER WORK

APPENDICES

NOTATION

A	Surface area	M^2
A_s	Surface area for heat transfer	M^2
B_i	Biot number	
C_p	Specific heat capacity	J/KgK
D	Diameter	M
E	Young's modulus	N/M^2
F_o	Fourier number	
h	Surface heat transfer coefficient	W/M^2K
h	Distance to neutral axis	M
k	Thermal conductivity	W/MK
q	Rate of heat transfer	W/M^2
r	Radius	M
R	Radius of curvature on neutral surface	M
t	Time	S
T	Temperature	K
u	Deformation	M
U	Overall heat transfer coefficient	W/M^2K
w	Thickness	M
x	Displacement	M
α	Thermal diffusivity	M^2/S
γ	Coefficient of thermal expansion	
ϵ	Strain	
θ	Angle	Radians
ν	Poisson's ratio	
ρ	Density	Kg/M^3
σ	Stress	N/M^2
τ	Shear stress	N/M^2
Φ	Shear strain	

subscripts

a	Axial
c	Circumferential
i	Instantaneous position
j	Instantaneous time
r	Radial
s	Surface

1 INTRODUCTION

1.1 THE USE OF CERAMICS TO INSULATE DIESEL ENGINE COMPONENTS

The concept of the adiabatic engine has been brought to the fore by Kamo at Cummins, and Bryzik of TARADCOM. [1,2] Their original theoretical work suggested that an uncooled diesel engine incorperating turbocompounding could attain a 48% thermal efficiency, whilst an unlubricated engine could achieve 56% efficiency. These claims may have seemed a little extravagant, but it is clear that appreciable efficiency gains can be made through insulation.

There are three main reasons for using insulation in the internal combustion engine:

i/ To increase the temperature in the combustion chamber, so lower quality fuels can be burnt with acceptable emission levels. This characteristic is important because the quality of diesel fuel has been worsening in recent years and will continue to do so for several reasons:

a) The increased demand for diesel fuels.
b) New areas of production are now available with a consequent change in quality.
c) In the future as the easily accessible and better quality fuels run low then fuel quality will drop.

Eventually substitutes for petroleum such as liquified coal, alcohol, and shale oil, may become the only available fuel sources.[3] If these substitutes are used a decrease in cetane rating will be expected. The use of insulation will allow the introduction of these alternative fuels.

ii/ Reducing the heat loss from the combustion chamber can lead to an increase in the thermodynamic efficiency. This follows as the

introduction of insulation reduces heat loss from the cylinder. In turn this leads to higher gas temperatures, and potentially to higher efficiencies. As the level of insulation increases, so do the surface temperatures in the combustion chamber. This leads to one of the main problems with thermal insulation: as air is drawn into the cylinder, it becomes heated by the combustion chamber surfaces, the accompanying decrease in volumetric efficiency lowers the potential output of the engine. It must also be recognised that there is little point in insulating an engine and thus increasing the exhaust enthalpy, unless this energy can be extracted in the form of work. With the naturally aspirated engine very little of the extra thermal energy is turned into shaft work. The naturally aspirated adiabatic engine therefore shows little improvement in thermal efficiency over the uninsulated equivalent: on the contrary, a worsening of performance often results. The full advantage of insulation is therefore not realised unless turbocharging or preferably compounding is used. This both corrects the lower volumetric efficiency, and can be used to extract the energy still available in the exhaust gases.

There are many different schemes which are available to extract this extra work, two of these are shown in figure 1.1,[4] together with three conventional uninsulated schemes. The high gas enthalpy available with these insulated designs is used to provide additional output power via the exhaust turbine. A further efficiency gain can be achieved through the use of the Rankine cycle, where further energy is extracted from the exhaust gases, through a vapour cycle turbine.

iii/ Less cooling equipment is needed. This is especially important in military vehicles where cooling equipment is sensitive to combat damage, and the power used by the cooling equipment is high. In road vehicles the reduction in radiator size, or its elimination can further increase overall efficiency levels through a gain in aerodynamic efficiency.

In addition to these advantages there are various other reasons to insulate the diesel engine:

a) Ceramics are often less dense than metals, so weight improvements are available.

b) Ceramics may not need as many cooling passages as their metal equivalents, so castings may be simpler.

c) The use of ceramics in the combustion chamber and exhaust ports can reduce the emission levels, particularly of hydrocarbons.

d) Ceramics can be used in areas such as the valve gear and bearings because of their high wear resistance. It may even be possible to dispense with lubricants in this area.

e) The high refractory nature of ceramics will ease the temperature limits in high BMEP engines.

Much of the early work directed towards the insulation of diesel engines was conducted using all metal components with air gaps incorporated into their structure to provide the required insulation. Metallic components were chosen in preference to ceramic because there was considerable doubt about the usable mechanical strength of ceramics. This is a satisfactory solution where low levels of insulation are required, but as the thermal resistance is increased so is the surface temperature of the metal, this will eventually pass the metalurgical limit. At these high temperatures ceramic materials offer the only realistic solution, their refractory nature making them ideal for this application. In addition many ceramics have low levels of thermal conductivity, therefore additional insulation though the use of air gaps may not be necessary. Ceramics with higher conductivity can make use of the air gap method to provide the required insulation, only if their mechanical strength is sufficient to maintain an unsupported region above the air gap.

1.2 TRULY ADIABATIC ENGINE OPERATION

The concept of the adiabatic engine, in which there is no heat transfer away from the combustion space, has existed for some time. However the term adiabatic in the context of this work is a misnomer, as there will always be heat loss to the surroundings. An adiabatic engine is generally taken to be one where attempts have been made to minimise the heat flow. It is not sufficient merely to reduce the

level of cooling, as heat will pass from the working fluid to the walls during the power stroke, and in the reverse direction during induction, this effect will limit efficiency grains. What is needed ideally is complete absence of heat flow from the gas to wall,[5] this can only occur when the wall temperature exactly follows the gas temperature. It thus follows that for high efficiency operation not only are low thermal conductivity materials required, but also low thermal capacity (density * specific heat). The term thermal inertia b, is used as an indication of the suitability of a material as an insulator, where;

$$b = k \rho C_p$$

where k = thermal conductivity
ρ = density
C_p = thermal capacity

Valland and Wyspianski[9] have examined the effect of thermal inertia using a cycle simulation program incorporating a thermal network. The wall temperature fluctuations are shown in figure 1.2. For zirconia, where $b=3.5 \times 10^6$, the temperature fluctuation is $\pm 50^{o}C$, whilst for steel with $b=2 \times 10^8$ the swing is around $\pm 10^{o}C$. It is therefore evident that true adiabatic operation is impossible to achieve in practice.

1.3 RESEARCH AT BATH UNIVERSITY INVOLVING THERMAL INSULATION

The work at Bath University has followed similar trends to many other research centres,[5,6,7,8] interested in the insulation of diesel engines. Initial investigations were intended to establish a theoretical understanding of the mechanism of insulation, using both computer based cycle simulations and Fourier analysis. Later this work was extended into two areas;

i) Experimental work: Following the initial theoretical study it was decided that an experimental programme was worth pursuing. Because little practical experience was available with ceramic

materials, the initial work made use of an air-gap all metal piston in a single cylinder Petter PH1W engine.[10] The resulting design is shown in figure 1.3, and makes use of a nimonic crown and aluminium piston body. To avoid direct attachment between nimonic and aluminium a collar was used into which bolts located. These bolts fix the crown to the collar, leaving the piston body free to take up any expansion mismatch. By scalloping the insert between crown and piston body the air gap was extended over virtually the whole of the underside of the crown, leading to a reduction in heat flow of over 50%. A moving arm linkage was used to provide instrumentation of the piston. This work has now been extended to include an insulated liner.

ii) Theoretical work: An in house finite element program written by Kao[11,12] was used to analyse the performance of the air gap piston mentioned above. A cycle simulation program, CSP[13] was used to examine the theoretical performance of various adiabatic engine schemes, and different insulating materials.

Work has since tended towards on a greater emphasis on the use of ceramics with the procurement of a range of test equipment capable of studying the performance of various ceramic materials and design concepts. The following three stage test schedule has been devised:

a/ Initial testing of ceramic samples in a mechanical proof test rig, and thermal shock rig. The proof test rig shown in figure 1.4, is capable of applying a known pressure drop across a ceramic disc. Large ceramic samples (80mm diameter) can therefore be tested at room temperature before insertion into the ceramic insuation test rig. The thermal shock rig uses high power Quartz Halogen lamps and focusing devices to heat a ceramic test piece for a controlled length of time before the sample is cooled. Similar thermal loadings should be attainable to that in an operating diesel engine. These two tests can be used as a simple check on the suitability of ceramic materials for the diesel engine environment.

b/ Use of a ceramic insulation test rig. This apparatus can produce a repeatable and controllable environment with pressure and temperature peaks comparable to that in a firing engine, and at a similar frequency. This rig can be used to test both material suitability for the diesel engine environment as well as proposed attachment methods. The design and commissioning of this rig form the practical side of the author's work and are discussed in more detail later.

c/ Component testing in a fired diesel engine. The Petter PH1W engine used for testing the air gap piston can, similarly be used for testing ceramic pistons and liners, once sufficient expertise has been established with the insulation test rig.

1.4 SUMMARY OF INVESTIGATION AND THESIS STRUCTURE

The first part of this thesis contains a literature review of work carried out into the use of ceramics in the diesel engine. Included in this section is a summary of the behavioural characteristics of ceramics. Engineers often complain that material scientists do not present the ceramic data available in a form which is of use to them, whilst material scientists complain that engineers do not tell them the form in which they require the data. This section therefore explores both the properties of ceramics and the best way for these properties to be presented, together with the most appropriate testing methods.

The second part covers the theoretical work pursued. This includes a description of a program written by the author for deriving transient and steady state stresses present in disc shaped components, together with a description of the finite element work undertaken.

a) This disc analysis although less adaptable than a finite element package, has a greatly reduced computer run time; to predict the transient temperature and stress distibutions in a ceramic disc subject to an oscillatory thermal boundary conditions over a real time of 20 seconds takes about 20 CPU seconds using this program. This represents a vast time saving over a transient finite element program whose run time for the same problem would amount to over one CPU

hour. The low run time of this program has been used to establish relationships that would otherwise take too long to discern, such as the effect on the predicted stress levels of an error in material property data, and to assess the residual stresses developed in zirconia coatings as a result of the plasma spraying process.

b) A large number of finite element runs were also undertaken using the finite element package ANSYS, further developing the concepts and trends established using the disc program mentioned above. Attempts were also made to set up simplified models of the cracking present in ceramic coatings. The purpose behind these investigations has been to find criteria under which the stresses in ceramic components can be minimised and hence life increased.

The third part is concerned with the construction of the ceramic insulation test rig. The aim of this rig was to provide a controllable and repeatable environment for the testing of ceramic specimens. The temperature and pressure were to be of a similar level to that in a firing engine, whilst providing a design which ensured that a failure of the ceramic would not cause damage to the rest of the engine structure. Unfortunately due to illness of workshop personnel associated with this work the initially envisaged schedule was delayed. In addition a rebuild of the test cell where the apparatus was sited was undertaken part way through the work causing further delays. The quantity of experimental tests originally envisaged has therefore not been achieved. Despite these problems the rig still forms an important addition to the equipment available at Bath.

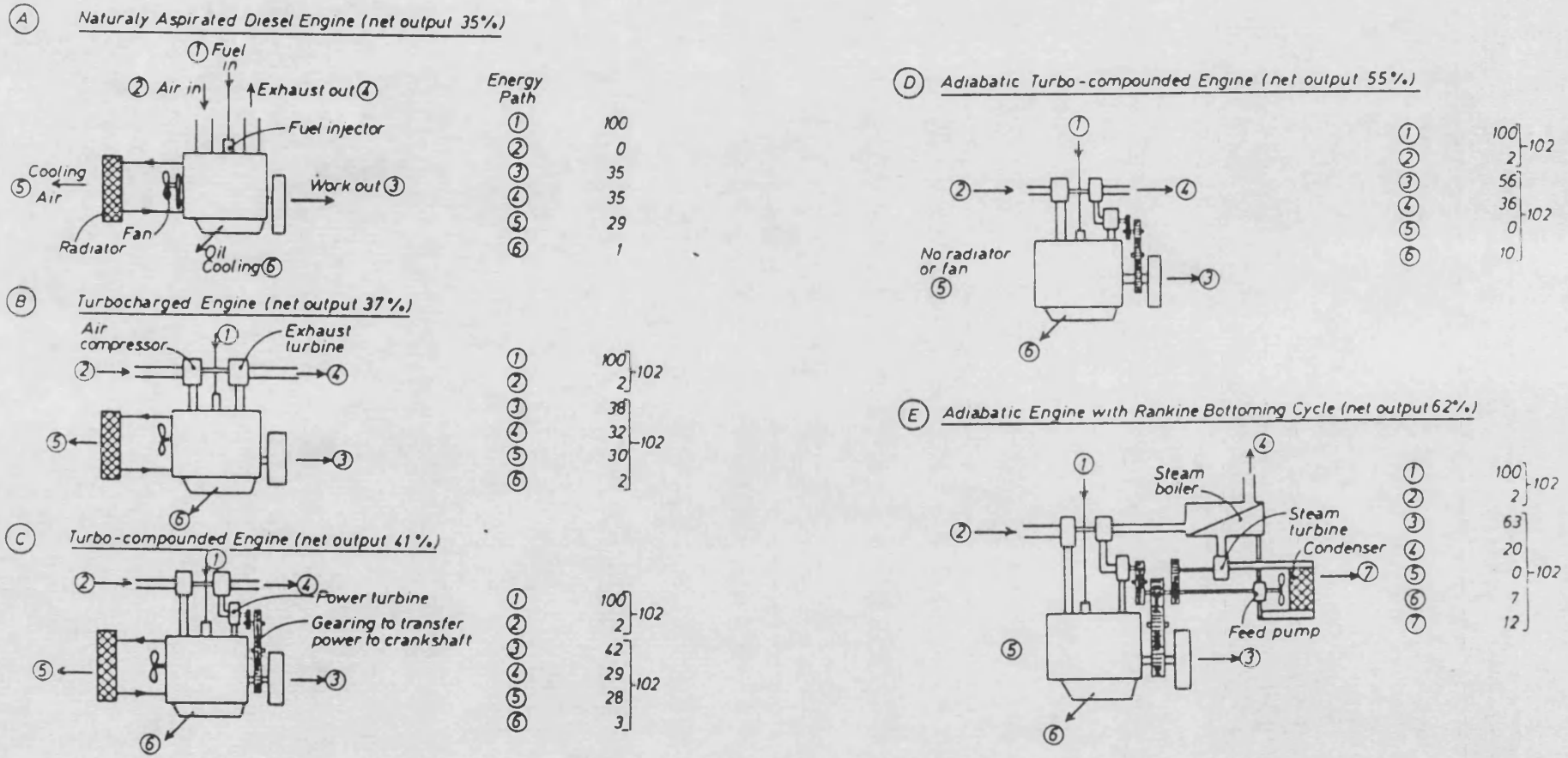

FIGURE 1.1 ENERGY BREAKDOWN FOR VARIOUS INTERNAL COMBUTION ENGINE SCHEMES

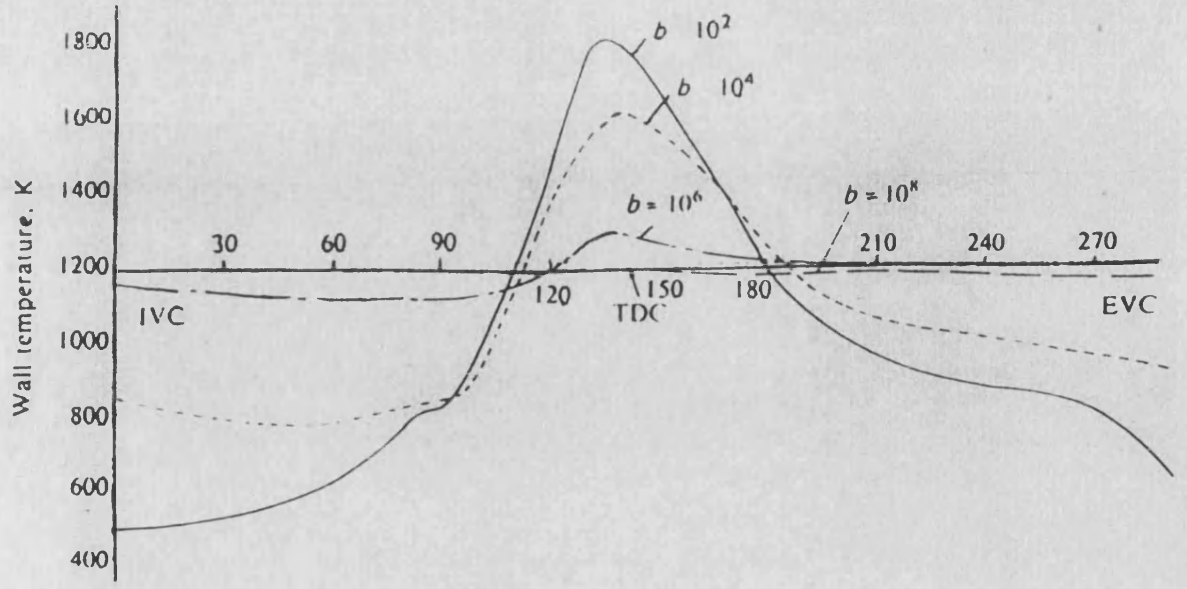

FIGURE 1.2 WALL TEMPERATURE FLUCTUATION FOR DIFFERENT VALUES OF b.

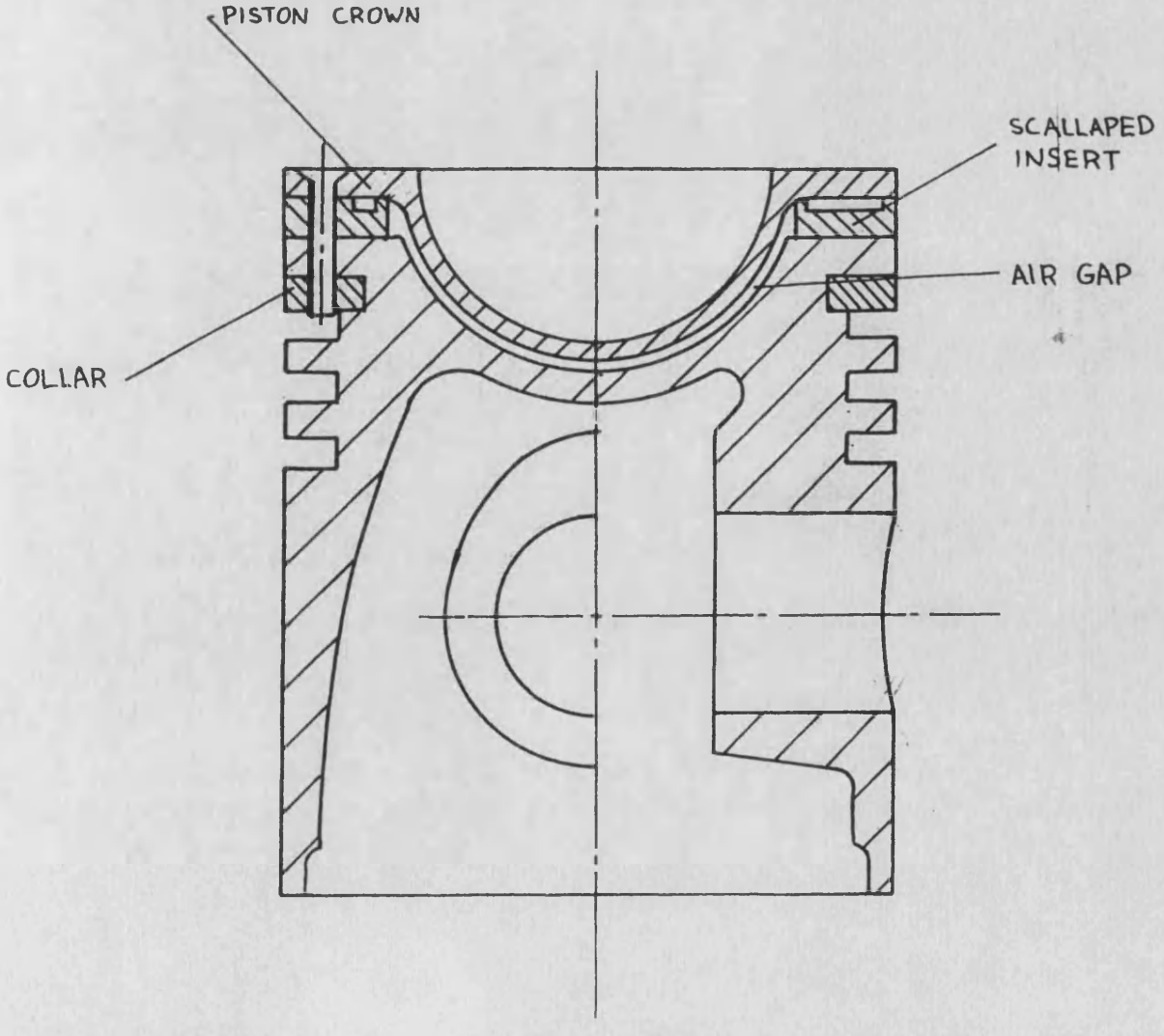

FIGURE 1.3 CROSS SECTION OF AIR GAP PISTON.

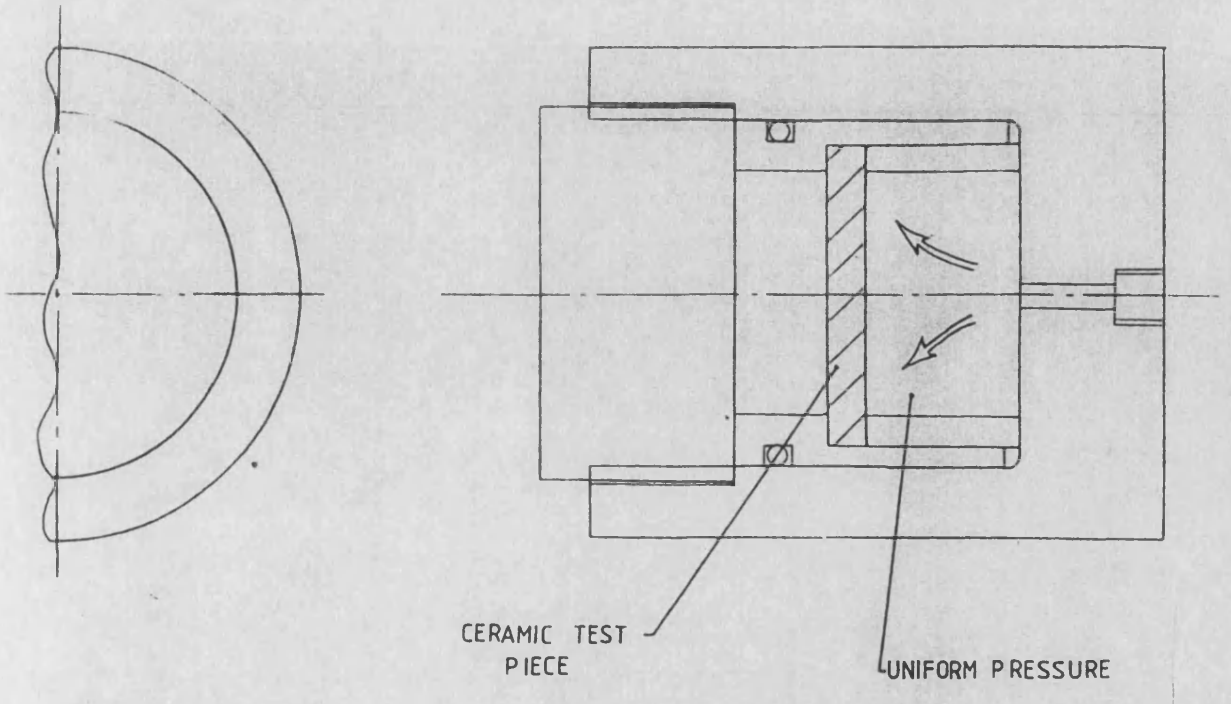

FIGURE 1.4 HYDRAULIC PROOF TEST RIG.

2 PROPERTIES OF CERAMICS

2.1 BONDING OF ATOMS

The difference in the behaviour of ceramics and metals can be explained by the dissimilarity of their atomic structures, which are in turn the consequence of their different types of atomic bonds. There are three main mechanisms through which atoms interact with one another to form atomic structures, these are referred to as metallic, ionic and covalent bonding.

a) Metallic bonding: Metals generally make use of metallic bonding, in which a cloud of free electrons is formed, leading to a net attraction between the nuclei. Densely packed structures generally result, helped by the fact that all the atoms in a pure metal are of the same size. This arrangement, for reasons explained later leads to the ability of metals to exhibit ductility and so redistribute loads.

Bonds which form in ceramics are usually ionic or covalent in character, although in practice both types of bond are present in the same structure.

b) Ionic bonding: This occurs where one atom permanently loses one or more electron to the atom of another material. Each of the atoms formed will have a charge, this holds them together as a molecule with a zero net charge. Other molecules will be attracted, forming a structure which minimises the total energy of the system, this is generally regular in form, so building up a crystal.

c) Covalent bonding: When two or more atoms share electrons a covalent bond is formed. A directional distribution of electrons and hence charge is formed, this leads to a regular orientation of the atoms and hence to the formation of a crystal.

Whilst ionic bonding will lead to a close packing of atoms, covalent bonding does not. Materials with ionic bonds have high strength, and melting temperatures, with low level thermal expansion. These properties arise from the atomic layout, as examined latter.

There are two types of atomic layout, found as a consequence of these different bonds. Close packed, which is a characteristic of ionic and metallic bonds where the distance between ions (charged atoms) is minimised, and not close packed structures, existing with covalent bonding.

As pure metals have atoms of regular size, the regular geometry of close packing is formed, as shown in figure 2.1. Materials with ionic bonding still attempt to form close packing, but the presence of more than one atom type leads to a less regular layout, as in figure 2.2, and a more open structure. This variability of atomic density is one of the factors leading to the difference in properties between the two material groups.

Not all atomic arrangements are as regular as the metals and ceramics mentioned above, a typical example of a non crystaline structure are the glasses. A glass is formed when a molten ceramic composition is cooled so rapidly that the atoms do not have time to re-arrange themselves in a periodic structure, as in figure 2.3. The glasses formed are often good thermal insulators with low thermal expansion.

2.2 EFFECT OF ATOMIC LAYOUT ON PHYSICAL PROPERTIES

2.2.1 THERMAL CONDUCTIVITY

Heat is carried through a solid material either by vibration of the atomic structure or via the movement of electrons. With metals the free electrons created by metallic bonding are able to act as heat carriers through the material. By adding alloying materials to pure metals the ease with which the electrons move through the atomic structure is reduced, so the conductivity is also lowered. In ceramics there are no free electons, so heat transfer can only occur through

vibration of the atomic structure (phonons). Their conductivity is therefore generally lower than that of metals. Radiation also can be a significant source of heat transfer in ceramics at high temperatures. Materials with a high level of porosity will therefore exhibit an increase in thermal conductivity at elevated temperatures. Despite this, porous materials are generally good insulators.

2.2.2 THERMAL EXPANSION

As the temperature of a material increases so does the vibration of the atomic structure. In metals the close packing leads to very little free space, consequently this vibration causes an appreciable expansion in component size. Ceramics however have a much more open structure, vibration can therefore be accomodated without a high level of expansion. Potentially materials with low thermal expansion can have a good resistance to thermal shocks, and can survive thermal cycling.

However, not all materials exhibit smooth, continually changing dimensions with temperature. Some materials called polymorphs can exist in more than one crystalline form. A switch between forms can be brought about by a temperature rise, which increases the level of atomic vibration to a point where the original structure is no longer stable. Zirconium oxide is an example of such a material, which changes form at about 1170^{o}C, accompanied by a 3% volume change.

2.2.3 DUCTILITY

In brittle failure fracture occurs when two adjacent layers of atoms become separated, without a large change in their position relative to the other atoms further into the material. With ductile failure, adjacent layers of atoms slide past each other, this does not alter the relative positions of atoms away from the flaw. So why do the layers of atoms present in ceramics crack apart and not slide past one another?

The first and most important reason is a consequnce of the way the atoms are arranged. Metallic bonds produce a regular structure, so there are a large number of different planes in which atom layers can slide past one another. Ceramics with mixed covalent and ionic bonding do not posess such a large number of slip planes. The ceramics which do have good atomic symmetry, and thus several slip planes, have the highest ductility. However yielding is controlled not only by the number of slip planes present in the atomic structure, but also by the level of imperfection. For slip to occur in a perfect crystal, the stress levels would be very high as all the atoms in one plane would simultaneously have to slide past one another. If a flaw exists, however, this dislocation can gradually move through the atomic plane, as in figure 2.4.[19] thus increasing the ability of creep to redistribute stresses.

These defects are of several types, a Frenkel defect is one in which an atom is moved from its original position. A Schottky defect exists where an atom is completely missing. It can be shown through thermodynamic equilibrium that any crystal at a temperature above absolute zero will contain these vacancies.

Another defect type exists where an atom of impurity has filled a vacancy. Entropy dictates that any pure crystal will disolve impurities it comes into contact with. These impurity atoms tend to block the ability of creep to take place.

2.2.4 YOUNG'S MODULUS

An applied tensile load will attempt to move atoms in the structure further apart. Where the attraction between these atoms is greatest, as in covalent bonding, then Young's Modulus will be high. In an ionically bonded structure the Young's Modulus is low. Since ceramics use both types of bonding structure the range of Young's Modulus exhibited is very large. Consequently despite the difference in atomic structure between metals and ceramics it is possible to select an example from each group where the moduli of elasticity are fairly close. So the deformation caused by an applied load in each case is similar.

2.2.5 CRACK GROWTH

In metals a crack large enough to cause a significant deviation in strength away from the mean can be detect by NDT. In ceramics cracks which are too small to be detected can significantly reduce the usable strength of a component. The reason for this difference again relates to the two types of atomic structure.

When energy is applied to a material this energy can cause an increase in the surface area of the component. Since the surface of a liquid or solid is in tension this process effectively stores the energy input. as in figure 2.5. Grifiths was the first to recognise a link between fracture and energy storage through an increase in area. (The propogation of a crack also increases the surface area of a component) He developed the idea and established a theoretical strength for a given material:

$$\sigma = 2\sqrt{\frac{G\,E}{x}}$$

where E = Young's Modulus
G = Surface energy of the solid $/m^2$
x = distance between atomic layers

We find from experimentation that:

$$G = \frac{E\,x}{20}$$

Allowing for the fact that Hooke's law is only approximate for large strains, then the strength of any solid should be around E/10 to E/5. Practical materials reach only a fraction of this theoretical strength. This is now known to be due to the presence of cracks in the material. These cracks have a very high stress concentration at their tip, any structure with a crack will therefore have a breaking strength much less than this theoretical limit. There are two stages in the formation and growth of these cracks.

i) Cracks can be introduced through surface damage, or can be generated through the process of plastic deformation where dislocations will pile up at grain boundaries. The crack will continue to grow in this manner until the critical crack size is reached, this process is called sub-critical crack growth.

ii) Once a crack of critical size is formed, the crack growth will accelerate rapidly. Griffiths observed that a crack will propagate if the elastic energy released by its passage (stored energy) is greater than the surface energy needed to extend it.

This critical crack size l_g can be shown to be equivalent to:

$$l_g = \frac{2\,G\,E}{\pi\,\sigma^2}$$

In reality the energy required to make a new surface is greater than the energy stored in the surface G. This is because it not only must cause the adjacent atoms to be torn apart, but energy will be absorbed when the atomic structure is disturbed at a greater depth. In practise:

$$l_g = \frac{2\,W\,E}{\pi\,\sigma^2}$$

where W is the work of fracture.

As metallic structures are close packed, the amount of damage done to the substructure by prising two atoms apart is very great, hence W is large, and the critical crack size is also large. With ceramics their less dense structure the atoms can be separated without disturbing those around them, W therefore approaches G, and the critical crack size becomes very small.

This is the important difference between ceramics and metals, critical crack length in a ceramic material will often be too small to detect, the first indication of its presence will be a catastrophic failure.

As a consequence of the random nature of the size and distribution of cracks the strength of a given ceramic material will be uncertain, and can only be expressed in terms of statistical analysis. This is something most engineers are not used to, but the aerospace industry for many years has been using statistical methods. The maximum stress a material can be subjected to, is chosen so that it has an acceptable probability of surviving under that condition. This probability is chosen according to how dangerous a component failure would be, where public safety is concerned very high probabilities are used.

2.2.6 OTHER PROPERTIES

The more open structure of ceramics helps to contribute towards the low densities generally domonstrated by ceramic materials. However the density is still mainly dictated by the atomic weight of the elements of which they are composed.

Similarly a low Poisson's ratio would be expected in an open structure, where movement in one plane has little effect on the dimensions in the other planes.

2.3 ENGINEERING PROPERTIES

Having examined the differences in the atomic structure of metals and ceramics, and how these effect their general behaviour we now need to examine the engineering properties of ceramics in greater depth to judge where their use is appropriate.

The mechanical behaviour of ceramics is generally divided into two regions, the low temperature region where plasticity is unimportant, and the high temperature region where plasticity takes place. Only the low temperature behaviour is well understood. Fortunately with most ceramics we shall be considering, the temperature at which creep becomes significant is outside the operating range likely to be encountered in the internal combustion engine.

2.3.1 TENSILE STRENGTH

When analysing the strength of ceramics there are two areas which must be considered:

i) Scatter: A far wider distribution of properties is exhibited by a ceramic material than a metal. Any description of the strength of a ceramic must include a guide to the range of properties likely to be encountered.

ii) Time dependance: the highest load is not always the most likely to cause a failure, a lighter load applied for a longer period of time can be more likely to lead to a failure.

The first of these two phenomena can be represented by the Weibull approach. This assumes a ceramic test piece under uniform stress will fail at the most severe flaw. Weibull proposed the following relationship, giving the probability of failure P, at a given stress as:

$$P = \left(\frac{\sigma - \sigma_\mu}{\sigma_o} \right)^m$$

where σ is the applied stress,
σ_μ is the stress at which the probability of failure is zero.
σ_o is the stress at which the probability of failure of 0.632
m is the Weibull modulus, and is a measure of the data scatter.

These constants are determined from large numbers of experimental tests, the resulting probability distribution being shown on Weibull paper as in figure 2.7.[15]

This approach can be extended to cover the effect of component size. It is obviously more likely to find a given sized flaw in a large specimen than a small one.

$$P(v) = e^{-v\left(\frac{\sigma - \sigma_\mu}{\sigma_o} \right)^m}$$

Where P(v) is the probability of failure in a given volume, v.

It follows that if two specimens are equally likely to fail then their volumes v_1, v_2 and their uniform stresses σ_1, σ_2 will be related by the equation:

$$\left(\frac{\sigma_1}{\sigma_2}\right) = \left(\frac{v_2}{v_1}\right)^{\frac{1}{m}}$$

The time dependence of strength can also be brought into this analysis. If a ceramic is subject to a load any cracks present will grow over a period of time. As the crack grows so does the stress concentration at its tip. The stress intensity factor at which the crack will propagate and lead to failure is called the critical stress intensity K_{ic} or the fracture toughness. It can be shown that:

$$\left(\frac{\sigma_1}{\sigma_2}\right)^n = \left(\frac{t_2}{t_1}\right)$$

t_1 is the time to failure at stress σ_1
t_2 is the time to failure at stress σ_2
n is a constant

This information can also be represented on a Weibull diagram as shown in figure 2.7.[15] The probability of failure for each load is given at various time steps (decades).

2.3.2 THERMAL SHOCK

In any situation where a ceramic is subject to rapid heating or cooling it is of value to consider thermal shock parameters. These give an indication of the crack initiation resistance of different materials. There are many different types of parameter, each with a slightly different formulation. It is clear that good thermal shock resistance is associated with high values of strength, and high thermal conductivity; similarly low values of Young's Modulus and coefficient of thermal expansion are required;

$$\text{hence} \qquad R' = \frac{K\,(1-\nu)}{\gamma\,E}\,\sigma$$

where K is the thermal conductivity

γ is the thermal expansion

ν is Poisson's ratio

However, these parameters do not always give a true indication of the fracture toughness. As an example partially stabilised transformation toughened ZrO_2 has a very high coefficient of thermal expansion, and only a moderate strength but has excellent thermal shock resistance due to its high fracture toughness. Which of the many parameters is most appropriate in a given situation is difficult to judge. Another criterion which takes into account how easily cracks propagate is as follows:

$$R''' = \frac{\beta\,E}{\sigma^2\,(1-\nu)}$$

where β is the fracture surface energy

2.3.3 POROSITY

Many methods of manufacture used in the fabrication of ceramic components inevitably lead to high levels of porosity. This porosity does lead to a reduction in conductivity, which is beneficial in many situations; however the pores are generally also the cause of difficulties. In particular the strength of ceramics is reduced by the presence of pores as they act as crack initiation sites, this reduction in strength is dependent on several factors;

i) The shape, and size of pore
ii) Their position with respect to the surface
iii) the distance between pores

Different microstructures are shown in figure 2.8. Evans and Tappin have produced an equation giving the theoretical strength of a material with a flaw in the surface, where the reduction in strength

is the greatest:

$$\sigma_f = \frac{Z}{Y}\left(\frac{2\,E\,\beta}{c}\right)^{\frac{1}{2}}$$

where Y is a constant dependent on flaw configuration $\simeq 1.5 \rightarrow 2.0$
Z is a constant dependent on flaw shape $\simeq 1 \rightarrow 2$

Using suitable values for the constant Y and Z this equation can adequately represent the effects of pore shape and size.

The analysis of flaws within the bulk of the material is more difficult and dependent on many factors. If the pore is close to the surface, the bridge of material supporting it from the surface may break, resulting in a flaw causing greater weakness than the original flaw, even if it was at the ceramics surface. Figure 2.9 shows the theoretical reduction in strength according to flaw size. [19]

If pores are close together there is a chance that the bridges between the flaws will crack creating a much larger flaw. The following all have the same theoretical effect on strength. [20]

crack size μm	No of cracks	distance between cracks (fraction of crack size)
477	1	-
95	5	0.3
40	∞	0.575

2.4 PROPERTY DETERMINATION

In recent years the range of ceramic materials available has increased dramatically. Many of these new materials display properties which make them potentially useful engineering materials. However before they can be used by engineers their properties must be accurately measured and the results published. Unfortunately the tests carried out by material scientists are generally for the purpose of comparing different ceramic materials, and the test methods are

often inappropriate for measuring the properties engineers need to know. This is unfortunate as there are often more appropriate testing methods available:

2.4.1 TENSILE STRENGTH

As has already been mentioned the strength of ceramics cannot be stated by a single figure. Instead the mean strength and an indication of the spread of strengths must be given. This type of information can only be obtained through an extensive test programme. The number of tests is not the only consideration, the strength of a ceramic is to a large extent dependent on the number and type of flaws; the number of flaws is in turn dependent on the volume of material tested. To obtain an accurate measure of the strength of a ceramic it is the cumulative volume of material that is tested which is important, not just the number of tests.

Engineers are used to having the tensile strength of a material characterised through the use of tensile tests. This is an excellent test method as it puts a large volume of the test piece under tension as shown in figure 2.10. Unfortunately the fabrication of these test pieces in ceramic is very expensive, and very exact alignment needs to be used when setting up the test.

The most frequently used method of characterising the strength of a ceramic material is through the bend, or flexural strength test. A variety of different specimen shapes, supports and loading mechanisms are employed, but they all have the same major weakness as a test method. Only a small volume of the test piece is subject to a high tensile load, as in figure 2.11. Typically the strength given by a bend test is two to three times that in a tensile test. An attempt has been made to include an allowance for this effect, using stress volume integrals, explained later. This does produce more realistic values of tensile strength, However, even this analysis assumes that the flaw density in a small test piece is the same as that in a large one. This is often unrealistic as the volume

tested in some test pieces is so small. (A 2-3mm thick disc in a bend test only has the bottom 1/2mm subject to high tensile loads) Similarly the manufacturing methods used are often best suited to small test pieces, which will inevitably have a lower flaw density than a large test piece.

The hydrostatic tensile test is perhaps the best test method for ceramic materials at room temperature. A ceramic cylinder is placed around a fluid filled bag, as in figure 2.12, hydrostatic pressure puts the entire volume under tension.

When determining which type of test method is appropriate it is important to recognise that it is the quality and not the quantity of tests which is important in establishing the tensile strength of ceramics. Wherever possible large test pieces should be used, with a test method that maximises the volume held in tension.

2.4.2 YOUNG'S MODULUS

There are two main methods of measuring Young's Modulus

The first can be carried out at the same time as the tensile test mentioned before, a graph of stress vs strain must be produced, and Young's Modulus measured from its gradient. This is an excellent test at room temperature where strain gauges are used to produce the load deflection diagram.

Young's Modulus can also be measured by using the relationship between the resonant frequency and Young's Modulus:

$$E = C\ M\ f^2$$

where f is the frequency of vibration
M is the mass
C is a constant dependent on the specimen size, shape and Poisson's ratio.

The resonant frequency is measured and used with published values

for the above constants. This method is more appropriate at higher temperatures where the strain gauges in the former method cannot be used.

2.4.3 CONDUCTIVITY

There are two basic types of conductivity measuring tests, static and dynamic.[78] Static methods measure the steady state temperature gradient in a material sample together with the heat flow. Dynamic methods employ transitory applied heat inputs; the temperature changes in the sample are then used in conjunction with the Fourier heat flow equation to calculate the conductivity.

There are two subsets within the range of static methods, these are longitudinal and radial flow methods. With the longitudinal method a known heat flow is conducted along a rod of fixed diameter. The temperatures at two stations are then recorded, enabling the conductivity to be calculated. Allowance for radial heat loss, and the alteration in heat flow caused by the temperature sensors must be made. Radial methods employ a heating source which is enclosed by a cylinder or sphere; again the temperature drop across the sample material is used to calculate conductivity.

Dynamic conductivity measuring methods can also be split into two types, those using a single heat input, and those incorporating a cyclic input. With both methods it is normal to monitor the imposed temperature and the temperature at another point in the structure. The thermal conductivity can then be calculated from these transient temperature fields.

2.5 CERAMIC MATERIALS APPLICABLE TO ENGINES

The ideal characteristics for thermal insulation materials are easily classified. The material must be light as well as strong at elevated temperatures, possess good thermal shock resistance and have low thermal conductivity. A thermal expansion coefficient comparable to the surrounding structure is also important, especially if coatings are considered. Ceramics are able to satisfy some of these demands easily, others represent a problem for many ceramics. It is obviously important to minimise these problems by choosing the correct material for a given situation. There will probably not be a single ideal material for use in the internal combustion engine, but different materials for each area which needs insulation. There are many contenders for use in the internal combustion engine, the most popular are probably silcon nitride and partially stabilised zirconia.

2.5.1 ZIRCONIA

As mentioned before zirconia is a polymorph, able to exist in more than one crystaline form.[22] Zirconia therefore cannot be used as an engineering material at temperatures where the change in crystaline form occurs, as the accompanying volume change will result in component failure. Fully stabilised zirconia uses MgO, CaO or Y_2O_3 to keep the cubic form stable over a wider temperature range. Partially stabilized zirconia (PSZ) uses lower levels of these additives so that a mixture of the stabilized cubic phase, and the monoclinic phase is formed. The temperature range for stability is shown in figure 2.13.[20]

PSZ has a very high fracture toughness, this occurs as the cubic structure has tetragonal particles within it. Any crack propagating through the material will transform these tetragonal particles into the cubic form at the crack front. The associated change in volume causes micro cracking, restricting further crack growth.

Zirconia has a high density and it is therefore mainly in the field of coatings where it has been of use. As a coating it has been used

In the gas turbine industry for some time. It has a low thermal conductivity, low emissivity, and a high enough coefficient of thermal expansion to avoid a large mismatch with the metal substrate. The following properties have been observed.

Property	300K	1200K	
Young's Modulus	180*	170	GPa
Poisson's ratio	0.23	0.23	
Thermal conductivity	2*		W/mK
Thermal expansion	10	10	$x10^{-6}$
Weibull Modulus	20	8	

* where high porosity is present this value will be lower.

These coatings are formed by plasma spraying the ceramic onto metal, using an intermediate bond layer such a nickel aluminide, or CoCrAlY (Cobalt-Chromium-Aluminium-Yttria) These provide an improved thermal expansion match and adherance.

The different types of stabilizer lead to different mechanical strengths. Yttria stabilised PSZ monoliths offer the greatest strength, once the surface is subject to abrasion. The surface layer is transformed to a cubic form by this action, creating a compressive layer. However there is doubt if Yttria stabilized PSZ is stable under the chemical attack arrising in the IC engine.

	Strength MPa	K_{1c}
Cubic	240	2.8
PSZ transformation* toughened	600-800	7.1
100% tetragonal Y_2O_3 stabilized	1200	12

* Transformation toughening occurs when particles of an additive are mixed with the main ceramic material. This additive is chosen such that during the cooling period after manufacture their relative

expansion creates local stressing and cracking, an increase in fracture toughness results.

2.5.2 SILICON NITRIDE

This is a well established material whose properties are fairly well understood. It is a strong high temperature ceramic with good thermal shock resistance, but it is a poor thermal insulator. It was originally developed for the gas turbine industry where its poor insulation properties were unimportant. For silicon nitride Si_3N_4 to be adopted for use in the adiabatic diesel engine additional insulation needs to be provided, this is generally gained through the use of an air gap. There are two main methods of preparing silicon nitride components, hot pressed and reaction bonded.

Reaction bonding: Silicon powder is formed into the required shape, and compacted. The component, said to be in the green state is then fired in a nitrogen or nitrogen/helium atmosphere. A complex firing schedule is necessary lasting up to 12 days at temperatures from 1200 to 1400^{o}C. The nitrogen reacts with the silicon to from silicon nitride.

Hot pressing: Hot iso-static pressing (HIP) subjects silicon nitride powder to simultaneous high pressure and temperature.

Both the above forming methods are discussed in section 2.6. Reaction bonding, although a time consuming precedure, has the advantage that the shrinkage during densification is less than 1%. Hot pressing can have a reduction in volume of up to 8:1. Reaction bonded components therefore require little final machining. Hot pressed silicon nitride has better mechanical properties, as shown in figure 2.14. The following are typical properties for silicon nitride.

	RBSN/HPSN	
Strength	580/145	MPa
Young's Modulus	310/690	GPa
Poisson's ratio	0.24/0.27	
Thermal conductivity	30/12	W/mK
Thermal expansion	2.5/2.4	$x10^{6}$

2.6.3 SILICON CARBIDE

Silicon carbide is another material which was first evaluated for use in the gas turbine industry. It has high strength and temperature stability, and like silicon nitride it has high conductivity and low thermal expansion. The main problem encountered is its hardness, it is difficult to finish machine, and for this reason is not thought of as the most likely material for use in the internal combution engine.

Strength	410MPa
Hardness	3300
Thermal expansion	$3.8x10^{-6}$
Young's Modulus	400GPa

The strength of SiC with temperature is shown in figure 2.14.

It is difficult to propose silicon carbide as an insulation material, given the availability of other materials, which have similar thermal conductivity without appreciably worse mechanical properties.

2.6.4 SIALON

Sialon's (Silicon-Aluminium-Oxygen-Nitrogen) are a range of materials with different compositions, and hence properties. It has similar conductivity and density to HPSN, with this high thermal conductivity air gaps would be necessary in components. Also the expansivity of $3x10^{6}$ is approximately that for RBSN and HPSN.

Strength	450MPa
Hardness	2000
Thermal expansion	$3x10^{6}$
Conductivity	20W/mK

2.6 FABRICATION

There are four stages in the formation of most ceramic monoliths, starting from a finely ground powder, with exactly controlled particle size and composition, to the final inspection of the completed component. These are:

i) Powder processing
ii) Compact formation
iii) Densification
iv) Final machining and inspection

2.6.1 POWDER PROCESSING

The object of any forming method is to achieve maximum density of particle packing and uniformity of structure. The powders used must be sized so that maximum density can be achieved. A single particle size produces high porosity. Analysis gives the following theoretical densities for uniform particle size:

Dense random packing	64% filled
Loose random packing	60% filled

By using a range of particle sizes a maximum density of over 75% can be achieved. Unfortunately raw materials are not usually available with an optimum particle size distribution. There are many ways of processing powders to produce the desired range of particle

sizes. These include Ball Milling, where the raw material is placed in a rotating cylinder containing a grinding media. Different processing times are used to produce a variety of size distributions. Fluid energy milling uses a mixture of ceramic and a high pressure fluid which is used to impact the particles against the wall of a grinding chamber.

To obtain the desired particle size distribution, powders may be sorted. The particles can be graded using a number of sorting screens, with decreasing aperture size. Air classification uses centrifugal forces set up by rotating air currents to grade the particles.

Additives where required are mixed with the ceramic at this stage, there are a variety of chemicals for different applications:

1/ Binders are added to give the formed compact enough strength to permit handling before firing.
2/ Lubricants are used to decrease friction during compaction and so help increase the final density.
3/ Sintering aids are included where activating agents are needed to promote densification (section 2.6.3)

2.6.2 COMPACTION

There are many methods of forming the powdered ceramic into the desired component shape, called the green state.

Pressing: Two main methods are used; Uniaxial and Isostatic pressing. Uniaxial pressing involves the use of a die where pressure is applied in a single direction through a plunger, this procedure is shown in figure 2.15.[16] This method has a very high output rate, but can suffer from high variations in compact density, die wear can also be significant. Isostatic pressing involves the application of pressure from all sides. The powder is enclosed in a non-ridged mould and fluid pressure applied, this arrangement is shown in figure 2.16. Components with good internal, but poor external tolerances are produced. A good density can be achieved, but production rates

are slower than with uniaxial pressing.

Casting: Ceramic particles held in suspension in a liquid are cast in a mould. In slip casting a porous mould is used to remove the fluid by capillary action. The ceramic suspension (slip) is poured in the mould, and left as the ceramic is deposited on the walls, this procedure is outlined in figure 2.17.[16] The mould preparation and deposition time must be carefully controlled. This method can produce complex shapes, but is difficult to automate and only low levels of output can be achieved. Slip casting can produce high tolerance components.

The lost wax method can be an excellent casting method for many situations. A wax pattern is formed using a mould, and filled with ceramic slip. After ceramic deposition is completed the wax is either disolved or melted. This production method can be automated, and used to produce components with excellent tolerances, the procedure is outlined in figure 2.18.

Plastic forming: A polymeric binder is added to the ceramic powder to create a mixture of the desired viscosity. A 10-30% liquid content is generally used, normally heat is provided to melt the binding agent. The resultant material is generally injection moulded or extruded whilst hot. In injection moulding a ram is used to force the material into a shaped cavity, the mould is then cooled, and the binder sets, the component can then be removed. The binder is burnt out later. Extrusion is an excellent method of forming green state ceramic, but shapes need to have a constant cross section.

These plastic forming methods can be used to create a variety of different ceramic shapes but unless the moulding equipment is correctly set up large pores can be formed in the ceramic.

2.6.3 DENSIFICATION

All ceramics have one common characteristic in the way they are made. A heating process is used which is not sufficient to melt the raw material completely, but instead causes the uniting of adjacent

particles. This process is called Sintering. The aim of densification is to remove all the gaps between the particles present in the green state, it therefore leads to component shrinkage.

Ceramic components are difficult to machine after densification; so machining should be carried out before this stage. However, when distortion occurs during the firing process then this may not be possible.

Solid state material transport is the main mechanism involved in sintering, through which ceramic particles grow together, and bonding between adjacent particles occurs. The driving force for sintering is provided by excess surface energy which a material possesses when it is divided into many parts. Heat is necessary to enable the surface energy of the system to be minimised, as the particles move together. The process of densification is initially rapid, but progressively slows, for low levels of porosity long firing times are generally necessary. Unless both dense and uniform packing were achieved in the construction of the compact shrinkage will be high, and significant porosity will result. To obtain maximum density the vacancies in the compact should be gas free, or allow any gas to defuse away.

Reaction bonding is a development of sintering which produces components without the high level of shrinkage associated with conventional sintering. Its main use is in the production of silicon nitride and silicon carbide components. In the former case a compact of pure silicon particles is formed, and fired in nitrogen. To form silicon carbide a mixture of SiC powder and carbon is fired in molten or vapour phase silicon. Both silicates undergo a dimensional change of less than 1% during densification.

Sometimes the processes of compaction and densification are combined as in the case of cold pressing and hot pressing.

- Cold pressing: Where soft materials are used, cold pressing in which pressure and not heat is applied can be used to produce a dense specimen. In this case densification is primarily

achieved through plastic flow.

Hot pressing: Pressure and heat are used during the densification process. An increase in the density is achieved in the latter stages of sintering using this method. This is bought about by plastic flow, and bulk diffusion.

2.6.4 FINAL MACHINING AND INSPECTION

Where possible the compact should be made to size using the previous methods, however dimensional tolerances may be too tight, or an improved surface finish required. The problem in machining fired ceramic components is two fold:

i) The difficulty in holding a brittle component while it is machined.
ii) The high hardness of ceramics forces the use of expensive and slow machining methods.

There are many methods of machining ceramic components, these include:

Mounted Abrasive Machining: This includes machining methods such as the use of grinding wheels. For very hard ceramics such as Si_3N_4 and SiC, diamond is the most efficient abrasive.

Free Abrasive Machining: Loose abrasive is placed on a soft material and used to lap the ceramic material. However, the ceramic removal rates are very low, and its main application is where mirror or bearing surfaces are required.

Impact Abrasion: Abrasive particles are impacted on the workpiece using compressed air. Al_2O_3 and SiO_3 are commonly used abrasives, this method is mainly used for cleaning the surface as close tolerances are difficult to achieve.

Machining ceramic components can dramatically reduce their

strength. The process of machining involves the breaking and deformation of the material, this creates cracks in the surface of the ceramic. It is possible to reduce the effect of machining. Grinding will introduce cracks parallel to the direction of relative movement, the component should therefore be machined so that the introduced flaws run parallel to the action of the applied load. Post machining processes such as lapping and surface compression can also be used to reduce the effect of these cracks.

The scatter exhibited by the properties of ceramics make the non destructive testing of ceramic components far more vital than it is with metal ones. The view is held in certain quarters that by using NDT to detect large flaws in ceramics the scatter can be reduced. Examining figure 2.9 showing the strength of RBSN against flaw size it would seem that testing for flaws of over 50μm would guarantee a strength of over 200MPa. This is misleading because several small flaws close together have the same weakening effect as a large flaw.

Another NDT method is to overstress a component, since a large load applied over a small time increment can represent the entire working life of a component at a lower stress level. By briefly overstressing a component in this way it will fail if a large flaw is present. However, this method will increase the crack size of any non critical length cracks, and so shorten the life of components that do pass this test.

2.6.5 PLASMA SPRAYING

This is the process through which molten material is sprayed onto a substrate. The spray/substrate material combination must be one in which adherance will be achieved. Zirconia and steel or aluminium are the combinations attracting interest for the insulation of the internal combustion engine. These thermal barrier coatings generally consist of a corrosion resistant metal coating with a plasma sprayed zirconia layer. The zirconia can either be a single thick layer, or can include a graded ceramic/bondcoat layer. Zirconia coatings formed by plasma spraying are full of pores, and generally cracks.

This porosity typically reduces the conductivity form 2 to 1W/mK. Young's Modulus is about one tenth of the monoliths value.

The process of plasma spraying makes use of a plasma torch which is fed with hydrogen and argon which are electrically heated to form a plasma. The zirconia is then fed into this plasma in the form of a fine powder (typically 20μm diameter) where it is melted. The substrate is cooled by air jets on the front or rear face to prevent over heating.

Achieving an optimum coating is a complex procedure, involving the setting many variables; as the process of plasma spraying is not fully understood these variables are generally set to levels that have been successfull in the past. There is little information available to optimise the coating for a given application. The variables which can be adjusted include; electrical power, plasma gas flow rate, cooling gas velocity, spraying distance, gun traverse rate, gas temperature and ceramic feed rate. By varying these it is possible to form a coating with graded porosity, and hence conductivity. By mixing the ceramic with a metal all the properties can be varied.

2.7 DESIGNING WITH CERAMICS

The design of components in brittle materials involves a different design philosophy from that in ductile materials. Simply to replace a metalic component with a ceramic equivalent without any design changes will give a high probability of failure. There are three rules which should be followed wherever possible in the designing of ceramic components.

i) Stresses should be kept compressive as this slows the rate of propagation of cracks.

ii) Direct contact between ceramic components should be avoided. Deformable soft metal elements should be used between the brittle ceramic components.

iii) The factors of safety must be larger than those employed in

metal components.

The main difference in design arises from the lack of experience engineers have in dealing with ceramics. Engineers generally only use high performance ceramics where metals cannot be used. The mechanical and thermal environment these ceramics are subject to is therefore invariably very hostile. Little background experience has been gained with high performance ceramics in situations where the loading is not so severe. In most design situations it is possible to refer to previous problems which have been successfully resolved, so new designs represent an excercise in extrapolating design trends. This approach is not yet possible with ceramic materials, because of the limited background available.

It is also difficult for an engineer to reach a definite conclusion as to whether a component will survive under given conditions using the traditional range of mathematical tools. The best that can be done is to give an indication as to the probability of survival.

There are two design approaches possible:

i) To accept that numerical results can only give an indication of the stresses that are likely to arise and to produce a series of designs. Each of these must be tested and an empirical store of knowledge built up. This approach can only be used when a large amount of machine shop time, and material is available.

ii) Develop methods of mathematical analysis which are appropriate to the study of ceramic materials, such as probabilistic analysis

It is likely that before ceramics find widespread commercial use in mechanically hostile environments both areas will need to be investigated

2.7.1 PROBABILISTIC DESIGN

By selecting a probability of component failure which is acceptable, the Weibull statistical method can be used to find the maximum stress which can be allowed.

The most useful design tool of recent years is the finite element method: its use in many engineering situations is now commonplace. Similarly Weibull analysis is one of the most useful concepts in the understanding of the behaviour of ceramics. Engineers have sought to combine both of these methods.

The finite element method is used to split the component being studied into a number of elements, and then calculate the stress present within each of these elements. Weibull statistics are then used to calculate the probability of failure wtihin each of these elements. This information can then be used to produce a plot showing the probability of failure throughout the component rather than the stress levels. Alternatively all the elements can be summed and the total probability for component failure produced.

There are two forms of this analysis

i) Assuming the component will fail due to the presence of flaws in the body of the material, a volume integral is used to find the probability of failure.

ii) If flaws in the surface are assumed to be far more likely to lead to failure than those in the rest of the component then surface integrals are used.

This design tool can be used to evaluate the likely performance of ceramic monliths. It should reduce the protracted hardware development time, which at the moment is necessary with ceramic components. However, like all numerical methods its accuracy is dependent on the availability of accurate and valid material property data.

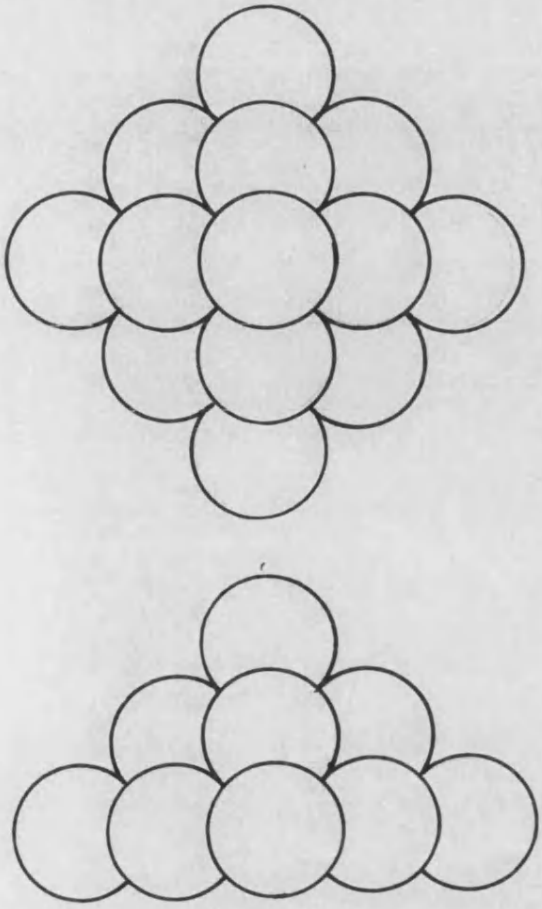

The regular structure exhibited by metals, where only one type of atom is present.

FIGURE 2.1 CLOSE PACKING OF ATOMS

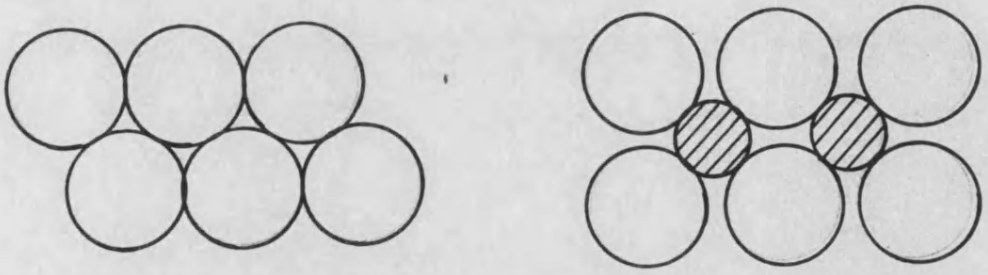

Ceramics have more than one atom type, so their structure is less dense.

FIGURE 2.2 IONIC BONDING WITH ONE OR TWO ATOM TYPES.

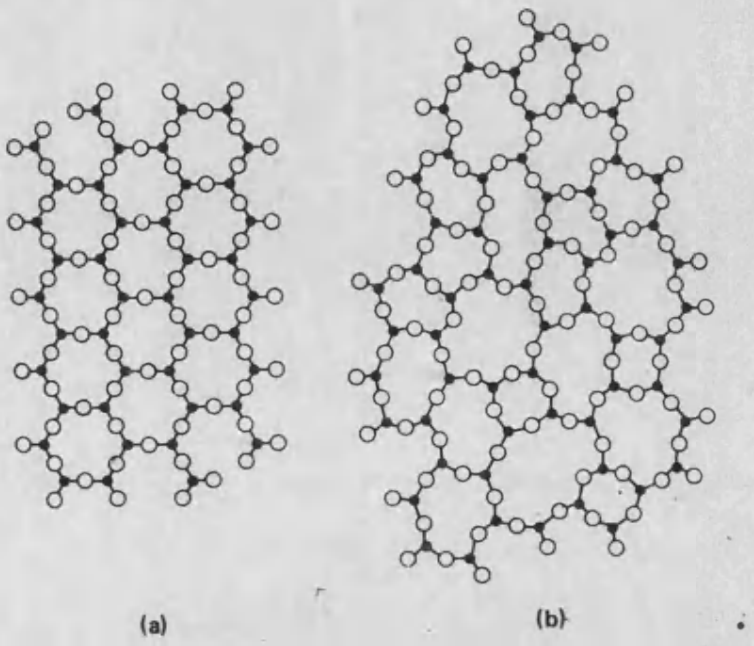

FIGURE 2.3 CRYSTALINE (a) AND NON-CRYSTALINE (b) ATOMIC STRUCTURE.

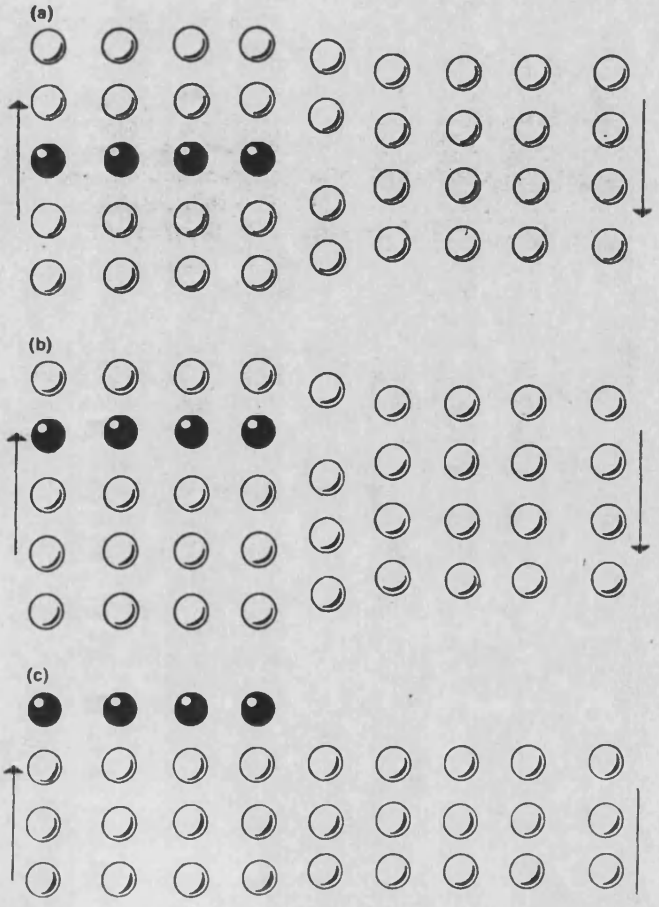

FIGURE 2.4 YIELDING THROUGH THE PROCESS OF DISLOCATION.

FIGURE 2.5 A LOAD ON A LIQUIDS SURFACE CAUSES AN INCREASE IN AREA.

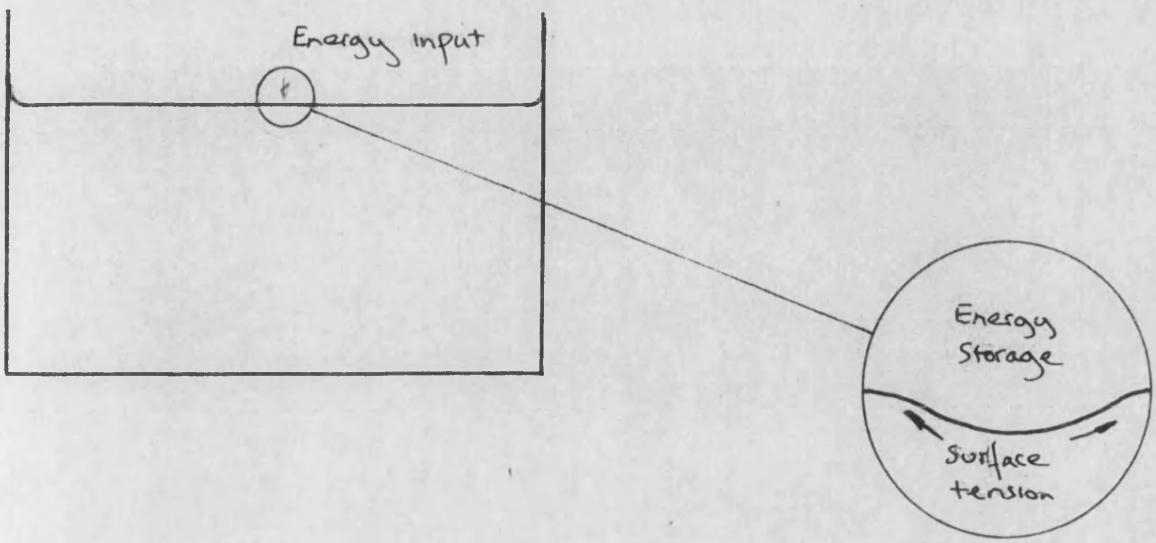

FIGURE 2.6 PROBABILITY OF FAILURE SHOWN ON WEIBULL PAPER.

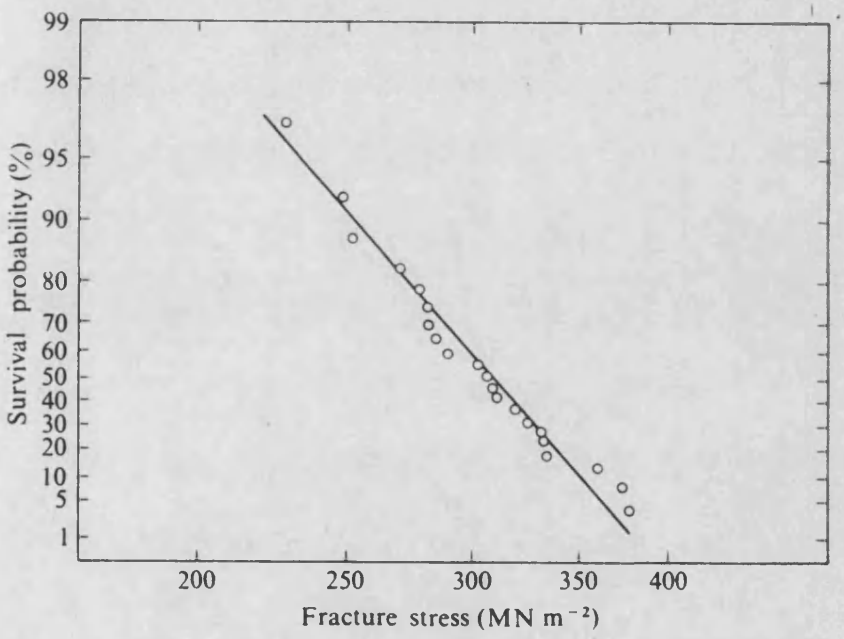

FIGURE 2.7 STRENGTH-PROBABILITY-TIME DIAGRAM ON WEIBULL PAPER

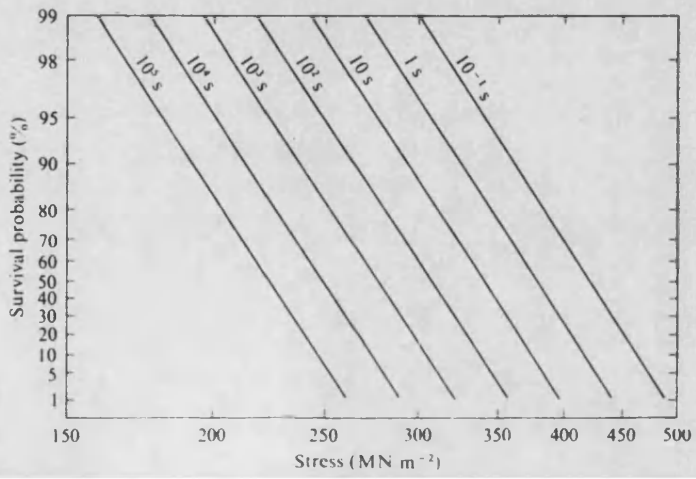

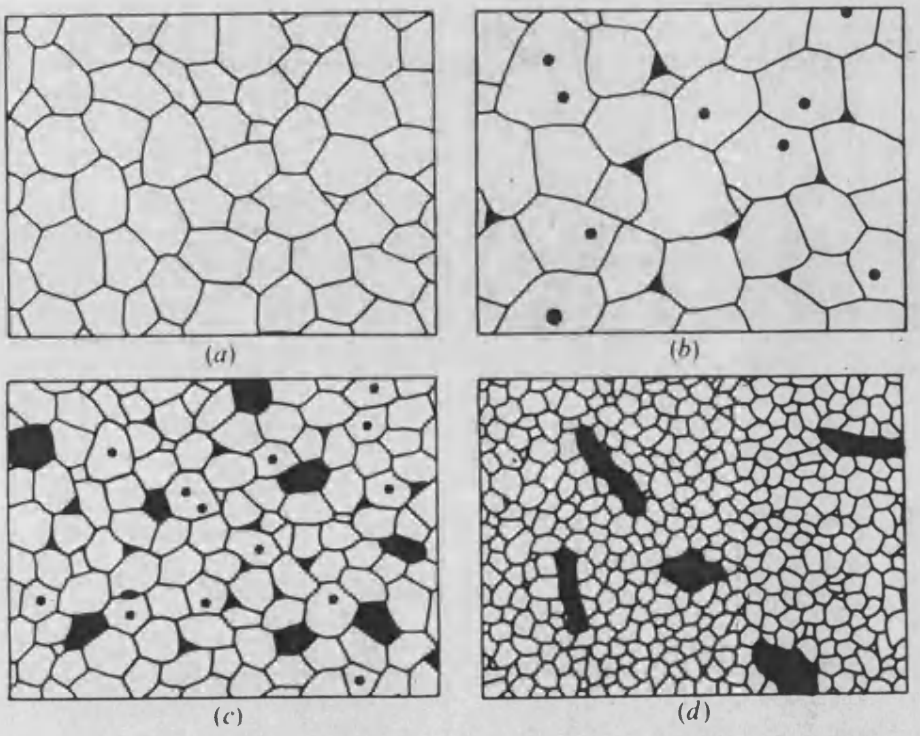

FIGURE 2.8 DIFFERENT POROSITY DISTRIBUTIONS IN CERAMICS

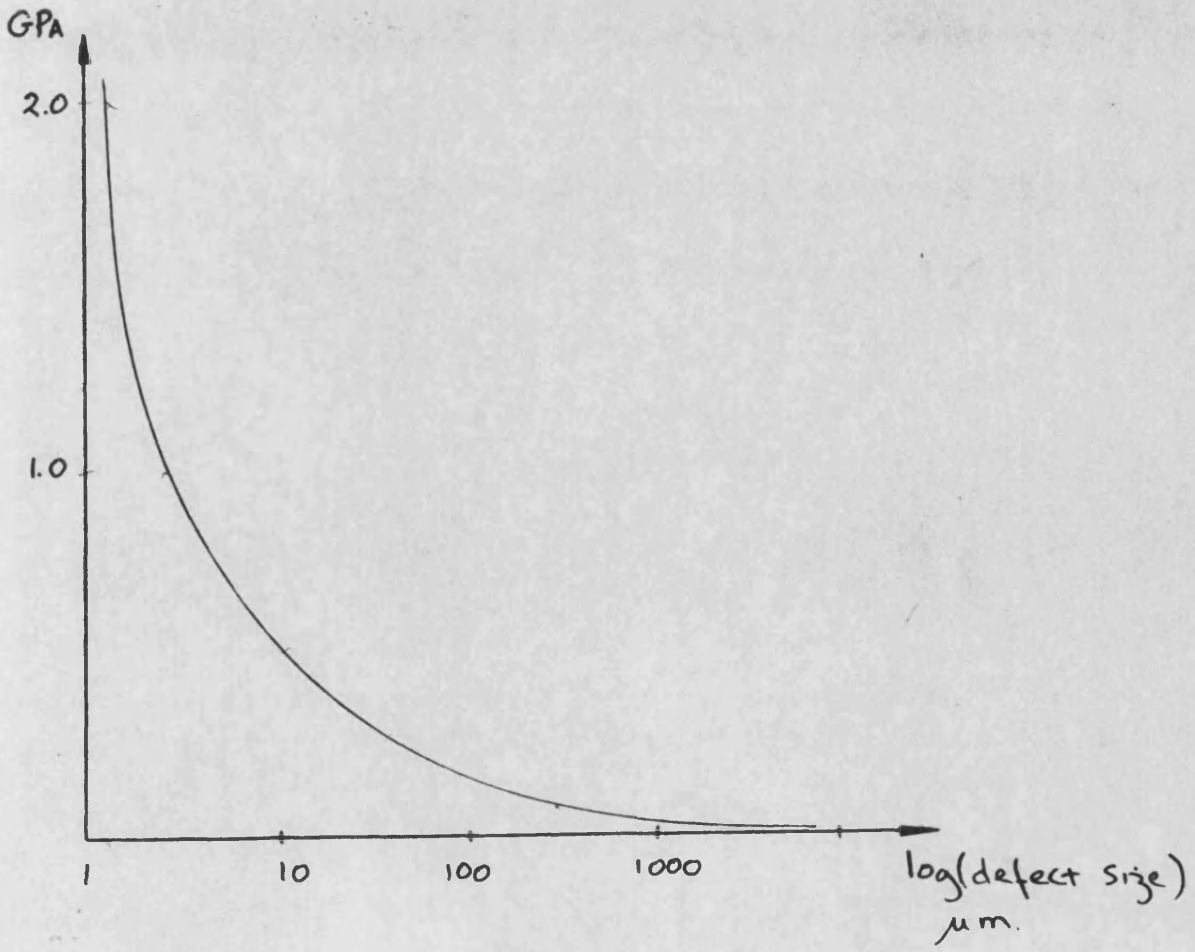

FIGURE 2.9 REDUCTION IN BULK STRENGTH CAUSED BY DEFECTS.

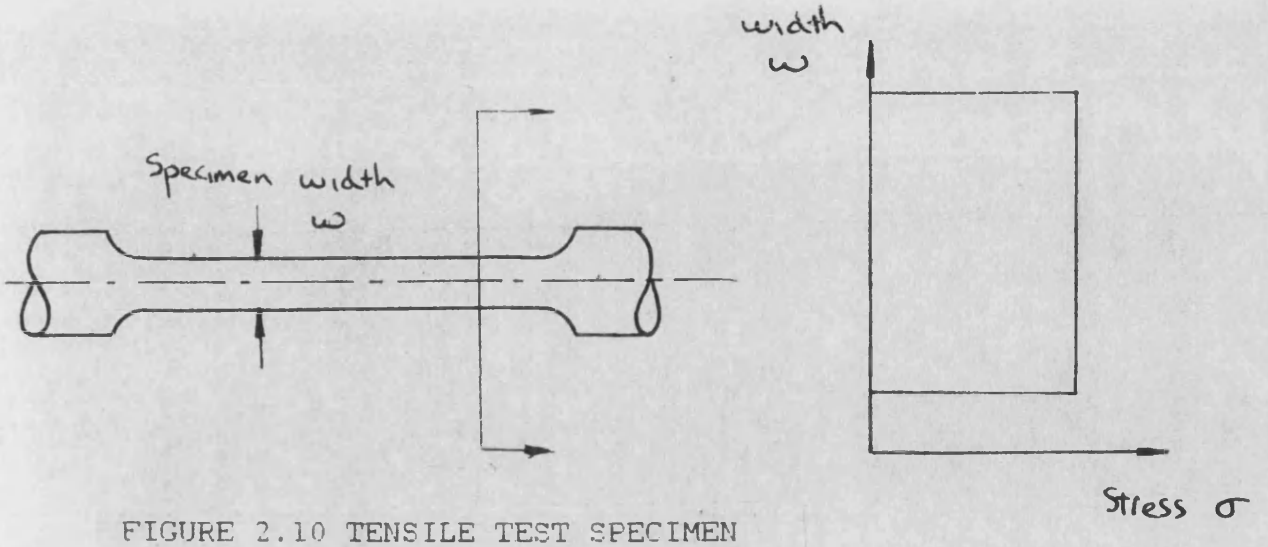

FIGURE 2.10 TENSILE TEST SPECIMEN

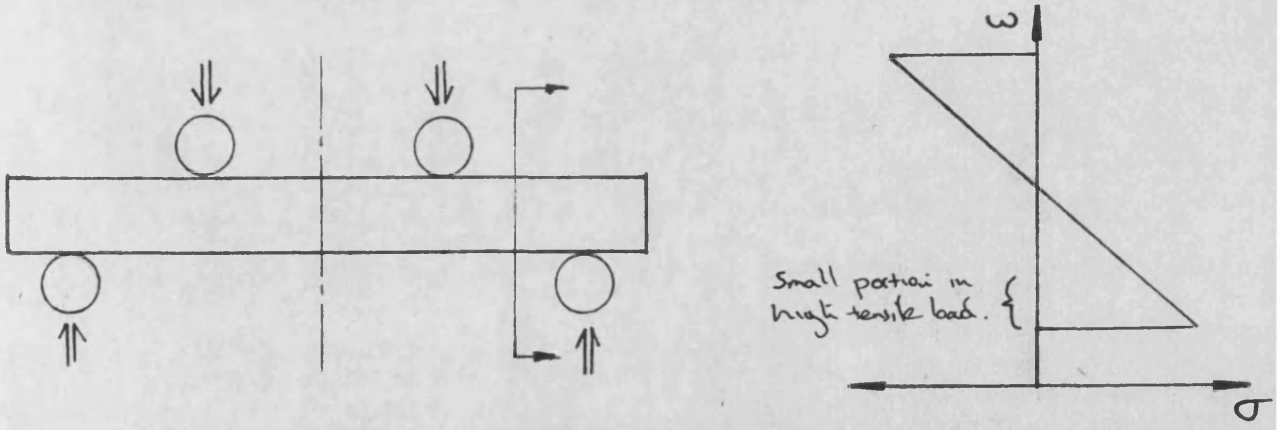

FIGURE 2.11 FLEXURAL STRENGTH TEST

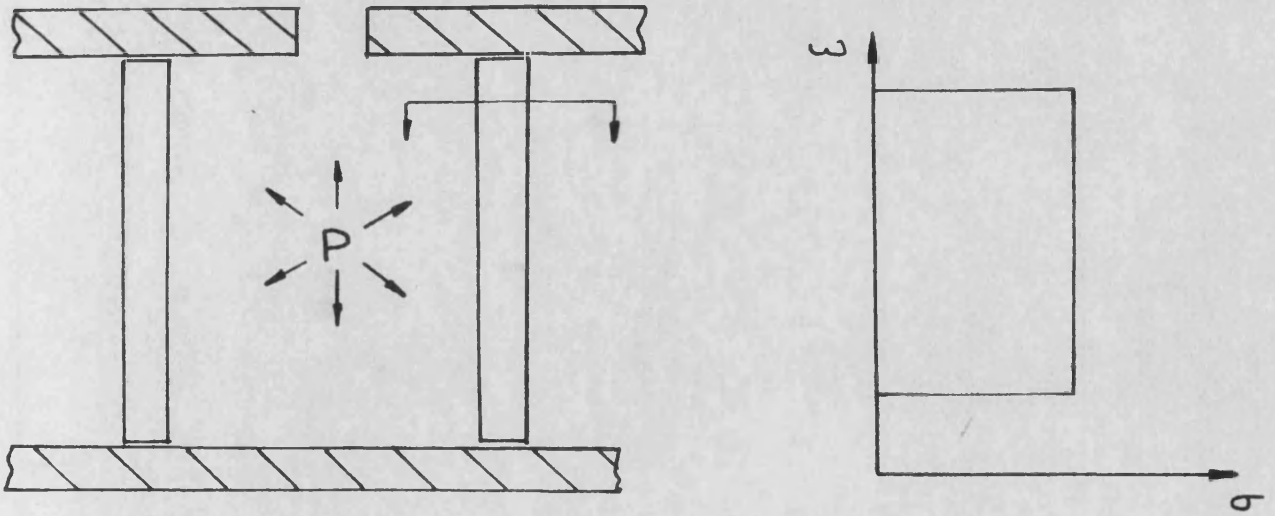

FIGURE 2.12 HYDROSTATIC TENSILE TEST

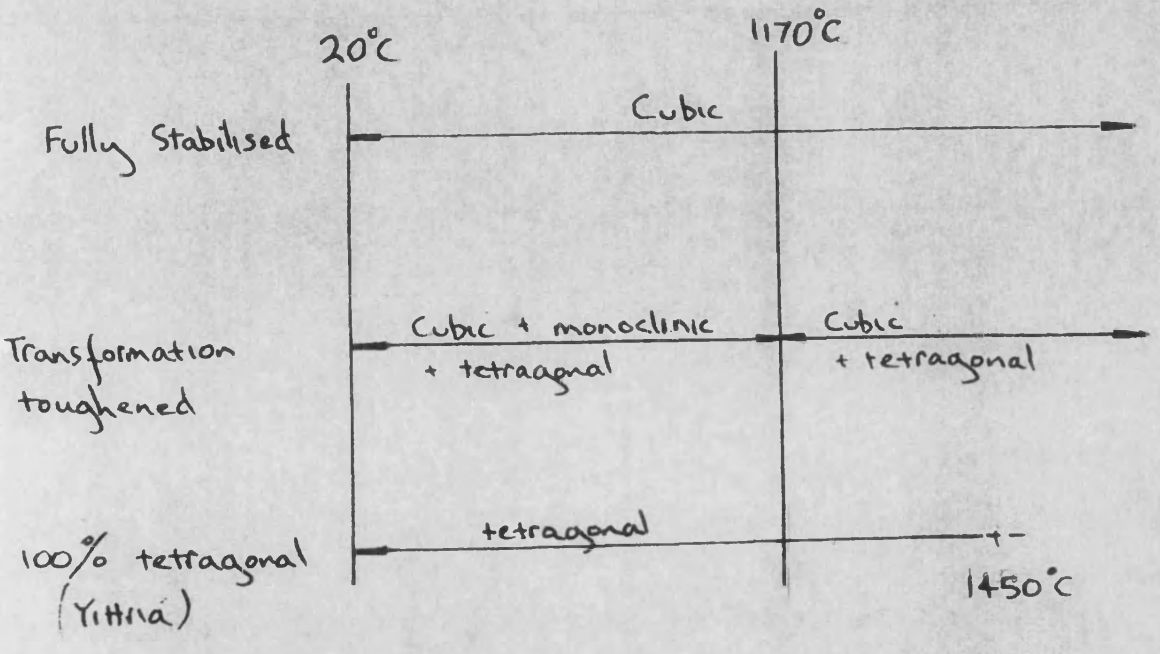

FIGURE 2.13 STABILITY OF STABILISED ZIRCONIA

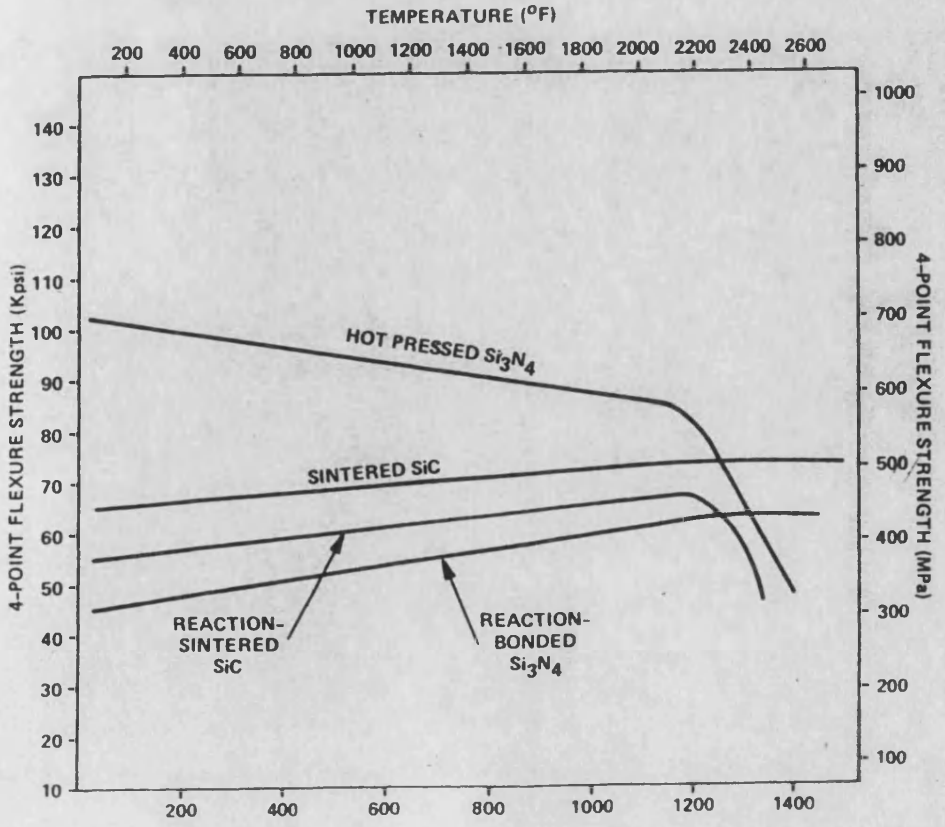

FIGURE 2.14 STRENGTH OF SiC AND Si_3N_4 WITH TEMPERATURE

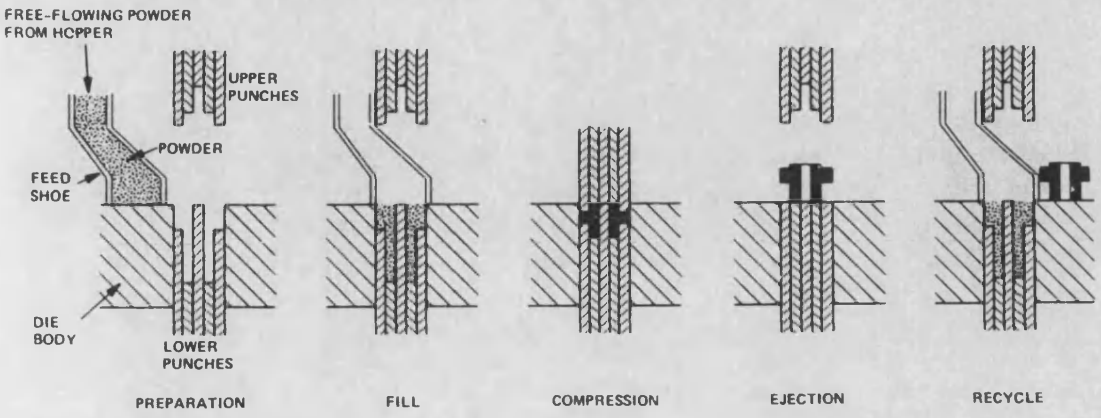

FIGURE 2.15 UNIAXIAL PRESSING.

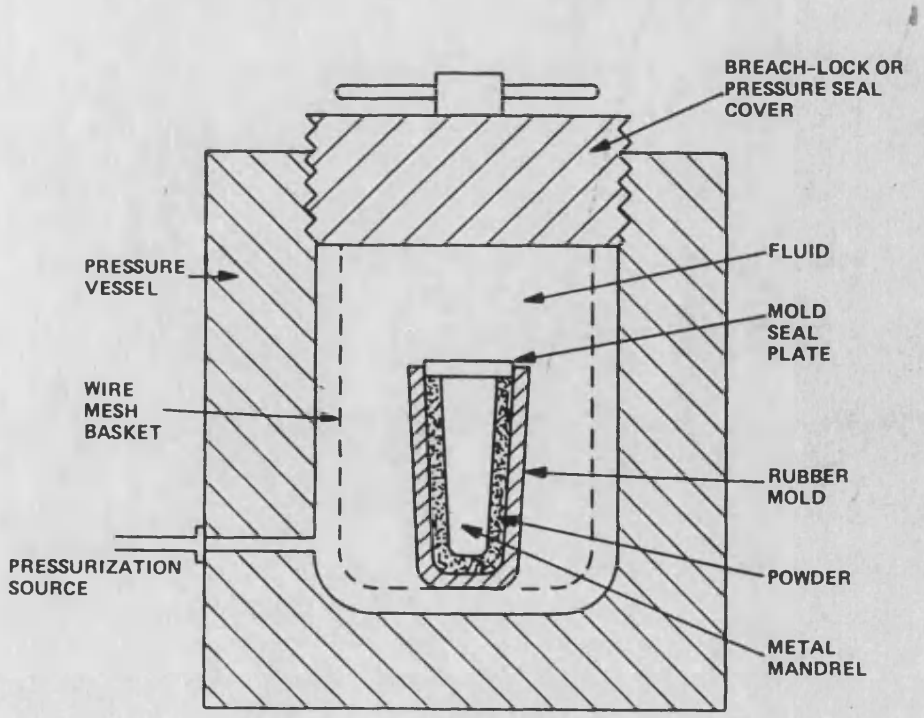

FIGURE 2.16 ISOSTATIC PRESSING.

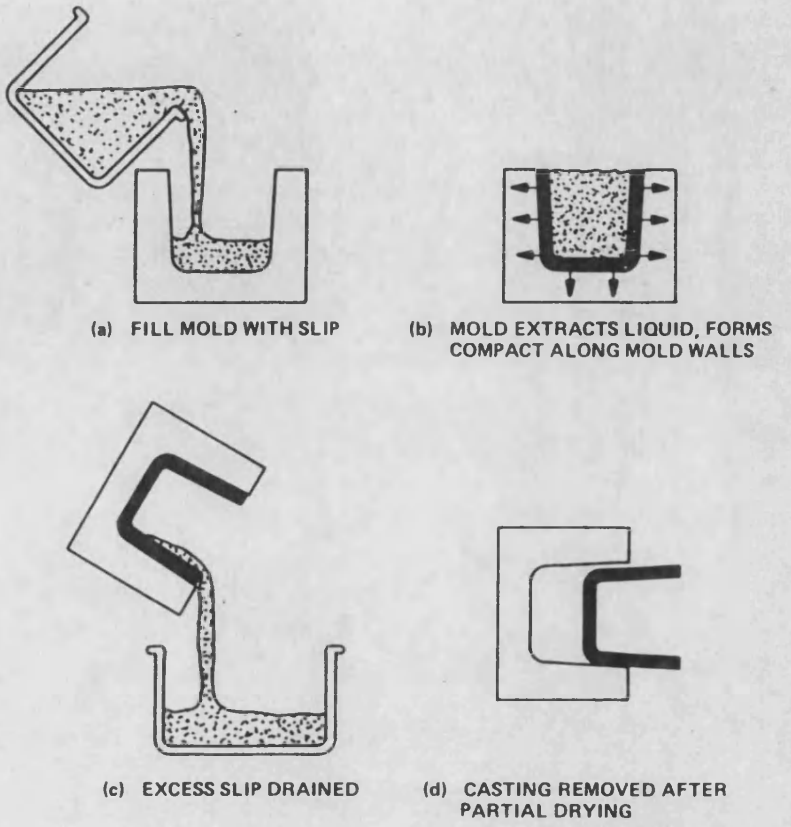

FIGURE 2.17 SLIP CASTING.

3.1THEORETICAL AND EXPERIMENTAL STUDIES TO ASSESS THE PERFORMANCE OF INSULATED DIESEL ENGINES

To achieve optimum operating efficiency in an adiabatic engine a complex compromise between insulation levels, surface temperatures, exhaust enthalpy, boost pressure, turbine and compressor geometries, level of cooling, and turbine and compressor gearing must be reached. This problem is further exacerbated as these variables must be optimised over a speed range. During the preliminary development of any design these factors can best be assessed through the use of a computer model. Computer simulations of the internal combustion engine have existed for some time, mainly following the same concepts as for conventional engines and using similar simplifications. The engine model is split into a number of sub models covering each of the systems elements, such as compressor, turbine and reciprocating engine, all of these need not be discussed here. However, the heat transfer model is of particular interest in the case of an insulated engine and is worth mentioning briefly.

3.1.1 HEAT TRANSFER MODEL

Heat loss in a diesel engine is the sum of four components, convective, radiative, conductive loss and unused exhaust enthalpy. The convective loss component is lowered through the introduction of insulation, whilst the radiative contribution may increase due to the higher gas temperature. Accurately representing this complex heat transfer phenomenon is one of the more difficult elements in diesel engine performance modelling. This involves an assessment of the temperature and heat transfer coefficients of both the working and cooling media, using either instantaneous values over the cycle or a constant approximation. A method of predicting the soot production and hence radiation is ideally required. Siegla and Amann[24] compared the heat rejection of a baseline and low heat rejection engine at 1000 rpm, the increased radiative component is clearly shown in figure 3.1. In addition the engines insulation properties

must be represented, this is generally achieved by calculating an equivalent thermal resistance for each component. Unfortunately the engine components are complex three dimensional shapes and are not easily described by one or two dimensional thermal resistances.

The problem of representing the heat transfer in an engine can thus be divided into three sections:

i) HEAT CONVECTION FROM GAS TO WALL: There are three main ways of representing the gas heat transfer coefficient and temperature:

a) Using spatially and temporally constant values. This is incorporated into very simple computer models and is not of sufficient accuracy to be of use when accurate heat losses and efficiency estimates are required.

b) A spatially variable time average value, this type of correlation is used in finite element programs when calculating the equivalent heat transfer coefficient.

c) A spatially constant but instantaneously variable representation such as the Woschni[25] correlation, this is the most frequently used representation in diesel engine simulations.

The Woschni heat transfer coefficient was used by Watson et al[26] to establish a spatially constant instantaneous heat transfer coefficient. An iterative loop is used to calculate the heat transfer through the combustion walls. A constant wall temperature is assumed at the start of the cycle. This value together with the predicted gas condition is used to estimate the associated heat flow. A more accurate estimate of the surface temperature can then be formulated and the calculations repeated. Cycle to cycle temperature transients are therefore ignored. At low levels of insulation this approximation is valid. However, when low conductivity materials are used these fluctuations of wall temperature become more critical.

In addition to the convective transfer the radiative component should be predicted. Accuracy is dependent on the assumed level of soot in the combustion products. General Motors Research Laboratories have used the Arrhenius expression[27] derived by Khan et al to assess soot formation. These equations are experimentally based and are held to be the best representation available although 'considerable uncertainty surrounds the validity of the soot model'. The radiative heat transfer thus calculated is shown in figure 3.1.

ii) HEAT TRANSFER THROUGH WALL: For the purpose of analysis it is generally assumed that heat flow can be represented by a number of one or two dimensional heat paths, and thus the thermal circuit can be represented by a simple electrical analogy. Each of the engine components is represented by an equivalent resistance. The temperature difference and heat flow are analogous to the voltage and current respectively. This thermal resistance is often calculated by the finite element method. The component under consideration is modelled with typical thermal boundary conditions; the analysis yields heat flow and subsequently the equivalent thermal resistance is found. However, the resistances calculated become increasingly inaccurate as the operating conditions are altered. This arises as the assumption of one dimentional heat flow introduces inaccuracies which increase away from the calculated operating condition.

iii) HEAT TRANSFER FROM WALL TO COOLANT: Empirically calculated heat transfer coefficients are used. Where water cooling is incorporated the heat transfer coefficient and temperature are constant throughout the cycle and theoretical representation is not as complex as that required from the combustion side.

3.1.2 COMPUTER PREDICTED PERFORMANCE

The initial theoretical study of Kamo and Bryziks[2] into the performance gains available through the use of thermal insulation revealed the potential for significant efficiency gains. The predicted efficiency of an uncooled turbocompound engine was given as 48%, whilst an unlubricated engine was expected to return 56%. Although these figures seemed optimistic, the initial aim of a 48% efficiency

has been achieved. Further theoretical studies have since been undertaken by other researchers. These, as expected, show that the increased wall temperatures resulting from an increase in insulation cause a lowering of the volumetric efficiency. This trend can be compensated for by using the increased exhaust enthalpy to raise the boost pressure. However, charge heating not only reduces the volumetric efficiency but also increase both compression and expansion work. Figure 3.5, from Ford[28] shwos the breakdown of the indicated work, into compression and expansion work.

Watson et al[26] have assessed the relative improvements predicted by various compound systems. The efficiency gains over the standard engine are shown in figure 3.3, all five engine configurations used a 40% insulation level. The turbo-compound system has a low efficiency at part loads due to turbine mismatch at these low speeds. Efficiency improvements at these low loadings are observed when a variable geometry turbine or variable gearing are used. Further theoretical work indicated that the increase in efficiency is approximately linear with the level of insulation, in a practical engine a 40% reduction, in heat loss to coolant would produce a 2.3% gain in efficiency at full power and 1.7% at 40% load. The extreme case of a truly adiabatic engine would have a 20% improvement in efficiency over a convential engine. However it should be recognised that the reduction in heat loss and thickness of insulation are not proportional: each unit increase in the insulation thickness produces a lower net effect.

The effect of increasing the thickness of an insulating PSZ coating has been examined by Vallad H. and Wyspianski G.K.[29] using a cycle simulation program. Figure 3.4 shows the energy balance. The value of thermal conductivity assumed was 2W/MK; although this value is that generally accepted for monolithic Zirconia, the high porosity in plasma sprayed zirconia reduces the conductivity to approximatley 1W/MK. Consequently the scale on the abscissa is in error approximately by a factor of two. The energy balance shows that only mimimal changes in heat to coolant occur for thicknesses over 5mm, this corresponds to approximately 2.5mm if the correct value of 1W/MK were used. This finding is broadly in agreement with

British Leyland who see little benefit in increasing coating thicknesses above 2mm.[20]

3.2 EXPERIMENTAL ASSESSMENT OF THE FEASIBILITY OF USING CERAMICS IN INTERNAL COMBUSTION ENGINES

Attention was attracted to the adiabatic engine by a number of adventurous engine tests with ceramic components. A less spectacular approach has now generally been adopted. As a result the majority of experimental work conforms to one of two patterns. One aproach, demonstrated by Timoney[4] and Godfrey[30] was to start by testing ceramic components in low rated but fired diesel engines. Other researchers such as Kamo[2] of Cummins and Fletcher-Jones et al[31] of Wellworthy have produced test procedures for the progressive development of ceramic materials and designs to a position where they are ready to be incorporated into a working engine.

3.2.1 PROGRESSIVE DEVELOPMENT OF CERAMIC COMPONENTS

This low risk approach, splits the problems associated with the introduction of ceramics into a number of solvable steps. Following the initial theoretical study by Kamo,[32] Cummins and TADCOM were sufficiently interested to initiate a practical investigation. The procedure used is shown in figure 3.5, and incorporates a four stage testing sequence.

I/ The non-distructive testing of ceramic components for flaws and out of tolerance dimensions.

II/ Bench tests in a low thermally loaded environment. This acts as a screening device and reduces the level of damage which is associated with failures in an operating diesel engine. The test rig used is based around a conventional reciprocating engine with the cylinder head replaced by a component containing a stationary ceramic test piece, as shown in figure 3.6. The engine is then cycled without firing taking place, the adiabatic compression and expansion providing the required

pressure peaks. The design also incorporates a screen below the test piece, which traps any ceramic fragments formed and prevents secondary damage to the engine structure. However this rig only simulates mechanical loads and speeds, not the thermal loadings present in a firing diesel engine.

iii/ The test pieces are now installed in a single cylinder firing engine for 250 hours of proof testing under typical operating conditions.

iv/ The surviving test pieces are used in a six cylinder engine, where the thermodynamic and mechanical performance of the engine are monitored.

Kamo and Bryzik used the above test procedure for evaluating a number of ceramic piston crown designs. The performance of these is reported in their 1981 paper,[32] each of these designs incorporating a different ceramic material.

Hot pressed silicon nitride	HPSN
Reaction bonded silicon nitride	RBSN
Sintered silicon nitride	SSN
Lithium alumium silicate	LAS
Stainless steel	

Only the HPSN cap survived the 250 hour proof testing. Due to the relatively high thermal conductivity of these materials, with the exception of the LAS, a pack of roughened metallic discs was used to provide an air gap. The designs used incorporated a central waspalloy bolt, which unfortunately acts as a stress raiser and a low thermal resistance heat path. When the pistons were used in the fired engine no other part of the combustion chamber volume was insulated, so the in cylinder conditions were fairly close to those encountered in an unmodified engine. With the more severe conditions encountered in a fully insulated engine the probability of this design surviving would be reduced.

The concept of proof testing ceramic components in less arduous

environments than are found in a firing engine has been advanced elsewhere. Wellworthy[31] have produced a test rig which fulfills the same function as Kamo's bench test described above. The apparatus used is shown in figure 3.7. One side of the test piston is subject to an oscillatory hydraulic pressure whilst the other has no applied load. Heaters are provided to increase the operating temperature. Although this design to a very limited extent can mimic the steady state thermal loading in a diesel engine the potentially more damaging transient thermal loads cannot be reproduced.

Komatsu ltd[3] of Japan also used a single cylinder engine to screen ceramic components before testing in a six cylinder engine.

3.2.2 TESTING OF CERAMIC COMPONENTS IN FIRED ENGINES

3.2.2a MONOLITHIC COMPONENTS

If a ceramic material with the right conductivity, strength and fracture tooughness could be found, then metal components could simply be substituted for ceramic ones. Perhaps the first successful engine component substitution was initiated by Godfrey of the Admiralty materials laboratory[30]. A 900W, 4 stroke air cooled engine was used as a test bed, in which the pistons, piston rings and gudgen pin were replaced with RBSN equivalents. Although with the first build the gudgeon pin failed, a later re-fit has survived many hours of operation. Subsequently Stone of the Royal Naval Engineering College[33] designed and ran a 108mm diameter RBSN piston which survived 94 hours in a 9kW, four stroke engine with a rating of 690kPa BMEP. These were very successful tests in that they indicated that ceramics can be used in fired diesel engines. However, there are two points which must be recognised.

i) 690kPa is a very low rating, a more typical pressure of approximately 1600kPa must be survivable by ceramic engine components.

ii) The maximum stresses predicted for the second design was approximately 100MPa, whilst the maximum survivable tensile load for large volumes of RBSN was taken to be 145 MPa. In a commercial engine a much higher factor of safety would be necessary.

If RBSN is used in an engine with the aim of reducing the heat loss to coolant then additional insulation must be provided. This can be achieved with a RBSN crown by incorporating an air gap. However, with a solid piston it is difficult to include the additional insulation required.

Timoney S.G. of Dublin University[4] was one of the first researchers to recognise the possibilities of using ceramics as an insulating material. Timoney also felt that ceramics could be used to solve some of the problems he had found with an earlier 'conventional' opposed piston engine. A ceramic engine was constructed using silica glass ceramic shown in figure 3.8. The cylinder liner makes use of a metal compression ring to reduce the tensile stresses. Initially motoring tests were run at a compression ratio of 20:1, these were completed without encountering any problems. The engine was then fired, and after three minutes the inlet piston fractured causing engine failure. Although the concept of using ceramics in opposed piston engines is very promising the choice of materials in this case was unfortunate. The flexural strength of silica glass is generally taken as about 100MPa, it is therefore unwise to assume a tensile strength greater than 50MPa. Once a realistic factor of safety is applied the maximum usable strength of this material is approximately 20MPa. It is difficult to see how a working piston can be designed with this stress limitation.

Subsequently the engine was rebuilt with a cast iron liner, HPSN pistons were installed but failed whilst motoring.[34] Successfull fired running was later achieved using silicon carbide pistons, after completion of 50 hours running an examination of the piston revealed no damage.

Despite Timoney's failure with HPSN other researchers have produced

working engines with silicon nitride components. In Japan interest in ceramics seems to have been inspired originally by the need to inhibit corrosion, and only later by its insulation properties. Hamano of the Kyoto Ceramic Company ltd[35] in Japan has used a variety of silicon nitride components in a 0.51 litre, eight hp engine of 85mm bore. The top of the cylinder liner (above top ring position), cylinder head and piston crown were all constructed from silicon nitride. After several design changes an engine construction was achieved which ran successfully for 300 hours at full loading. Also in Japan, Komatsu ltd[3] have developed a six cylinder turbocharged Si_3N_4 insulated engine. In this design greater use was made of air gaps to provide insulation and the exhaust port was constructed from ceramic. No failures were reported in a 250 hour test schedule which included a maximum BMEP of 1470kPa. One difficulty with these designs is the low level of insulation afforded by silicon nitride. Consequently although the two Japanese designs should be successful in reducing corrosion the effect on performance will be small.

A study of the literature reveals that there have been many other successful trials of silicon nitride and silicon carbide engine components.[36,37] The critisism levelled a few years ago that these ceramic components had only been tried in low rated engines is no longer valid. The main difficulty which now prevents the widespread use of the materials is their high thermal conductivity. Air gaps must be included. With monoliths this type of construction is difficult to achieve. In addition the introduction of air gaps inevitably leads to regions of unsupported ceramic and hence stress raisers.

Where a separate ceramic crown or insert is used the introduction of an air gap is easier. However, the problems associated with the attachment of crown to piston are not easily solved. Of the two methods most often employed, the first involves the use of bolts through the ceramic and into the piston body. This type of design should be avoided as the bolt holes are stress raisers and the metal shafts act as heat sinks. Similarly the second solution often adopted of a shrink fit ring around a ceramic body such that the metal is visable from the combustion space is undesirable. With this design, as in figure 3.9, the metal ring becomes almost as hot as the

ceramic. To prevent the difference in thermal expansion causing separation a large shrink fit is needed. The type of design shown in figure 3.10 has none of these problems, although it is best suited to IDI engines. This layout results in a low metal temperature, and high ceramic temperature, the initial shrink fit required is therefore small. There is also no ring to provide a heat path away from the combustion space. Although this type of design has been suggested by different groups such a SICERI, there is little practical experence of its use available.

To avoid the problem of the high thermal conductivity of silicon nitride some researchers have used monolithic PSZ components. Karl Schmidt GmbH[38] have examined the use of zirconia piston crowns, held by a shrink fit steel ring which is screwed into an aluminium piston body. This type of design leads to two problems:

i) The outer steel ring provides a heat sink reducing the effectiveness of the insulation.

ii) The technique of attaching aluminium to steel using a screw thread would lead to very high stress concentrations.

Woods and Oda of Cummins[39] used a PSZ insert in an iron piston, avoiding the problem of an aluminium-iron interface. They also used a Y_2O_3 stabilised zirconia cylinder liner insert and cylinder head plate. However, both these designs suffer from the high density of PSZ at 5.8, which makes monoliths very heavy.

The use of PSZ monoliths can solve some of the problems associated with SiC and Si_3N_4 However, its high density and cost may preclude its use for large engine components.

3.2.2b CERAMIC COATINGS

The attraction of ceramic coatings lie in their conceptual simplicity. Potentially all the components requiring insulation in the diesel engine can be coated, with little design change. With a low percentage of ceramic present in the engine, crack propogation represents less of

a problem. However, coatings create their own unique difficulties.

There are many materials which could be used as an insulative coating. Murray[40] of Oklahoma State University examined various coatings which can be used as insulation materials in both compression and spark ignition engines. The figures given for three of the materials considered were:

	K (W/mK)	$\gamma x10^{-6}$
Zirconium Oxide	1.16	3.0
Aluminium Oxide	4.18	2.28
Chromium Oxide	4.18	2.78

Yittria stabilised zirconia was chosen as the best prospect for a coating material, despite the rather unique measured value of thermal expansion ($3.0x10^{-6}$). Tests were conducted in a four cylinder engine, with PSZ coated cast iron cylinder head and aluminium piston. Coatings of 0.51 to 0.76mm thickness survived over 100 hours without apparent degradation. Coatings of this thickness are unlikely to affect heat flow significantly, especially as the liner was not insulated.

British Leyland[20] have also used PSZ coatings on valves, cylinder head and pistons. The cast iron cylinder head was used with a 1mm coating reducing the bulk metal temperature by 50K, a feathered coating was used around the valve seat.

Perhaps the greatest success with PSZ coatings has been achieved in the TADCOM/Cumins ablabatic engine program[41]. The first trials were conducted using a 140mm diameter piston with 0.5 and 1.5mm thick coatings. The 0.5mm coating survived 30 hours without failure, whilst the 1.5mm coating lasted 17 hours at which time a 50mm diameter portion flaked off. This region of failure coincided with the position of maximum stress predicted by a finite element analysis. As part of the same program zirconia coated pistons were tested at Yanmar diesel[3] 1.5 and 2.5mm coatings were used, these pistons

had embedded thermocouples for performance monitoring. The 1.5mm coating failed after 30 hours.

More recently a 240 HP adiabatic engine has been developed at Cummins using plasma sprayed zirconia coated pistons, cylinder liners and head, all being iron components. The reported thermal efficiency of this engine is 48%. Work at the moment is based on a 500-750 HP engine incorporating mainly zirconia insulation. Both coatings and monolithic inserts are to be tried. Work is also continuing into a minimum friction engine using ringless pistons, dry ceramic bearings and solid lubricants. With the complete elimination of the oil system the projected thermal efficiency is 54%.

3.2.2c VALVES AND VALVE SEATS

In a four valve cylinder the valve surface areas represents over 50% of the exposed surface of the cylinder head. In an insulated engine it is therefore very important to provide insulation for the valves. Asnani and Knonen[43] have examined monolithic SIALON and PSZ valves using theoretical and experimental methods. The initial theoretical comparison of the production metal valves with the PSZ replacements yielded the following values:

Valve configuration	Maximum tensile stress (MPa)	
	Principal	Hoop
Production valve, metal seat	135	167
PSZ valve, metal seat	148	485
PSZ valve, PSZ seat	147	191

The decrease in hoop stresses observed through the use of a PSZ seat is caused by the modification of the temperature distribution. The PSZ valve seats were chilled before insertion, this created an interference fit and reduced the maximum tensile stresses. However one of the most important rules to observe in the design of ceramic components is that ceramic surfaces should not contact one another, and intermediate soft material should be used. A PSZ valve on PSZ

seat breaks this rule. The PSZ valves tested typically lasted 2-4 hours. the reason given for these failures was thermal shock. An increase in life was observed when a PSZ coating was used on top of the PSZ monolith. In this case a life of up to 24 hours was reported. This coating has high porosity and hence reduces the temperature swing in the body of the valve.

One difficulty with low thermal conductivity monolithic valves is that non axisymmetric temperature distributions can be produced. During transients such as those present at start up one side of the valve stem will have a different temperature from the other. This effect will be more marked in low than high thermal conductivity materials where there will be a quicker redistribution of temperature. A non symmetrical temperature distribution will cause misalignment of the valve. Where a ceramic seat is used then the offset loading that is produced cannot be redistributed, and fracture can result. The high porosity PSZ coating may have improved the valve life through an ability to be crushed at the ceramic-ceramic interface and so prevent high loading of the valve.

The SIALON valves were more successful, of the six valves tested only one failed: at the lock groove: up to 1000 hours of testing were completed.

As an alternative to the monolithic valves British Leyland[20] amongst others have used ceramic coatings on metal valves. In one test a PSZ coating of less than 1mm was used, these valves survived a 150 hour test without apparent degradation.

3.3 MONITORING OF THE PERFORMANCE OF TEST ENGINES

Engine tests with ceramic components must examine not only the life of the new component, but also the change in performance of the engine package. The work carried out by different research centres to assess the performance change derived from the use of thermal insulation can be divided into two areas.

i) Partially insulated engines: Frequently test engines run with only the piston insulated. In this and similar situations where only one component is insulated there is a tendency to increase the heat flow through the uninsulated portions of the engine. The observed performance can therefore be misleading.

ii) Extensively insulated engines: One of the difficulties with the introduction of high levels of insulation is that the engine is not optimised for these conditions. The injection timing, valve timing, valve size, etc are all set for optimum uninsulated performance. Inferring performance gains through this type of test can therefore also be difficult.

3.3.1 PARTIALLY INSULATED TEST ENGINES

Yanmar diesel[3] have monitored the performance of a single cylinder naturally aspirated test engine rated at 650kPa. The piston used was 95mm diameter by 106mm stroke, with a 1.5mm zirconia coating. The engine was run under air fuel ratios between 100 and 20. An exhaust gas temperature increase of 30^{o}C was recorded across the entire air fuel range. Both the volumetric efficiency and fuel consumption were worse in the insulated case, particularly at high air fuel ratios.

Similar observations were made during the work carried out at Bath University. Wallace et al[5] have used an air gap all metal piston in a Petter PH1W engine with a 86mm diameter bore. The introduction of the insulated piston again saw a reduction in volumetric and thermal efficiencies. The heat loss to coolant was up by approximately 25%, this it was felt was due to an increase in the gas

temperature, which gave rise to an increase in the heat rejection through the combustion surfaces.

Cole and Arkidas[48] of General Motors Research Laboratories felt heat rejection increased primarily because of a gain in exhaust port heat transfer. To check this theory they developed an engine which has four independent cooling zones, three in the cylinder head and one in the liner. An insulated all metal air gap piston of diameter 103mm was used. This was constructed using a metal crown attached by four bolts, disc springs allowing movement between crown and piston body. The engine was run in both insulated and uninsulated configurations to establish the change in heat transfer to each of the cooling regions. They confirmed that the heat rejection through the exhaust port area increased, while the heat rejection through the liner decreased by between 12% and 15%. A decrease in volumetric efficiency of 2% was measured, this was less than was expected, probably because of the lack of induced swirl in the cylinder, reducing the heat flow to the gas. However, it may not be sensible to read these results across to similar work as the overall heat rejection to coolant was reduced by between 3% and 7%. This is the reverse of the trend generally observed and this is difficult to reconcile, especially as a low boost pressure was used. Emissions of CO and HC decreased while NO_x increased. This was expected, and is often predicted as higher gas temperatures are encountered.

3.3.2 EXTENSIVELY INSULATED TEST ENGINES

A detailed experimental study was undertaken by Wade et al of Ford Motor Company[28] using an experimental, uncooled insulated single cylinder engine. Zirconia coatings were used in the cylinder head and valves, whilst the cylinder liner was insulated using a zirconia monolith ring. An articulated piston with ring steel crown and aluminium skirt was used, of the type shown in figure 3.11, using a crown formed with a fork in its lower surface.[49] this connects through the gudgeon pin to the piston body. The heat flow between these two components is small, and in addition the lower conductivity of the cast iron contributes towards the performance gains with this

piston design. In addition the weight of this piston is reported as equal or less than an aluminium equivalent.

To compensate for the reduction in volumetric efficiency encountered with insulated engines Ford used a low boost pressure. This was adjusted to maintain the same volumetric efficiency as that in the unmodified engine, and the exhaust back pressure was adjusted in unison. An improvement in specific fuel consumption of 4% at 1700rpm to 7% at 1000rpm was noted. A drop was recorded in NO_x production, and at light loads HC emissions were reduced. Under heavier loadings HC emissions increased, this was probably due to the inappropriate fuel spray and air swirl patterns which were optimised for uninsulated operation. Reductions in both HC and NO_x emissions were expected by Ford as the premixed combustion fraction was reduced by approximately 50%. It has been shown that HC and NO_x emissions are governed by the fuel present in the premixed combustion mode. Ford felt that this effect would be dominant over the increase in NO_x production associated with higher combustion temperatures.

It was further noted that the ignition delay was reduced by approximately 50% compared with the standard engine. This results from the charge heating. Consequently the maximum rate of pressure rise was lower in the uncooled engine. As this influences the overall noise levels it is to be expected that the adiabatic engine should be quieter than its conventional equivalent.

Komatsu ltd[3] have also monitered the performance of their six cylinder turbocharged engine, with PSZ coated liner, cylinder head, valves and piston. An exhaust port liner was also used. The resulting engine had an efficiency of 48%, representing a 6% improvement over the base line engine. This was achieved through a 35% reduction in heat rejection. With this level of insulation the liner temperature in the top ring position was 350^{o}C, and a synthetic oil could therefore be used without difficulty. A higher insulation rate of 50% could yield a temperature beyond the lubricants capacity.

3.4 ENGINE PERFORMANCE WITH LOW QUALITY FUELS

One possible justification for reaseach into the adiabatic engine it its ability to use low quality fuels. The effect on emission levels and on performance of these low cetane fuels has been examined by various researchers. Komatsu ltd[3] have tested a six cylinder turbocharged engine without water cooling. This was run with three fuels, diesel fuels of 52 and 30 cetane ratings, and a liquified coal fuel. The coal based fuel was used in the insulated engine without the occurrence of knocking, except at idle, when the combustion chamber surface temperature dropped to levels where the gas temperature after compression was to low too maintain satisfactory performance. The ignition delay and rate of pressure rise are both worse with the coal based fuel in the standard engine. The low cetane fuel was used in the insulated engine over the entire operating range without misfiring.

The adiabatic engine provides higher compression temperatures with reduced ignition delay. This is necessary when low cetane fuels are to be used. The following characteristics of insulated engines were observed by Yoshimstu el al[3].

a) The rate of heat release during the main combustion period is lower. This arises as the quantity of air and fuel mixed before ignition starts is lower, being a consequence of the reduced ignition delay.

b) During the later stages of combustion the heat release is increased and is accompained by an extension of the combustion period. This is caused because the fuel injected after the initial combustion passes through the existing flame region, losing mixing momentum.

These factors necessitate the alteration of the combustion chamber and inlet port to accelerate the mixing.

Murray R.G. of Oklahoma State University[40] has examined how different combustion chamber surfaces affect combustion through

catalytic action. It was proposed that by introducing catalytic substances into zirconia insulation the combustion characteristics could be changed. Unexpectedly the use of these catalysts did not appear to initiate pre-flame reactions and hence reduce ignition delay. However it was suggested that the reduction in power output exhibited by unboosted adiabatic engines was not only due to the drop in the volumetric efficiency but also derived from:

i) A change in the pre-combustion (catalytic) reactions at the surface which could delay and inhibit combustion.

ii) The absorption of impinging fuel by the porous ceramic coating.

It remains unclear to what extent these factors may affect the combustion in insulated engines. Most researchers who study combustion in the adiabatic engine note a decrease in ignition delay. Delays caused by catalytic actions are therefore not a dominant effect. In addition if the second point mentioned above was significant we would expect an increase in the HC emissions fron the engine, and this is not found to occur.

3.5 LUBRICATION OF THE ADIABATIC ENGINE

The lubricants normally used in the internal combustion engine have temperature limits which makes their use in the adiabatic engine impossible. There are three routes through which this problem may be overcome.

i) By insulating just the top portion of the cylinder liner only a small performance loss is to be expected, as the effect on heat rejection rates of insulating the liner below the top ring position is minimal. When the uninsulated region of the liner is uncovered by the piston motion then the gas temperature has dropped sufficiently for heat loss to be small. This procedure will also limit the ring pack temperature and conventional lubricants may still be used.

ii) By developing new lubricants which are stable at the high operating temperatures required. The synthetic lubricants so far produced[44] have exhibited very high oil consumption and the temperature limits could still prove too low. Alternatively solid lubricants can be incorporated, these have high temporature limits but have the difficulty of not being self renewing.

iii) By the use of a lubricant free engine: If this can be achieved without seizure then the efficiency of the engine will be improved through the elimination of fluid friction present with lubricants.

Yoshimitsu et al of Komatsu ltd[50] used an insulated six cylinder engine to examine the possibility of using low cetane fuel in the adiabatic engine. Various oils were tried in this engine which had an insulated liner, leading to a temperature at the top ring position of above 400^{o}C. The limiting value in a normal engine to prevent oil break down is around 200^{o}C. A graph of liner temperature distribution with the rate of heat insulation was produced to accompany the practical work and is shown in figure 3.12. The level of insulation achieved with the Komatsu engine must therefore be assumed to be around 30%. With a 50% insulation level a peak liner temperature of 600^{o}C is predicted.

To assess the suitability of various lubricants Komatsu ltd used a hot tube test in which oil is drawn through a glass tube and heated for a set time period. The oil recovered is given a rating from 10 for transparent to 0 for very black. The colour is regarded as having a close relationship with its anti-scuffing performance. Different synthetic and mineral oils were tested. Some of these were used in the above insulated engine and the test results stated as satisfactory. However, this engine has a low level of insulation. A more realistic 50% insulation level will increase the liner temperature by a further 200^{o}C, placing the environment beyond the limit of the oils used.

Similar work has been carried out by Radovanovic and Kamo[44] who examined various synthetic lubricants at these intermediate

temperatures. For this purpose they developed a minimally cooled metal engine which ran for 250 hours at a 298kW rating. They noted that previously tested synthetic lubricants have shown high oil consumption. However, a polyester based oil was tried which gave a good oil consumption of 0.6% of the fuel rate. Typical oil consumption figures in diesel engines are 0.2 to 0.5% of the fuel consumption. A liner top ring temperature of 371 ^{o}C was recorded. Analysis of the oil showed a higher iron content than would normally be expected but no other problems were evident. The following oil consumptions were reported for different oils:

	Oil consumption Kg/hr
Dralkylbenzene	1.160
Polyolester	0.413
Ester and synthetic chain HC	0.522
Polyolester and synthetic HC	0.340
Polyalfaelefin	0.399

Although successful test runs have been concluded using synthetic lubricants in minimally insulated engines it is unlikely that satisfactory performance will be achieved with a 50% insulation level. Elimination of the oil system and the use of solid lubricants, dry ceramic bearings etc seem to offer the greatest hope.

The liner temperatures predicted by Komatsu ltd[3] in figure 3.12 are broadly in agreement with those of Cummins [44] who predict a top ring liner temperature in an insulated engine of 530 to 650^{o}C for their turbocompound uncooled engine. They regard this temperature as above the limit for all liquid based organic lubricants. Solid lubricants were seen as having the best chance of success under these conditions. A button test was used, as shown in figure 3.13 to test the different candidate ring materials. Tribaloy 800 (17% Cr, 28% Mo cast material) was used for the buttons, and silicon nitride for the disc. These tests were conducted at successively increasing temperatures from 200 to 650 ^{o}C. Synthetic oils were used but they had been burned off by 425 ^{o}C. The coefficient of friction reduced for increased load and temperature. This behaviour is believed to

result from the formation of low friction oxide films on cobalt containing alloys. These oxide films are self healing, and so these lubricants can be thought of as self renewing.

Moorhouse et al[45] have also sought to use solid lubricants through the development of special piston ring construction. The piston ring has small (0.5mm diameter) holes switched into the surface, these holes are filled with a solid lubricant. The most promising of these lubricants was molybdenum disulphide or lithium fluoride plus copper. Although these techniques provide lubrication at high temperatures it is unclear how long these solid lubricants will last in an operating diesel engine as they are not self renewing.

Running an engine unlubricated is an attractive proposition since fluid friction is eliminated increasing efficiency by up to 6%.[44] Timoney and Flynn[34] have used the opposed piston engine to evaluate the performance of a lubricant free engine. Initially a lithium-alumino-silicate construction was used. The engine was motored and the friction losses measured, these were found to be 8 to 10% less than those in a conventional engine. Unfortunately the engine failed before further tests could be carried out. Later a SiC liner and pair of pistons were installed. Fired testing was concluded satisfactorily, and the authors concluded that unlubricated silicon carbide reciprocating parts can run with less friction than conventionally lubricated metal parts. However, a study in Japan reached a different conclusion investigating ceramic sliding interfaces. Shimauchi et al[46] conducted various tests under dry conditions where all the ceramic materials tried seized under low loadings.

The difficulties associated with the lubrication of the adiabatic engine remain unsolved at the present time. Of the various methods which have been tried it is unclear which, if any, offer a workable solution in a firing engine.

3.6 DO COATINGS OR MONOLITHS HAVE THE BEST POTENTIAL AS INSULATION?

One of the questions that has arisen with respect to the use of ceramics in the internal combustion engine is whether ceramic coatings or monoliths offer the best prospects for a reliable insulation medium. In some areas it is possible to provide a reasonably confident answer. In IDI engines the pre-combustion bowl develops such high temperatures and pollutant levels that a PSZ coating is unlikely to survive. A ceramic monolithic insert is the only realistic design solution in this case. Similarly to insulate the cylinder head with a monolithic insert, or construct the entire cylinder head of ceramic is probably unrealistic. The bridge between the valves represents too great a stress concentration and a ceramic coating is generally held to be the best solution. In other areas the best choice is less easy to define.

3.6.1 CERAMIC COATINGS

The use of ceramic coatings has been mainly restricted to the application of partially stabilised zirconia. Typically the coatings tested so far have been in the range of 0.1 to 0.5mm thickness. Where thicker coatings have been used the failures have far outnumbered the successes. Before the required 50% insulation can be achieved thicker coatings must be used. Approximately 2mm of PSZ is generally thought to be necessary, beyond this point a further decrease in heat loss to coolant is difficult to achieve.

Despite these problems zirconia coatings of up to 3.5mm have been tested successfully in fired diesel engines.[41] The difficulty exists in extending the lifetimes from less than fifty hours to the thousands of hours required. For this to be achieved methods must be found to reduce the chemical attack on:

i) The stabilisers
ii) The bond layer.

At the present time it is unclear how this can be accomplished.

3.6.2 CERAMIC MONOLITHS

If the main problem with PSZ coatings can be said to be achieving an acceptable life, then the main difficulty with most monoliths is their inappropriate properties. With a few exceptions such as PSZ and LAS the thermal conductivity of most potential ceramic monolith materials is too high. If their use is to be contemplated then further insulation must be provided. These materials can therefore only be used in situations where it is possible to incorporate an air gap. This can be accomplished in the case of the piston by using a ceramic cap attached by an interference fit or through the use of bolts. However, the liner design design is more difficult. If an intermediate layer of low thermal conductivity material is used, heat flow occurs down the axis of the ceramic as in figure 3.12. This further lowers the volumetric efficiency, increases ring pack temperature and causes an increase in heat transfer to the piston sides. For the liner a low thermal conductivity material must be used on the gas face. Although LAS has a suitable thermal conductivity its low strength does not recommend its use. Partially stabilised zirconia has both low thermal conductivity and moderate strength. A shrink fit metal ring can therefore be used around a monolithic zirconia insert, this provides a satisfactory solution and has been used by Cummins[42] The use of large PSZ monolithic components does have some problems, mainly because of its high density and also due to the cost of the stabilising materials.

It is therefore possible to set down the alternatives which are likely solutions for each of the areas which need insulation in the internal combustion engine.

Insulation area	Possible solutions
Cylinder head	PSZ coating
Cylinder liner	PSZ coating
	PSZ insert
	Si_3N_4 or SiC + air gap
Piston	PSZ coating
	Si_3N_4 or SiC with air gap

	PSZ cap
Exhaust ports	Large number of monoliths (due to low stresses)
Valves	PSZ coating on ~~Steels~~
	PSZ coating on PSZ monoliths
	SiC or Si_3N_4 monoliths
Pre-combustion bowl	SiC or Si_3N_4 monoliths

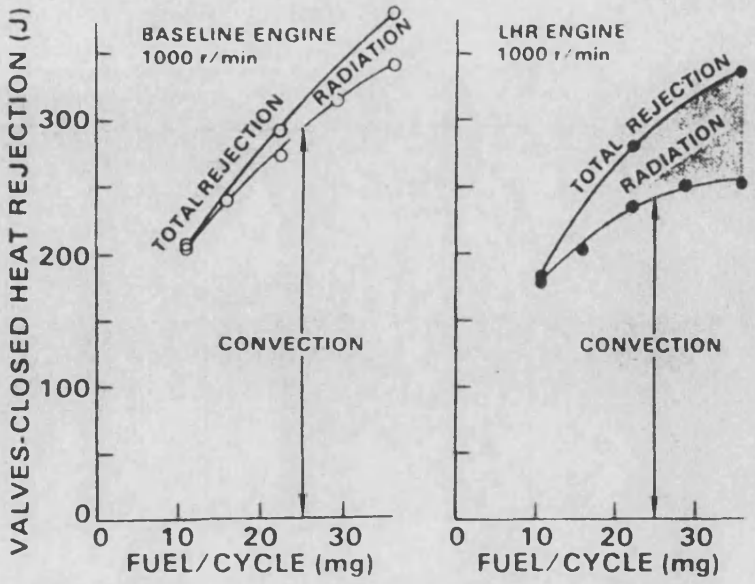

FIGURE 3.1 HEAT REJECTION IN A BASELINE AND LOW HEAT REJECTION ENGINE.

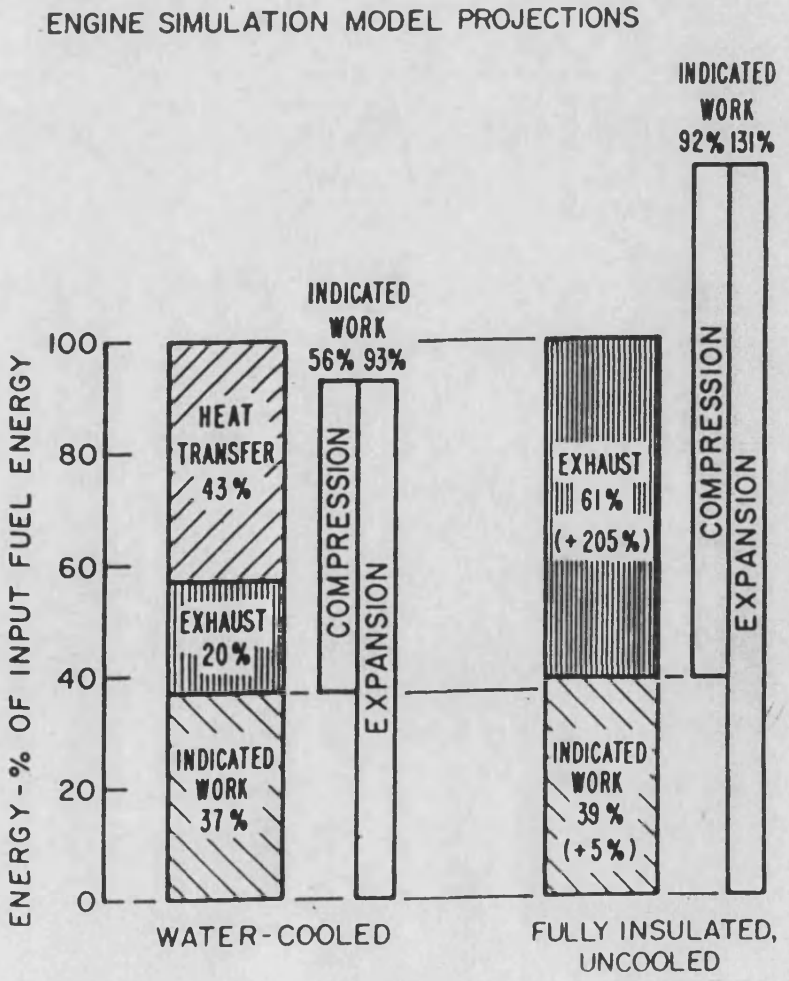

FIGURE 3.2 BREAK DOWN BETWEEN INDICATED, COMPRESSION AND EXPANSION WORK.

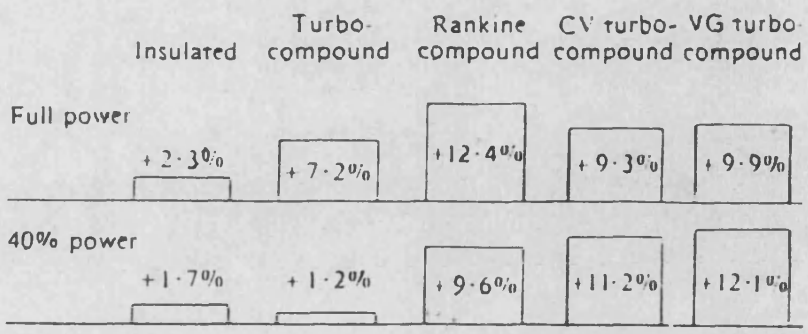

FIGURE 3.3 SUMMARY OF SPECIFIC FUEL CONSUMPTION IMPROVEMENTS PREDICTED WITH VARIOUS COMPOUND SYSTEMS.

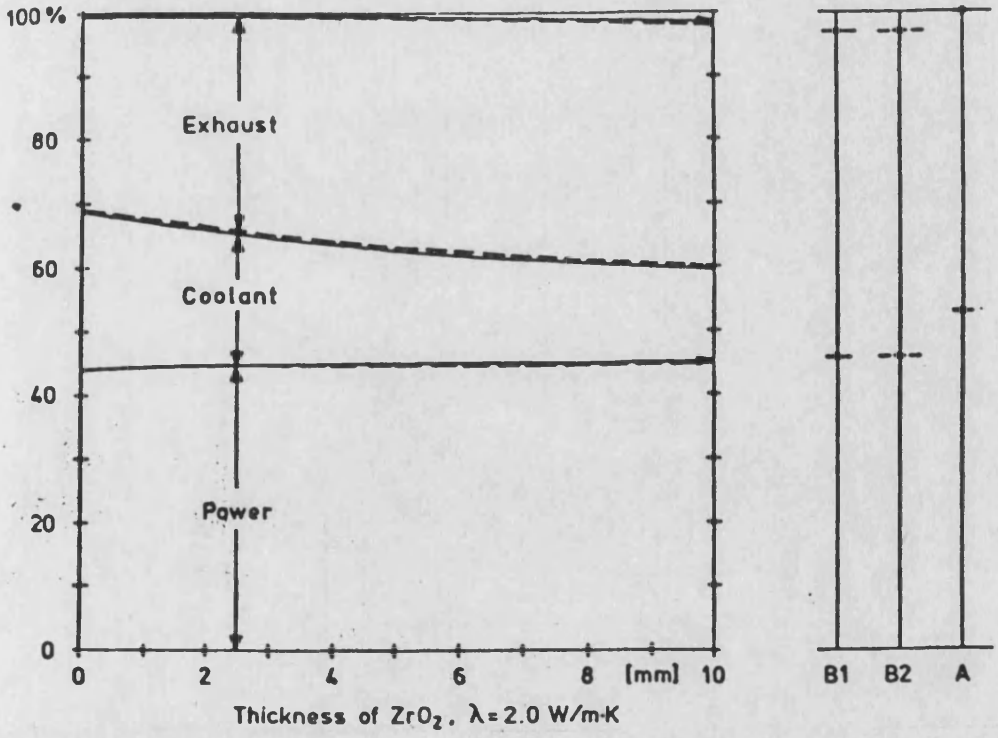

FIGURE 3.4 ENERGY BALANCE CREATED WITH DIFFERENT PSZ COATING THICKNESSES.

FIGURE 3.5 TESTING PROCEDURE FOR CERAMIC COMPONENTS.

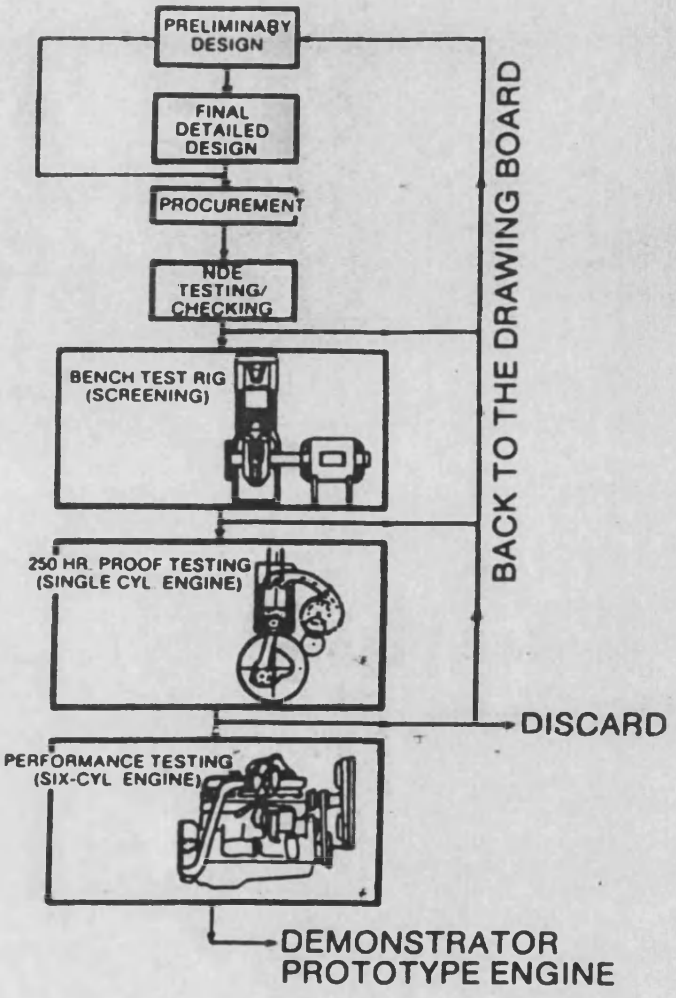

FIGURE 3.6 BENCH TESTING OF CERAMIC SAMPLES (SCREENING).

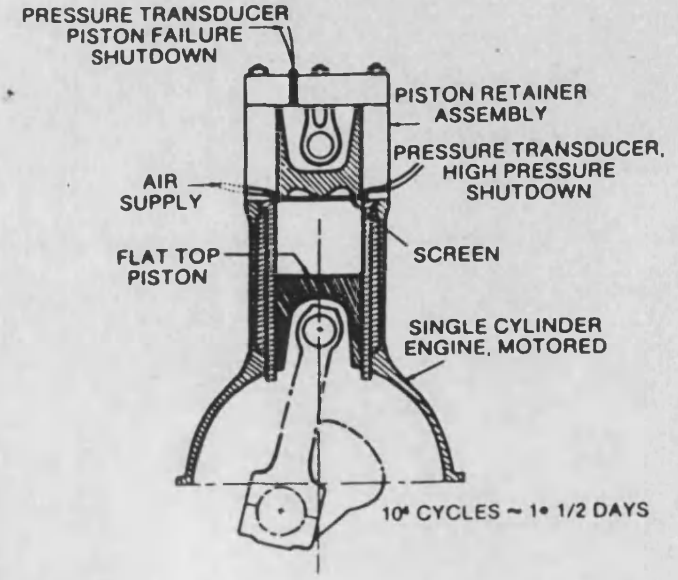

FIGURE 3.7 WELLWORTHY'S PROOF TEST RIG.

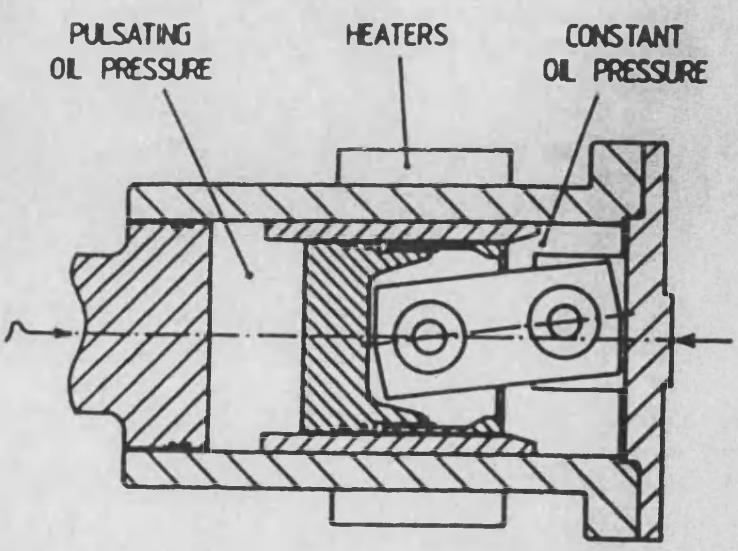

FIGURE 3.8 OPPOSED PISTON ENGINE CONSTRUCTED FROM CERAMIC.

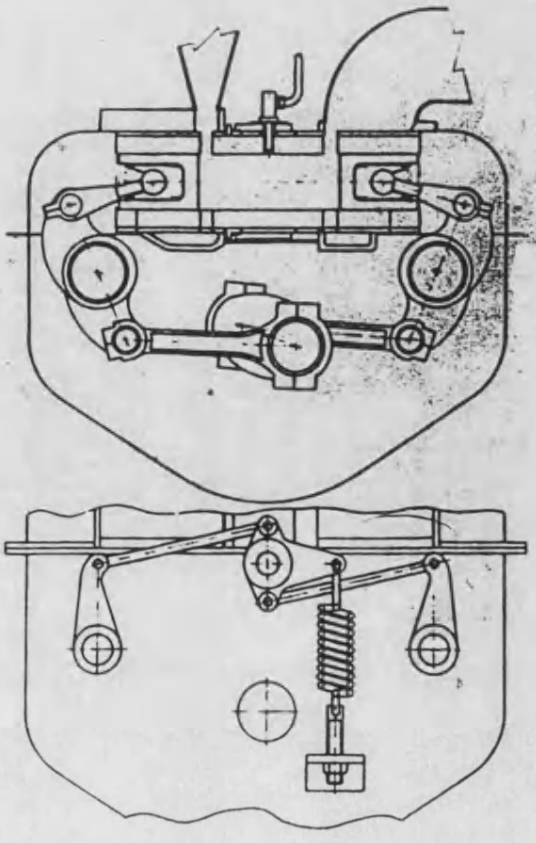

FIGURE 3.9 SHRINK FIT RING AROUND CERAMIC BOWL.

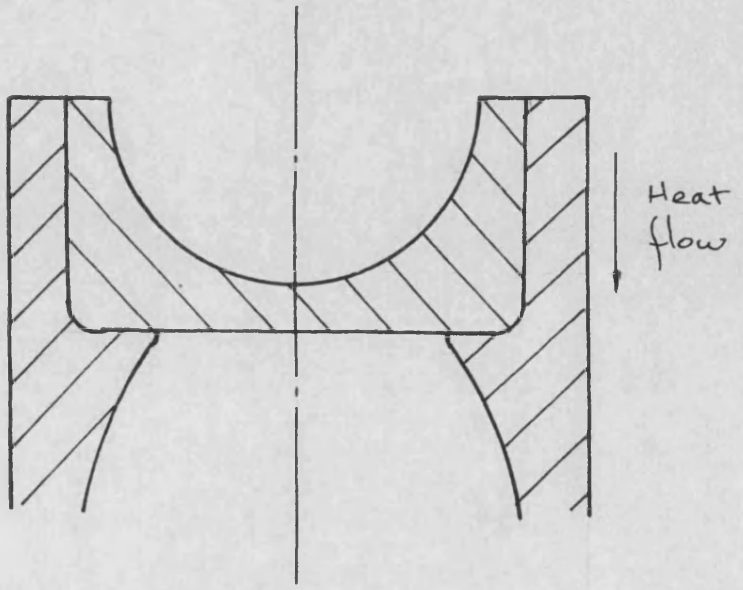

FIGURE 3.10 CERAMIC CROWN WITH SHRINK FIT BASE.

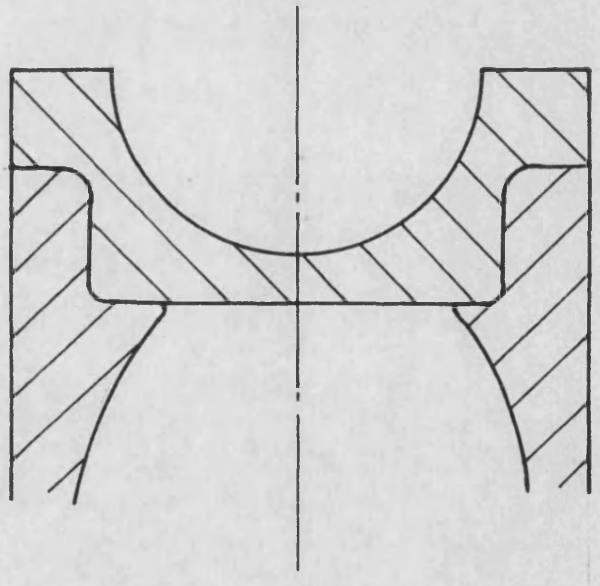

FIGURE 3.11 ARTICULATED PISTON.

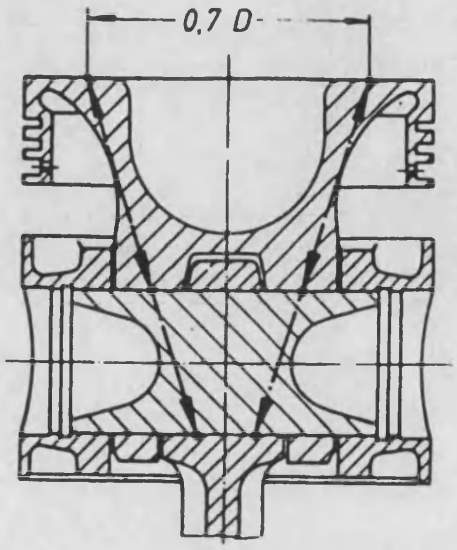

FIGURE 3.12 LINER TEMPERATURE DISTRIBUTION WITH RATE OF HEAT INSULATION.

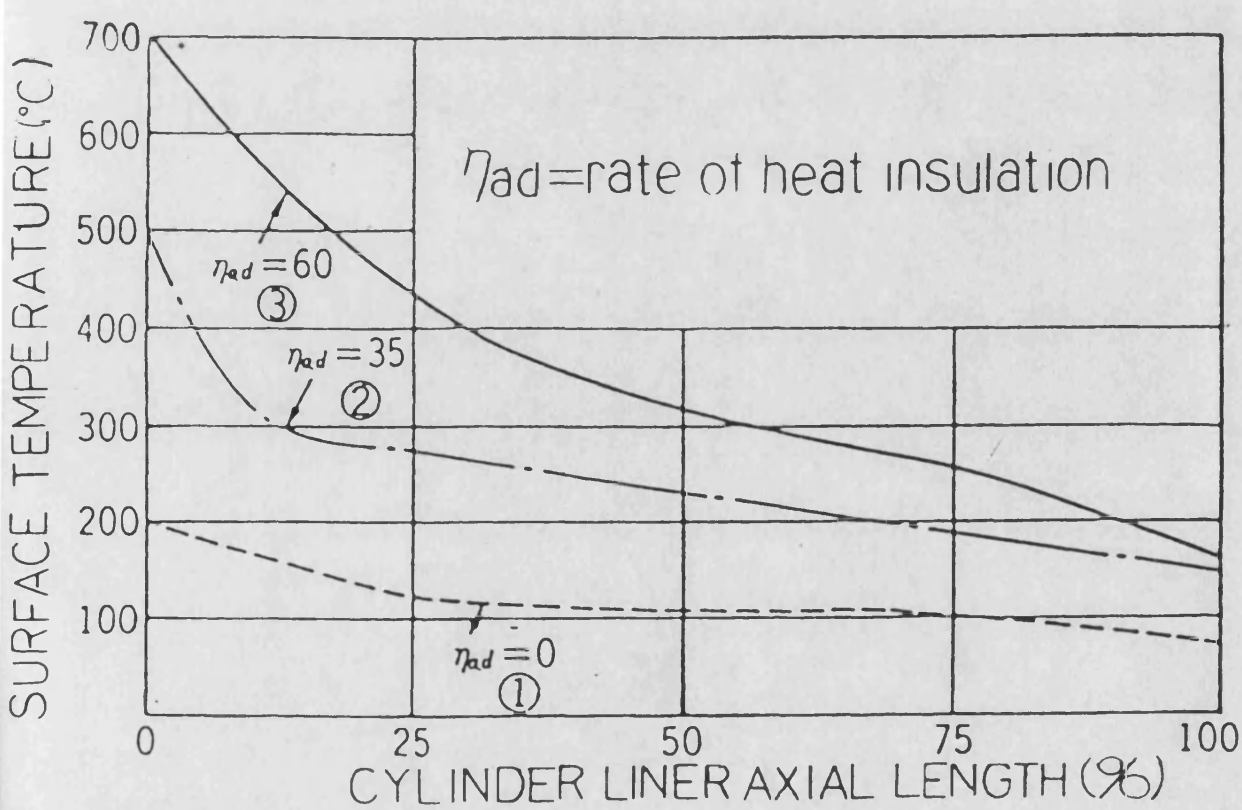

FIGURE 3.13 BUTTON TEST FOR SOLID LUBRICANTS.

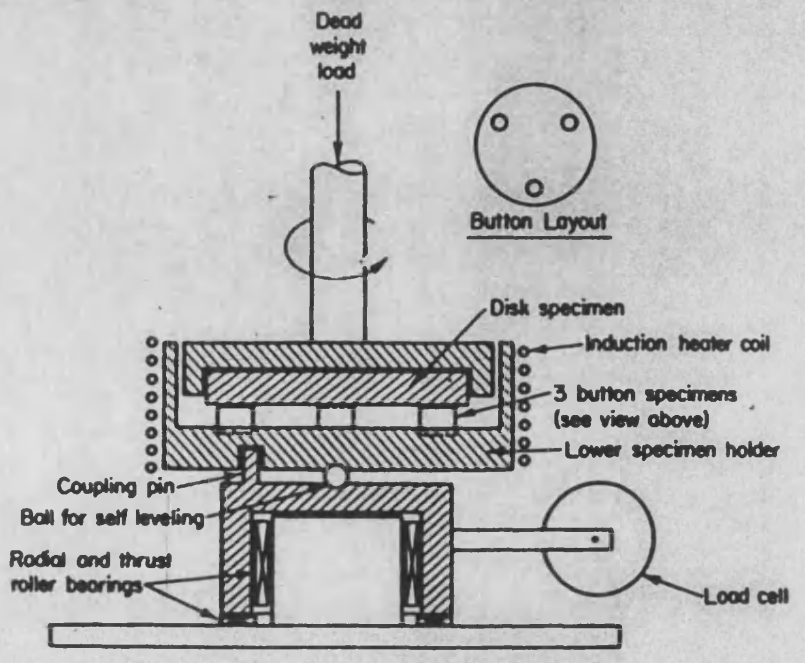

FIGURE 3.14 HEAT FLOW DOWN LINER AXIS.

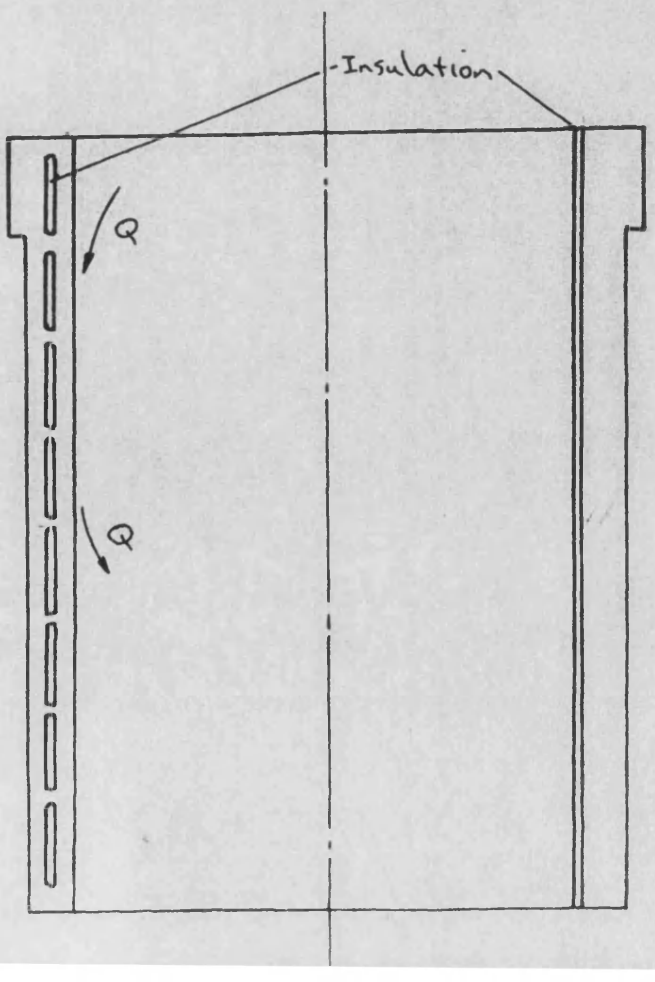

4.1 STEADY STATE AND TRANSIENT THERMAL ANALYSIS OF DISCS

This analysis was introduced to provide a quick method of gauging the temperature and stress distributions which arise within disc shaped components. Both steady state and transient loadings can be investigated to provide an insight into the way thermal stresses occur within ceramic coatings or ceramic inserts.

The steady state stresses arising within ceramic coatings can be reduced by careful management of the substrate temperature during the coating of the disc. and by controling the extent to which the disc is allowed to deform. Transient stress distributions are more difficult to minimise in this way. controlling the rate of change of gas conditions during start up and shut down is more likely to provide an effective way of increasing component life. The cycle to cycle stress variations are not likely to significantly affect component performance.

The analysis has further indicated that while evaluating the stress distributions within ceramic components using a numerical analysis it is vital to have access to accurate figures for the properties of the ceramic materials and the way these change through their operational life.

4.2 THE STUDY OF STRESSES WITHIN ENGINE COMPONENTS

When studying the thermal loading of engine components it is often assumed that the complex variation of gas conditions within a firing engine can be represented by steady state values. A mean gas temperature, and heat transfer coefficient are taken as acting on the cylinder surfaces. This assumption is made to simplify the numerical analysis needed to predict the stress distribution within the engine components. For a more complete analysis it is necessary to take into account the transient thermal effects which exist in a firing engine.

The most significant are:

1/ The large temperature rise during start up when the engine components are cold.

2/ The cycle to cycle fluctuations in temperature, caused by the gas compression and combustion. In this case the temperature of the engine components will oscillate about a mean value.

It is important to know which of these conditions is the most demanding for any given material. A ceramic component must be designed to survive under the most severe conditions it will encounter. To produce an item only knowing its steady state loading could lead to its failure, or the use of factors of safety which may be inappropriate.

There are many finite element packages available, some of which are capable of predicting transient behaviour. However these are general purpose programs and the data preparation and computer run time are prohibitively long. Many of the test pieces that can be incorporated into the ceramic rig (chapter 7) such as monolithic disc inserts, or metalic discs with a ceramic coating some, due to their simple shape do not require these very complex numerical solutions.

A quick method of gauging the steady state and transient, temperature and stress fields developed within these simple components has many uses particularly when comparisons can yield relevant data. The numerical analysis of a standard component can be used to gauge the suitability of various ceramic materials for the diesel engine environment.

Inconsistencies are exhibited in published ceramic property data, this results from a lack of standard test types, and the limited scale of material testing. This variability casts doubt on results derived from a numerical analysis of stress, which utilises only a single set of property data. Results can be better interpreted if the relationship between an error in material property data and the resulting change in maximum stress is known. This interrelationship is best established through the use of a simple numerical method.

A further use of this type of analysis is to judge the relative levels of stress resulting from transient and steady state temperature loadings.

The reults yielded by these numerical investigations can therefore be used to:

1/ Highlight areas where material properties need to be known with a high degree of accuracy, so optimising the funding available for materials research.

2/ Gauge when further, more complex analysis is needed and to provide a good starting point for the iterative development of the design.

3/ Develop realistic factors of safety for interpreting the results from other numerical methods.

4.3 THE STRESS DISTRIBUTION WITHIN A DISC

The two dimensional axi-symmetric disc is the standard component configuration for use within the insulation test rig. This simple shape can be analysed using specialised numerical methods, optimised for this specific problem, whilst the representative shape can yield useful results.

The stress distribution within a multimaterial disc can be a complex function. The presence of material boundaries causes instantaneous changes in stress levels, and transient temperature loadings result in parabolic stress distributions. We are concerned only with a two dimensional axi-symmetric shape with a one dimensional property distribution. Similarly the resultant stress field in such a system is one dimensional.

The relevant equations for the stress-strain relationship within a single material disc are:

$$E\frac{du}{dr} = \sigma_r - \nu\sigma_c - \nu\sigma_a + \Delta T\gamma E \qquad 4.3.1.$$

$$E\frac{u}{r} = \sigma_c - \nu\sigma_r - \nu\sigma_a + \Delta T\gamma E \qquad 4.3.2.$$

where u is the radial shift, as shown in appendix 4.1.

and ΔT is the change in temperature from the datum.

γ coefficient of thermal expansion.

σ stress.

ν poisson's ratio.

r radius.

subscripts c,r,a are the circumferential, radial, and axial components.

The radial expansion in a disc being a function of the temperature and stresses only.

4.4 FORCE BALANCE APPROACH

The problem analysed in this section is that of computing the value of forces and deformations within a solid disc subject to a variety of thermal and mechanical loadings.

Development of the theory is based on the following assumptions:

1/ The plate is flat, of uniform thickness and can be represented by a one dimensional axial property distribution.

2/ Maximum disc deflection is not more than one half the thickness of the disc.

3/ At no point is the disc stressed beyond its elastic limit.

4/ Straight lines in the plate that were originally vertical remain straight but become inclined.

An analytical method has been developed to predict the stress distribution that arises within a single material disc. When a disc has an axial property distribution the anlysis can be applied repeatedly on discrete layers, each of which is assumed to have uniform properties. This is shown in figure 4.1. Similarly the temperature of each element is taken to be uniform. Any thermal or mechanical loads which are applied to the disc will affect the deformation of all these discrete layers. Each layer will exert a force on its neighbours and act against any restraining surfaces. We know that when a body is in equilibrium applied and reactive forces must balance. With the force balance method this relationship is used to evaluate the system of axial, radial and circumferential stresses within the disc. The disc studied by the numerical method will deform to a shape where it is in equilibrium.

Using this procedure the material properties can be specified for any element, or any group of elements. This facility can be used to incorporate temperature dependent properties into the analysis,

provided empirical relationships can be developed for the property variation.

Similarly the process of discretisation can be used to find the temperature distribution, derived from steady state or transient thermal loadings. The temperature field may be derived from the temperature of the outer elements, or the fluid conditions at the disc boundaries. With one dimensional analysis no radial heat transfer is incorporated, the radial boundary being taken as adiabatic.

4.5 THE NUMERICAL METHOD

As outlined in section 4.3 the system of stresses in each element is governed by its temperature and the radial deformation. The deformation is determined by the equilibrium conditions and mechanical loading. The temperature is derived from the thermal loading.

Before either type of loading is applied it is assumed that there exists a uniform temperature at which there are no residual stresses. Similarly there is no force developed between adjacent discs, or between the elemental discs and their boundaries. This condition is taken as a datum, all thermal and mechanical loading is analysed with reference to this point. At this datum condition all the elemental discs are taken to be flat with a common external diameter. As outlined earlier each layer has a uniform temperature and set of poperties which can, if desired, be different from the adjacent layers.

The analytical procedure follows the theory of superposition of strains. Each of the applied loadings causes a strain within the elemental discs. These strains are summed and the stresses derived from this cumulative strain. The method is best described by studying each of these deformations and their causes.

4.5.1 The initial condition has no associated residual stresses at a datum temperature level and a common outer diameter. This

arrangement is shown in figure 4.2. It is now necessary to impose the applied temperature distribution on this datum condition.

4.5.2 There are two methods used to predict the temperature field within the structure. The first is valid for steady state heat transfer, the second is appropriate if transient thermal loadings are being considered.

a) For steady state analysis a simple resistive network is used. With one dimensional heat conduction the thermal energy is transferred through each elemental disc in series. In the steady state the heat flow through each element must be equal, therefore:

$$Q = \frac{-k_i A(T_{i+1} - T_i)}{w_i}$$

for $i = 1,2,3,4.....N$

where N is the number of elemental discs
A is the contact area between discs
w is the width of each elemental disc
T is the uniform temperature of each disc
k is the thermal conductivity

The temperature at the N nodes can therefore be found by solving the N simultaneous equations.

A simpler approach can be developed by introducing the concept of the overall heat transfer coefficient:

where:

$$Q = -UA(T_n - T_1)$$

U is the overall heat transfer coefficient

This analysis can be developed to include convection. It can be shown that:

$$\frac{1}{UA} = \frac{1}{h_a A} + \sum_{i=1}^{n} \frac{w_i}{k_i A} + \frac{1}{h_b A}$$

where $Q = -UA(T_b - T_a)$

h is the surface heat transfer coefficient.
subscripts a and b donate the fluid conditions on either side of the disc.

Each of the N+2 elements within this equation can be thought of as a resistance in series, forming a resistive network. 1/UA is therefore the total thermal resistance. This approach can be used to find the nodal temperatures under all the appropriate boundary conditions.

b) When transient heat transfer is considered the analysis is more complicated. In this case a finite difference method has been introduced to predict the temperature field. This approach is outlined in section 4.9.

The temperature field found from a) or b) is now imposed on the stress analysis as shown in figure 4.3. The elemental discs are allowed to expand freely to their equilibrium position. The outer diameter is now a function of the temperature distribution and the coefficient of thermal expansion.

4.5.3 The third stage in the analysis involves setting a common external diameter compatible with radial equilibrium. This process is shown in figure 4.6.

a) Initially all the elemental discs are restrained to their datum diameter, which is defined in 4.5.1. The radial shift in each element resulting from this confinement is labelled Δr_c.

b) This outer diameter is now varied until the net radial force is zero. Typically some of the elements will be in compression and others in tension. The change of radius in each element arrising from this equilibrium criterion is called Δr_f. So the total change of radius is now $\Delta r_c + \Delta r_f$.

The resulting configuration is shown in figure 4.4.

It should be recognised that although the body is now in radial equilibrium it is rare for axial equilibrium to be satisfied. The physical significance of this situation is that a bending moment must be developed about the neutral surface to maintain this position. If the body is prevented from axially deforming then this bending moment is applied by the external constraints. Should the body be free to deform it will assume a position where the bending moment is zero.

4.5.4 The fourth stage of the analysis is only initiated if the body is unrestrained, and therefore able to deform axially, or if forced by an external load to deform. The change in radius within each element caused by this deformation is denoted the symbol Δr_l, and is at its maximum at the disc boundaries. Each elemental disc will deform such that it forms a section of a sphere radius R, shown in figure 4.5. This radius of curvature can be set to that required for equilibrium, when the applied bending moment is zero. Alternatively the deformation may be imposed by external restraints.

The parameters Δr_c, Δr_f, Δr_l *and* R *will assume the values required for the disc to attain equilibrium.* The disc has two degrees of freedom, to expand radially, and to deform axially, these correspond to Δr_f and R. The values taken for these varibles are therefore adjusted until the equilibrium conditions are satisfied.

4.6.1 FORMULATION

The seperate radial shifts discussed in section 4.5 (Δr_c. Δr_f. Δr_l) are summed and the stresses derived from the cummulative strain using the following formula. These stresses are then used to ascertain whether equilibrium is achieved with the values chosen for Δr_f and R. The derivation of the formula used is shown in appendix 4.1, and is summarised below.

It should be noted that the radial and circumferential stresses within a disc are equal, as shown in appendix 4.1 The radial stress in each element is therefore:

$$\sigma_r = \frac{2E(\Delta r_c + \Delta r_f + \Delta r_l + \Delta r_a)}{D(1-\nu)} + \frac{\nu\sigma_a}{(1-\nu)} \qquad 4.6.1.$$

Where D is the disc diameter,

Δr_a is the radial shift due to the axial loading of each element

The radial stress is therefore a function of the temperature, deformation and axial stress in each element. Similarly for radial equilibrium to be satisfied the algebraic sum of the elemental radial forces must be zero.

$$\Sigma F_r = \sum_{i=1}^{n}\left(\frac{\pi\, w_i E(\Delta r_c + \Delta r_f + \Delta r_l + \Delta r_a)_i}{(1-\nu)} + \frac{D\,\pi w_i \nu_i \sigma_{a.i}}{(1-\nu)}\right) = 0 \qquad 4.6.2.$$

where there are N elemental discs in the body considered and w_i is the width of the elemental disc.

The axial stress must also be found, the appropriate equation is:

$$\sigma_{a.i} = \frac{\sigma_{a.i-1}\left(\frac{1}{2} - \frac{\nu_{i-1}}{1-\nu_{i-1}}(F/D^2)\right) + B(F/D) + AC}{\frac{1}{2} - \frac{\nu_i}{1-\nu_i}C} \qquad 4.6.3.$$

$$A = 12 \left(\frac{2E(\Delta r_c + \Delta r_f + \Delta r_i + \Delta r_a)}{D(1-\nu)} \right)_i$$

$$B = 12 \left(\frac{2E(\Delta r_c + \Delta r_f + \Delta r_i + \Delta r_a)}{D(1-\nu)} \right)_{i-1}$$

$$C = \frac{24 w_i h_i}{D^2} - 12 \frac{F}{D^2}$$

$$F = h_i + \frac{2}{3} w_i$$

where h_i is the distance from the neutral surface to the element centre line.

For axial equilibrium to be satisfied then the applied bending moment must be zero.

4.6.4.

$$\Sigma BM_r = \sum_{i=1}^{n} \left(\frac{\pi h_i w_i E(\Delta r_c + \Delta r_f + \Delta r_i + \Delta r_a)_i}{(1-\nu_i)} + \frac{D h_i \pi w_i \nu_i \sigma_{a.i}}{(1-\nu_i)} \right) = 0$$

The radial shifts must be such that the equations 4.6.2 and 4.6.4 are satisfied.

4.6.2 MATERIAL BOUNDARIES

Complications arise where material boundaries are investigated, there is an instantaneous change in stress levels where the preceding equations cannot be used. A complementary theory has therefore been developed to analyse this step function, based on equilibrium considerations. The procedure is best explained if we examine a disc

made of two materials. The first material is split into *n* elements, while the second is divided into *m* elements. As shown in Appendix 4.1 it follows from equilibrium that:

$$\sum_{i=1}^{n}((\pi w_i\ \sigma_{r.i-1})h_i + (w_i/12)(\sigma_{r.i-1} - \sigma_{r.i})w_i\pi)$$
$$+ \sum_{i=n+1}^{n+m}((\pi w_i\ \sigma_{r.i-1})h_i + (w_i/12)(\sigma_{r.i-1} - \sigma_{r.i})w_i\pi) = 0$$

The axial loading at the top face, arising from gas pressure, will be known. The first term in this expression can therefore be evaluated using the analysis outlined in section 4.5. The second term will only be equal to the first when the stresses used in the *n+1 th* disc are correct, these stresses however are not known. The stresses in elements *n*+2 to *n+m* can be calculated once these values are established. Different values of $\sigma_{a.n+1}$ (and hence $\sigma_{r.n+1}$) can therefore be tried until the two terms are equal.

4.7 PROGRAM STRUCTURE

This package is designed to be run interactively although batch operation can be specified. However, the computer time required is low and unless multiple transient analyses are desired there is little to be gained through batch operation.

In use the program presents the operator with a series of options. A selection is made according to the nature of the problem to be solved. In addition material data will be requested, together with any relevant boundary conditions. The program assumes all the data used is dimensionally consistent. Format and detail required in the output is similarly user specified.

The program is subdivided into a series of sections, these have been labelled A to L on the flow chart shown in figure 4.7. A simplified flow chart is shown in figure 4.8. These sections are best discussed

sequentially while following the flow diagram presented in figure 4.7. The program is shown in Appendix 4.2.

The first section (area A) is concerned with the specification of the disc size and the input of the mechanical and thermal loading which are to be applied to the disc. The user is presented with the following options:

1a/ Is disc free to deform to its equilibrium position?
1b/ If not, what is the radius of deformation?
2/ Are temperature dependent properties to be entered using a user-written subroutine?
3/ Is a transient analysis required, and if so how many sets of results are desired?
4/ Is the disc formed from more than two layers, each with its own properties?

Depending on the response received to these enquiries the program will decide what further information it requires.

In section B, the properties of each material used must be entered. This includes:

Poisson's ratio.
Young's modulus.
Thermal conductivity.
Coefficient of thermal expansion.

In addition when a transient analysis is pursued it is necessary to know:

Density
Heat capacity.

The values given are stored in matrices, so the properties pertaining to each elemental disc are stored separately.

Subroutine *properties* is used if a multilayer structure is analysed, as in option 4 above. This has a more convenient data input structure

if many sets of material property data must be entered.

Alternatively the material data may be set using a user-definable subroutine, called *section*. This can either pass fixed material properties back to the main program, or be used to define temperature dependent properties. The temperature of each elemental disc is passed to this subroutine and the corresponding set of properties calculated. Since the temperature is itself dependent on the properties, an iterative loop is used if this method is adopted for defining the properties. An initial estimate of the temperature distribution is formed and the property distribution calculated. These properties are then used to form a better estimate of the temperature field. The loop is repeated until the required accuracy is obtained. If this subroutine is used all the required properties must be set within the subroutine. It is not possible to set some material properties using another input facility whilst specifying the remainder through the use of subrountine *section*.

If steady state conditions are to be established the temperature distribution is calculated using the resistive network theory as shown in section C. If a transient analysis is being developed subroutine *temppro* is used. Temppro forms a matrix containing the time-temperature-depth distribution, this stores the temperature of each element within the disc at a series of time steps. Subsequently for each analysis pursued a single temperature field is taken from this matrix, and used to establish the resulting stress distribution. This procedure is further explained in section 4.9.

After the temperature and property matrices are set the program proceedes to calculate the position of the neutral surface as shown in subdivision D, using the formula outlined in Appendix 4.1. The free expansion in each element is similarly evaluated, and again recorded in a matrix; this corresponds to the theory in section 4.9.2.

Following section E in the flow chart the program now establishes the restraining conditions which are applied to the disc, the options available are:

1/ If the disc is axially restrained, or a known central deflection is applied then an estimate of Δr_f will be taken, this value is adjusted until the radial force is found to be zero. (Δr_f is the radial shift required for radial equilibrium as shown in 4.5.3)

2/ In the case where the disc is given freedom of axial movement to reach axial equilibrium, the program will take an estimate of both the radius of deformation R on the neutral surface, and the radial expansion Δr_f. Both of these will be adjusted until the radial force and the net applied bending moment are zero.

Convergence to these equilibrium conditions is iterative, achieved using a shooting method.

4.7.1 EVALUATION OF THE STRESS DISTRIBUTION

Once a value for Δr_f, and if appropriate R, has been established the resulting stress distribution can be derived. These stress levels are recorded in matrices, together with the radial force and the bending moment contributed by each of the elemental discs. The analysis proceeds from the top face (combustion chamber side) where the gas pressure and hence the surface axial stress is known. The stresses in each successive elemental disc are evaluated using formula 4.6.1 and 4.6.3, as indicated in division F.

Once a material boundary is encountered the associated change in stress levels is calculated. As outlined in section 4.62 the exact solution for the change in stress across the material boundary is found through iteration. When equation 4.6.3 is satisfied then the correct stress distribution has been found.

4.7.2 AXIAL AND RADIAL DEFORMATION

Once the stress distribution throughout the disc is finalised the cumulative radial force and bending moments are found. It should be emphasised that these stresses are those resulting for the values of R and Δr_f which were assumed. If the algebraic sum of the elemental radial forces is not zero then a new value of Δr_f is formed using a shooting method. the procedure is shown in section J.

After radial equilibrium has been achieved at a given value of Δr_f and there is no radial force developed by the disc, then the program checks if axial equilibrium is required. If the disc is free to assume its axial equilibrium position, then the applied bending moment should be zero. The value of the radius of deformation R is varied until the sum of the elemental bending moments is zero.

4.7.3 TABULATED OUTPUT

When the correct values of the axial and radial deformations have been established, together with the associated stress levels the program will output the results as shown in section K using the format which has been previously requested by the user.

This has three forms:

1/ A summary of the stress levels can be produced. The maximum and minimum circumferential and axial stresses present within each material are recorded, together with the conditions to which the disc is subject and the material properties.

2/ A full output listing, which includes the stress within each elemental disc, and a list of the properties for each of the materials used.

3/ If a multiple material disc or temperature dependent properties are being studied then the output will state both the properties and the stresses within every elemental disc.

4.7.4 MULTIPLE ANALYSIS

If more than one disc is being studied, or a transient analysis is pursued then the program will repeat the above procedure (as shown in section L). In the case of a transient analysis the time-temperature-depth matrix is used to obtain the temperature field appropriate to the next time step. The analysis is repeated from section D. If a second run is requested the program will be initiated from section A.

4.8 VALIDITY OF STRESS ANALYSIS

Three methods have been introduced to monitor the accuracy of the force balance method.

1/ Use of independently developed theoretical equations. There are two sets of formulae which have been used, valid for different loadings, and material configurations.

i) The stresses arising from a linear temperature distribution, and forced displacements of a single material disc can be calculated.

ii) For bi-material discs the stresses at the disc surfaces can be found for forced central displacements and a uniform temperature rise from a zero stress level.

2/ When a disc is free to deform in all axes the axial stress at both faces will be equal since equilibrium will be maintained. This relationship has not been used within the program, and so provides

a check on the validity of the stress distribution under this condition.

Appendix 4.3 shows examples of numerical output using the force balance program to study various discs, under different loadings. These are compared with values obtained from theoretical formulae.

4.8.1 The first of these tests is conducted with a 20mm thick Silicon Nitride disc, external diameter 86mm. A linear temperature drop is imposed between the two faces. This particular case is of interest because when the body is free to deform, it is able to assume a stress free condition. This arises since the linear temperature field results in a linear radial strain through the disc. Similarly the strain relief as a result of deformation is linear, given uniform material properties. Equilibrium is reached when the component strains are equal and opposite. The radius of deformation, at which this occurs can be calculated using the relevant formula. This value was compared with that given by the computer program, using 100 elements.

The agreement between the curvature given by the computer model and theoretical analysis is such that they agree to all significant figures given in the computer output: ie 67.34m.

Figure 4.9 shows the effect of varying the number of elements used in this computer model. The computer and theoretical values converge, the accuracy obtained is therefore a function of the computer time that can be devoted to the analysis.

4.8.2 The second test is conducted on a bi-material disc subject to a uniform temperature rise from its stress free condition, the body is free to deform. Both the theoretical equations and the axial equilibrium criteria can therefore be used as comparisons.

4.8.3 To check the accuracy of the axial stress formulation 4.6.3 the same disc as in 4.8.1 is subject to a forced central deflection of 0.231mm, corresponding to a radius of curvature of 4m.

There are various methods of entering data into this program, the analytical sequence is slightly different in each case. In this example two methods of data entry have been used:

1/ Assuming the disc to made of two materials, or

2/ Four materials.

In both these cases the material properties in each layer are identical, so the stress levels predicted should be identical.

Again there is close agreement between the theoretical equations and the computer model, both methods of data input produce solutions that are within 2% of the theoretical formula. The alternative output format is shown in this example.

4.8.4 The last two results show the effect of a temperature drop between the disc faces. These can be checked using the equilibrium criteria in 4.8.

In addition,

$$\sum \sigma D\pi t = 0$$

and $$\sum \sigma D\pi th = 0$$

All these conditions are satisfied.

3/ A zirconia coated disc subject to a fixed temperature gradient was analysed using the finite element code ANSYS (discused in chapter five) and the results compared with those given by the disc analysis program.

The stress and temperature distribution in a 86mm diameter zirconia coated disc are shown in figure 4.10, these are output plots from ANSYS. They are axi-symmetric studies, the left edge of the disc

being the axis of symmetry. An adiabatic radial wall was used to maintain compatability with the disc analysis program. The isotherms are therefore parallel with the top surface.

The radial stress distribution is shown, there is a fall off in stress levels towards the outside of the disc, caused by the effect of shear introduced at the boundary. Most of the disc is subject to isostresses running parallel to the surface, and the peak tensile and compressive stresses occur in a plain.

A comparison between the finite element analysis and the disc analysis is shown in figure 4.12. The stress levels shown for the finite element analysis are the centre line values. A close correlation is obtained (<1% error) between the two numerical methods.

4.9.1 COMPUTER SIMULATION OF TRANSIENT TEMPERATURE DISTRIBUTIONS

With transient heat conduction the temperature profile in the solid material is a function of both the spacial coordinates and time. Its analysis leads to partial differential equations that are parabolic rather than eliptic.

We are concerned only with one dimensional transient conduction in rectangular coordinates. The governing equation reduces to the following parabolic form:

$$\frac{\partial T}{\partial t} = \alpha \frac{\partial^2 T}{\partial x^2}$$

There are many different finite difference methods that are suitable for solving the above problem but they can all be divided into two catagories:

1/ Explicit methods

2/ Implicit methods

Both of these result in a set of algebraic equations, but each has its own inherent advantages and disadvantages. The final choice is dependent not only on the geometry of the problem, but the required accuracy, and the computational time which can be committed to the solution. Further consideration must be given to the range over which the solutions are stable. In order to obtain a numerical solution to this problem we divide the x and t domains in a series of elements each with an internal node as shown in figure 4.12. This space time grid can now be analysed using either of the two previously mentioned finite difference methods.

4.9.2 EXPLICIT METHOD

Using finite difference anlaysis we derive the formula:

$$T_{i,j+1} = F_o[T_{i+1,j} + T_{i-1,j} + (\frac{1}{F_o} - 2)T_{i,j}]$$

where F_o is the Fourier number

It is assumed when developing this formula that during the small time increment considered, the heat conduction across the surface of the element is constant. The accuracy will therefore increase with the fineness of the time mesh. The main advantage associated with this method is that the equations are uncoupled and easy to solve, cutting the required computer run time for a given solution.

Examination of the above formula reveals that if the $1/F_o$ term is less than 2 the coefficient of $T_{i,j}$ will be negative. To examine the physical significance of this characteristic suppose at any instant j, the temperatures $T_{i+1,j}$ $T_{i-1,j}$ are equal but less than $T_{i,j}$. Then if the time step is chosen such that $1/F_o < 2$, the temperature $T_{i,j+1}$ will be less than that of the neighbouring nodes, but this is not possible thermodynamically. Therefore to obtain meaningful solutions

the value of the parameter $1/F_o$ should be chosen such that:

$$0 < F_o < 0.5$$

4.9.3 IMPLICIT METHOD

The finite difference explicit method described above has the disadvantage that, if a small space step Δx is chosen to improve the accuracy of the calculations the computational problem increases because the time step Δt must also be very small due to the stability consideration.

In order to remove this restriction it is necessary to use an implicit method of finite differencing. There are many implicit schemes, the *fully implicit* method gives the equation:

$$T_{i,j+1} - T_{i,j} = \alpha\left(\frac{T_{i-1,j+1} + T_{i+1,j+1} - 2T_{i,j+1}}{\Delta x^2}\right)\Delta t$$

This expression is of the same form as that for the implicit method, but the right hand terms are evaluated at the time step j+1, rather than at j in the implicit form. The fully implicit method, though stable for any Δt is not as accurate per unit of computer run time as the more general implicit method, where a weighted average of T_j and T_{j+1} is used:

$$T_{i,j+1} - T_{i,j}$$

$$= \alpha\Delta t\left[(1-\lambda)\left(\frac{T_{i+1,j+1} - 2T_{i,j} + T_{i-1,j+1}}{\Delta x}\right) + \lambda\left(\frac{T_{i+1,j} - 2T_{i,j} + T_{i-1,j}}{\Delta x}\right)\right]$$

Putting $\lambda=0$ gives the explicit form, $\lambda=1$ gives the fully implicit form. If there are complications in the system being solved, for example

where variable conductivity is considered, the λ should be chosen close to 1, for this choice generates the most stable solution. Lower values of λ produce better levels of local truncation error and accuracy, but if

$$0 \leq \lambda < 0.5$$

then the solution is only stable if

$$F_o \leq \frac{0.5}{(1-2\lambda)}$$

With the geometry and time increment that are being considered this is too great a limitation, except where $\lambda \simeq 0.5$. For this reason the *Crank-Nicholson* method was chosen, which has the lowest accumulated truncation error whilst maintaining unconditional stability.

$$T_{i,j+1} - T_{i,j}$$

$$= \alpha \Delta t \left[\left(\frac{T_{i+1,j+1} - 2T_{i,j} + T_{i-1,j+1}}{2\Delta x^2} \right) + \left(\frac{T_{i+1,j} - 2T_{i,j} + T_{i-1,j}}{2\Delta x^2} \right) \right]$$

The derivation of the Crank-Nicholson form is shown in Appendix 4.4.

Each of these implicit methods involves the solution of a set of equations, each with three unknowns, except the first and last with two unknowns. They can be assembled into matrix form:

$$\begin{bmatrix} (2+2F_o) & -F_o & 0 & 0 \\ -F_o & (2+2F_o) & -F_o & 0 \\ 0 & -F_o & (2+2F_o) & -F_o \\ 0 & 0 & -F_o & (2+2F_o) \\ 0 & 0 & 0 & -F_o \end{bmatrix} \begin{bmatrix} T_{1,j+1} \\ T_{2,j+1} \\ T_{3,j+1} \\ T_{4,j+1} \\ T_{5,j+1} \end{bmatrix} = \begin{bmatrix} (2-2F_o) & F_o & 0 & 0 \\ F_o & (2-2F_o) & F_o & 0 \\ 0 & F_o & (2-2F_o) & F_o \\ 0 & 0 & F_o & (2-2F_o) \\ 0 & 0 & 0 & F_o \end{bmatrix} \begin{bmatrix} T_{1,j} \\ T_{2,j} \\ T_{3,j} \\ T_{4,j} \\ T_{5,j} \end{bmatrix}$$

The temperatures $T_{1,j}, T_{2,j} \ldots\ldots T_{n,j}$ are the initial conditions, and are known. The n algebraic equations are simultaneously solved, using the algorithm shown in Appendix 4.5, and the temperatures $T_{1,j+1}, T_{2,j+1} \ldots\ldots\ldots T_{n,j+1}$ found. The temperatures at the rest of the time steps are computed in a similar manner.

Further formulae are needed for a finite-difference representation of the boundary conditions, in Crank-Nicholson form these are

$$-B_i F_o T_{f,j+1} + (B_i F_o + 1) T_{s,j+1} - F_o T_{2,j+1}$$

$$= B_i F_o T_{f,j} + (B_i F_o - 1) T_{s,j} + F_o 2,j$$

where T_s is the surface temperature
and T_f is the fluid temperature.

In addition the presence of internal material interfaces alters the Crank-Nicholson equations derived earlier, although they maintain the same format. The final form of the tri-diagonal matrix derived with this method is shown on the next page.

$$
\begin{bmatrix}
1+F_1(1+B_1) & -2\bar{F}_1 & 0 & 0 & 0 & \cdots & 0 & 0 & 0 \\
-F & (1+(1+RC))\bar{F} & -RC\bar{F} & 0 & 0 & \cdots & 0 & 0 & 0 \\
0 & -F & (1+(1+RC))\bar{F} & -RC\bar{F} & 0 & \cdots & 0 & 0 & 0 \\
0 & 0 & -\bar{F} & (1+(1+RC))\bar{F} & -RC\bar{F} & \cdots & 0 & 0 & 0 \\
\vdots & \vdots & \vdots & \vdots & \vdots & & \vdots & \vdots & \vdots \\
0 & 0 & 0 & 0 & 0 & \cdots & -\bar{F} & (1+(1+RC))\bar{F} & -RC\bar{F} \\
0 & 0 & 0 & 0 & 0 & \cdots & 0 & 2F_2 & 1+F_2(1+B_2)
\end{bmatrix}
\begin{bmatrix}
T_{s,j+1} \\ T_{1,j+1} \\ T_{2,j+1} \\ T_{3,j+1} \\ \vdots \\ T_{n-1,j+1} \\ T_{n,j+1}
\end{bmatrix}
=
$$

$$
\begin{bmatrix}
1-F_1(1+B_1) & 2F_1 & 0 & 0 & 0 & \cdots & 0 & 0 \\
\bar{F} & (1-(1+RC))\bar{F} & RC\bar{F} & 0 & 0 & \cdots & 0 & 0 \\
0 & \bar{F} & (1-(1+RC))\bar{F} & RC\bar{F} & 0 & \cdots & 0 & 0 \\
0 & 0 & \bar{F} & (1-(1+RC))\bar{F} & RC\bar{F} & \cdots & 0 & 0 \\
\vdots & \vdots & \vdots & \vdots & \vdots & & \vdots & \vdots \\
0 & 0 & 0 & 0 & 0 & \cdots & (1-(1+RC))\bar{F} & RC\bar{F} \\
0 & 0 & 0 & 0 & 0 & \cdots & 2F_2 & 1-F_2(1+B_2)
\end{bmatrix}
\begin{bmatrix}
T_{s,j} \\ T_{1,j} \\ T_{2,j} \\ T_{3,j} \\ \vdots \\ T_{n-1,j} \\ T_{n,j}
\end{bmatrix}
+
\begin{bmatrix}
B_1F_1T_{j+1} \\ 0 \\ 0 \\ 0 \\ \vdots \\ 0 \\ B_nF_nT_{j+1}
\end{bmatrix}
$$

(83)

4.10 OPERATION OF TRANSIENT TEMPERATURE PROGRAM

During its initialisation procedure the main program will enquire if a transient analysis should be developed. If the operator requests a transient solution the input data must contain the density and specific heat capacity of each material used. This program will calculate the temperature distribution at a number of time steps.

The transient analysis program is called only once, regardless of the number of temperature fields requested. A matrix is formed of the depth-temperature-time distribution. This contains the temperature of the nodal point in each of the elemental discs, at each of the time increments specified. The same elemental grid is used with the thermal analysis as in the force balance method.

The material data, boundary conditions and grid dimensions are transferred to the thermal analysis package contained in subroutine *temppro*. This package will then operate independently of the stress program, until all the temperature distributions are calculated. Some or all of these temperature fields are recorded in the matrix. This data is then transferred back to the main program which calculates and records the stress distribution at each of the time increments.

Program structure is shown in the flow chart figure 4.13, and the program listing is shown in Appendix 4.6. As mentioned above the first action is to define the material data, in addition the thermal boundary conditions must be set. Either in terms of the wall temperature, or the fluid flow conditions on the disc faces. These can be set as constants or as time dependent variables. The applied thermal loading will probably be a complex time dependent function of engine crank-angle, and inlet gas temperature. In this case the user must set up a subroutine called *tempbound*. This subroutine should calculate the applied thermal boundary conditions in response to an input of time.

Once the initialisation is completed the program assembles the system of simultaneous equations for each of the time increment considered. These are then solved using the tridiagonal matrix algorithm outlined in Appendix 4.5. The relevant subroutine is called *tridig*.

To achieve high accuracy results it is neccessary to use a small time increment, especially if the applied thermal conditions are oscillatory. It is, however, not neccessary to calculate the stress distribution at each of the time increments. The program therefore selects only a few of the calculated temperature fields for recording in the depth-temperature-time matrix.

Once the pre-set number of cycles has been performed control is then returned to the force balance program.

4.11 VALIDITY OF TRANSIENT ANALYSIS

There are two areas which can be checked, both the predicted transient temperature field and the final steady state distribution.

The example given in Appendix 4.7 is for a ceramic material

Thermal conductivity	=	30 W/mK
Density	=	3800 kg/m^2
Heat capacity	=	800 J/Kg

A 20mm thick specimen is taken at a uniform initial temperature of 200^{o}C. One side is maintained at 200^{o}C whilst the other is left open to gas, at a temperature of 1200^{o}C and a heat transfer coefficient of 1100W/m^2.

The program is used to output the temperature field to a data file at

specified time increments, the tabulated output for this example is shown. The temperature field is recorded at 2.7 second time intervals and at 2mm depth intervals.

It is nesessary to validate the transient response. A hand calculated finite difference explicit method was used, with spatial and time increments chosen for stability. The stability criterion forced the use of a very coarse spatial grid, so inaccuracies are inevitable. Despite this limitation the agreement between the explicit and implicit methods is good as shown.

In addition the steady state distribution can easily be checked using a one dimensional thermal network. The example given shows the temperature field predicted by the implicit method to have stabilised after about 100 seconds, at this point the agreement with the steady state temperature given by the thermal network is shown in Appendix 4.7.

4.12 GRAPHICAL OUTPUT

When using the force balance method to study the transient behaviour of discs a large quantity of numerical data is produced. Although this is tabulated in the same way as the steady state analysis, it is none the less difficult to isolate the trends exhibited by the data. To best show the transient behaviour a graphics subroutine has been produced which can show the progression of the temperature and stress distributions within the disc. The standard tabulated output from the stress program is used as the input for this graphics package. The operator only needs to specify the number of transient responses which are to be plotted. The remaining criteria are set by the program.

Three graphs are produced:

Temperature	vs	depth
Radial stress	vs	depth
Axial stress	vs	depth

The axes are automatically set. example outputs are shown in figures 4.27 to 4.30.

The program listing is shown in Appendix 4.8. and uses the plot_ routines with multics fortran.

4.13.1 PREDICTED STEADY STATE THERMAL CHARACTERISTICS

The stresses arising within engine components are the result of two types of imposed loading. these being thermal and mechanical. Mechanical loading of stationary components is produced either by gas pressure or mechanical restraints. Also the thermal loading has two causes. Firstly that resulting from an increase in bulk material temperature above that at which the component was formed. Secondly a temperature difference across the material will give rise to thermal stresses. The stress analysis program has been used to examine the effects of these two thermal loadings.

Two examples have been taken:

1/ A 2mm thick layer of Silicon Nitride on a 21mm thick base of steel. disc diameter 86mm.

	Si N	Steel	
Young's modulus	290	200	GPa
Thermal conductivity	20	30	W/M^2
Thermal expansion	2.5	14	$x10^{-6}$
Poissons ratio	0.23	0.3	

2/ A 2mm thick layer of Partially Stabilised Zirconia on a 21mm thick

base of steel, disc diameter 86mm.

	PSZ	Steel	
Young's modulus	220	200	GPa
Thermal conductivity	3	30	W/M^2
Thermal expansion	10	10	$x10^{-6}$
Poissons ratio	0.23	0.3	

The above figures are typical of the published material property data.

Silicon Nitride is not a practical coating material but studying this case can give an insight into certain characteristics.

Figures 4.14 and 4.15 show the stresses developed within the two example discs from both of the temperature distributions mentioned. In these examples both the discs are unrestrained, and axial movement is allowed, this corresponds to the design shown in figure 4.14b.

Due to the close matching of thermal expansivity the stress distribution that arises with the PSZ example is less that that in the Silicon Nitride. However a more important effect, is that with the PSZ the two thermal radial thermal stresses can be arranged to cancel one another. A uniform temperature rise in the disc causes both tensile and compressive loadings in the Zirconia coating, while a temperature difference between the faces causes a compressive loading. By choosing the temperature at which the coating is formed it is possible to minimise the stresses within the coating, and to ensure the loading is compressive. If this approach is used it will be necessary to ensure that the disc is not subject to stresses at atmospheric conditions which would cause yielding.

The same two discs as above are examined in figures 4.16 and 4.17, but are not allowed to axially deform, a design which

represents this is shown in figure 4.18a. The Silicon Nitride again develops higher magnitudes of stress than the Zirconia. The unrestrained Zirconia disc will develop lower radial stresses than the unrestrined example, unless the two thermal stresses can be used to counter one another.

In neither case are the axial stresses likely to prove critical.

Figure 4.19 shows the radial stresses that arise by imposing a given radius of curvature (or central deflection). The smaller the radius of curvature the greater the stresses produced. Since there is a linear radial stress distribution through the disc the graph only records the stresses that ar ise at the top and bottom of the ceramic face. Also shown is the effect of the two types of thermal loading, both of which are independent of the radius of curvature. These correspond to a $100^{o}C$ temperature drop between opposite faces, and a $100^{o}C$ uniform temperature rise. As mentioned above, it can be seen that is is possible with the Zirconia coating to arrange the thermal stresses to relieve each other.

The effect of the radius of curvature is further examined in figure 4.20 and 4.21, a disc having a fixed temperature distribution of 800K on the ceramic surface and 200K on the rear face (relative to a zero stress position). Figure 4.20 shows that by allowing the disc freedom to deform the resulting axial stresses are kept close to their minimum. However the radial stresses are not at their optimum at this condition, as shown in figure 4.21. By reducing the central deflection that is permitted the radial stresses are reduced. In the case of the PSZ coating limiting the radius of curvature to 15m significantly reduces the tensile radial loading within the coating, while only slightly increasing the axial stress.

Figures 4.22 and 4.23 show the effect of increasing the coating thickness on the radial stresses, in both the restrained and unrestrained states. In both examples a disc of 86mm diameter and 23mm thickness was taken. The ceramic face is open to gas T=1500K, $h=1100W/M^{2}K$ the rear face is held at 500K. It is assumed that the disc is stress free at 300K.

With Silicon Nitride the effect of increasing the coating thickness is to reduce the stress levels. This behaviour arrises because the thin coatings are forced to deform to a position imposed by the metalic base. The thicker coatings are able to assume a compromise position transfering more of the load to the base. With a thicker PSZ coating a greatly increased temperature drop is developed across the ceramic. This increases the thermal mismatch, resulting in higher stress levels. However at very high coating thicknesses the temperature drop has almost stabilised The predominant effect with these thickest coatings is the way the Zirconia is able to transfer its loading by straining the metal base.

4.13.2 THE EFFECT OF INACCURATE MATERIAL PROPERY DATA

As discussed in section 4.2 there are inconsistencies within the published ceramic property data. When analysing the stresses which are derived within ceramic components it is necessary to allow for the range of properties which can be exhibited.

The force balance method can be used to establish the relationship between an error in material property data and the resulting change in maximum stresses. Figures 4.24 to 4.27 show the percentage change in stress against a percentage error in property data used in the analysis. This percentage change is defined as the change in stress at a given point divided by the maximum stress within the material. On all graphs a ±20% error in material property data is shown. This range is not excessive and represents the range which can result from both inacuurate/inappropriate property measurement, coupled with the changes in ceramic properties which arrise over time, especially in a hostile environment, such as that within the diesel engine.

The properties examined are:

Poison's ratio
Thermal expansion

Thermal conductivity
and Young's modulus

The behaviour is shown for both restrained and unrestrained discs (correspnding to figures 4.18a and 4.18b). The same disc configuration and properties are used as discussed in 4.13.1.

Figures 4.24 to 4.25 examine the case of axially restrained discs. In all cases a given error in a material property produces a less than proportional change in the maximum stress, except with the coefficient of thermal expansion. A 10% error in this property causes an error of approx 25% in the stress calculated at the top face.

Similar behaviour is produced with the unrestrained discs, shown in figures 4.26 to 4.27. The effect of an error in Young's modulus with Silicon Nitride is reduced, whilst the effect of the coefficient of thermal expansion in PSZ is increased. In this case a 10% error in the property data leads to a 30% error in the stresses predicted at the top face.

These percentage figures can however be misleading, under some situations a tensile load can be developd within the ceramic when the analysis (performed with inaccurate data) gives a compressive load.

4.13.3 TRANSIENT RESPONSE OF MONOLITHS

The computer output from two transient analyses is shown in figures 4.28 to 4.31. The two cases considered are of a PSZ disc and a Silicon Nitride disc. Both are 86mm diameter and 20mm thick, each is made of a single material, the properties of which are recorded in section 4.13.1. One side of the disc is subject to a fluctuating gas temperature, corresponding to the environment created with the insulation test rig operating at its minimum temperature rating.

Gas inlet temperature	$23o_C$
Maximum in cylinder temperature	721^oC
Rear face held at	200^oC
Initial ceramic temperature	200^oC
Engine speed	1200rpm

pressure loading ignored, no mechanical restraints taken.

There are two effects to monitor, those resulting from the initial gas temperature rise, and that arrising from the cycle to cycle fluctuations. These are shown in figures 4.32a and 4.32b.

The transient temperature distribution within the PSZ disc from 0.5 to 5 seconds and from 2 to 20 seconds are shown in figure 4.28. All the readings are taken at TDC corresponding to position A on figures 4.32. From figure 4.28 the gas side surface temperature can be seen to be approximately 200^oC after 0.5 seconds. The two graphs therefore show the progress of the temperature wave through the material.

Figure 4.29 show the radial stress distribution from 0.5 to 20 seconds. Initially the peak tensile load is increasing and moving through the material. At approximately 10 seconds the maximum tensile stress of about 70KPa is reached, after this time although the stress wave continues through the material it decreases in intensity. In the steady state the disc is able to assume a stress free position. The axial stress distribution is shown in figure 4.30, the stress levels shown are all low. The peak radial stress occurs in conjunction with the peak axial stress and marks the depth the temperature wave has reached. As with the radial stresses the maximum level is reached at about 10 seconds, after which the levels recede.

The cycle to cycle fluctuations in temperature and radial stress are shown in figure 4.31. A single engine revolution has been analysed, at a point 6 seconds after start up. There is approximately a $\pm 8^oC$ variation in surface temperature which penetrates to a depth of less than 1mm. The change in radial stress is about ±20KPa, however since the material is in continual

compression it may not to present a fatigue problem.

Figure 4.33 shows the transient response of the Silicon Nitride disc, the behaviour is similar to that of the PSZ disc. The temperatures are recorded at BDC corresponding to point B in figure 4.32. There is consequently a drop in the temperature gradient at the surface caused by the cycle to cycle gas temperature variation. In this example the steady state temperature distribution is approximated after 10 seconds. Since the temperature gradient in the Silicon Nitride disc is not as steep as in PSZ, the peak stresses are consequently lower. The peak radial stress of 3KPa has been reached at 2 seconds at a depth of 8mm, this is approximately 5% of that arrising in the PSZ under identical conditions.

4.13.4 TRANSIENT RESPONSE OF ZIRCONIA COATING

The transient temperature and stress distributions in an 86mm diameter zirconia coated disc are shown in figures 4.34 to 4.36. A 1mm coating on a 1cm thick steel substrate is used. This disc is initially at a uniform temperature of $20^{o}C$. The following boundary conditions were instantaneously imposed.

Heat transfer coefficient of water	$1000W/M^2K$
Water temperature	$80^{o}C$
Heat transfer coefficient of Gas	$500W/M^2K$
Gas temperature	$900^{o}C$

Time intervals of 0.2 seconds are used for the temperature and stress plots shown. Over the 2 second scale shown in figure 4.34 the temperature of the ceramic at the gas surface has risen by 265K, whilst the interface has risen by only 30K.

The stresses developed within the coating over this time are all compressive. This behaviour is expected as the insulative ability of the ceramic will ensure the temperature rise in the metal will be small in relation to that in the ceramic. The higher thermal expansion of the base material will therefore have little effect on the stress distribution. Consequently only compressive stresses will be

produced in the coating.

Maximum tensile stresses within the coating will occur in the steady state. A transient analysis of a zirconia coating therefore reveals little information to warrant a protracted investigation. The stresses derived when the coating is being cooled would present a more critical situation, but to model this an assessment would have to made of the air temperature and heat transfer coefficient during shut down, and the appropriate data is not available.

FIGURE 4.1 DISCRETISATION OF DISC

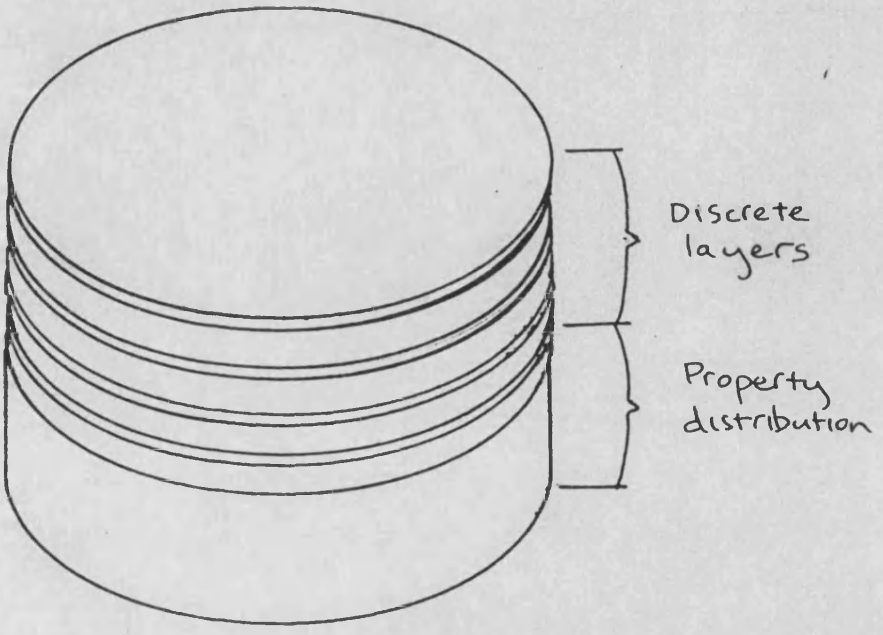

FIGURE 4.2 STRESS AND TEMPERATURE DATUM IN DISC

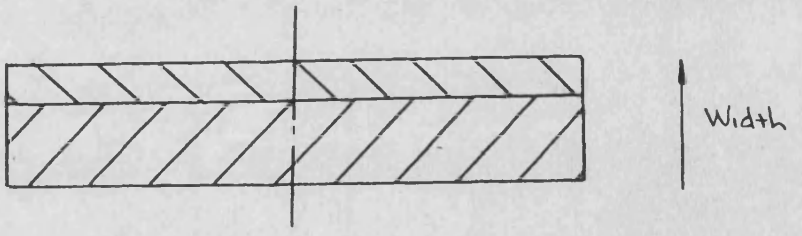

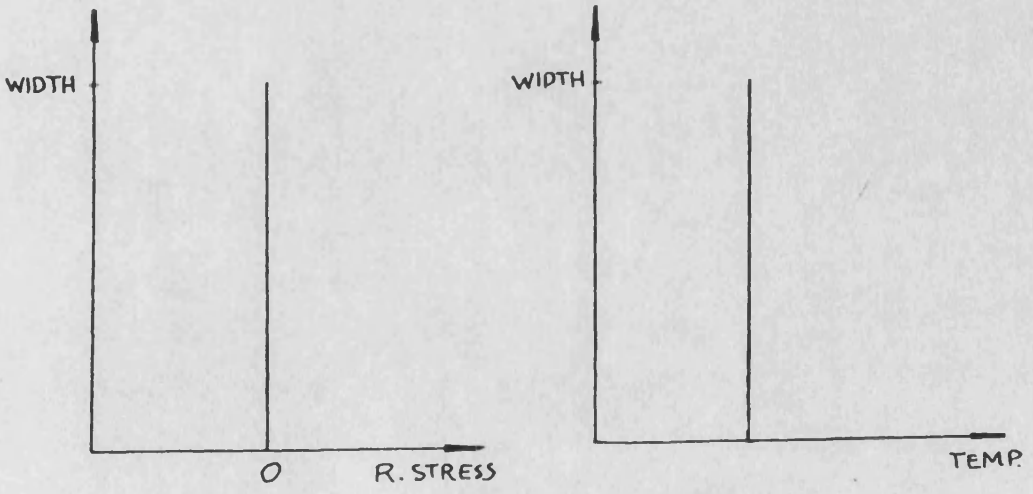

FIGURE 4.3 STRESS FREE DISC WITH IMPOSED TEMPERATURE FIELD

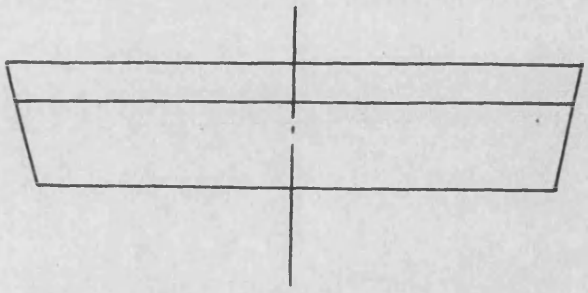

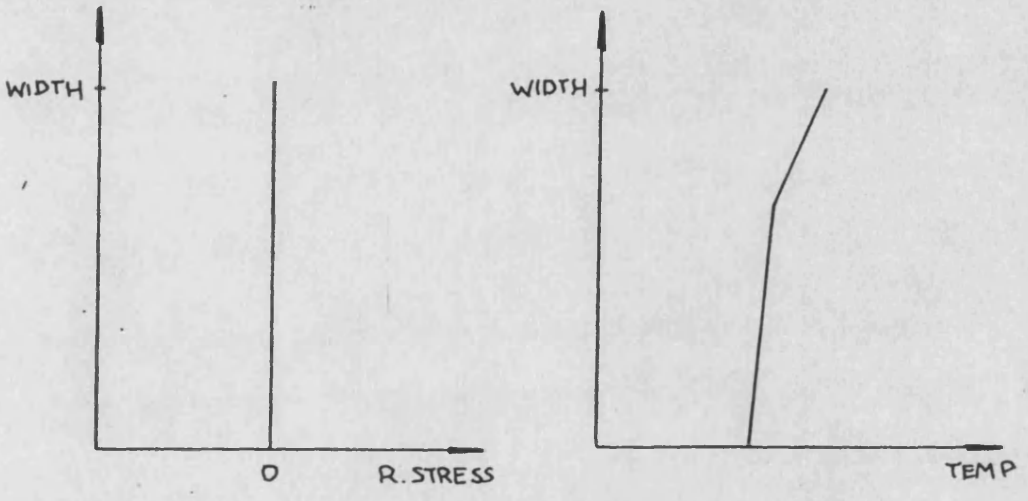

FIGURE 4.4 STRESS AND TEMPERATURE DISTRIBUTION WITH RESTRAINED DISC

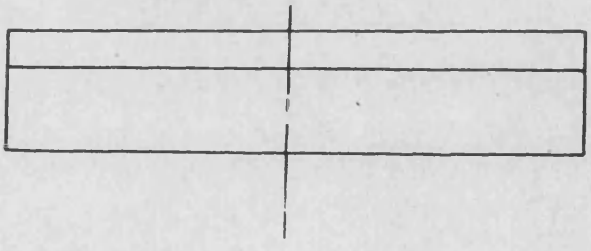

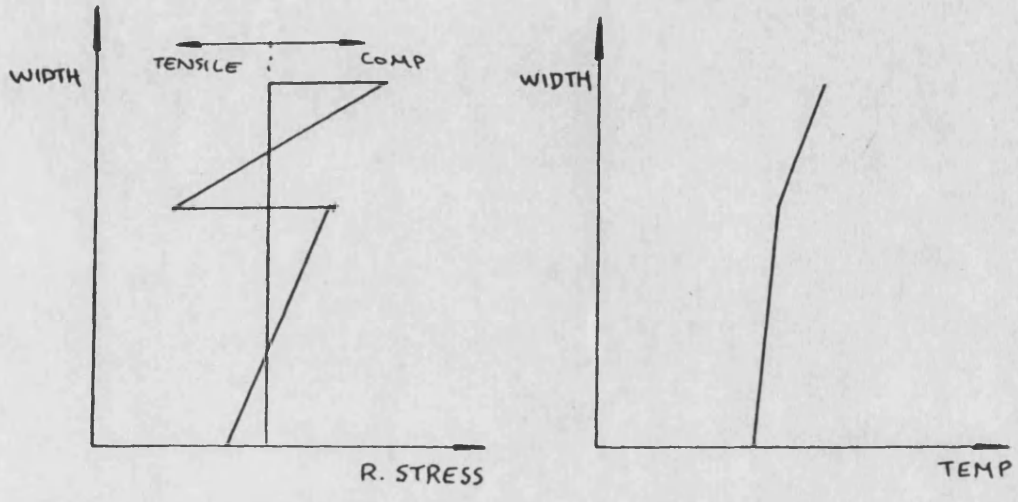

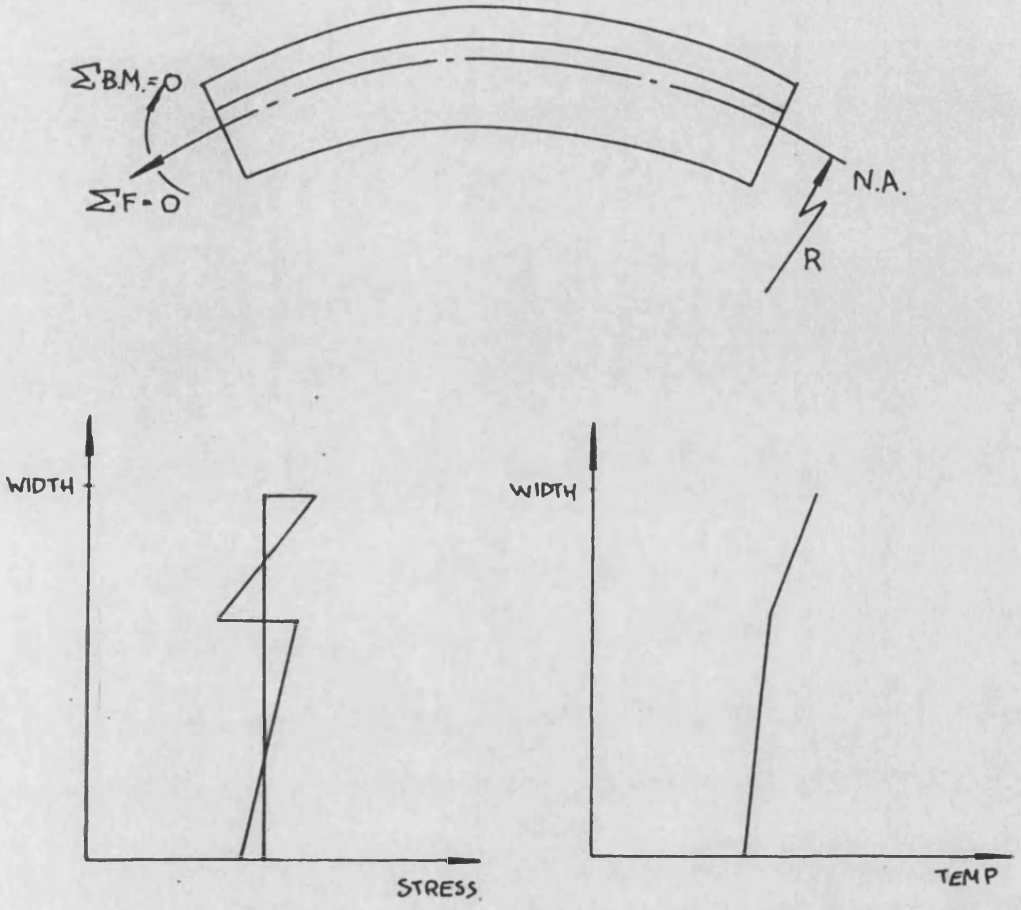

FIGURE 4.5 STRESS AND TEMPERATURE DISTRIBUTION WITH UNPESTRAINED DISC

a) When the disc is subject to a temperature difference between faces, each elemental disc will try to expand to its free diameter. If constrained to its original diameter then effective change in radius is Δr_c

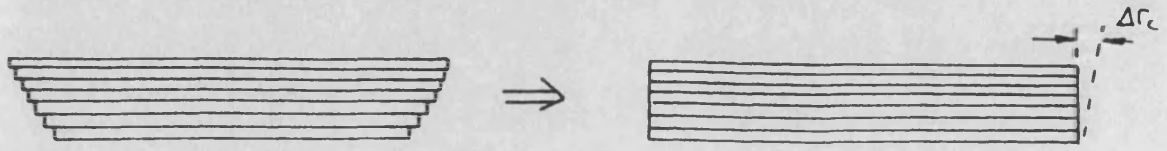

b) Δr_f is the change in radius required for radial equilibrium

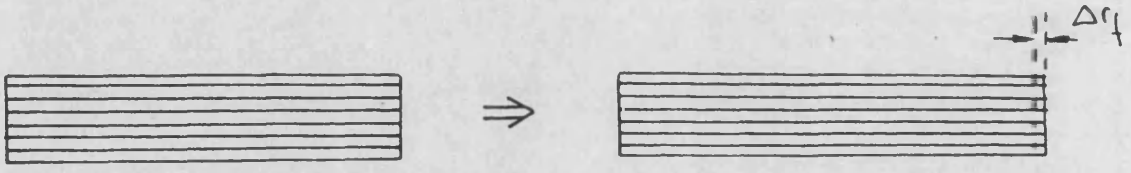

c) If disc is unrestrained then Δr_i is the change in radius of each elemental disc due to axial deformation.

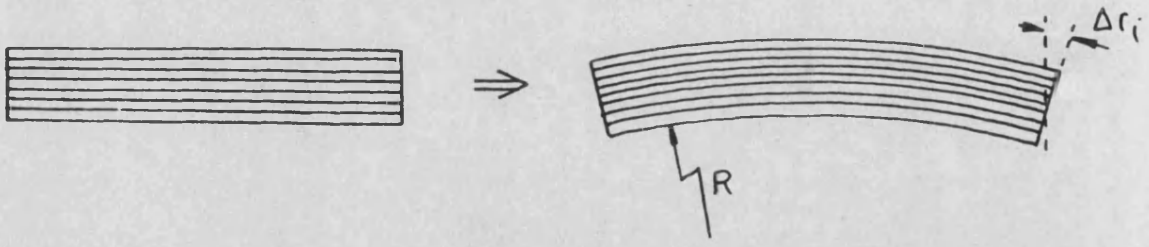

FIGURE 4.6 SETTING EXTERNAL DIAMETER FOR DISC

FIGURE 4.7 FULL FLOW CHART OF STRESS ANALYSIS

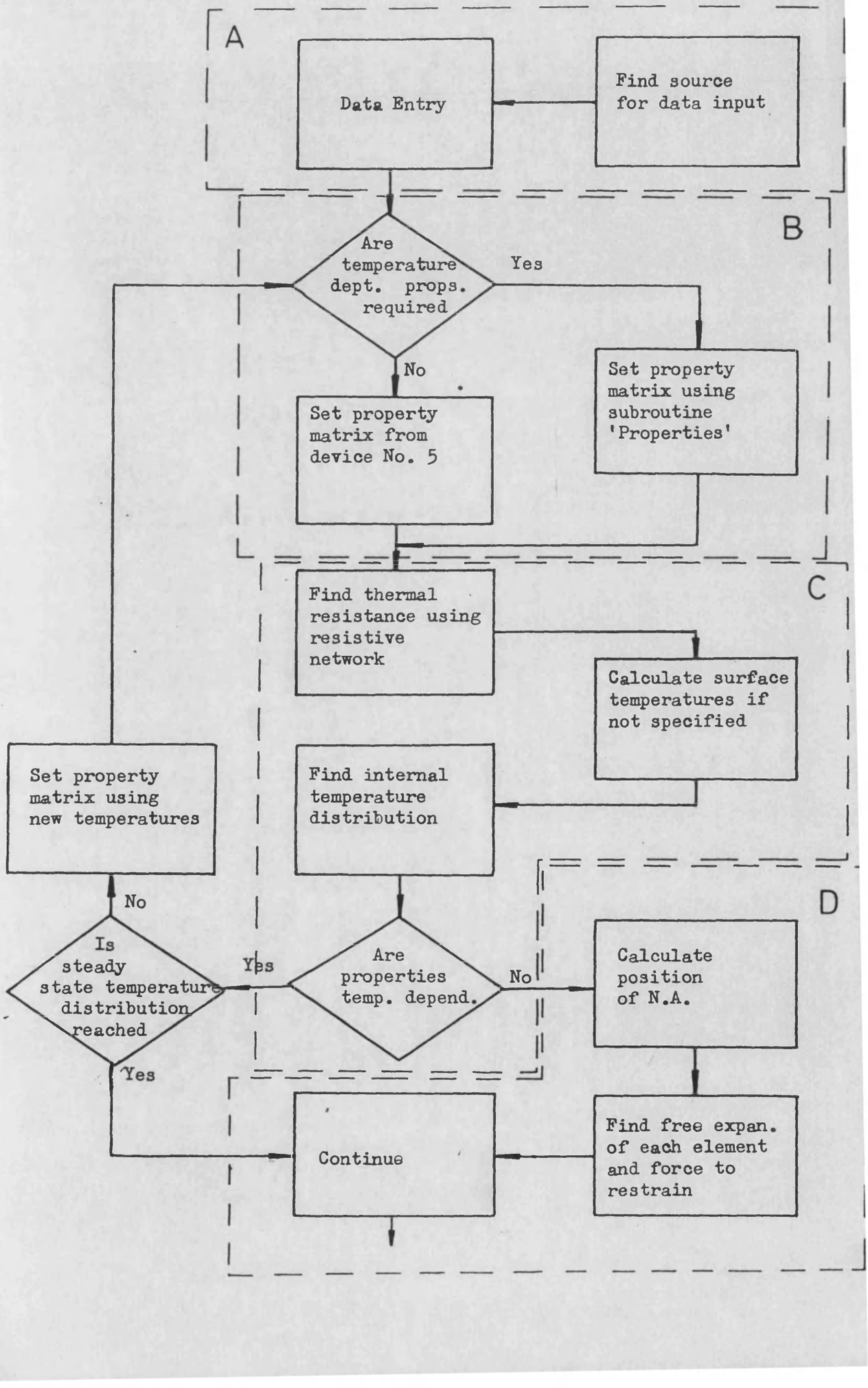

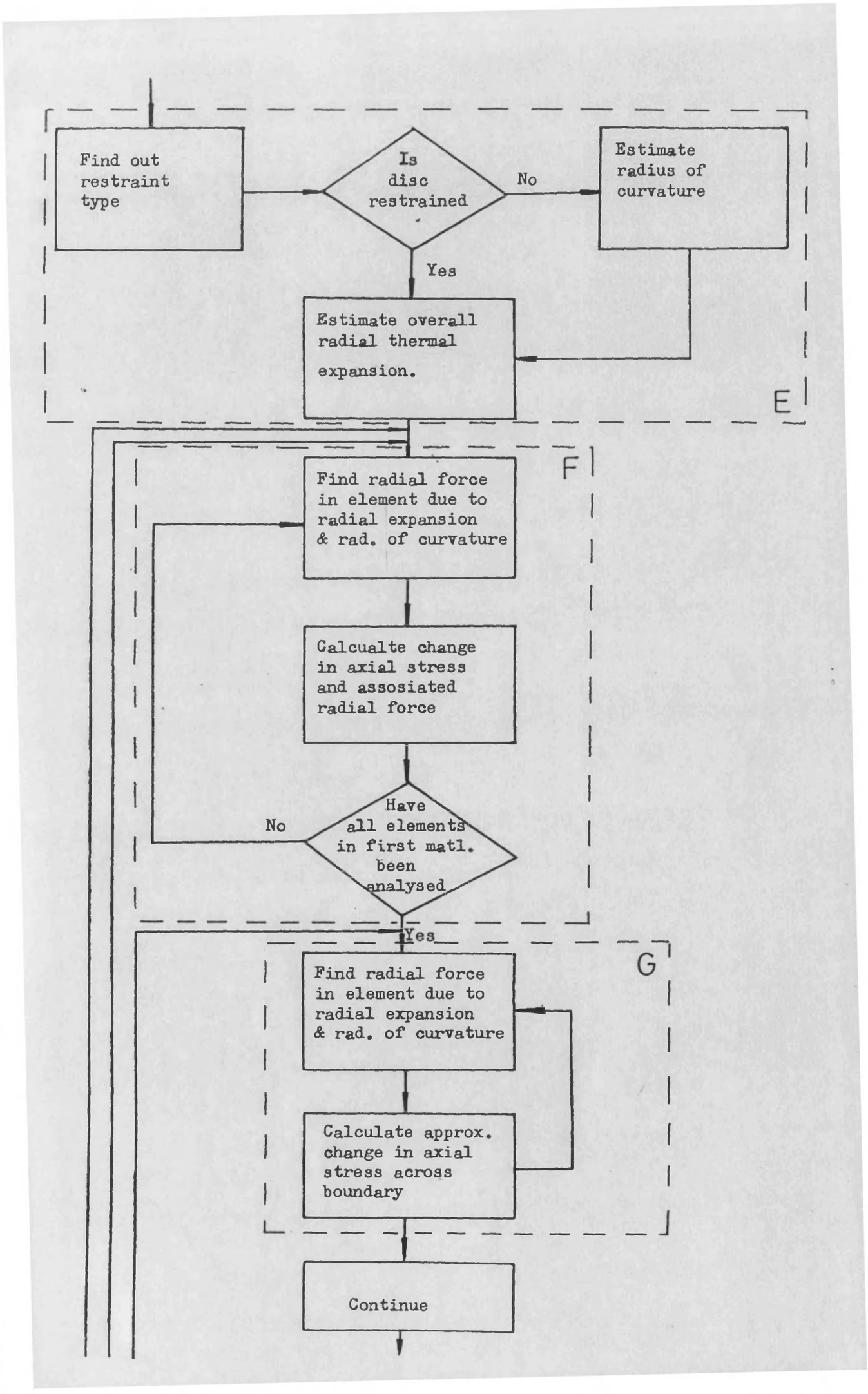
Find out restraint type
Is disc restrained
No
Estimate radius of curvature
Yes
Estimate overall radial thermal expansion.
E
F
Find radial force in element due to radial expansion & rad. of curvature
Calcualte change in axial stress and assosiated radial force
Have all elements in first matl. been analysed
No
Yes
G
Find radial force in element due to radial expansion & rad. of curvature
Calculate approx. change in axial stress across boundary
Continue

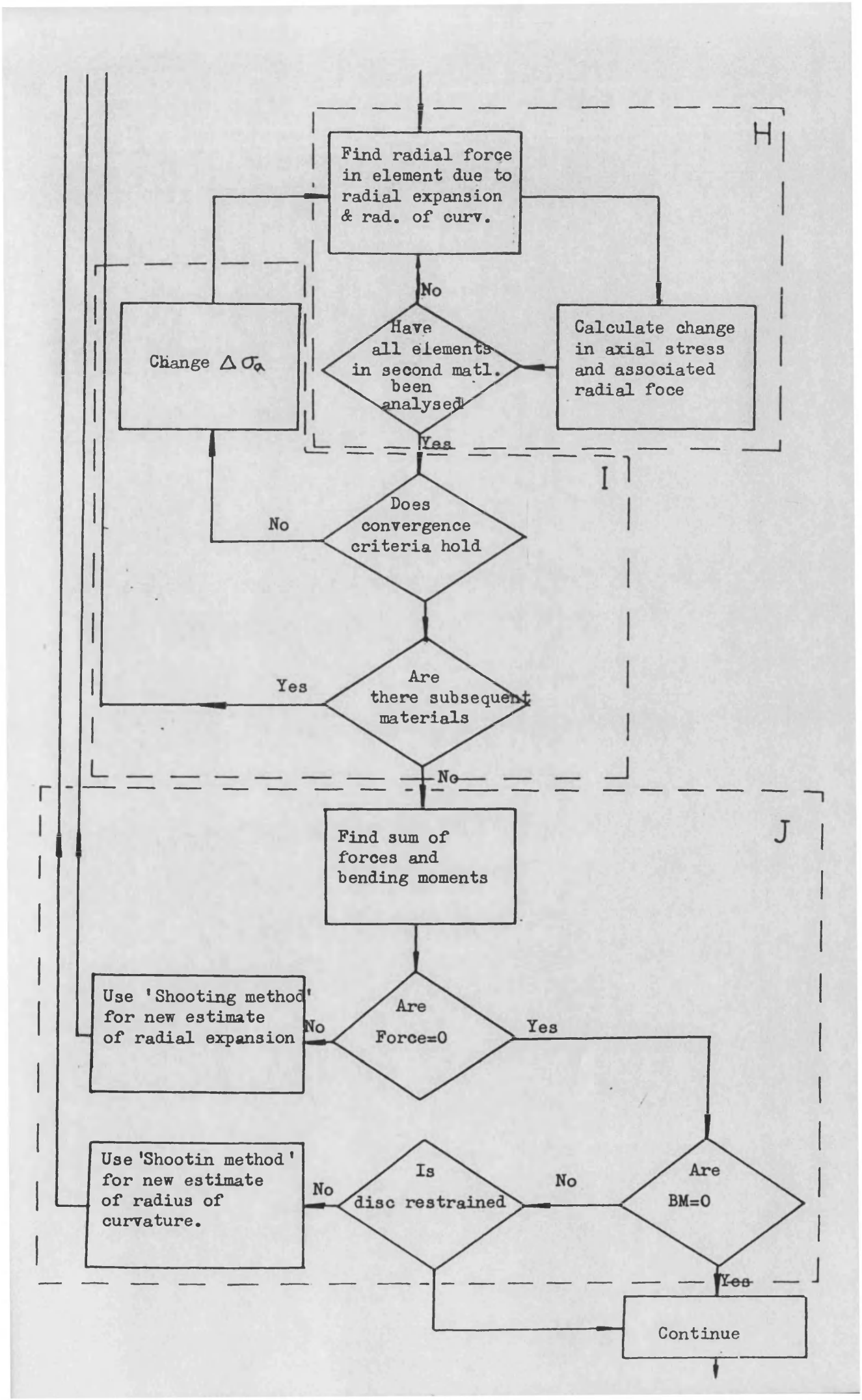
H
Find radial force in element due to radial expansion & rad. of curv.
No
Have all elements in second matl. been analysed
Calculate change in axial stress and associated radial foce
Change Δσa
Yes
I
Does convergence criteria hold
No
Are there subsequent materials
Yes
No
J
Find sum of forces and bending moments
Use 'Shooting method' for new estimate of radial expansion
No
Are Force=0
Yes
Use 'Shootin method' for new estimate of radius of curvature.
No
Is disc restrained
No
Are BM=0
Yes
Continue

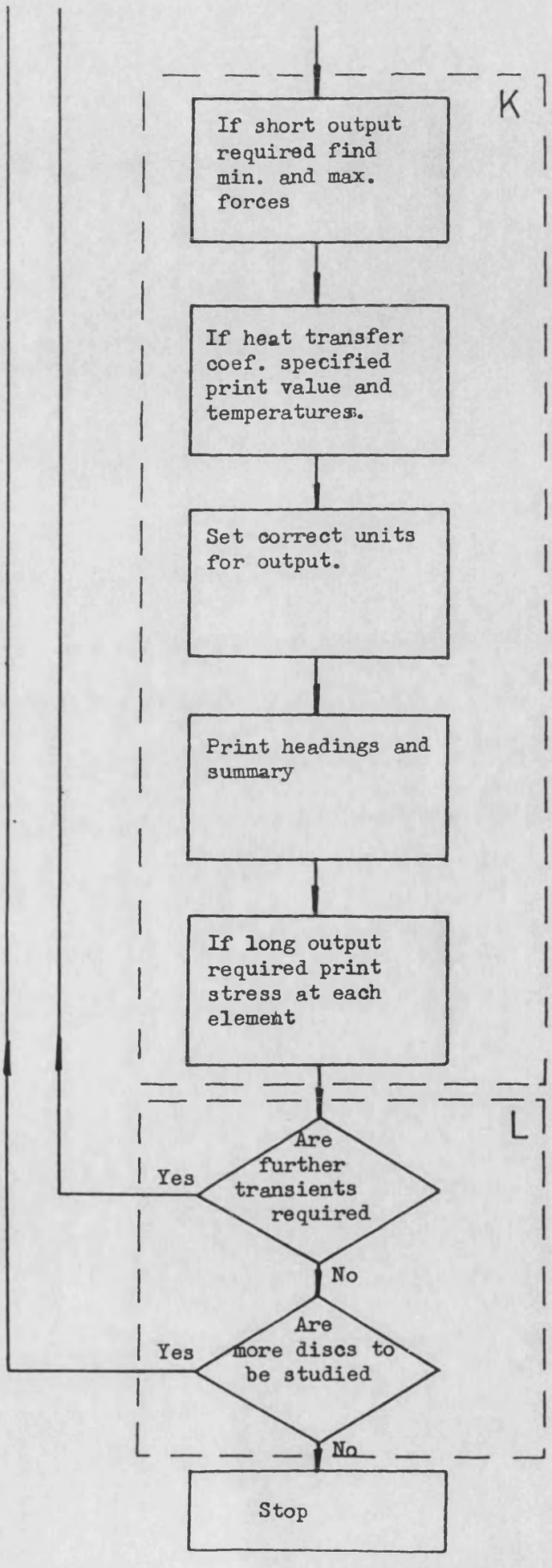
K
If short output required find min. and max. forces
If heat transfer coef. specified print value and temperatures.
Set correct units for output.
Print headings and summary
If long output required print stress at each element
L
Are further transients required
Yes
No
Are more discs to be studied
Yes
No
Stop

FIGURE 4.8 SIMPLIFIED FLOW CHART OF STRESS ANALYSIS

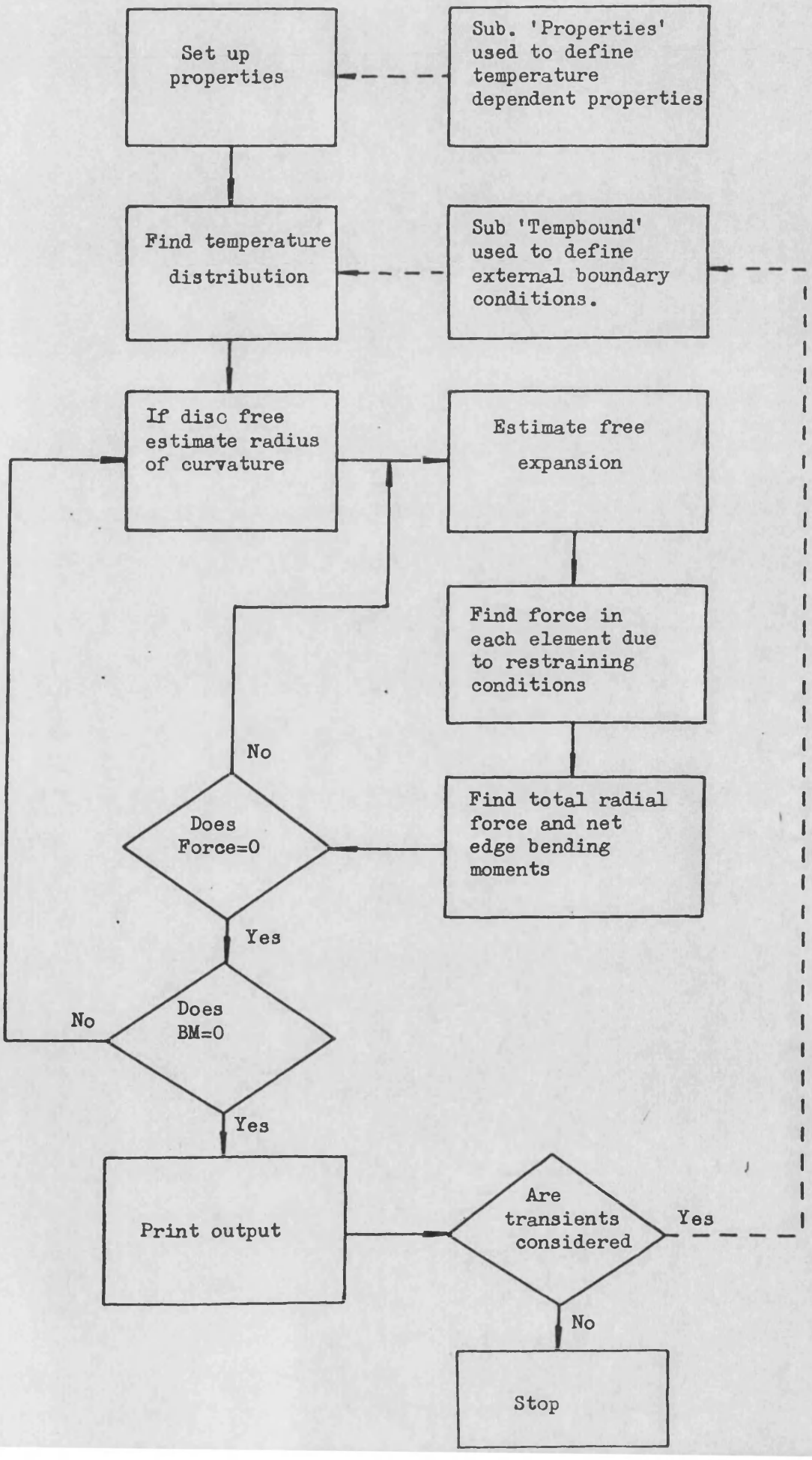

FIGURE 4.9 COMPARISON OF THEORETICAL FORMULA AND COMPUTER MODEL

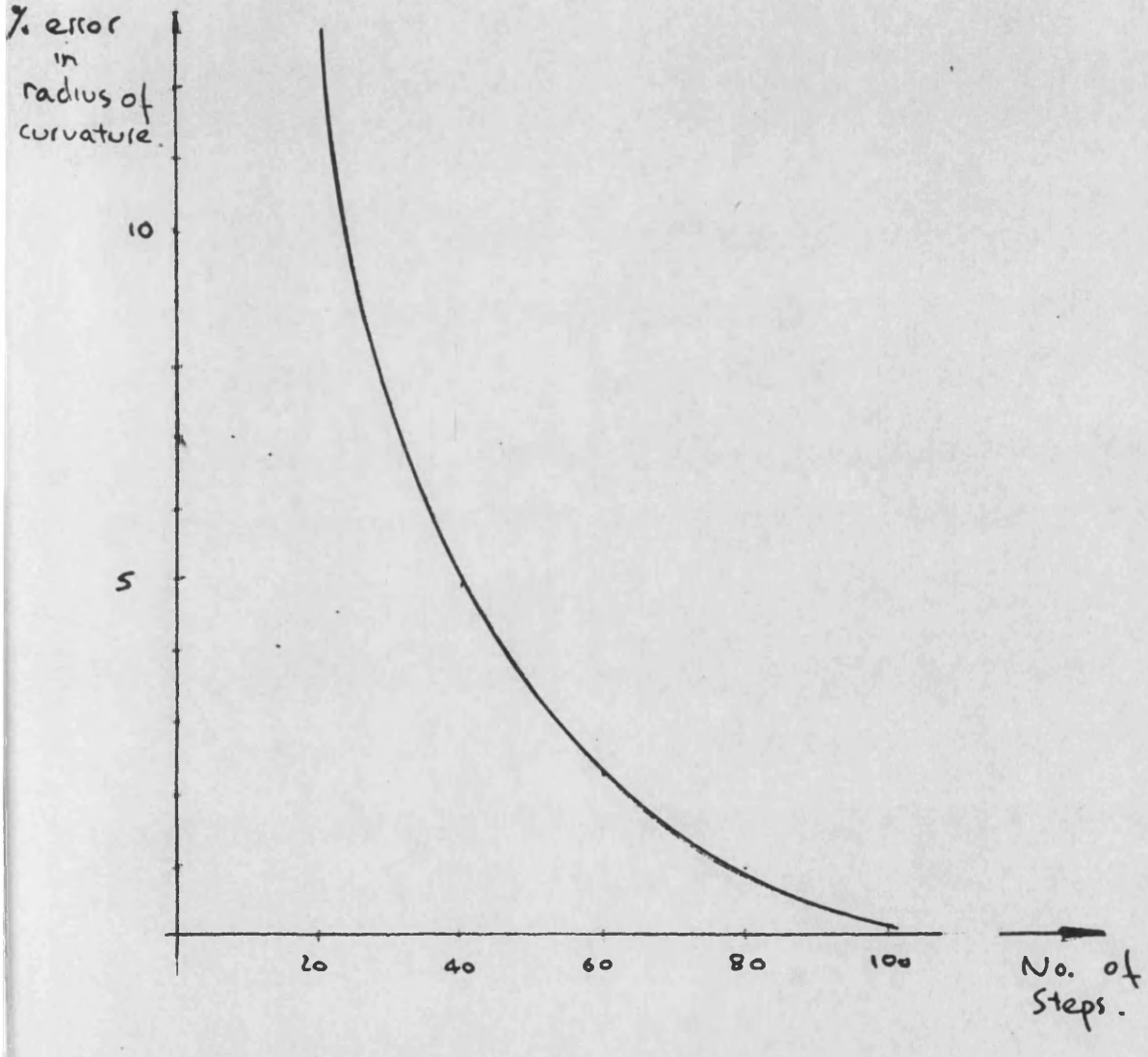

FIGURE 4.10 AXISYMMETRIC DISC ANALYSED ON ANSYS

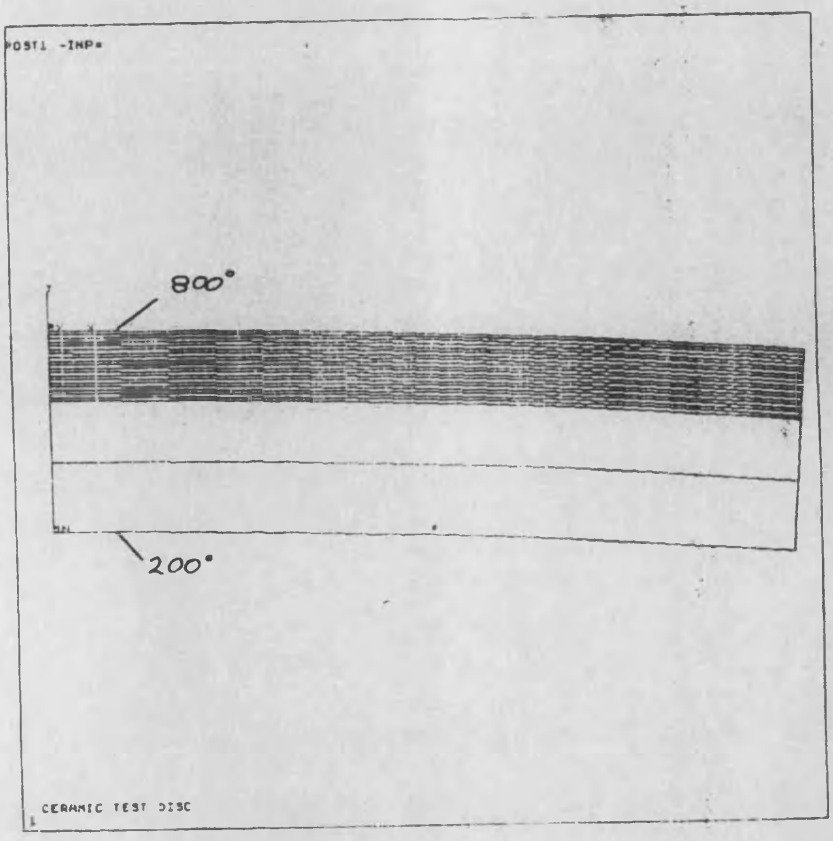

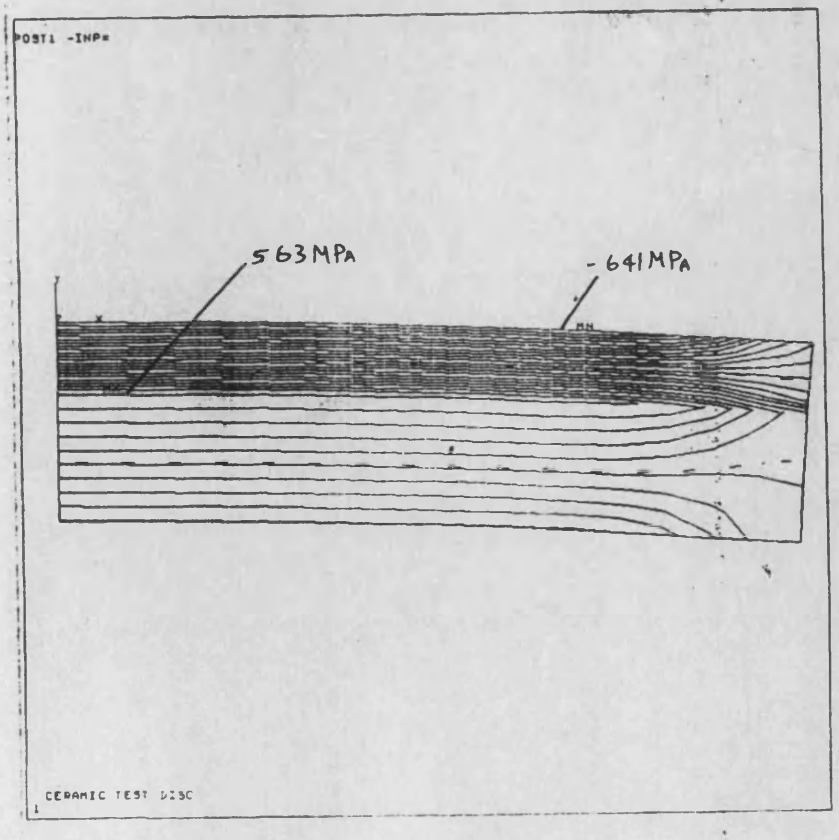

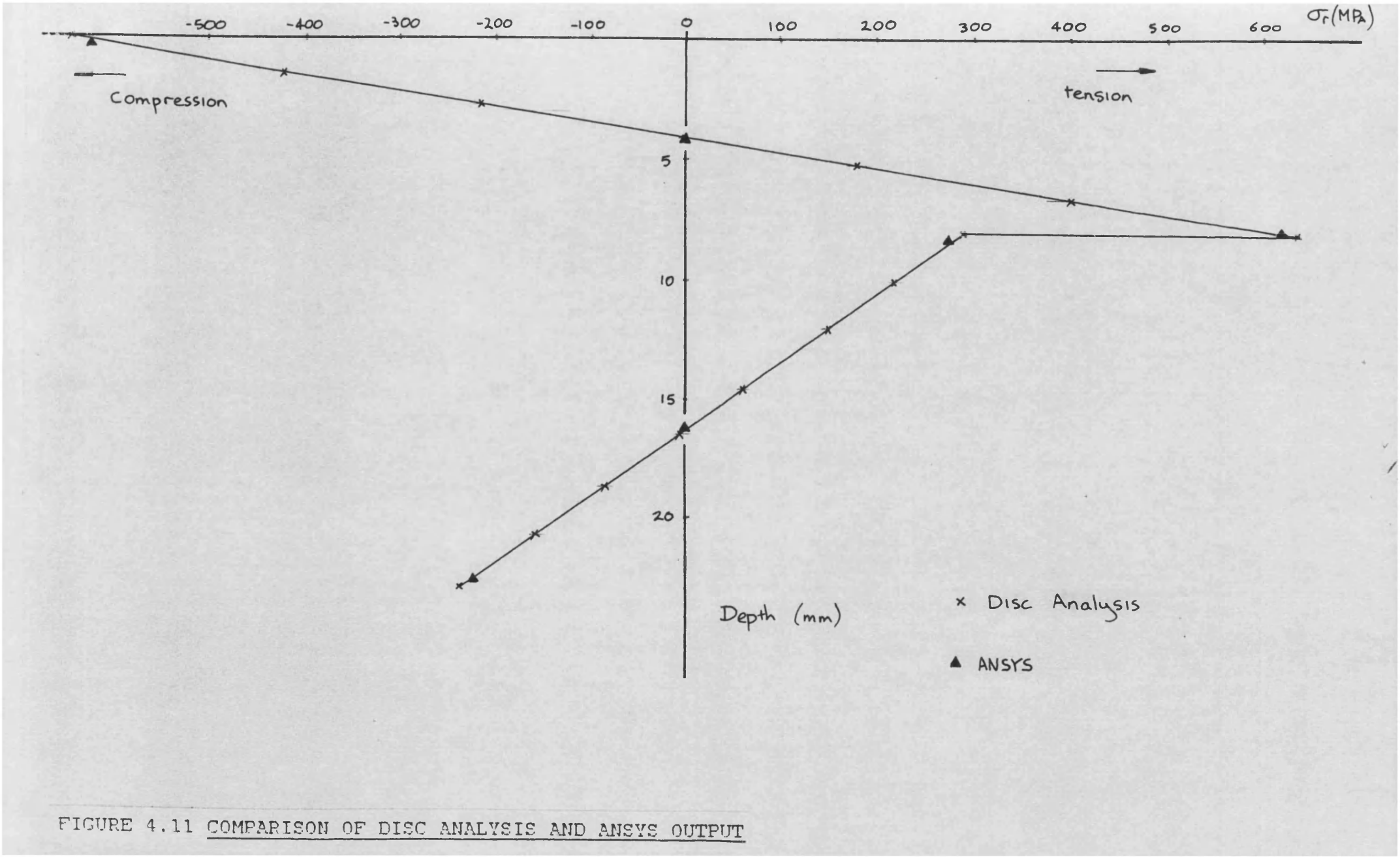

FIGURE 4.11 COMPARISON OF DISC ANALYSIS AND ANSYS OUTPUT

FIGURE 4.12 SPATIAL AND TIME DOMAINS USED IN FINITE DIFFERENCE METHODS

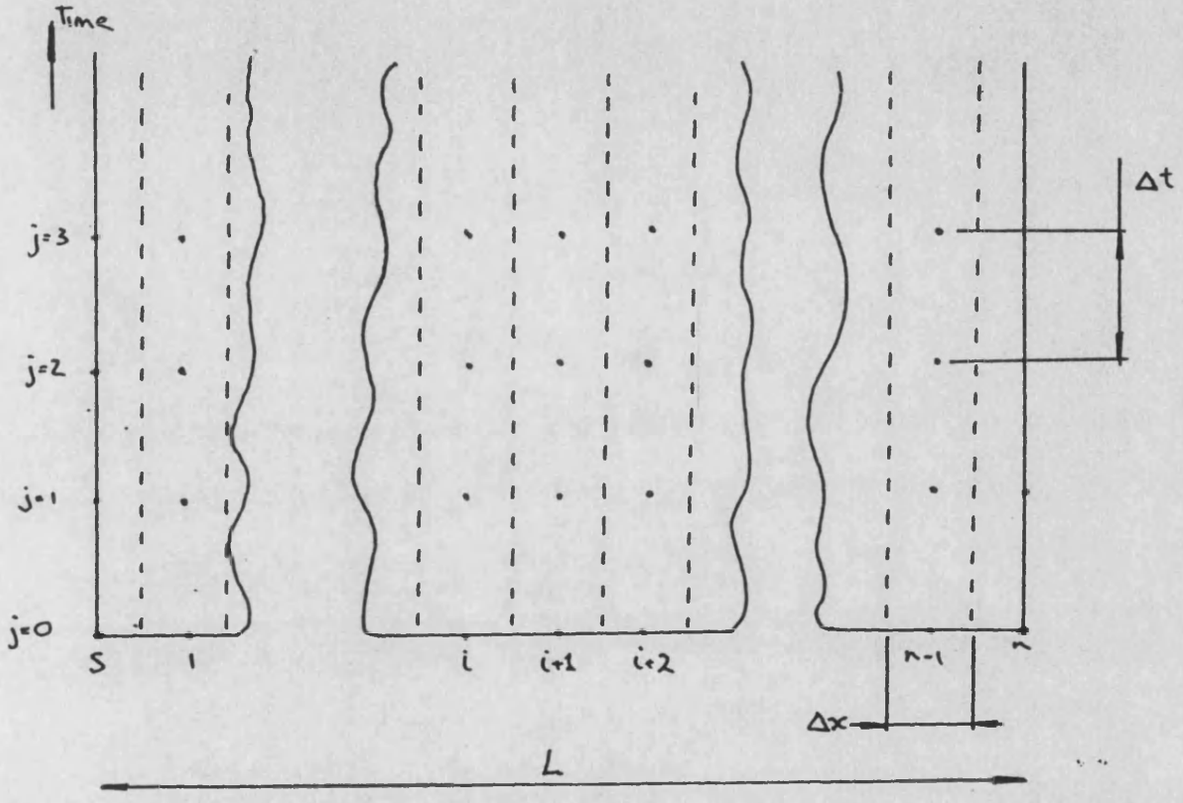

$x = i.\Delta x$ $\quad i = S, 1, 2 \cdots\cdots N$ $\quad$ where $\quad L = N.\Delta x$

$t = j.\Delta t$ $\quad j = 0, 1, 2, 3 \cdots\cdots$

FIGURE 4.13 FLOW CHART OF TRANSIENT TEMPERATURE ANALYSIS

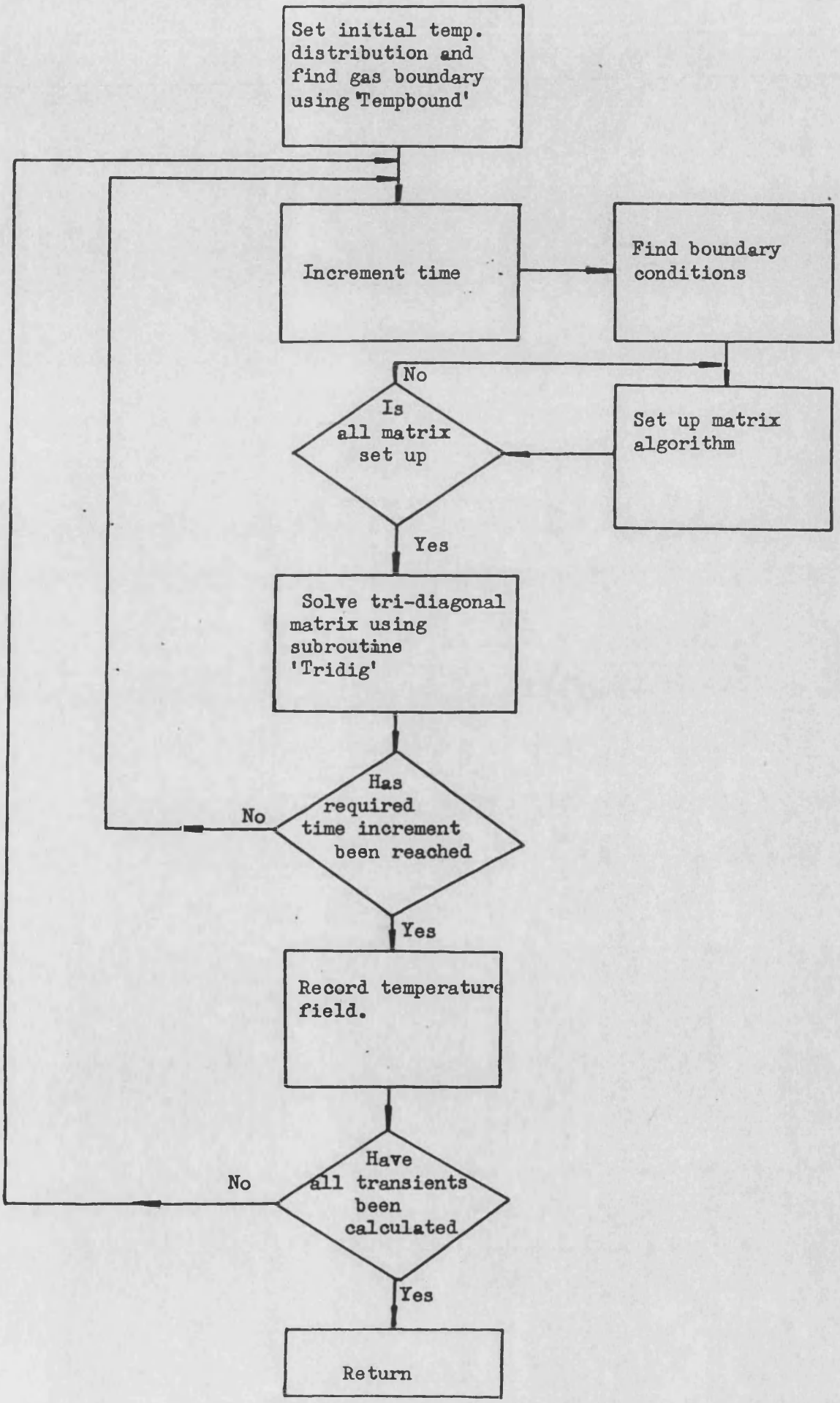

FIGURE 4.14 STANDARDISED STRESS DISTRIBUTION WITH SILICON NITRIDE COATED DISC

-Axially free to deform

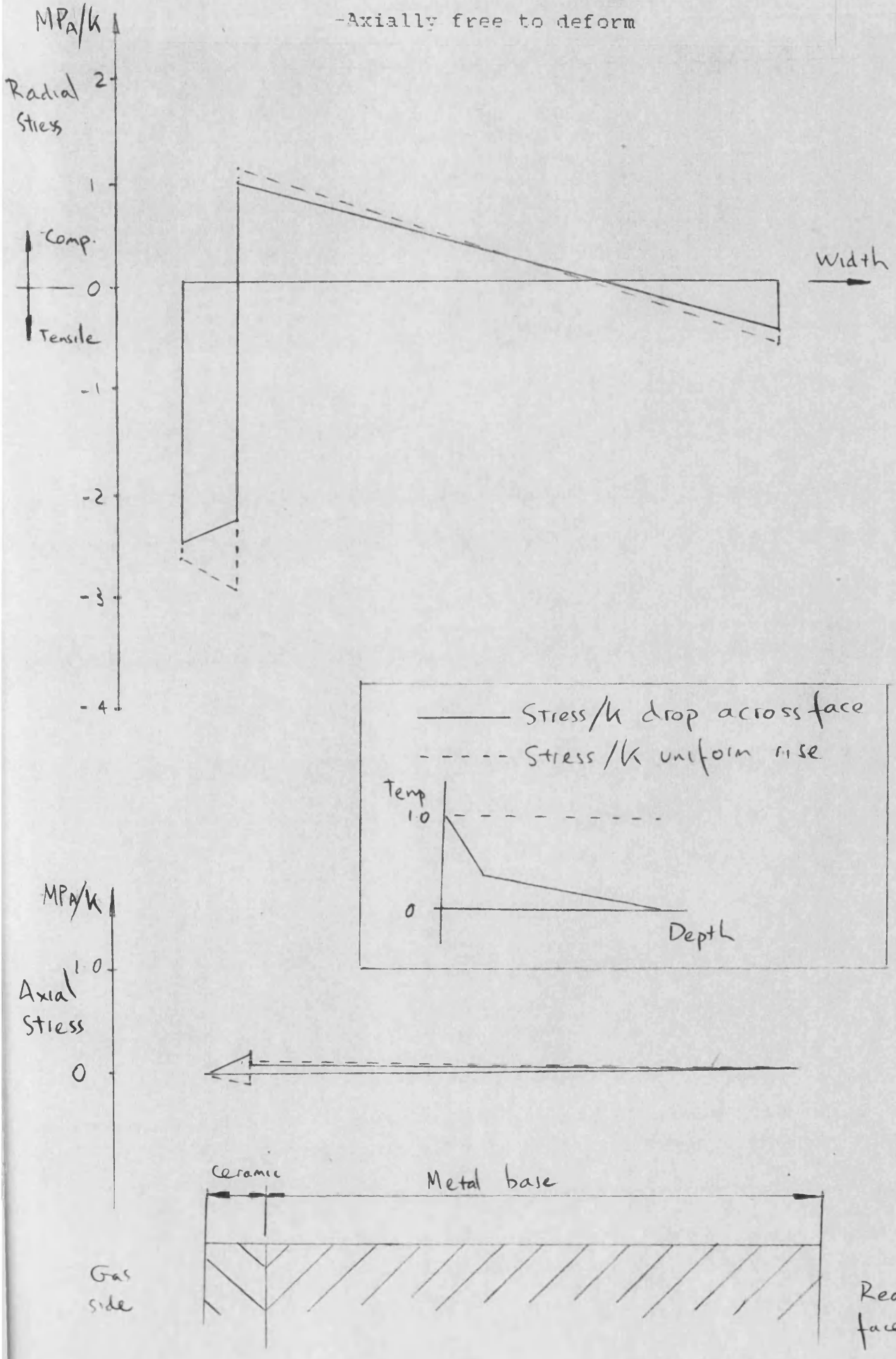

FIGURE 4.15 STANDARDISED STRESS DISTRIBUTION WITH PSZ COATED DISC

-Axially free to deform

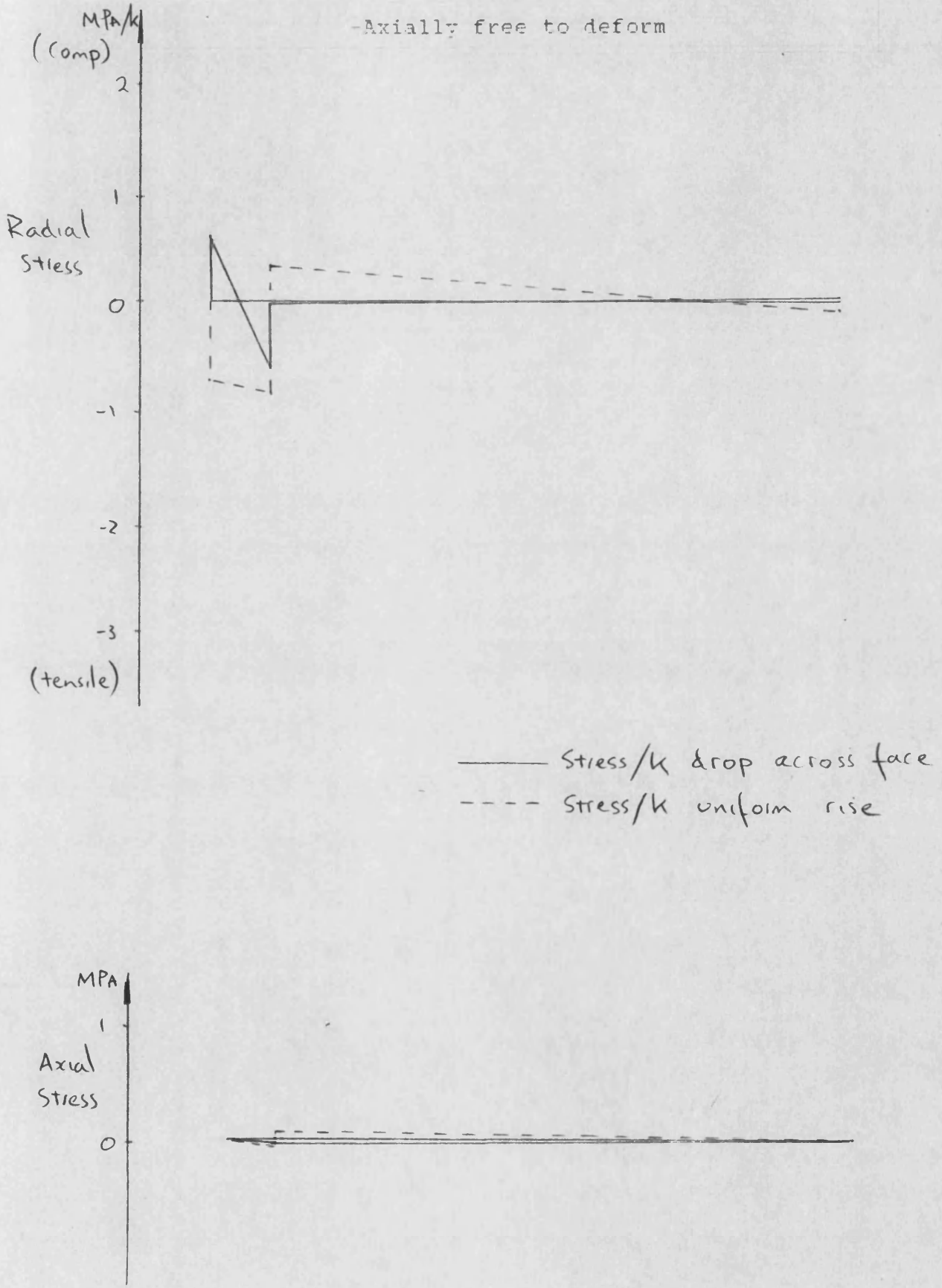

FIGURE 4.16 STANDARDISED STRESS DISTRIBUTION WITH SILICON NITRIDE COATED DISC

-Axial movement prevented

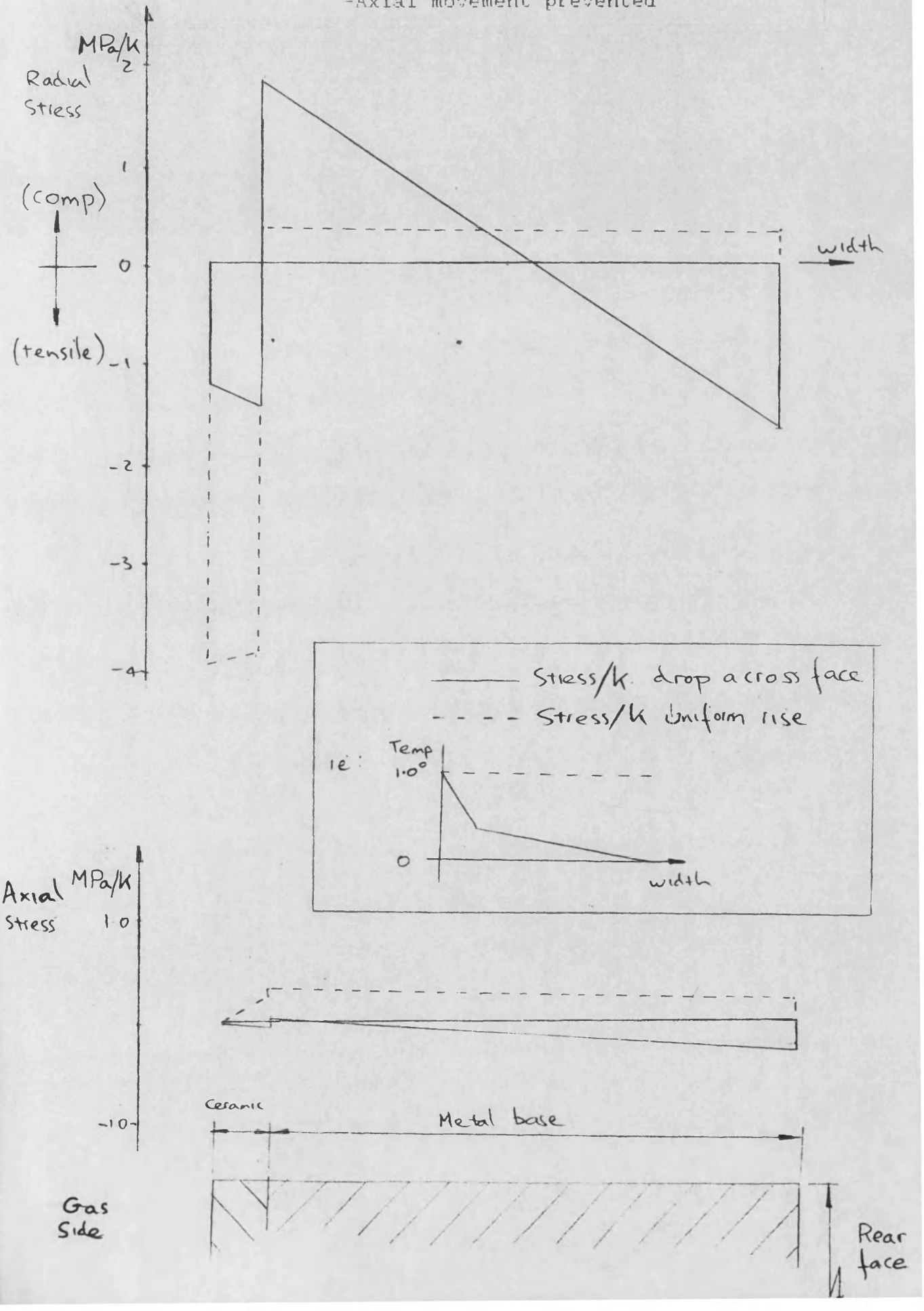

FIGURE 4.17 STANDARDISED STRESS DISTRIBUTION WITH PSZ COATED DISC

-Axial movement prevented

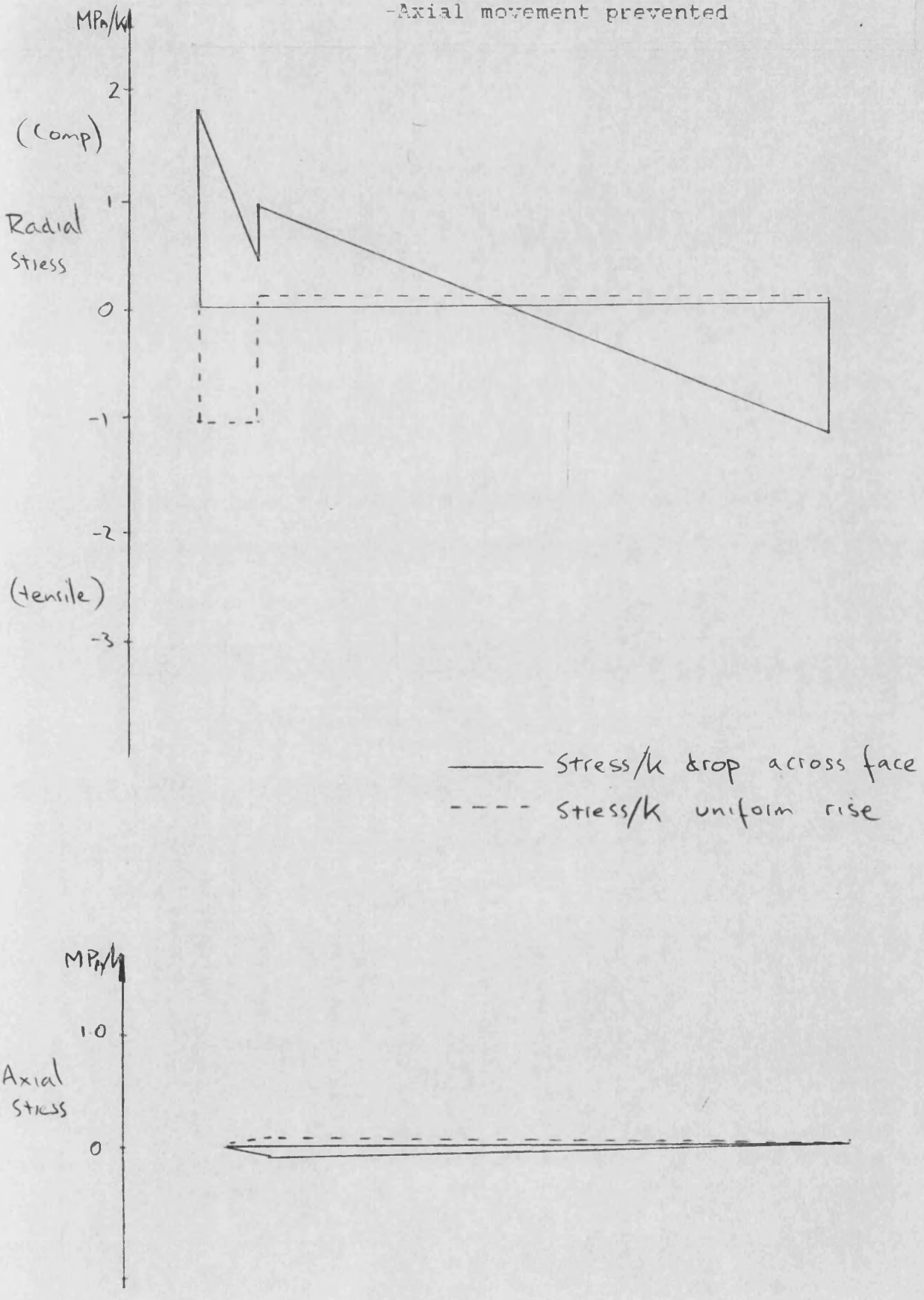

FIGURE 4.18a BI-MATERIAL DISC WITH AXIAL RESTRAINT

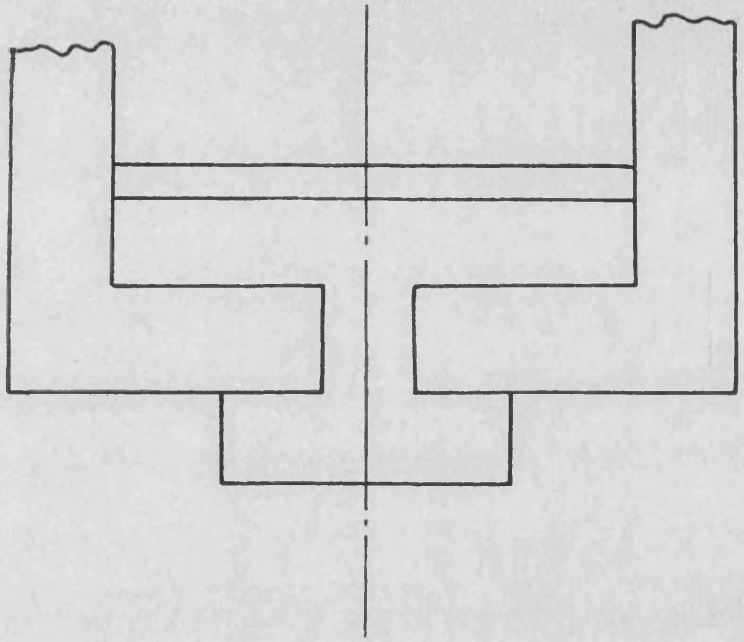

FIGURE 4.18b BI-MATERIAL DISC WITHOUT AXIAL RESTRAINT

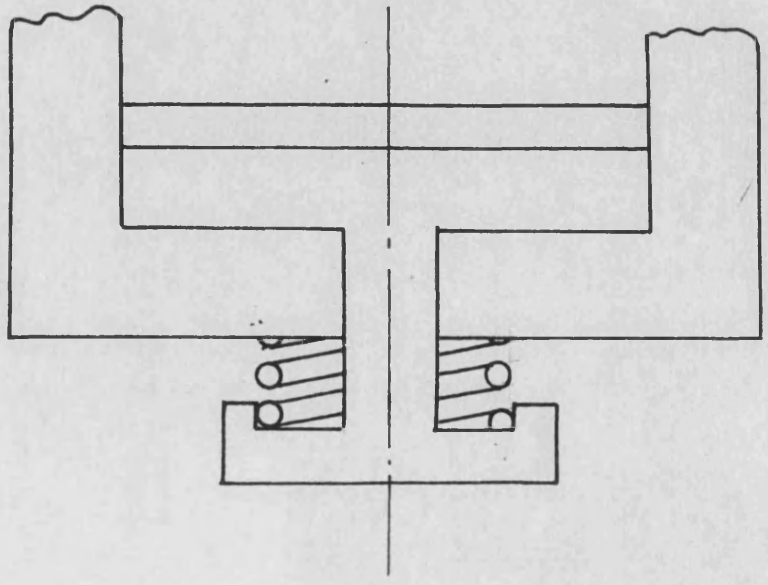

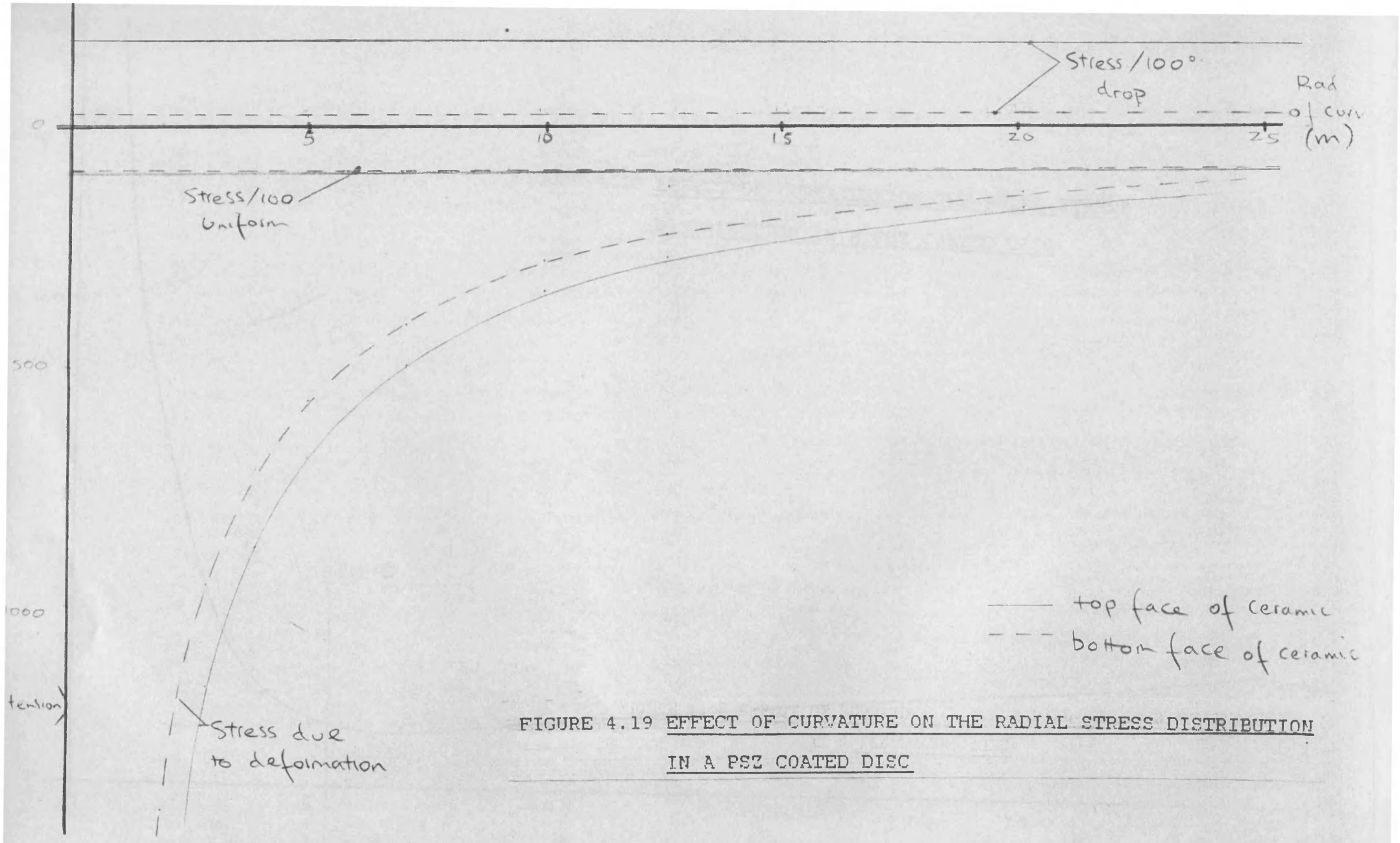

FIGURE 4.19 EFFECT OF CURVATURE ON THE RADIAL STRESS DISTRIBUTION IN A PSZ COATED DISC

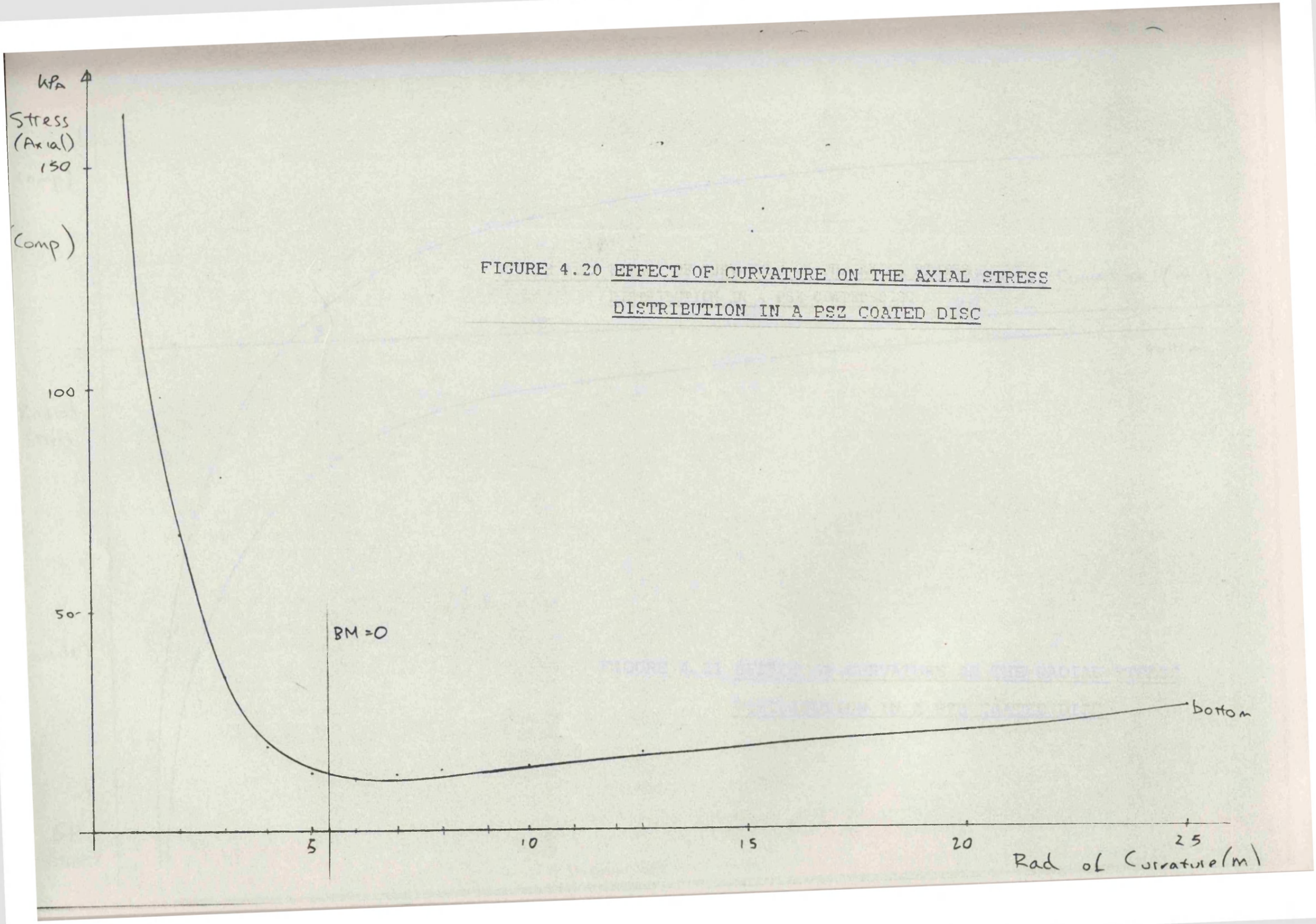

FIGURE 4.20 EFFECT OF CURVATURE ON THE AXIAL STRESS DISTRIBUTION IN A PSZ COATED DISC

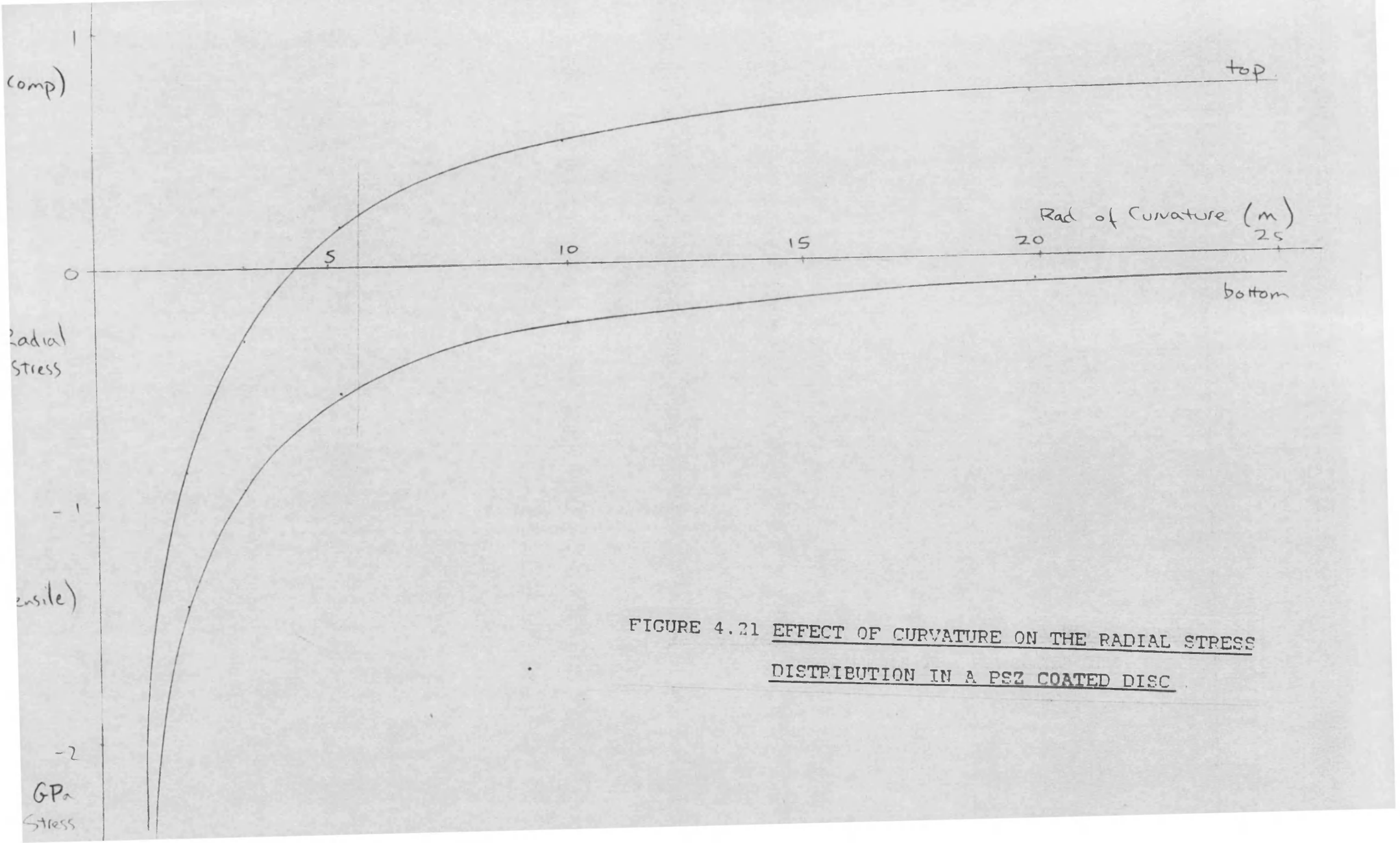

FIGURE 4.21 EFFECT OF CURVATURE ON THE RADIAL STRESS DISTRIBUTION IN A PSZ COATED DISC

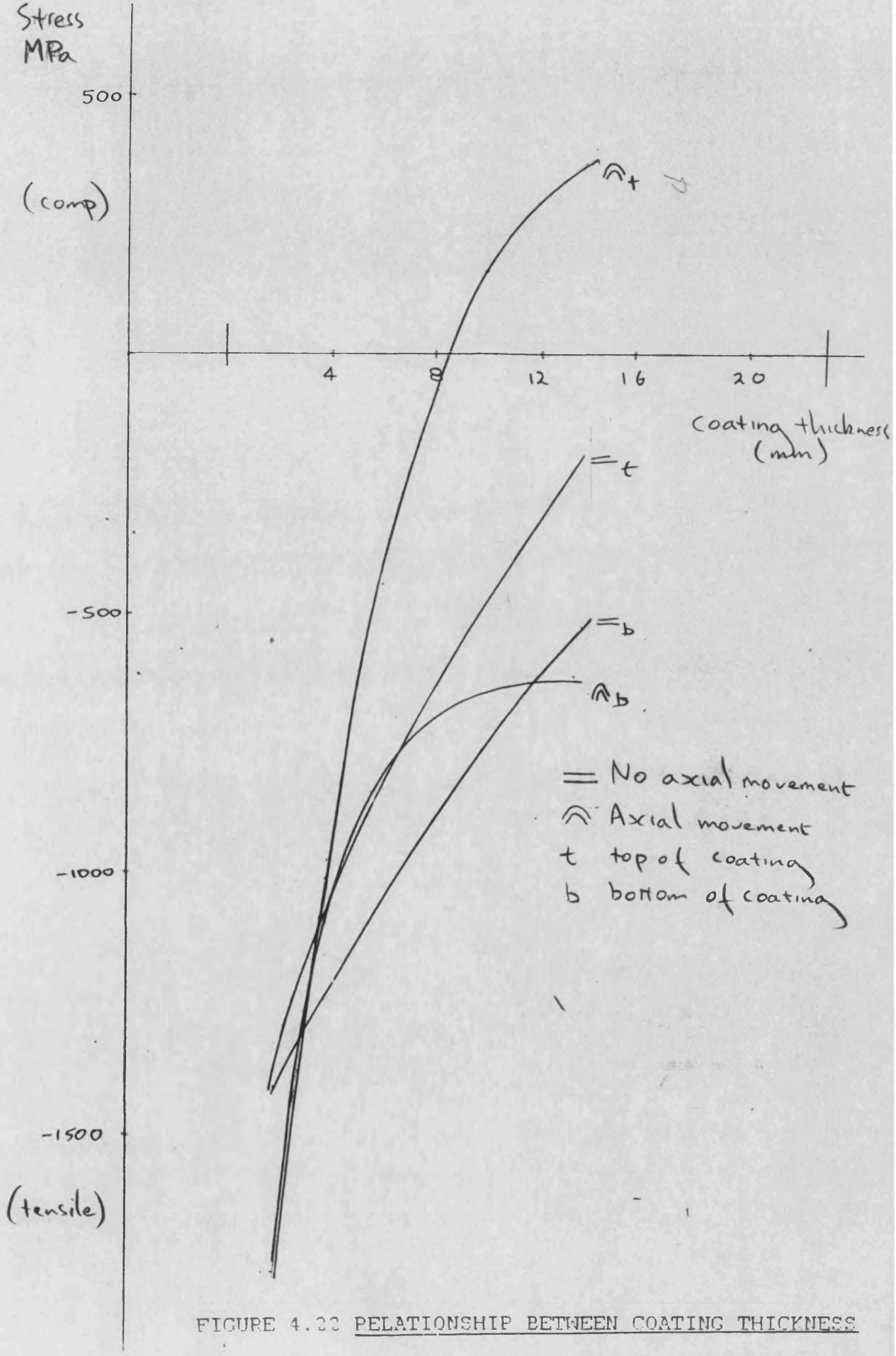

FIGURE 4.22 RELATIONSHIP BETWEEN COATING THICKNESS AND RADIAL STRESS WITH SILICON NITRIDE

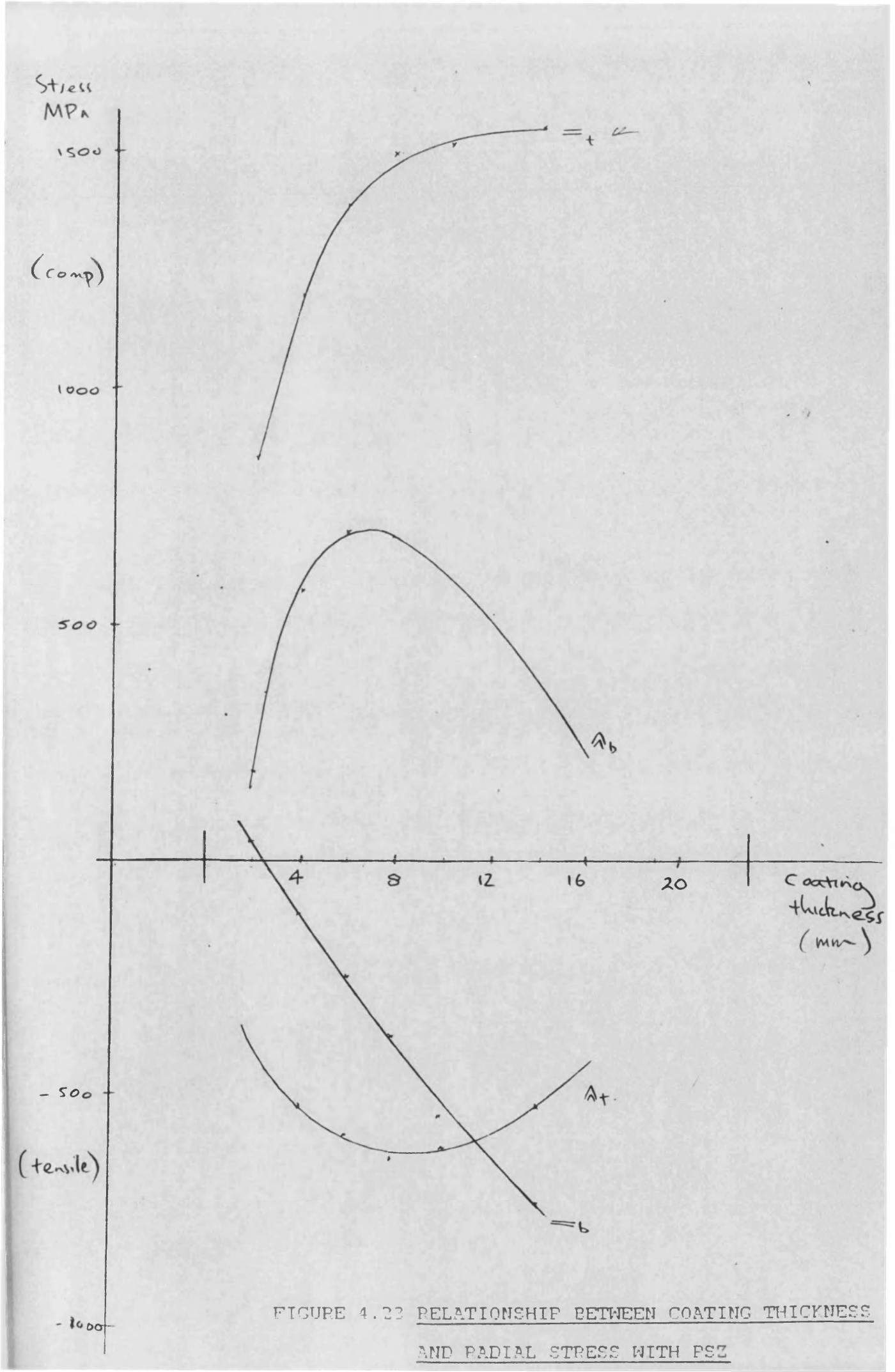

FIGURE 4.23 RELATIONSHIP BETWEEN COATING THICKNESS AND RADIAL STRESS WITH PSZ

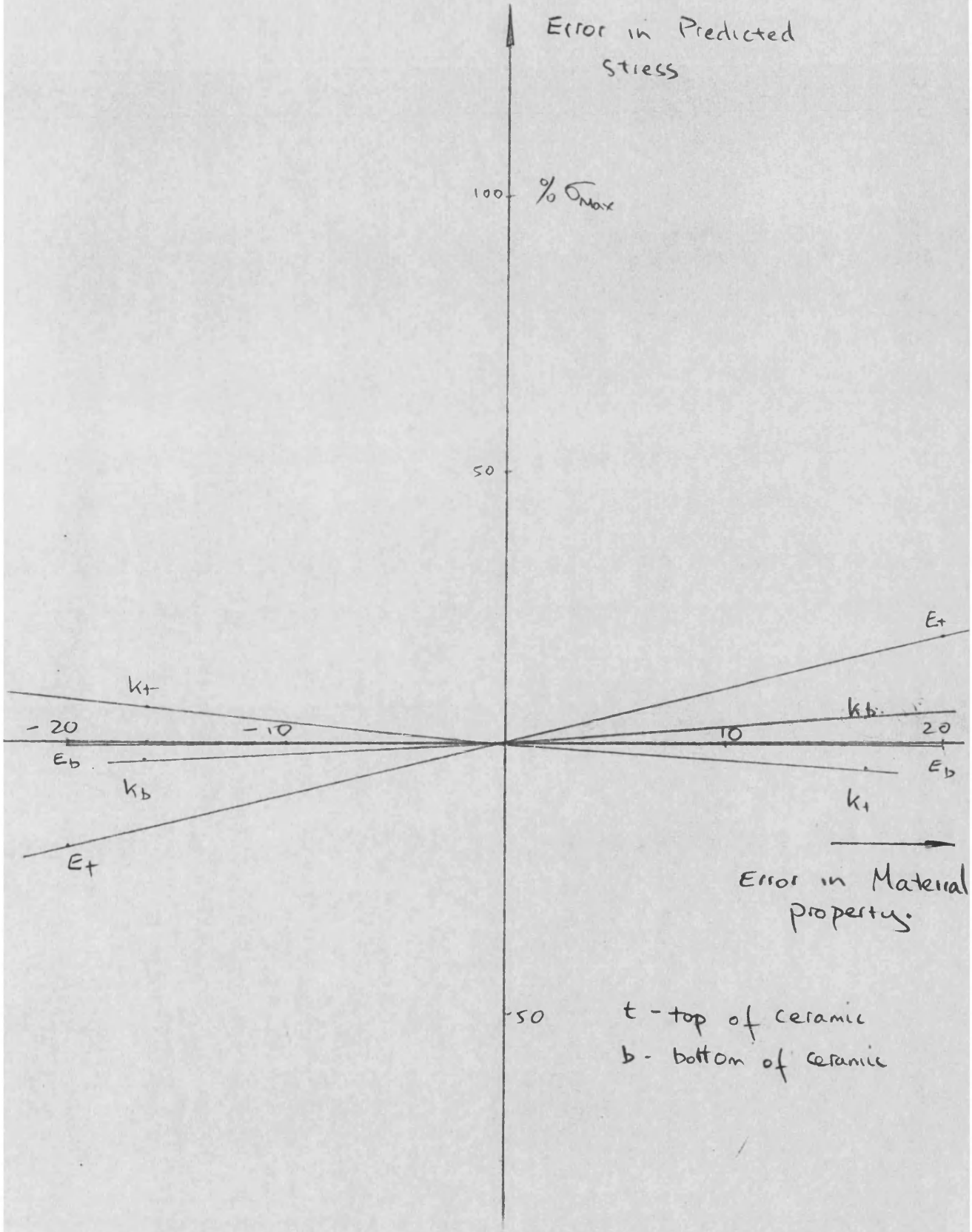

FIGURE 4.24 RESULT OF PROPERTY VARIATIONS WITHIN PSZ COATED DISCS

-Axial movement prevented

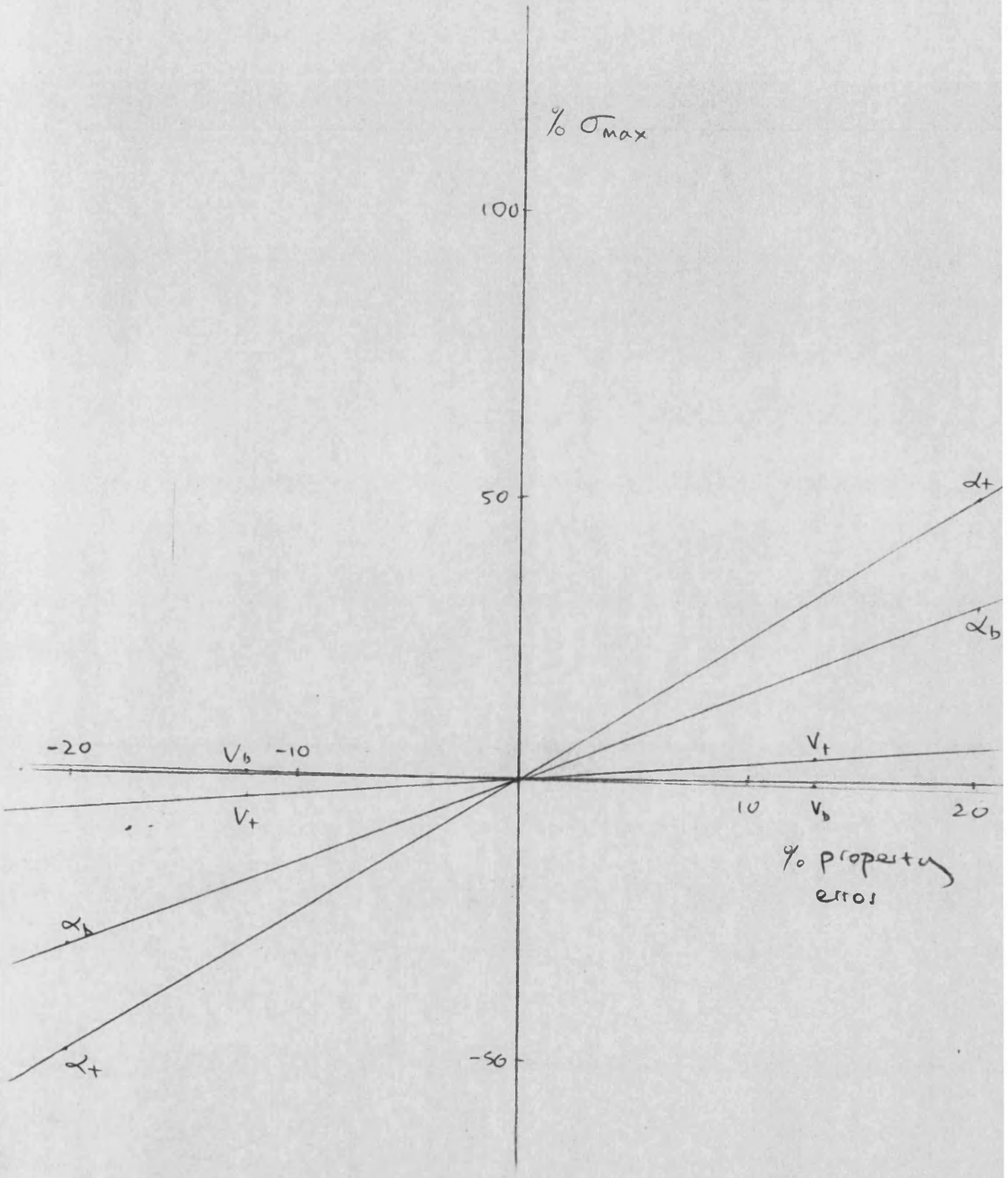

FIGURE 4.25 RESULT OF PROPERTY VARIATIONS WITHIN PSZ COATED DISCS

-Axial movement prevented

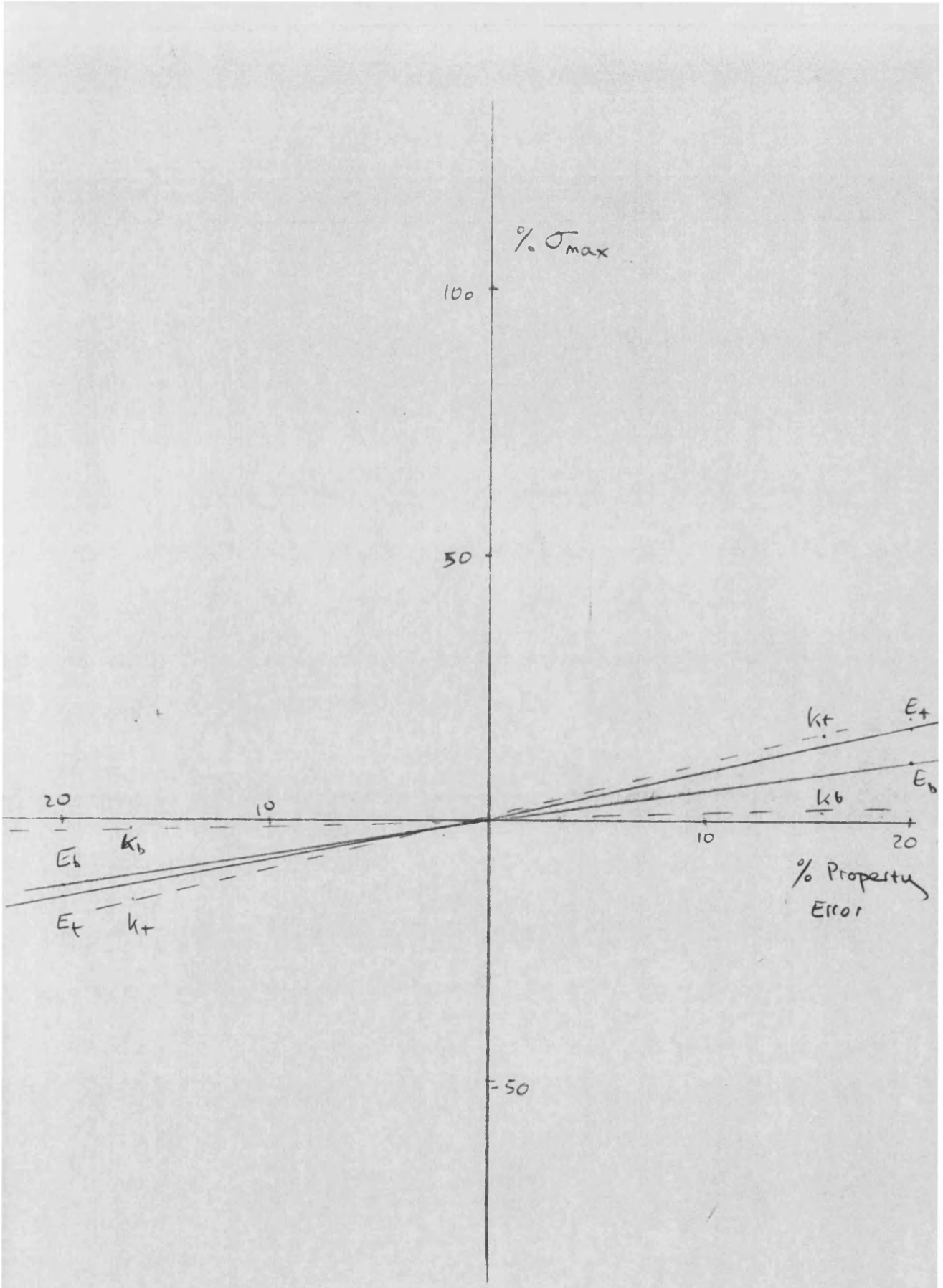

FIGURE 4.26 RESULT OF PROPERTY VARIATIONS WITHIN PSZ COATED DISCS

-Axially free to deform

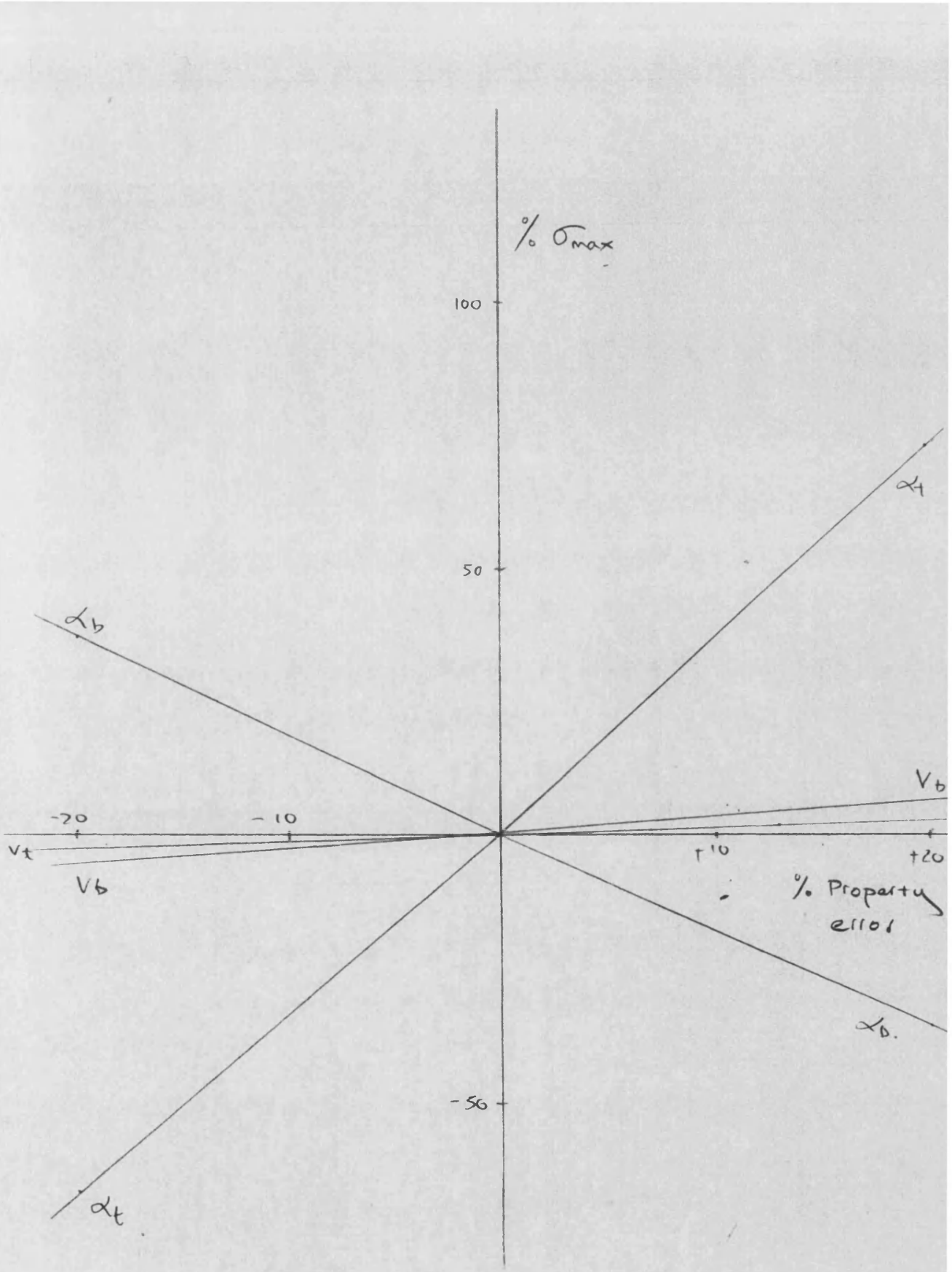

FIGURE 4.27 RESULT OF PROPERTY VARIATIONS WITHIN

PSZ COATED DISCS

-Axially free to deform

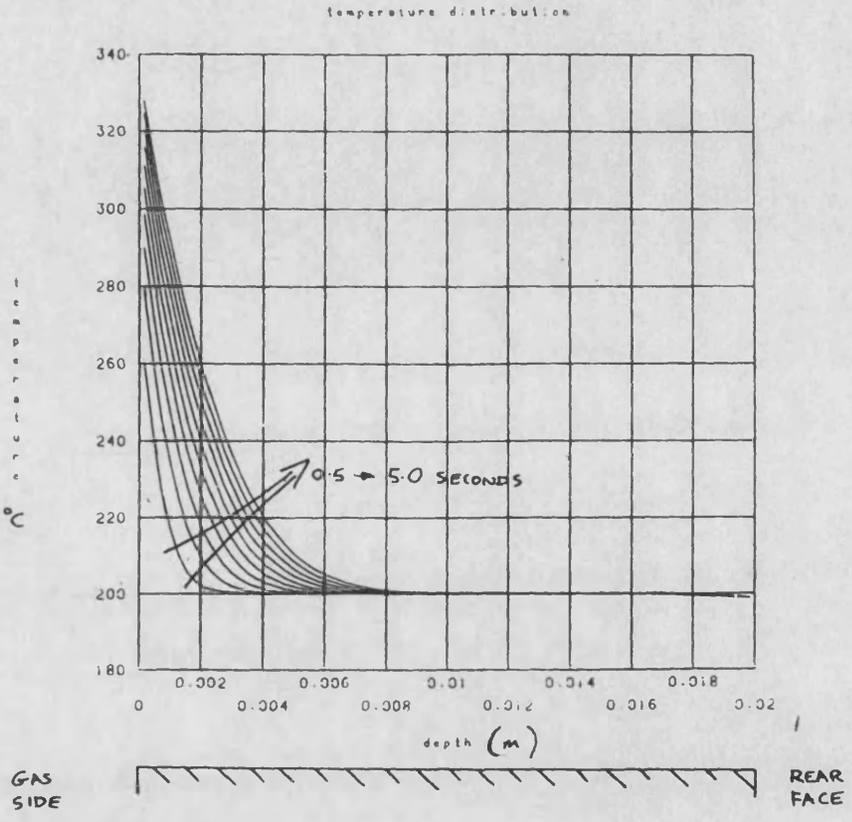

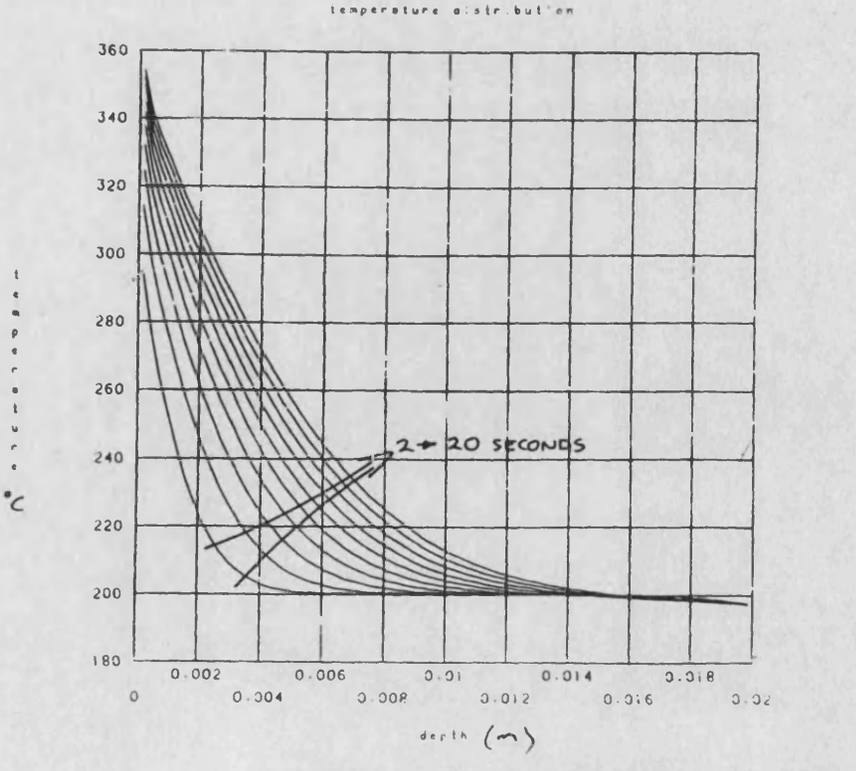

FIGURE 4.22 TRANSIENT TEMPERATURE DISTRIBUTIONS IN PSZ DISC

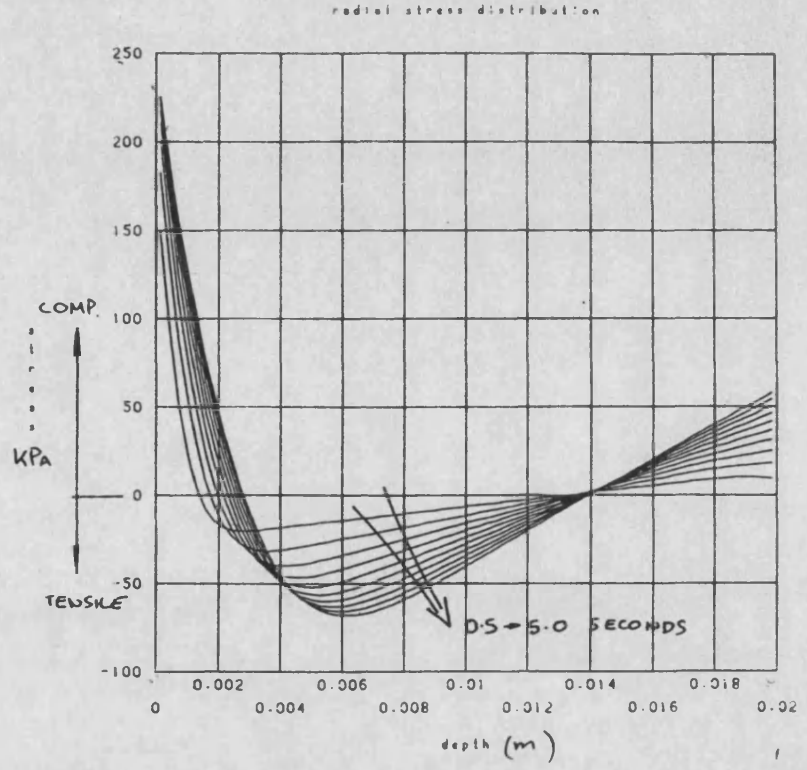

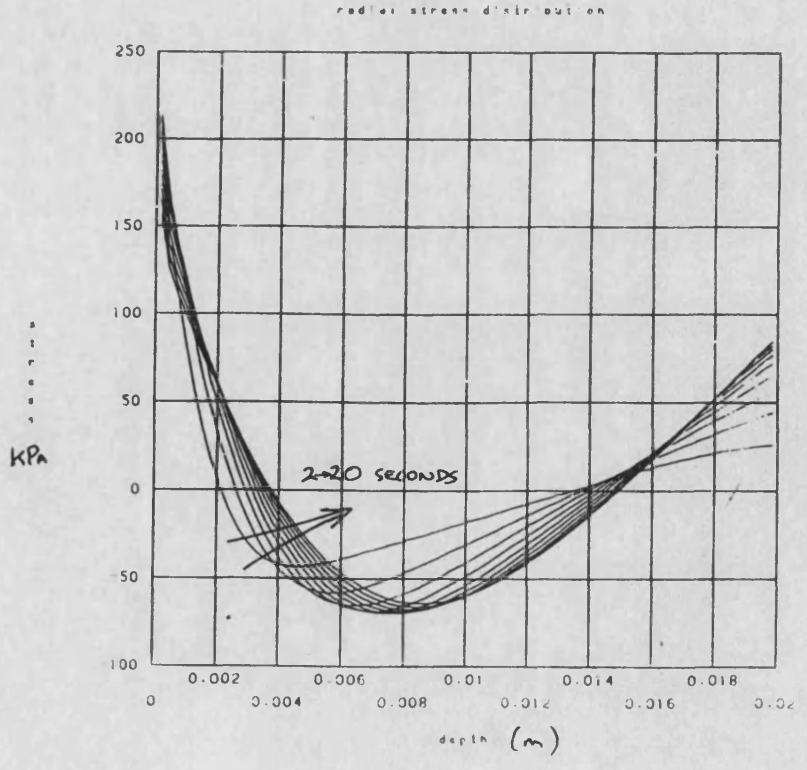

FIGURE 4.29 TRANSIENT RADIAL STRESS DISTRIBUTIONS IN PSZ DISC

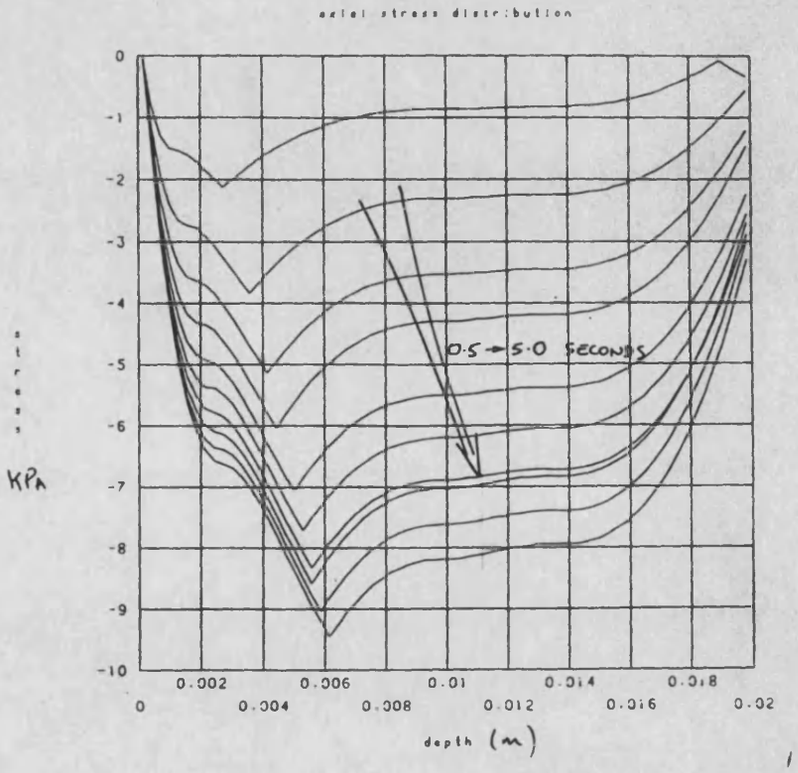

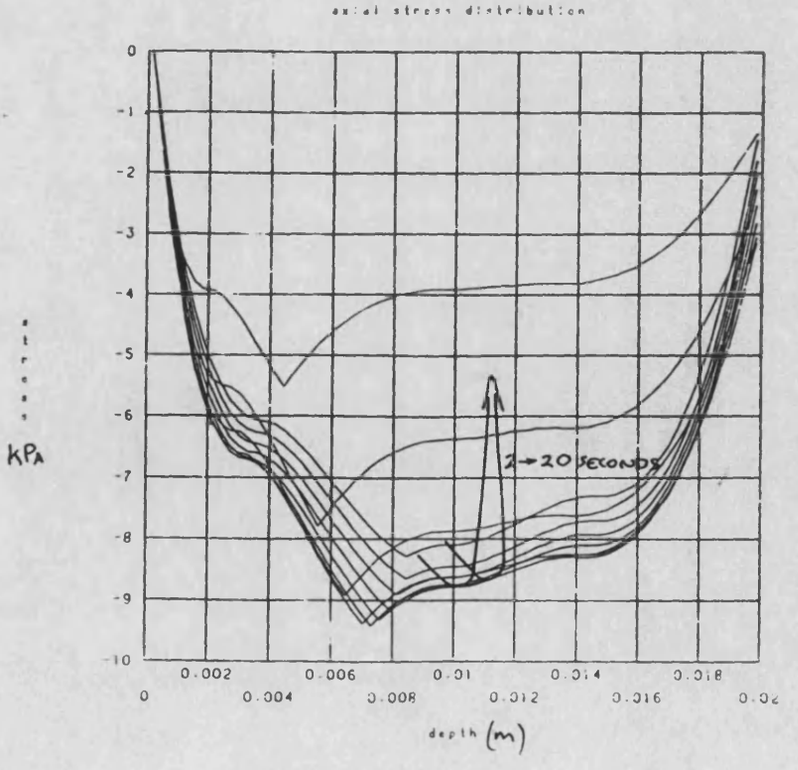

FIGURE 4.30 TRANSIENT AXIAL STRESS DISTRIBUTIONS IN PSZ DISC

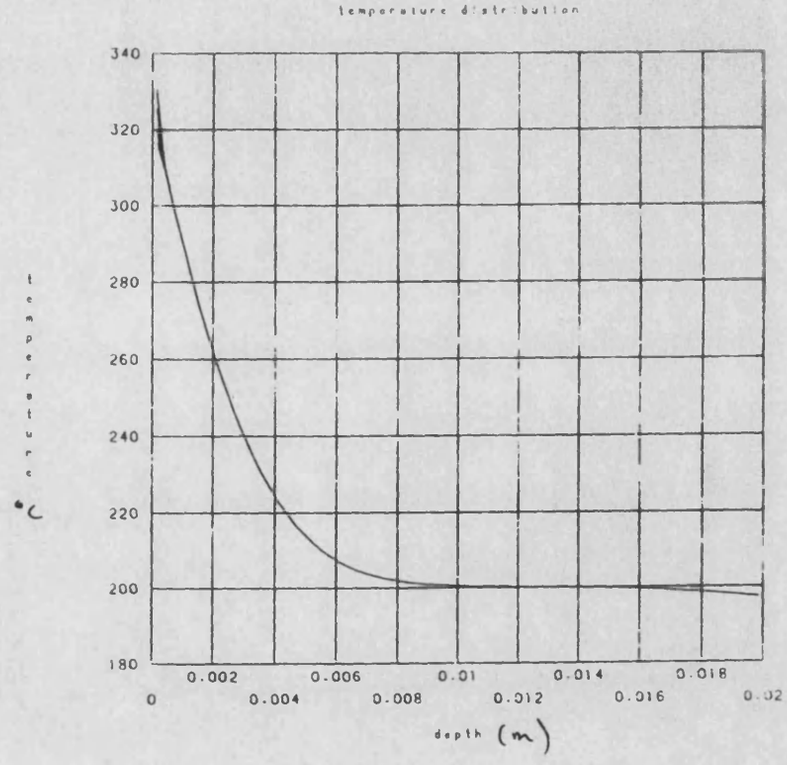

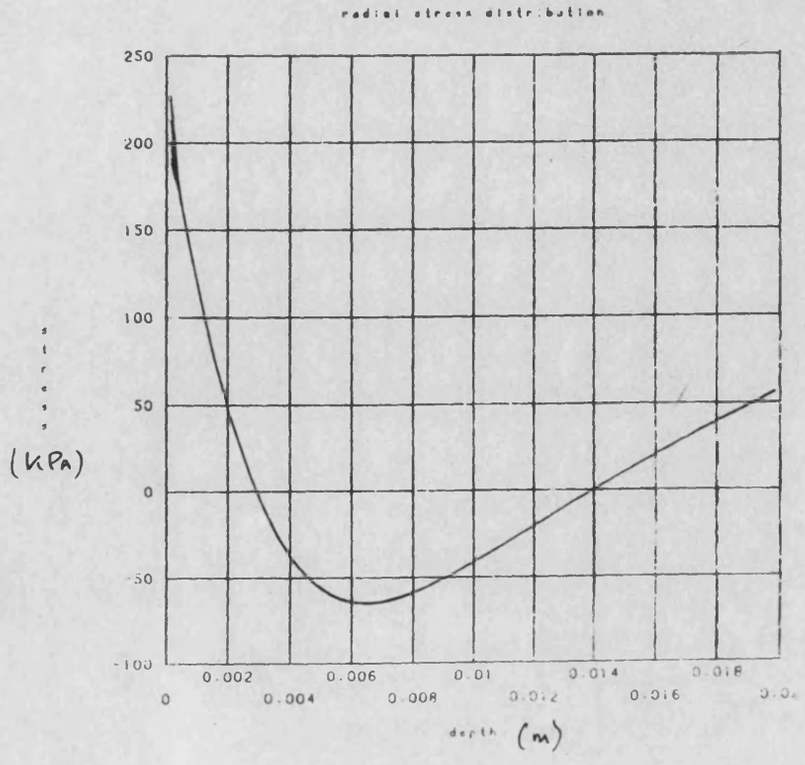

FIGURE 4.31 CYCLE TO CYCLE VARIATIONS IN PSZ DISC

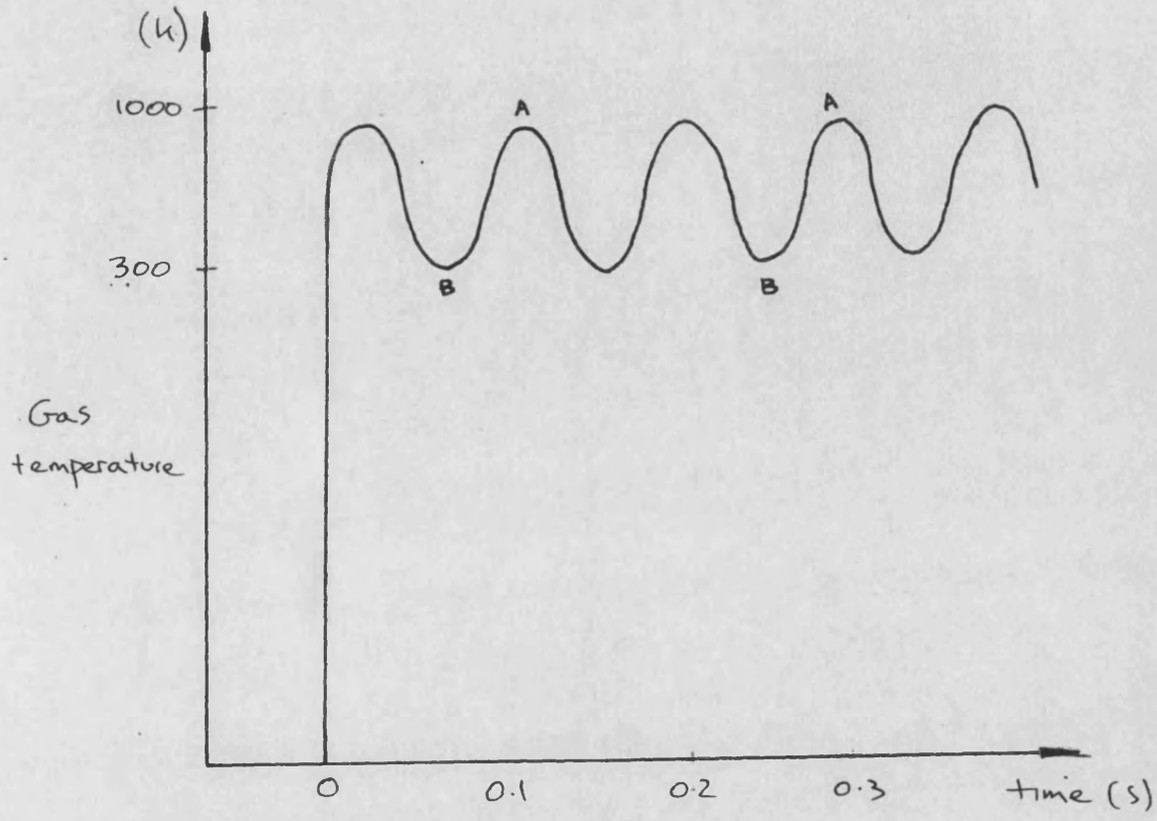

FIGURE 4.32a GAS TEMPERATURE VARIATION

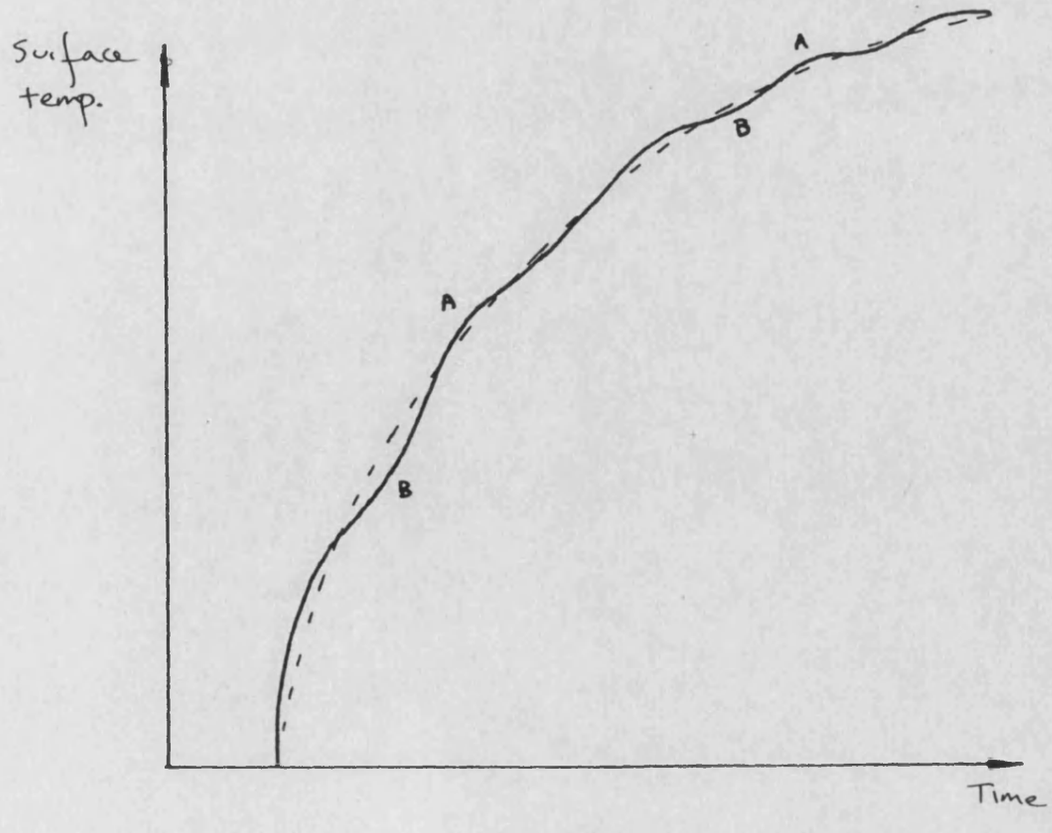

FIGURE 4.32b SURFACE TEMPERATURE VARIATION

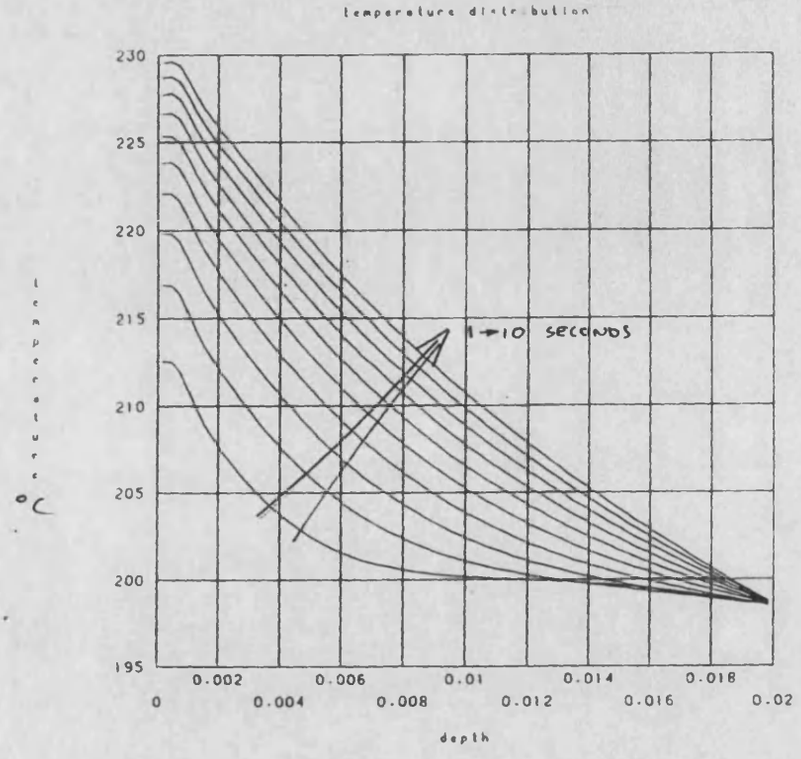

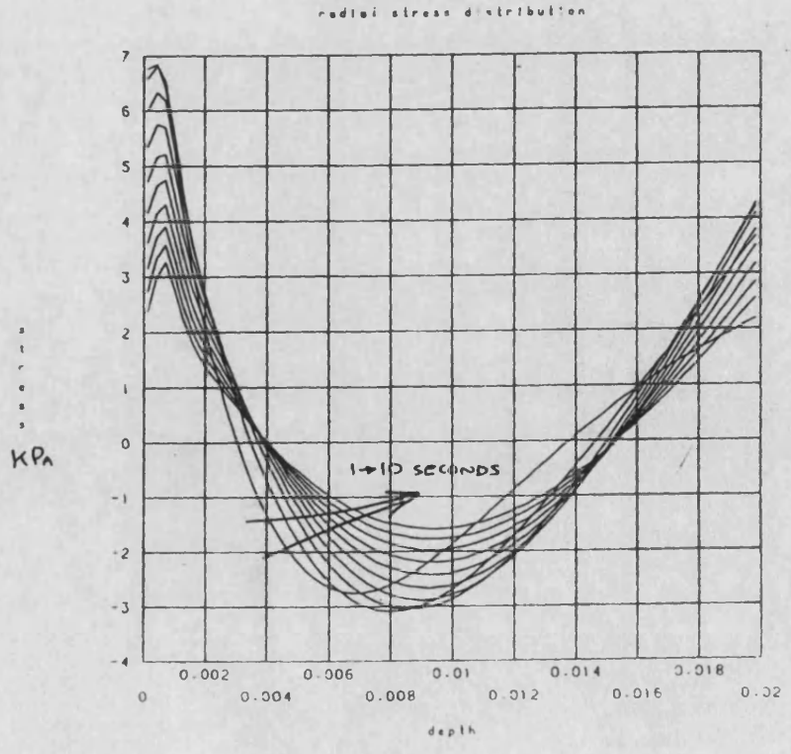

FIGURE 4.33 TRANSIENT DISTRIBUTIONS IN SILICON NITRIDE DISC

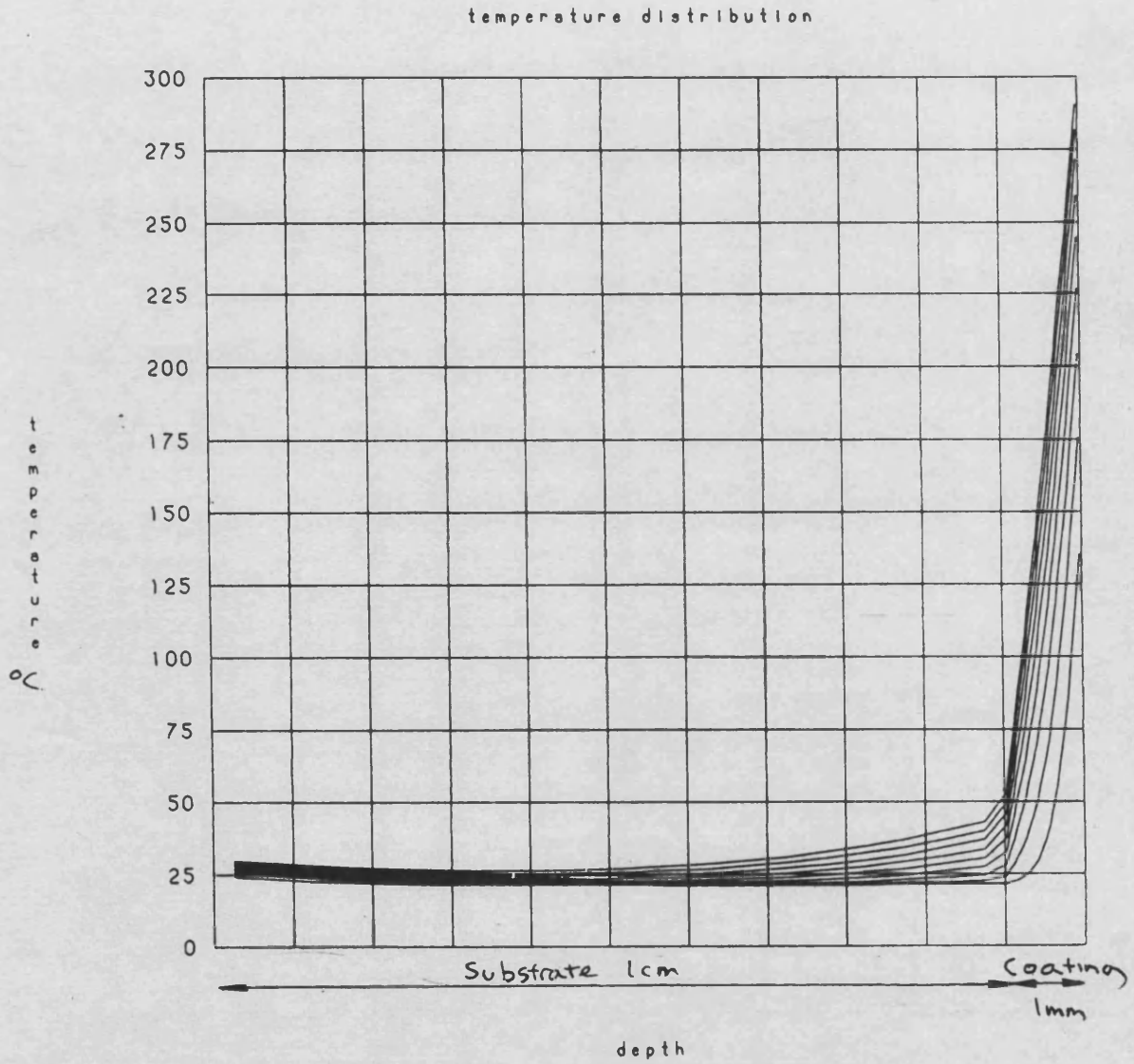

FIGURE 4.34 TEMPERATURE DISTRIBUTION IN PSZ COATED DISC

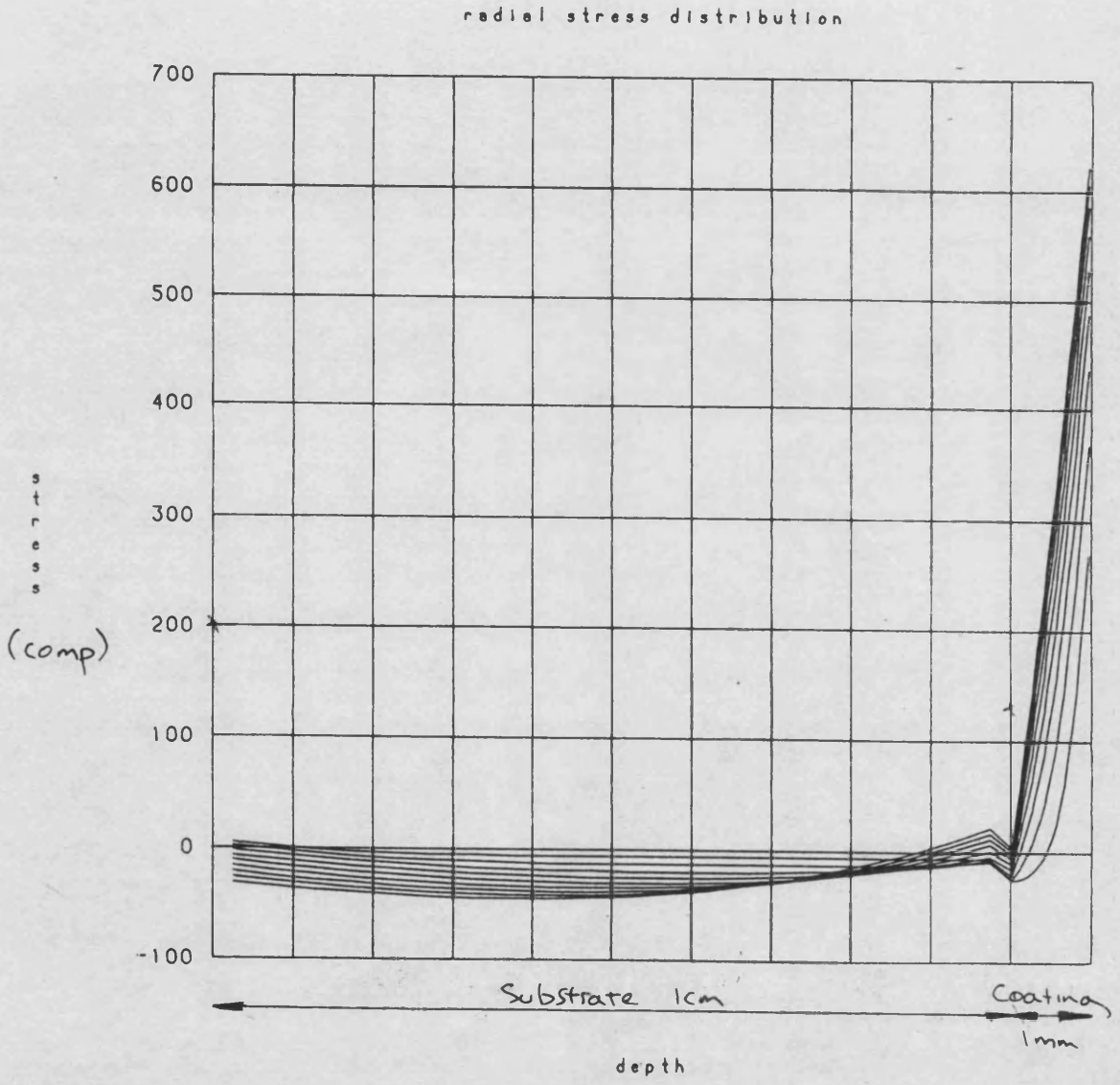

FIGURE 4.35 RADIAL STRESS DISTRIBUTION IN PSZ COATED DISC

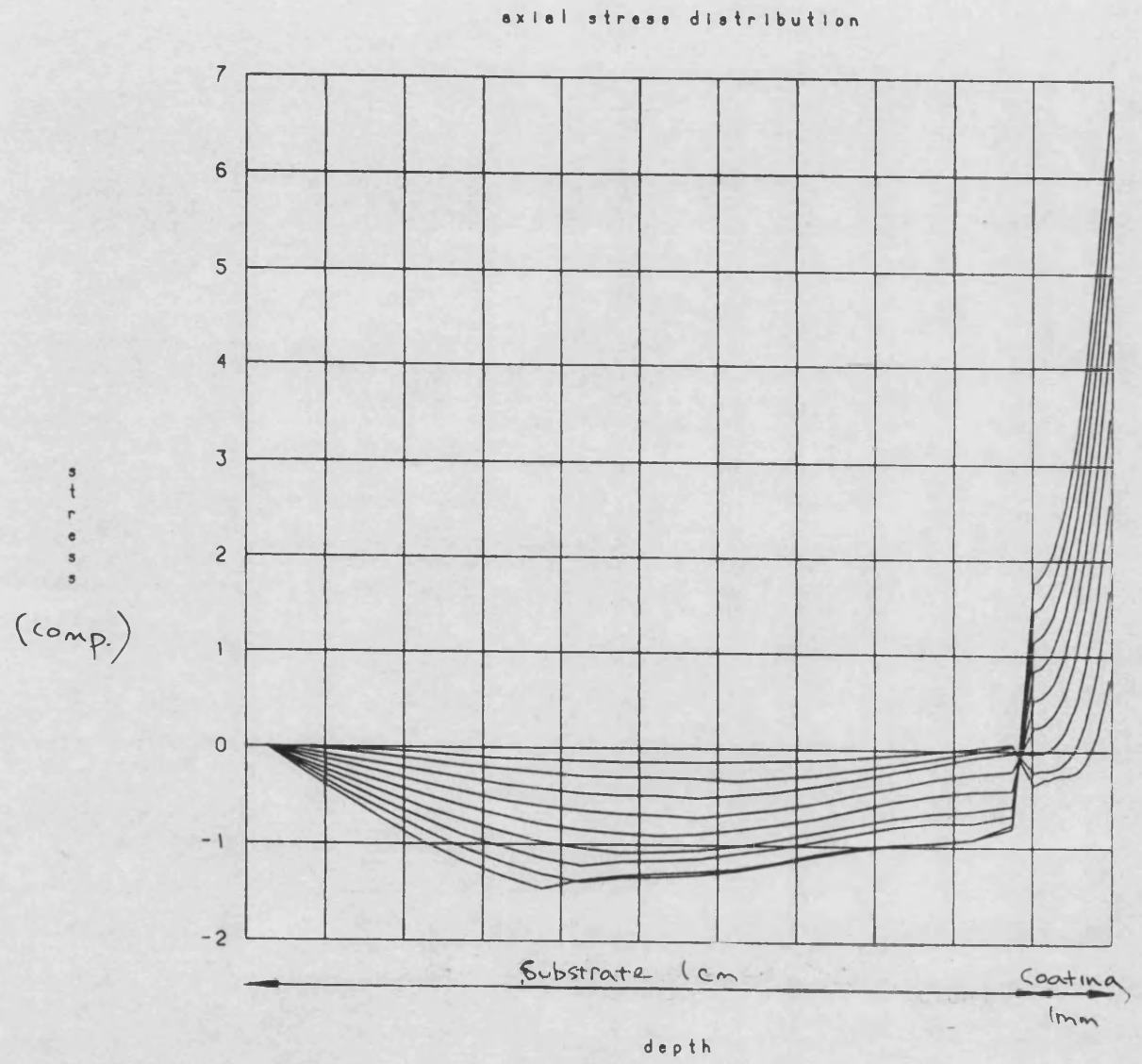

FIGURE 4.36 AXIAL STRESS DISCTRIBUTION IN PSZ COATED DISC

5.1 APPLICATION OF THE FINITE ELEMENT METHOD TO THE STUDY OF CERAMIC MONOLITHS AND COATINGS

The finite element package ANSYS has been used to study both ceramic coatings and monoliths using two dimensional, two dimensional axisymmetric and three dimensional models of engine components. The concept of running a single finite element model with a spread of material data and boundary conditions has been advanced. This procedure makes allowance for the possibility that the material property data and the boundary conditions may be inaccurate. In this way the worst conditions that can arise will be found rather than just the average. If an analysis of this depth is not persued then a large factor of safety must be incorporated. This application of a large global factor of safety is only a method of allowing for inaccuracies and variables the engineer cannot properly represent, the less thorough the investigation the larger this factor must be. Similarly individual aspects of the design should be varied (such as radii and section widths) so that the basic characteristics of a particular design can be recognised, not only revealing the position and cause of a stress concentration but also possible methods for minimising these stresses. Stress concentrations are not always the result of a single design feature and often arise as a result of a variety of factors. A single finite element run will generally fail to uncover these causal-relationships.

The problems with the finite element method are further exacerbated when ceramics are studied, as the data base of material properties is both unreliable and limited in coverage. Also ceramics exhibit properties which can only be represented accurately through the use of statistical analysis. The spread of properties is increased further where ceramic coatings as opposed to monoliths are used. The presence of large numbers of micro cracks in plasma sprayed coatings produce very different stress levels from those which would arise in a fully dense coating. When interpreting the finite element results these effects must be taken into account.

It follows as a consequence of these areas of uncertainty that the

stresses predicted for a ceramic component will rarely be accurate. All that can be achieved is to ascertain the positions of stress concentrations, and evaluate methods for lowering these stress peaks. Finding exact stress levels throughout a ceramic component is often not achievable.

5.2 THE DEVELOPMENT AND USE OF FINITE ELEMENT PROGRAMS

The finite element method was developed within the Aerospace industry in the 1950's for structural mechanics. Over the next thirty years this numerical procedure has been developed to produce a number of multipurpose computer programs capable of analysing thermal, mechanical, and electrical systems, under both transient and steady state conditions. This advance was originally achieved as a consequence of the need for a more accurate analysis of aircraft frames and the development of high speed computers. The finite element method is concerned with the replacement of continuous functions with piecewise approximations, usually polynomials. The power of the computer is needed not only to solve the piecewise equations, but also to assist in the discretisation of the model and the presentation of the results. Without recent developments in computer science the finite element method could not be used except on the simplest structures.

As these mathematical tools have become generally available it has become increasingly important to make the large programs user friendly and so accessible to the non-specialist. Engineers with little or no theoretical understanding of the finite element method are now able to operate these programs. To achieve this level of user friendliness the codes written for the mesh generation, and result presentation facilities have become as complex as the finite element code itself. The commercial success or failure of the program depends to a large extent on these pre and post processors.

However, the excellent presentation of results which is produced by the large finite element codes may be a source of other problems. The very clear result presentation gives the impression that the

problem has been correctly set up and solved, when this may not be the case. The engineer often lacks even a basic knowledge of the finite element method and fails to recognise its limitations. An ability to interpret correctly the graphical and numerical output can only be acquired through experience. Similarly for accurate results both the mesh used, and element type must be appropriate to the particular problem under consideration. This difficulty in setting up the model and interpreting the results is increased as the material properties, operating conditions, and dimensions are often not known accurately, and approximations or at the best average values have to be used.

5.3 THE FINITE ELEMENT METHOD

Engineers are often concerned with the effects of externally applied loads on a given component. These loads include pressures, thermal fluxes and applied mechanical loadings. The resulting deformations, stresses and temperatures need to be evaluated to assess the suitability of a given design. The finite element method is used to find the distribution of these effects or displacements (thermal or mechanical). It is necessary to recognise the strengths and weaknesses of the finite element method before an assessment can be made of where its use is appropriate. Similarly the conditions under which high accuracy answers are obtainable must be known. For this to be achieved a theoretical understanding of the finite element method must be gained.

There are a number of conceptual stages in the use of the finite element method, shown as a flow chart in figure 5.1.

Firstly the body is divided into a number of regions, as a consequence the distribution of the continuously variable displacement (such as temperature or strain) is similarly discretised. These subdivided elements are easier to analyse than the complete system. Generally the elements are triangular or quadrilateral when a two dimensional analysis is pursued or a hexahedron in three

dimensions. Figure 5.2 shows some typical finite elements. These elements have nodes in each corner with straight sides between the nodes. Although any body can be divided into a large number of these regularly shaped elements, often the boundary shape is better represented using a second order isoparametric element. The boundary of these isoparametric elements is described by a polynomial function, with nodes along the element boundary as shown in figure 5.3.

Once the body is divided into a number of elements the finite element method concerns itself with approximating a continuous function over a single element. A series of mathematical functions, generally polynomials, are used to describe the shape of the displacement over the element. Where the polynomial used is linear the element is described as simplex. The value of the displacement over the element can be represented diagramatically as in figure 5.4. The polynomial discribing the displacement over this area is called an interpolating polynomial. [55]

$$u = \alpha_a + \alpha_b x + \alpha_c y + \alpha_d xy$$

where α_a to α_d are constants.

It follows that at node 1, where $x=X_1$, $y=Y_1$, $u=U_1$

$u=U_1$	at	$x=X_1$, $y=Y_1$
$u=U_2$	at	$x=X_2$, $y=Y_2$
$u=U_3$	at	$x=X_3$, $y=Y_3$
$u=U_4$	at	$x=X_4$, $y=Y_4$

These conditions can be used to produce the element equation

$$u = N_1U_1 + N_2U_2 + N_3U_3 + N_4U_4$$

Where expressions $N_1 \rightarrow N_4$ can be derived from the conditions at the nodes.

or more generally, for m nodes

$$u = N_1U_1 + N_2U_2 + \cdots\cdots\cdots + N_mU_m$$

Where $U_1 \cdots\cdots\cdots U_m$ are the displacements at the nodal points.

and $N_1 \cdots\cdots\cdots N_m$ are the shape functions

Such that at node 1 $N_1 = 1$: while $N_2 \rightarrow N_m = 0$

and at node 2 $N_2 = 1$: while N_1 & $N_3 \rightarrow N_m = 0$

As an alternative to the simplex element where a linear interpolation polynomial is used a quadratic or cubic form can be utilised, represented graphically in figure 5.5. The interpolating polynomial takes the form;

$$u = \alpha_a + \alpha_b x + \alpha_c y + \alpha_d xy + \alpha_e x^2 + \alpha_f y^2 + \alpha_g x^2 y + \alpha_h xy^2$$

This equation can be rearranged to produce the element equation

$$u = N_1 u_1 + N_2 u_2 + N_3U_3 + \cdots\cdots\cdots U_8N_8$$

with eight shape functions $N_1 \rightarrow N_8$

If only one type of displacement is possible at a node (ie: a temperature displacement), then there are as many terms as nodes. If the node has two or more degrees of freedom (ie: physical displacement in the x and y directions) then the equation will contain a term for each of these displacements. A different polynomial is defined for each element. Each polynomial is selected in such a way that continuity is maintained along the element boundaries. If all the governing equations can be formulated in terms of a first

derivative then for continuity only the values of displacement at the nodes need be identical. When the governing equations contain second derivatives the necessary continuity is achieved when the first derivative of the approximating function is continuous between elements.[52] These two cases are shown in figures 5.6i and 5.6ii. By completing this process a piecewise continuous function for the entire region is formed.

For the two elements shown in figure 5.6i

$$u^1 = N_1^1 U_1 + N_2^1 U_2 + N_3^1 U_3 + N_4^1 U_4$$

$$u^2 = N_1^2 U_1 + N_4^2 U_4 + N_5^2 U_5 + N_6^2 U_6$$

where the superscript represents the element number.

5.4.0 PIECEWISE CONTINUOUS FUNCTIONS

The theory for individual elements is now expanded to form a set of element equations covering a complete body. The nodal displacements can be scalar (ie: temperature) or vector. (ie: pysical displacements)

i) Examining a four element domain with scalar dispacement only, shown in figure 5.7. There are nine degrees of freedom $U_1 \rightarrow U_9$, and four element equations which can be arranged in matrix form:

$$\begin{bmatrix} u^1 \\ u^2 \\ u^3 \\ u^4 \end{bmatrix} = \begin{bmatrix} N_1^1 & N_2^1 & N_3^1 & N_4^1 & 0 & 0 & 0 & 0 & 0 \\ 0 & N_2^2 & N_3^2 & 0 & N_5^2 & N_6^2 & 0 & 0 & 0 \\ 0 & N_2^3 & 0 & 0 & N_5^3 & 0 & N_7^3 & N_8^3 & 0 \\ N_1^4 & N_2^4 & 0 & 0 & 0 & 0 & N_7^4 & 0 & N_9^4 \end{bmatrix} \begin{bmatrix} U^1 \\ U^2 \\ U^3 \\ U^4 \end{bmatrix}$$

ii) Similarly with vector displacements, as shown in figure 5.8 with eighteen degrees of freedom. This produces the element equation:

$$u_x^1 = N_1^1 U_{x1} + N_2^1 U_{x2} + N_3^1 U_{x3} + N_4^1 U_{x4}$$

$$u_y^1 = N_1^1 U_{y1} + N_2^1 U_{y2} + N_3^1 U_{y3} + N_4^1 U_{y4}$$

this can be rearranged:

$$\begin{bmatrix} u_x' \\ u_y' \end{bmatrix} = \begin{bmatrix} N_1' & 0 & N_2' & 0 & N_3' & 0 & N_4' & 0 \\ 0 & N_1' & 0 & N_2' & 0 & N_3' & 0 & N_4' \end{bmatrix} \begin{bmatrix} U_{x1} \\ U_{y1} \\ U_{x2} \\ U_{y2} \\ U_{x3} \\ U_{y3} \\ U_{x4} \\ U_{y4} \end{bmatrix}$$

Or over the entire domain:

$$\begin{bmatrix} u \end{bmatrix} = \begin{bmatrix} N \end{bmatrix} \begin{bmatrix} U \end{bmatrix}$$

5.5 SOLUTION OF ELEMENT EQUATION

The element equations are now developed by assuming a shape of displacement that satisfies the external boundaries together with the principles and laws of the physical situation. In the early stages of the development of the finite element method a property related to the physical process under consideration was integrated under conditions which minimise the answer. In a mechanical problem the potential energy of the system was thus minimised. A number of additional methods are now available including the variational technique and more recently the Galerkin method. [53]

With the variational technique the integral of a function is minimised. This functional must have the property that any function which makes it a minimum also satisfies the governing differential equation and the boundary conditions. Variational calculus is used when finding the stationary values of functionals. In the case of a two dimensional thermal conductivity the minimising procedure produces a set of linear equations that can be solved for the nodal values. Considering the case of heat transfer in two dimensions, the governing equation for this problem is; [54]

$$\frac{\partial}{\partial x}\left(K_{xx}\frac{\partial T}{\partial x}\right)+\frac{\partial}{\partial y}\left(K_{yy}\frac{\partial T}{\partial y}\right) \quad + Q \quad = \quad 0$$

xx and yy donate the x and y planes.
where the temperature T, is continuous through the body. Keeping the previous notation u for displacement then:

$$\frac{\partial}{\partial x}\left(K_{xx}\frac{\partial u}{\partial x}\right)+\frac{\partial}{\partial y}\left(K_{yy}\frac{\partial u}{\partial y}\right) \quad + Q \quad = \quad 0$$

where u is the temperature.

The functional formulation equivalent to this expression is derived.

$$\Psi = \frac{1}{2}\int_V \left[K_{xx}\left[\frac{\partial u}{\partial x}\right] + K_{yy}\left[\frac{\partial u}{\partial y}\right] - 2Qu \right] dV$$

This equation must be minimised with respect to the set of nodal values u. The functional can thus be re-written for element e.

$$\Psi^e = \int_v \frac{1}{2}\left[\left[g^e\right]\left[K^e\right]\left[g^e\right] - 2u^eQ^e \right] dV$$

where

$$\left[g^e\right] = \left[\left[\frac{\partial u}{\partial x}\right]^e, \left[\frac{\partial u}{\partial y}\right]^e \right]$$

$$\left[K^e\right] = \begin{bmatrix} K^e_{xx} & 0 \\ 0 & K^e_{yy} \end{bmatrix}$$

Since our model consists of four elements each with its own continuous functions then;

$$\Psi = \Psi^1 + \cdots\cdots\cdots + \Psi^4 = F\,\Psi^e$$

Ψ is minimised when $\frac{\partial \Psi}{\partial u} = 0$.

The previously derived matrix 5.1 for u is now used to solve this system of matrices.

More recently the system of nodal equations has been formed by a weighted residual method such as Galerkin's method. The Galerkin method is a procedure for finding an approximate solution to a differential equation. This is used to find solutions to the initial governing differential equation without the need for a formulation of the physical problem as with the variational formulation.

5.6 MESH FORMATION WHEN ANALYSING A CERAMIC STRUCTURE

When assembling the mesh used in a finite element analysis it is not sufficient merely to fill the models boundaries with the type, size and distribution of elements which are the most convenient. The engineer must make an assessment as to where the steepest stress gradients will be encountered, and in this region a fine mesh structure must be used. Similarly consideration must be given to the type of element which is to be used.

With the more sophisticated finite element packages the user has to choose between a large number of element types. The choice between a thermal solid, membrane shell, fluid element, or structural solid is easily made according to the nature of the problem. Two further choices need to be made:

i) The number of dimensions to be modelled.
ii) The element order.

Often the geometry of the component being studied forces the use of either one dimensional, two dimensional, two dimensional axisymmetric or three dimensional elements. However with many components it is possible to simplify the problem. Pistons are often approximated to a two dimensional axisymmetric equivalent. Reasonable accuracy is produced in this way provided the aRea of investigation is away from the site of the gudgeon pin. The number of elements still available to the user could still be more than six. The decision as to which to use will depend on the steepness of the stress gradients and on which shape of element is best suited to filling the component layout.

High order elements should be used where the second derivative of displacement with position is large, as fewer elements are necessary in this case to produce high accuracy as shown in figure 5.9. Rectangular elements are often the easiest to build a model from but in some cases, especially where curved boundaries are present triangular elements may be better as in figure 5.10. The best choice

may involve a mixture of various elements provided the program ensures continuity across the junctions. A further factor which must be considered is the ease with which the program code can generate a mesh of the desired form. Experience of when each element should be used is important, and a series of trial runs should be undertaken by the inexperienced operator so the accuracy of each type can be assessed in the situations likely to be encountered.

Similarly the shape of each element is an important factor, they should not have a high ratio of length to width, or the accuracy will be impaired. Figures 5.11 and 5.12 show the meshes used to analyse a ceramic coated piston crown. In comparison the mesh used in 5.13 and 5.14 produces as much as a 20% error in calculating stresses and temperatures. This error arrises because in the second example thin elements where used in the coating, whilst the first used a higher width/length ratio. In addition the range of included angles between adjacent sides is often limited. For complex models involving many curved surfaces these limitations make the construction of a mesh a complicated task. These difficulties also arise when studying ceramic coatings, the thin layer of ceramic has a very steep stress gradient within it. It is therefore necessary to incorporate a large number of elements through the coating width. Since the length/width ratio is limited this leads to a large number of elements being used along the coating length The completed model involves a large number of elements, and this increases the computer run time. The model shown in 5.11 uses approximately 3000 CPU seconds on the VAX 11/750 computer to calculate the stress and temperature fields.

The engineer often studies systems involving two materials, in this case particular consideration must be given to the way these materials interact. This is important not only in the case of two separate components in contact (through an applied load or an interference fit) but also where two materials are directly bonded. In the case of a ceramic coated component there are two ways of forming the mesh at the interface. Both materials can have a common set of nodes at the boundary, or a double set can be used occupying the same spatial co-ordinates; this is shown in figure

5.15. Where a double set of nodes is used each pair of nodes must be coupled. In both cases the finite element method produces the same set of calculated values. However the graphics packages are often unable to plot the iso-stresses correctly at points close to the boundary when a single set of nodes are used. This difficulty arrises because the displacement of each node is calculated, the stresses are then found from this value using the relevant material properties. The set of nodes along the boundary only has a single corresponding set of material property data. The graphics packages therefore calculate a single stress value at that node. However, the node on the boundary should be considered as overlapping the material boundary and hence processing both sets of material properties, and therefore have two sets of stresses. This problem is examined in figure 5.25. Where a double set of nodes is used, then the four nodes on the element examined have stresses of -10, 40, 60 and 20 MPa and the isostresses can easily be plotted. With a single set of nodes the four stress levels predicted are 125, 170, 60 and 20 MPa, the iso stress lines in one material will therefore attempt to join with the same value iso stress line in the second material producing a very misleading plot. It should be recognised that the stress lines away from the boundary will be identical in either case. When only the stresses away from the boundary are of interest then a single set of nodes can be used, as this is the simplest of the two approaches to analyse.

5.7 ZIRCONIA CERAMIC COATINGS ON PISTONS

This finite element study of ceramic coatings includes two dimensional and two dimensional axi-symmetric representations of pistons. The approach used in both these cases has been initially to take simplified components and study the stress patterns that arise by altering features of the design. More complete representations of pistons have subsequently been used to provide a more accurate overall picture of the stress behaviour.

Many different models have been studied with a variety of ceramic properties, base materials and coating thicknesses. An attempt has been made to examine the effect of a variation in the temperature of the matallic base during the plasma spraying. Very large reductions in the peak tensile stress can be achieved in this way, but only at the expense of increasing the residual stresses present in the sample at room temperature. However even using this method to minimise the stress levels, they are still sufficient to cause the coating to fail.

This behaviour is expected as we know from practical work that micro-cracking of the coating occurs either during the coating formation, or at the latest during the first thermal cycle. The way these micro cracks affect the stress patterns needs to be examined. Unfortunately it is not possible to create a model of an entire piston complete with micro cracking as the computer run time for such a study would be excessive. Instead a two dimensional analysis has been pursued to investigate the stresses that arise in small two dimensional sections of the coating, containing just a few micro cracks.

5.8 EFFECT OF MICRO CRACKING

Due to the high level of porosity and cracks present in all PSZ coatings the stresses predicted by a simple finite element study will be inaccurate. It is only possible to predict general regions where high stresses will occur. However this is of significance since it is in these regions where high levels of microcracking will develop.

This micro cracking will develop as the loading increases until the stresses are reduced to below the maximum strength of the materials. A high level of cracks will in turn lead to easier chemical attack of the bond layer, which will cause coating failure. It is therefore important to reduce cracking by lowering the overall stress levels.

5.8.1 MESH GENERATION

Thick partially stabilised Zirconia coatings generally develop micro cracks running vertically through the coating. This cracking develops at right angles to the predominant stress. A series of finite element models have been used to study the way in which these cracks alter the stress distribution within the coatings. In this analysis a series of vertical cracks have been introduced into a 1mm PSZ coating at regular intervals. This coating is attached to a 10mm thick base, via an intermediate layer. Although these cracks will in reality follow grain boundaries and so not be exactly vertical, the predominant stress parallel with the surface will ensure that the general direction is vertical.

5.8.2 STRESS PATTERNS IN MICRO CRACKED COATINGS

A series of finite element models have been created with regular crack spacing of 1/4, 1/2 and 1mm. The substrate used is cast iron. So that the resulting stress fields can be interpreted, a crack free sample has been analysed as a datum. Figures 5.16 to 5.22 show the finite element isotherm and isostress plots produced for a few of these crack free examples. conditions used on either side of the specimen are shown on figure 5.16. The sides of coating section are adiabatic surfaces, the isotherms are therefore parallel to the gas surfaces. The maximum temperature in the Zirconia is 618°C with a temperature drop of approximately 105°C across the 1mm of insulator. The graphical output prepared by ANSYS shows the maximum and minimum levels of stress or temperature using the labels MX or MN. Lines of zero stress are shown using a broken isotress line. Deflections are also shown, the plotting routine used magnifies the calculated deflection so they are always drawn as a

fixed percentage of the overall component size. This can be confusing as small distortions are shown as about 5% of the specimen size. Figure 5.17 and 5.18 show the stresses in the x and y directions respectively. The dominant stresses are those parallel to the ceramic-metal interface (x), by comparison the perpendicular stresses (y) can be ignored. These finite element studies represent a slice from a larger specimen, hence edge effects are of little importance, the center line stesses are of most interest. In addition the edge of the ceramic coating can be feathered, the end effects will therefore be minimised. The maximum tensile stress in the ceramic is 340 MPa whilst the compressive stress is 130 MPa. The metallic base is subject to a peak compressive loading of 250 MPa. These loadings are sufficient to cause the coatings to fail.

Inherant in all finite element work is the idea that a component has a stress free condition. This is generally taken to be at room temperature, any change in temperature away from this condition will give rise to stresses. In PSZ coatings this is unlikely to be true, an attempt to represent the residual stresses present at room temperature has been made in chapter 6. However, here a simplified analysis has been used to represent the presence of these residual stresses when using the finite element results.

The remaining crack free samples shown in figures 5.19 to 5.22 show the effect of increasing the temperature at which the sample is assumed to be stress free from 20°C to 420°C. The assumption that there exists a stress free temperature is likely to produce inaccuracies, but some simplifying assumption must be made and the ansiysis shows the general effect of altering the temperature at which spraying occurs. Figures 5.19 and 5.20 show appreciable reductions in stresses over those shown in 5.17 and 5.18 under identical gas conditions. The stresses in the base are reduced to a very low level, whilst the tensile loading in the coating has been lowered by 210 MPa. The stresses σ_x parallel to the interface are still dominant. The problem with this method of reducing the stresses in the ceramic coating is that residual stresses are developed in the specimen. These are shown in figure 5.21, corresponding to a room temperature of 20°C. The stresses shown

are higher than those at the operating conditions. The coating develops a compressive loading at the interface, whilst the base is in tension, this configuration will probably lead to yielding in the base, negating the effect of raising the temperature during spraying. A temperature for plasma spraying must be chosen such that this yielding will not occur. The finite element model has therefore been used with different datum temperatures, these are summarised in figure 5.22. A condition can therefore be chosen from this graph to minimise the stresses derived in the coating. However, even after this process the stesses are still sufficient to cause micro cracking of the sample.

The remaining figures from 5.23 to 5.32 show the effect of introducing vertical cracks into the ceramic material. It has been assumed that the inside surfaces of the cracks are adiabatic: this will be valid if the surfaces forming the crack do not separate far enough to allow a free movement of gases. Figure 5.23 shows the temperature distribution in a 1mm coating with 1mm spaced cracks. The isotherms are again parallel with the gas surfaces, the peak temperatures are the same as in the datum example in figure 5.16. Figure 5.24 shows the stress in the x direction, while 5.26 show that in the y direction; figures 5.25 and 5.27 show close ups of these two stress patterns. The peak tensile stress developed in the ceramic at the interface has been reduced by approximately 15%, whilst the compressive loading present in the upper section of the ceramic has been removed by the introduction of the cracks. The large number of broken contours shown in the metallic base are the zero isostress lines, and only serve to show that the bulk of the material in this configuration is almost stress free. The higher levels of σ_y recorded at the crack tip would either lead to yielding of the metal in this region or the development of the crack into the base. The stress σ_x is still high in this example, and a higher crack density would be certain to occur than is represented by this example. The level of micro cracking that arises will be that necessary to reduce the stress levels to below the breaking stress for the ceramic.

Further finite element models were created using different crack spacing in each case, the results are summarised in table 5.1.

This crack spacing was varied from 1mm to 1/4mm. To reduce the computer run time each model studied used only the width taken up by four cracks. The model used for the 1/4mm case is therefore only 1.25mm wide. Three different datum crack free models had to be created for comparison to predict the stresses in a crack free sample. The table shows the maximum stresses developed in the coating and the base, in both the cracked and crack free conditions. The percentage reduction in stress levels caused by the micro cracking is also shown. Appreciable reductions in the tensile loading in the ceramic occur with fine crack spacing. However, to reduce the stress level to that which the ceramic can survive the crack spacing will be very small in relation to the depth of ceramic. If these cracks propagated all the way through the ceramic they would inevitably link up and cause separation of coating and base. However, it should be noted that even when coarse crack spacing is used the stresses in the upper part of the coating are very low. Chapter 6 examines the residual stresses present in sprayed coatings. Both empirical and theoretical data suggests the bottom part of the coating contains a residual compressive stress. It is therefore possible that the high crack density proposed at the boundary to reduce the stresses is not necessary. The stresses in the bulk of the material can be satisfactorily relieved through a low crack density. This is substantiated by figure 5.28, which shows vertical cracks developing in a zirconia coating, but not as far as the ceramic-metal boundary.

A long life coating will be one in which these vertical cracks occur regularly. If too many develop in a single region they will link up and the coating will fail. A large number of crack initiation sites along the interface may therefore be desirable. Normally the micro cracking distribution which arises during the coating formation and the first thermal cycle must be accepted. But if the initial thermal cycle is controlled a better distribution of micro cracks may be achievable. There are other methods which may facilitate the formation of desirable micro crack distributions.

The zirconia coating could be formed in two stages, firstly a thin layer of PSZ could be applied. This component could then be heat

treated to promote a high level of micro cracking. This first thermal cycle could be quite severe as coating separation with thinner layers is unlikely. Subsequently the remainder of the PSZ coating could be applied. The high density of small micro cracks produced in the original coating should sufficiently reduce the stress at the boundary to limit the number of through cracks which develop. Similarly sufficient nucleation sites would be provided for these through cracks to ensure a uniform distribution rather than merely being concentrated in regions where flaws are present.

By using a high level of porosity in the zirconia adjacent to the interface a large number of crack initiation sites will be provided.

The analysis of thin coating sections was continued, examining the effect of using elevated teperatures for the base during plasma spraying. Figures 5.29 to 5.32 show the effect of raising this base temperature to 220^{o}C. The finite element method assumes that at this temperature the component is stress free. The stress patterns shown in figures 5.29 and 5.30 arise when the coating sample is subject to the same gas conditions as in the previous examples. The stress patterns are the same form as before, except that the peak stress σ_x is reduced from 292MPa to 182MPa, a reduction of 38%. A similar level of stress reduction is observed in tension and compression in both the x and y directions. The residual stresses present in the material are shown in figures 5.31 and 5.32. The stress levels arising in the micro cracked sample are close to those in the crack free section. The combined effect of introducing 1mm microcracks and raising the base temperature to 220^{o}C reduces the peak σ_x value from 343MPa in the datum crack free sample to 182MPa. Increasing the spray temperature to 420^{o}C further reduces the stress levels, but the residual stresses become too large. This is shown in table 5.2 which contains the maximum stresses in the coating, σ_x and σ_y. Tables 5.3 and 5.4 show the stresses occurring with 1/2 and 1/4mm crack distributions respectively. The residual stresses change only minimally with the crack density, while the operating stresses are further reduced. With a 1/4mm crack density and a 420^{o}C stress free temperature

the stress level σ_x is reduced by 85% from its datum. The residual stresses in the base would cause creep under these conditions. However, at a more realistic residual stress level the stresses in the coating can still be reduced by 60% with 1/4mm crack spacing.

5.9 PARTIALLY STABILISED ZIRCONIA COATED PISTON

Two dimensional axisymmetric representations of PSZ coated pistons have been examined in the steady-state condition. Part pistons and complete pistons have been modelled, using different coating thicknesses, and material properties. These finite element models assume the coating is crack free, as the computer run time associated with a model of a piston complete with micro cracks would be impractical. The stress levels predicted must therefore be interpreted using the previous analysis which examined the effects of micro cracking. Despite this the following finite element results can be of considerable use for the purpose of comparison and the examination of general trends.

As was shown in chapter four, accurate results can only be achieved with accurate material property data. Unfortunately the PSZ samples used for property determination are generally micro crack free. Materials with a high level of micro cracking have very different properties from a fully dense structure. The measured value of Young's Modulus in a micro cracked sample can be an order of magnitude lower than that given in published data. It is also expected that the rate of micro cracking is dependent on the stress distribution, and hence on the geometry of the component. Therefore the material properties cannot be considered as constant but dependent on the component they will be sprayed onto. In addition it should be recognised that there are two types of property, an average value taken for large material samples, including many micro cracks and flaws, and a local value for the small volumes between these flaws. Which of these two values should be used in

a particular finite element model depends on what part of the structure is being considered.

i) If the stress distribution in the metal piston body away from the coating-metal interface is of interest, then the average material property data should be used. This will produce accurate levels of distortion in the piston body, and hence also of stresses. However at the boundary the localised effects will be dominant and the stress levels predicted will be highly inaccurate.

ii) Using the localised values of material properties the analysis gives the stress values that would occur without micro cracking. Where the predicted stresses are above the fracture strength of the material micro cracking will develop until the stresses are sufficiently reduced. This type of analysis therefore shows where high levels of micro cracking occur, and hence where failure is most likely. Multiple computer runs can be used to indicate how these stress concentrations can be minimised.

5.9.1 SIMPLIFIED FINITE ELEMENT MODELS OF PISTONS

Simplified piston models were analysed to establish general trends in the way ceramic coated pistons behave. A piston crown, 86mm diameter, with a bowl diameter of 40mm was used, as shown in figure 5.33. The bowl lip incorporates a radius, and the coating is feathered on the outer edge. The thermal boundary conditions shown were given by an inhouse program called CSP when modelling a turbocharged partially insulated engine. As a result of the geometry of the component, and the steepness of the stress gradients a very fine mesh structure had to be used incorporating 1652 elements. This level of complexity resulted in a total computer run time of around 3000 CPU seconds on the VAX 11/750 computer. Total computer run time for the two dimensional axi-symmetric study outlined here was around 200,000 CPU seconds.

There are eight main cases studied using this simplified representation of a piston, incorperating different coating thicknesses

and base materials.

base material	coating thickness	thermal conductivity
Aluminium	1mm	1W/mK
Aluminium	1mm	2W/mK
Aluminium	2mm	1W/mK
Aluminium	2mm	2W/mK
Steel	1mm	1W/mK
Steel	1mm	2W/mK
Steel	2mm	1W/mK
Steel	1mm	2W/mK

Two values for thermal conductivity of the PSZ layer were used as it is possible to vary the porosity by changing the variables in the plasma spraying process. All other material properties were fixed.

Property	Aluminium	Steel	PSZ	
Thermal conductivity	202	46	1 & 2	W/mK
Poisson's ratio	0.3	0.3	0.23	
Young's Modulus	70	200	300	GPa
Thermal expansion	23	14	10	$x10^{6}$

The eight material/thickness combinations each have their own temperature distribution, two of these are shown in figures 5.34 and 5.35. In all cases the maximum temperature occurs at the bowl lip, with the isotherms in the coating closely spaced and roughly parallel to the surface. The temperature drop across the ceramic varies from 100 to 200 K/mm. The highest temperature gradients occur with the aluminium base, the lowest with the steel. As discussed in chapter four, thermal stresses arise from two sources, thermal expansion mismatch and because of the temperature gradient. The stresses that arise in the aluminium based piston crown should be higher than in the steel substrate because the temperature gradient within the ceramic is steeper, and because of the larger thermal mismatch. The isotherms in the steel substrate are spaced at approx 7K/mm and

in the aluminium at 1.5K/mm. The piston crowns made from a steel substrate have a peak temperature about 30°C higher than those with aluminium.

5.9.1a ONE MILLIMETER PSZ COATINGS ON STEEL

The coating/base combinations shown in the two isotherm plots are further examined in figures 5.36 to 5.41. Figures 5.36 to 5.38 cover the case of a 1mm PSZ coating, thermal conductivity 2W/mK on a steel piston crown. The broken lines indicate zero isostress lines, the isostress spacing is 50MPa. The coating is in tension through its entire volume, with the maximum values of σ_x, σ_y and τ_{xy} (radial stress, axial stress and shear stress) occuring at the bowl lip. The flat portion of the piston crown has isostress lines parallel to the surface, whilst the bowl does not. This arises since the stresses plotted are σ_x, and σ_y and not the stress normal to the ceramic-metal interface which would show parallel isostress lines throughout the coating. Figure 5.39 shows this effect with σ_x reaching a minimum where σ_y is at its maximum. The effect of changing the radius at the bowl lip is therefore of interest, and in section 5.10 different lip radii have been studied.

The value for thermal conductivity of solid PSZ is generally given as about 2W/mK, however, the high level of porosity present in the sprayed coatings adds further insulation, reducing the conductivity to around 1W/mK. The effect of these pores can be represented by using the bulk property of 1W/mK in the finite element analysis, as shown in figure 5.40. Region A has closely spaced isotherms due to the low conductivity. Region B however has widely spaced isotherms even though the conductivity is low this arises since the heat flow through the gap between the pores is low. The average temperature gradient in both cases is identical, but with the sprayed coating the gradient will not be constant. This in turn leads to local variations in the stress field through the layer, but a value of 1W/mK will give the correct mismatch error between coating and substrate. However an allowance must be made for the fact that additional localised stress concentrations will occur due to the corner effects of each pore.

Figure 5.41 examines the same piston crown as above but using a thermal conductivity of 1W/mK for the PSZ instead of 2W/mK. There are two types of stress present in these coatings, arising from expansion mismatch and a temperature gradient. The expansion mismatch producing a mainly tensile loading while the temperature gradient can give both compressive and tensile stresses. The decrease in conductivity from 2 to 1W/mK increases the temperature gradient, with the result that the surface layer of ceramic tries to expand more, but is prevented from doing so. The ceramic layer is therefore not uniformly in tension as before, but is in compression at the surface, and in tension at the interface, as shown in the plots of σ_x.

The compressive surface effect shown in the figure 5.41 may reduce corrosion attack deeper into the ceramic layer as any fine surface cracks will be closed. Micro cracking, as mentioned before will reduce the tensile stresses present in the layer. However, the compressive load will not be lowered as effectively. The predicted compressive stress σ_x of -353.8MPa can therefore be regarded as fairly accurate. A high compressive load in a porous structure will lead to a high tensile load at the pore corners, cracking of the ceramic surface could occur. A high compressive stress in the surface of a ceramic coating may therefore not always be desirable.

In both the above cases using 1mm PSZ coatings the compressive stresses predicted for the metalic part of the crown coupled with the elevated temperatures will lead to slight creep. This would lead to a reduction in the stresses present under operating conditions, but a residual stress will occur at room temperature.

5.9.1b TWO MILLIMETER PSZ COATINGS ON STEEL

Coating thicknesses of this depth have had greater difficulty remaining in contact with the substrate. However, a study of the stress levels predicted may lead to sufficient understanding of the processes involved to make these thicker coatings a more realistic goal.

The 2mm, 2W/mK example shows an increase in the stresses present in the ceramic layer over that occurring in the 1mm layer. Figures 5.42 to 5.44 show these stresses, the radial tensile stress σ_x has changed little from 604MPa to 566MPa, the same is true of the axial tensile stress σ_y which changes from 559MPa to 484MPa. (These stresses will be substantially reduced by micro cracking) The compressive radial stress has changed from -170MPa to -331MPa, and the axial component from -50MPa to -150MPa. The change in stress levels produced by an increase in coating thickness is probably too small to expect an appreciable decrease in life. Instead the short lives found with thick coatings may be caused by the residual stresses or the increased probability of micro cracks joining up and causing coating failure.

The use of 1W/mK ceramic rather than 2W/mK in the 1mm thick coating produced an increase in the compressive loadings. The same is true in the 2mm thick layer, as shown in figure 5.45. The tensile stresses change very little with thermal conductivity, but the compressive radial and axial loadings have increased by over 100%. These stresses will not be lowered through micro cracking and could lead to tension failure at pore corners. The high stress levels could be reduced by using graded coatings, if the top coating layers have a lower coefficient of thermal expansion then the high compressive loads could be reduced in the surface. A similar effect could be achieved by using a high thermal expansion layer at the interface.

With both of these 2mm coating examples the stresses predicted in the metallic base are slightly lower than in the 1mm examples, however creep may still occur, but its effects will not significantly alter the high stress levels predicted.

5.9.1c PSZ COATINGS ON ALUMINIUM

Aluminium is the prefered material in automobile piston construction, mainly because of its low weight. However, the thermal expansion mismatch between PSZ and aluminium is 3.25 times as great as that between PSZ and steel. It is important to recognise that there are two types of thermal stress, that resulting from thermal expansion

mismatch, and that derived from the presence of temperature gradient. The stresses in the coating on an aluminium piston are therefore not necessarily three times greater than that in a steel one.

Figures 5.46 and 5.47 show the stresses present in a 1mm PSZ coating on aluminium. A similar stress pattern is revealed to that in the steel based example. However, all the stresses are significantly increased. The radial tensile stress σ_x has increased by 135%, and the axial tensile stress σ_y by 90%. This large increase in tensile stresses indicates that the stresses from thermal mismatch are greater than from the temperature gradient. (A 200% increase would be expected if the stresses were only derived from thermal mismatch.) To relieve these stresses through the use of micro cracking to a level that can be supported by the zirconia the crack density must be very fine. As seen in section 5.8 a 1/4mm crack spacing lowered the tensile stress by 32%. A much finer crack spacing therefore needs to be developed in this case. However if the process of spraying at an elevated temperature is used a theoretical reduction in peak tensile stresses of 58% was achieved with the same crack spacing. For a thick coating on aluminium to have sufficient life for its use in an internal combustion engine to be contemplated then a method such as this must be used to reduce the tensile stresses.

Examination of a 2mm layer on aluminium shows little increase in the tensile loadings predicted but the surface layer of ceramic is in compression, these stresses can be reduced through the use of graded coatings.

5.10 EFFECT OF ELEVATED SUBSTRATE TEMPERATURES DURING COATING FORMATION

To simulate the effect of using an elevated base temperaure during coating formation, the temperature used by ANSYS to represent the stress free condition was raised. The previous piston crown examples were re-run with this temperature set at 200°C and 400°C. the results obtained are summarised in tables 5.6 to 5.7. Only the case

of a 2mm PSZ layer on steel, with k=1W/mK is shown graphicaly in figures 5.48 and 5.49. The figure 5.48 shows the conditions arising within the normal operating environment, assuming a stress free temperature of 400^{o}C. Figure 5.49 shows the residual stress present at room temperature assuming the same stress free condition. Examining figure 5.48 showing σ_x: the distortion indicated by this plot is misleading, as the ANSYS package always displays the maximum level of distortion as a fixed percentage of component size, actual distortion levels are very small. The characteristic isostress distribution observed with the standard piston crown is stil present, but compressive loading of the coating has been increased to 1306MPa, whilst the tensile loading has lowered to 221MPa. Using elevated temperatures during the formation of coatings this thick obviously does not reduce the stresses to a manageable level. The use of a 2mm coating does not seem a realistic proposition without graded coatings. However the use of graded material coatings under these conditions could present difficulties as the residual stress levels would also be affected by their use, as examined in section 5.13.

In this case with uniform material properties the residual stresses at room temperature, (figures 5.48 and 5.49) show high levels of compressive and tensile stresses. The residual stresses predicted by the finite element method for the piston crown at room temperature show isostress lines perpendicular to the surface, rather than parallel at elevated temperatures. This illustrates the two types of thermal stress mentioned in the last sub-section, those from the thermal expansion mismatch, and those from a temperature drop across the ceramic. The stresses present at room temperature arise only as a result of the thermal mismatch, while those at elevated temperatures also arise from the temperature drop. The stress produced by a temperature gradient will always be greatest at the surfaces of the ceramic coating, and so the isostresses will be parallel with the surfaces. A different stress pattern arises from thermal mismatch. Figure 5.50 examines why these stresses occur. Where the surface is horizontal a uniform compressive stress σ_r would be expected. When the surface is vertical a large value of compressive stress σ_a is produced. These effects combine in the piston crown to

produce isostress lines vertical to the coating at the centre and rim with
σ_r a maximum, while σ_a is a maximum close to the bowl lip. These patterns are confirmed by the finite element analysis.

Tables 5.5 to 5.6 show the peak stresses recorded in 1mm and 2mm thick PSZ coatings, all with k=1W/mK. The first row in each table shows the stress arising in the piston crown under normal operating conditions if it is assumed to be stress free at 20^{o}C. The second and third rows show these operational stresses if the stress free condition is 200^{o}C and 400^{o}C respectively, corresponding to an increase in the base temperature during coating formation of the same level. The next two rows show the residual stresses present at room temperature, ie 20^{o}C, for the 200^{o}C and 400^{o}C stress free conditions. Table 5.5 shows a steady reduction in the maximum tensile stresses developed in a 1mm coating under normal operating conditions as the stress free temperature is raised. This is accompanied by an increase in the compressive stress. Both the tensile and compressive loadings at room temperature increase. There are two ways in which such information can be useful:

i) If graded material properties are to be used this analysis provides an indication as to the depth, and properties desired in various parts of the coating, either for the purpose of further theoretical analysis, or for setting the spray parameters during coating formation without this more detailed study.

ii) The maximum compressive stress the coating can withstand both at room temperature, and for the shorter time it will be at the operating condition should be assessed experimentally. The tabulated results can then be used to give a temperature for spraying at which this stress is achieved. The tensile loads at this condition will be the minimum that can be attained practically.

Table 5.6 for a 2mm coating shows the same pattern of behaviour as that in table 5.5, except that the tensile stress levels cannot be reduced as significantly as in the 1mm case. The use of a 400^{o}C

elevated temperature is the example examined previously and shown in figures 5.48 and 5.49.

5.11 EFFECT OF BOWL LIP RADIUS

The finite element models of the piston crown examined so far all possess a bowl lip radius of 6mm, the maximum stresses invariably occurring around this lip. The finite element grids previously used were therefore repeated using 4mm and 8mm radi at the bowl lip. These models were then studied with 1mm and 2mm thick PSZ coatings, using thermal conductivities of 1 and 2W/mK. These form a total of 12 different finite element models, the associated graphical output is not shown, but the peak stresses are recorded on tables 5.7 through 5.10. Where 1mm thick coatings are used the effect of these alterations represent a change of less than 2% of the peak stress. In the case of 2mm coatings the change is around 6%. The stress concentration occuring at the bowl lip seems to result purely from the change in direction of the coating, and not from the distance over which this is achieved. There seems no easy way of relieving this particular stress concentration.

5.12 AXI-SYMMETRIC REPRESENTATION OF A COMPLETE PISTON

The previous finite element study of a piston crown, was intended to establish basic behavioural trends. For a theoretical study to be of use cause and effect must be linked. This is not easy in a complex structure, where a stress concentration can arise as a result of several design features, so a simplified piston model was used. Having established a few identifiable stress patterns and their causes, it is now realistic to study a more complete piston model. The complete axi-symmetric model shown in figure 5.51 of a coated piston was therefore developed. The dimensions chosen were close to those used in the Petter PH1W engine, diameter 87mm, length 106mm, with a bowl diameter of 25mm. A 6mm bowl lip was used and the ceramic coating feathered on the outer edge. The thermal boundary conditions used are shown. The mechanical boundary conditions used in this case are more realistic than in the simplified model, as only one node needs to be fixed to prevent rigid body motion. The crown model fixed the bottom plane in the axial but not radial direction, as shown in figure 5.52. As in the previous analysis this model has been run with different material specifications, and coating thicknesses, ie;

Base material	Coating thickness mm	Thermal conductivity W/mK
Steel	1	1
Steel	2	1
Steel	1	2
Steel	2	2
Aluminium	1	1
Aluminium	2	1

The isotherm distribution for two of these cases is shown in figure 5.53 and 5.54. Similar peak temperatures are recorded in the examples listed above, as with the piston crown equivalents examined earlier. The temperature distributions developed in the metal bases are also similar to their simplified counterparts. The thermal

boundary conditions chosen in the piston crown study are therefore compatible with those used in the full piston analysis. The peak temperature again occurs at the bowl lip with closely spaced isotherms. The temperature gradient is steepest with the low thermal conductivity coatings, and where aluminium is used as a base material.

A steel piston with a 1mm coating of 1W/mK PSZ is examined in figures 5.55 and 5.56. As the coating is relatively thin compared with the piston size little detail of the stress patterns can be seen in the main plot. The windowing facility on ANSYS has therefore been used to show the isostress lines at the bowl base, and lip. Figure 5.55 shows the stresses derived using an identical material/thickness combination to the idealised crown in figure 5.41. The radial stress levels in both cases are similar σ_x=558/-460MPa in the piston and 583/-352MPa in the crown, the largest discrepancy occurring in the centre of the bowl, the smallest at the pistons plateau. This is because the mechanical boundary conditions used with the piston crown are at their least appropriate under the bowl, as in the complete piston the thinner metal section at this point is able to deform slightly, as in figure 5.52. The loading shown in the piston body is mainly compressive, up to 260MPa, at the radius joining bowl and the side of the piston.

The difference in stress levels accompanying a change in substrate material from steel to aluminium is shown in tables 5.12 and 5.13 for 1mm PSZ coatings, and 5.15 and 5.16 for 2mm coatings. In all cases thetensile stresses are approximately doubled, although the compressive stresses are reduced. The 1mm, 1W/mK PSZ coating is also shown on an aluminium piston body in figure 5.57. A very high tensile stress is again recorded in the coating which will result in a very high level of microcracking with the associated high probability of failure. Summarising, there are two main methods which can be used to reduce this stress level:

I) By increasing the number and regularity of micro cracks. Such as the use of heat treatment to create a cracked sublayer of PSZ, with subsequent spraying of a fully dense upper layer.

ii) By using a raised substrate temperature during coating formation the tensile stresses may be reduced, at the expense of creating a high compressive surface loading. The effect of increasing substrate temperature to 200°C is shown in table 5.11 and 5.14 for 1mm and 2mm coatings respectively. A reduction of approximately 40% in tensile stress is achievable.

These two methods can be used with both aluminium and steel based pistons, although the stress levels encountered in the case of steel are not so severe. The effect of increasing the stress free temperature too 200°C in a 1mm, 1W/mK coated steel piston is shown in figures 5.58 to 5.59. The stresses arising under normal operating conditions are shown in the first figure. This represents an attainable ceramic coating, if the above stress minimising techniques are used. The residual stresses in figure 5.59 are also low enough to be acceptable. Again there is little difference in the stress levels and patterns arising in this more complex piston model than the simplified piston bowl study discussed earlier.

5.13. EFFECT OF GRADED MATERIAL PROPERTIES

The stresses arising in ceramic coatings occur for two reasons, the difference in thermal expansion between coating and substrate, and the temperature gradient created by thermal conductivity. It would seem that the closer the properties of the ceramic and metal coincide the lower the stress levels will be. This, however, is an over simplification, for as already has been noticed thick ceramic coatings, and ceramic coatings where a raised base temperature has been used during plasma spraying can develop compressive stresses in the upper part of the coating. The use of a ceramic with a lower coefficient of thermal expansion in this upper layer could reduce, or eliminate this compressive stress. A similar effect can be achieved by using a ceramic with increased conductivity in the top layer of the coating. This will reduce the temperature gradient in the ceramic, and hence lower the stress levels.

The finite element mesh describing a piston crown has been further developed so that a graded coating can be included in the analysis. Two cases have been examined, the first using a 2mm PSZ layer on a steel substrate, the second using a 1mm, PSZ layer on an aluminium substrate. Different property distributions have been examined, yielding a total of six finite element studies.

The first example involves a 2mm coating on steel. A coating with a variable coefficient of thermal expansion is used, ranging from 5e-6 at the gas surface to 10e-6 at the interface, using a linear variation with depth. As a comparison the same example was studied using a constant thermal expansion of 10e-6, this was shown in figure 5.45. The stresses arising within this new graded coating are shown in figures 5.60 to 5.62. A significant reduction in the compressive stresses has occurred, the radial stress σ_x has reduced from -790MPa to -163MPa, similarly the compressive axial stress is reduced from -516MPa to -116MPa. This change was expected, as the compressive region in the top part of the coating can be relieved by using low expansivity materials. In addition the tensile stresses have been reduced, σ_x is reduced from 568MPa to 423MPa, while σ_y is reduced from 500MPa to 374MPa. The coating is now in tension throughout its volume, the maximum tensile stress occuring at the edges of the ceramic, with the mimimum at the centre. Using graduated material properties a coating depth of 2mm is no longer theoretically impossible to achieve. But further stress reductions may be achievable if the effects of graduated properties are combined with the effects of using an elevated substrate temperature during coating formation. This analysis indicates that the high thermal expansion of zirconia is not necessarily an advantage. A ceramic with a lower expansion when used as a graded coating can develop lower stresses.

The same finite element analysis was repeated but assuming a stress free temperature of 200^{o}C, corresponding to a substrate temperature of 200^{o}C during coating formation. The stresses arising in this case are shown in figures 5.63 and 5.64. As in previous examples this has reduced the tensile stresses, whilst increasing the compressive. The peak tensile stress is now 255MPa, the peak compressive

-242MPa. This represents a further improvement in the original stress levels of 568 and -780MPa. Difficulties arise when the residual stresses are examined; large compressive stresses have been developed in the coating surface, the radial stress peak is -409MPa. These stress levels are clearly undesirable in a component that will be left in this condition for most of the time. A further reduction in the coefficient of thermal expansion at the surface would alleviate this problem.

Similar reductions in compressive stress can be achieved through the use of high thermal conductivity layers in the top part of the ceramic layer. This effect has been examined using the previous finite element model, but taking a variation in K from 2W/mK in the surface to 1W/mK at the interface. This produces unequal spacing in the isotherms, as shown in figure 5.65. Its effect on the stress levels however is less than with a change in thermal expansion, the radial stresses σ_x have changed from peaks of 568/-790MPa to 378/-778MPa while σ_y is changed from 500/-778MPa to 343/-468MPa. These stresses are shown in figures 5.66 and 5.67. Although most of the coating is subject to a low stress gradient the bottom 0.5mm develops very steep stress gradients.

By optimising the formation temperature and the coefficent of thermal expansion it is clear that very large reductions in the stress levels can be achieved. With careful management the stresses given theoretically can be set so that coatings of 2mm are theoretically possible. However, the residual stresses set up during the formation are likely to be greatest with these thick coatings, and a theoretical study can only roughly indicate the route that should be taken.

Further finite element work examining graded coatings has shown that the introduction of a coating structure which would 'intuitively' be expected to reduce stress levels, can have the opposite effect. Under certain circumstances an exact matching of the coefficients of thermal expansion at the interface can produce an increase in stress levels over the values produced with uniform coating properties.

5.14 FINITE ELEMENT ANALYSIS OF CERAMIC MONOLITHS

Two dimensional axisymmetric and three dimensional models have been used in the study of ceramic monoliths.

In common with the examination of coatings the main difficulty arising with this F.E. analysis is the representation of the methods used to attach the ceramic to the engine structure. In the case of monoliths these problems are at their worst when contact stresses between two components need to be calculated. These problems are increased because most potential ceramic materials have very low coefficients of thermal expansion, hence large shrink fits are needed, leading to high stresses.

To represent the performance of a monolith accurately there are two difficult areas which must be modelled.

i) The contact stress between components. It will often be necessary to incorporate a shrink fit into the analysis. Special elements are available for this purpose in finite element packages. A further area needing numerical analysis is the level to which mating surfaces can slip, to achieve this an accurate measure of the friction between the surfaces must be achieved.

ii) If an air gap is included (even if only the trapped layer between mating surfaces) its insulative properties must be included. For high accuracy radiative heat transfer should be represented, as this will significantly affect the insulative ability. The emissivity of these surfaces are likely to change during their working life due to deposition of soot.

At the start of this work it was proposed to study a large number of ceramic monoliths. This programme had to be restricted because most of the designs envisaged could only be accurately represented by a full three dimensional analysis. The version of ANSYS available for this work was intended for research use only, and came with an internal trigger which prevents problems over a certain size from being studied. The three dimensional shapes, with shrink fitting and

air gaps were over the size limitation, making their analysis impossible.

5.14.1 MESH GENERATION

In the steady state condition the temperature and the stress gradients through ceramic monoliths are far lower than with coatings. The mesh density is therefore less critical and so computer run times are reduced. Element shape is still critical, and the angle between element boundaries must be carfully controlled.

Where two or more mating surfaces are used an interferance fit element should be used, this allows for the introduction of residual stresses into the ceramic component.

5.15 SIMPLIFIED FINITE ELEMENT MODEL OF PISTON CROWN

The computer model used to represent the top portion of a piston crown in section 5.9.1 has been adapted to examine the behaviour of monoliths. The piston crowns studied were made from silicon nitride with the following properties.

Thermal conductivity	20W/mK
Thermal expansion	2.5e-6
Young's modulus	290GPa
Poison's ratio	0.23

Figure 5.68 shows the isotherms produced with the boundary conditions taken previously, as shown in figure 5.33. The maximum temperature of 577^{o}C compares with a range from 600 to 688^{o}C with the 1 and 2mm zirconia coatings studied previously. The stress levels developed within a monolith are highly dependent on the mechanical boundary conditions used. In this case the assumption of zero axial displacement, and free radial displacement at the boundary has been kept. This was found to be a good representation of the way a piston crown behaved in section 5.9. With these boundary conditions the stresses developed would be close to those observed with a complete monolithic piston. The stresses are shown

In figure 5.69 to 5.71. The maximum tensile radial stress is 10MPa, and axially 54MPa. These tensile stresses are low, and certainly within the limits of silicon nitride. The radial stress is particularly low, the majority of the component being in compression. Axial stresses show compressive, or near zero stresses at the material surface, this is also desirable as flaws at a material surface are likely to cause failure if in tension. Figure 5.71 shows the principal stress, this has the maximum stresses occurring at the base of the bowl, however the plot is misleading as it fails to discriminate between tensile and compresive stresses.

The bowl lip develops only compressive stresses and this is helpful as the lip is likely to be a region where flaws are most likely to occur due to the difficulty of manufacture in this region.

5.15 FINITE ELEMENT MODELS WITH AN INTERFERENCE FIT

The assessment of the correct interference fit in bimaterial structures is of critical importance. Not only must the tolerances insure that there is no separation at high temperatures, but also that the load is evenly distributed at both room temperature and at the operating condtion. A silicon nitride-aluminium piston is examined in figure 5.72, this shows two points of stress concentrations on the interference fit. By using the finite element analysis it should be possible to find a design of interference fit which requires little modification in the hardware development stages.

An attempt has been made to model the behaviour of the sample holder installed in the ceramic insulation test rig. The holder is made from six components. The ceramic disc is held in place by three clamps of the type shown in figure 5.73 and 5.74. These show the clamps in psition with the ceramic disc. A shaft locates into the rear of these three clamps, and a shrink fit ring fits around these to form a compressive load on the ceramic, as shown in figure 5.75.

It was initially intended to use a finite element model to establish the optimum shrink fit on the ring, and what taper should be used at the

ceramics edge. Unfortunately, the problem proved too large to be handled by our version of ANSYS, and the desired mesh density could not be achieved.

	σ_x Max. & Min stress (MPa)	σ_y Max & Min Stress (MPA)
Crack free	342.99 -255.87	170.61 -176.4
1mm Cracks	292.23 (-14.8%) -263.1 (+2.8%)	128.1 (-24.9%) -149.5 (-19.2%)
Crack free	335.21 -280.75	169.53 -230.89
½ mm Cracks	255.11 (-23.9%) -286.12 (+1.9%)	89.58 (-47.2%) -119.78 (-48.2%)
Crack free	294.49 -300.39	157.7 -245.91
¼ mm Cracks	200.24 (-32.0%) -308.89 (+2.8%)	84.36 (-46.5%) -81.45 (-66.9%)

TABLE 5.1 STRESS RELIEF THROUGH INCREASING CRACK DENSITY.

	σ_x Max & Min (MPA)	σ_y Max & Min (MPA)	Stress Free Temperature °C
Operating Stresses	292.23/-263.1	128.1/-149.5	20
	182.01/-156.79	70.46/-98.10	220
	71.79/-50.49	161.3/-49.45	420
Residual Stresses	106.3/-110.22	51.82/-57.68	220
	212.60/-220.45	103.63/-115.37	420

TABLE 5.2 EFFECT OF INCREASING SUBSTRATE TEMPERATURE DURING COATING FORMATION, WITH 1mm CRACKS.

	σ_x Max & Min (MPA)	σ_y Max & Min (MPA)	Stress free Temperature °C
Operating Stresses	255.11/-286.12	89.58/-119.77	20
	156.04/-117.39	51.10/-75.93	220
	56.98/-56.65	129.82/-32.08	420
Residual Stresses	114.73/-99.07	43.85/-39.46	220
	229.5/-198.13	87.69/-78.92	420

TABLE 5.3 EFFECT OF INCREASING SUBSTRATE TEMPERATURE DURING COATING FORMATION, WITH 1/2mm CRACKS.

	σ_x Max & Min (MPA)	σ_y Max & Min (MPA)	Stress Free Temperature °C
Operating Stresses	200.24/-308.89	84.35/-81.45	20
	121.23/-185.38	49.79/-50.26	220
	42.21/-61.87	15.22/-19.06	420
Residual Stresses	123.5/-79.01	31.19/-34.56	220
	247.02/-158.03	62.39/-69.13	420

TABLE 5.4 EFFECT OF INCREASING SUBSTRATE TEMPERATURE DURING COATING FORMATION. WITH 1/4mm CRACKS.

	σ_r Max & Min (MPa)	σ_a Max & Min (MPa)	Stress Free Temperature °C
Operating Stresses	583.8/-352.4	537.8/-120.1	20
	355.5/-610.9	328.6/-308.2	200
	110.85/-898.1	96.07/-530.8	400
Residual Stresses.	87.36/-258.5	37.7/-209.2	200
	184.4/-545.6	79.59/-441.7	400

TABLE 5.5 RADIAL AND AXIAL STRESSES IN PISTON CROWN, 1mm PSZ, 1W/mK, STEEL SUBSTRATE.

	σ_r Max & Min (MPa)	σ_a Max & Min (MPa)	Stress free Temperature °C
Operating Stresses	567.9/-790.3	500.4/-515.8	20
	385.3/-1034.5	336.3/-685.7	200
	221.3/-1305.9	156.1/-874.3	400
Residual Stresses	96.85/-244.2	61.21/-169.81	200
	204.5/-515.6	129.22/-358.5	400

TABLE 5.6 RADIAL AND AXIAL STRESSES IN PISTON CROWN, 2mm PSZ, 1W/mK, STEEL SUBSTRATE.

Bowl lip radi (mm)	σ_r Max & Min (MPA)	σ_a Max & Min (MPA)
4	603.8 / -168.5	589.3 / -95.7
6	604.1 / -170.5	559.1 / -75.36
8	607.75 / -170.26	516.7 / -71.37

TABLE 5.7 EFFECT OF BOWL LIP RADI STRESS DISTRIBUTION. 1mm PSZ. 2W/mK

Bowl lip radi (mm)	σ_r Max & Min (MPA)	σ_a Max & Min (MPA)
4	596.1 / -349.1	571.1 / -132.9
6	583.8 / -352.4	537.8 / -120.1
8	582.2 / -368.9	503.3 / -164.2

TABLE 5.8 EFFECT OF BOWL LIP RADI ON THE STRESS DISTRIBUTION.
1mm PSZ. 1W/mK.

Bowl lip radi (mm)	σ_r Max & Min (MPA)	σ_a Max & Min (MPA)
4	586.4/-327.8	508.1/-161.8
6	565.9/-331.4	483.6/-150.0
8	552.8/-331.3	470.1/-148.1

TABLE 5.9 EFFECT OF BOWL LIP RADI ON THE STRESS DISTRIBUTION.
2mm PSZ. 1W/mK.

Bowl lip radi (mm)	σ_r Max & Min (MPA)	σ_a Max & Min (MPA)
4	582.6/-784.8	545.6/-530.5
6	567.9/-790.3	500.4/-515.8
8	558.1/-789.0	479.1/-525.4

TABLE 5.10 EFFECT OF BOWL LIP RADI ON THE STRESS DISTRIBUTION.
2mm PSZ. 1W/mK.

	σ_r Max & Min (MPa)	σ_a Max & Min (MPa)	Stress Free Temperature °C
Operating Stresses	558.5/-459.4	525.3/-168.3	20
	343.0/-712.5	321.2/-349.5	200
Residual Stresses	85.2/-253.1	42.9/-204.2	200

TABLE 5.11 RADIAL AND AXIAL STRESSES IN PISTON, 1W/mK, STEEL SUBSTRATE.

Substrate Material	σ_r Max & Min (MPa)	σ_a Max & Min (MPa)
Steel	565.6/-351.7	537.0/-169.9
Aluminium	1065.7/-245.5	969.5/-152.3

TABLE 5.12 COMPARISON BETWEEN STRESSES IN STEEL AND ALUMINIUM PISTONS. 1mm PSZ. 2W/mK.

Substrate Material	σ_r Max & Min (MPa)	σ_a Max & Min (MPa)
Steel	558.5/-459.4	525.3/-168.3
Aluminium	1054.5/-219.5	968.3/-113.4

TABLE 5.13 COMPARISON BETWEEN STRESSES IN STEEL AND ALUMINIUM PISTONS. 1mm PSZ. 2W/mK.

	σ_r Max & Min (MPA)	σ_a Max & Min (MPA)	Stress Free Temperature °C
Operating Stresses	573.4/-842.8	519.3/-535.9	20
	411.8/-1073.7	359.6/-667.6	200
Residual Stresses	109.1/-230.9	605.0/-132.2	200

TABLE 5.14 RADIAL AND AXIAL STRESSES IN PISTON. 1mm PSZ. 1W/mK. STEEL SUBSTRATE.

Substrate Material	σ_r Max & Min (MPA)	σ_a Max & Min (MPA)
Steel	542.9/-429.8	486.3/-189.4
Aluminium	989.9/-404.4	854.9/-191.3

TABLE 5.15 COMPARISON BETWEEN STRESSES IN STEEL AND ALUMINIUM PISTONS. 2mm PSZ. 2W/mK.

Substrate Material	σ_r Max & Min (MPA)	σ_a Max & Min (MPA)
Steel	573.4/-842.8	519.3/-535.9
Aluminium	1026.8/-578.9	902.8/-460.5

TABLE 5.16 COMPARISON BETWEEN STRESSES IN STEEL AND ALUMINIUM PISTONS. 2mm PSZ. 1W/mK.

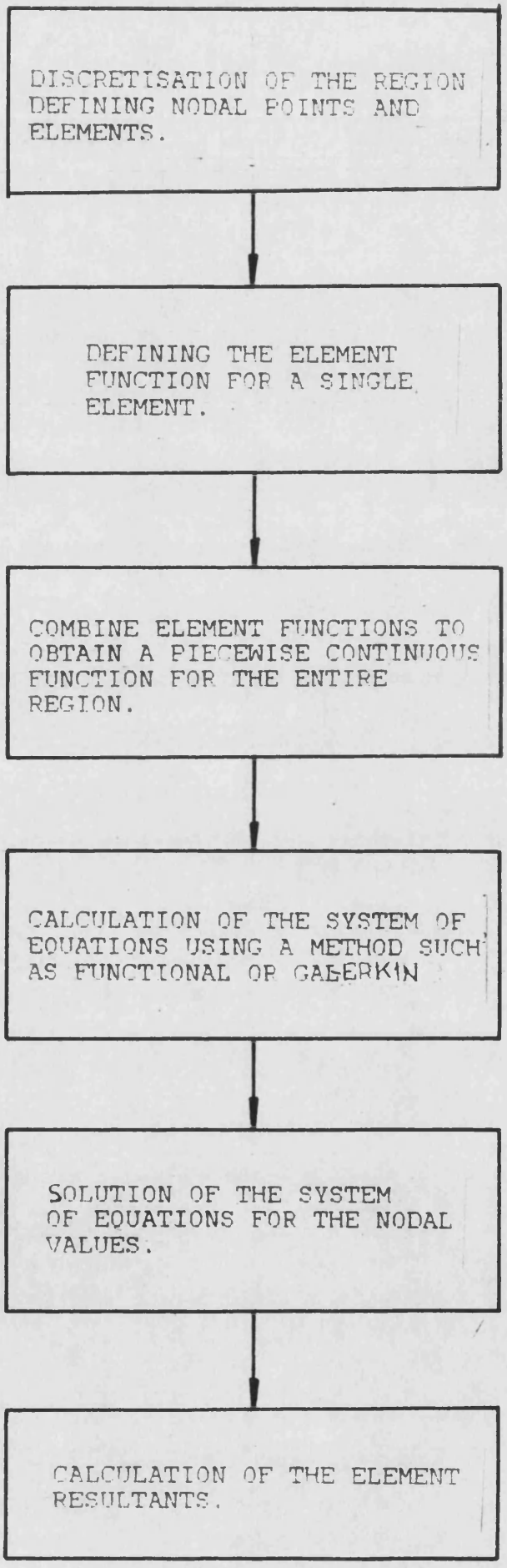

FIGURE 5.1 STAGES IN THE USE OF THE FINITE ELEMENT METHOD

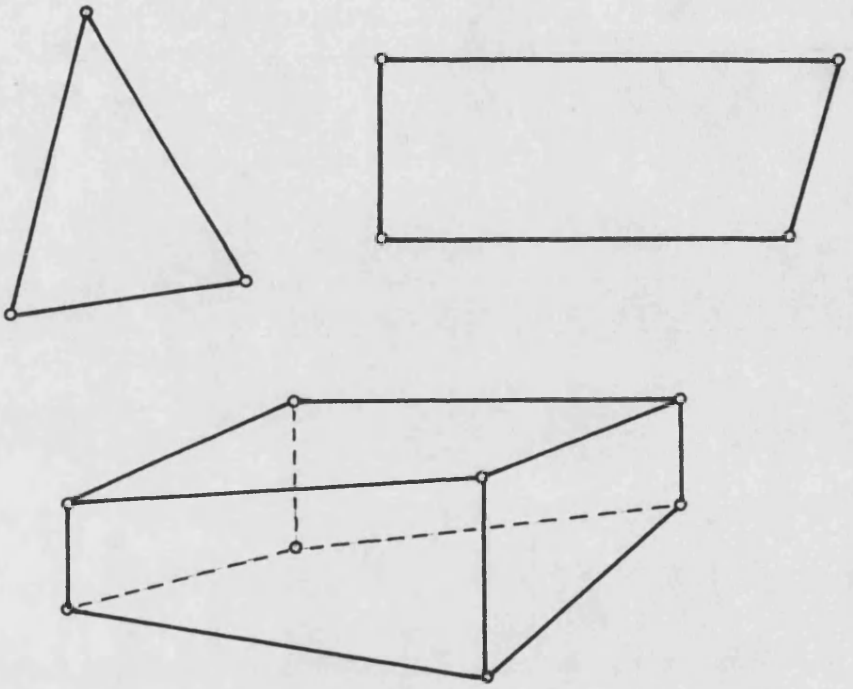

FIGURE 5.2 TRIANGULAR, QUADRILATERAL AND HEXAHEDRAL ELEMENTS

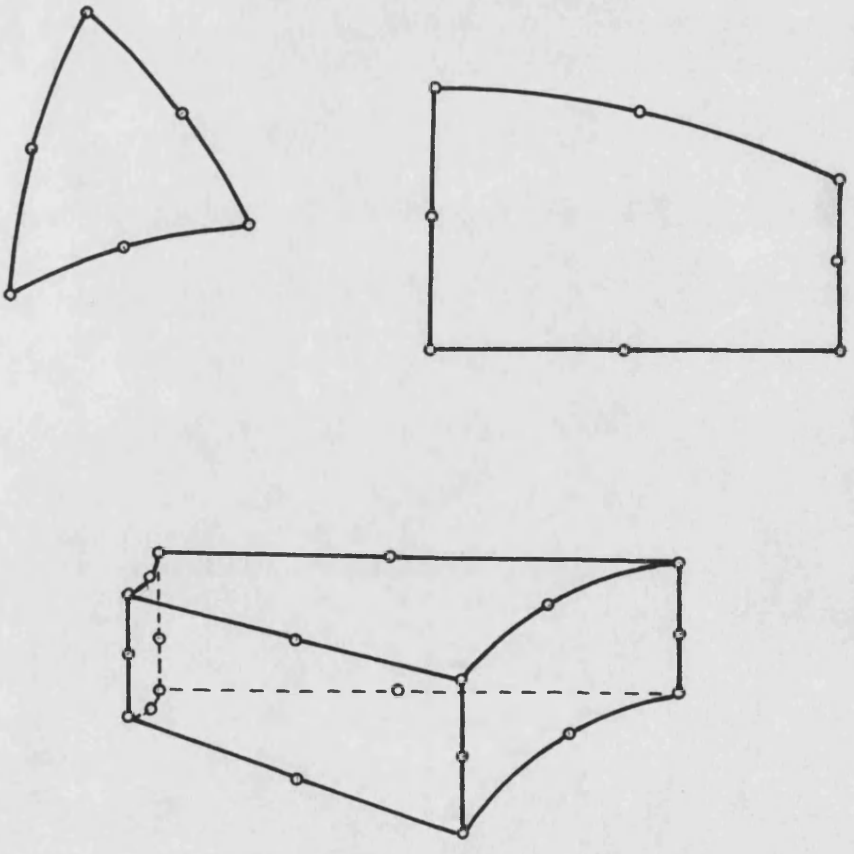

FIGURE 5.3 ISOPARMETRIC ELEMENTS

FIGURE 5.4 DISPLACEMENT SHAPES OVER SIMPLEX QUADRILATERAL ELEMENTS.

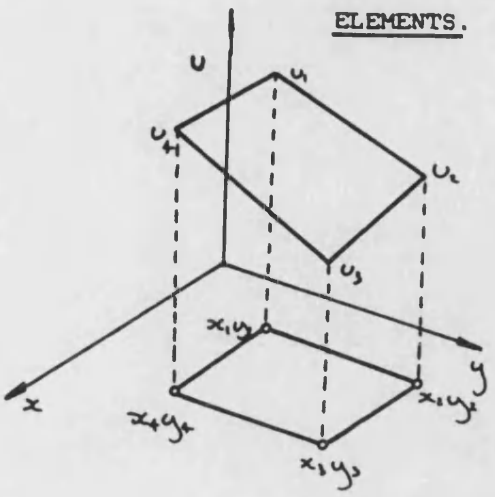

where u is the displacement

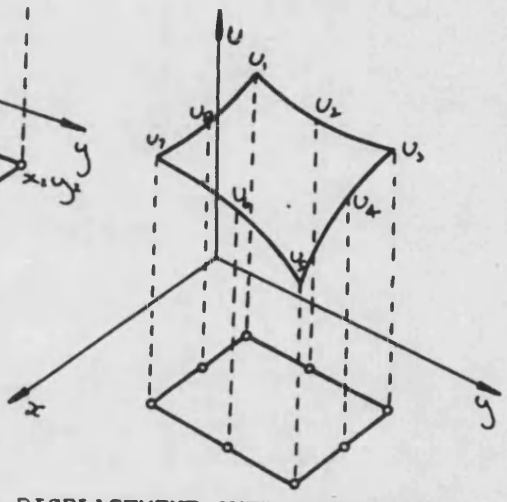

FIGURE 5.5 DISPLACEMENT OVER QUADRATIC QUADRILATERAL ELEMENTS.

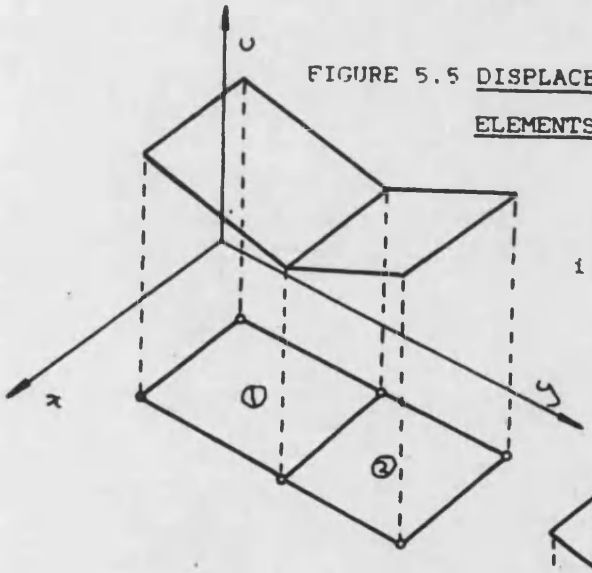

i) SIMPLEX

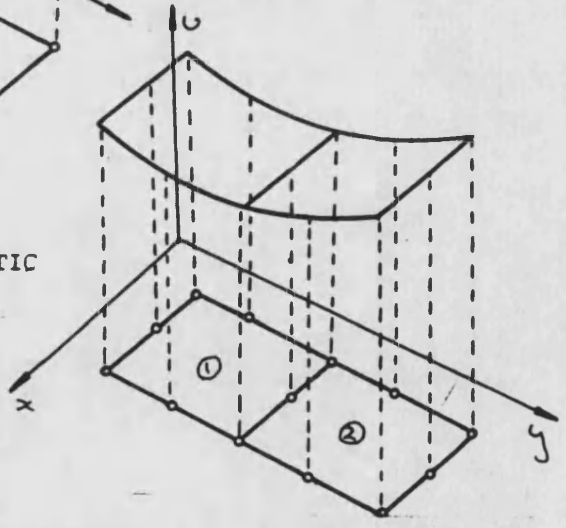

ii) QUADRATIC

FIGURE 5.6 MAINTAINING CONTINUITY ACROSS ELEMENT BOUNDARIES.

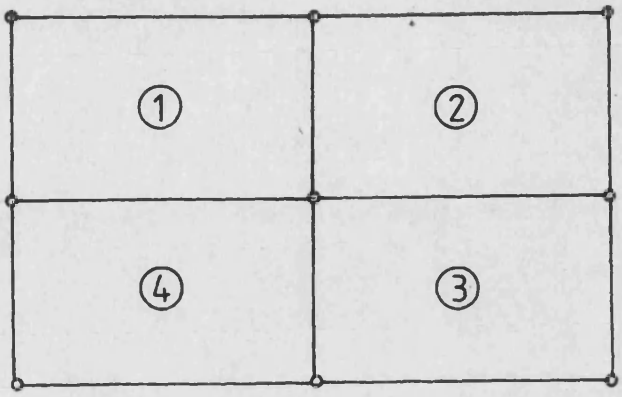

FIGURE 5.7 SCALAR DISPLACEMENT AT NODES

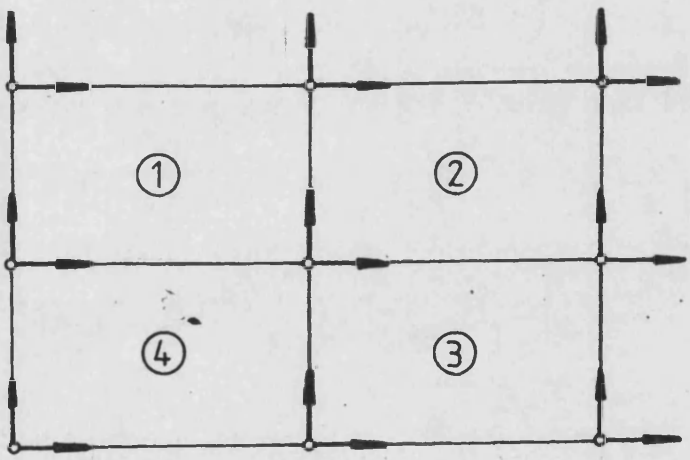

FIGURE 5.8 VECTOR DISPLACEMENT AT NODES

FIGURE 5.9 DISPLACEMENT FORM WITH SIMPLEX AND QUADRILATERAL ELEMENTS.

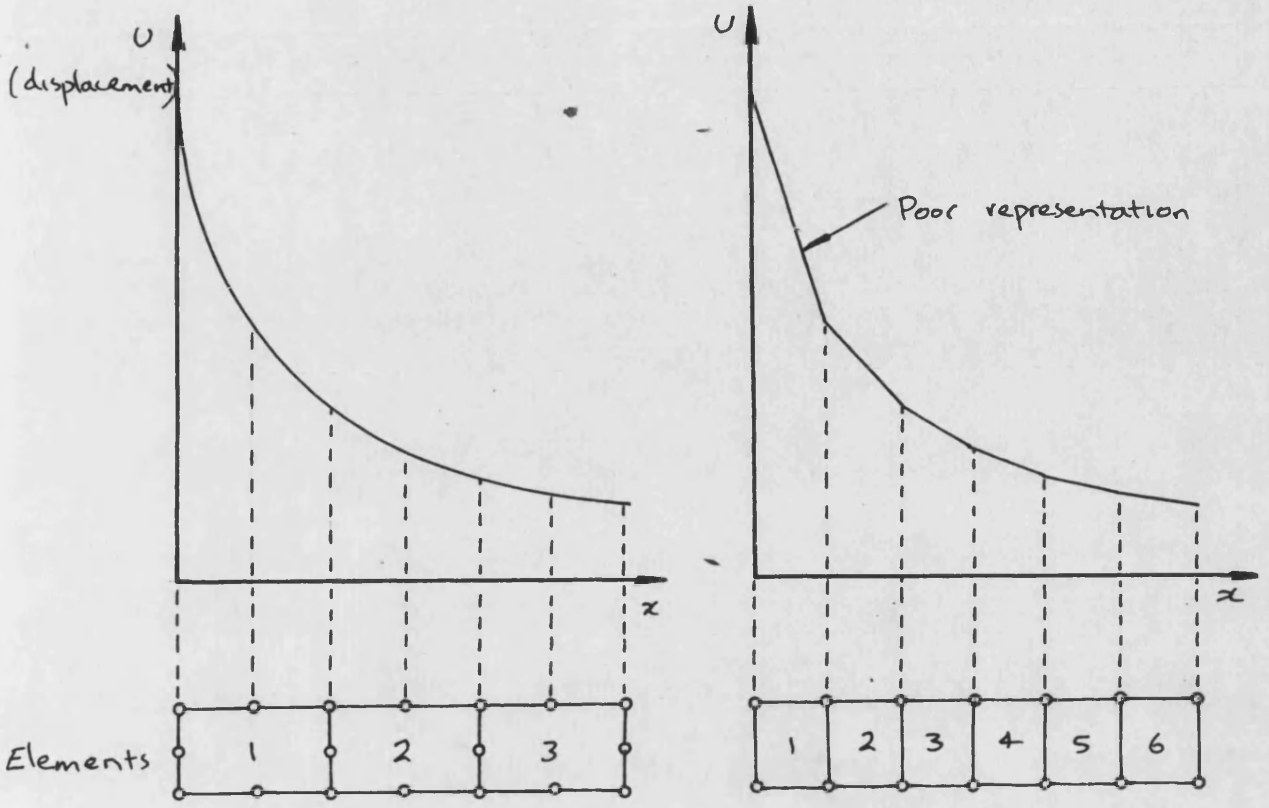

Quadratic element best with high $\frac{d^2U}{dx^2}$

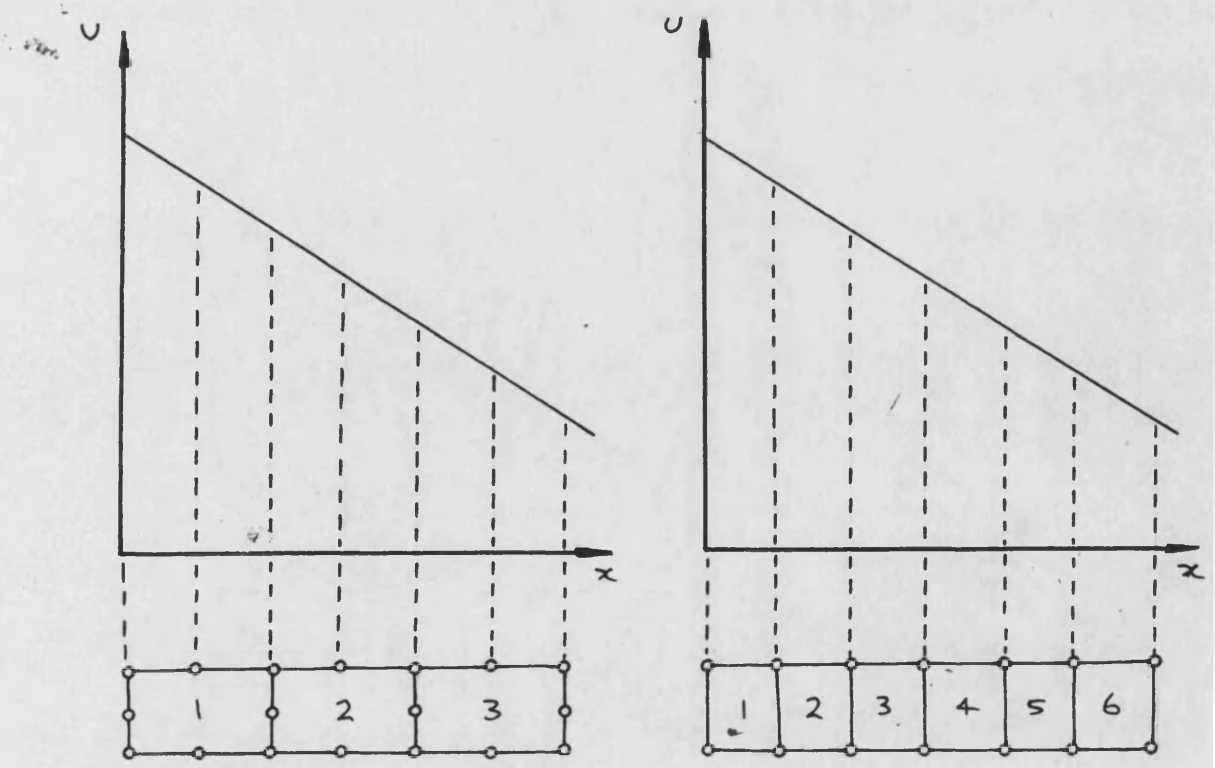

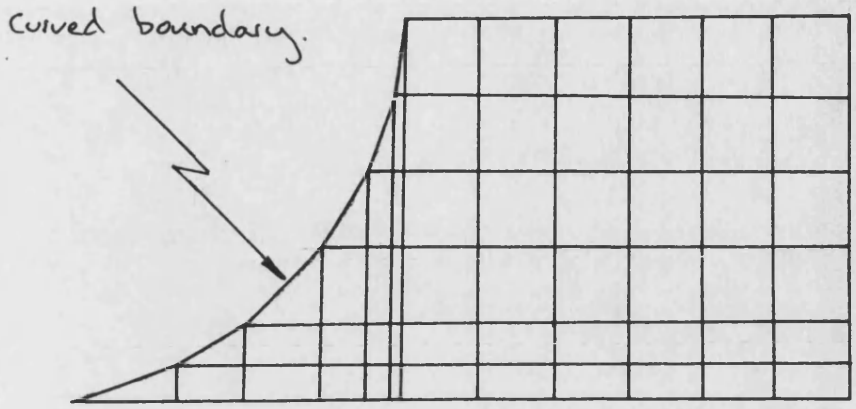

FIGURE 5.10 USE OF TRIANGULAR AND RECTANGULAR ELEMENTS AT CURVED BOUNDARY.

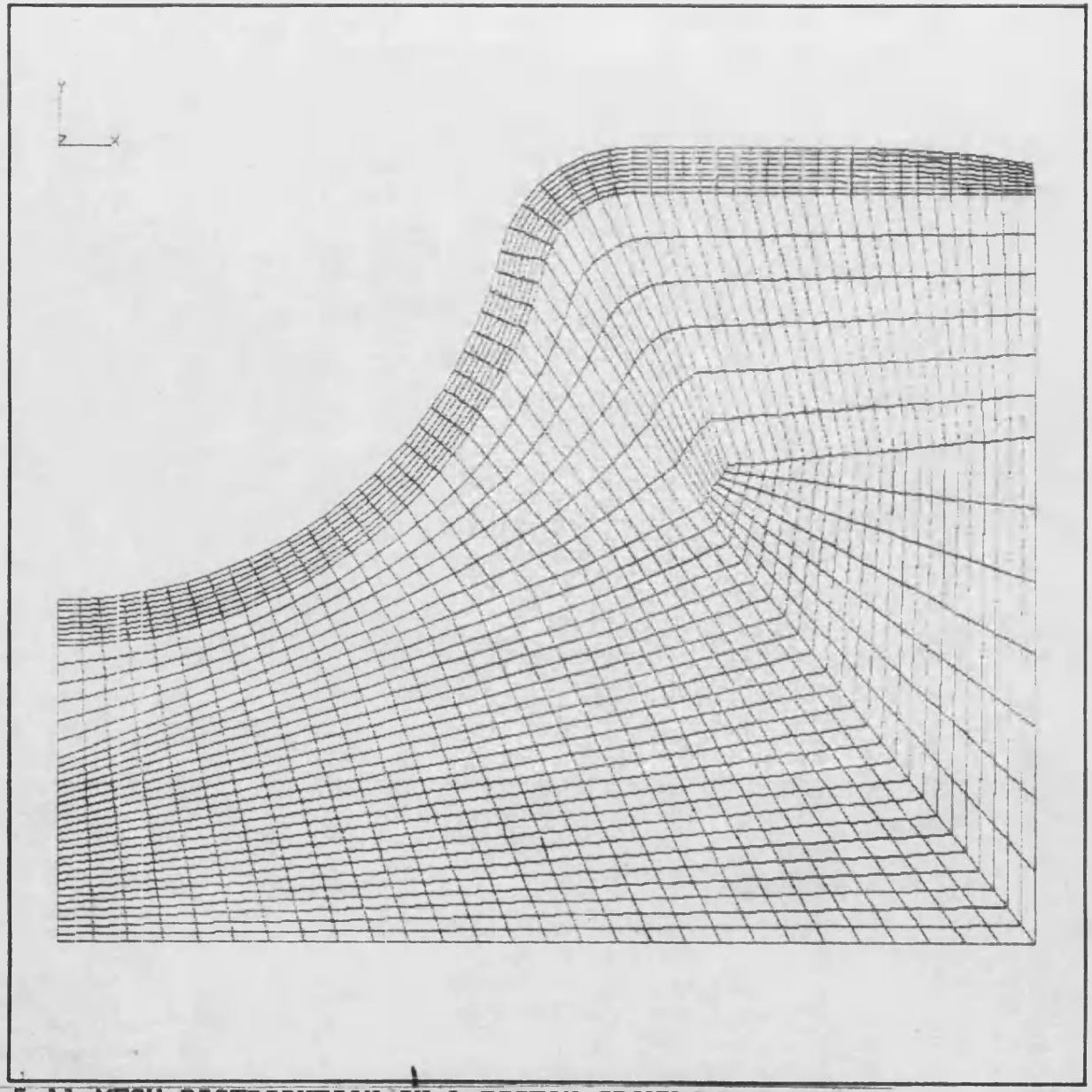

FIGURE 5.11 MESH DISTRIBUTION IN A PISTON CROWN.

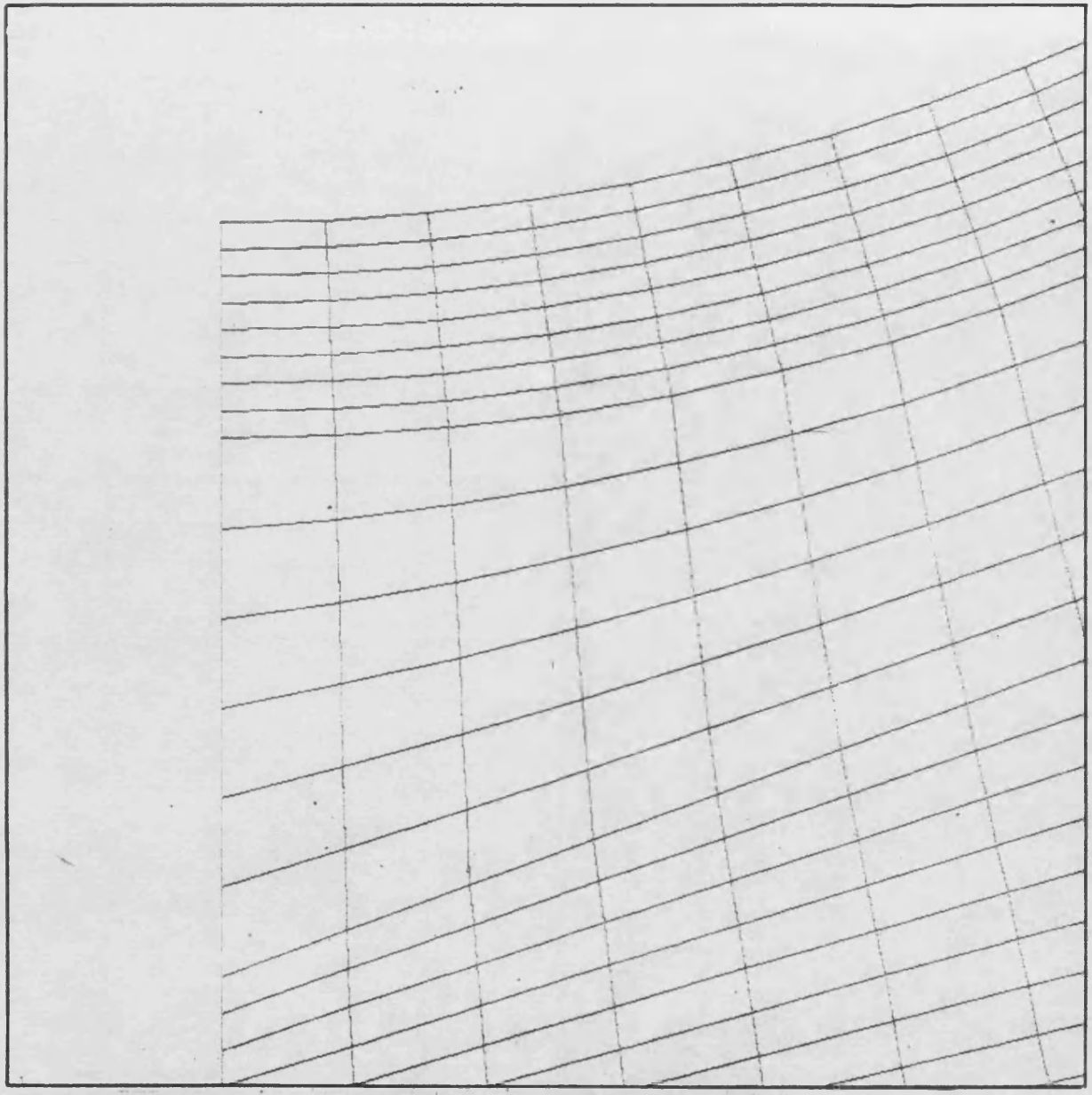

FIGURE 5.12 LOCAL MESH DISTRIBUTION IN A PISTON CROWN.

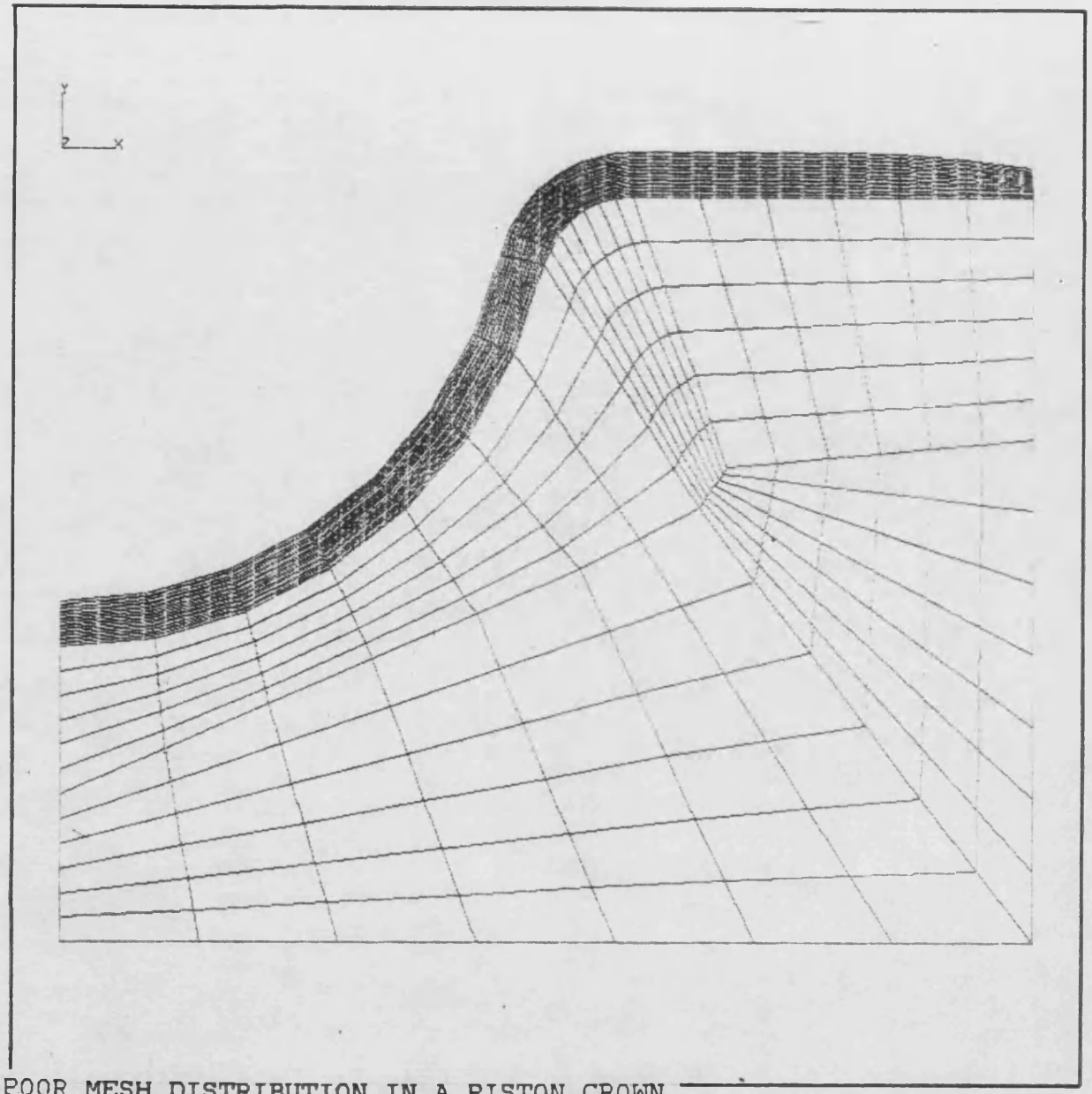

FIGURE 5.13 POOR MESH DISTRIBUTION IN A PISTON CROWN.

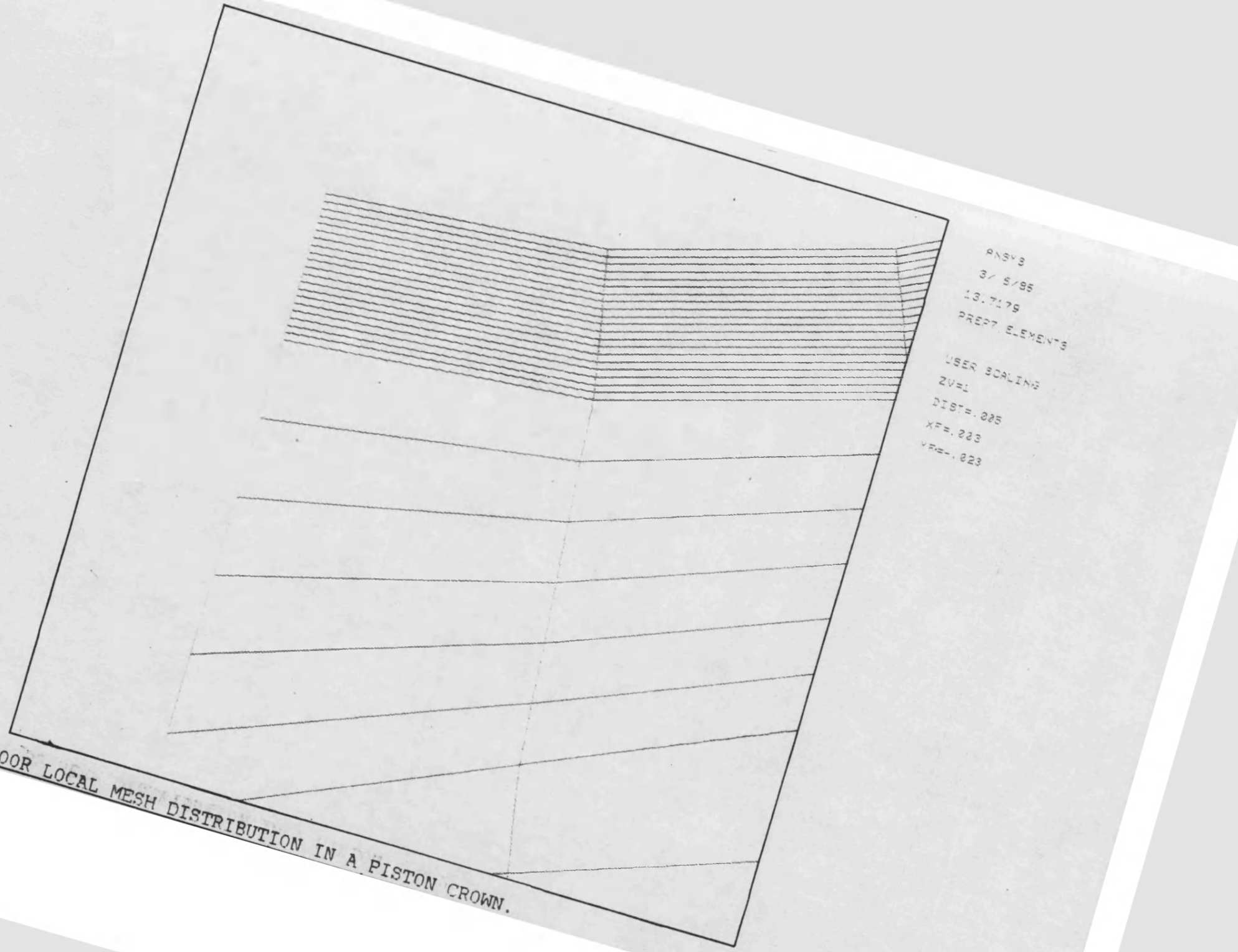

FIGURE 5.14 POOR LOCAL MESH DISTRIBUTION IN A PISTON CROWN.

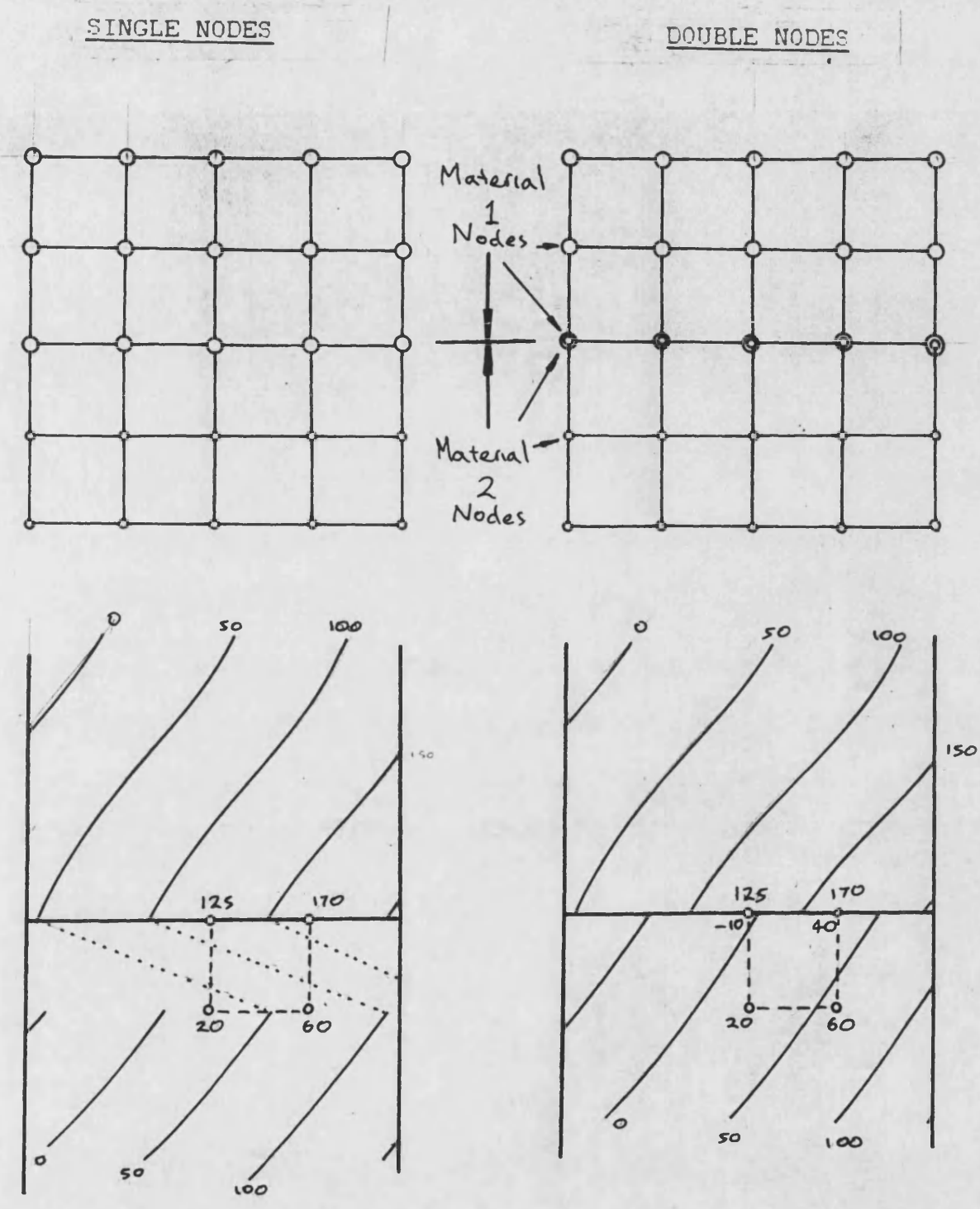

FIGURE 5.15 THE RESULT OF USING SINGLE OR DOUBLE NODES AT A MATERIAL BOUNDARY.

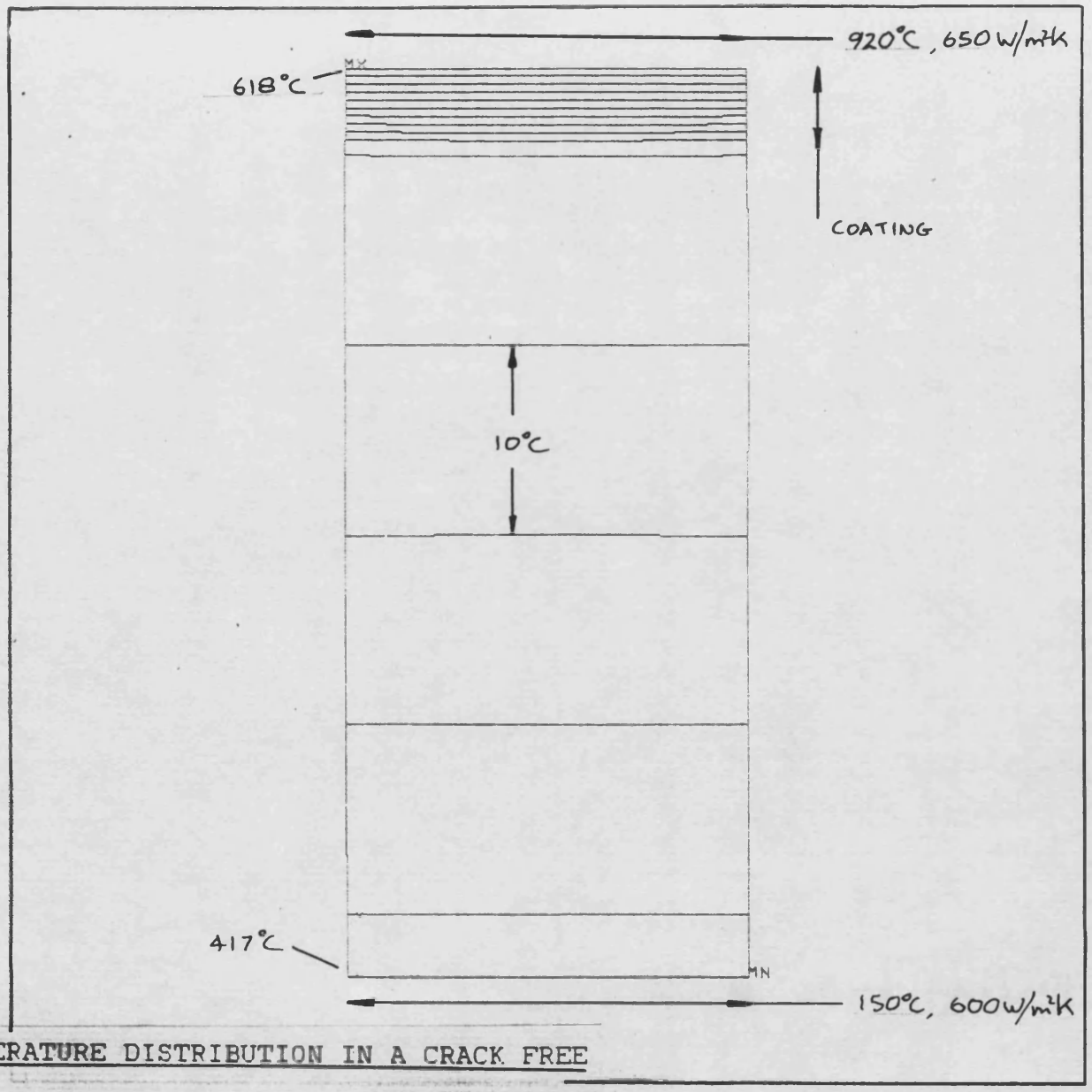

FIGURE 5.16 TEMPERATURE DISTRIBUTION IN A CRACK FREE ZIRCONIA COATING.

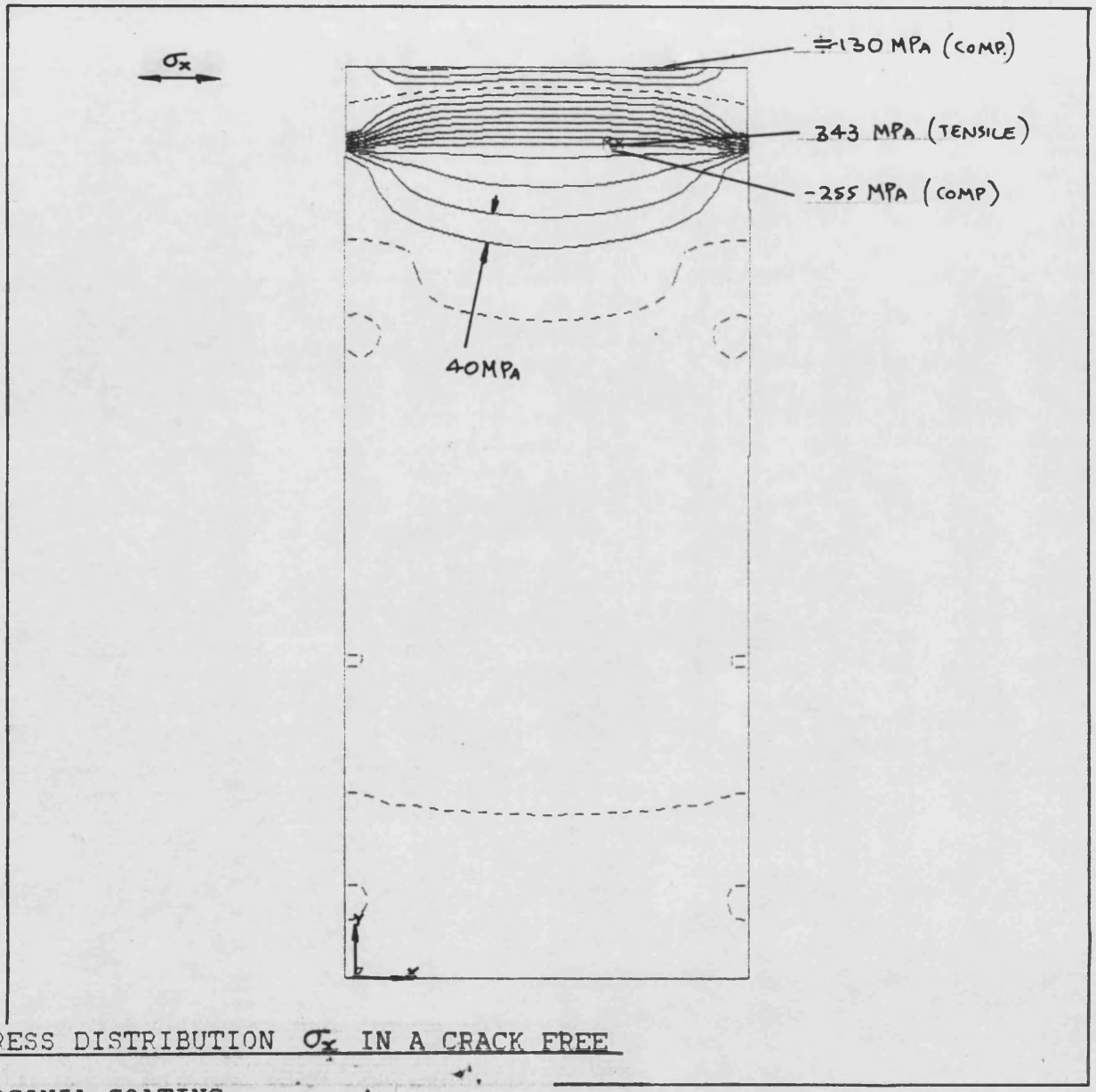

FIGURE 5.17 STRESS DISTRIBUTION σ_x IN A CRACK FREE ZIRCONIA COATING.

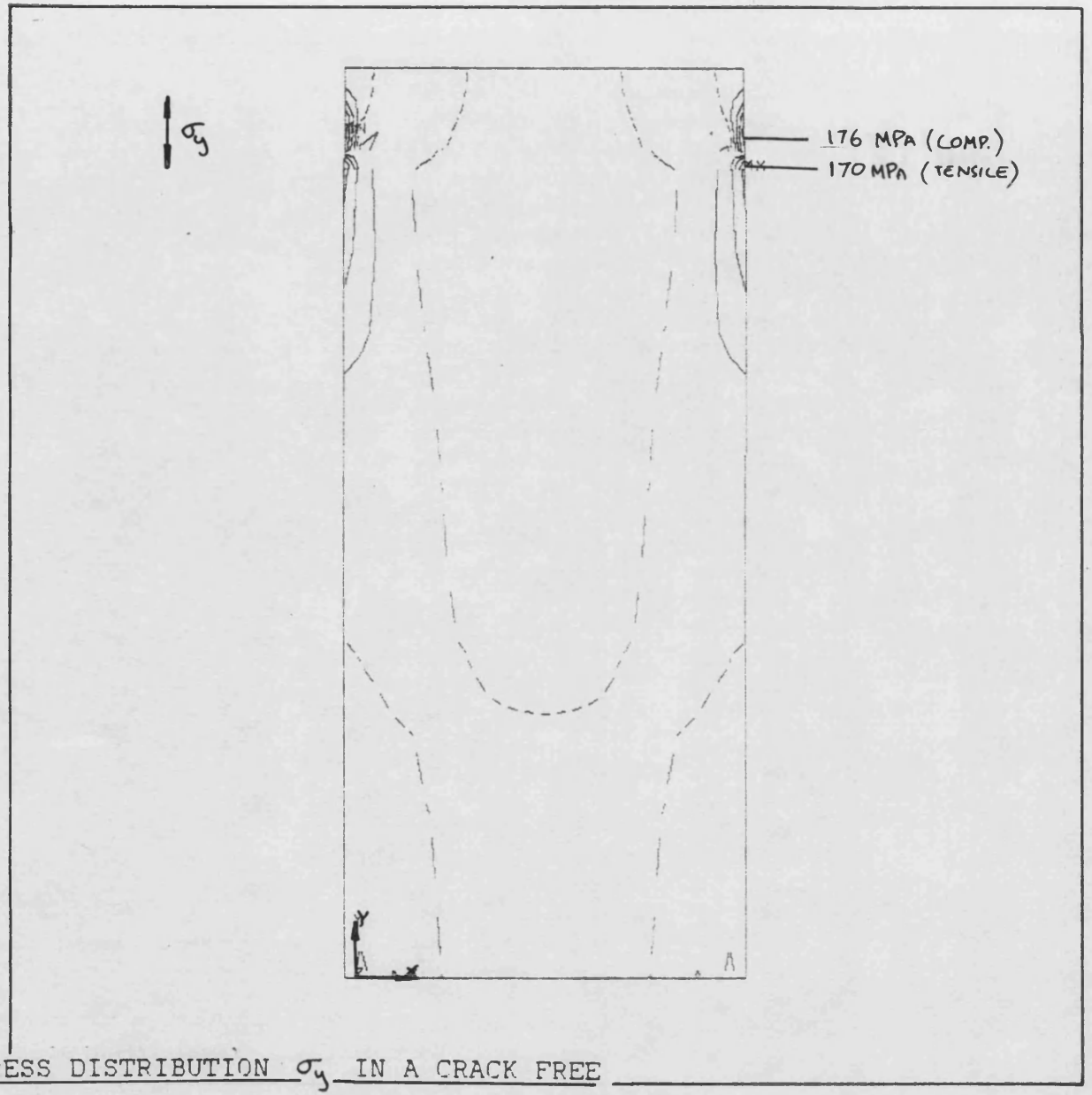

FIGURE 5.18 STRESS DISTRIBUTION σ_y IN A CRACK FREE ZIRCONIA COATING.

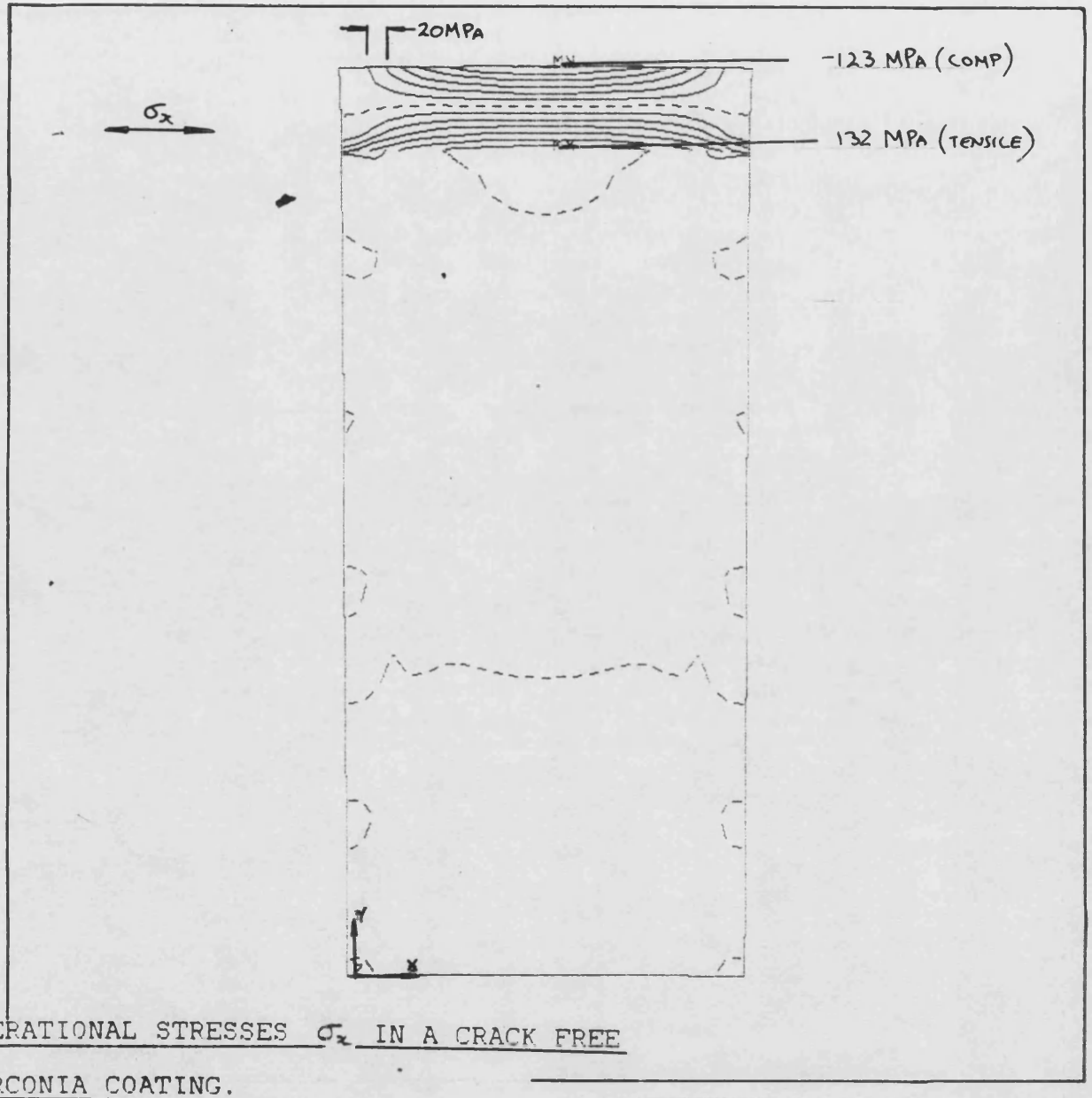

FIGURE 5.19 OPERATIONAL STRESSES σ_z IN A CRACK FREE ZIRCONIA COATING.

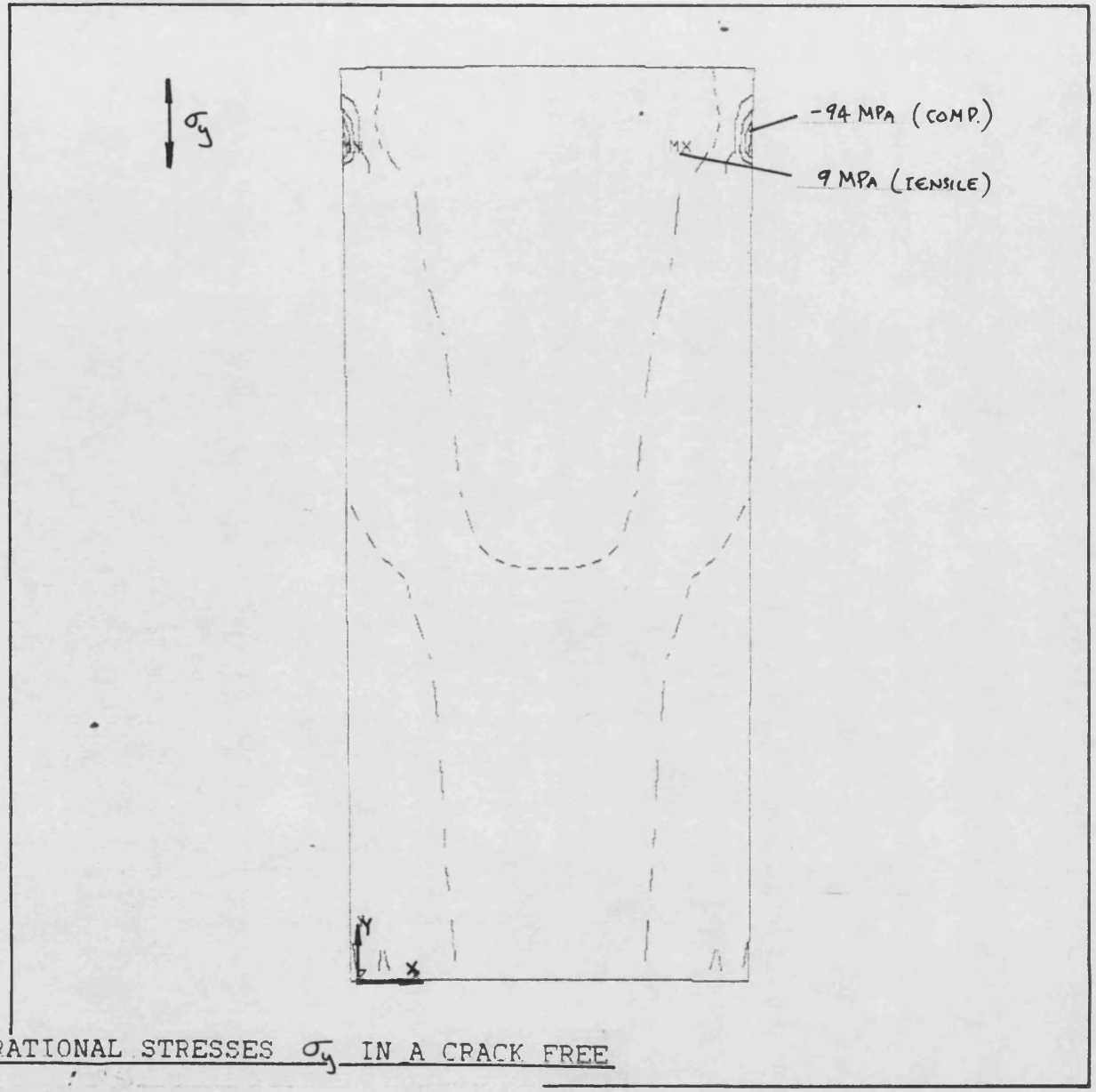

ANSYS
2/ 1/85
14.3544
POST1
STEP=1
ITER=1
STRESS PLOT
SY

USER SCALING
ZV=1
DIST=.007
XF=.2825
YF=.28553
EDGE
MX=58487228
MN=-94622142
INC=20000000

FIGURE 5.20 OPERATIONAL STRESSES σ_y IN A CRACK FREE ZIRCONIA COATING.

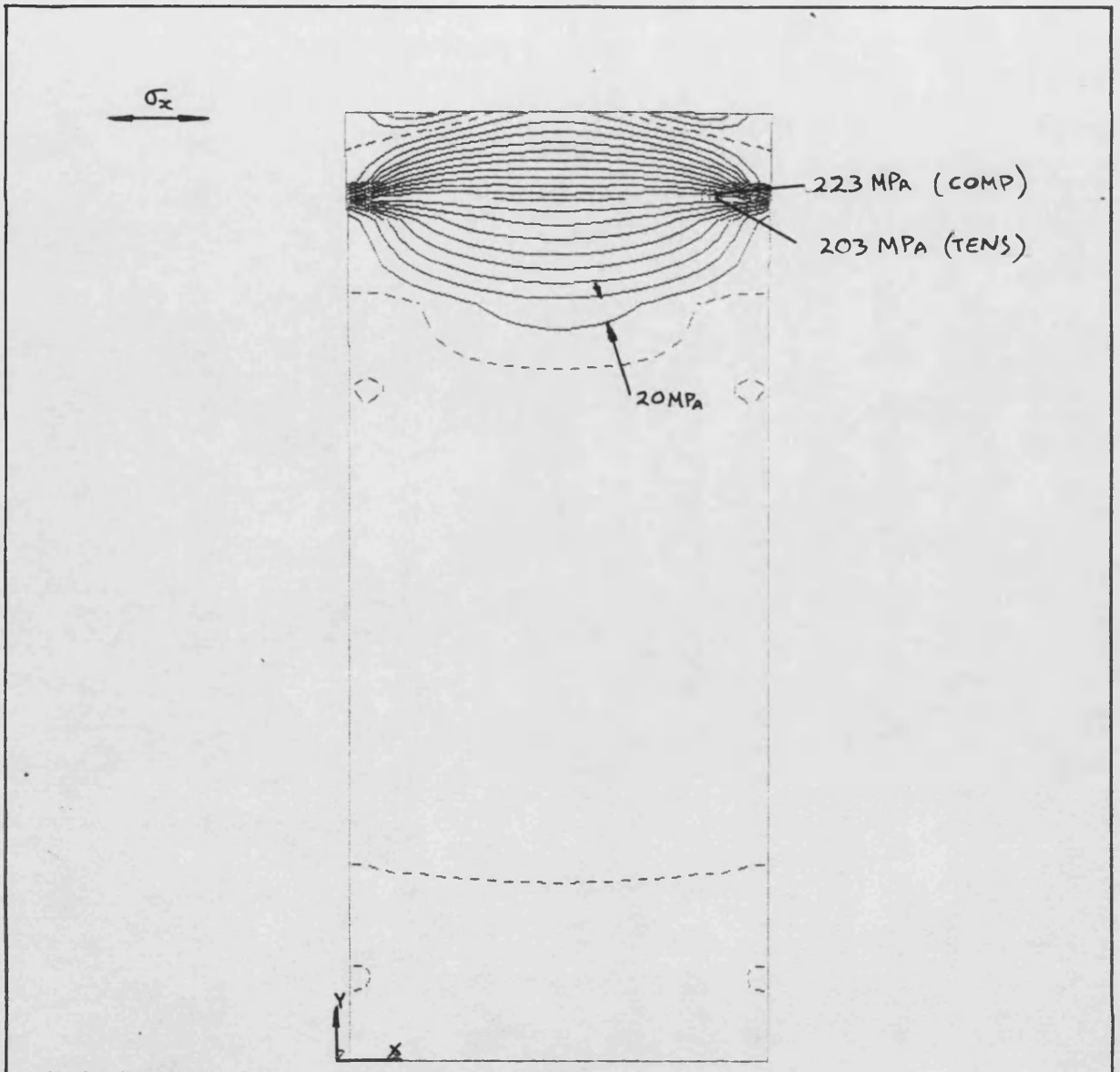

ANSYS
2/ 4/85
16.1742
POST1
STEP=1
ITER=1
STRESS PLOT
SX

AUTO SCALING
ZV=1
DIST=.00619
XF=.0025
YF=.22553
EDGE
MX=223036364
MN=-223634497
INC=20020002

FIGURE 5.21 RESIDUAL STRESSES σ_x IN A CRACK FREE

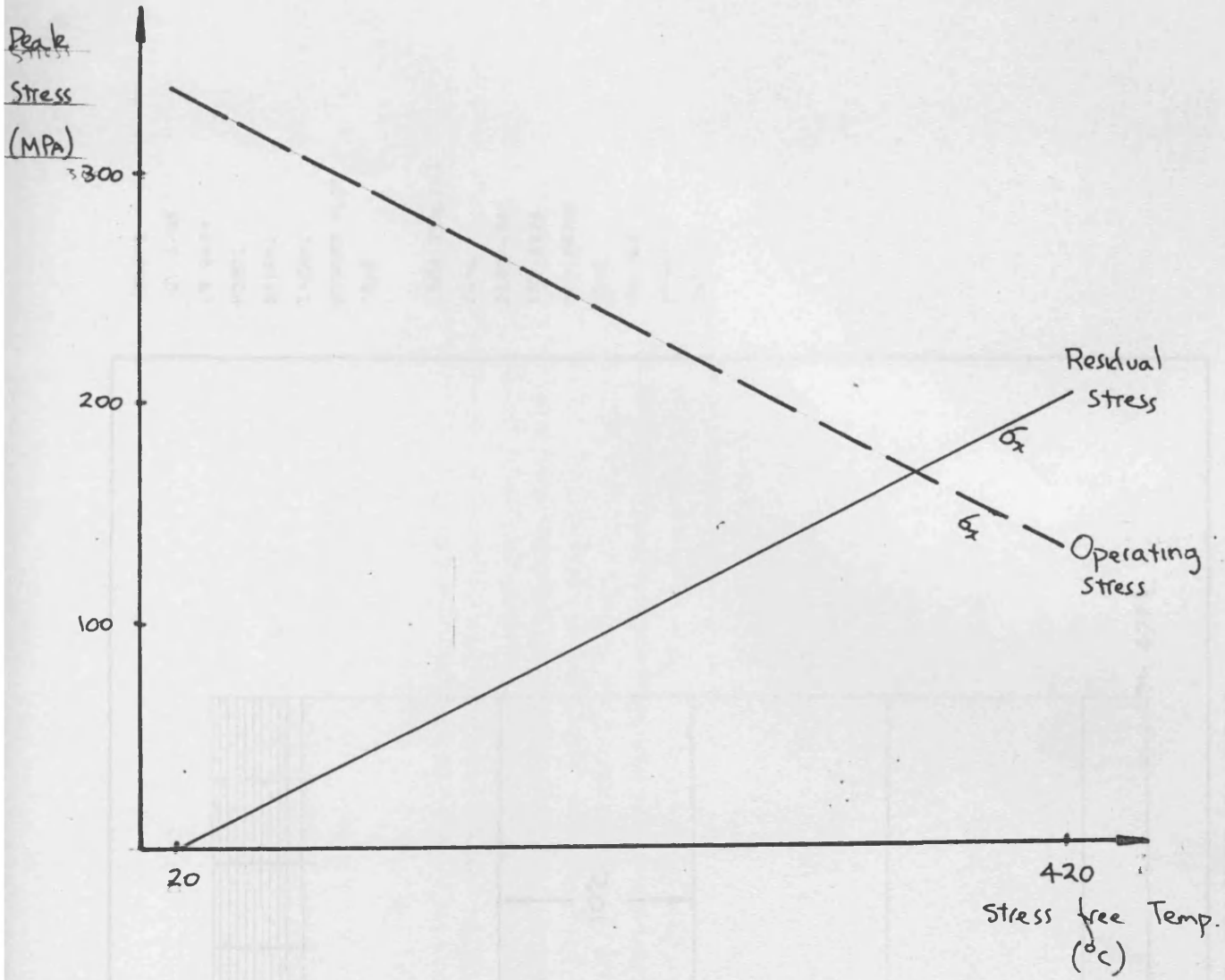

FIGURE 5.22 PEAK STRESSES RECORDED AS A RESULT OF A CHANGE IN STRESS FREE TEMPERATURE.

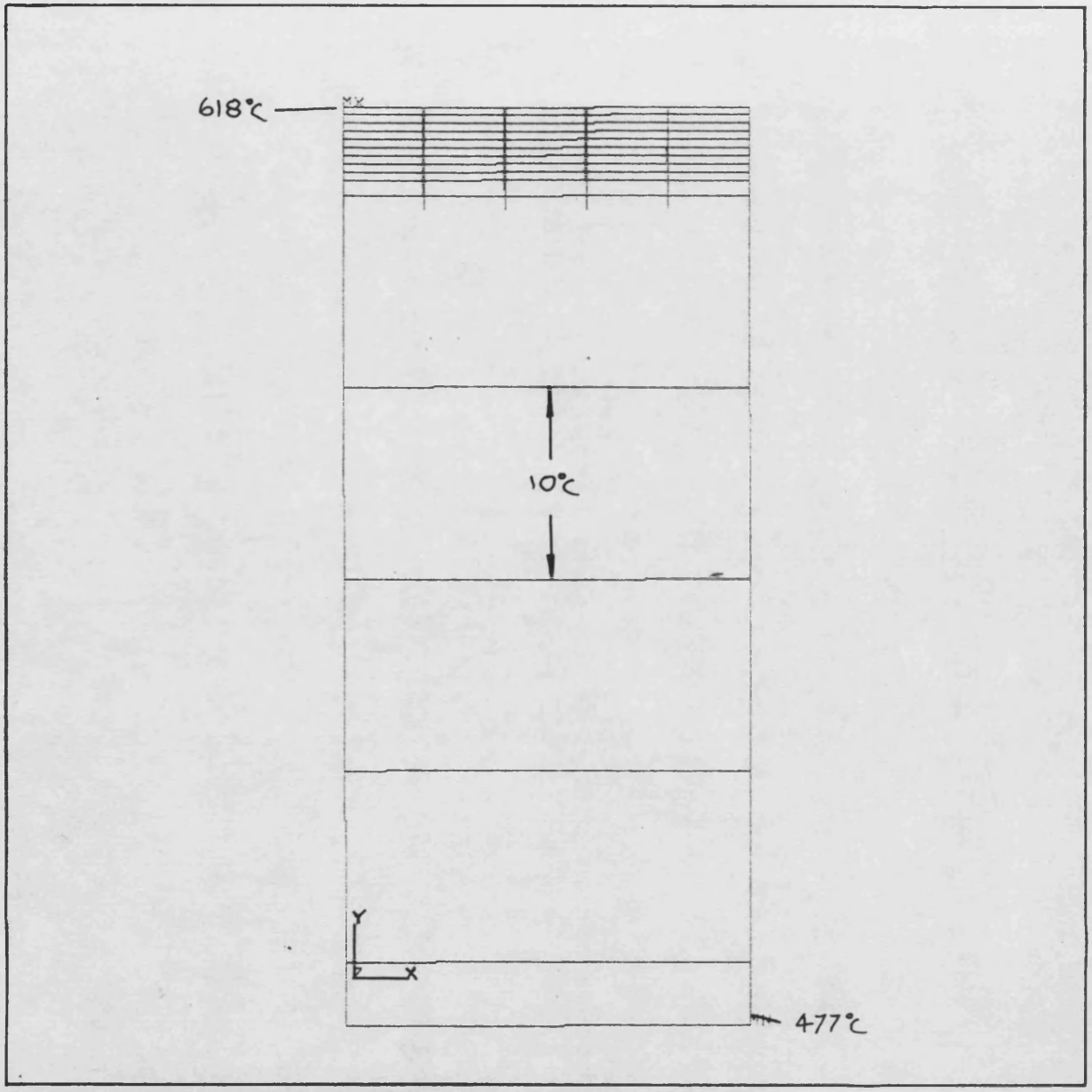

FIGURE 5.23 TEMPERATURE DISTRIBUTION IN A MICRO CRACKED COATING.

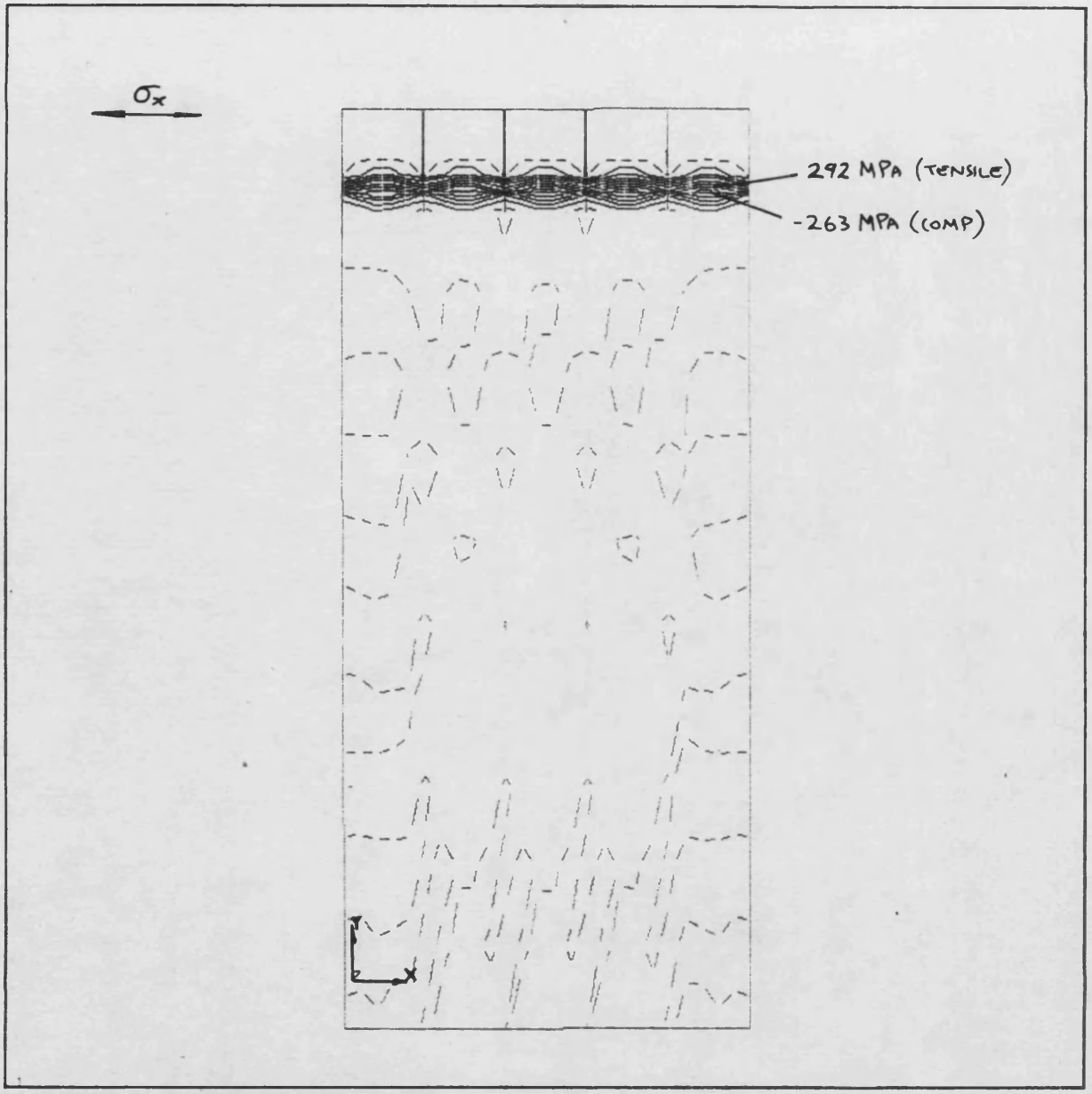

FIGURE 5.24 STRESSES σ_x IN A CRACKED ZIRCONIA COATING.

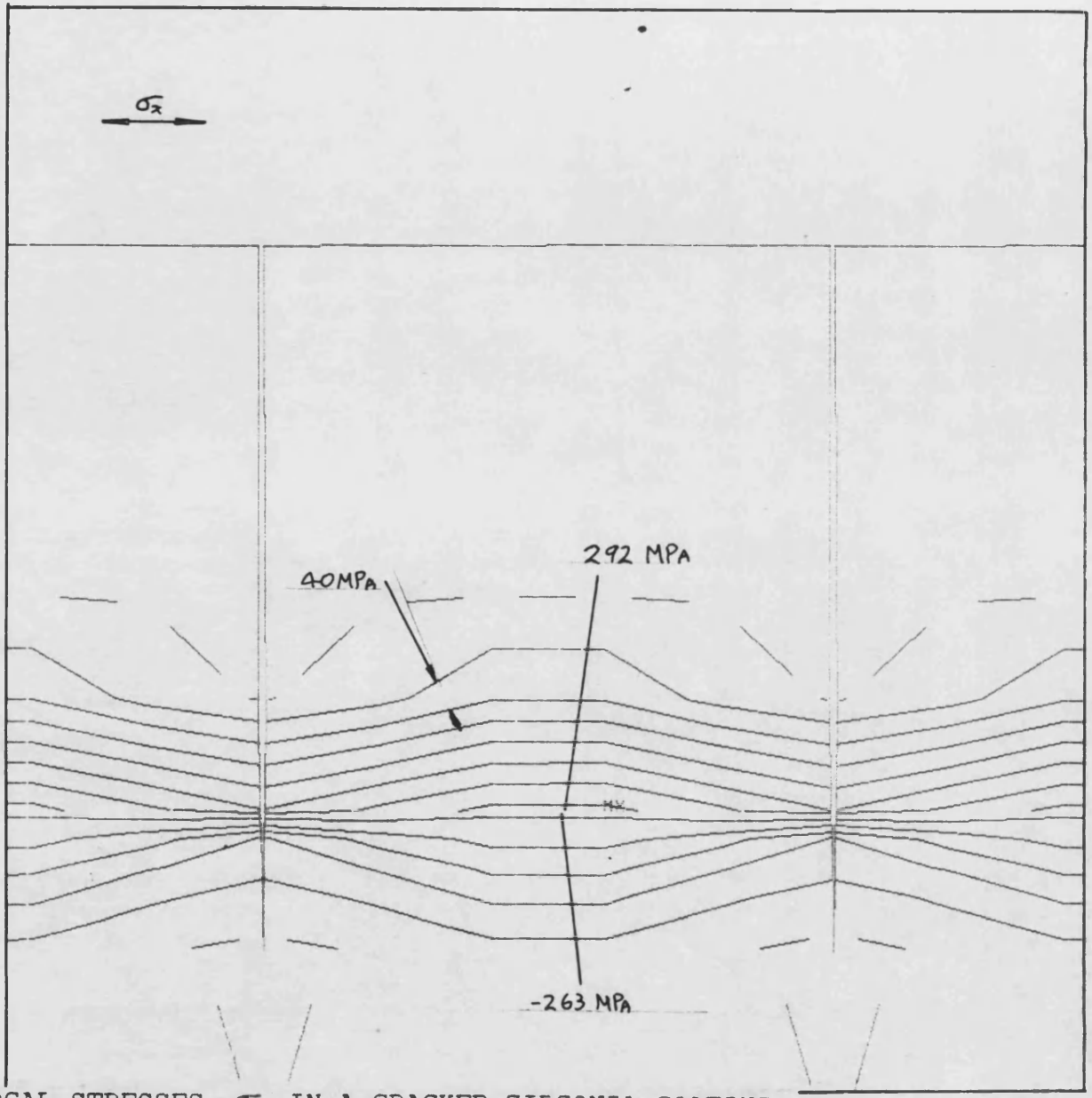

FIGURE 5.25 LOCAL STRESSES σ_x IN A CRACKED ZIRCONIA COATING.

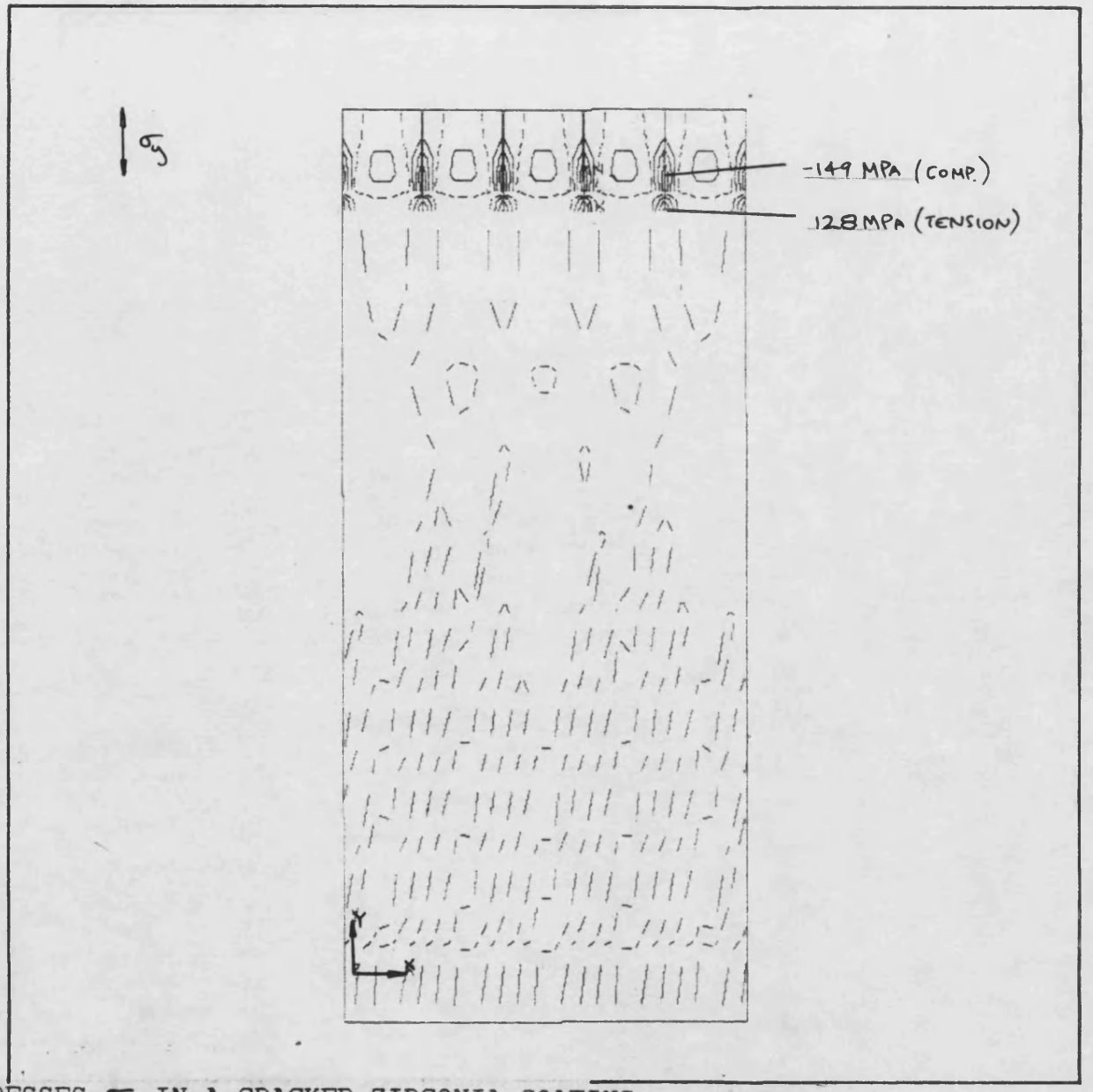

ANSYS
2/ 1/85
15:18:19
POST1
STEP=1
ITER=1
STRESS PLOT
SY

USER SCALING
ZV=1
DIST=.007
XF=.0025
YF=.20553
EDGE
MX=128141245
MN=-149492626
INC=40000200

FIGURE 5.26 STRESSES σ_y IN A CRACKED ZIRCONIA COATING.

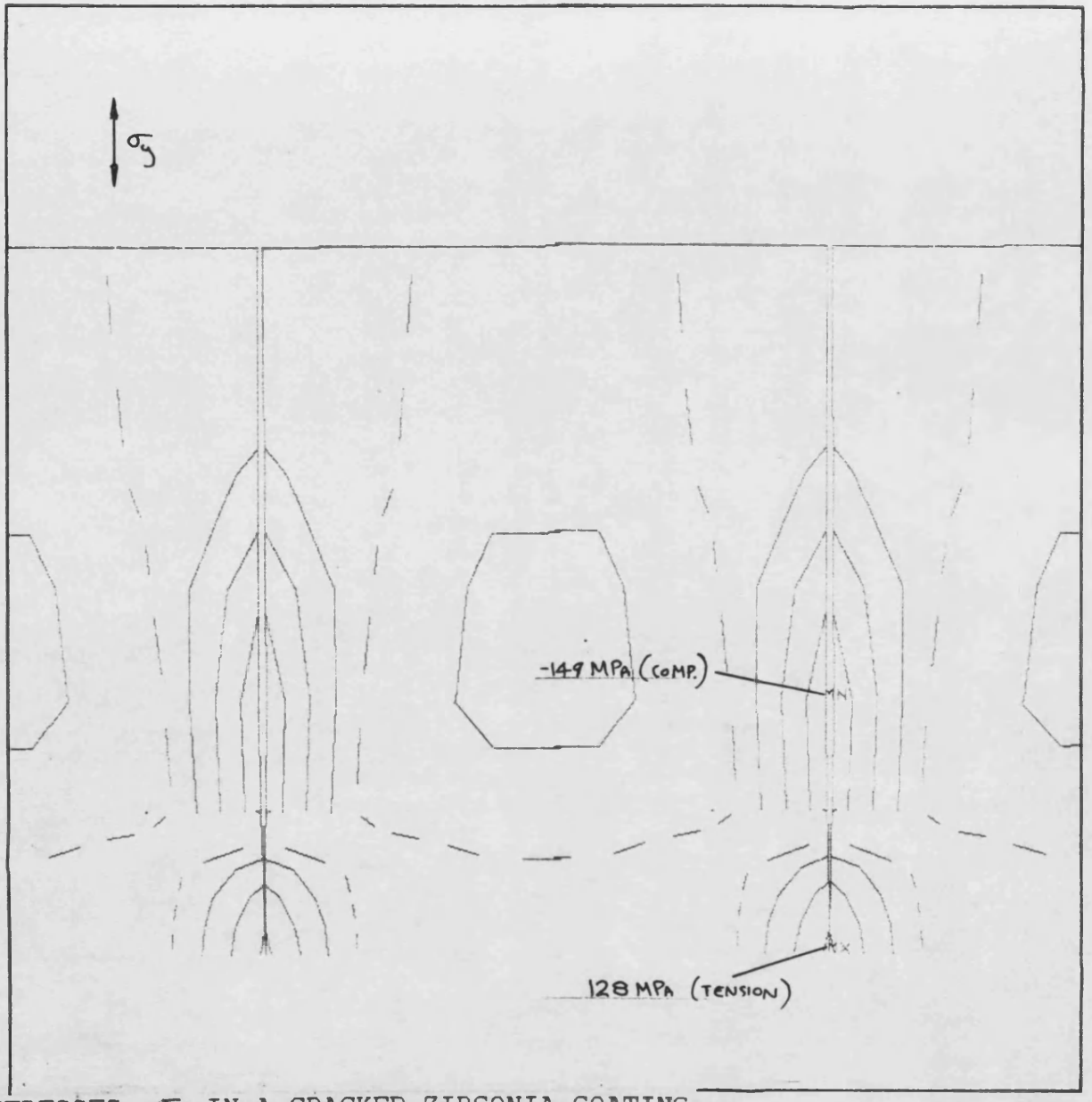

FIGURE 5.27 LOCAL STRESSES σ_y IN A CRACKED ZIRCONIA COATING.

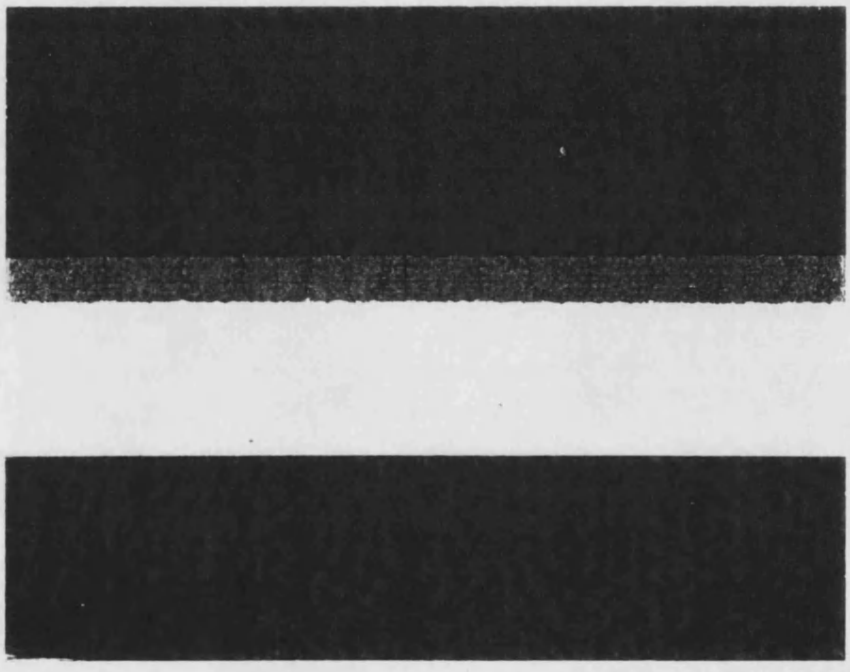

Average spacing = 1·2 mm.

FIGURE 5 28 CRACK DISTRIBUTION

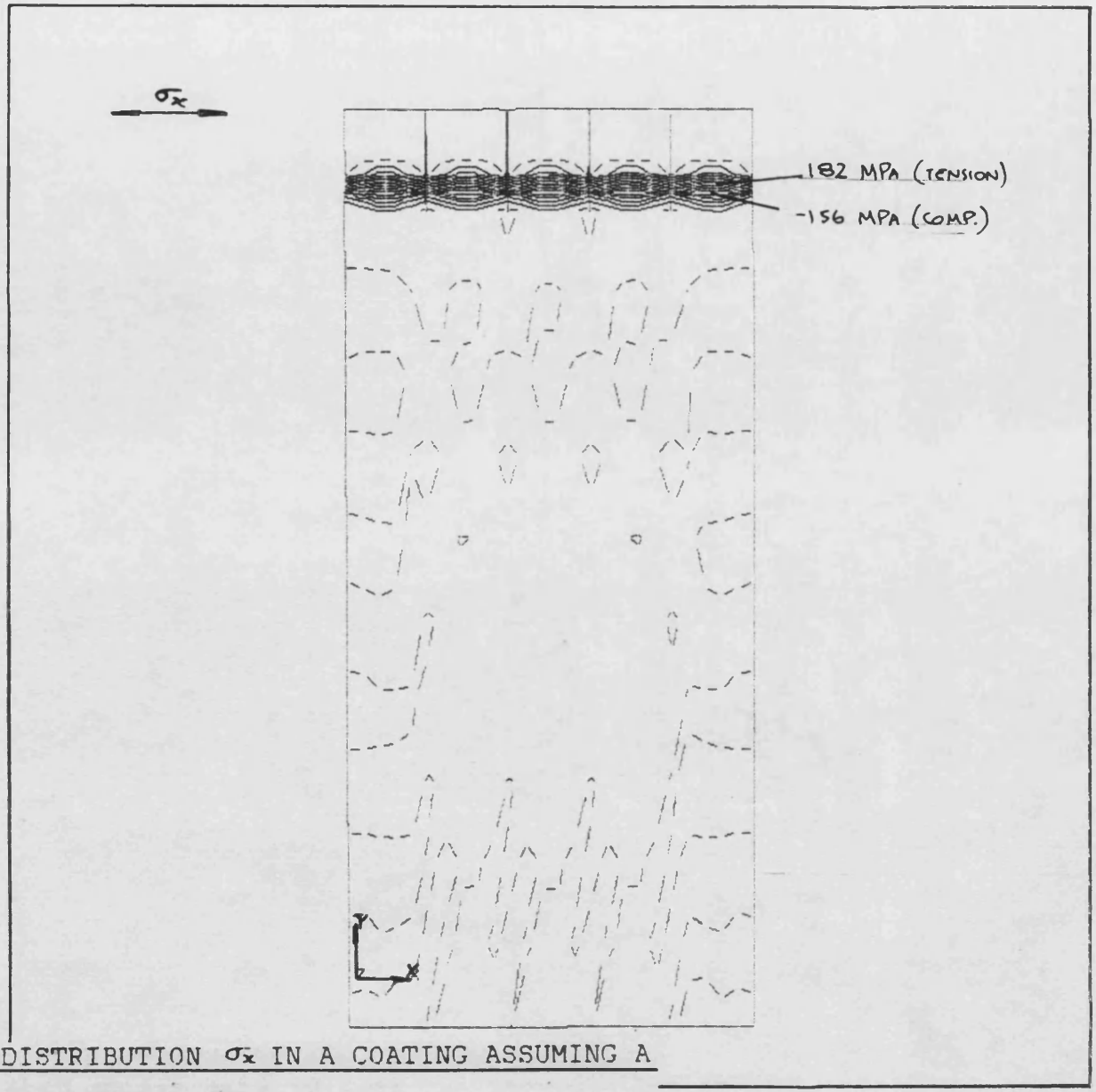

FIGURE 5.29 STRESS DISTRIBUTION σ_x IN A COATING ASSUMING A STRESS FREE TEMPERATURE OF 220C.

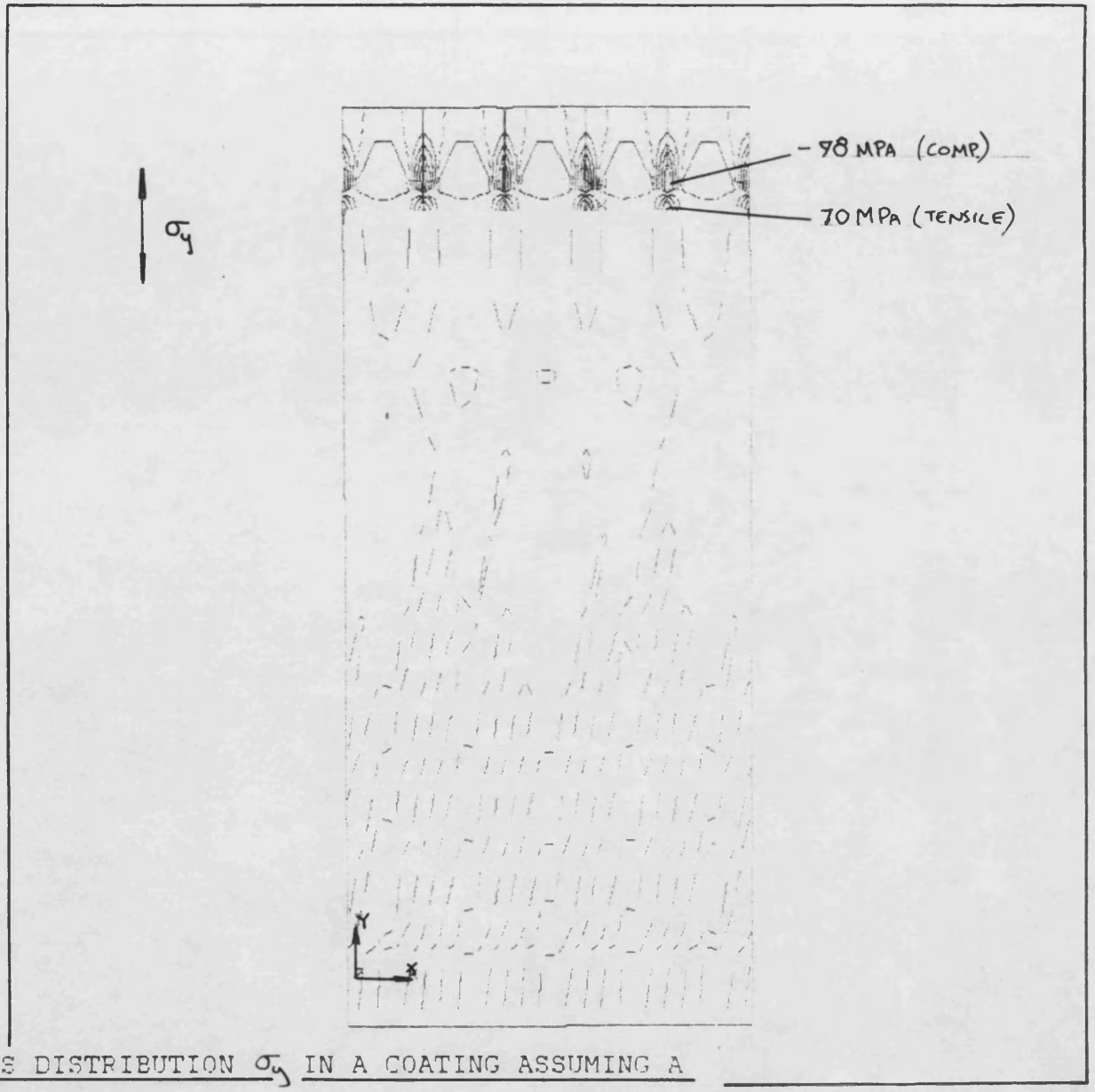

FIGURE 5.30 STRESS DISTRIBUTION σ_y IN A COATING ASSUMING A STRESS FREE TEMPERATURE OF 220C.

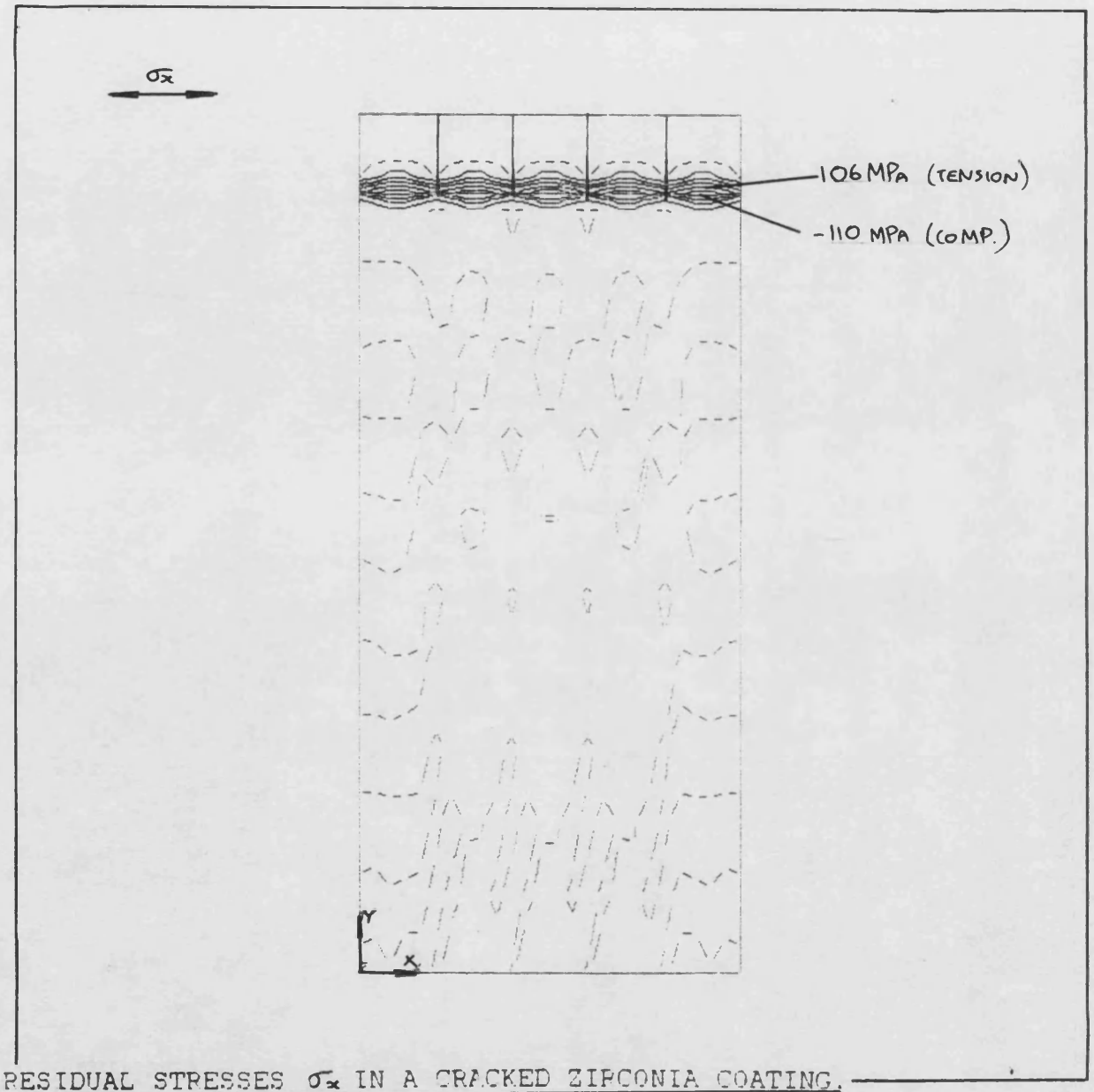

FIGURE 5.31 RESIDUAL STRESSES σ_x IN A CRACKED ZIRCONIA COATING.

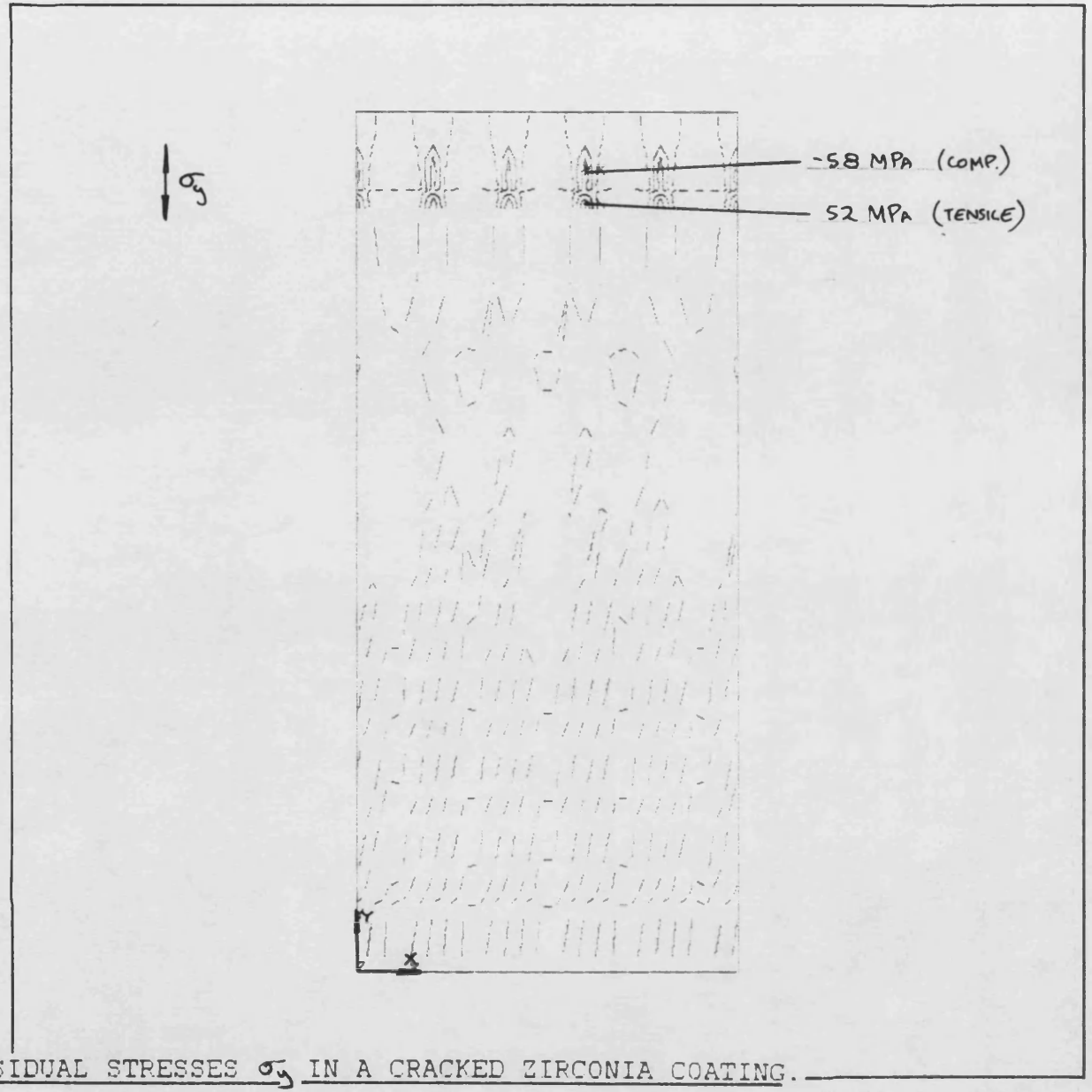

FIGURE 5.32 RESIDUAL STRESSES σ_y IN A CRACKED ZIRCONIA COATING.

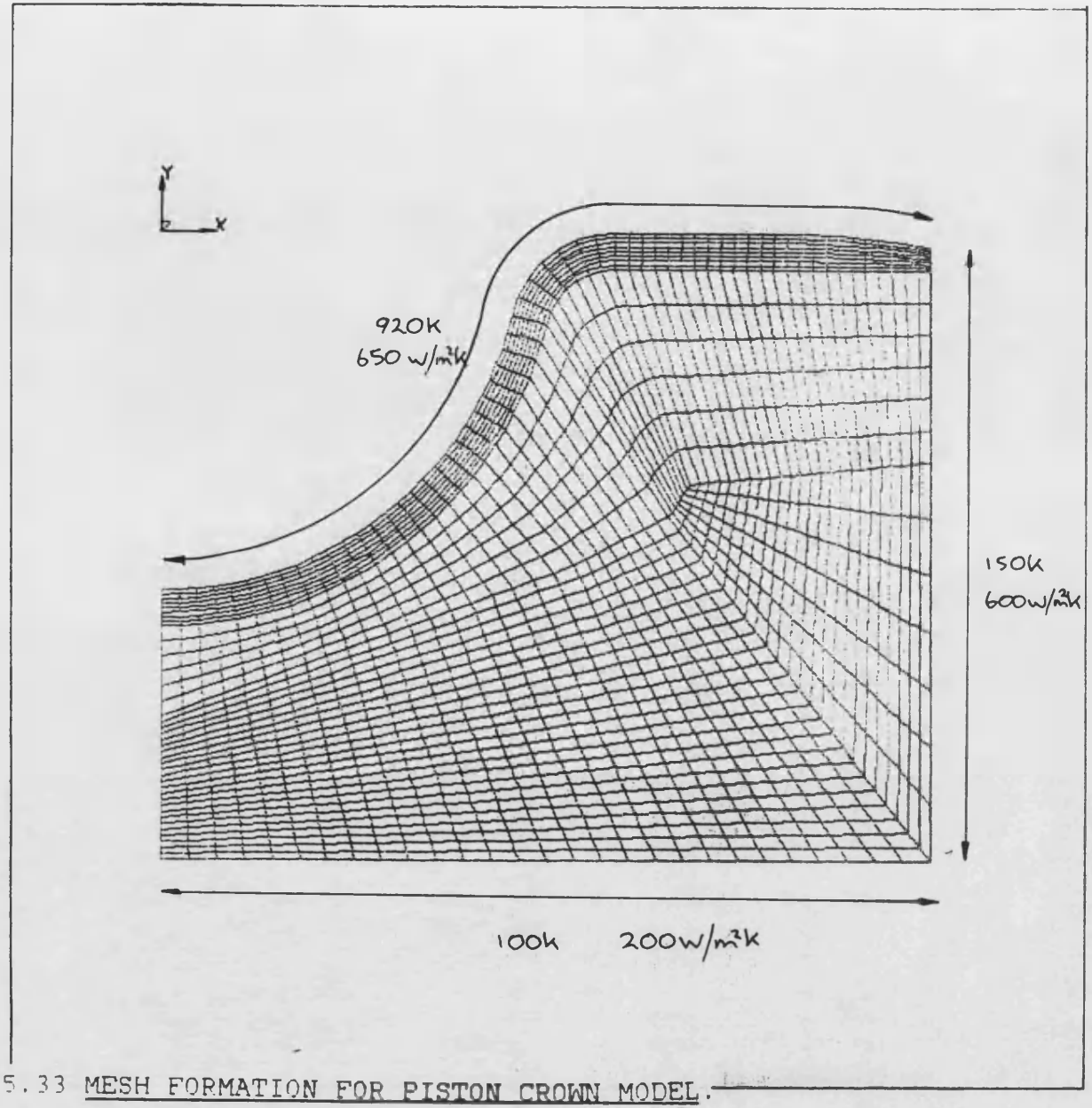

PNSYS
3/ 5/85
13.4655
PREP7 ELEMENTS

USER SCALING
ZV=1
DIST=.83
XF=.2215
YF=-.2175

FIGURE 5.33 MESH FORMATION FOR PISTON CROWN MODEL.

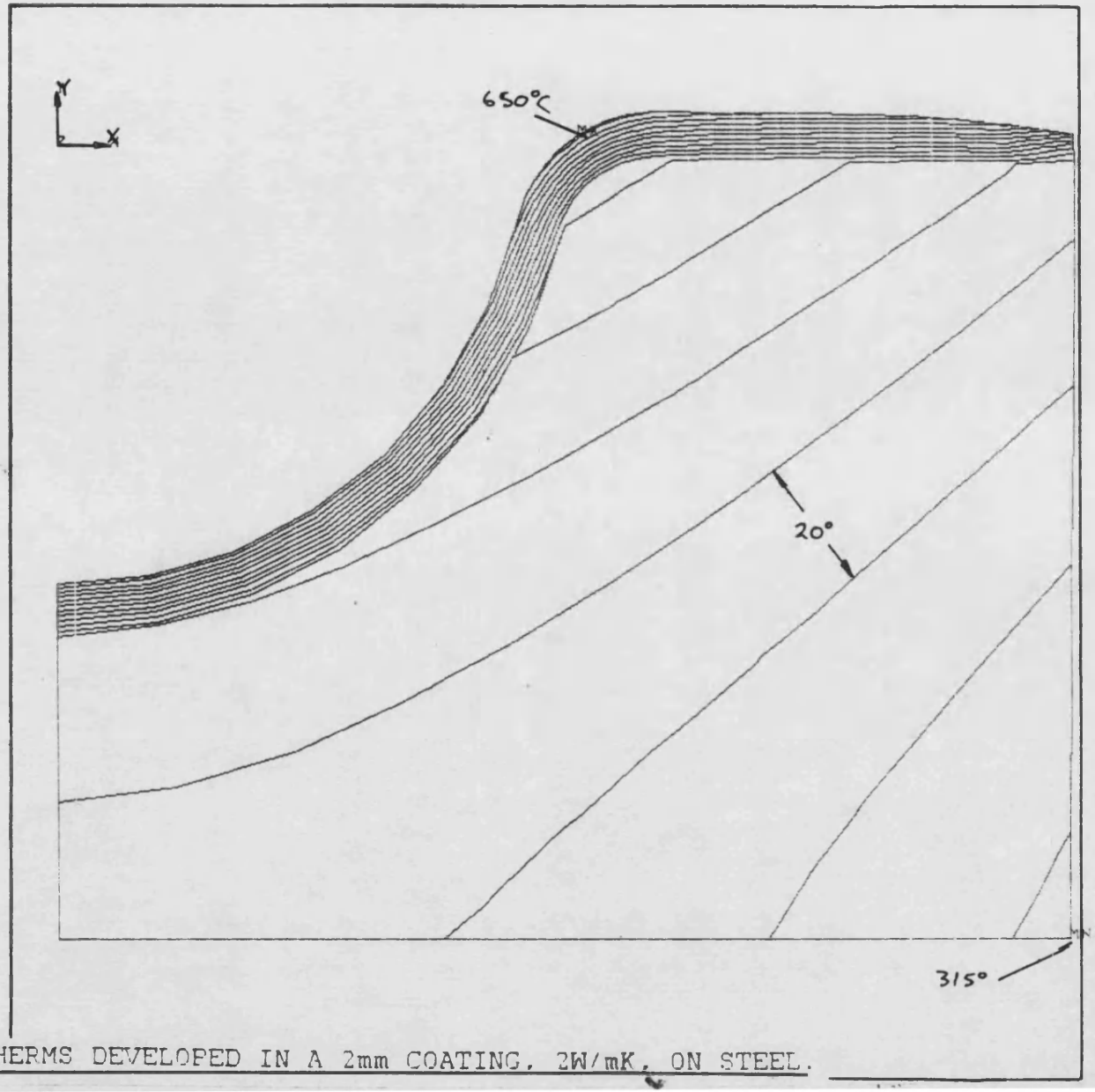

FIGURE 5.34 ISOTHERMS DEVELOPED IN A 2mm COATING, 2W/mK, ON STEEL.

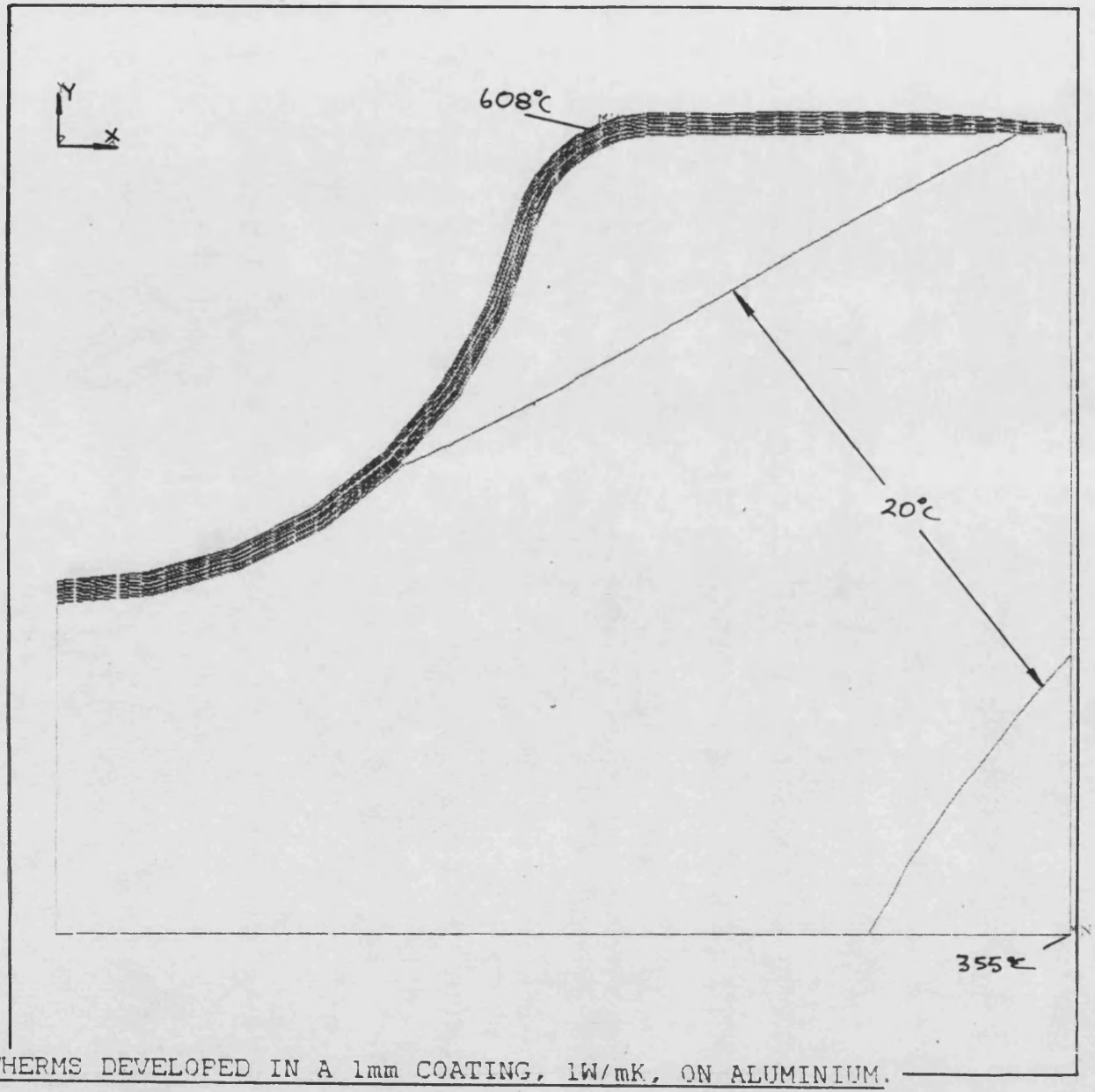

FIGURE 5.35 ISOTHERMS DEVELOPED IN A 1mm COATING, 1W/mK, ON ALUMINIUM.

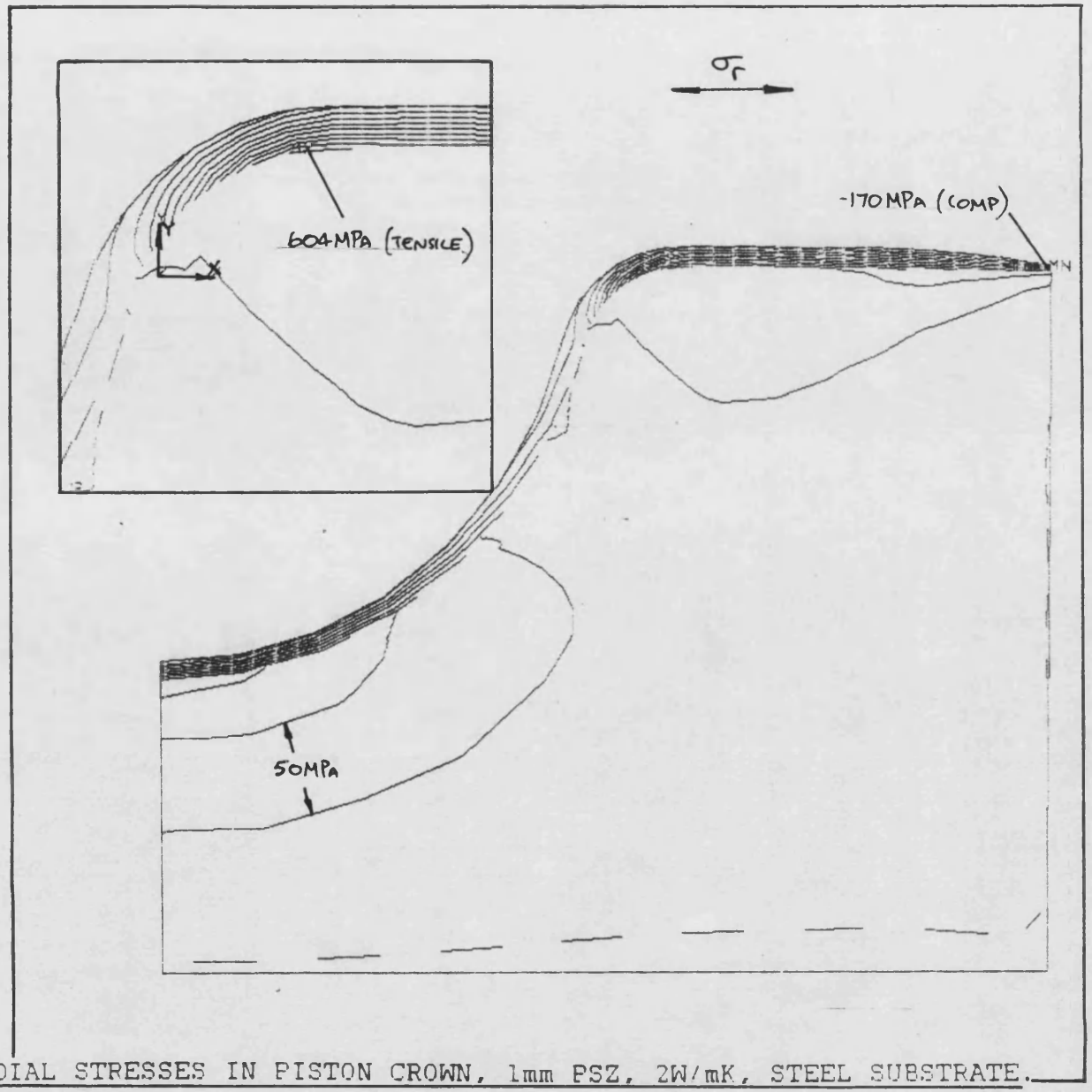

PLOT NO. 1
PNSYS
1/22/85
11.5305
POST1
STEP=1
ITER=1
STRESS PLOT
SX

USER SCALING
ZV=1
DIST=.027
XF=.0195
YF=-.0135
EDGE
MX=604107489
MN=-170495580
INC=50000002

WIND=2
USER SCALING
ZV=1
DIST=.005
XF=.024
YF=-.004
EDGE
MX=504107489
MN=-170495580
INC=50000002

FIGURE 5.36 RADIAL STRESSES IN PISTON CROWN, 1mm PSZ, 2W/mK, STEEL SUBSTRATE.

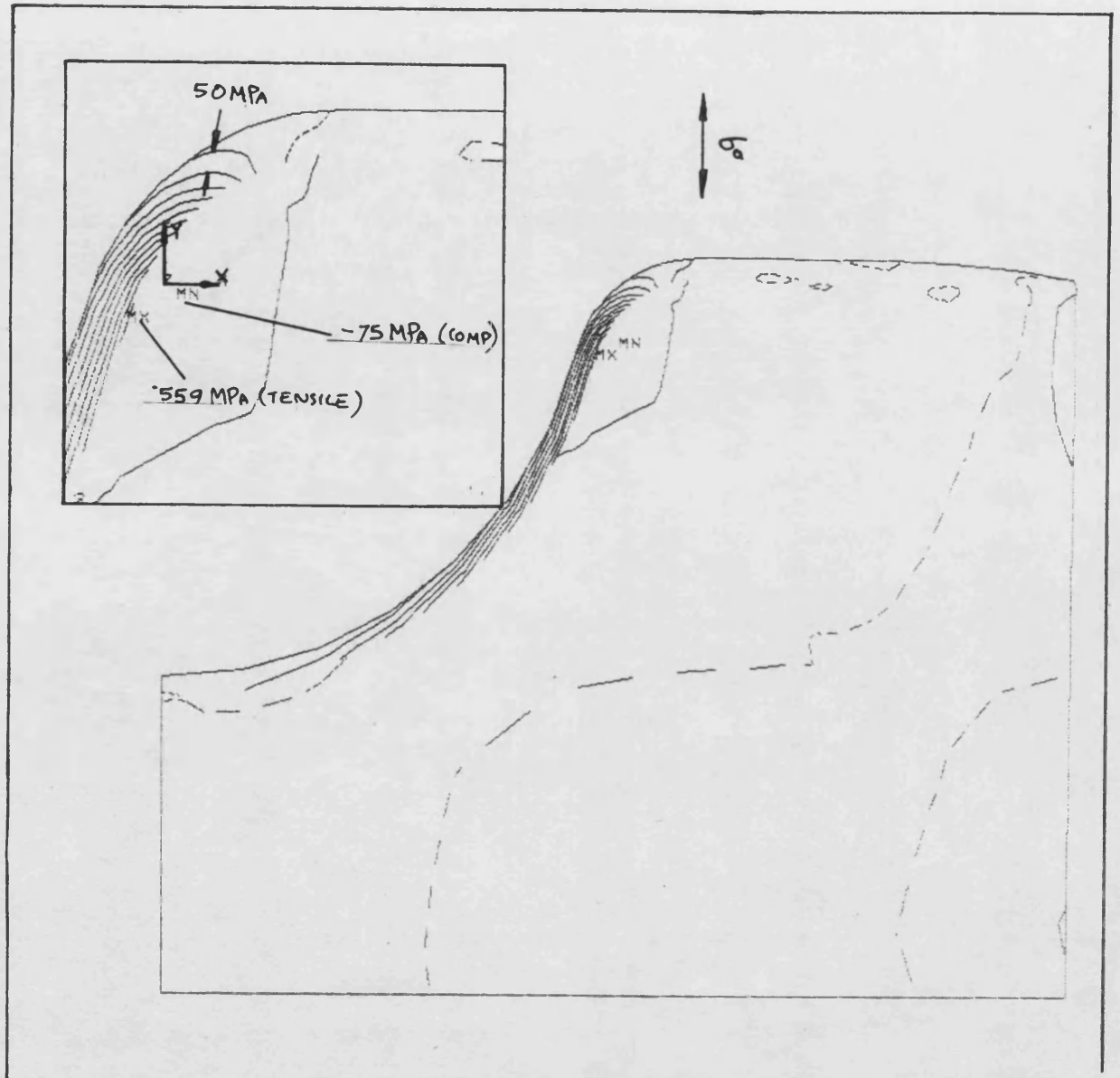

FIGURE 5.37 AXIAL STRESSES IN PISTON CROWN, 1mm PSZ, 2W/mK, STEEL SUBSTRATE.

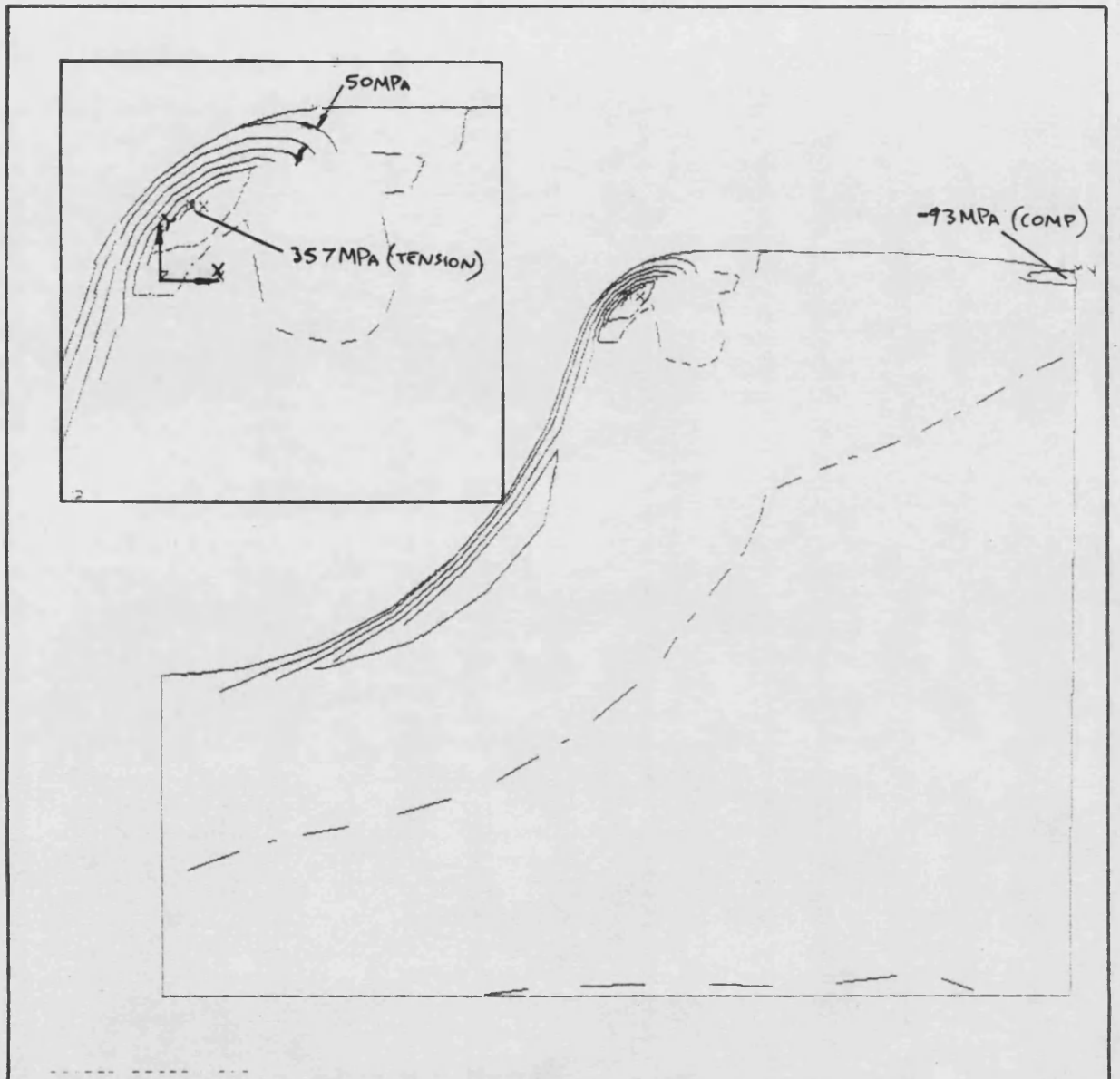

FIGURE 5.38 SHEAR STRESSES IN PISTON CROWN, 1mm PSZ, 2W/mK, STEEL SUBSTATE.

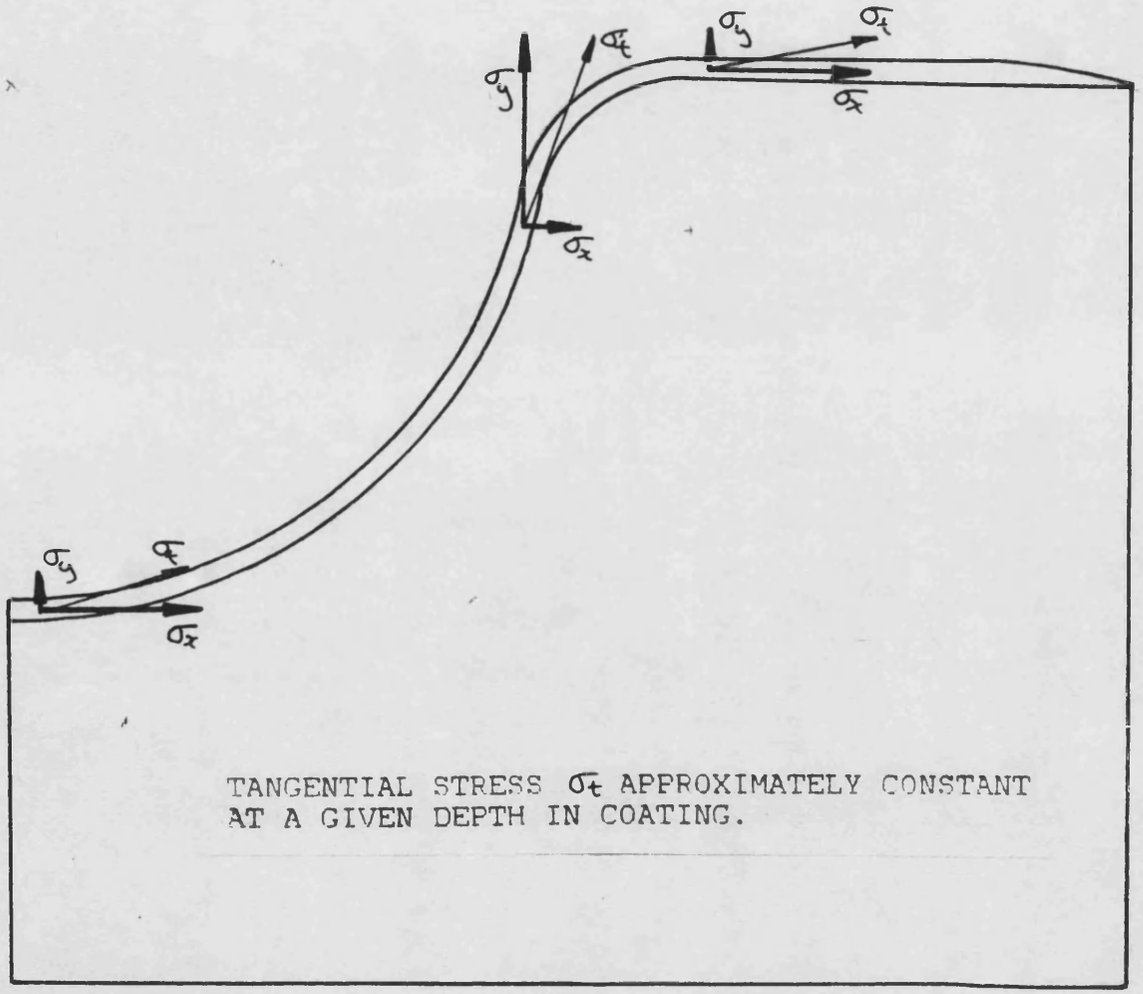

FIGURE 5.39 GENERAL STRESS DISTRIBUTION IN PISTON CROWN.

FIGURE 5.40 TEMPERATURE DISTRIBUTION IN POROUS AND NON-POROUS MATERIALS.

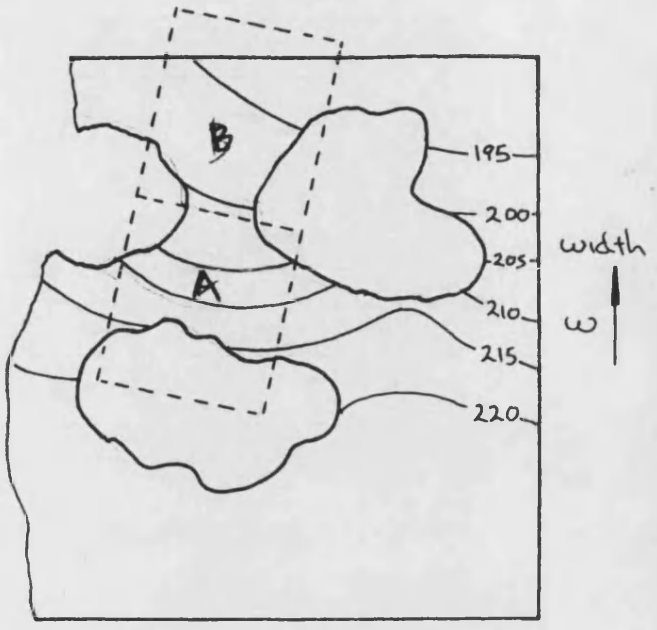

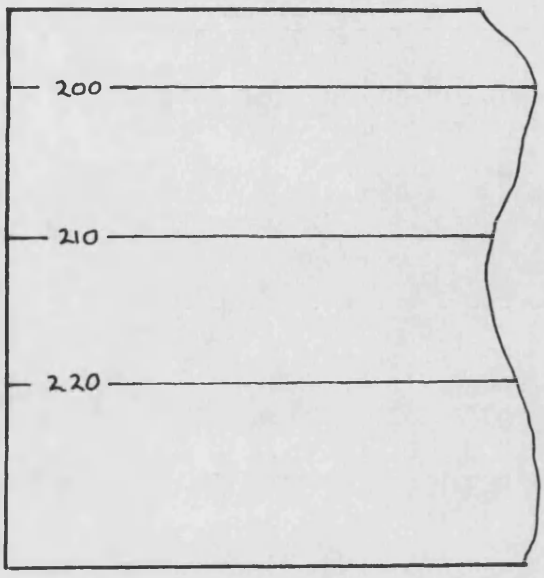

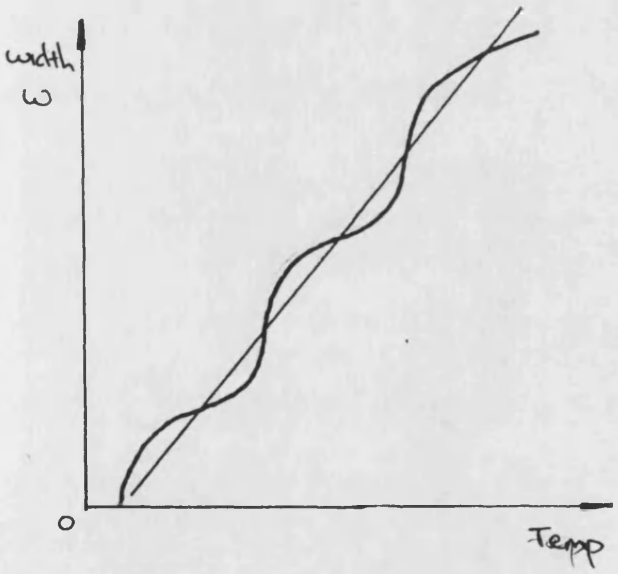

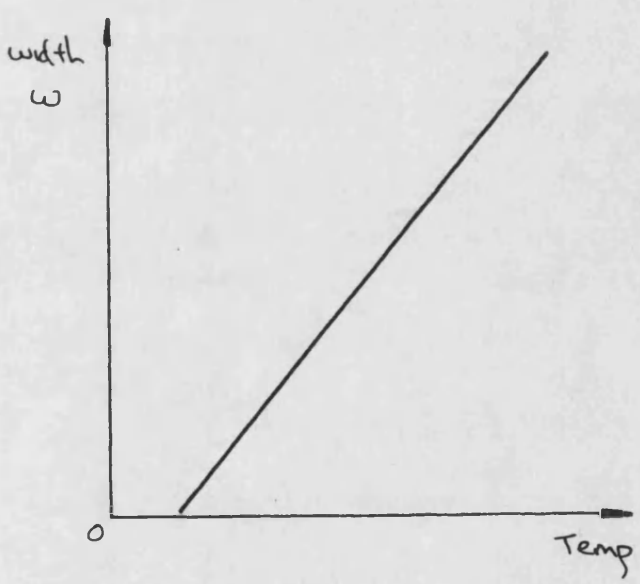

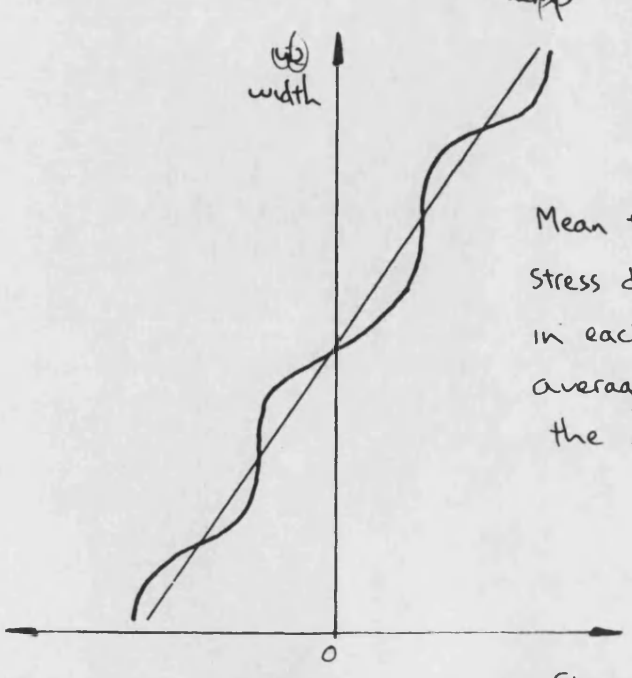

Mean temperature and stress distribution same in each case if average thermal conductivity the same.

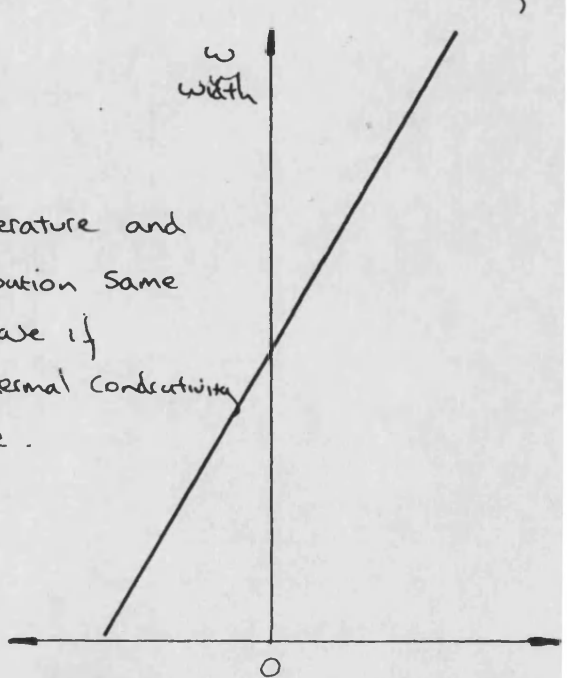

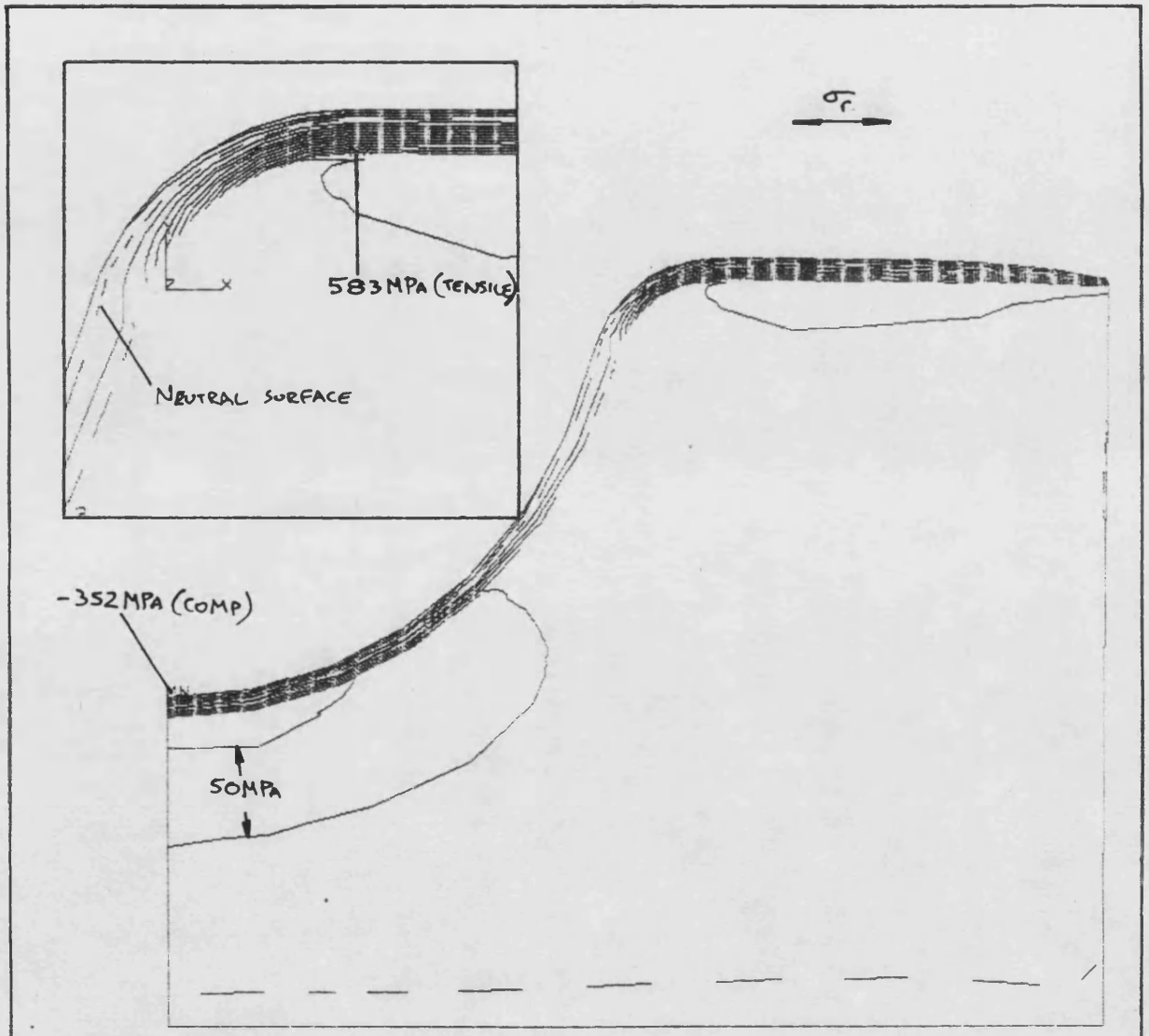

PLOT NO. 1
NODAL SOLUTION
STEP=1
ITER=1
RADIAL STRESS
SX

USER SCALING
ZV=1
DIST=.027
XF=.2195
YF=-.0135
EDGE
MX=583811729
MN=-352430816
INC=50000002

WIND=2
USER SCALING
ZV=1
DIST=.005
XF=.024
YF=-.004
EDGE
MX=583811729
MN=-352430816
INC=50000002

FIGURE 5.41 RADIAL STRESSES IN PISTON CROWN, 1mm PSZ, 1W/mK, STEEL BASE.

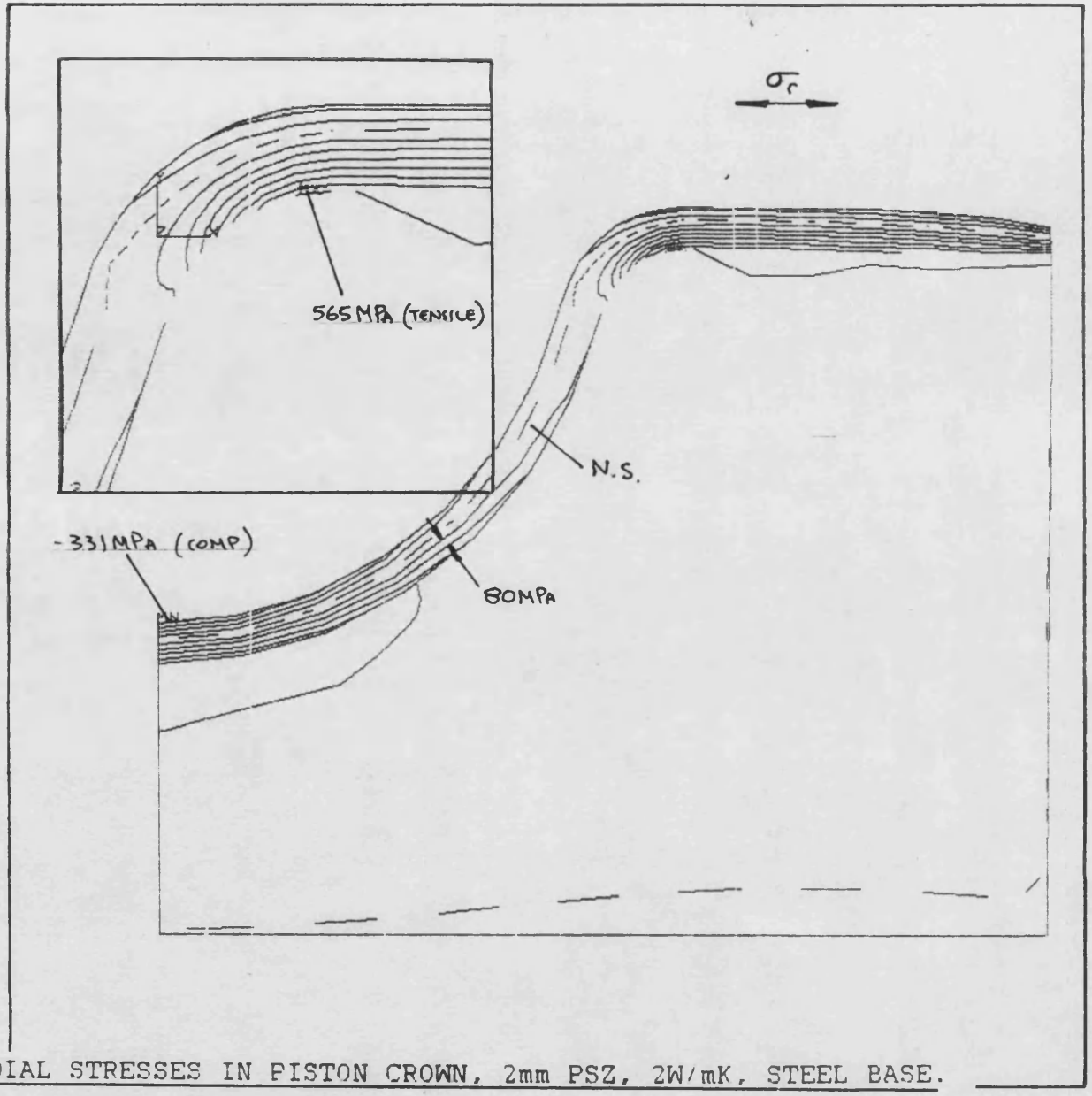

FIGURE 5.42 RADIAL STRESSES IN PISTON CROWN, 2mm PSZ, 2W/mK, STEEL BASE.

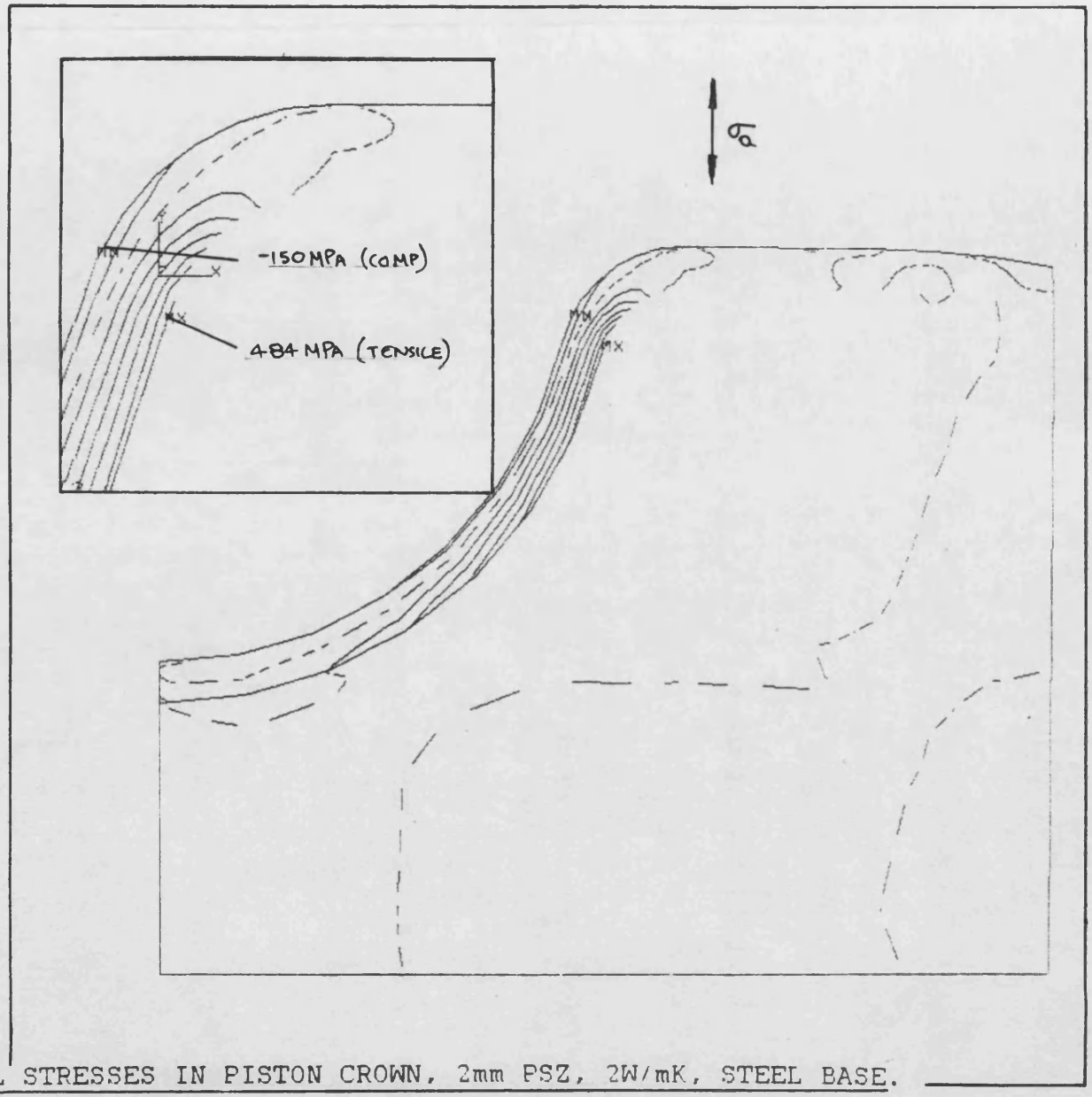

ANSYS
1/15/85
22.2186
POST1
STEP=1
ITER=1
STRESS PLOT
SY

USER SCALING
ZV=1
DIST=.027
XF=.0195
YF=-.0135
EDGE
MX=483555771
MN=-150027623
INC=80000000

WIND=2
USER SCALING
ZV=1
DIST=.005
XF=.224
YF=-.004
EDGE
MX=483555771
MN=-150027623
INC=80000000

FIGURE 5.43 AXIAL STRESSES IN PISTON CROWN, 2mm PSZ, 2W/mK, STEEL BASE.

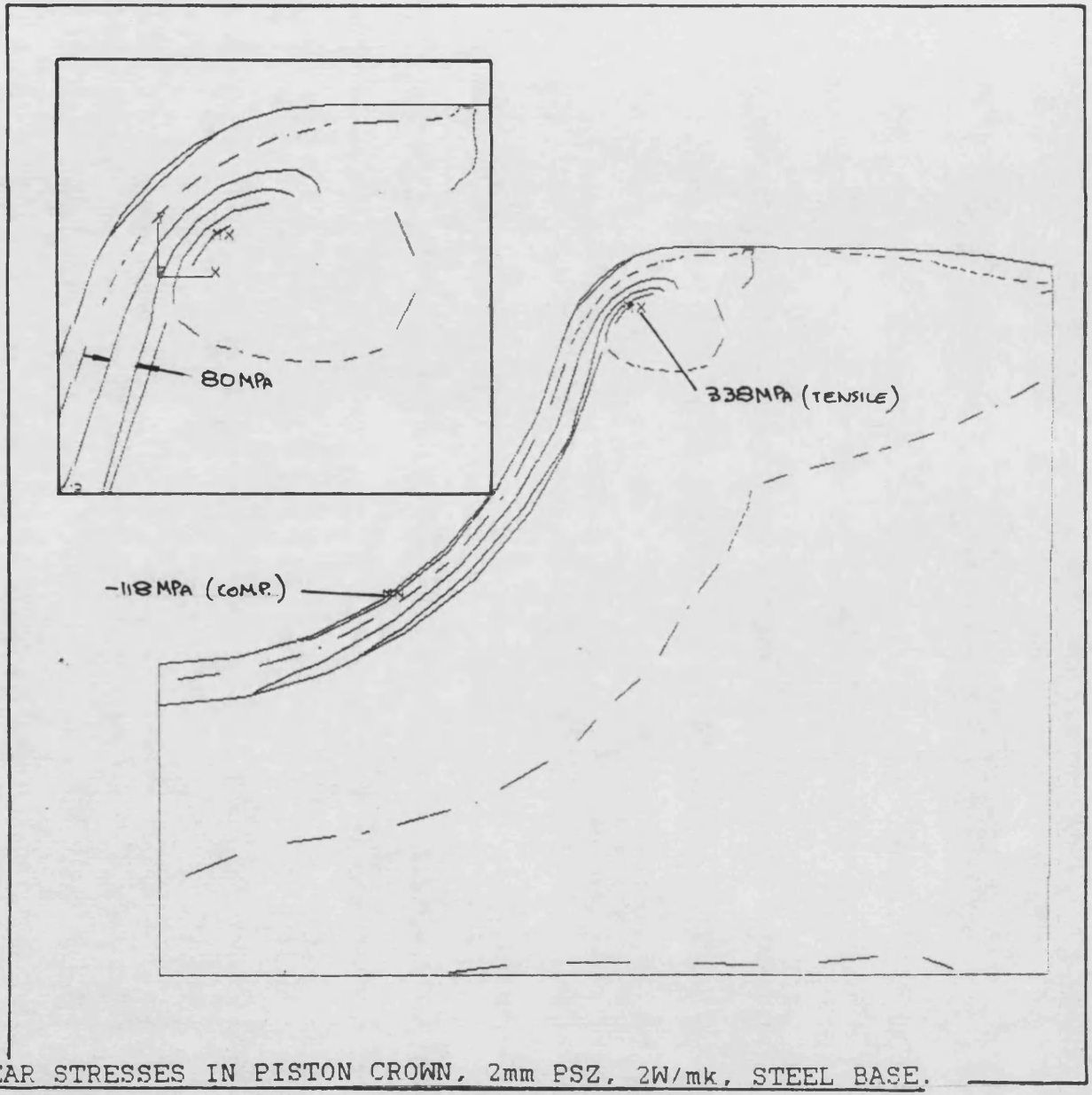

FIGURE 5.44 SHEAR STRESSES IN PISTON CROWN, 2mm PSZ, 2W/mk, STEEL BASE.

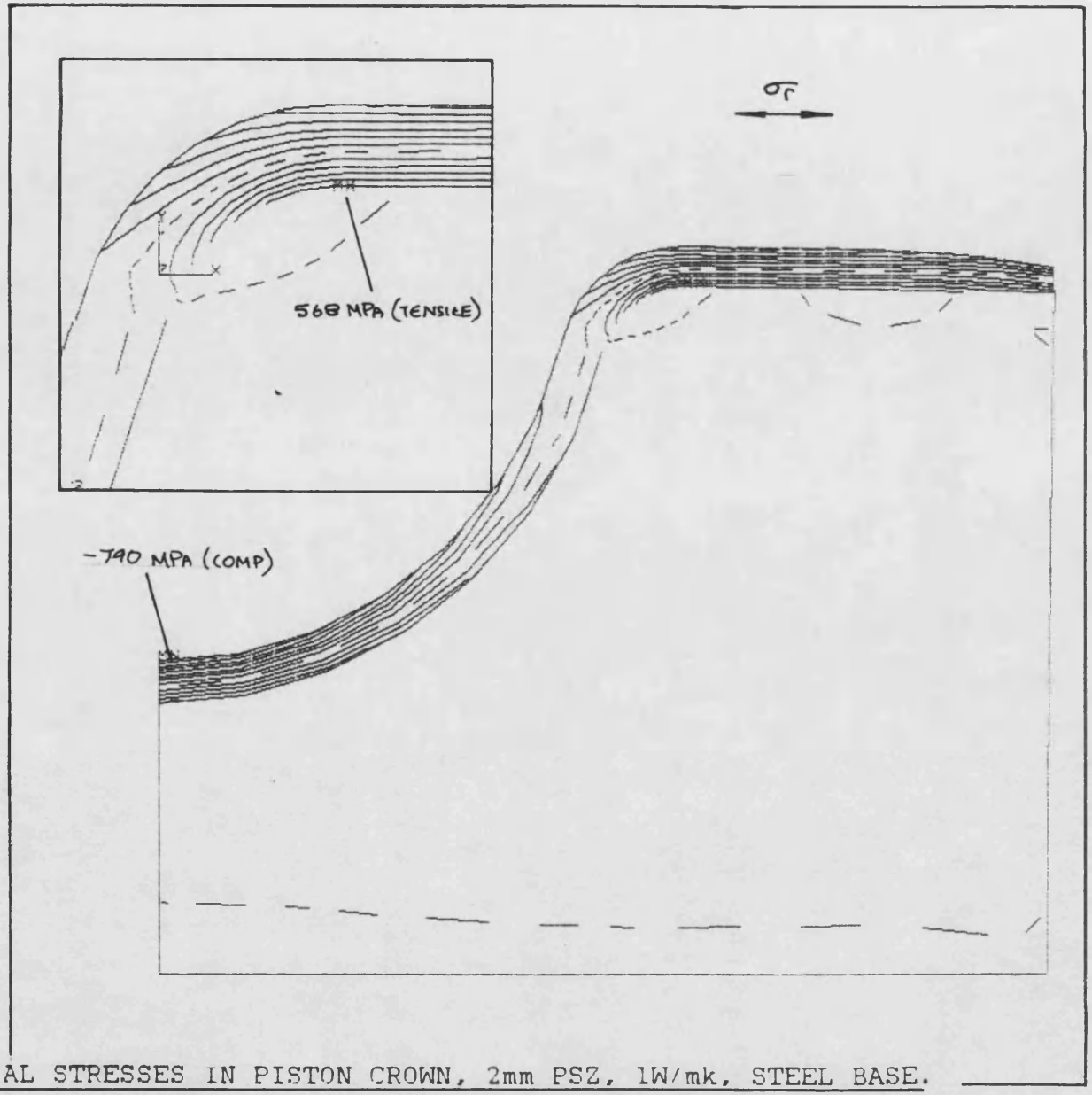

FIGURE 5.45 RADIAL STRESSES IN PISTON CROWN, 2mm PSZ, 1W/mk, STEEL BASE.

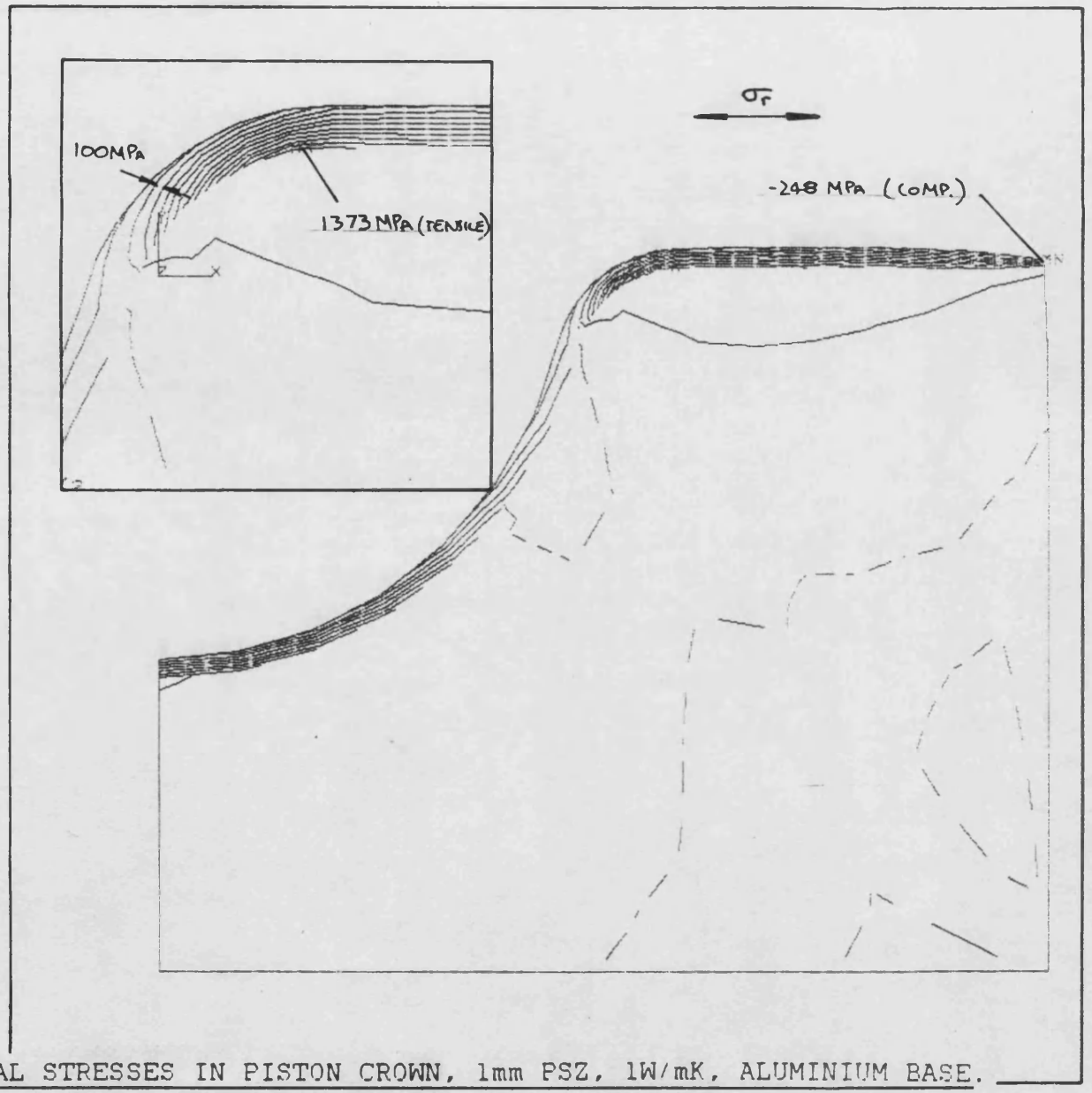

FIGURE 5.46 RADIAL STRESSES IN PISTON CROWN, 1mm PSZ, 1W/mK, ALUMINIUM BASE.

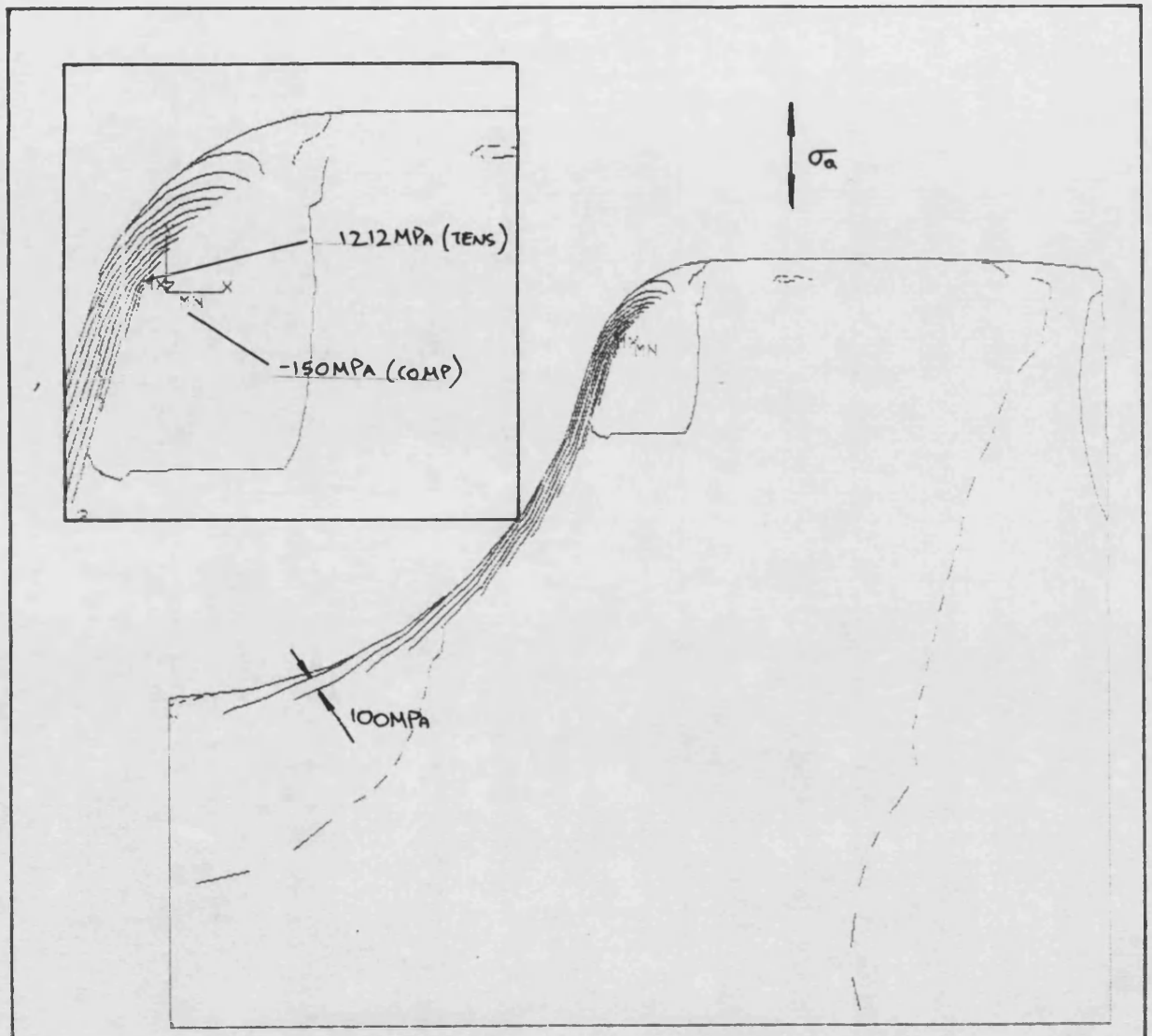

FIGURE 5.47 AXIAL STRESSES IN PISTON CROWN, 1mm PSZ, 1W/mK, ALUMINIUM BASE.

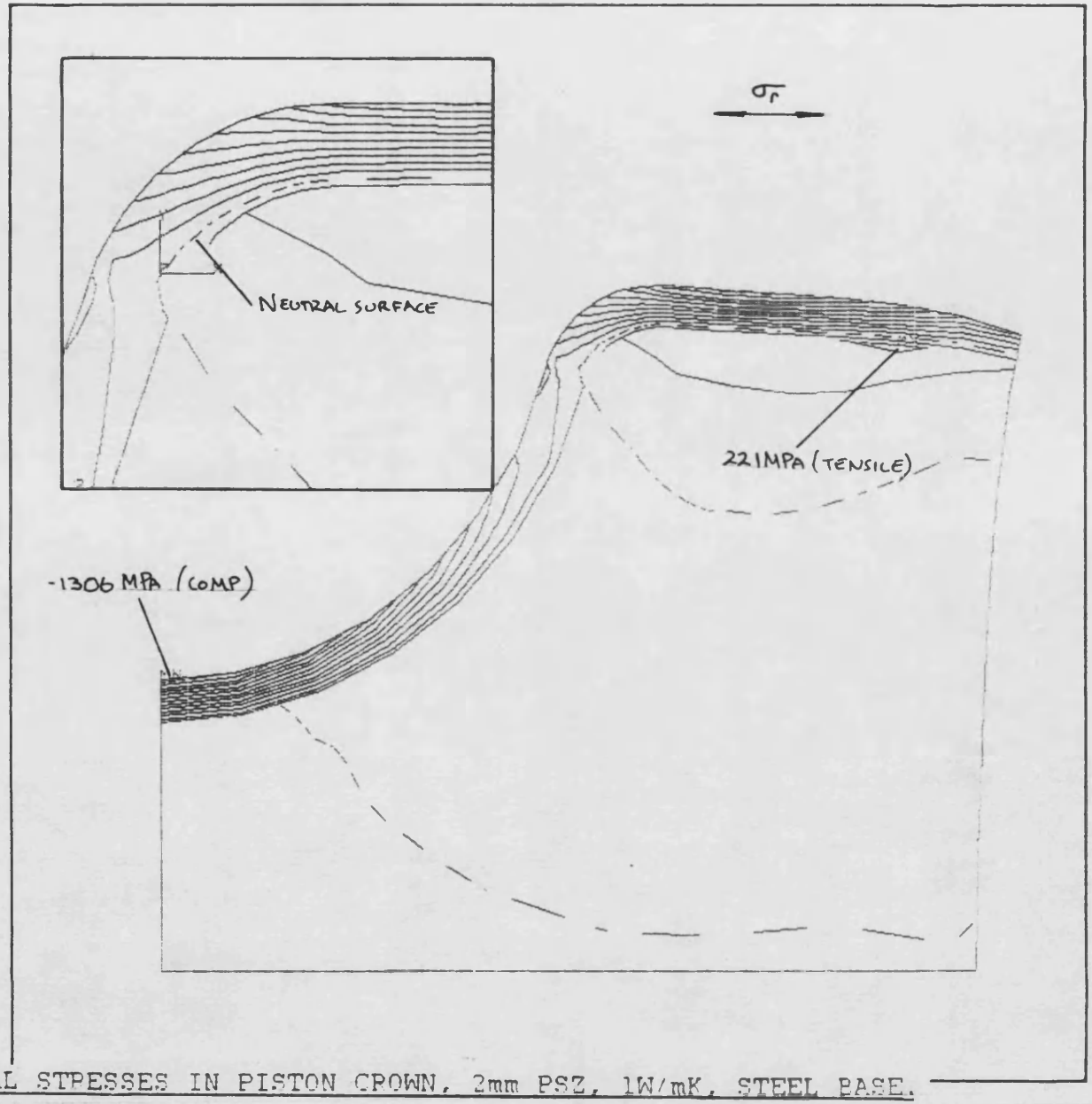

PNSYS
1/31/85
.3765
POST1
STEP=1
ITER=1
STRESS PLOT
SX

USER SCALING
ZV=1
DIST=.027
XF=.2195
YF=-.0135
EDGE
MX=221344395
MN=1325872257
INC=100220022

WIND=2
USER SCALING
ZV=1
DIST=.025
XF=.224
YF=-.284
EDGE
MX=221344395
MN=1325872257
INC=100220022

FIGURE 5.48 RADIAL STRESSES IN PISTON CROWN, 2mm PSZ, 1W/mK, STEEL BASE.

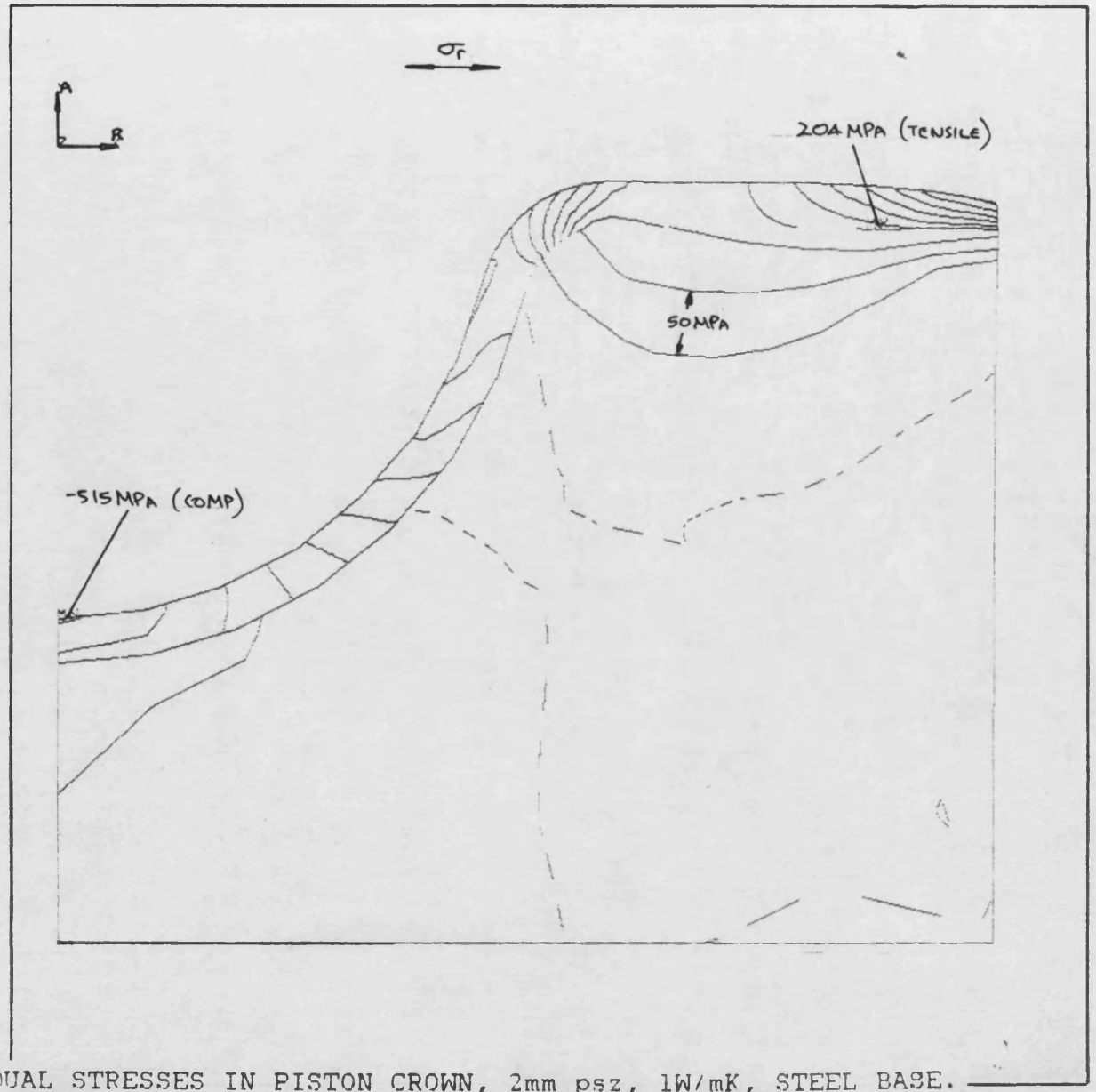

FIGURE 5.49 RESIDUAL STRESSES IN PISTON CROWN, 2mm psz, 1W/mK, STEEL BASE.

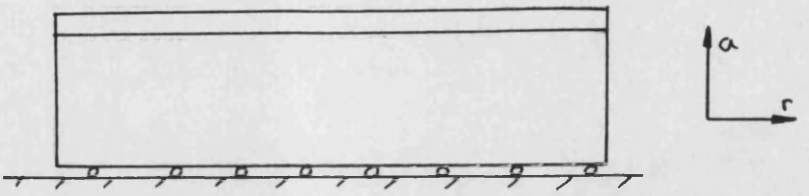

In horizontal coating a uniform compressive stress σ_r is created. $\sigma_a \neq 0$

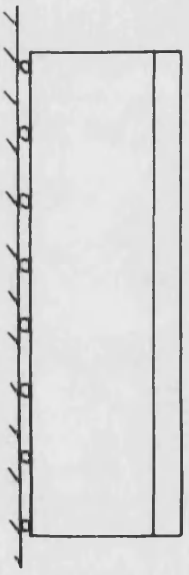

In Vertical coating a uniform compress stress σ_a is created. $\sigma_r \neq 0$

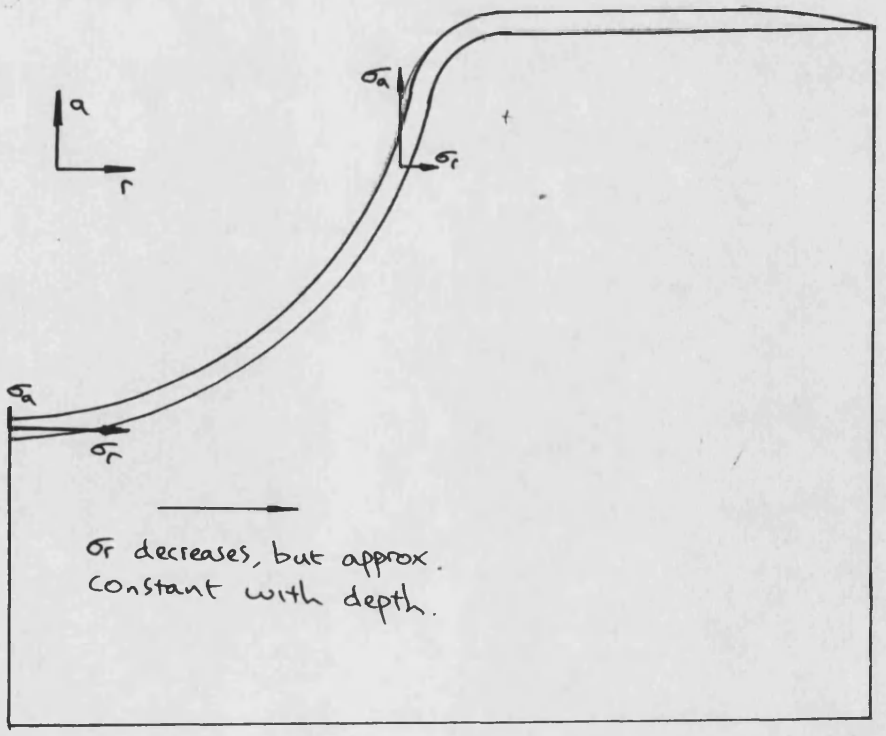

FIGURE 5.50 THERMAL MIS-MATCH STRESS DISTRIBUTION.

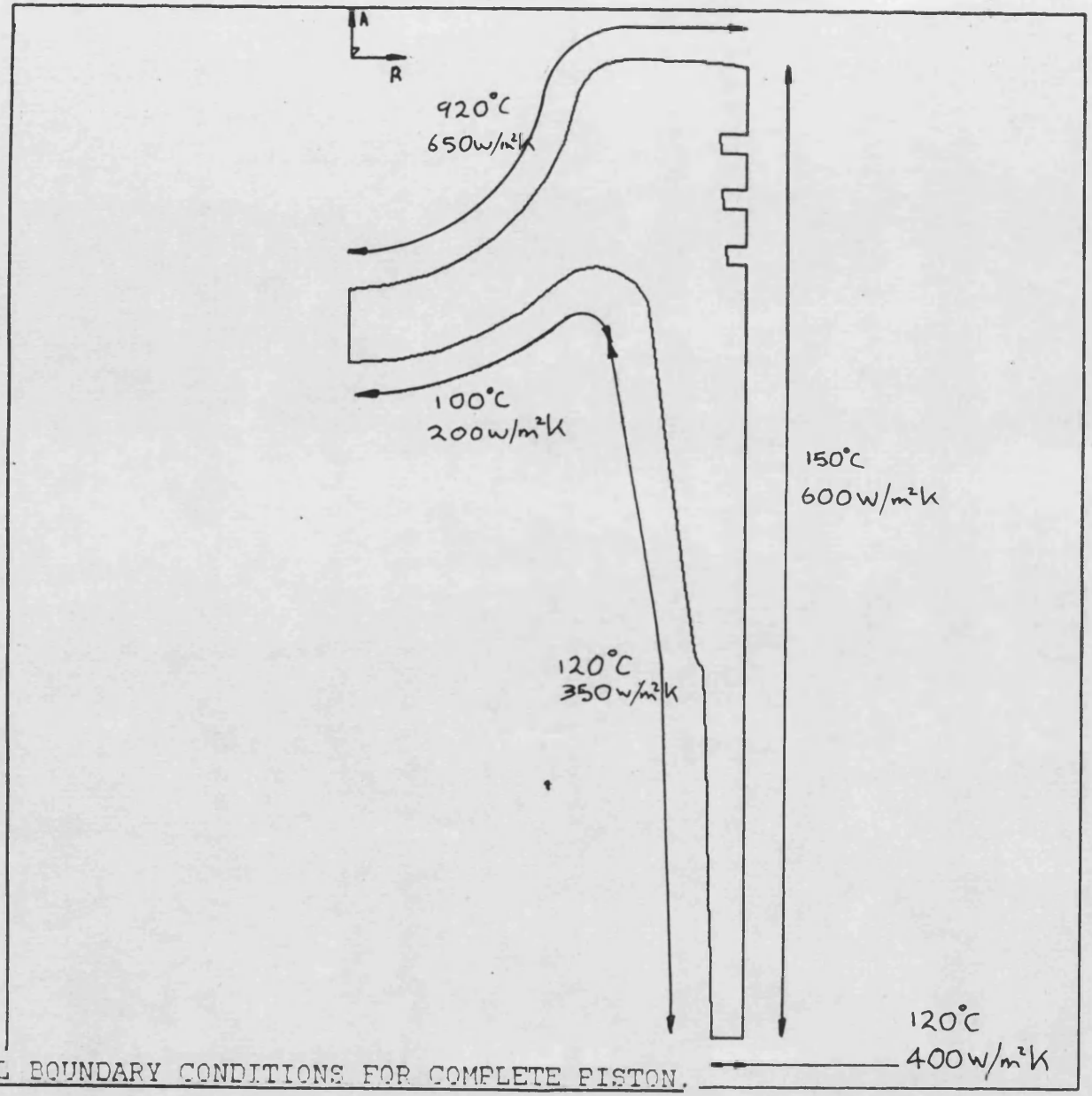

FIGURE 5.51 THERMAL BOUNDARY CONDITIONS FOR COMPLETE PISTON.

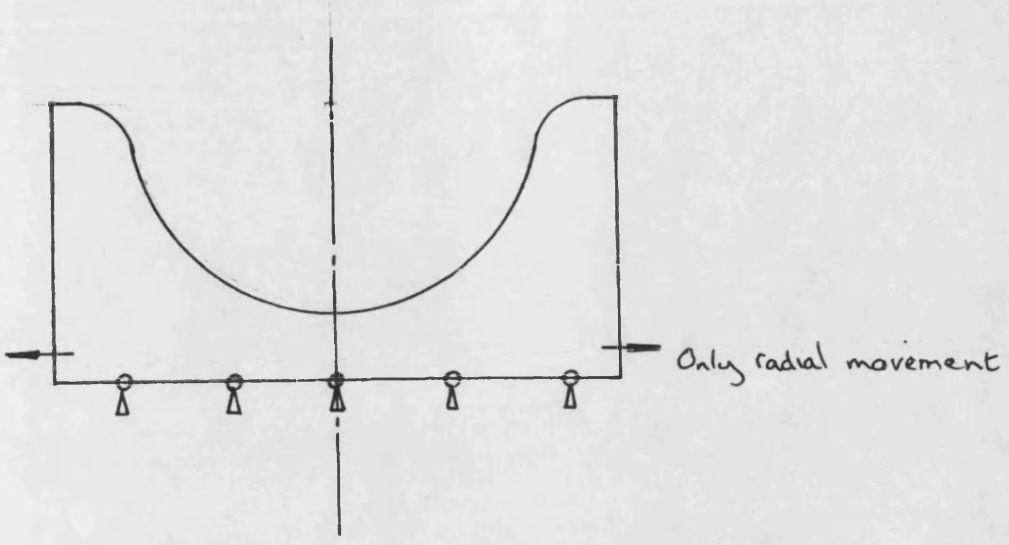

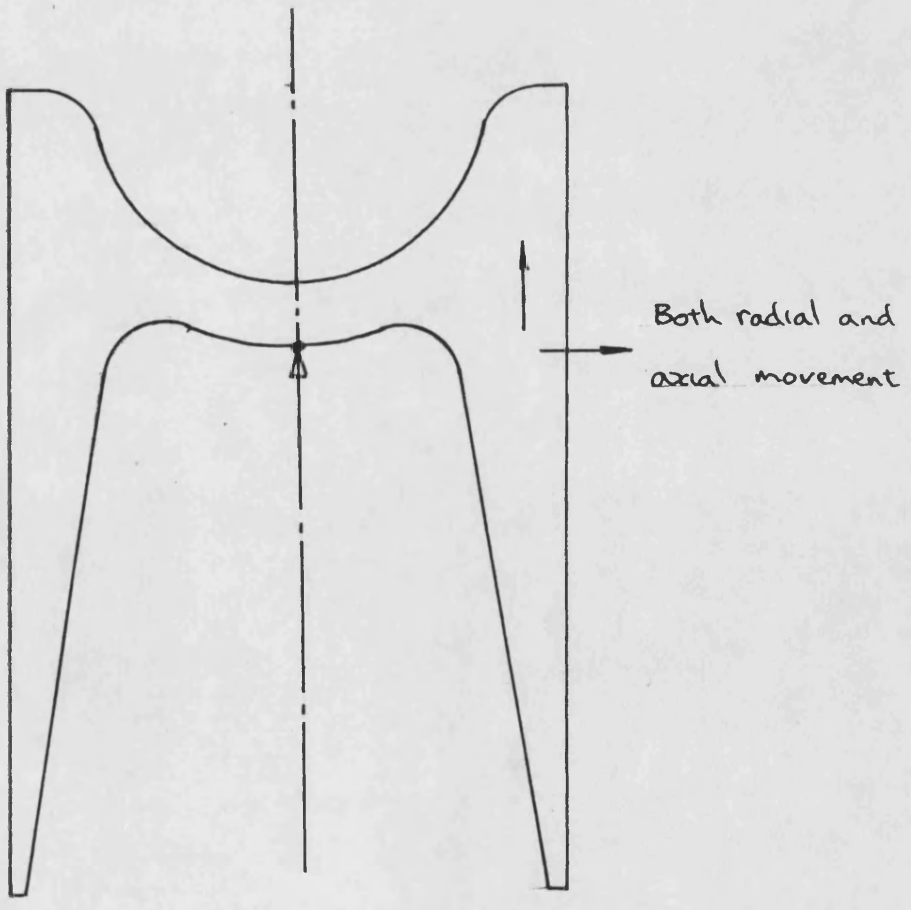

FIGURE 5.52 MECHANICAL BOUNDARY CONDITIONS FOR PISTON CROWN AND COMPLETE PISTON.

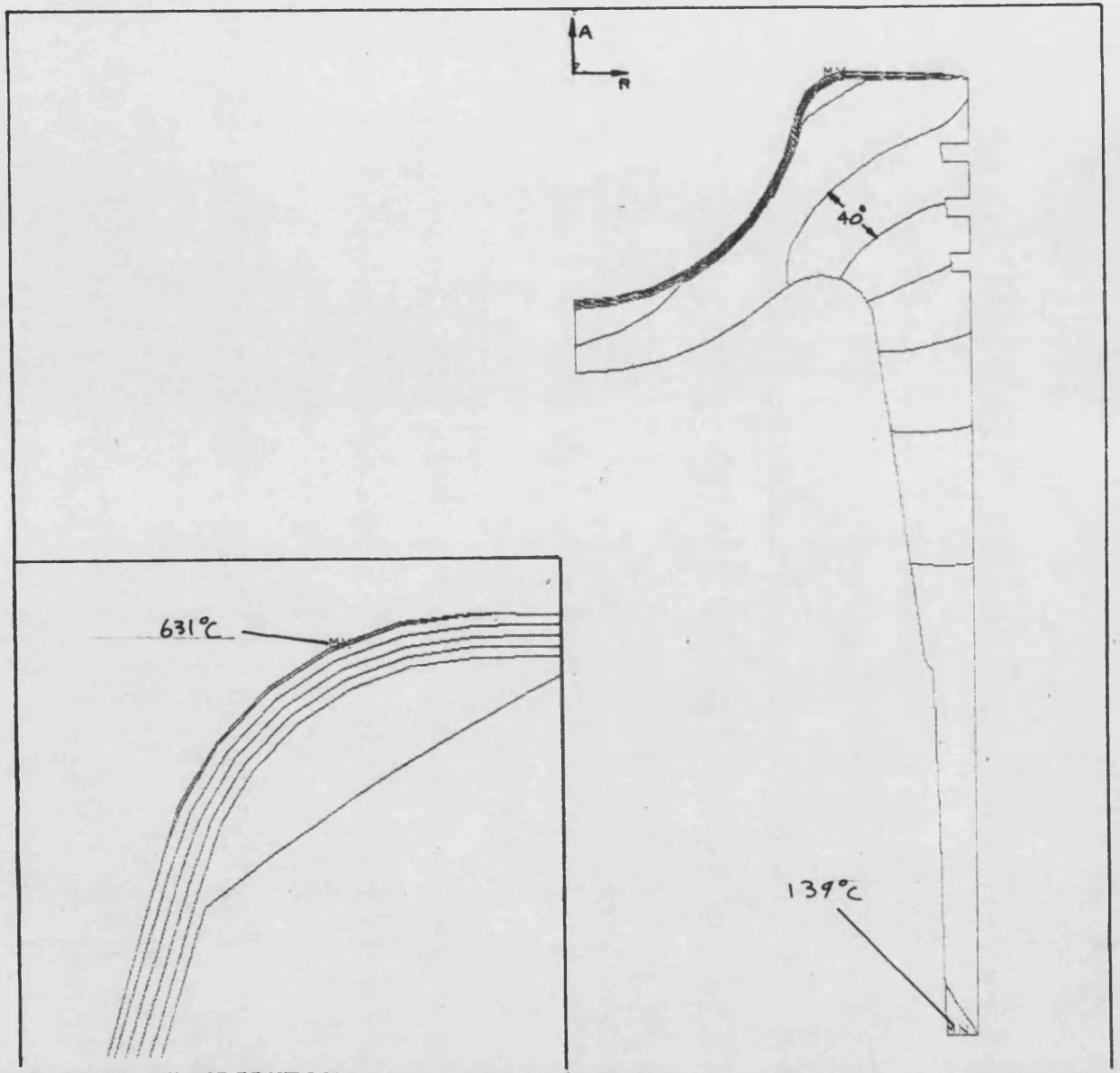

ANSYS
1/30/85
15.4812
POST1
STEP=1
ITER=1
STRESS PLOT
TEMP

USER SCALING
ZV=1
DIST=.06
XF=-.002
YF=-.053
EDGE
MX=631
MN=139
INC=40

WIND=2
USER SCALING
ZV=1
DIST=.005
XF=.027
YF=-.004
EDGE
MX=631
MN=139
INC=40

FIGURE 5.53 TEMPERATURE DISTRIBUTION FOR COATED PISTON, 1mm PSZ, 1W/mK STEEL SUBSTRATE.

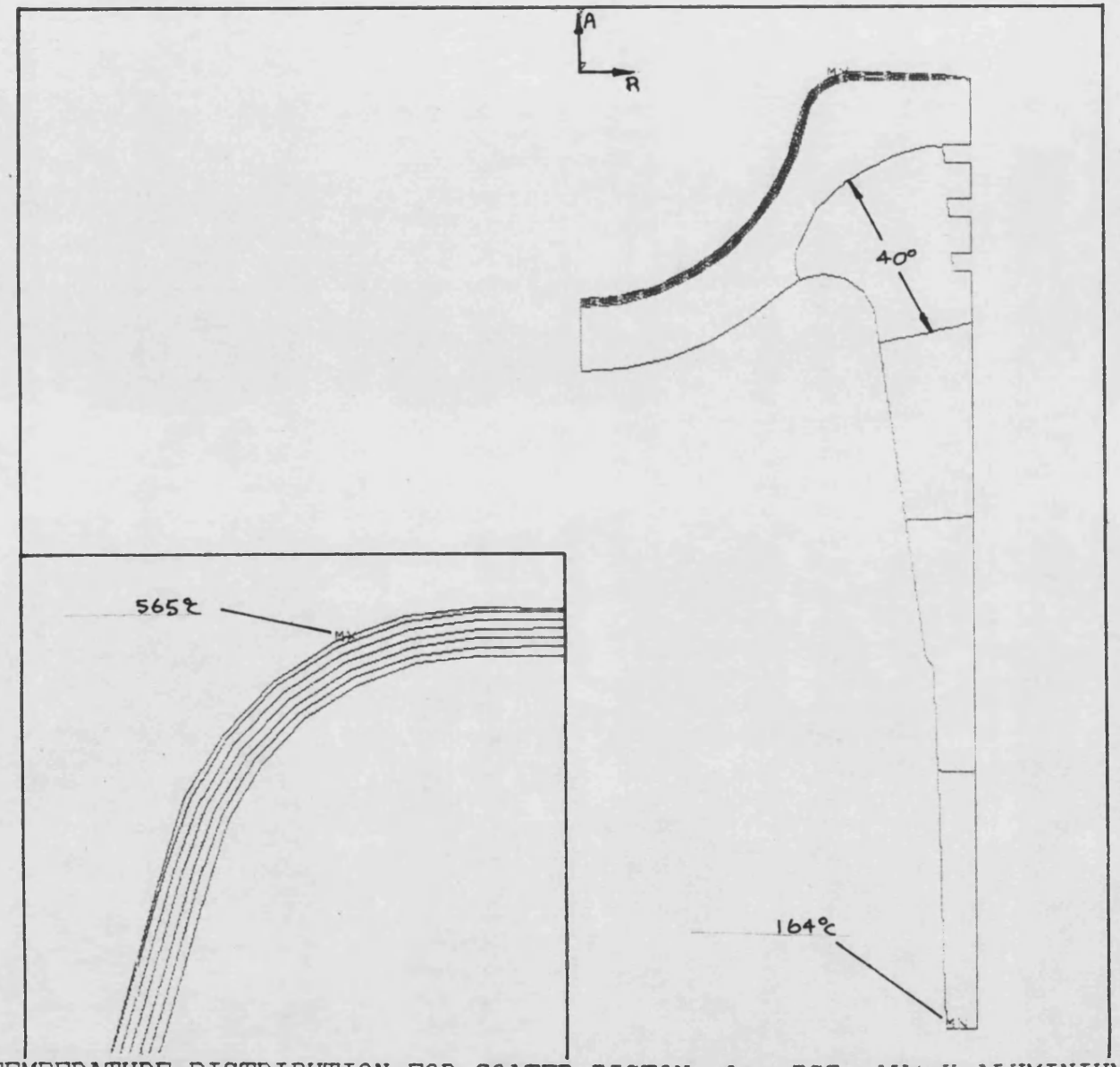

FIGURE 5.54 TEMPERATURE DISTRIBUTION FOR COATED PISTON, 1mm PSZ, 1W/mK ALUMINIUM SUBSTRATE.

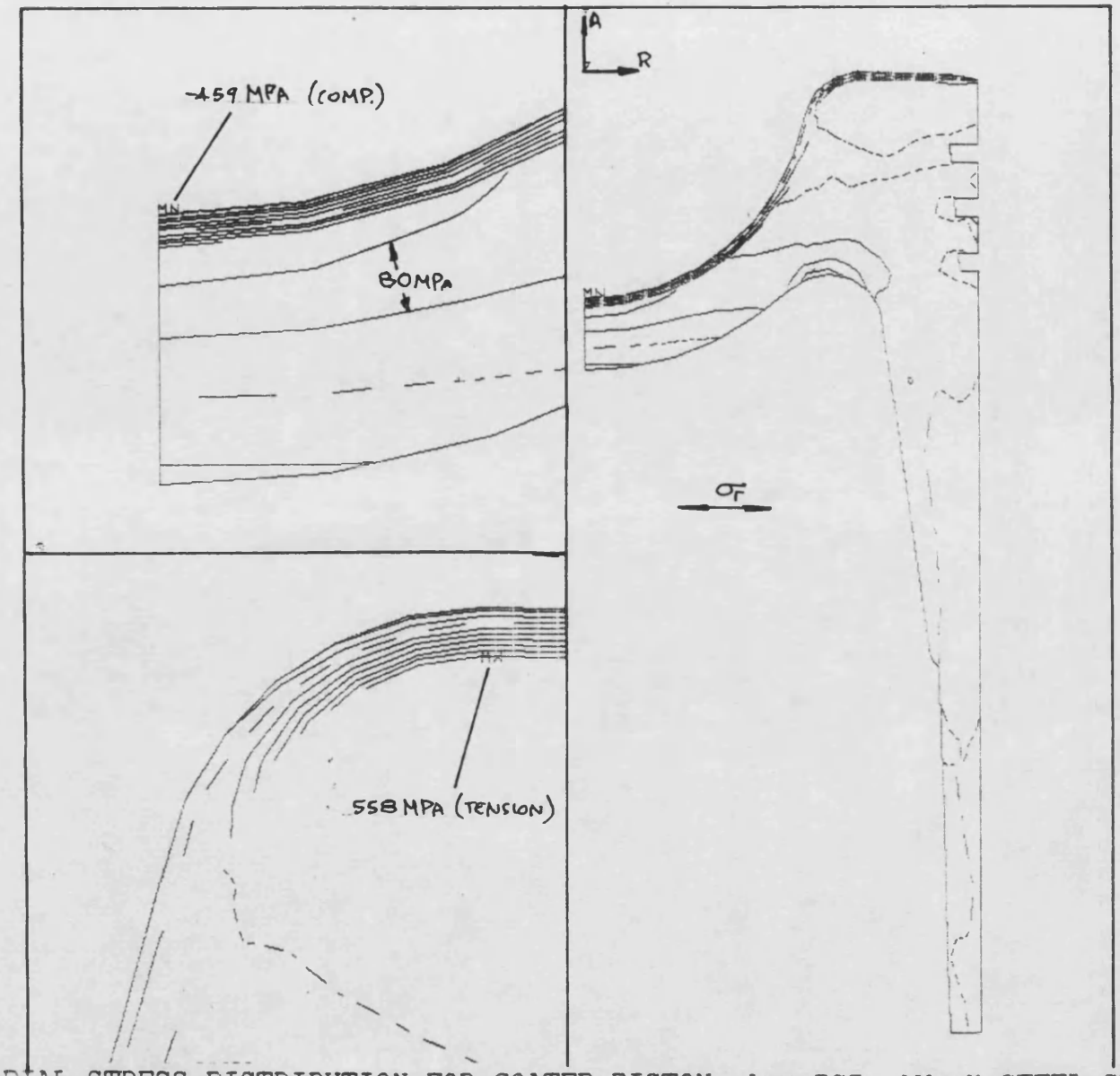

FIGURE 5.55 RADIAL STRESS DISTRIBUTION FOR COATED PISTON, 1mm PSZ, 1W/mK STEEL SUBSTRATE.

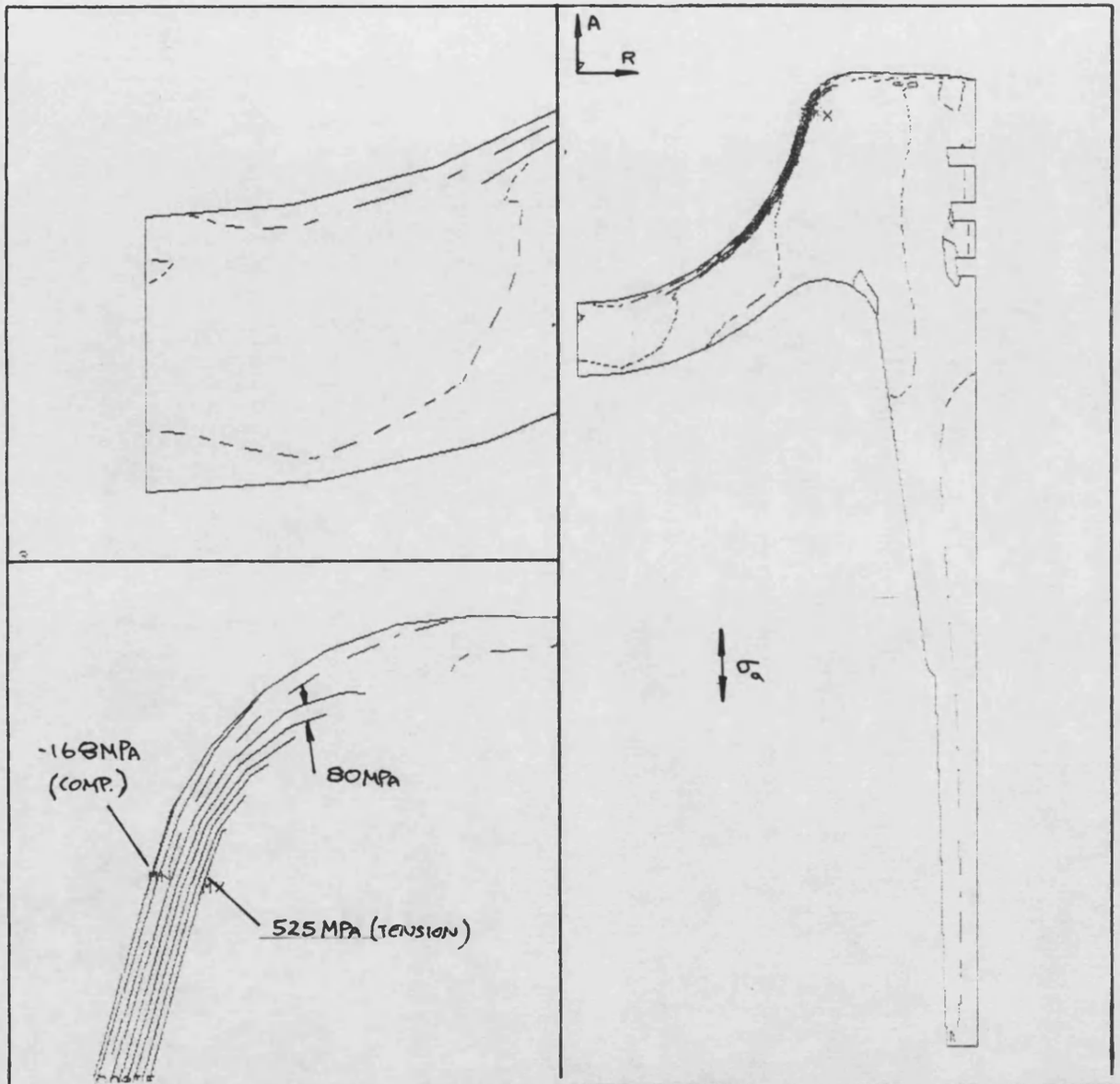

FIGURE 5.56 AXIAL STRESS DISTRIBUTION FOR COATED PISTON, 1mm PSZ, 1W/mK STEEL SUBSTRATE.

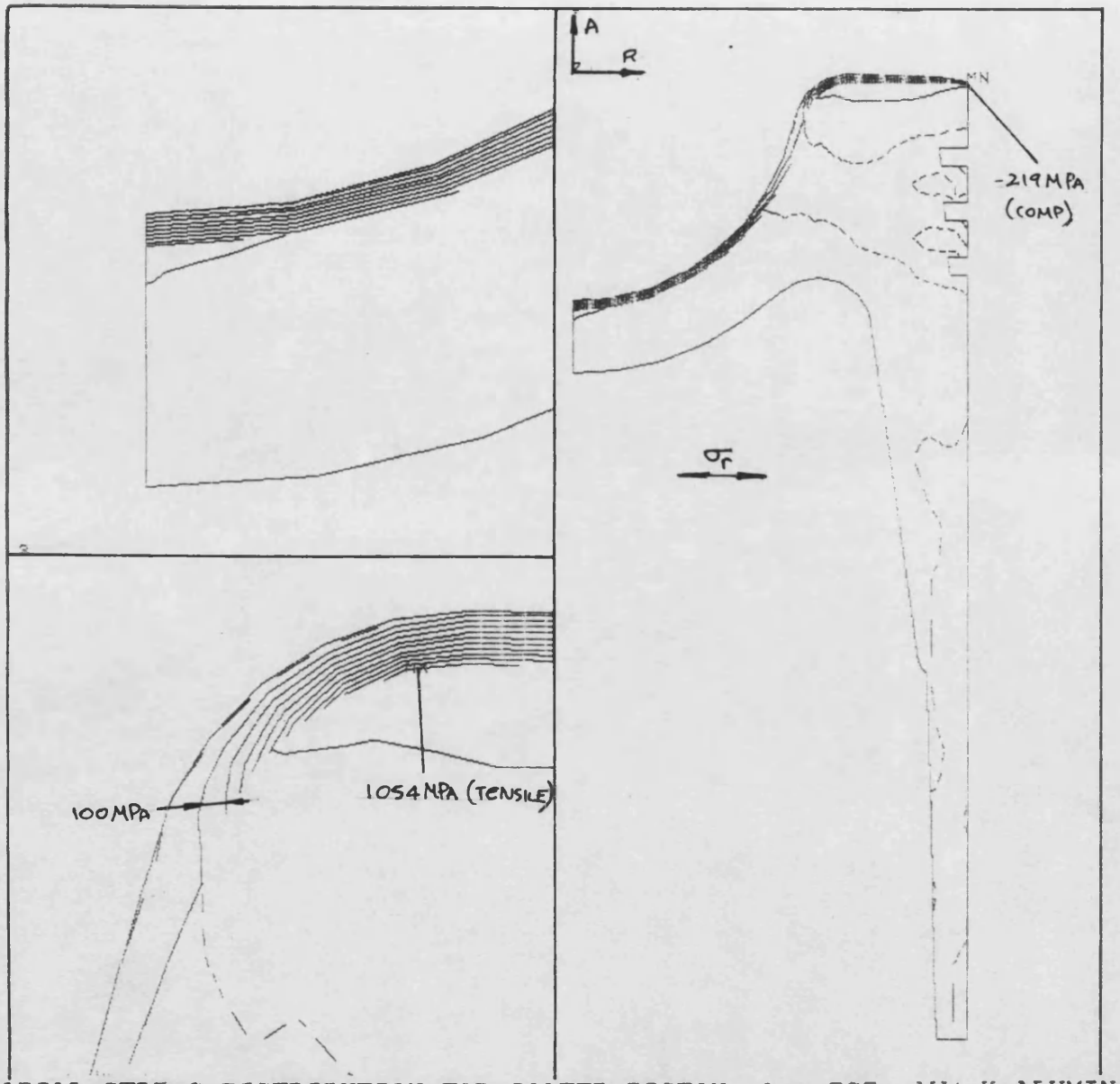

FIGURE 5.57 RADIAL STRESS DISTRIBUTION,FOR COATED PISTON, 1mm PSZ, 1W/mK ALUMINIUM SUBSTRATE.

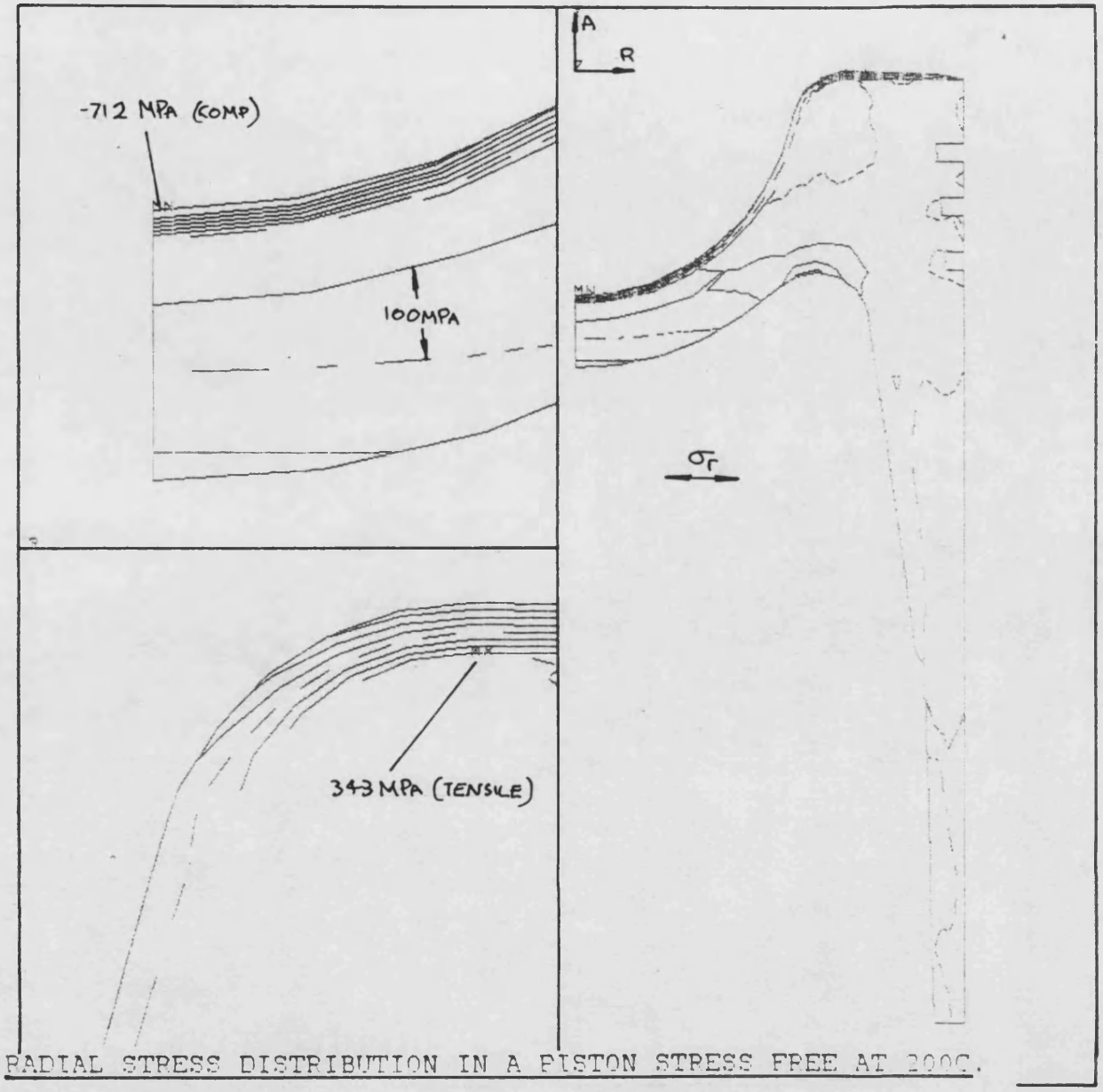

FIGURE 5.58 RADIAL STRESS DISTRIBUTION IN A PISTON STRESS FREE AT 200C.

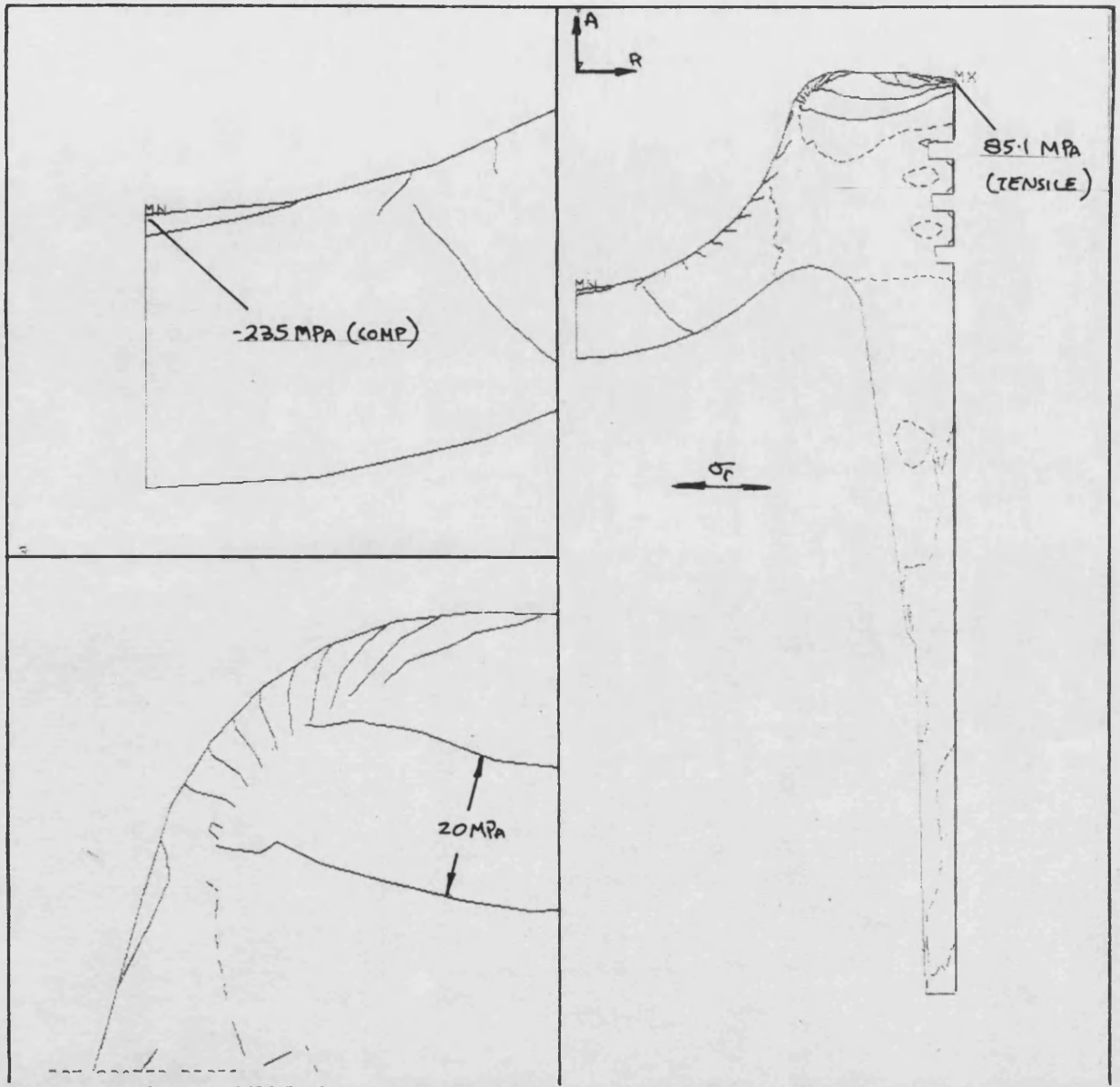

ANSYS
1/31/85
4.9164
POST1
STEP=1
ITER=1
STRESS PLOT
SX

USER SCALING
ZV=1
DIST=.06
XF=-.002
YF=-.053
EDGE
MX=85157152
MN=-253078735
INC=22000002

WIND=2
USER SCALING
ZV=1
DIST=.005
XF=.027
YF=-.004
EDGE
MX=85157152
MN=-253078735
INC=22000002

WIND=3
USER SCALING

FIGURE 5.59 RESIDUAL RADIAL STRESS DISTRIBUTION IN A PISTON STRESS FREE AT 200C.

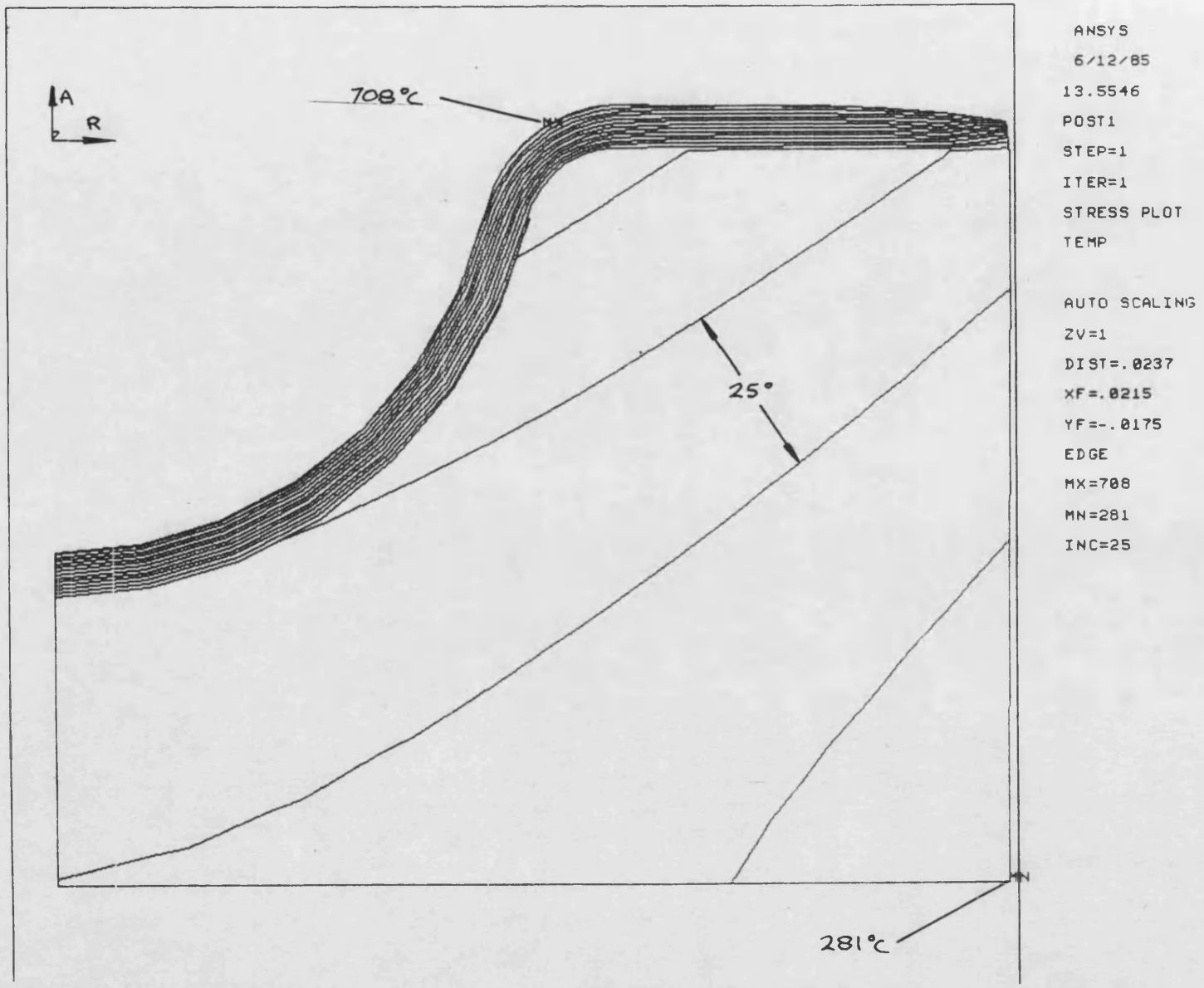

FIGURE 5.60 TEMPERATURE DISTRIBUTION IN A PISTON CROWN USING GRADED THERMAL EXPANSION.

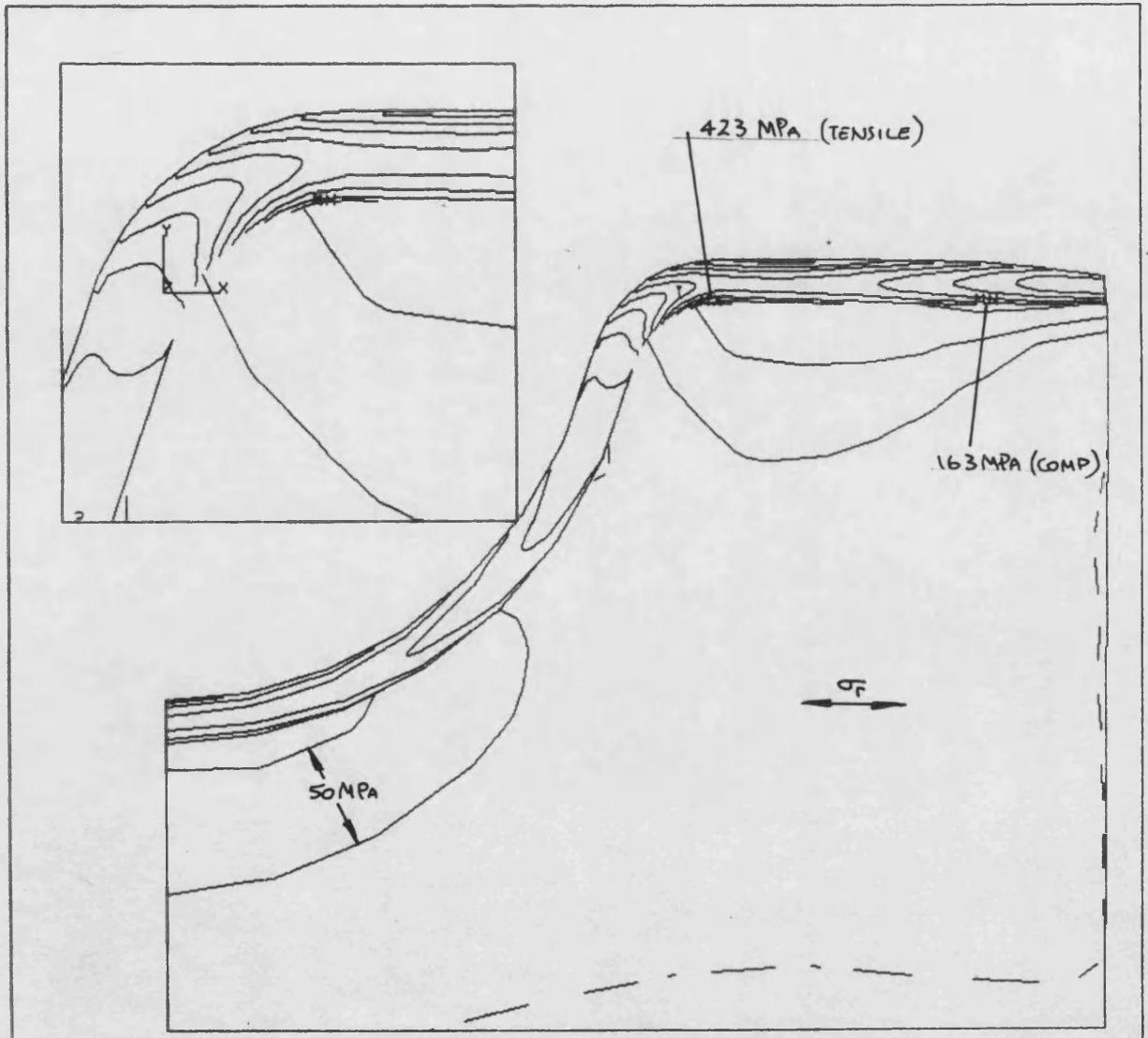

FIGURE 5.61 RADIAL STRESSES IN A PISTON CROWN USING GRADED THERMAL EXPANSION.

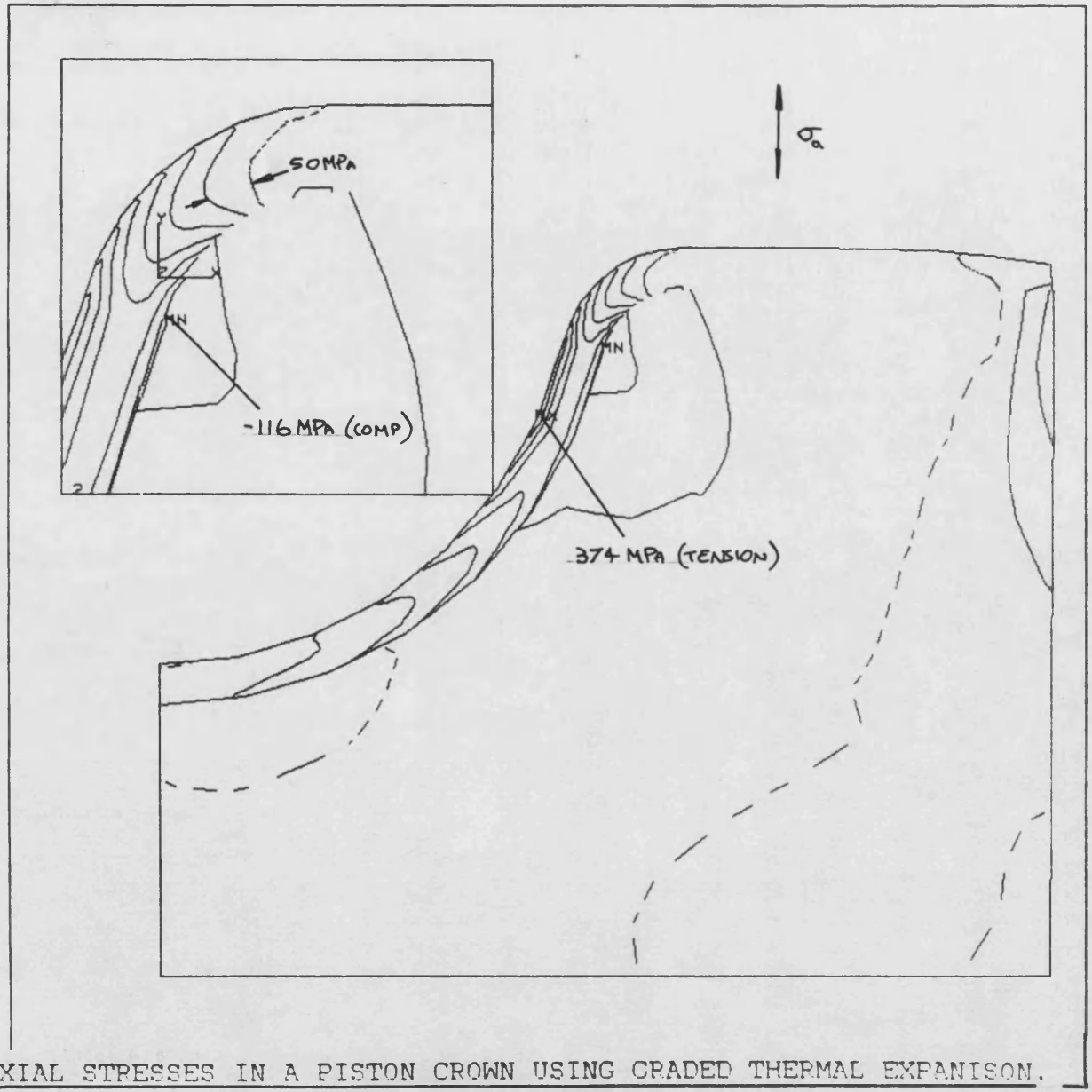

ANSYS
6/12/85
13.9047
POST1
STEP=1
ITER=1
STRESS PLOT
SY

USER SCALING
ZV=1
DIST=.027
XF=.0195
YF=-.0135
EDGE
MX=374721905
MN=-116475095
INC=50000000

WIND=2
USER SCALING
ZV=1
DIST=.005
XF=.024
YF=-.004
EDGE
MX=374721905
MN=-116475095
INC=50000000

FIGURE 5.62 AXIAL STRESSES IN A PISTON CROWN USING GRADED THERMAL EXPANISON.

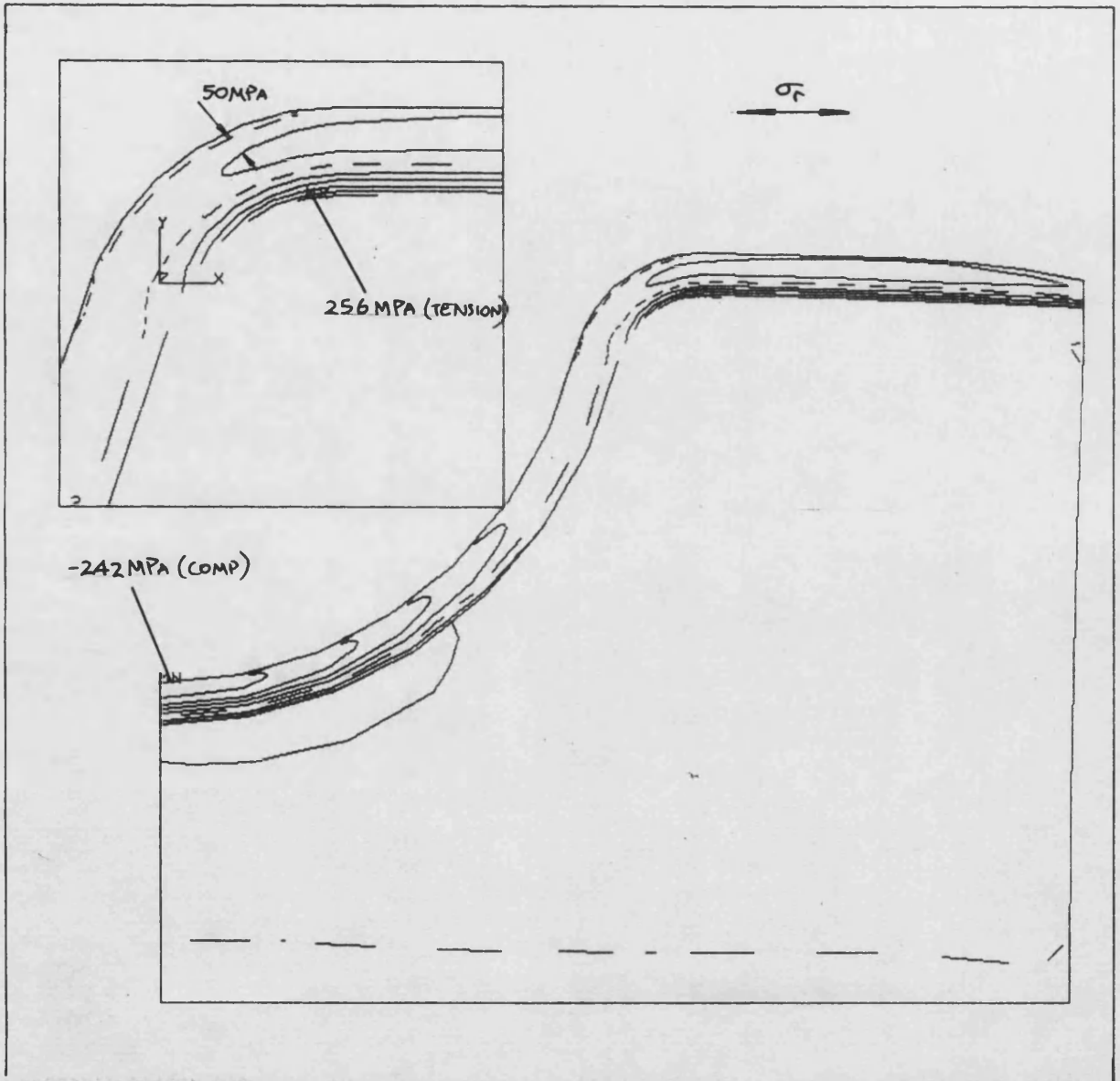

FIGURE 5.63 RADIAL STRESSES USING GRADED THERMAL EXPANSION, STRESS FREE AT 200C.

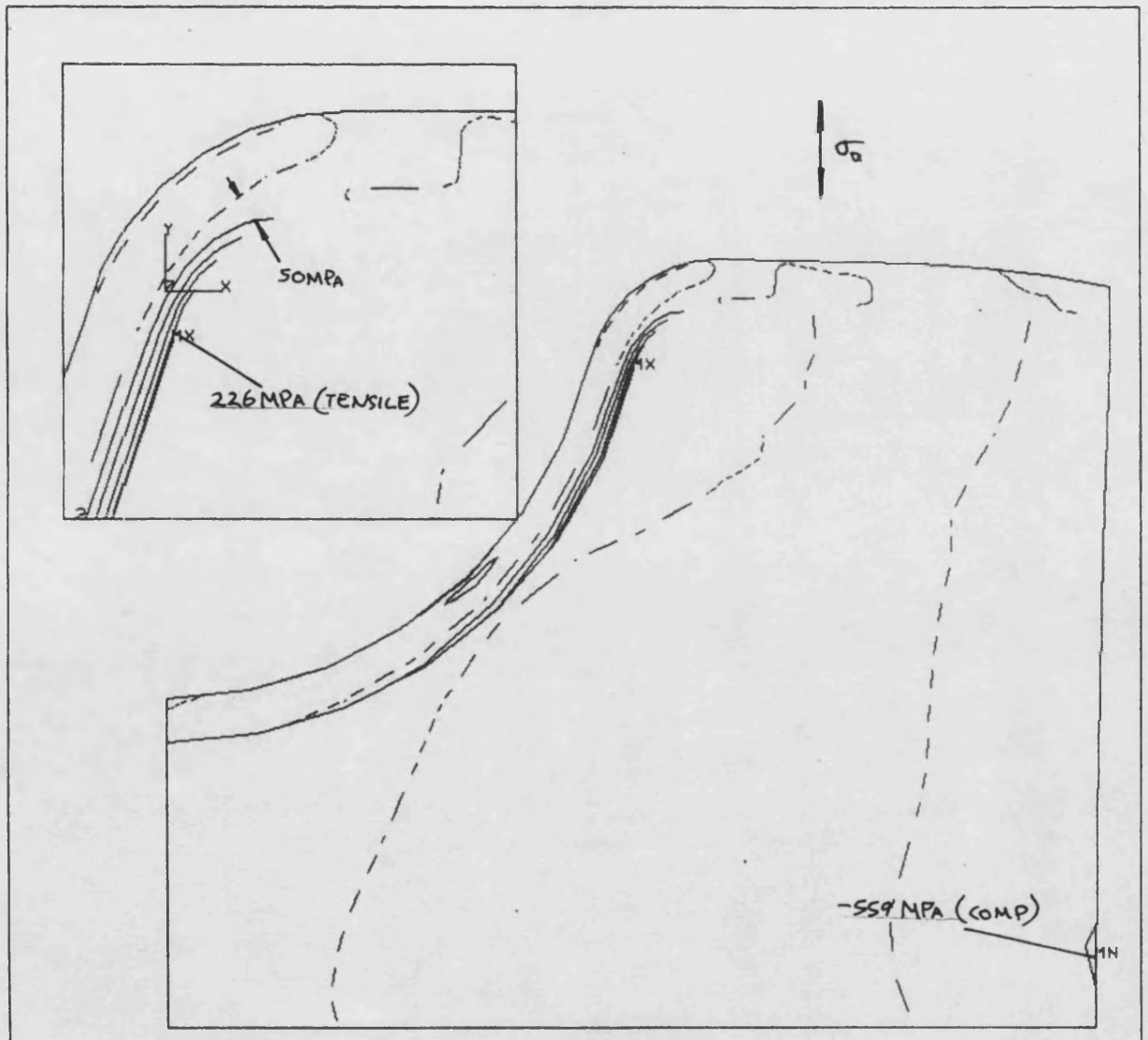

ANSYS
6/12/85
15.4572
POST1
STEP=1
ITER=1
STRESS PLOT
SY

USER SCALING
ZV=1
DIST=.027
XF=.0195
YF=-.0135
EDGE
MX=226529018
MN=-55872545
INC=50000000

WIND=2
USER SCALING
ZV=1
DIST=.005
XF=.024
YF=-.004
EDGE
MX=226529018
MN=-55872545
INC=50000000

FIGURE 5.64 AXIAL STRESSES USING GRADED THERMAL EXPANSION, STRESS FREE AT 200C.

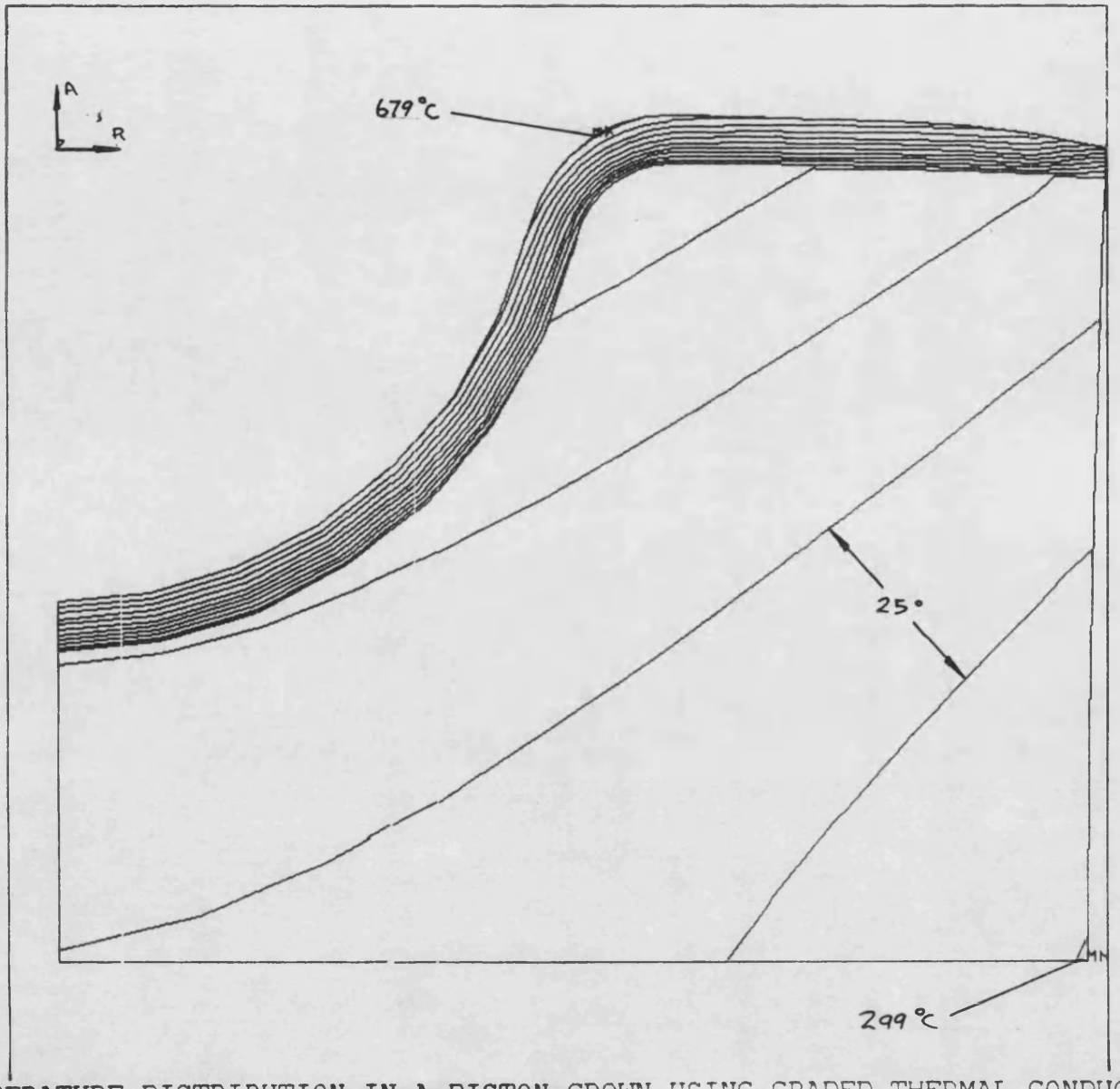

FIGURE 5.65 TEMPERATURE DISTRIBUTION IN A PISTON CROWN USING GRADED THERMAL CONDUCTIVITY.

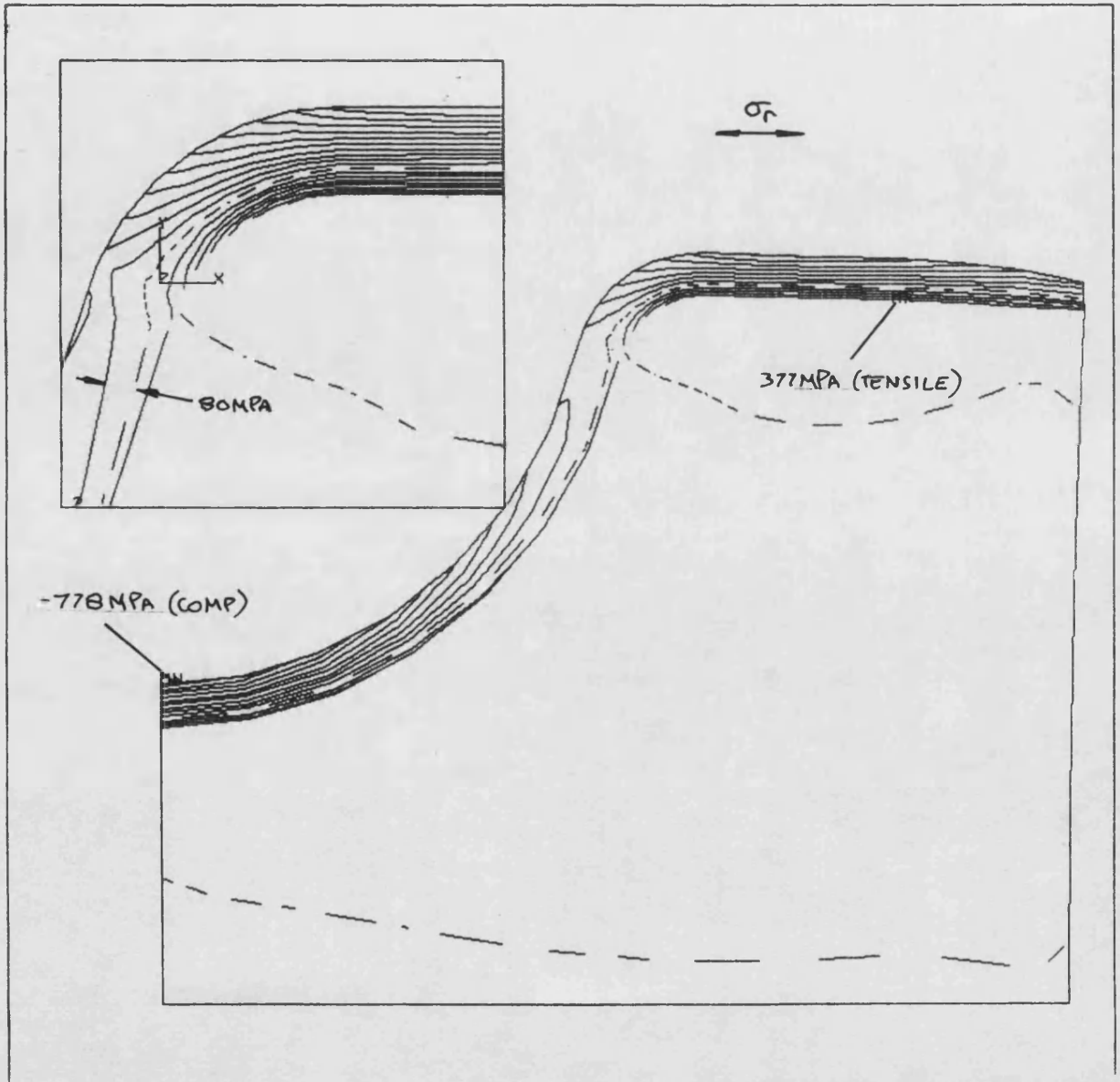

FIGURE 5.66 RADIAL STRESSES IN A PISTON CROWN USING GRADED THERMAL CONDICTIVITY.

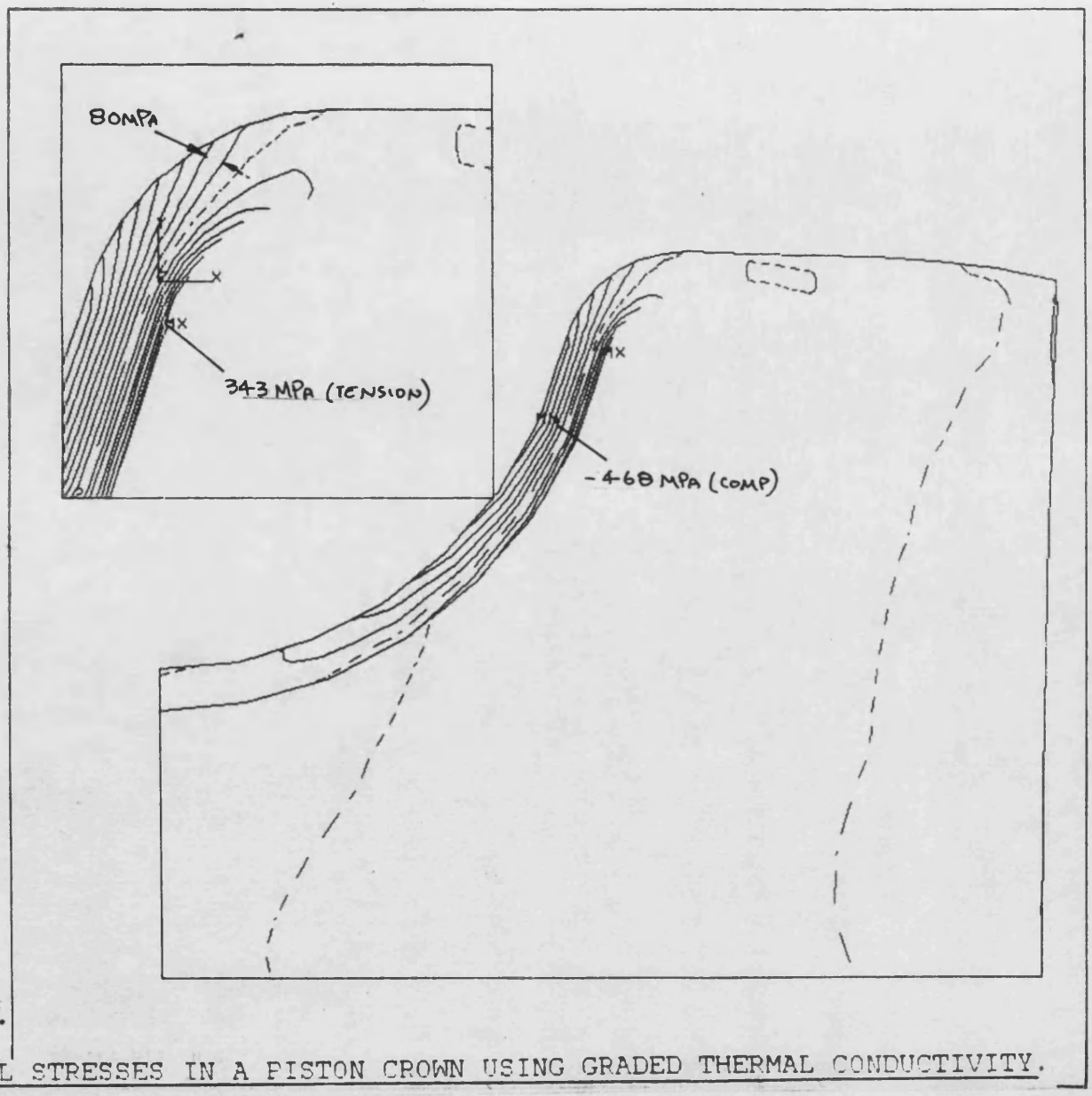

ANSYS
6/12/85
18.8660
POST1
STEP=1
ITER=1
STRESS PLOT
SY

USER SCALING
ZV=1
DIST=.027
XF=.0195
YF=-.0135
EDGE
MX=343723336
MN=-468209925
INC=80000000

WIND=2
USER SCALING
ZV=1
DIST=.005
XF=.024
YF=-.004
EDGE
MX=343723336
MN=-468209925
INC=50000000

FIGURE 5.67 AXIAL STRESSES IN A PISTON CROWN USING GRADED THERMAL CONDUCTIVITY.

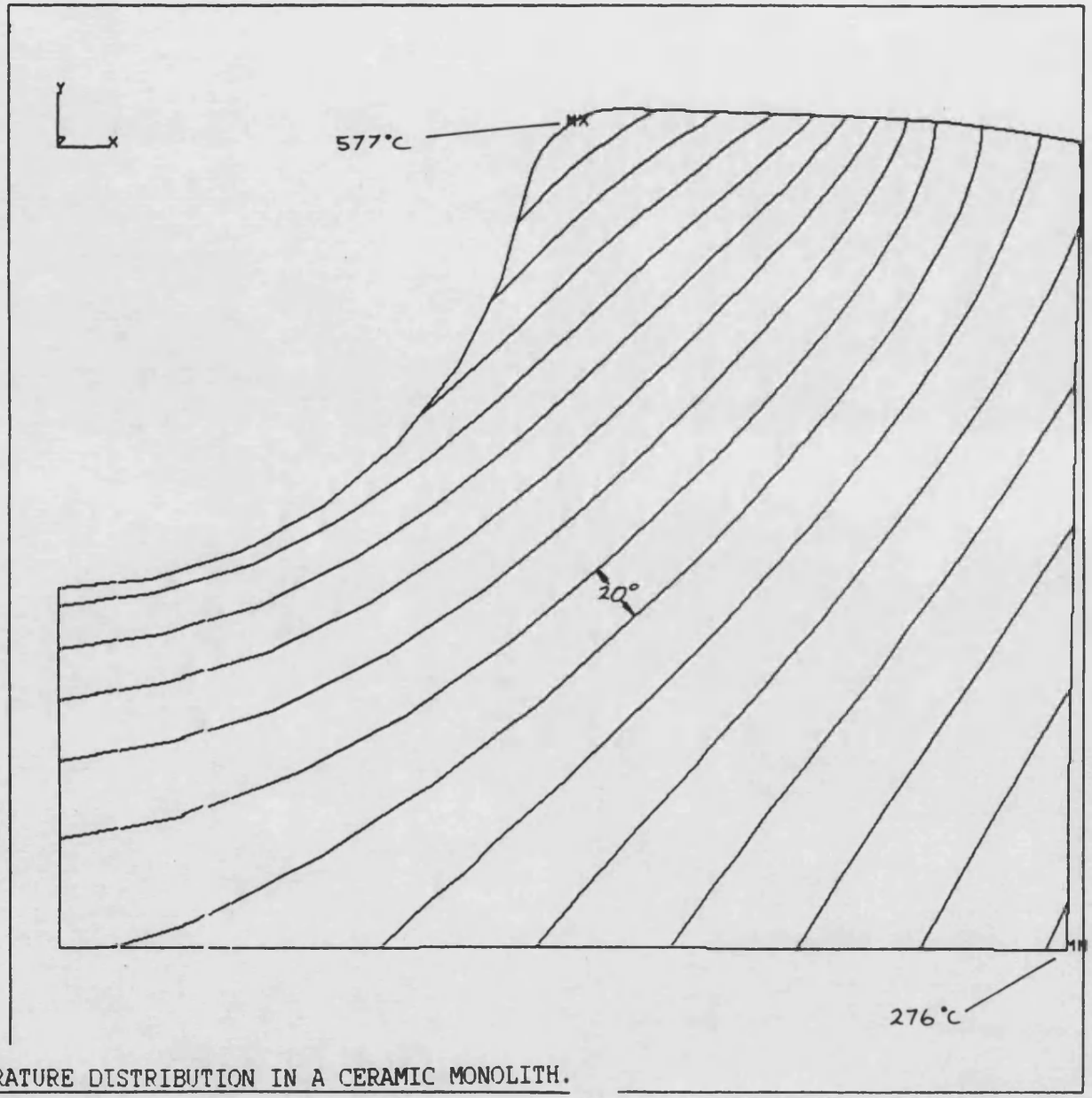

FIGURE 5.68 TEMPERATURE DISTRIBUTION IN A CERAMIC MONOLITH.

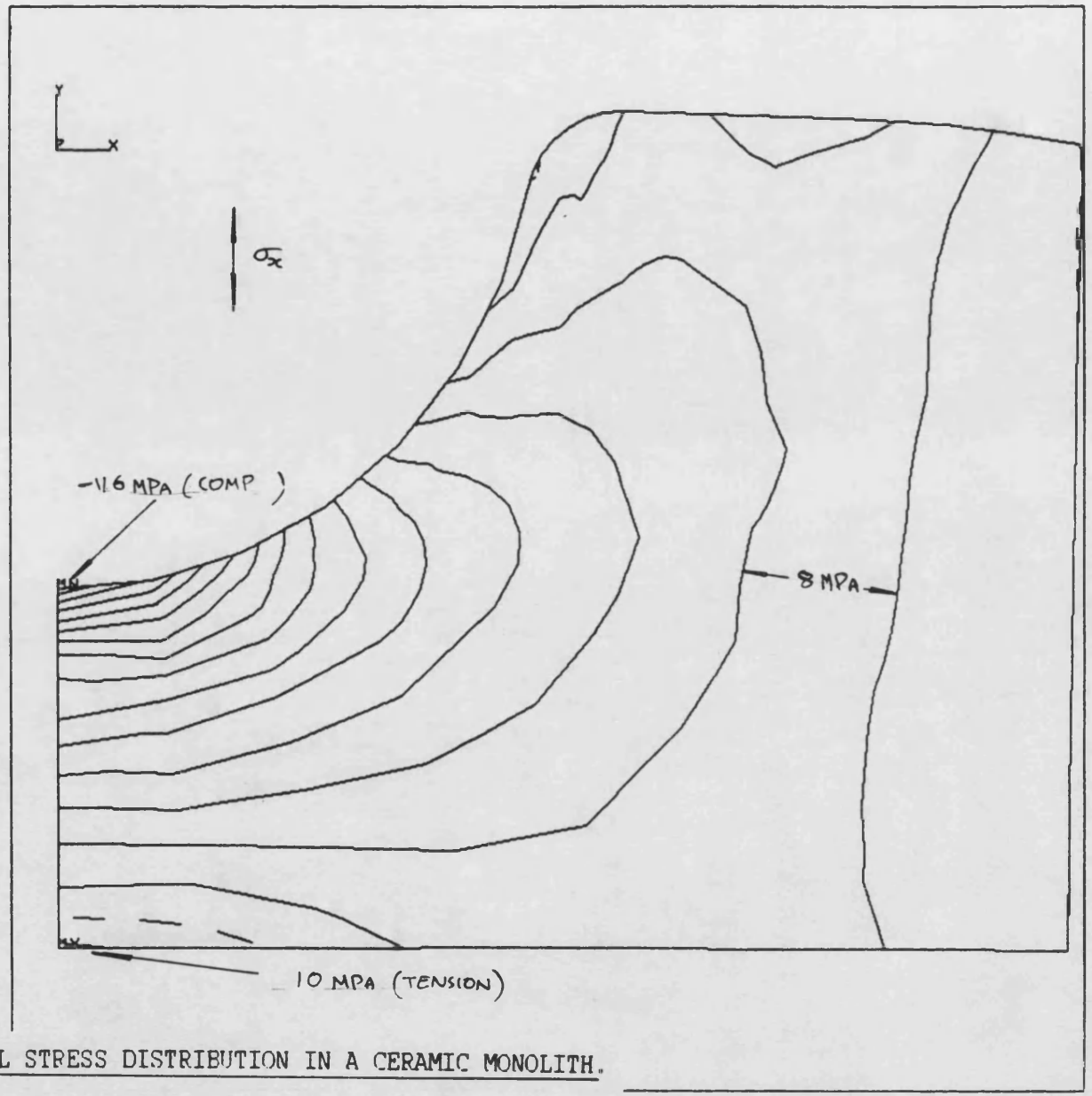

FIGURE 5.69 RADIAL STRESS DISTRIBUTION IN A CERAMIC MONOLITH.

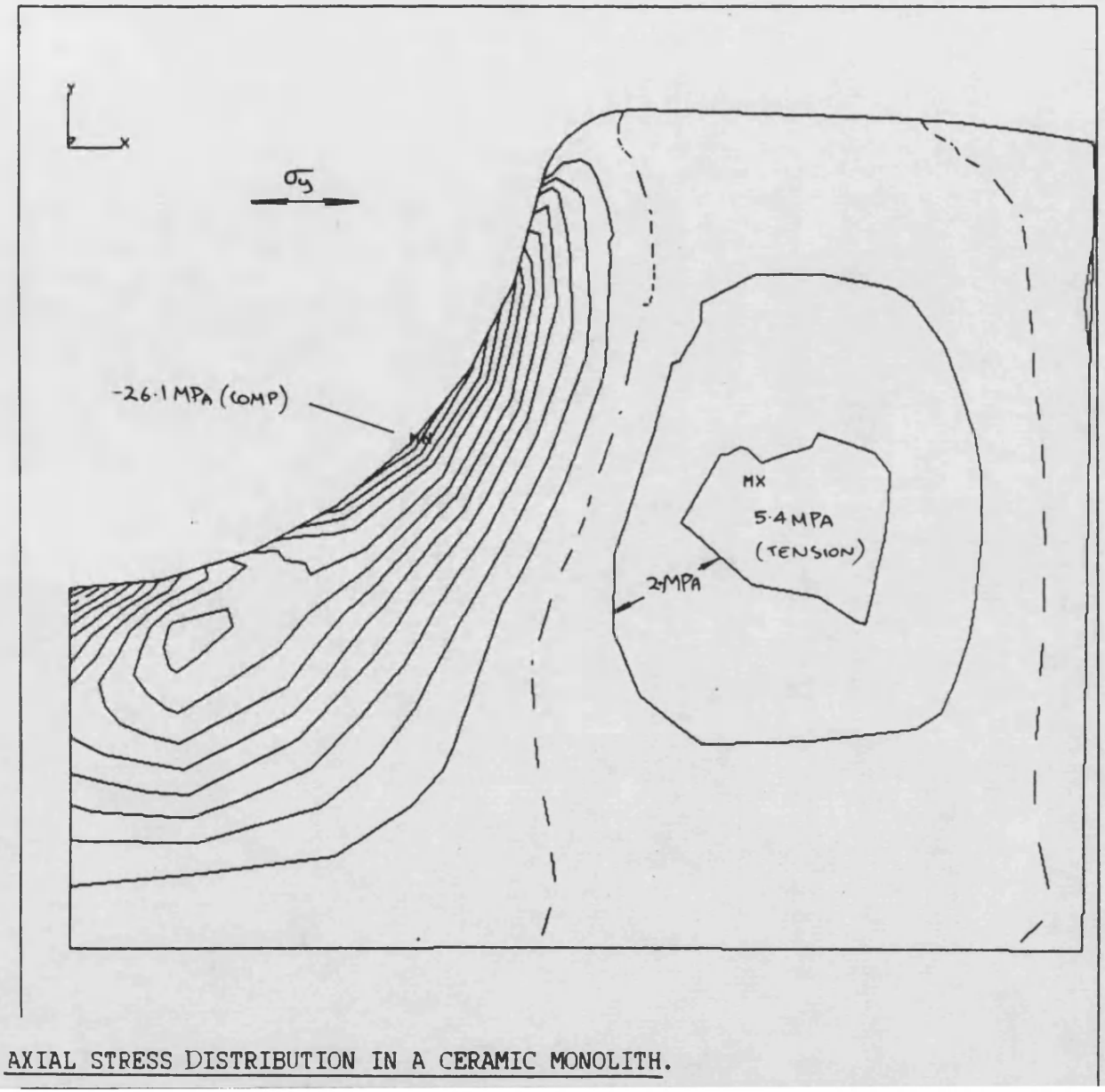

FIGURE 5.70 AXIAL STRESS DISTRIBUTION IN A CERAMIC MONOLITH.

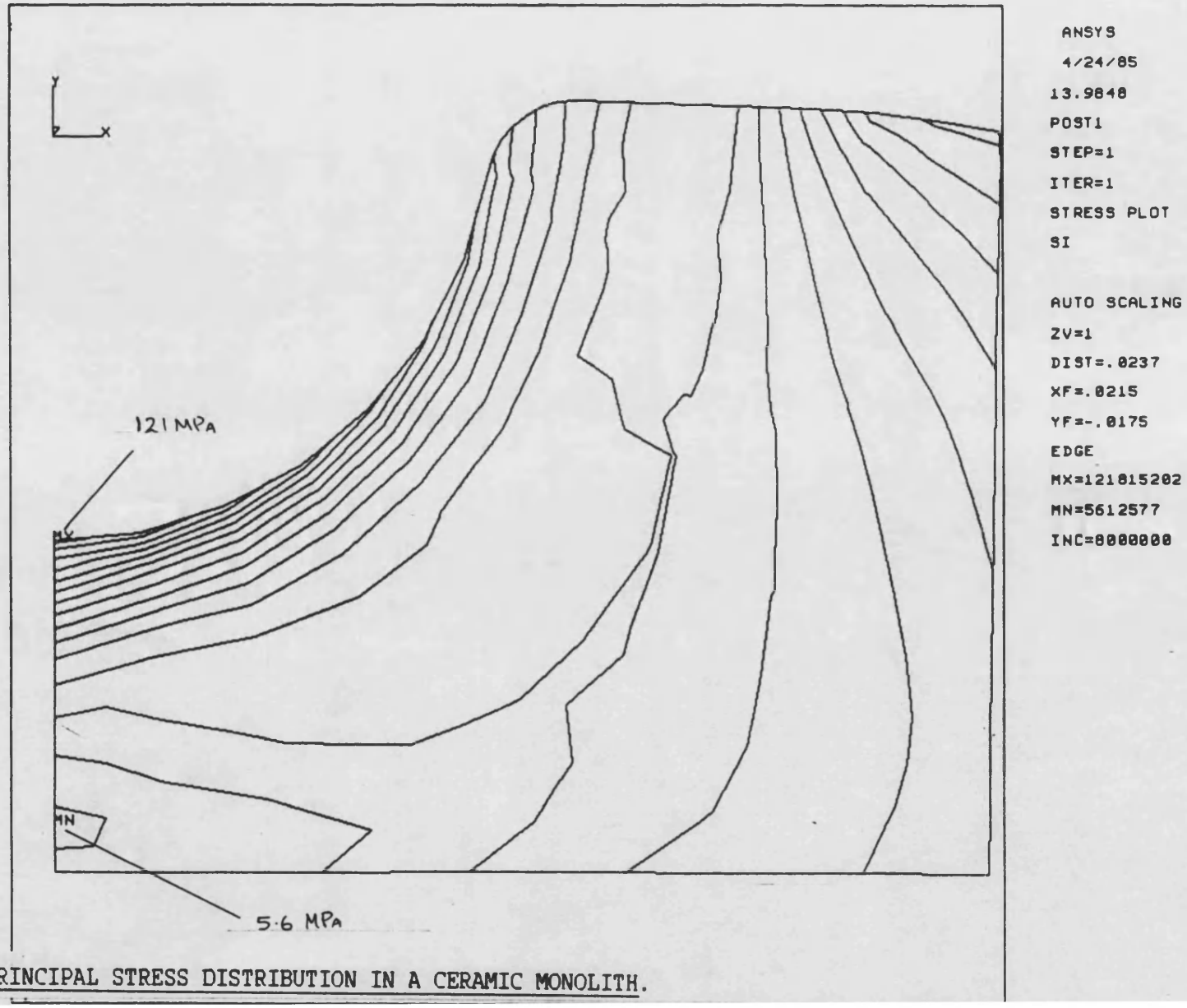

FIGURE 5.71 PRINCIPAL STRESS DISTRIBUTION IN A CERAMIC MONOLITH.

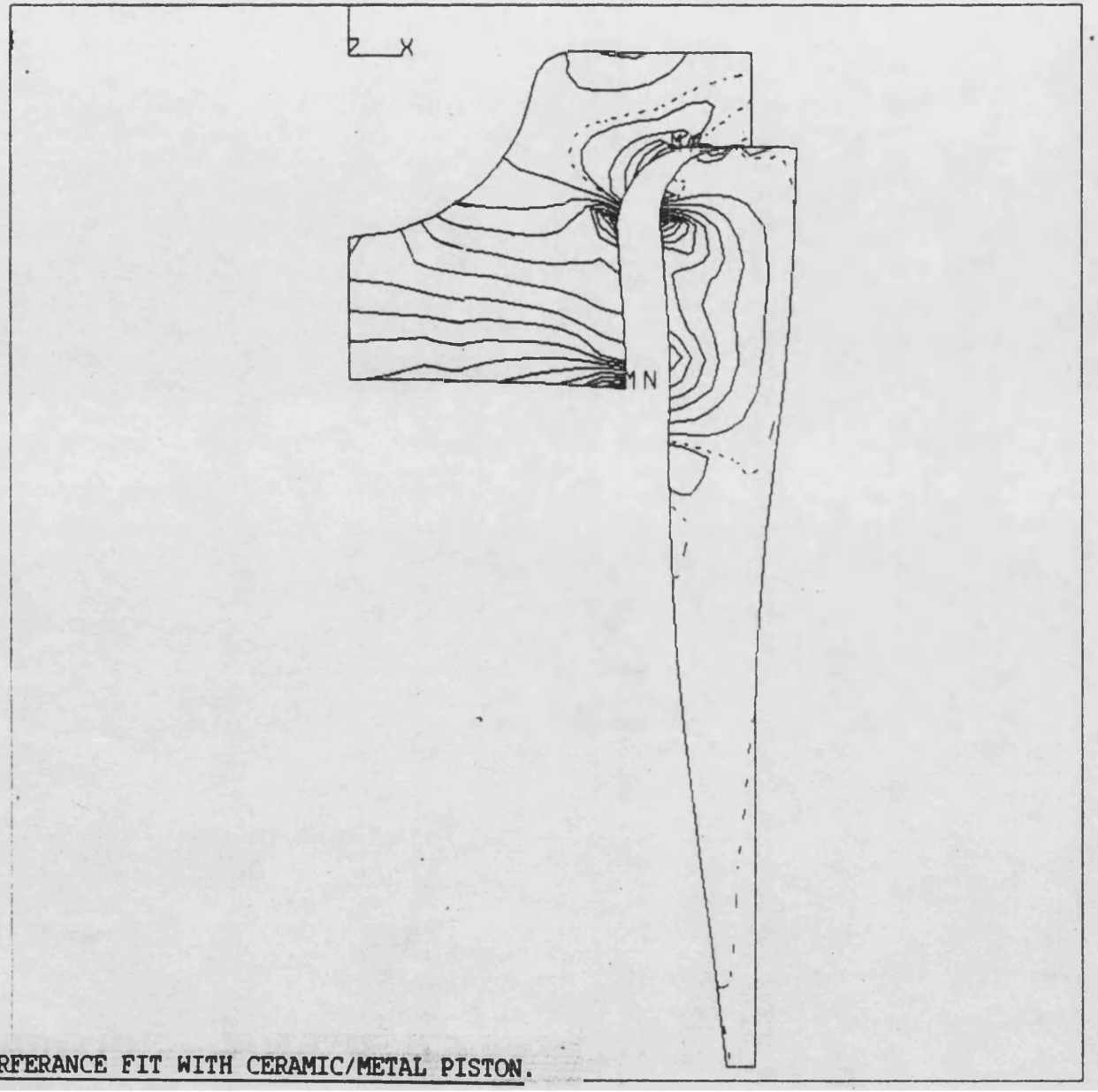

ANSYS 4.2
APR 11 1986
15:12:03
POST1 STRESS
STEP=1
ITER=20
SX
STRESS GLOBAL

ZV=1
DIST=.0583
XF=.0215
YF=-.053
EDGE
MX=341 1791
MN=101 03065

FIGURE 5.72 INTERFERANCE FIT WITH CERAMIC/METAL PISTON.

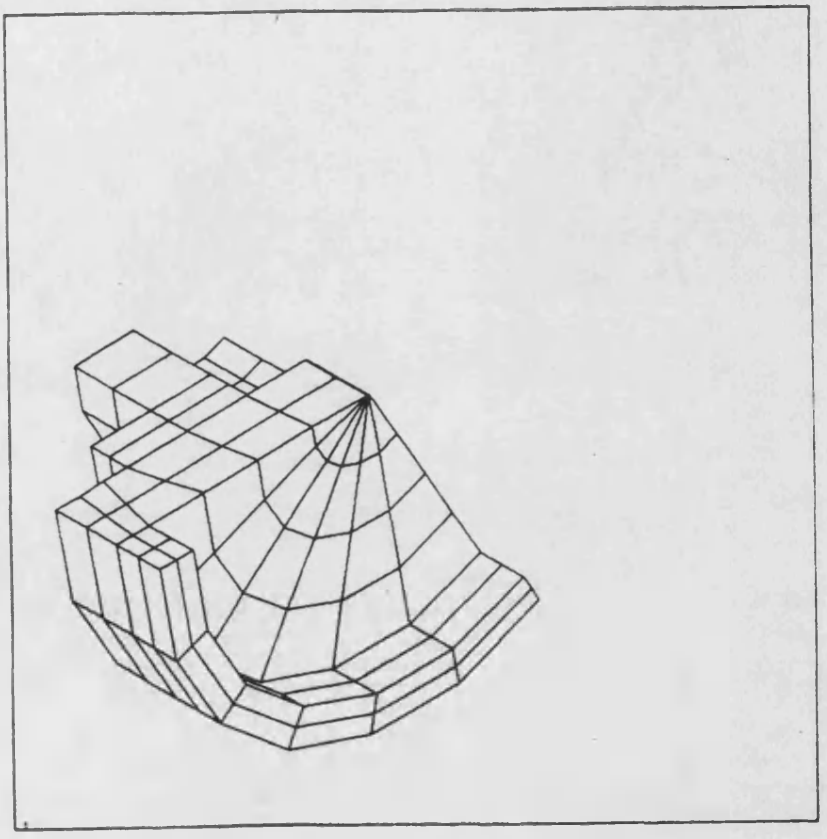

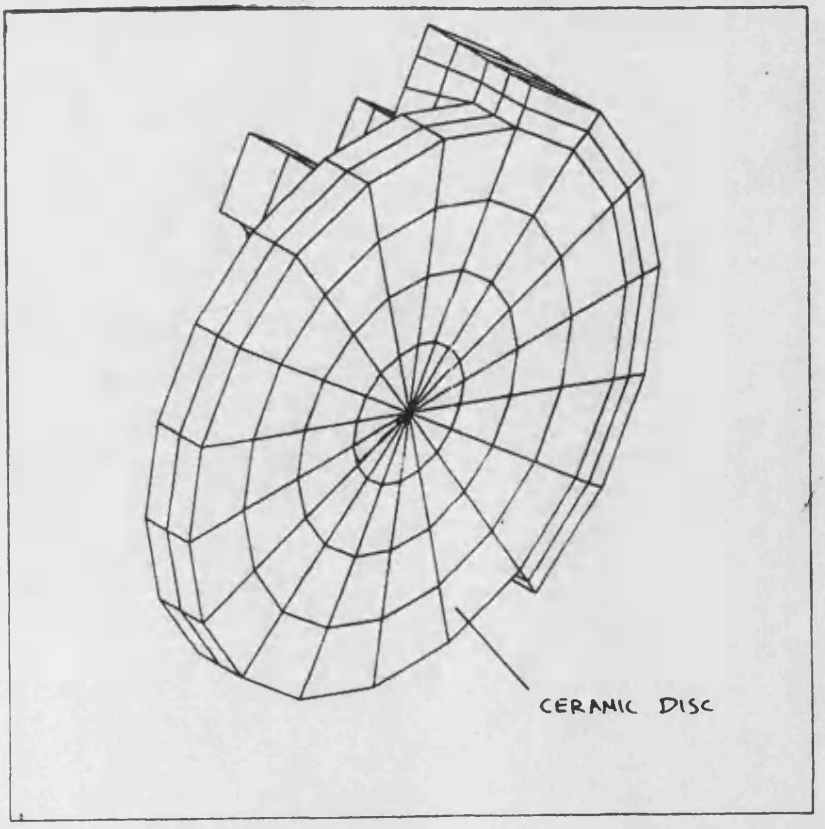

FIGURE 5.73 THREE DIMENSINAL FINITE ELEMENT ANALYSIS OF CERAMIC CLAMP.

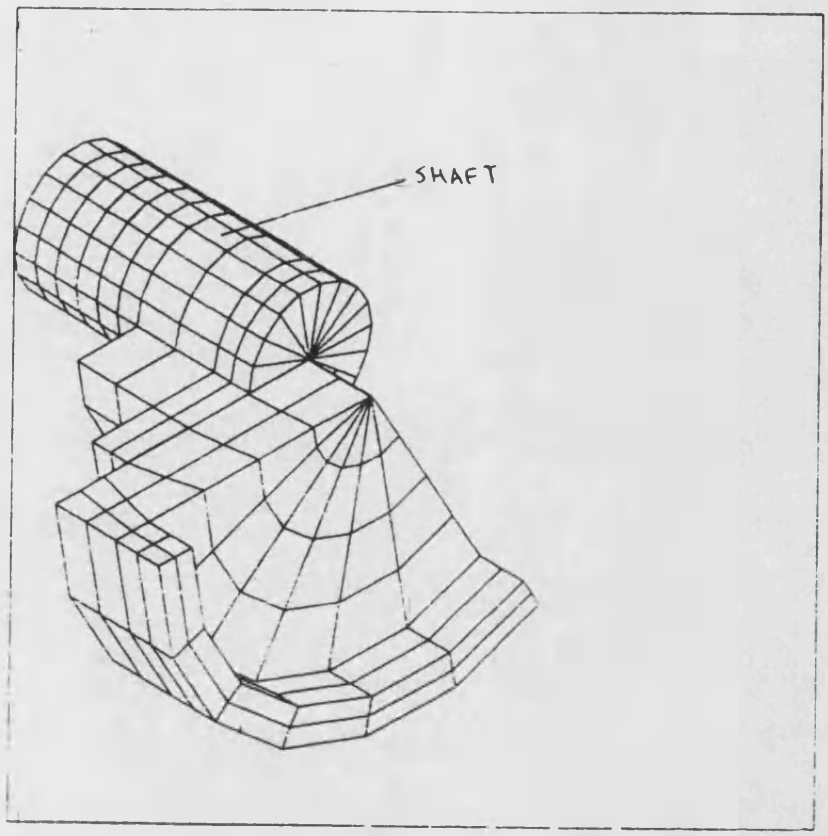

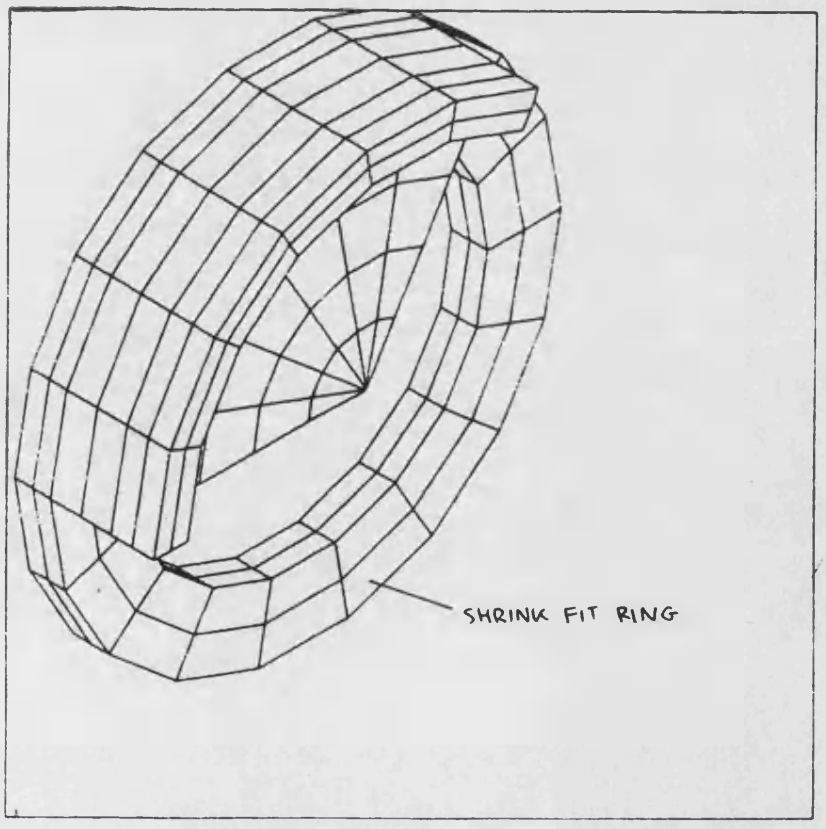

FIGURE 5.74 THREE DIMENSIONAL FINITE ELEMENT ANALYSIS OF CERAMIC CLAMP.

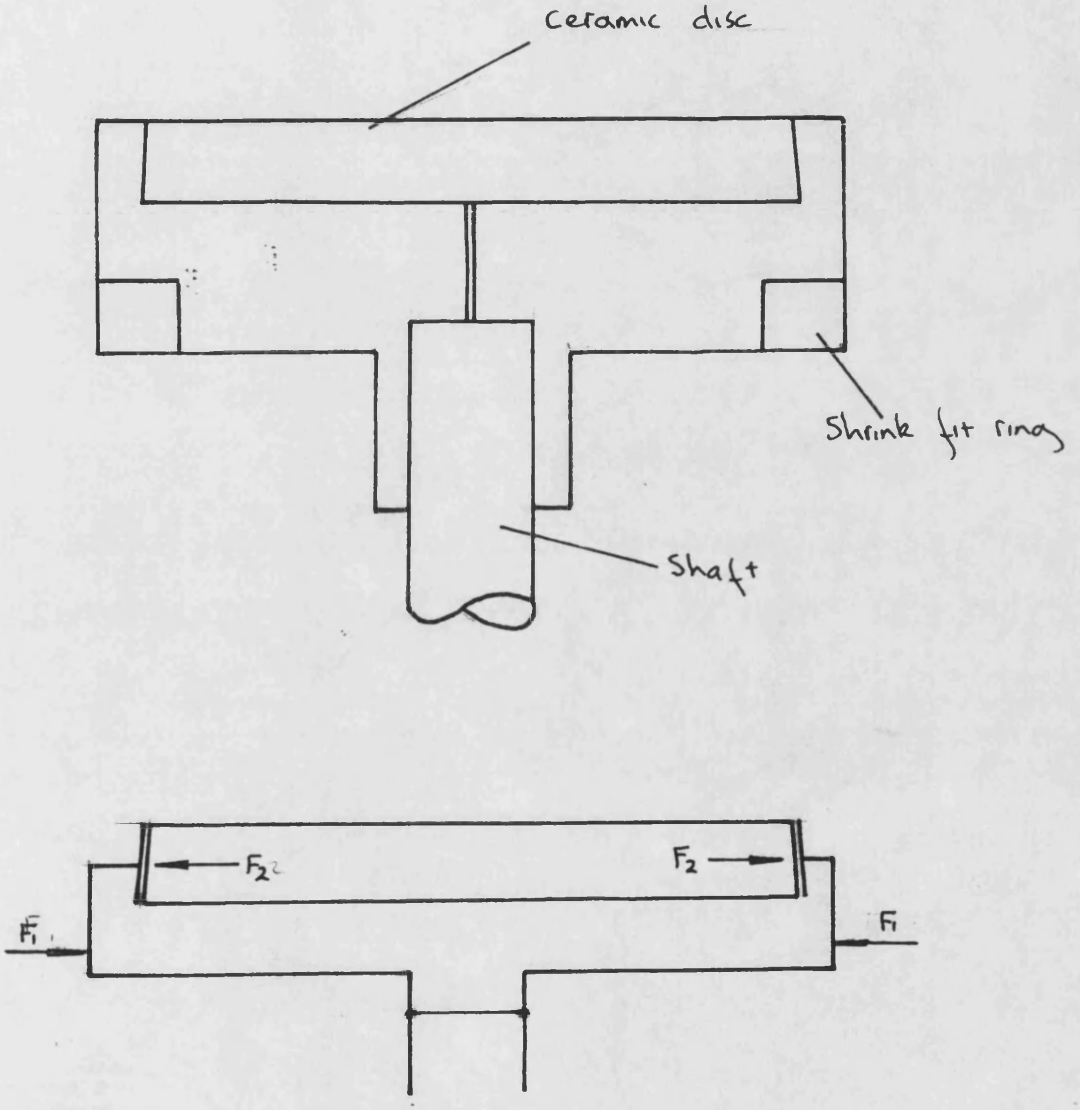

FIGURE 5.75 COMPRESSION FIT ON CERAMIC TEST PIECE HOLDER.

6.1 PREDICTION OF THE RESIDUAL STRESSES IN ZIRCONIA COATINGS

An examination of thick zirconia coatings generally reveals the presence of vertical cracking, even before they undergo thermal loading in an engine. Delamination can also develop between consecutive layers. As these imperfections significantly affect coating life, it is important to be able to assess why they form, and hence deduce the best way of maximising coating life.

With the process of plasma spraying there are many parameters which can be varied, including zirconia feed rate, distance between substrate and spray head and spray head traverse rate. At present these variables are set to values which experience has demonstrated can produce satifactory coatings, without any real appreciation of the reasons for success or failure. However, as coating thickness increases it has become necessary to gain a clearer understanding of how the variation of these parameters affects the coating. An attempt has therefore been made to assess theoretically the effect of these variables.

6.2 THEORETICAL ASSESSMENT OF COATING BEHAVIOUR

A simplified theoretical analysis of the residual stresses in a coated disc, as shown in Appendix 6.1, predicts very high stress levels. If we assume the substrate dimensions are unchanged by the plasma spraying then the stress levels present in a coated disc will simply be:

$$\sigma_r = \frac{\Delta T \gamma E}{(1-\upsilon)}$$

assuming axial stresses can be ignored.

Where ΔT is the difference between the substrates temperature and the temperature at which the zirconia can be assumed to behave elastically.

γ, E and ν are the thermal expansion, Young's Modulus and Poisson's ratio for the zirconia coating.

A temperature of approximately 2500^{o}C can be assumed for the end point of elastic properties. With these simplifications the stress levels developed in the coating can be expected to be of the order 6.5GPa for both steel and aluminium substrates. Although these are only approximate values it is evident that tension failure will occur.

The author has found little work where a satisfactory assessment of the residual stress distributions in ceramic coatings has been made. Accurate models of the temperature distribution[59,60] have been produced, but attempts to predict the corresponding stress levels have made assumptions which seem to be unsound,[61,62] such as assuming a linear variation of stress through the coating thickness. Before a numerical study of these stresses can be initiated it is important to examine the type of phenomenon which may effect the stress distibution through the coating.

The processes associated with the plasma spraying of zirconia coatings are very complicated, and they are best examined in a series of simple steps, initially making a large number of simplifications and subsequently examining the effects of introducing more realistic assumptions.

Figure 6.1 takes the case of an infinitely thick circular substrate, where there is no radiative or convective heat loss from the ceramic top surface. Edge effects are similarly ignored and it is assumed that the temperature and stresses in the substrate at no time rise above a level where plastic deformation will take place.

Zirconia coatings are built up by a series of passes with a plasma spray gun, each pass adding an increment of coating thickness. This examination is best initiated at the point where the first of these layers arrives at the substrate surface. Initially the zirconia layer can be assumed to be at a uniform temperature, above its melting point,

whilst the substrate will be at room temperature (unless it is pre-heated). Similarly the component will be stress free. This condition is shown in the first row in the sequence of diagrams shown in figure 6.1.

The temperature of the material adjacent to the interface will be affected first, as shown in the second row. The temperature increase in the metal is labelled ΔT_m and in the ceramic ΔT_c.
Elastic behaviour is assumed to start only below a temperature labelled T_E
Stresses are therefore developed only in the portion of the ceramic below T_E. The stresses are, in the ceramic:

$$\sigma_r = \frac{\Delta T_c \gamma_c E_c}{(1-\upsilon_c)}$$

and in the substrate:

$$\sigma_r = \frac{\Delta T_m \gamma_m E_m}{(1-\upsilon_m)}$$

as shown.

This process continues in row three, with the stress in the coating and substrate increasing. The final row shows the end condition with a uniform temperature through the coating and substrate. The stress in the coating is also uniform.

$$\sigma_r = \frac{\Delta T_c \gamma_c E_c}{(1-\upsilon)}$$

Where ΔT_c is the difference in temperature between the plastic-elastic change over temperature T_E and the final uniform temperature. With an infinite substrate thickness the stress derived within the substrate will be infinitely small.

In figure 6.2 the assumption that the metal temperature does not rise above a level where plastic deformation occurs is removed. The first column of diagrams sequentially shows the temperature distribution,

the second represents the stresses that would occur without plastic deformation of the base, and the third column shows the stress distribution with plastic deformation. Once plastic deformation takes place the zirconia coating will be able to contract freely towards a position where the net radial force is zero, ie $\sum F=0$. Part of the coating will therefore be in tension and part in compression, as shown in the first diagram in the third column. The stress in the substrate will be lost (or reduced) due to plastic deformation. This process will continue until the temperature in the substrate once again drops below the plastic limit. From this time onwards, in row three, the radial stress distribution will not be in equilibrium. The temperature drop indicated, ΔT_c, will cause an increase in radial stress above the equilibrium condition indicated in row three. Consequently the compressive component of stress in the coating will be reduced. Although it is possible that part of the zirconia layer will remain in compression the net radial force will be tensile.

During plasma spraying convective cooling of the top surface is used, as this has been found to improve coating performance. The consequence of this cooling is examined in figure 6.3, which also allows for plastic deformation of the base, but still assumes an infinitely thick substrate. The first column of diagrams shows the temperature distribution whilst the second plots the stress distribution derived in figure 6.2, where an adiabatic upper surface was assumed. The third column shows the additional effect of convective cooling. Initially the consequence of the convective cooling will be small in relation to the high heat transfer through the interface. But as the temperature difference between the substrate and coating reduces, the heat convection from the coating will become significant. This change becomes evident in the second row of diagrams, where the compressive stress will be reduced and hence a different equilibrium condition is reached. Once the elastic-plastic transformation temperature is reached in the substrate, as in row three then radial equilibrium will no longer apply, and a condition similar to that shown in row four will be reached. Tensile stresses will exist at the top surface and interface, with a compressive component centrally. The net radial force will still be tensile.

In practice the assumption that the substrate will not deform may be invalid, consequently the behaviour of a coating on a thin substrate is examined in figure 6.4. The second column shows the stresses arrising without component deformation, whilst the third demonstrates the effect introduced as a result of deformation. Initially the heat transfer will affect only a small region of the substrate, and deformation of the thin plate will not take place. However after the first time increment the substrate will have deformed in the manner shown. This will make little difference to the radial stress levels in the coating, as radial equilibrium will still be satisfied, but a compressive stress will be developed in the substrate. Once the substrate temperature returns to normal the component will resume its initial shape, this process will introduce a compressive stress in the coating as shown.

On subsequent coating passes the stresses built up will be different to that in the first layer, due to the insulating effect of the first ceramic layer. These stresses are shown in figure 6.5. The initial conditions are shown in the first row, with residual stresses still present in the first layer. Subsequently the heat input will diffuse through the structure. However, due to the insulating effect of the first zirconia layer the substrate will not reach as high a temperature as it did during the first pass. This is because the rate of heat flow into the metal will be reduced. Consequently more time is available to conduct the heat through the structure before high temperatures can be developed. In this case it is less likely that the temperature will rise above the plastic-elastic region.

During the transient the compressive stress in the second layer will be decreased by:

$$\sigma_r = \frac{\Delta T_2 \gamma_c E_c}{(1-\upsilon_c)}$$

Whilst a tensile stress will be introduced in the top layer:

$$\sigma_r = \frac{\Delta T_1 \gamma_c E_c}{(1-\upsilon_c)}$$

This process will continue until a uniform temperature is reached. As in the case examined in figure 6.1, a uniform tensile stress will be developed in the top coating. The bottom coating layer will return to its starting condition.

If the substrate deforms before the ceramics temperature drops to that where elastic properties dominate, then the tensile stress in the top layer will be reduced. However, with the effect of the insulative ceramic layer this is unlikely.

It is difficult to quantify the stress levels produced during coating formation through this theory. However, the nature of the stress distributions predicted in the previous analysis can be corroborated through experimental work; this is examined in section 6.4.

6.3 COMPUTER ASSESSMENT OF THE RESIDUAL STRESS DISTRIBUTIONS IN CERAMIC COATINGS

A complex study of the stress patterns present during coating formation was felt to be inappropriate. The number of variables which could not be established, or modelled accurately is too high. Instead a simplified study using the disc analysis program outlined in chapter four was used in conjunction with the program 'resid' shown in appendix 6.2. The following assumptions were made.

i) Each plasma sprayed layer was of uniform thickness, and applied instantaneously over the entire surface of the specimen.
ii) The time allowed between the application of each layer of zirconia was sufficient to allow a linear temperature distribution to be established.
iii) Convective cooling/heating of the front face was ignored.
iv) There was no plastic deformation within the substrate.
v) Elastic deformation of the substrate is prevented, this simplification corresponds to that of using an infinately thick plate.

These simplifications are those that were examined in figure 6.1.

The analysis used the following constants:

Melting point of zirconia	= 2700^{o}C
Latent heat of fusion	= 680J/gm
Deposition temperature	= 3000^{o}C

The temperature for the elastic-plastic transformation T_E was varied from 2500^{o}C to 2000^{o}C. Above this temperature the ability of the ceramic to hold a stress was assumed to be negligible.

Typical properties were chosen for the steel substrate and zirconia coating.

Figures 6.6 to 6.8 show the temperature and stress distributions derived during the formation of the first zirconia layer, assuming a elastic-plastic change over temperature, T_E of 2000^{o}C. The temperature distribution is shown in figure 6.6, decaying from a constant 3000^{o}C in the coating. A temperature plateau is reached at 2700^{o}C. This arises as the latent heat of fusion must be drawn from the material at this temperature. The maximum temperature occurring in the substrate is 450^{o}C. (A similar temperature was reached in the case of aluminium, and this would be more than sufficient to cause yielding)

The radial stress distribution is shown in figure 6.7, with the stress converging towards a constant value of 4.7GPa (tension). At no point are compressive stresses produced in the coating. Figure 6.8 indicates the axial stresses, which are all of a low level.

The previous analysis was repeated with T_E of 2500^{o}C, the residual stress distribution is shown in figure 6.9. In this case the stress levels converge to a value of 6GPa, without changing the characteristics of the curves.

The effect of applying a second layer of zirconia is demonstrated in figures 6.10 and 6.11. The rate at which the heat is transferred to the substrate is much lower than in the previous example, and conseqently the maximum temperature reached is 350^{o}C. the

yielding in the substrate will consequently be lowered, or eliminated. The radial stresses again reach a peak in the steady state.

6.4 COMPARISON WITH EMPIRICAL DATA

The Material Science Department at Bath Univerity have carried out a series of tests to establish the effect of changing the spraying parameters on the residual stress levels. In these tests most of the spraying parameters have been kept constant, changing only plasma gun traverse rate, gun-substrate separation and the material feed rate. The substrate size used for these trials was 100 x 25 x 3mm thick.

To establish the residual stress levels developed in the coating, the zirconia is separated from the substrate. This is achieved by dissolving the substrate in an acid which does not affect the ceramic. The length of the ceramic strip when attached to the substrate, and its free length can be used together with its curvature to establish the mean stress distribution, as in figure 6.12. This data can therefore be used to check the validity of the model described earlier in this chapter.

The effects of changing the spraying parameters and substrate materials are best discussed separately.

i) General stress distribution through coating: When the substrate is dissolved leaving coating and bond layer, the coating is observed to bend away from the substrate and increase in length. This behaviour indicates that the coating had a net compressive loading, with the lowest compressive (perhaps tensile) loading present in the bond coat or adjacent ceramic layer. When the bond coat is subsequently removed there is a further expansion in length, and the direction of curvature changes, this is shown in figure 6.13.

Both of these characteristics are in agreement with the model proposed. As was seen in figure 6.4, a tensile stress should be developed in the bond coat. Once this bond coat has been removed then the stress distribution proposed in figure 6.5, (both compressive

and tensile layers) causes the change in the direction of curvature observed.

However, as a net expansion in length is observed, then compressive stresses must dominate the ceramic when it is still attached to the substrate. This suggests that a high degree of curvature is exhibited by the specimen during the elastic-plastic change over period. Once this specimen has cooled a net compressive stress will therefore be introduced. The effect of this curvature will be greatest in thin substrates as they will deform most. Spraying onto a piston crown would not produce such large curvatures and so compressive stresses may not dominate the stress distribution in a more realistic application.

ii) Varying spray gun-substrate separation: Figure 6.14 shows that the curvature increases (radius increases), with spray distance. As curvature increases the difference in stress levels between the top and bottom of the coating reduces.

This behaviour is to be expected as a decrease in distance between spray gun and target will increase the local heat transfer. This will be accompanied by an increase in local substrate temperature, and hence depth to which plastic deformation will occur. Under this condition the behaviour indicated in figure 6.4, will be exhibited; with a compressive lower layer of ceramic and a tensile upper region, causing higher curvature. As the spray gap is increased the ability of the substrate to yield and redistribute the stresses will be lestened, and the compressive first layer will not develop, the level of curvature will therefore be reduced.

iii) Variation in the gun traverse rate: To maintain a uniform coating thickness throughout the test samples the number of passes was increased. As the travel rate is increased the radius of curvature is observed to increase to a maximum value, as in figure 6.15. This behaviour occurs for similar reasons to ii) above: an increase in traverse rate leads to a reduction in local heat flow, and a reduction in the plastic deformation, hence a reduction in the stress gradient and curvature.

The decrease in curvature shown with higher spray rates is likely to be caused by the increased number of passes made by the spray gun, which was used to maintain uniform thickness throughout this test. The stress distribution proposed in figure 6.4, would explain this behaviour. The first ceramic layer will be in compression, the rest in tension, therefore the more passes made the less effect the first layer will have on the coatings behaviour, thus decreasing the radius of curvature.

iv) Effect of different substrate materials: Constant spray rates, speeds and distances were maintained for three substrate materials aluminium, copper and mild steel. The sprayed layer on mild steel exhibited the largest radius of curvature, the aluminium the smallest. Once again this can be explained in terms of the plastic behaviour of the substrate. The lower the melting point of the material the more plastic deformation will take place, maximising the stress gradient, and hence reducing the radius of curvature.

This work indicates the validity of the assumptions made in the analysis. However, sever.al further points should be made

a) The substrates used by Materials Science were thin, easily deformed structures. Spraying onto a piston, or similar structure will prevent the deformation which led to the net compressive stresses in the ceramic layer.

b) If a bond coat is used on aluminium then the ability of the substrate to accommodate contractions of the coating will be reduced as the bond coat has a high melting point.

Despite these limitations it is obvious that several effects which occur during coating formation are desirable.

c) A compressive layer of zirconia next to the interface is beneficial as it will prevent cracks propagating to the interface, thus reducing access for chemical attack.

d) Pre-heating of the substrate will increase the region which

will undergo plastic deformation.

6.5 MAXIMISING COATING LIFE THROUGH THE MODIFICATION OF RESIDUAL STRESS PATTERNS

Although this work has been unable to predict exact stress levels produced during coating formation several conclusions can be drawn:

Experimentation with the plasma spraying process has shown that cooling of the front face increases coating life. Cooling of the rear face does not have this effect. From the theoretical analysis the opposite trend would be expected. Back face cooling would increase the deformation of the substrate, thus increasing compressive stresses in the coating on cooling. Similarly front face cooling would reduce the plastic deformation of the substrate, leading to higher tensile stresses in the coating. There are two effects which can account for this contradiction.

i) If the front face becomes too hot chemical attack of the bond layer will occur during coating formation.

ii) If compressive stresses are introduced throughout the coating few cracks will develop. This has been shown to reduce life in an engine, as the cracks act as stress lowering agents as examined in chapter five.

Back face cooling in an inert atmosphere will reduce the problem of chemical attack of the bond coating, and may offer a possible method of increasing coating life.

Increasing the substrate temperature during coating formation is another method which has been advanced to increase coating life. Obviously this can only be attempted in an inert environment or chemical attack of the bond layer will be severe. This increase of the substrate temperature would decrease the tensile stresses in the coating, as the complete component would contract during cooling. In addition the depth to which the substrate deforms plastically could

be increased. If this were coupled with controlled front/rear face cooling it may be possible to maintain this plastic region throughout the formation of the second and subsequent coating layers, thus producing coatings entirely in compression.

The effects of using graded coatings would be very complex, and it is unclear how they would affect residual stress formation.

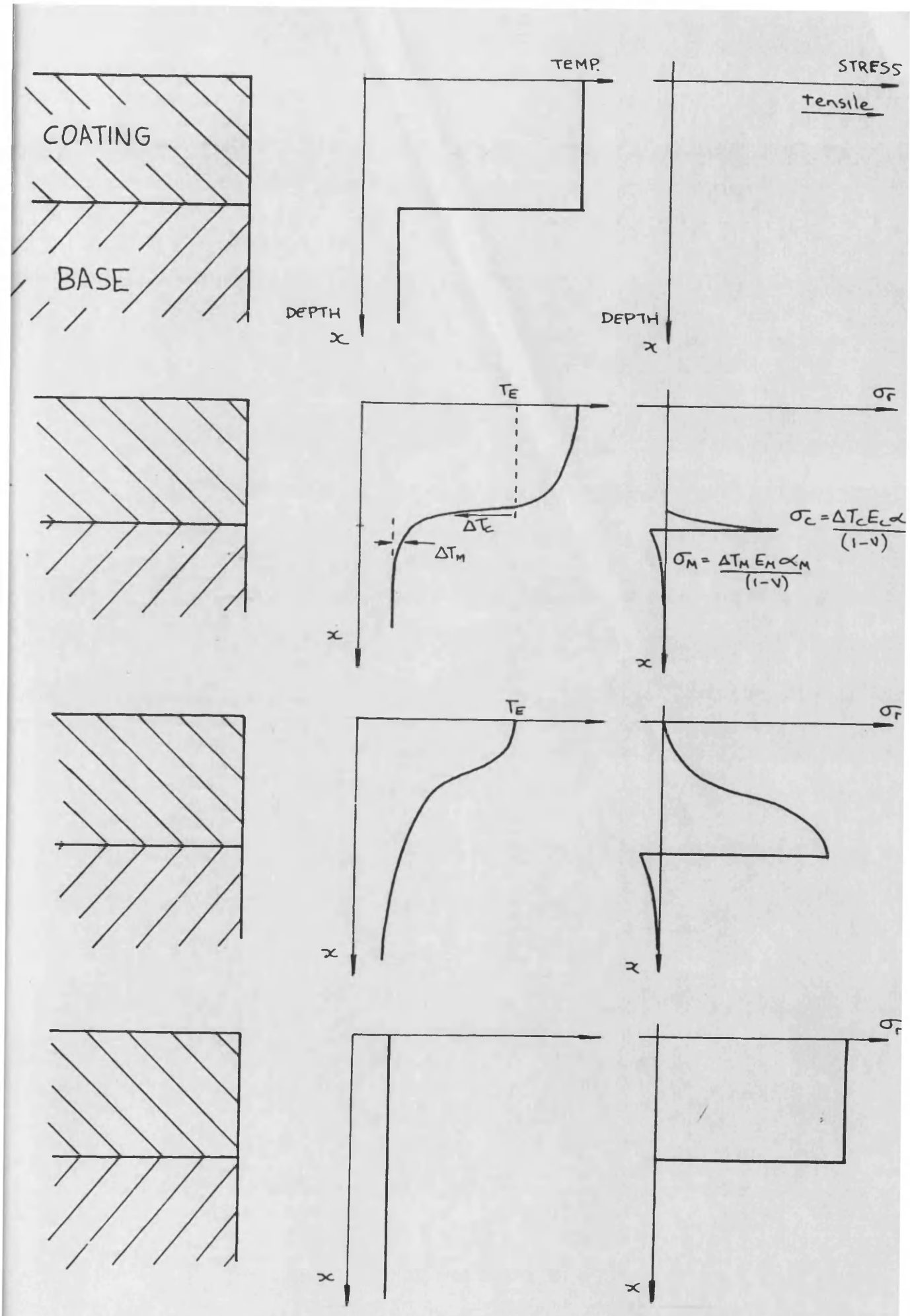

FIGURE 6.1 DEVELOPMENT OF RESIDUAL STRESSES. ASSUMING AN INFINITE PLATE, AND NO PLASTIC DEFORMATION.

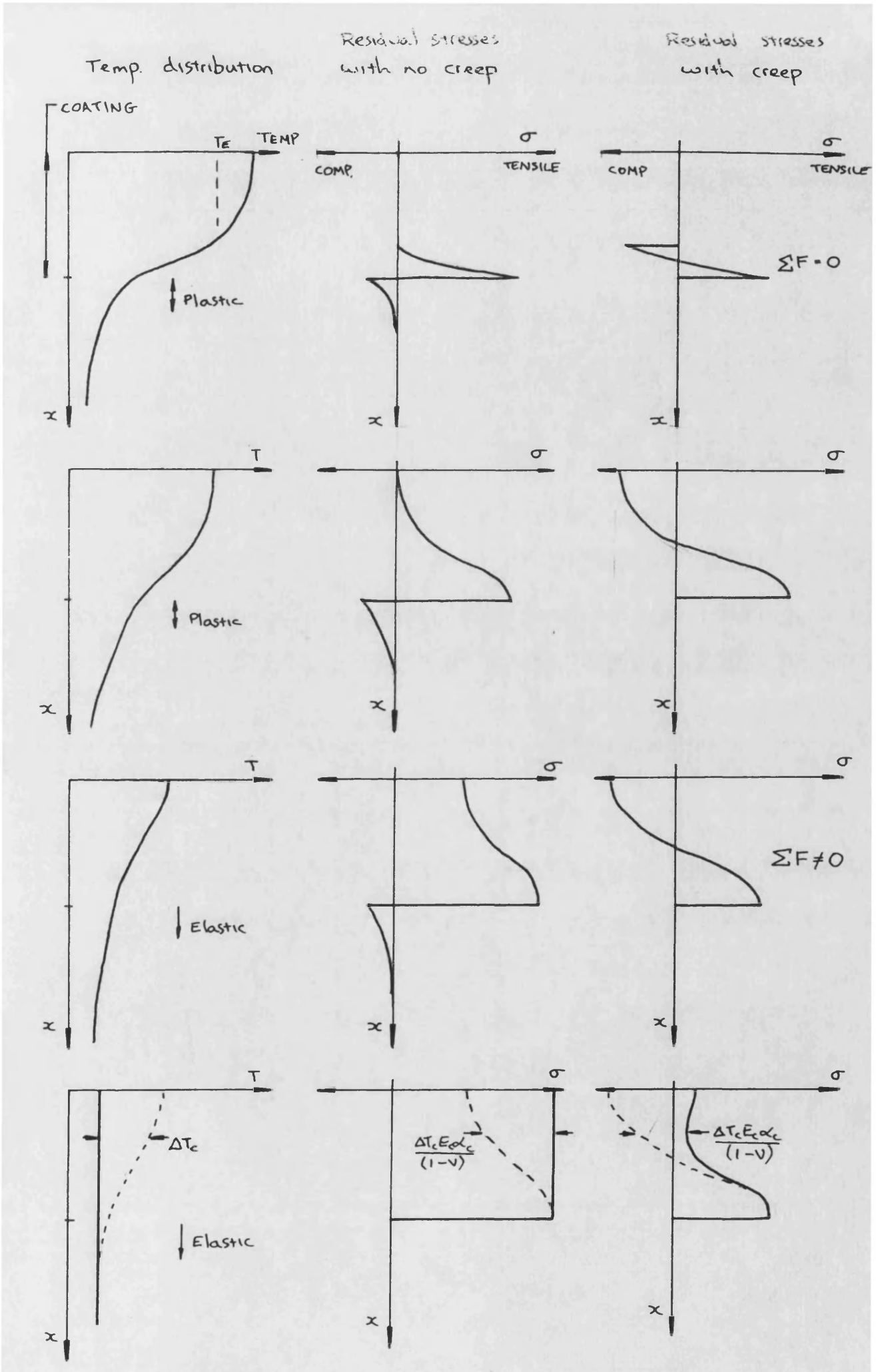

FIGURE 6.2 DEVELOPMENT OF RESIDUAL STRESSES, IN AN INFINITE PLATE

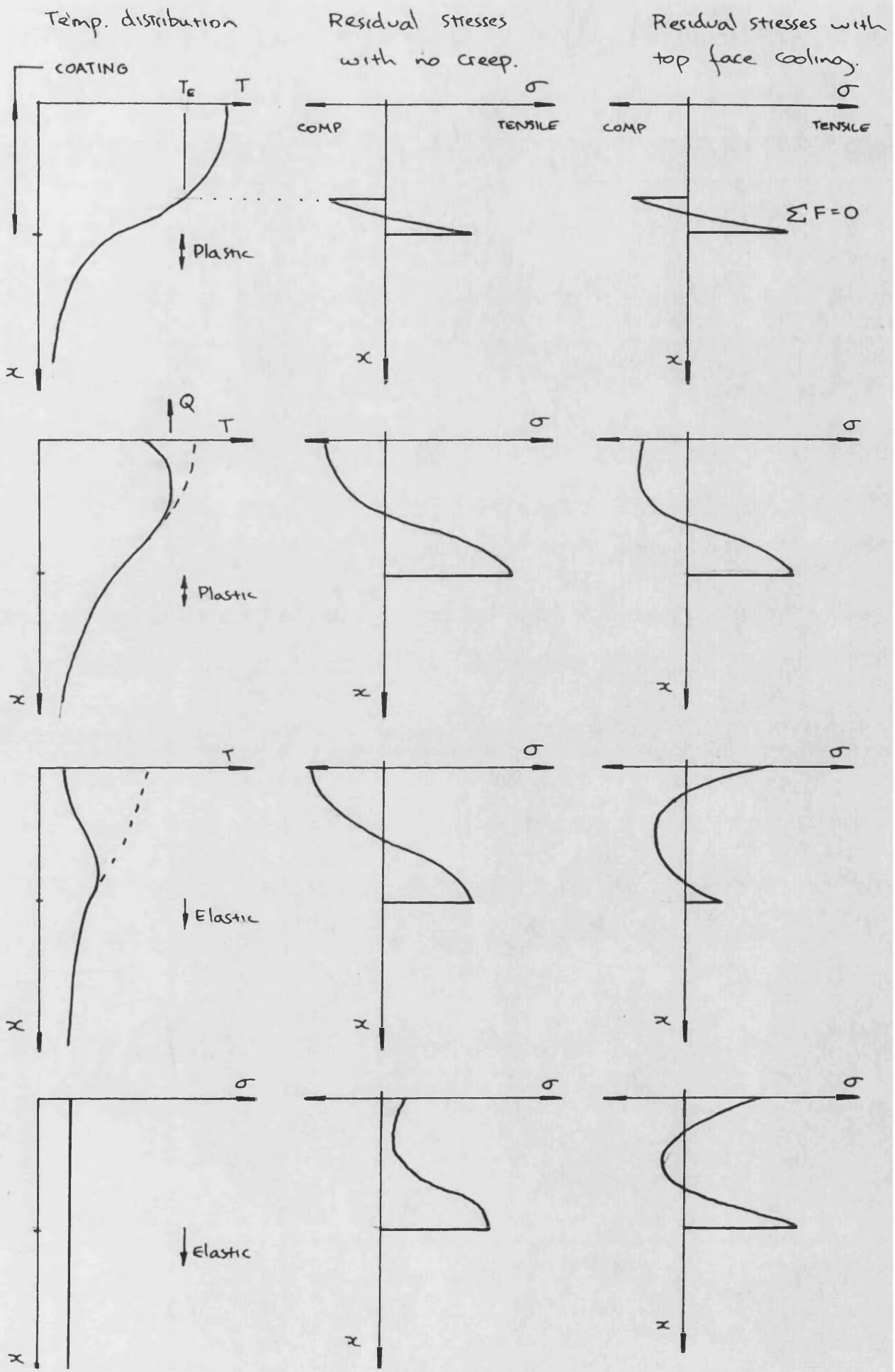

FIGURE 6.3 RESIDUAL STRESSES IN A COOLED COATING, ASSUMING AN INFINITE PLATE

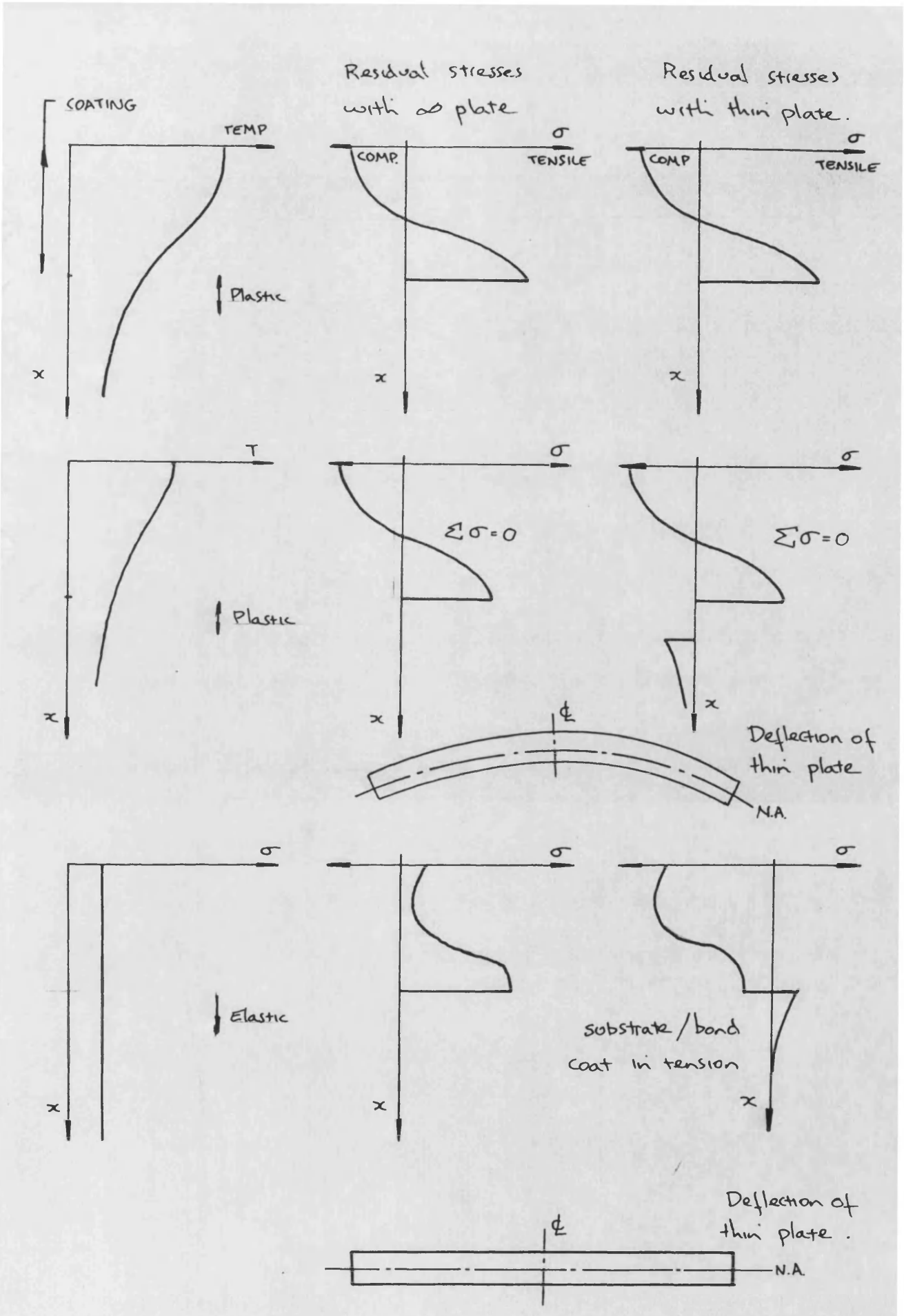

FIGURE 6.4 RESIDUAL STRESSES IN A FINITE THICKNESS PLATE, WITH PLASTIC DEFORMATION.

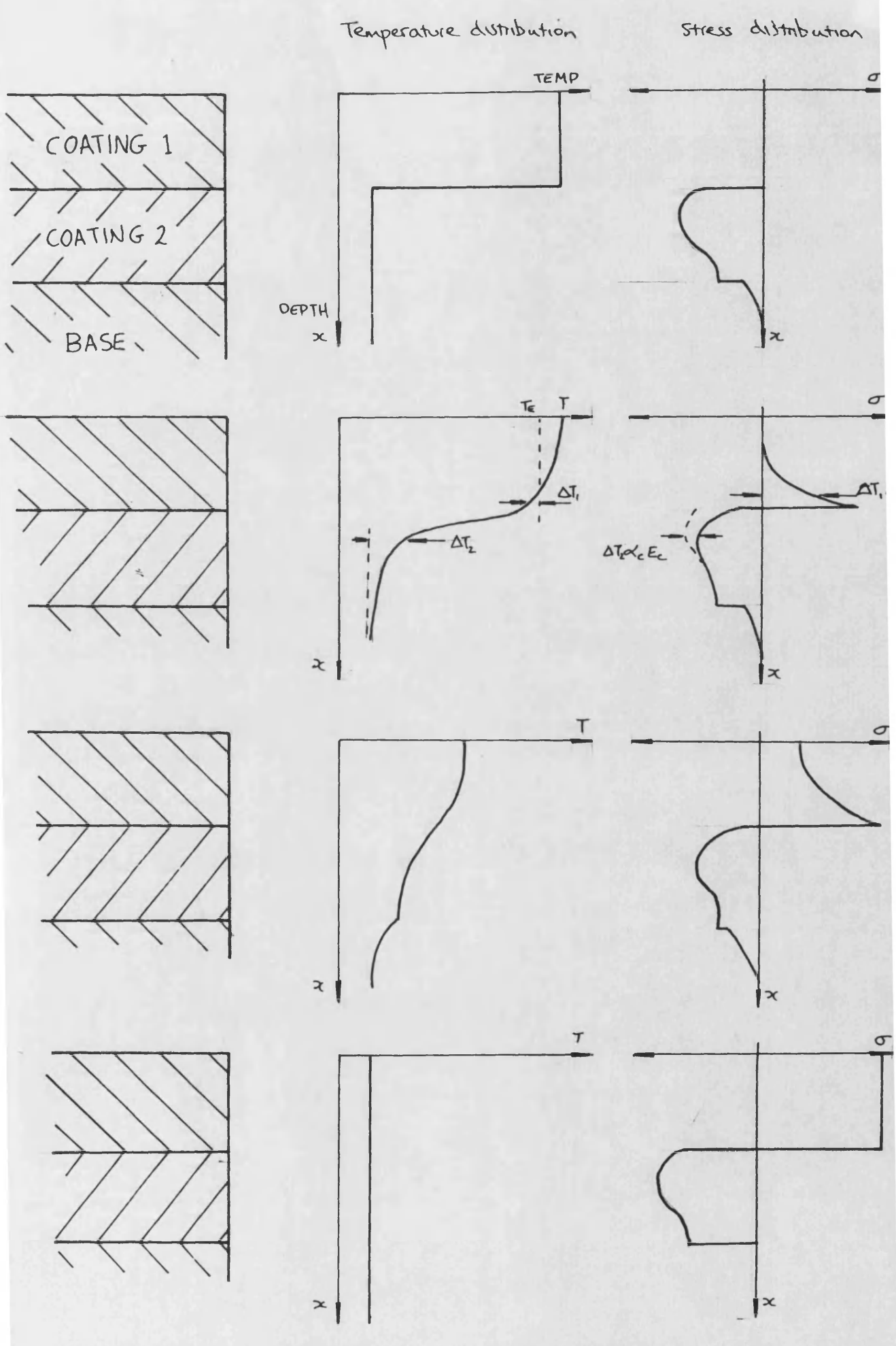

FIGURE 6.5 RESIDUAL STRESSES PRODUCED BY SUBSEQUENT SPRAY PASSES.

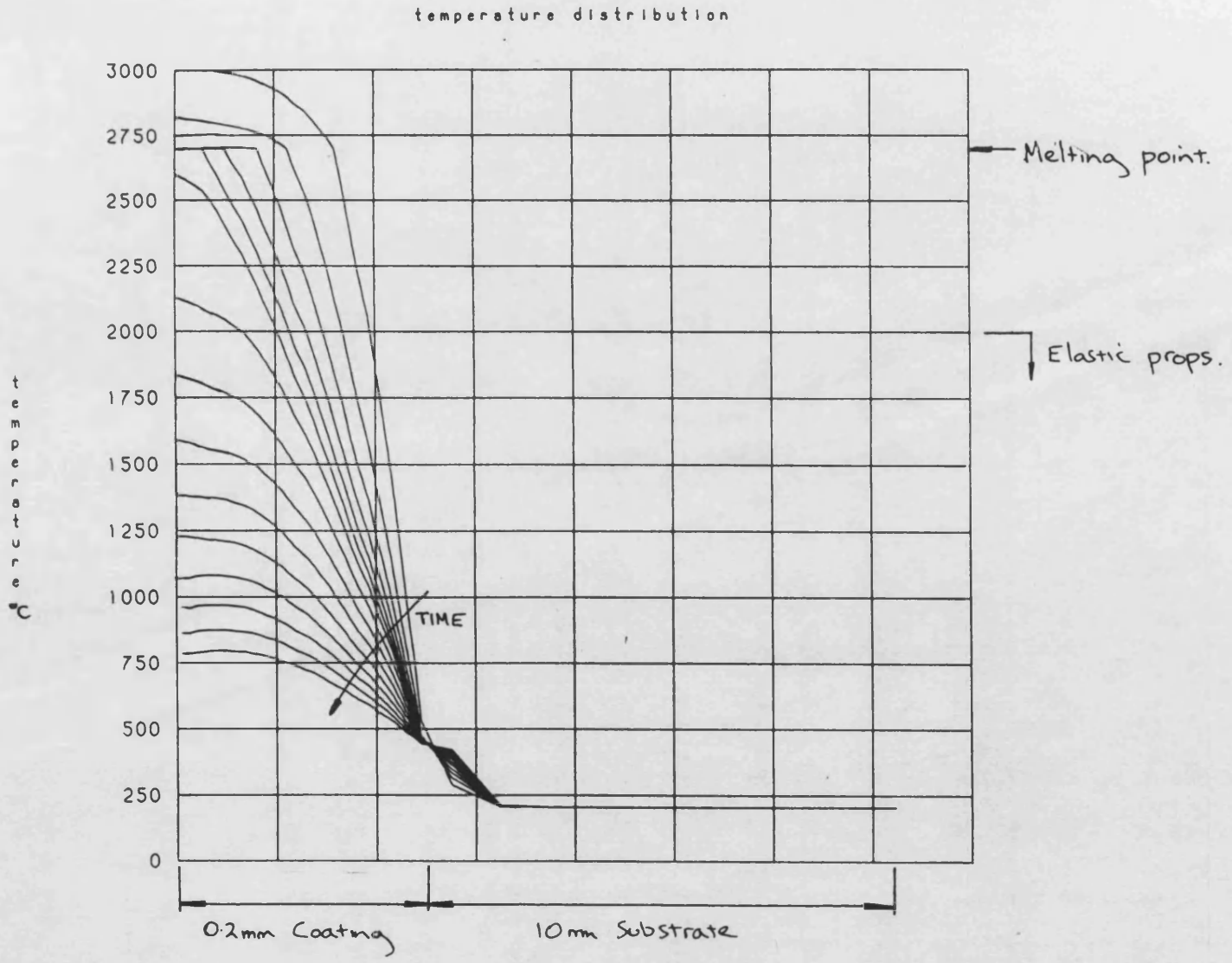

FIGURE 6.6 TEMPERATURE TRANSIENTS DURING COOLING OF A 0.2mm ZIRCONIA COATING.

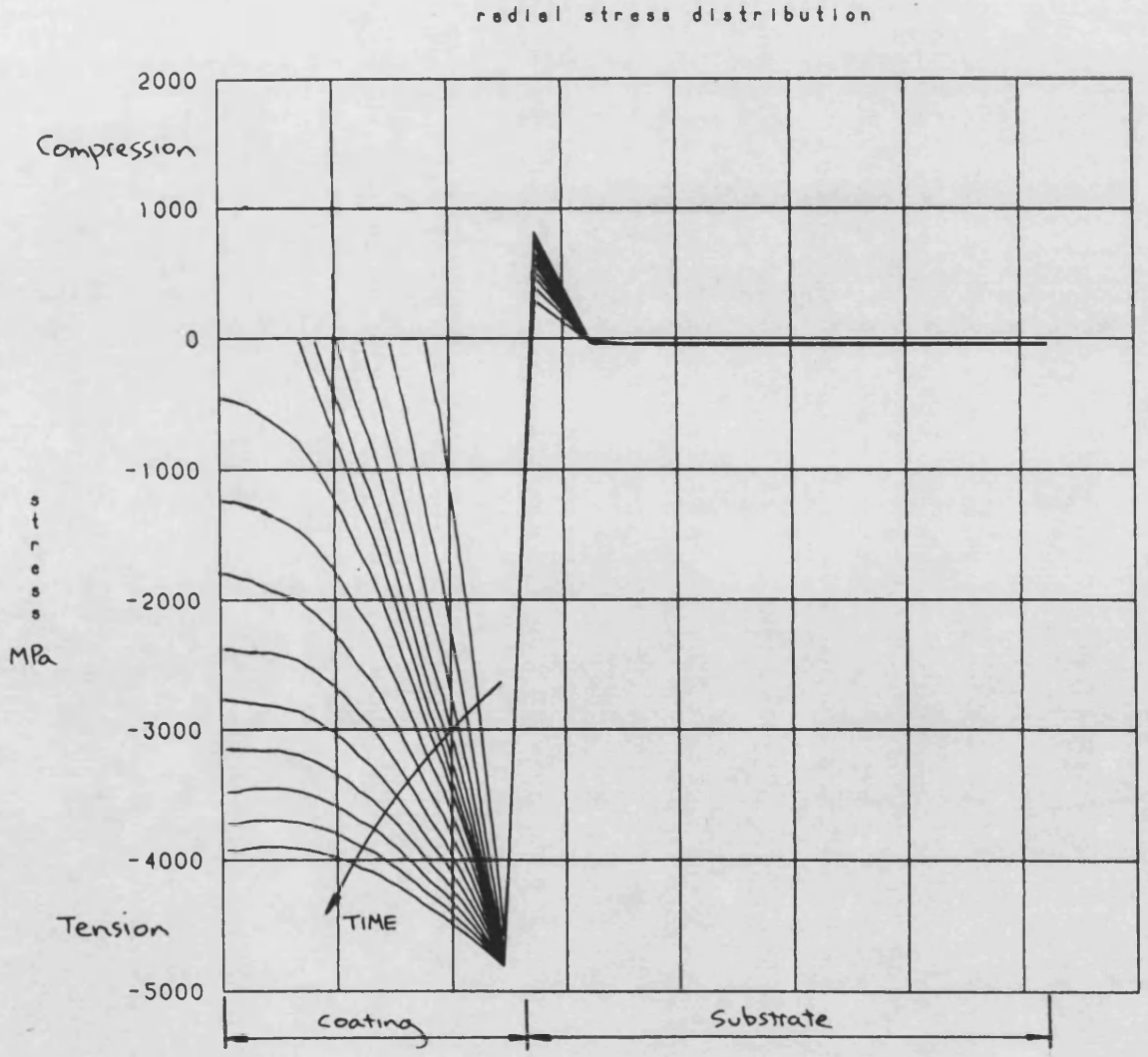

FIGURE 6.7 RADIAL STRESS TRANSIENT DURING COOLING OF A 0.2mm ZIRCONIA COATING (Te=2000 C)

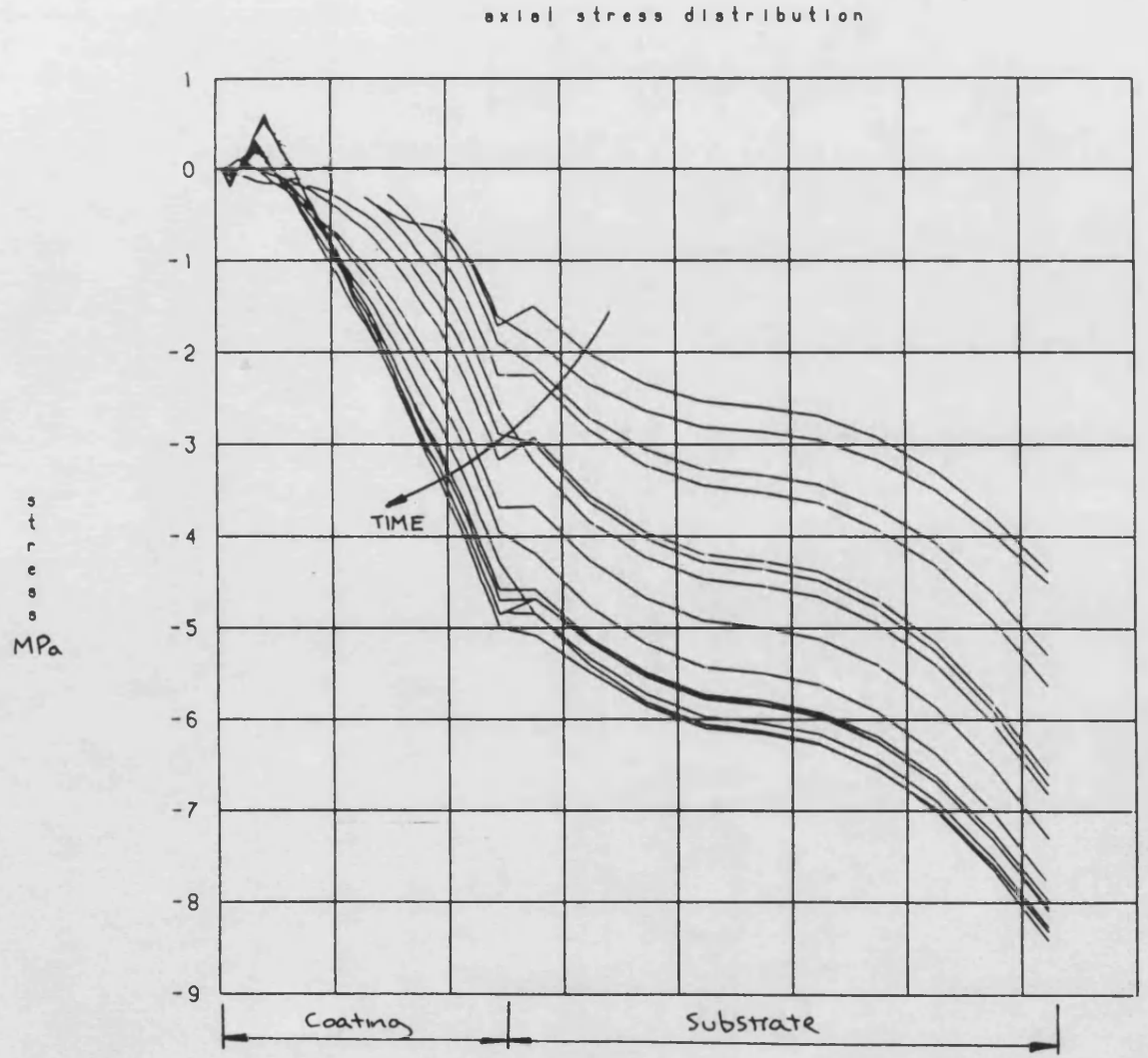

FIGURE 6.8 AXIAL STRESS TRANSIENT DURING COOLING OF A 0.2mm ZIRCONIA COATING. (Te=2000 C)

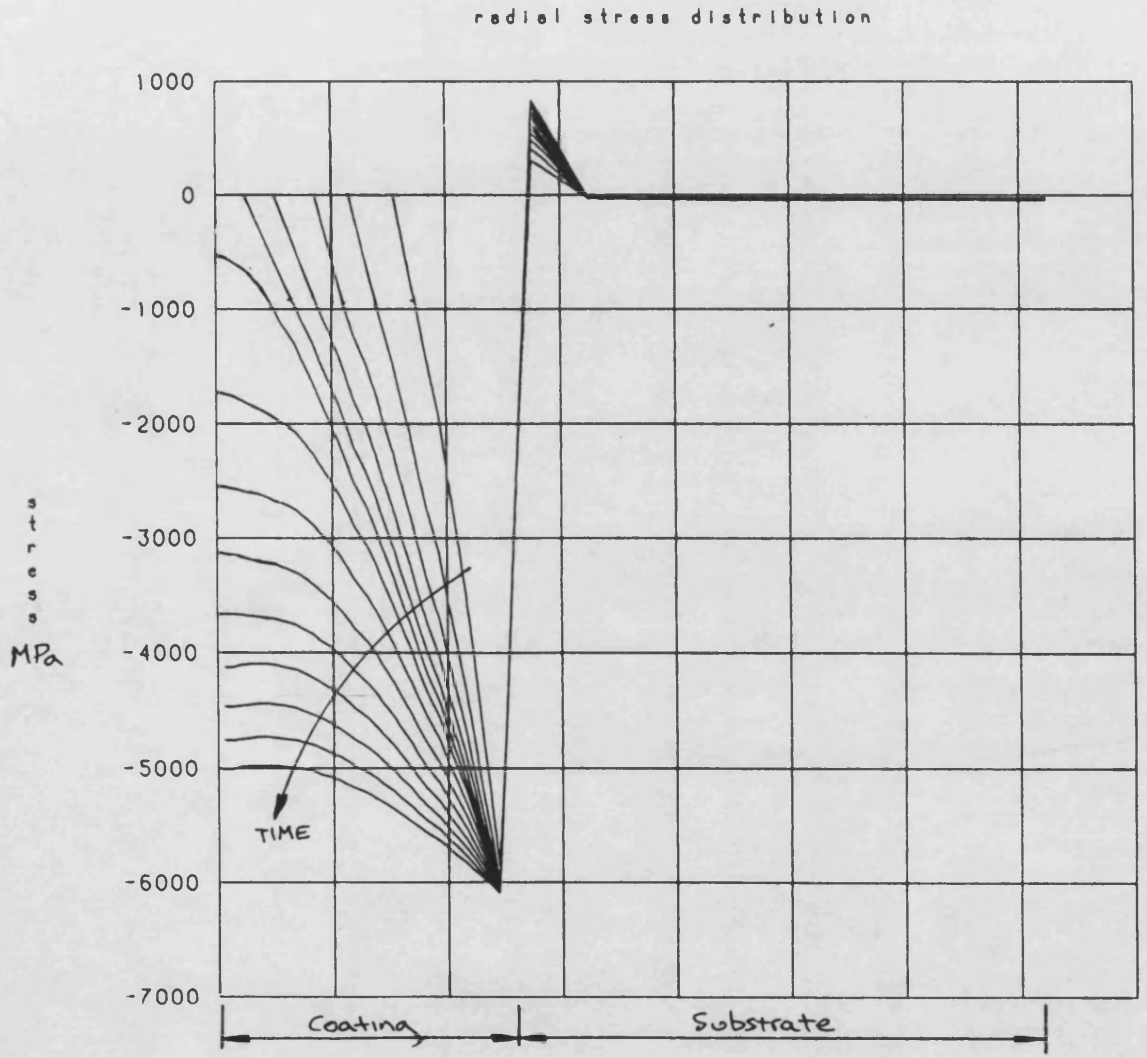

FIGURE 6.9 RADIAL STRESS TRANSIENT DURING COOLING OF A 0.2mm ZIRCONIA COATING. (Te=2500C)

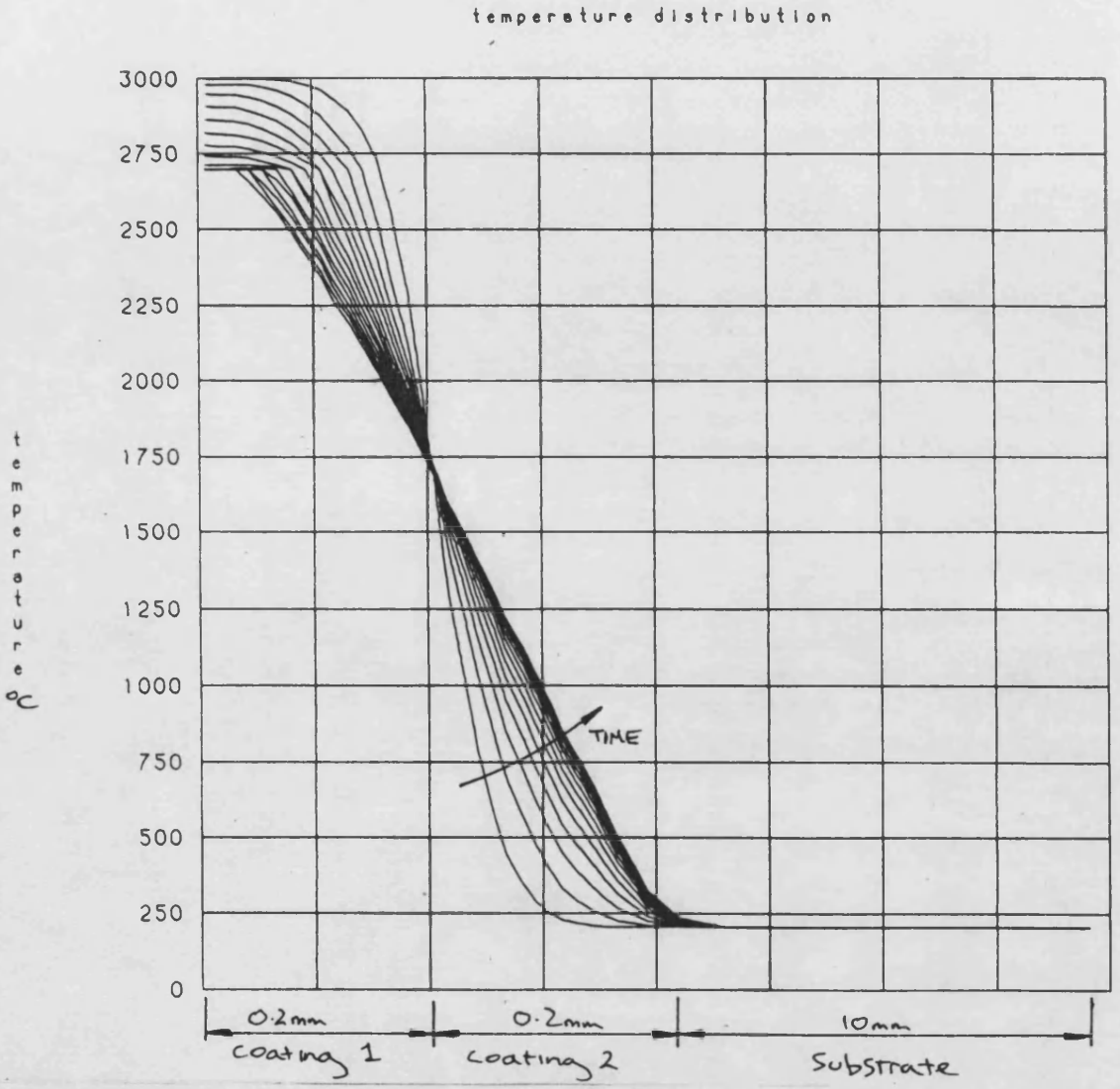

FIGURE 6.10 TEMPERATURE TRANSIENT DURING COOLING OF A SECOND 0.2mm ZICONIA COATING. (Te=2500 C)

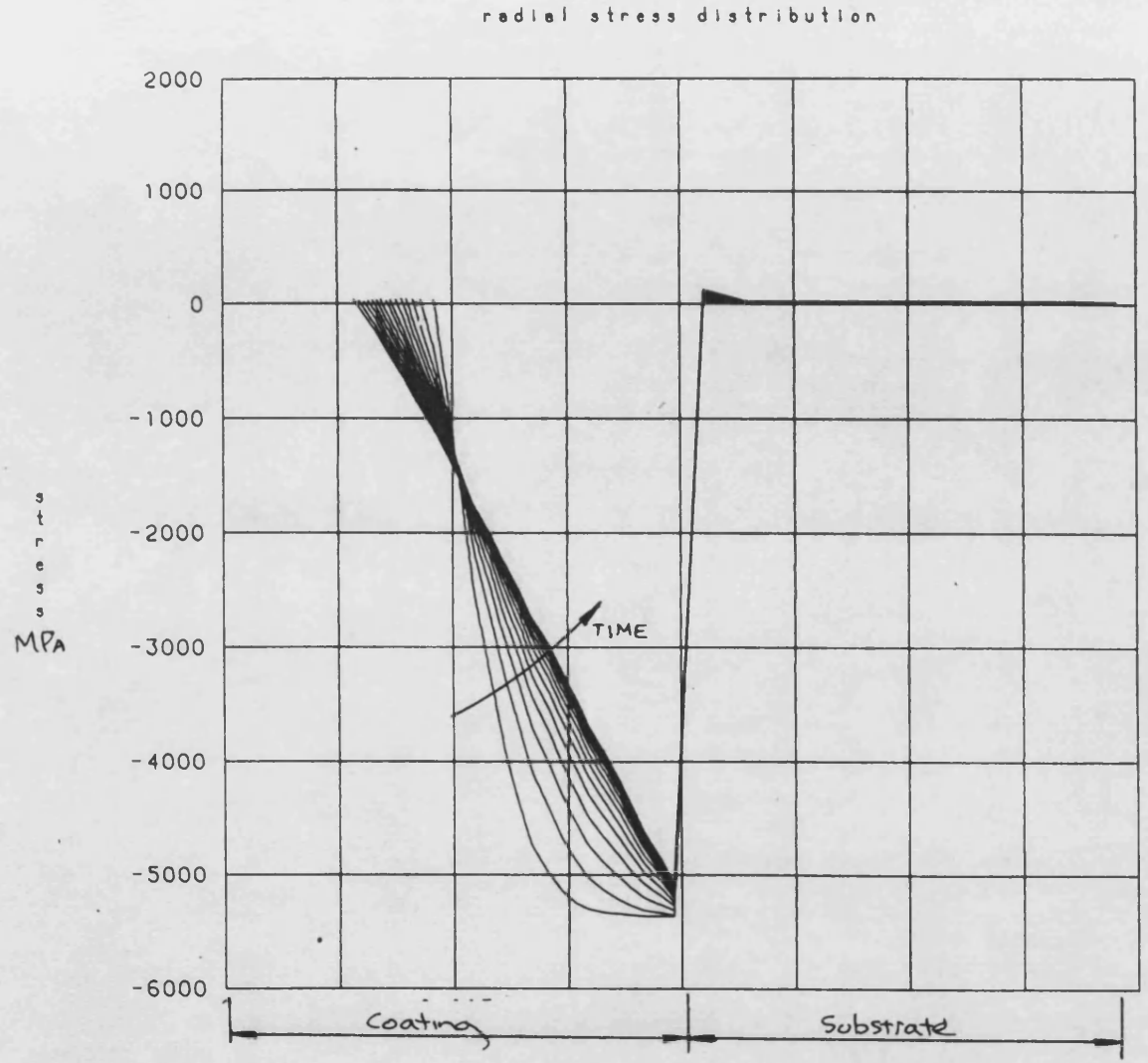

FIGURE 6.11 RADIAL STRESS TRANSIENT DURING COOLING OF A SECOND 0.2mm ZICONIA COATING. (Te=2500 C)

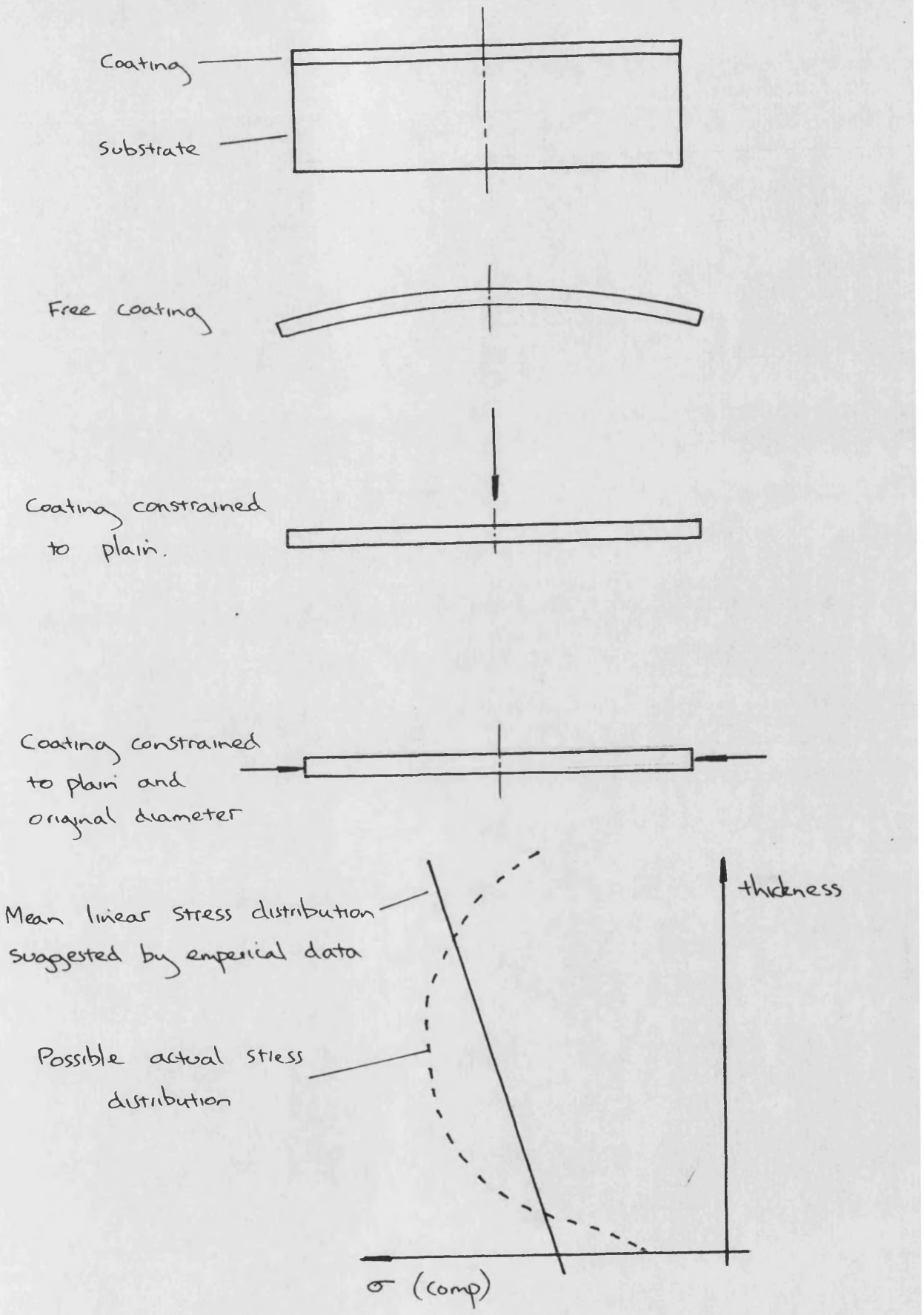

FIGURE 6.12 CALCULATION OF MEAN STRESS DISTRIBUTION IN A COATING FROM EMPERICAL DATA.

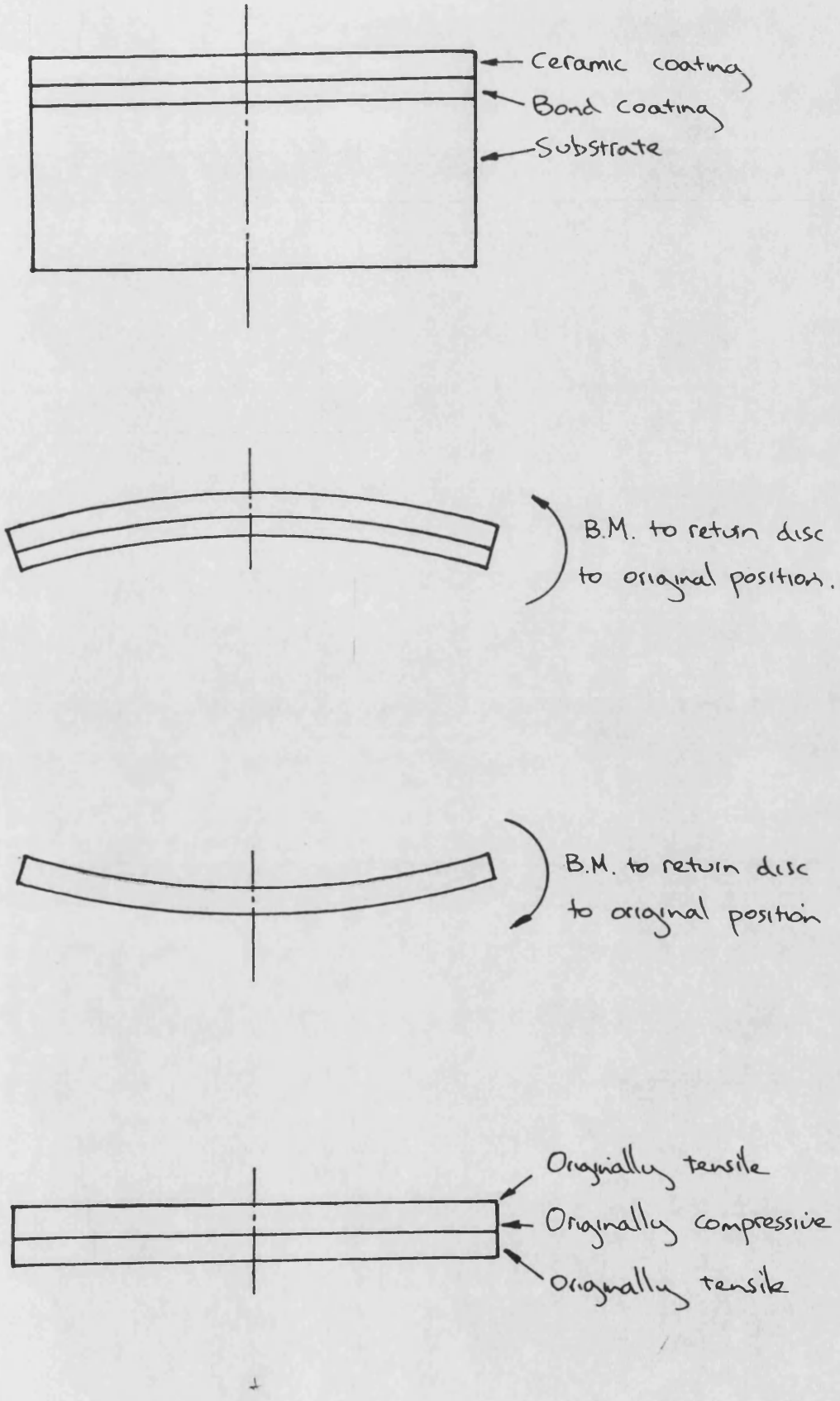

FIGURE 6.13 CHANGE IN CURVATURE OF A ZIRCONIA COATING WHEN REMMOVED FROM ITS SUBSTRATE.

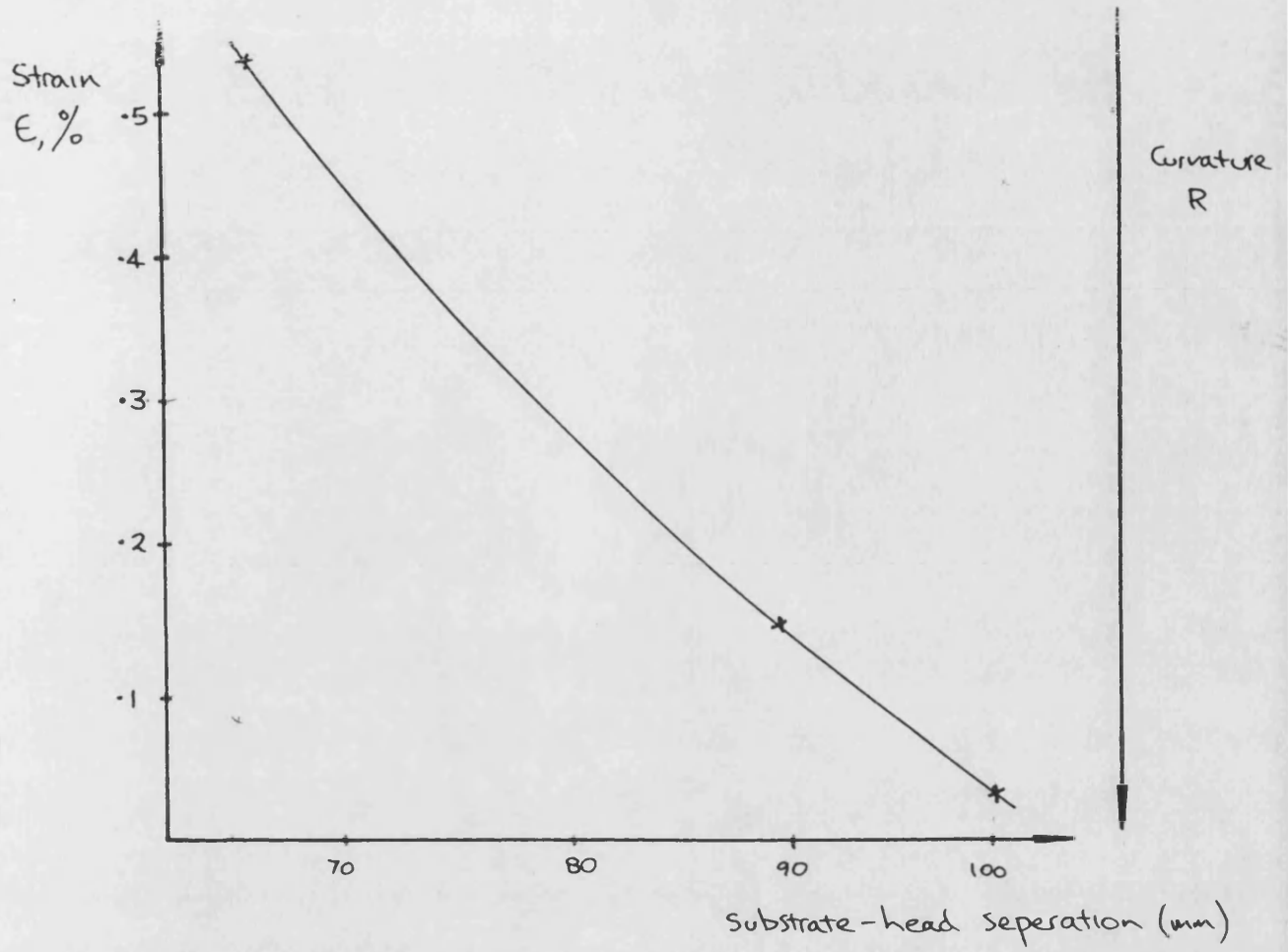

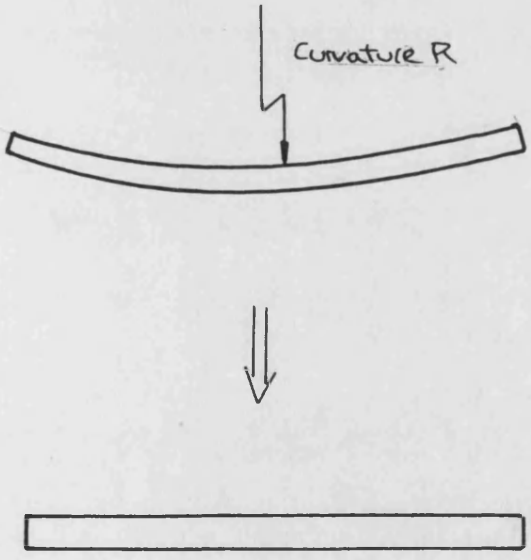

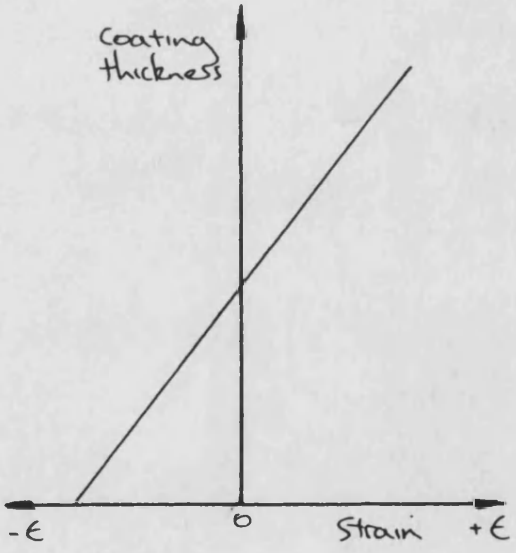

Flattening out the coating recreates the difference in Strain between the top and bottom surfaces, this strain is shown above.

FIGURE 6.14 STRAIN PRODUCED BY VARYING SPRAY GUN - SUBSTRATE SEPERATION.

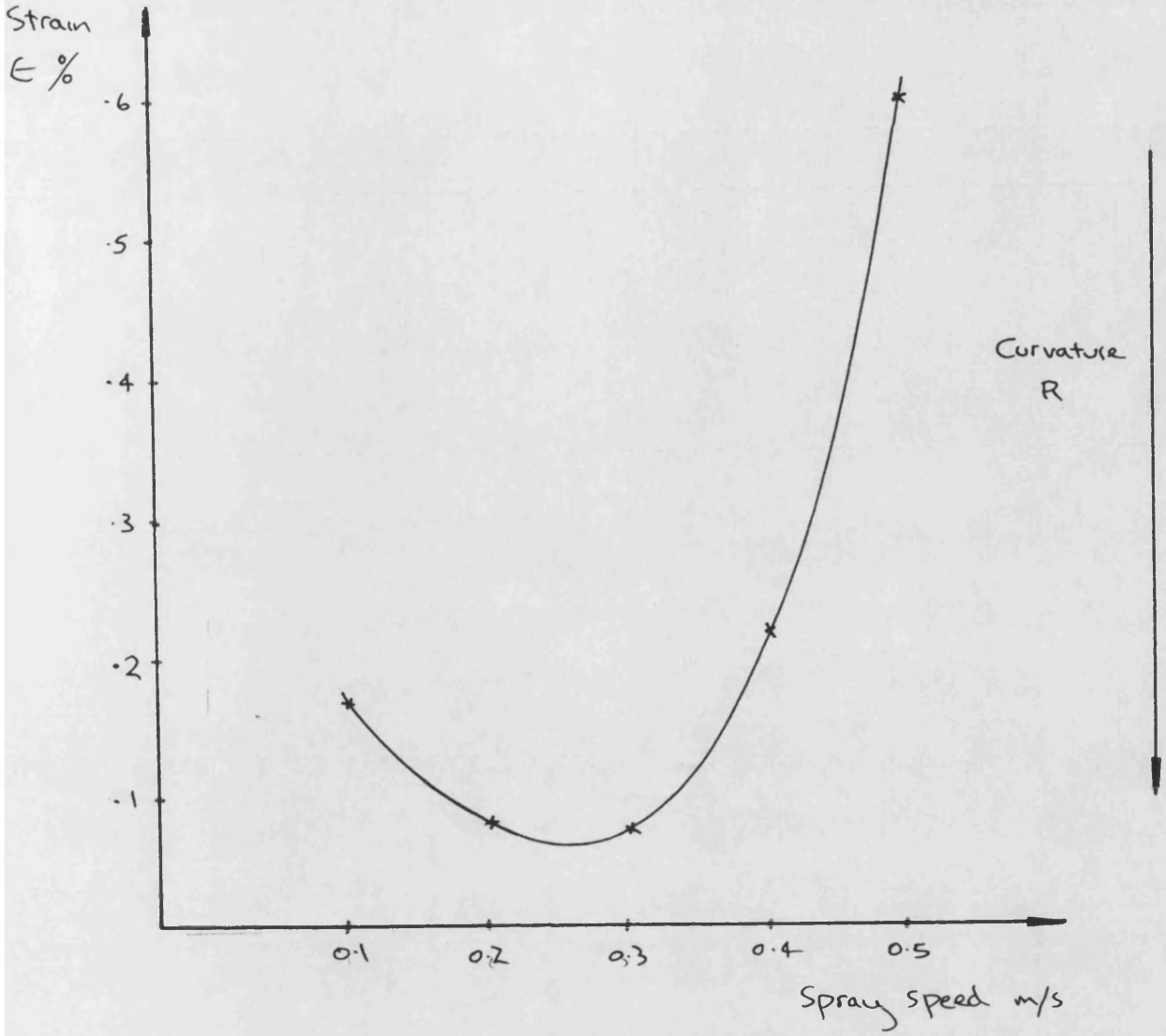

FIGURE 6.15 STRAIN PRODUCED BY VARYING GUN TRAVERSE RATE.

7.1 CERAMIC INSULATION TEST RIG

This apparatus is designed to mimic the temperature and pressure fluctuations present in a firing diesel engine, with provision for stationary mounting of selected insulated components. These ceramic components are positioned to minimise the level of secondary damage sustained in the event of a failure. This security makes it possible to assess the suitability of various ceramic materials for the diesel engine environment as well as judge the various methods of attaching the coatings and inserts to the engine structure.

In addition to providing endurance testing of ceramic materials the rig is intended to be used to provide data for accurate finite element analysis. Measurement of the temperatures and stresses will enable the boundary conditions used in finite element work to be chosen to provide accurate results.

7.2 EXPERIMENTAL ASSESSMENT OF THERMAL BARRIERS IN DIESEL ENGINES

In the search for higher efficiency diesel engines the concept of thermal insulation has attracted great interest. The high temperature strength and low thermal conductivity of many ceramic materials offer an advantage over the more traditional engineering materials. The laboratory measured properties of these high performance ceramics are such that their use in diesel engines can be contemplated. However it is unclear how well these materials will perform under highly loaded operating conditions.

Several tests have been conducted already with ceramic components in firing engines, but due to the limited availability of reliable material property data, and limited design experience these have often resulted in material failure. The catastrophic nature of these failures prevents the quantitative assessment of the materials or designs used. Often little information is gained to judge the level of over or under design present in a particular component configuration. What is required before these trials, is a test which subjects a material sample to realistic thermal and pressure loadings but does not require the component to be a functioning, load carrying part of the engine. In this case the apparatus can be configured so that the failure of a ceramic component will not necessarily lead to large scale damage of the test rig. This reduces the level of design complexity and eases the assessment of the ceramic materials.

Thus there are two distinct types of test:

1/ To judge the material specification and its suitability for the diesel engine environment.

2/ To assess the various methods of attaching the ceramic coatings and inserts to the engine structure, whilst monitoring the various ways of machining and finishing the components.

It is important at the development stage that these areas can be separated, the investigation can therefore proceed in a logical and progressive manner as technical problems can be isolated.

Failure of ceramic components in an operational engine often results in a high level of secondary damage sustained by other engine components and the ceramic test piece itself. Often the ceramic components are so badly damaged during the shut down period that it is impossible to diagnose the reason for failure. If ceramic fragments can be retained, or cracks detected during propagation then this secondary damage can be prevented. This will enable the failure mechanism to be traced back to its origin, which may arise from the manufacturing method, material inclusions, poor design or inappropriate material properties. Areas of weakness can therefore be identified and subsequent designs can be improved through feed back.

The introduction of a test capable of placing standard test pieces in a realistic and repeatable thermal and mechanical environment can produce useful results. Different ceramic materials can be compared in a more realistic manner than by collating laboratory measured properties. Salvaging these test pieces free of secondary damage will make it possible to ascertain the extent to which the high spread of properties exhibited by ceramics is attributable to poor quality control, poor design, finishing processes or bad handling.

The environment within a firing diesel engine has extreme temperature and pressure peaks. In the initial stages of assessing the suitability of individual ceramic materials these conditions are likely to be too severe, the test pieces not lasting long enough to provide useful results. Ideally the environment should be controllable, and capable of being made progressively more severe as the tests proceed: from small pressure and temperature ratios, to the levels present in a firing engine. This flexibility would allow designs to develop, difficulties and weak areas in the design can be rectified before the test piece is subject to the extreme thermal and pressure loadings.

Apparatus capable of fulfilling these needs has been suggested by Kamo and Bryzik.[2] In their design the cylinder head of an existing diesel engine is replaced by a piston retainer assembly (figure 7.1), which holds a stationary test piece. The engine is then cycled without firing, the adiabatic compression and expansion providing the environment required for simulating the mechanical loadings in a firing engine. A pressurised air supply is used for replacing air lost through blow-by. The use of this rig for various materials testing applications was discussed. However, it was recognised that this design could only simulate mechanical loadings and not the thermal loading found in diesel engines. Kamo's design has been developed by the author and his colleague W. Alexander at Bath to provide higher thermal loadings. This was achieved by maintaining the four stroke cycle of an existing engine, and heating the incoming charge air using an electrical heater. This configuration is shown schematically in figure 7.2.

With this design the test piece can be extensively instrumented to monitor the temperature and stress fields which will arise within the ceramic test pieces. The data can be used with finite element work to provide a detailed assessment of many ceramic components.

7.3 LAYOUT OF CERAMIC INSULATION RIG

The ceramic insulation rig is based on a development of the Kamo design, shown in figure 7.2. The apparatus is built around a replacement cylinder head mounted on a Petter PH1W diesel engine. This single cylinder diesel engine has:

Bore	87.3mm
Stroke	110mm
Compression ratio	16.5:1

This engine was chosen because of the reliability, and flexible operating range exhibited by a similar model used previously for the adiabatic project work.

A variety of ceramic material types and configurations can be mounted within the replacement head. The area reserved for the ceramic inserts is directly above the cylinder, providing a site 88mm in diameter and 25mm deep. The position of the inlet/oultet ports therefore had to be changed. The only satisfactory design involved the use of a single side valve, positioned as in figure 7.3. Because of the large trapped volume arising at T.D.C. with side valving the compression ratio would be too low if two poppet valves were used. Consequently a single valve was used, achieving a compression ratio of 19.5:1.

A retaining grid is incorporated immediately below the test piece to prevent any ceramic fragments from entering the cylinder space. Water cooling is provided at key positions within the head design, especially where high heat transfer coefficients will be encountered. The cylinder head design is further examined in section 7.3.

There are four sub-systems built around the replacement cylinder head, these are are shown in figure 7.4 and outlined below.

1/ Air flow system. In the Kamo design the air is trapped within the cylinder, and a pressurised supply used to replace blow by. The mean gas temperature will stabilise at a point where the heat loss will equal the energy derived from fluid and mechanical friction. To attain a mean gas temperature comparable to that in a firing diesel engine an additional heat input is required. With the author's design this heat input is supplied using an external electrical heater and maintaining the four stroke cycle of the diesel engine, as shown in figure 7.2. As only a single poppet valve could be encorporated into the replacement head, it was necessary to use two reed valves to provide a single direction for the air flow. A closed system is used to minimise the heat input required, and to enable the apparatus to be pressurised to increase the mechanical loading on the test piece. This is shown in figure 7.4.

2/ Water cooling: A closed system was again used, to maintain realistic water inlet temperatures. The heat exchanger provides a low temperature reservoir to an external water supply. An immersion

heater is used to achieve steady state operating conditions quickly.

3/ Engine speed control: A three phase electrical motor

speed	1420 rpm
power	4 KW

is used as a power source and a variable speed belt drive sytem incorporated to adjust the engine speed. This engine speed control is further explained in section 7.5.

4/ Instrumentation: The ease of access afforded with this cylinder head design ensures that the surface temperatures and stresses can be extensively monitored using thin film thermocouples. These will be formed be sputtering each of the metalic layers onto the ceramic surface. Two masks will be constructed for use with this sputtering process to form the fine network of leads needed. Spring contacts are used for making external contact with the instrumented ceramic blocks. The instrumentation is further discussed in section 7.6. A photograph of the rig is shown in figure 7.5.

7.4.1 OVERALL CYLINDER HEAD DESIGN

The replacement cylinder head is exposed to high temperatures, and pressures (1300K and 120bar) in addition high heat transfer rates will be developed, especially around the single poppet valve, leading to high thermal stresses. The cylinder head is manufactured in three main parts all of EN58E which was chosen for its good strength at elevated temperatures.

The cylinder head design was developed with the intention of leaving the rest of the Petter engine unmodified. The position of the push rods, water connection passages, and restraining bolts remain the same as in the existing cylinder head. This placed restrictions on the layout of the cylinder head but modification of the existing engine was

felt to be undesirable. The layout developed resulted from three further considerations.

1/ The need to keep the trapped volume of air between the two reed valves and poppet valve to a minimum (volume 2 in figure 7.2): if this volume becomes too large then the air will be cycled back and forth to the cyclinder. The quantity of hot replacement charge provided through the reed valve will be reduced, and hence the in cylinder mean gas temperature will drop.

2/ The position and design of the rocker arms and poppet valve was critical to avoid developing side loading on the valve guide.

3/ Water cooling has to be provided to the valve site where high heat transfer coefficients will be developed, and also to the rear of the ceramic location site. Since stress is related to the temperature drop across a component it is necessary to keep the rear face of the ceramic cool to provide the severest loading for any given gas condition.

A cross section of the head is shown in figure 7.3, and a photograph shows the general layout in figure 7.6. The following technical data applies.

Volume ratio	19.5:1
Bore	87.3mm
Stroke	110mm
Reserved ceramic test area	25mm x 88mm dia

This gives a datum pressure ratio of 64, and datum temperature ratio of 3.3. With a pressurised air flow system including heat input, the maximum cylinder conditions are:

Pressure	120bar
Temperature	1300K

These conditions although not as severe as those within a firing

engine are sufficient to provide a rigorous environment for the testing of ceramic components.

7.4.2 TEST PIECE LOCATION

Where ceramics have been tested in diesel engines if has become the general practice to attach the test piece to the piston or use a monolithic ceramic piston. This approach has three important limitations:

1/ For the experimental study to yield relevant information the ceramic component needs to be instrumented to monitor the temperature and stress fields. Instrumentation of a moving component is a complex task. In the case of an instrumented piston moving arm linkages are frequently employed. These are very expensive both to purchase and to maintain due to the frequent refurnishing which is needed. Maintaining this type of equipment for the prolonged running time envisaged is beyond the budget of this project.

2/ The reciprocating motion increases the probability of a catastrophic failure occurring as the component may make contact with loose particles within the cylinder. In addition no satisfactory method of retaining the debris during a component failure has been found.

3/ The test piece must also fulfil a load carrying role. and cannot. if desired be treated as an independant part of the engine. The design is therefore more complex and faults are more difficult to rectify.

The design chosen incorporates a cylindrical test site within the replacement cylinder head: this configuration is free of the problems associated with the piston sited test piece. In addition this layout affords easy access for instrumentation, and since the test piece is static a retaining grid can be introduced to prevent secondary damage. This can be seen in the cross section shown in figure 7.3.

The cylindrical specimen site can be used to test both ceramic caps and coatings. These can be developed until the designs are ready to be used within a firing diesel engine. This degree of flexibility has not, hitherto, been present in ceramic testing equipment.

7.4.3 AIR FLOW CONTROL

As discussed in section 7.4 the design of cylinder head developed incorporates a single poppet valve, and two reed valves, the layout is shown in figure 7.2.
There are three areas to consider:

i) Rocker assembly: In the standard cylinder head design, the camshaft and push rod assemblies are configured such that each of the two poppet valves is activated once every two crankshaft revolutions. With the test rig, only one valve is employed, the action of either push rod must be able to activate this valve. The desired timing is shown in figure 7.7; it was not considered practical to develop a design using only a single push rod, since this would involve operating the camshaft at twice the normal speed, or redesigning the cam profile.

To avoid the necessity of redesigning the camshaft or its drive a design was developed which allows the motion ot the push rods to be combined. Of the various configurations considered the one offering the most durable solution involved a system of three rocker arms, as shown in figure 7.8. Either of the two outer rocker arms when activated by the respective push rod will deflect the central rocker

arm, and so open the poppet valve. This arrangement ensures that no side loading is developed on the valve guide. It should be noted that a frictional force will be produced between the activated rocker pair, and the stationary side rocker. There will therefore be a tendency for this stationary rocker to lift and lose contact with its push rod. This is obviously undesirable, and to prevent this lifting the side rockers are spring loaded immediately above the valve adjusters as shown in figure 7.3, using the rocker arm retention mechanism.

The moment of inertia of these new rocker arms is slightly higher than with the standard design. Therefore the total stiffness of the springs needs to be correspondingly increased. This additional stiffness is provided by the two extra springs used in the rocker retaining assembly mentioned above, together with the standard springs used on the poppet valve. The associated increase of load on the cam was felt to be within the design limits of this engine.

The rocker arm assembly is bolted directly onto the cylinder head, as shown in figure 7.3. An oil feed is used which supplies oil firstly to the rocker arm block, and then to each of the bimetallic bushes used in the rocker arms. Oil is also directed towards the poppet valve, and rocker arm retention mechanism through a small bore tube.

ii) Poppet valve configuration: To facilitate the construction of the water and air passages, it was necessary to construct the cylinder head from three sections. This approach resulted in the valve guide passing through two of these pieces. These two blocks were constructed to ensure that the head can be dismantled without causing problems with misalignment of the valve guide. Islands of metal are provided, to create metal to metal contact, ensuring correct vertical alignment, the rest of the surface is sealed using a gasket. The correct horizontal position is ensured through the use of metal dowels.

The angled air inlet passage leading to the popet valve is shaped to minimise air flow losses, within the limitations posed by the necessity of maintaining a high compression ratio. To machine the valve seat

and air passage, the cylinder head is split as shown. Sealing between the two blocks is provided by a wire re-enforced gasket.

iii) Reed valves: Reed valves were chosen to provide the uni-directional air flow because they offer a high speed response to a pressure differential and have already been developed to provide the flow characteristics desired. Standard motorcycle reed valves could therefore be used obviating the necessity of developing a flow control valve. Other solutions investigated involved mechanical actuation, or designs whose flow characteristics could not easily be predicted.

The two reed valves are open at the positions indicated on the timing diagram figure 7.7. The reed valve blocks are those used on the Yamaha RT750 motorcycle. Each reed valve assembly includes two reeds, and eight inlet passages with a total free flow area of 680mm^2. They are mounted directly onto the cylinder head to keep the trapped air volume as small as possible as mentioned in section 7.4.1. Figure 7.9 shows the position of the inlet and outlet passages on the cylinder head.

7.4.4 WATER COOLING

The water cooling in the cylinder head is provided for two reasons, firstly to keep the bulk material temperature low minimising the resultant stresses, and secondly to ensure there is a large temperature drop across the ceramic test piece.

With most cylinder head designs the critical area in terms of thermal stresses normally occurs in the bridge between the two valves. The cylinder head developed for the ceramic testing rig has only one valve, the critical area occuring between the valve and ceramic location site. Three water cooling passages are incorporated to reduce the temperature level in this region. The maximum derived stresses are likely to be lower in this design for several reasons. The cycle to cyle fluctuations will be less severe, as both the inlet

and exhaust gas temperatures are comparable. In addition the fluid conditions will be more uniform over the surface and the localised temperature peak will be lower. due to the absence of a fuel burn.

In the standard cylinder head design water cooling passages are created using inserts in the casting mould. Since the replacement head was not to be cast the water passages were more difficult to incorporate. By constructing the head from three seporate machined blocks all the required passages could be formed.

The water flow enters the cylinder head from the cylinder block and passes over the rear of the ceramic test site. (Arrow A on figure 7.10 which is an off centre cross section of the cylinder head) Calculations of the heat flow suggested that the maximum size of water passage that could be incorperated would be insufficient to maintain the desired temperature drop across across the ceramic. For this reason fins (1) are provided in the water passages to increase the heat transfer rate. The coolant is next passed to the upper cylinder head block (B). In doing so the valve guide is cooled. In the upper cylinder head block cooling of the reed valve volume takes place (C). The critical area surrounding the poppet valve air inlet passage is similarly cooled as the water flow is directed into the lower cylinder head block (D). The water now leaves the cylinder head to be cooled and re-cycled.

7.4.5 RETAINING GRID

To prevent secondary damage occurring to both the ceramic test piece and engine components in general the rig design includes a retaining grid sited below the test piece. This grid must be able to retain any ceramic fragments over a wide temperature range preventing them from contacting the piston or cylinder walls. It was recognised that due to volumetric restrictions any distortion of the grid in the axial direction would result in contact between the piston and grid. This would lead to failure of the grid itself. and damage

to any surface instrumentation on the ceramic test piece. The presence of the inlet port also meant the grid would have to function unsupported for part of the circumference as shown in figure 7.11.

Many gauzes and grids are currently available but due to the non-uniformity of the temperature across the cylinder all these designs would distort axially. To meet the combination of restrictions a design was developed which would ensure that the thermal distortion would only take place radially. The configuration used is shown in figure 7.12. and photographically in figure 7.13. A number of curved metallic strips are held over the ceramic surface. Each of these strips is rectangular and thickest in the axial direction. The combination of these two features ensures that any thermal distortion takes place in the radial direction only. The grid will therefore not interfere with the piston or test piece.

The possibility of manufacturing this grid by electromachining was investigated but two significant difficulties were envisaged:

1/ Examining the grid in plan, the free flow area to material area needs to be high to avoid significant alteration of the air flow characteristics in the vicinity of the test piece. In the extreme case a dead space would be created where film insulation would significantly affect the heat transfer in the head. The mechanism of electomachining results in tapering of the cut material edge. Since the material section must be thin this tapering would produce an unacceptably weak component.

2/ The material grain structure would not be suited to the final shape of the component. The electromachined grid would therefore be mechanically weak.

To overcome these problems the grid was constructed as shown in figure 7.12. each of the strips is pre-cut from a sheet of Incoloy 800 alloy. These strips are held in a horse shoe shaped clamp of EN58E, with small balls held between each parallel strip of material.

to act as spacers. The horseshoe shaped design ensures that all the ceramic face can be covered despite the position of the air inlet passage which restricts the room that is available.

7.4.6 PISTON CROWN

The piston bowl on the standard piston must be filled because of the high volume ratio required in the ceramic insulation test rig. The simplest way of achieving this is by attaching a flat crown to the top of the piston. If this crown is bolted directly onto the piston, stress concentrations will occur due to thermal mismatch. A method of clamping crown and piston together was therefore devised to ensure the absence of stress concentrations. the design is shown in figure 7.14. A split threaded insert (1) is assembled inside the piston body (2). The piston crown (3) is then screwed into this insert, clamping crown and piston together.

This type of construction has two further advantages:

1/ An air gap can be incorporated between the crown and piston, reducing heat loss through the piston.

2/ A metallic 'O' ring seal can be incorporated into the assembly to prevent the build up of carbon deposits within the piston. Without this precaution the heat transfer through the piston will increase during its operational life as the air gaps become blocked.

A cross sectional view is provided in figure 7.3

7.5 SPEED CONTROL

A manually operated variable speed belt drive system is used to power the insulation test rig. It is set to achieve ratios from of 0.14:1 to 0.5:1. Using two pulleys of 240mm and 110mm diameter, the engine can be driven at speeds between 200rpm and 700rpm. These pulleys may be changed if a different speed range is required. A soft starter is provided with the electrical motor for ease of start up. Similarly the cylinder is equipped with a decompressor.

There are five important safety circuits built into the engine drive to stop the engine in the event of failure.

a/ Low speed detection circuit: if the engine speed should drop below a preset value, as in the case of engine seizure the power to the electrical motor is cut.

b/ A flow detection switch is fitted in the water circuit. If the water supply fails then the engine drive is cut, thus preventing the cylinder head overheating.

c/ The electrical heater's temperature is also monitored, and a cut out incorperated.

The following circuits are intended to be installed in the future.

d/ The power can be cut if a pressure rise is recorded at the back of the ceramic test piece, this would occur if a crack propagates through the ceramic specimen.

e/ Surface gauging on the ceramic test piece will record any surface cracks that develop; this signal can be used as a power cut out.

7.6 INSTRUMENTATION

To monitor the performance of the ceramic and to provide a method of cross checking the theoretically derived temperature and stress distributions it is necessary to study the temperatures and strains present in the ceramic test pieces. The ease of access afforded with this design of head enables the test piece to be extensively instrumented. Generally the measuring systems used in internal combustion engines involve the use of thermocouples set into the surface. Since such a site would provide a point for crack initiation with ceramics, its use cannot be considered. Surface sensors do not present the same difficulties but little practical experience is available with the temperature levels envisaged for the ceramic insulation rig.

The use of thin film surface thermocouples has been investigated in the gas turbine industry for the measurement of surface temperatures and strains in turbine blades. Work in this area suggests that noble metal layers can be used to form a thermocouple ie: Platinum/ Platinum-Rhodium.[58] However, if Platinum/Platinum-Rhodium gauges are used then the connecting leads and connections must also be of the same material to avoid the creation of secondary junctions. This would be prohibitively expensive, so Nickel/Nickel-Chromium thermocouples are to be used. Two masks will be made to form the network of leads needed to form the thermocouple junctions on the ceramic, as in figure 7.15. Spring contacts will be used for making external contacts with the instrumented ceramic block.

7.6.1 FAILURE DETECTION CIRCUITRY

The insulation test rig is designed for long term cyclic loading, it will therefore be necessary to leave the rig running unattended for long periods of time. So that a component failure will not cause secondary damage before the rig can be manually stopped, a failure detection circuit is installed which continually monitors the rigs performance. Eight failure detection channels are available, as long

as each of these maintains a closed circuit the rig will continue running. If a failure is indicated by an open circuit then the power to the electrical motor will be cut. A photograph of the failure detection circuit is given in figure 7.16.

It is possible to set the circuitry to ignore any one of these failure detection cannels, so that spurious signals can be overridden.

NOR gates are used to combine these inputs in the desired fashion as shown if figures 7.17 and 7.18. If any of the switches (A) are open the accompanying input is ignored. LED drives (B) are used to indicate the state of each line. The control rack is shown in figure 7.16. It should be noted that this system is fail safe.

A latching relay is used to ensure that a failure will stop the motor until the circuit is manually reset. An intermittent failure signal such as that resulting from an air leak occuring only at peak pressures will therefore not cause the motor to switch itself off and on repeatedly. The relay can be reset with a switch mounted on the control panel.

If the 12 volt power supply to the detection circuit fails then the input line to the electrical motor will also fail, and the motor stop. Similarly if the three phase supply should fail, the motor will only restart if it is manually switched on.

Since any of the failure inputs can be cut, it is important to have a visual method of indicating which lines are inactive. Another LED (C) is triggered if an input line is deactivated.

7.6.2 THERMOCOUPLE FORMATION

There are two methods of producing the metallic layers needed for the instrumentation, evaporation and sputtering. Both of these methods are carried out in a vacuum.

With the evaporation technique a source of coating material is heated in a vacuum near the substrate. When the metal reaches a given

temperature atoms evaporate from the source. These atoms come into contact with the cool surface of the substrate or chamber walls and adhere. Different source materials have different evaporation temperatures and pressures, thus under similar conditions different materials will have different deposition rates. As it is required to deposit thermocouple materials, which are alloys then the evaporation technique would yield thermocouples having a different composition from the source materials. For this reason sputtering was chosen.

Sputtering also makes use of low pressures. The vacuum chamber is generally filled with an inert gas, at a pressure of around 100mTorr. When a sufficient voltage is placed across the vacuum a glow discharge will form as electrons are ejected from the cathode surface. The electron-atom collisions that occur result in the formation of ions. When these ions impinge on a surface they can cause surface atoms to be ejected. These ejected atoms will coat any nearby surfaces. The source material, or target is made from the thermocouple material. This process should lead to a similar material composition in the deposited layer as in the target.

The vacuum equipment is shown diagramatically in figure 7.19. Initially attempts to form the metallic layers required made use of glass slides as a substrate material. Although the glow discharge, characteristic of sputtering was present during operation, the layers deposited were found to be non-conductive, and very thin. Due to the equipment's age and its inability to hold a vacuum this was initially felt to be due to the presence of oxygen in the chamber, as this would oxidise the metallic layers. A great deal of time was spent investigating leaks and trying a variety of targets, unfortunately without improving the coating. Eventually the problem was traced to an electrical fault, caused by the failure of a high tension lead. This was repaired, but by this stage too much time had elapsed for the author to develop the thermocouples for use in the insulation test rig. However, it is intended that this work be continued, and these thermocouples installed at a later date.

7.7 COMPUTER PREDICTION OF PERFORMANCE

The engine simulation program SPICE[64] was used to predict the performance of the insulation test rig. This computer code proved sufficiently flexible to model the performance of the rig which incorporates reed valves, a single poppet valve and an electrical heater. Initial estimates of the gas temperature at inlet, and electrical power were made, the program then uses these to converge automatically to the steady state operating condition. The computer predictions are shown in figure 7.20 and 7.21, the peak gas conditions are 142bar, 1240K at a boost pressure of 2bar.

As the volumetric efficiency observed in the operating engine was lower than that expected, as discussed in 7.8, the peak gas conditions are likely to be approximately 120bar and 1300K. The peak temperature is improved as the reed valves exhibited a higher than expected temperature ceiling, and a correspondingly higher preheat temperature could be used.

7.8 RIG COMMISSIONING

Initial running was performed without air boost or pre-heat. A steel disc coated with 1/2mm PSZ was installed and ran for approximately four hours at 600rpm. The cylinder head and test piece were then removed and examined, no signs of wear were found. Subsequently a silicon nitride disc, supplied by ARE was installed in the engine and ran briefly with air boost, again no problems were encountered. This disc is shown in figure 7.22.

Endurance testing was then commensed. The rig was run without air boost, but with air pre-heat on; an air inlet temperature of 140^{o}C and engine speed of 600rpm was used. During this period the water pump failed, and as the relevant failure detection circuit was not yet installed the rig was left running for approximately one hour before this was detected. There appeared to be no damage sustained, but during later running under boost conditions air was forced into the water system. This was not serious in itself as the leakage showed no signs of increasing, and the quantities involved were small, but

these air bubbles caused the water pump to cut out frequently.

At this time a AVL 8QP piezo-electric quartz transducer was fitted to the engine, as shown in figure 7.23. The peak pressures were recorded and found to be only 20bar under unboosted conditions. A low volumetric efficiency was suspected as the cause of this low pressure. Subsequently the air flow passage leading to the single poppet valve was enlarged, and the cylinder head refitted. The new pressure peak was found to be 43bar at 700rpm. This compares with a theoretical value ot 59bar if blowby is ignored, and 100% volumetric efficiency is assumed. At 700rpm 43 bar is therefore a realistic value.

The rig was then run for about 300 hours with pre-heat and no air boost, during this time the silicon nitride disc survived without failure. Mid way through this trial the water pump stopped again, and after restarting the air leak was far worse, with air pulsing into the water even under normally aspirated conditions. The head was stripped down, and one of the gaskets was found to have failed. It was replaced with a wire re-enforced material. The water pump was also replaced. Although the air leaking into the water supply was stopped during naturally aspirated conditions, with boost low leakage rates still occured. After these repairs endurance testing was resumed.

During the rig's operation it was noted that oil was being lost in the form of mist through the oulet reed valve. Although no more than the normal level of oil loss was encounted the oil built up in the closed loop air circuit. Due to the presence of the electrical heater in this loop there was a risk of the oil mist being ignited. In the sealed air circuit this could have caused an explosion, and therefore an air filter will be fitted after the inlet valve. After the first 300 hours of running the rig was therefore not opperated with preheat.

At the time of writing the air filter has been purchased but not installed. Once it is in place running with preheat will resume. Due to the air leakage into the water supply maximum in cylinder

conditions are limited to approximately 60bar and 1300K.

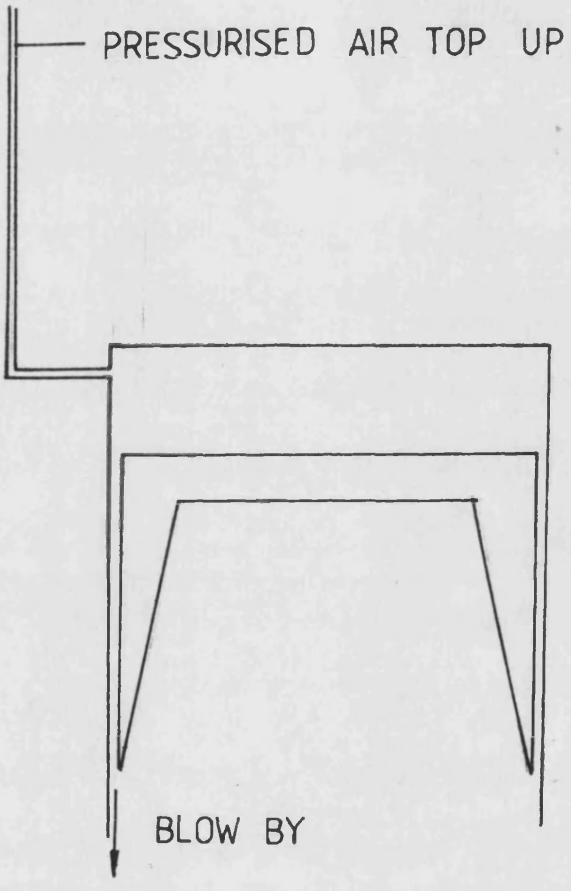

FIGURE 7.1 KAMO'S INSULATION TEST RIG.

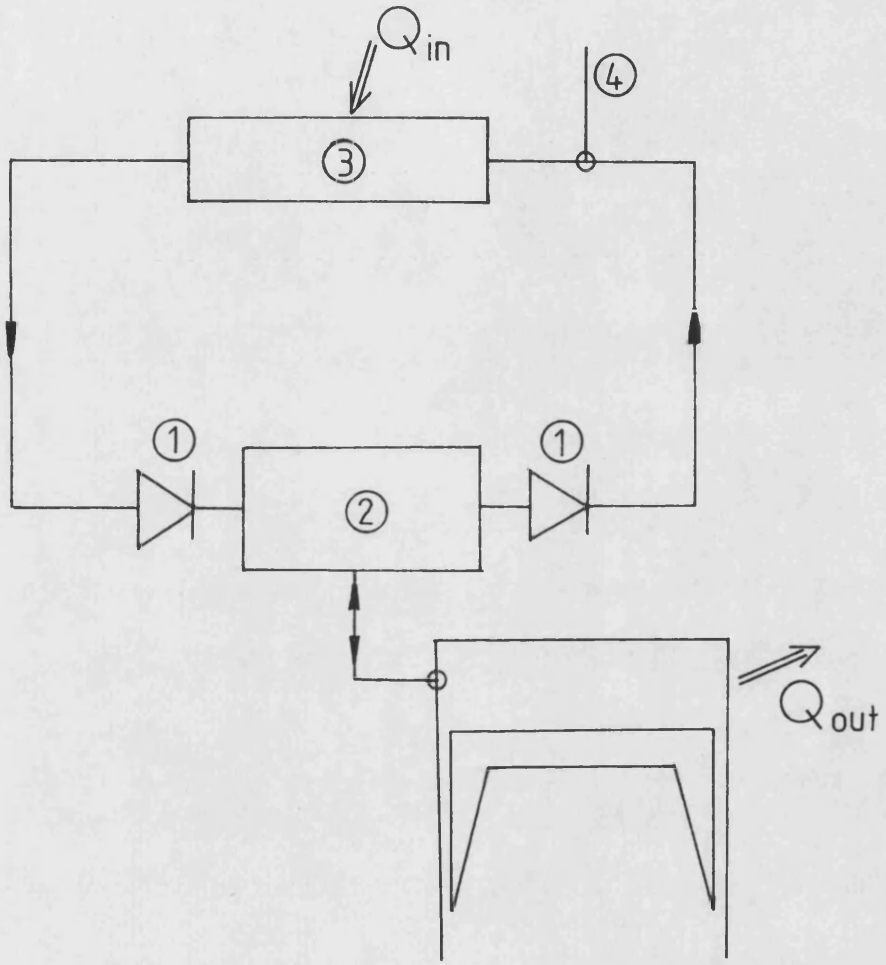

1 REED VALVES

2 POPPET VALVE

3 AIR HEATER

4 PRESSURISED AIR TOP UP

FIGURE 7.2 IMPPOVED INSULATION TEST RIG.

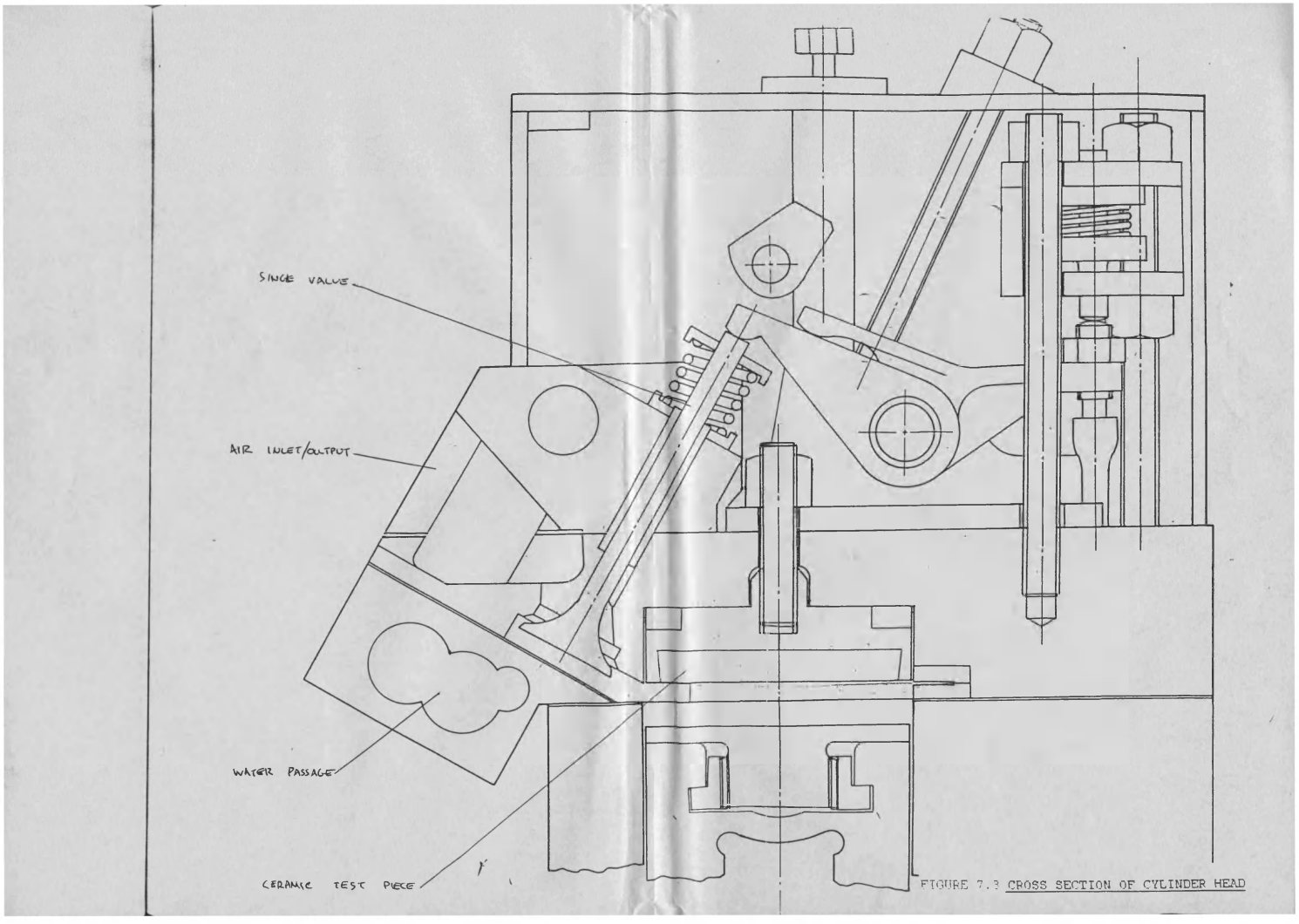

FIGURE 7.3 CROSS SECTION OF CYLINDER HEAD

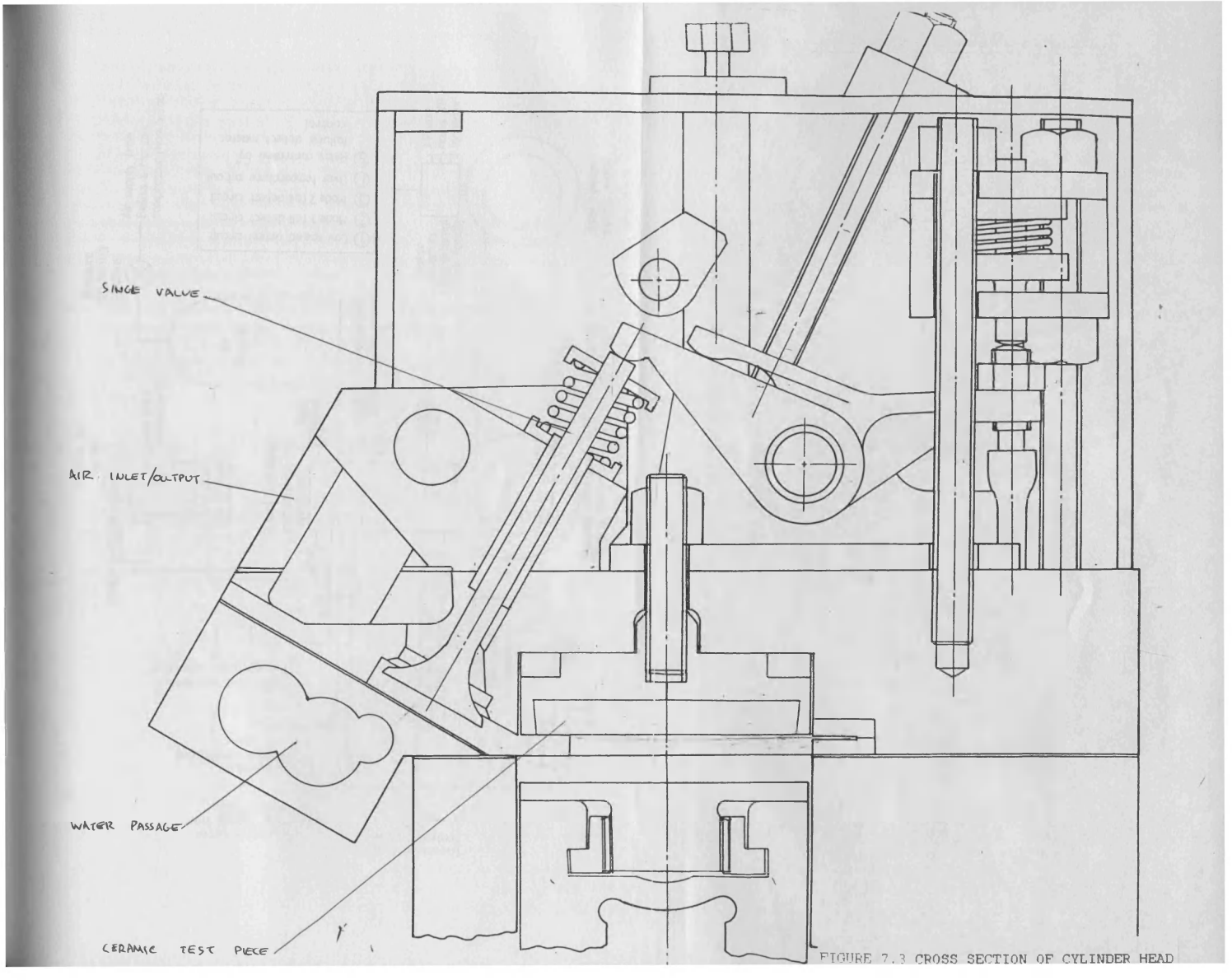

FIGURE 7.3 CROSS SECTION OF CYLINDER HEAD

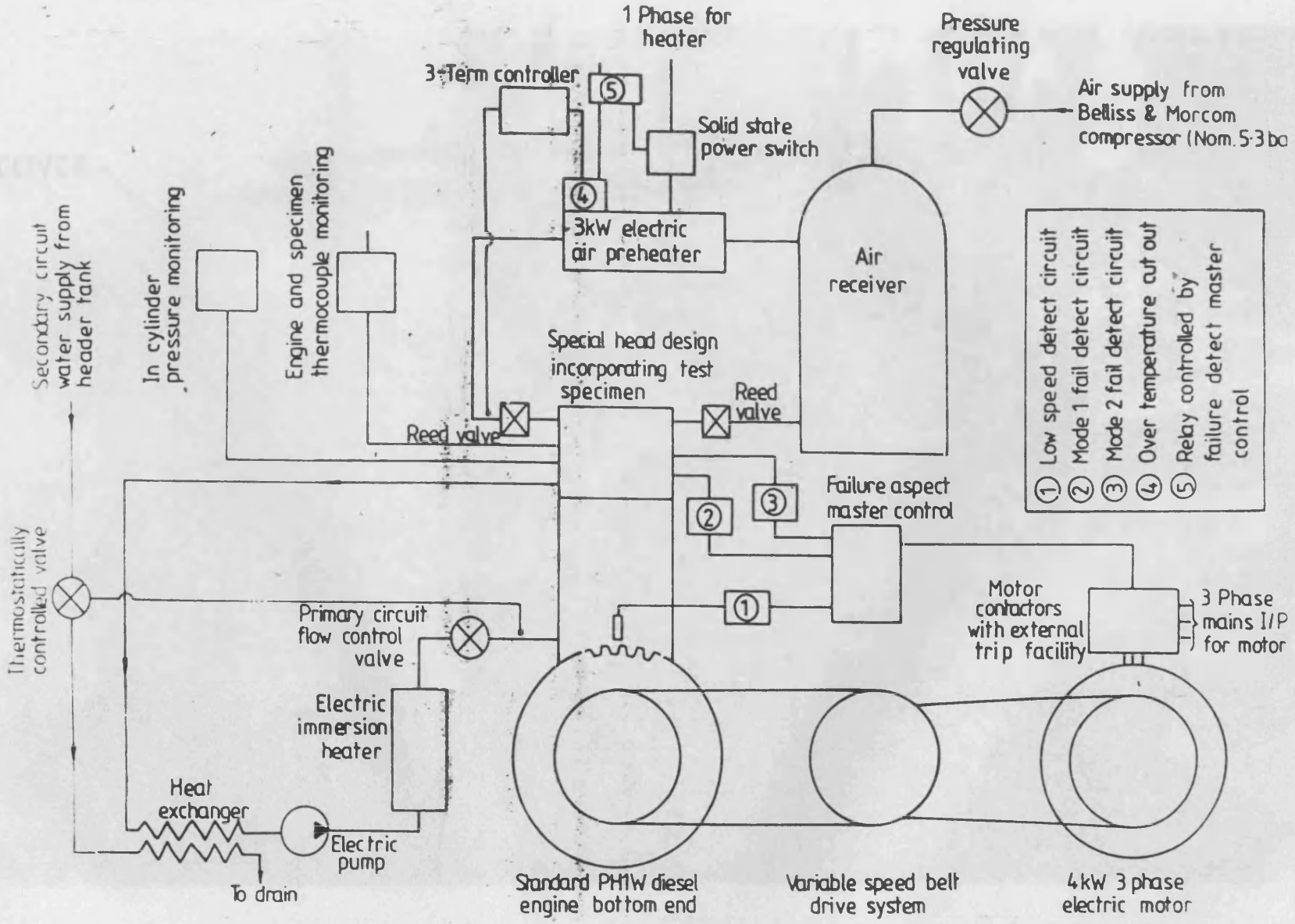

FIGURE 7.4 SCHEMATIC LAYOUT OF THE INSULATION TEST RIG.

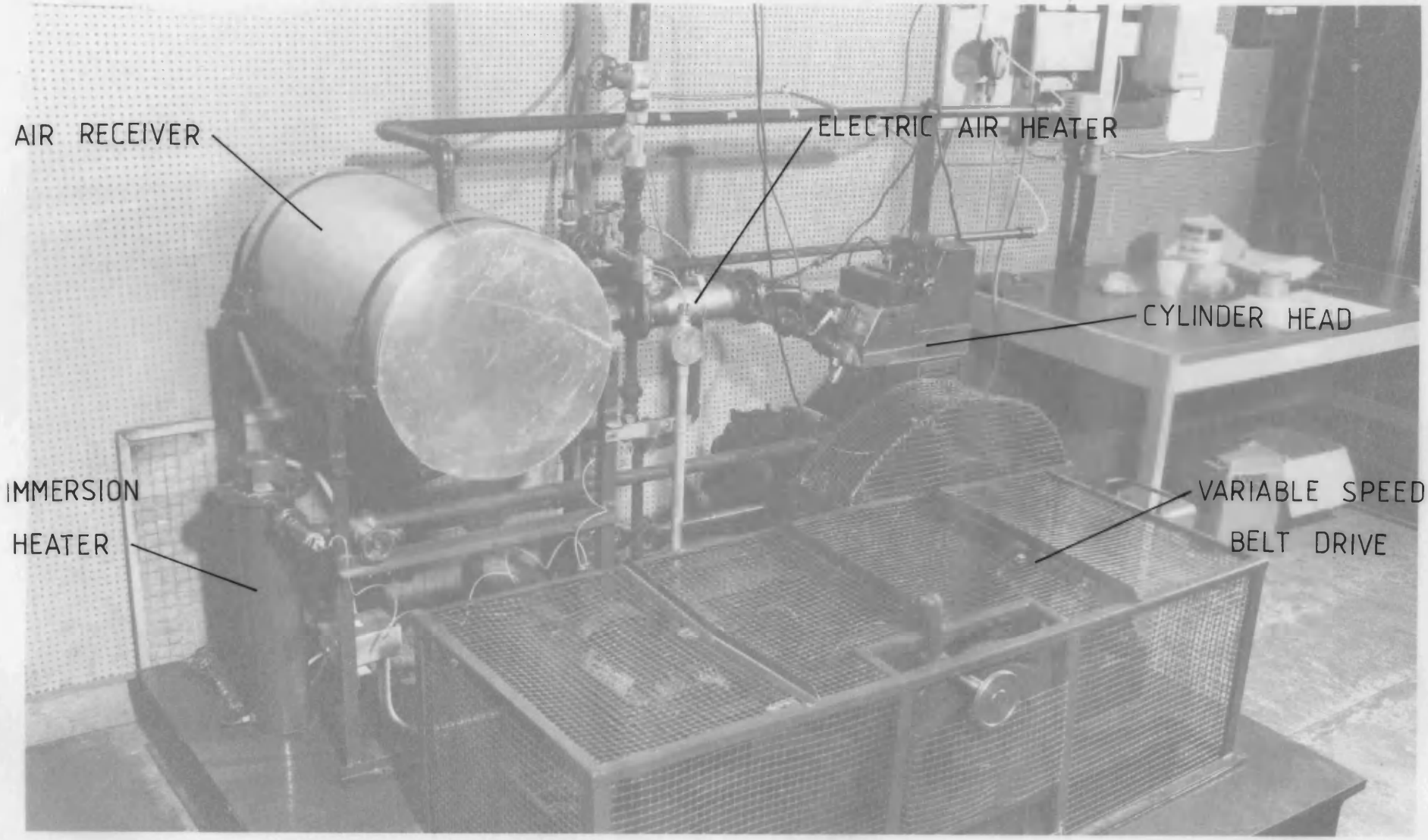

FIGURE 7.5 CERAMIC INSULATION TEST RIG

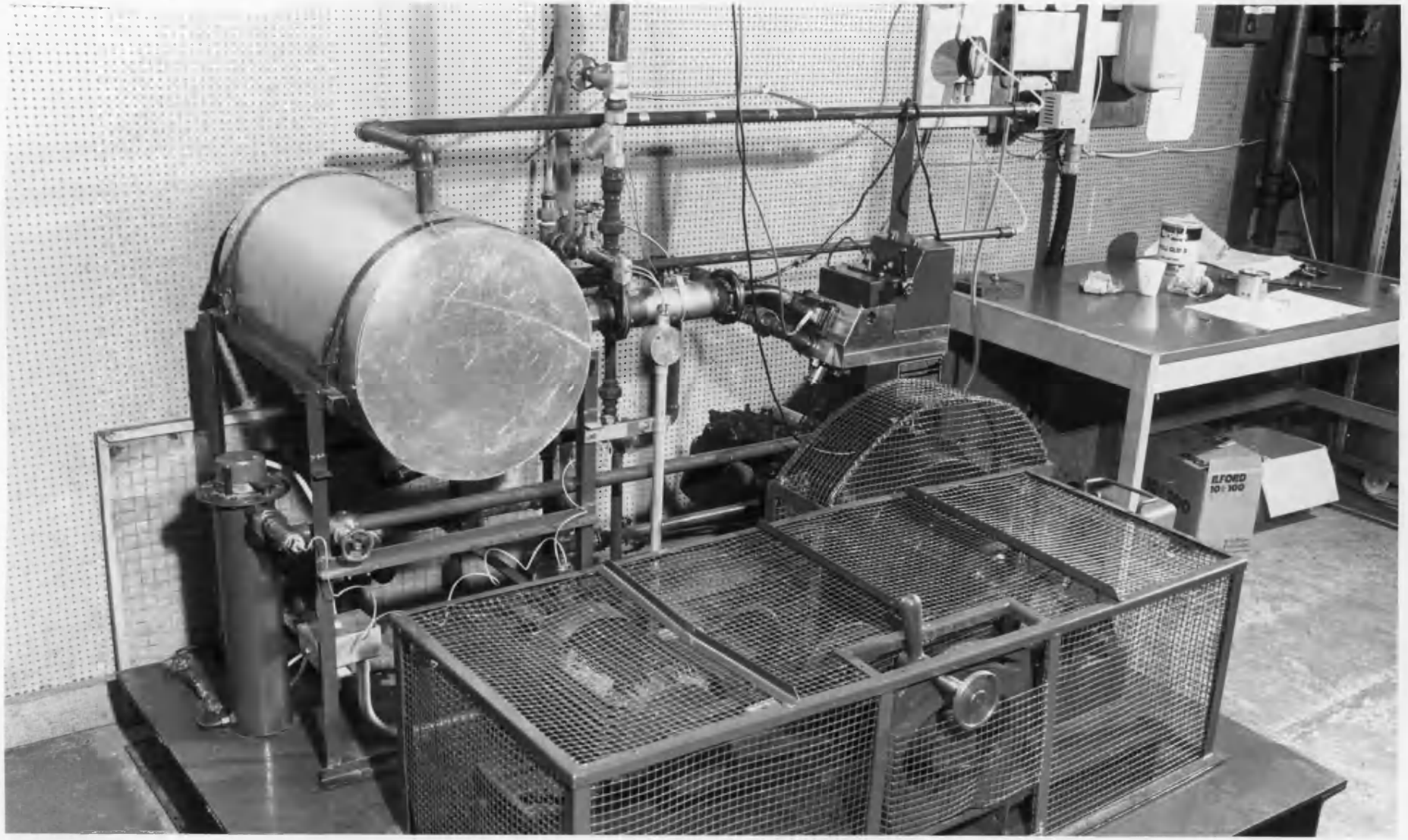
ILFORD
10 : 100

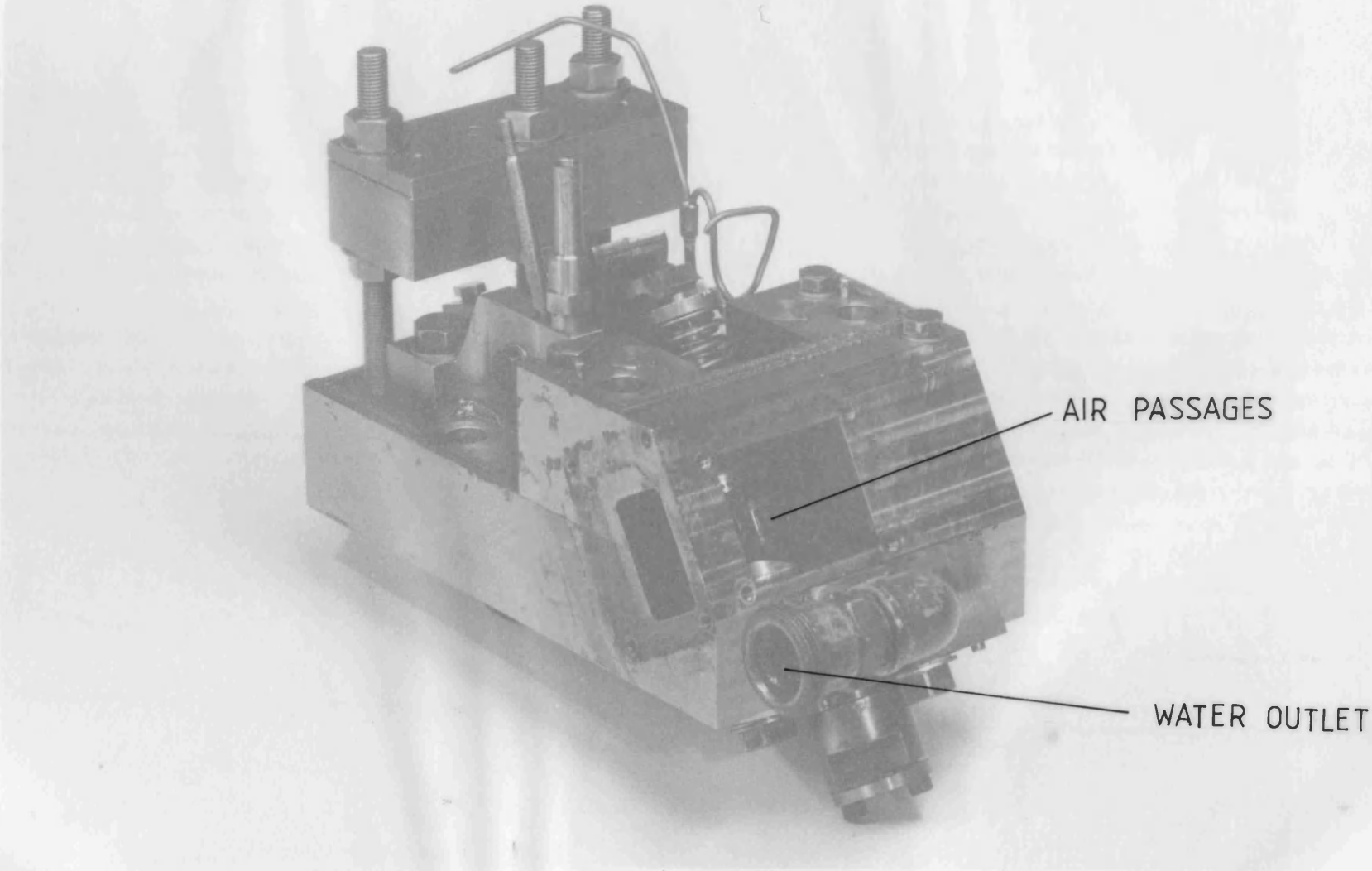

FIGURE 7.6 CYLINDER HEAD

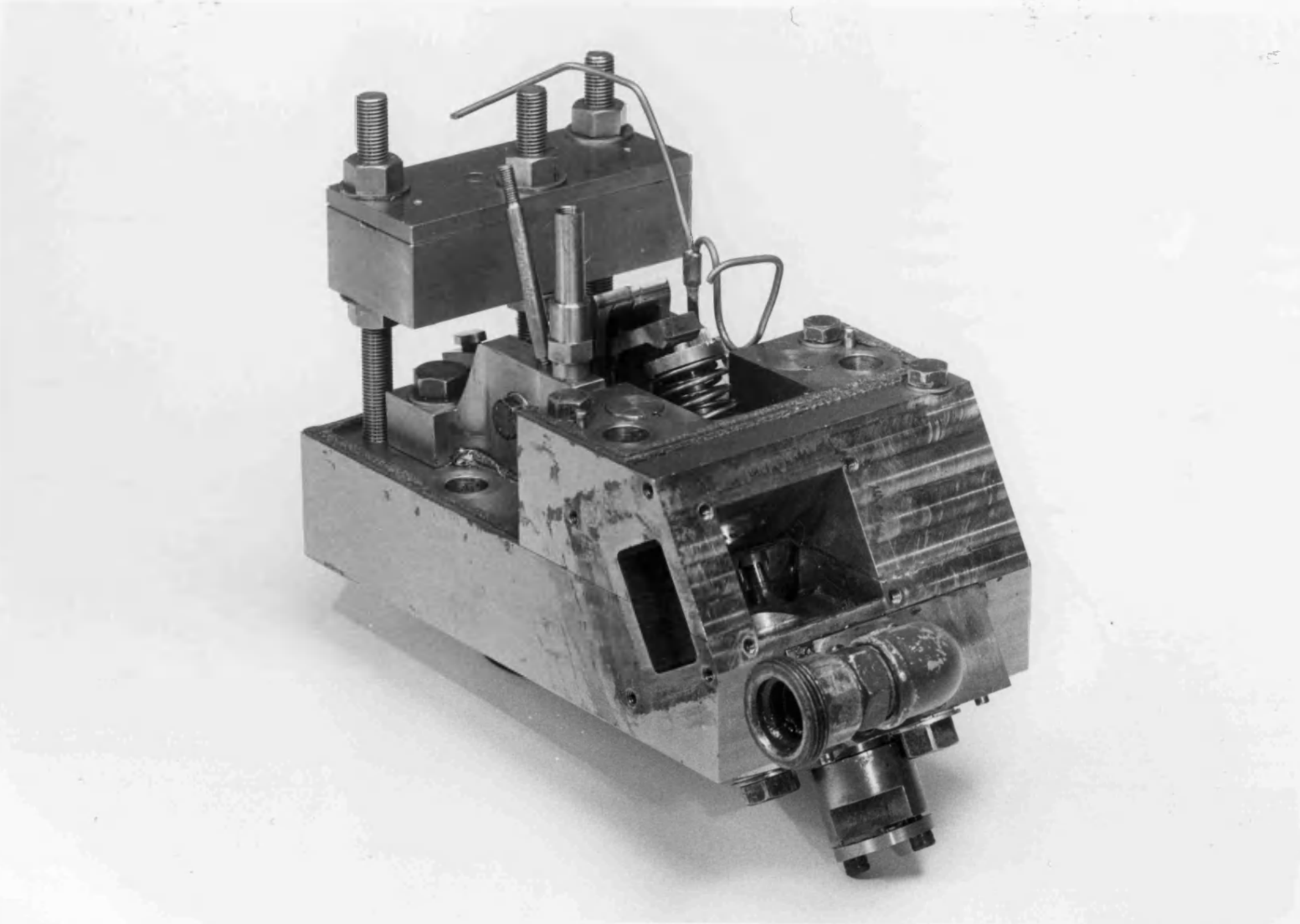

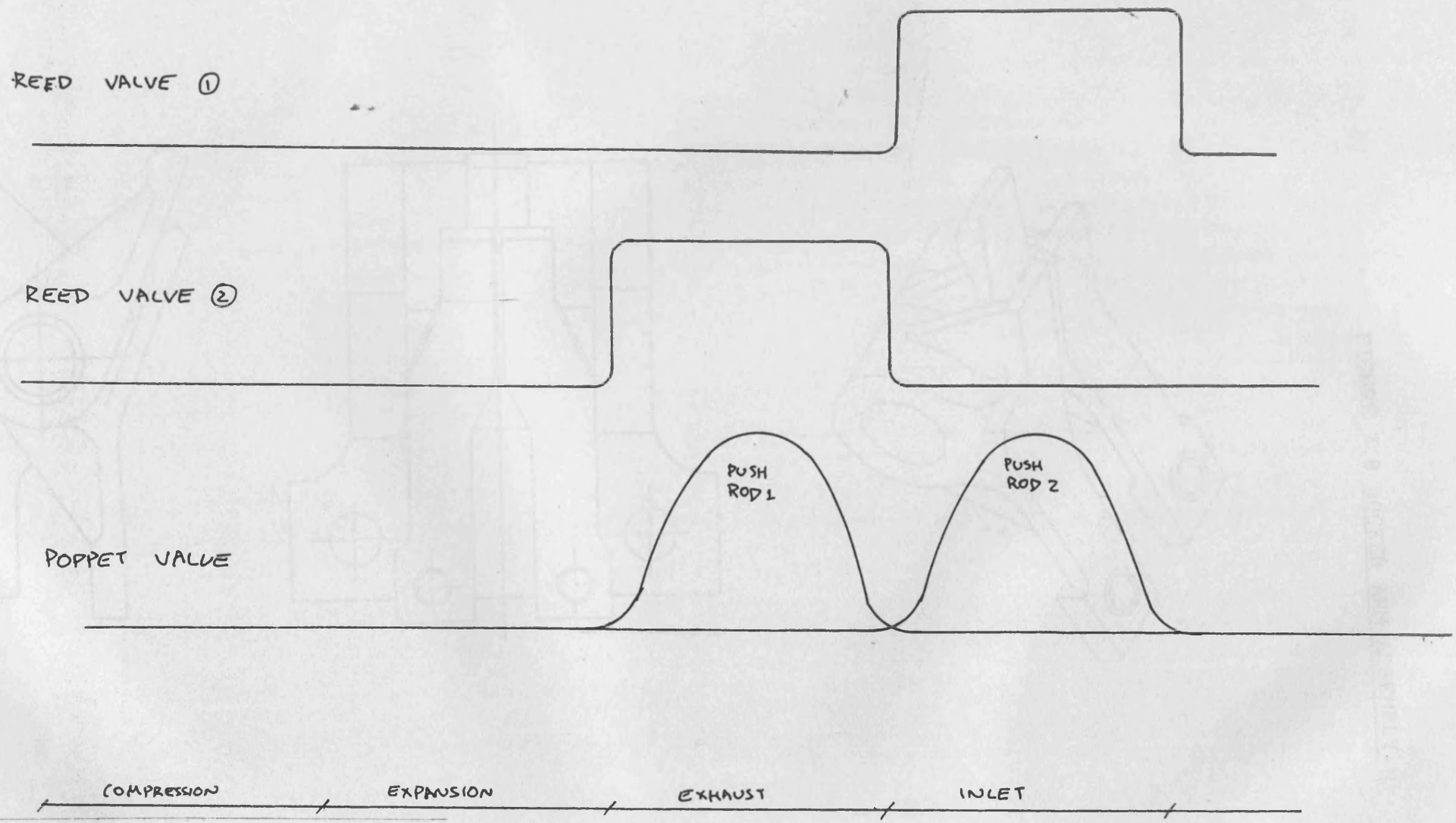

FIGURE 7.7 VALVE TIMING ON TEST RIG.

FIGURE 7.8 ROCKER ARM ASSEMBLY.

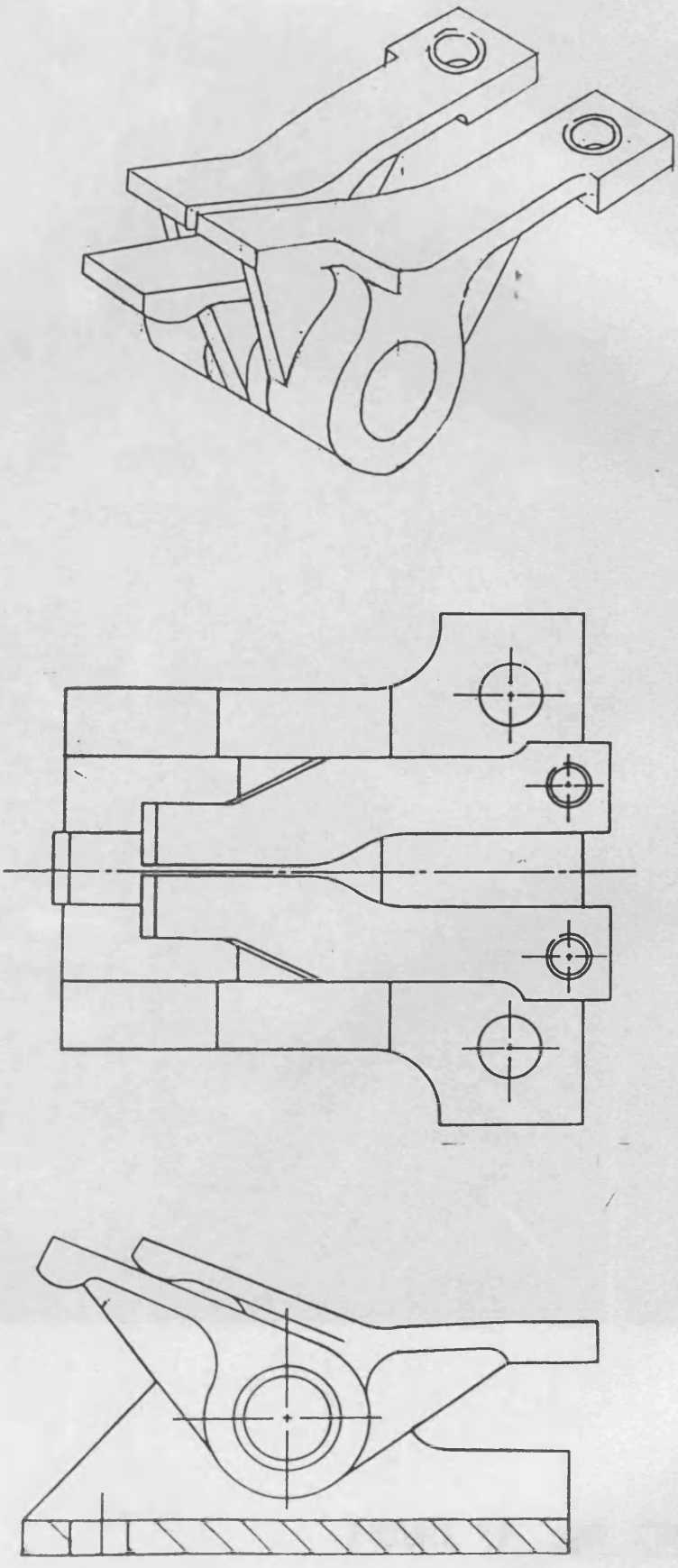

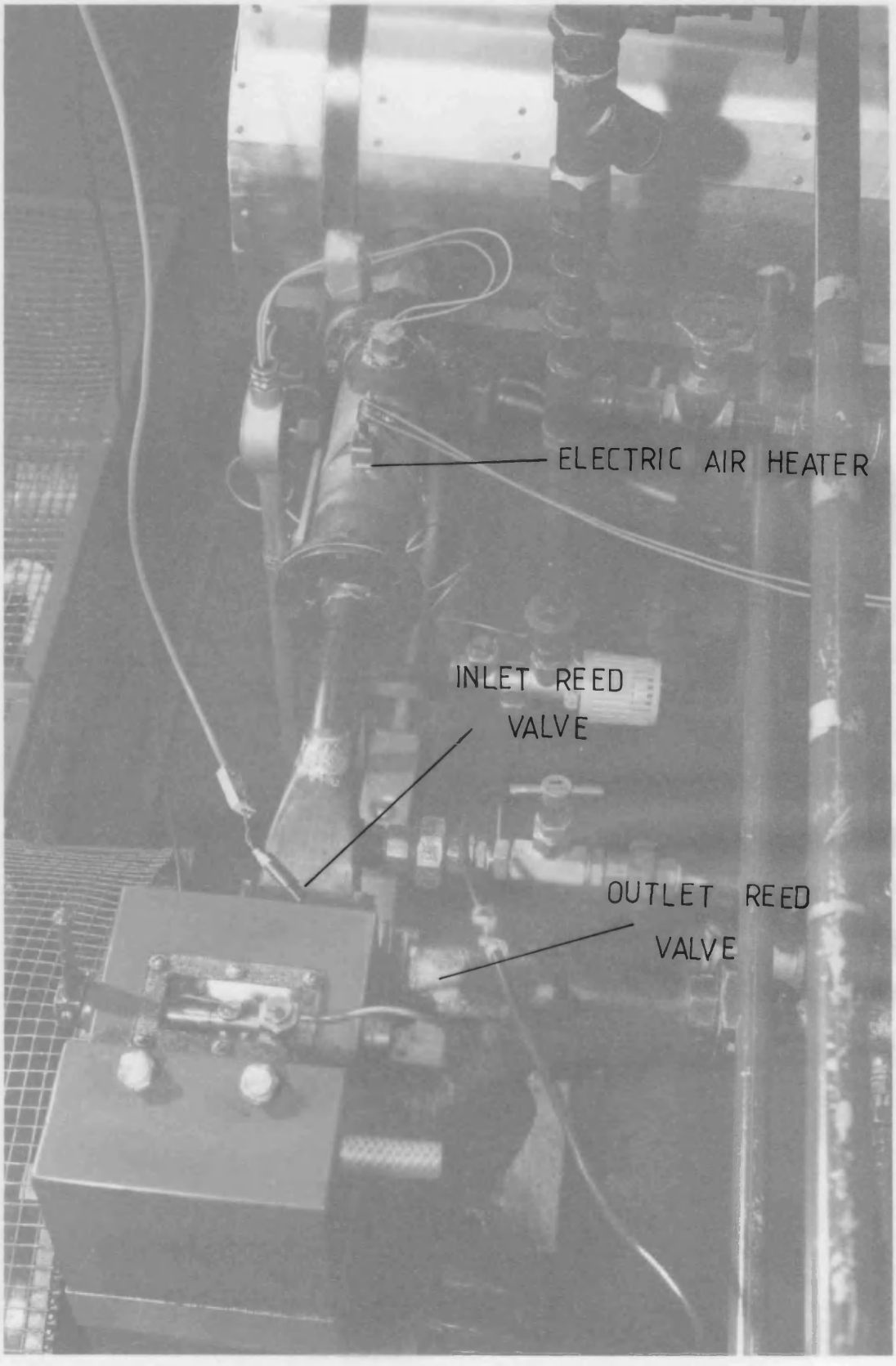

FIGURE 7.9 AIR CIRCUIT

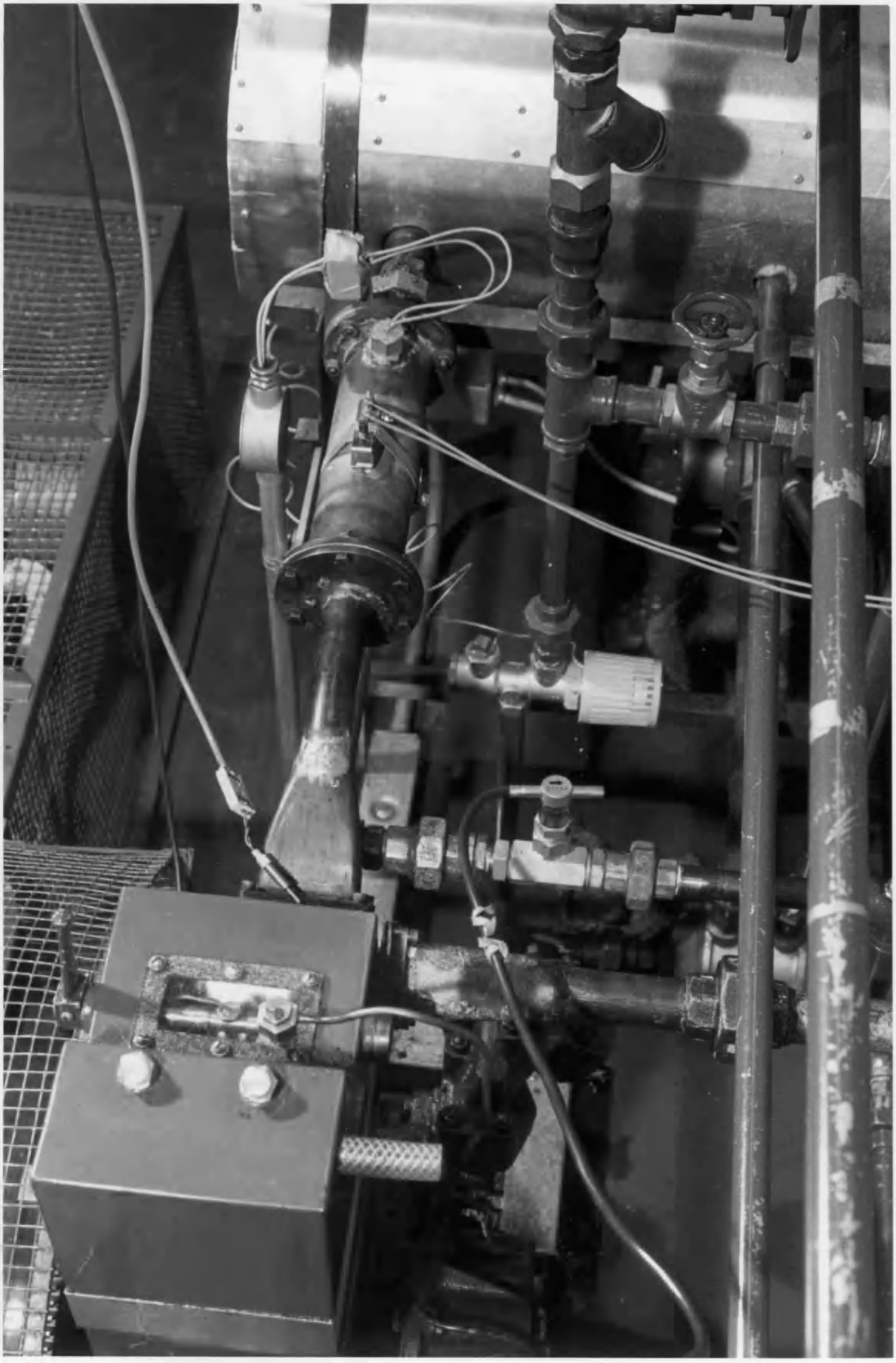

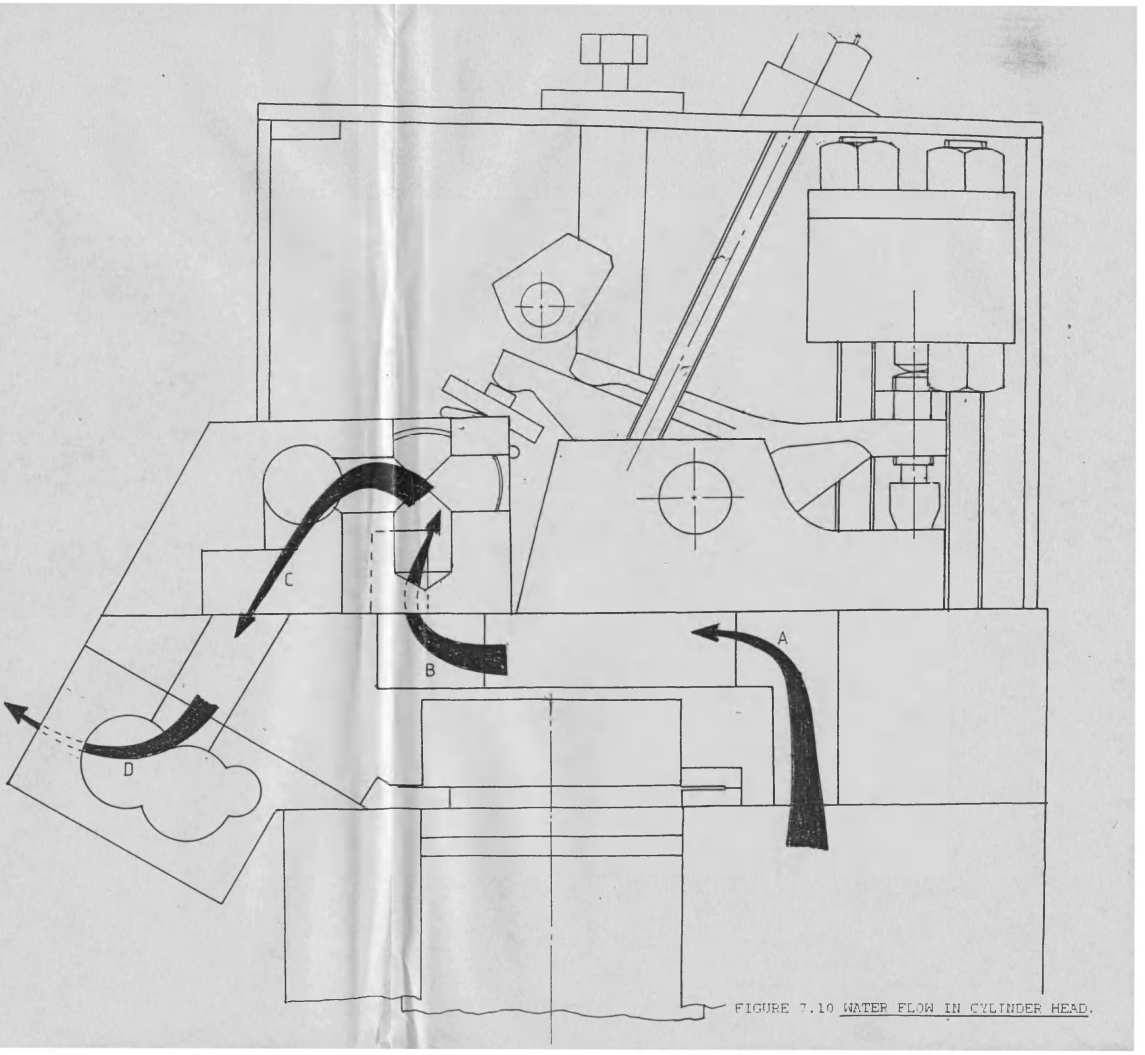

FIGURE 7.10 WATER FLOW IN CYLINDER HEAD.

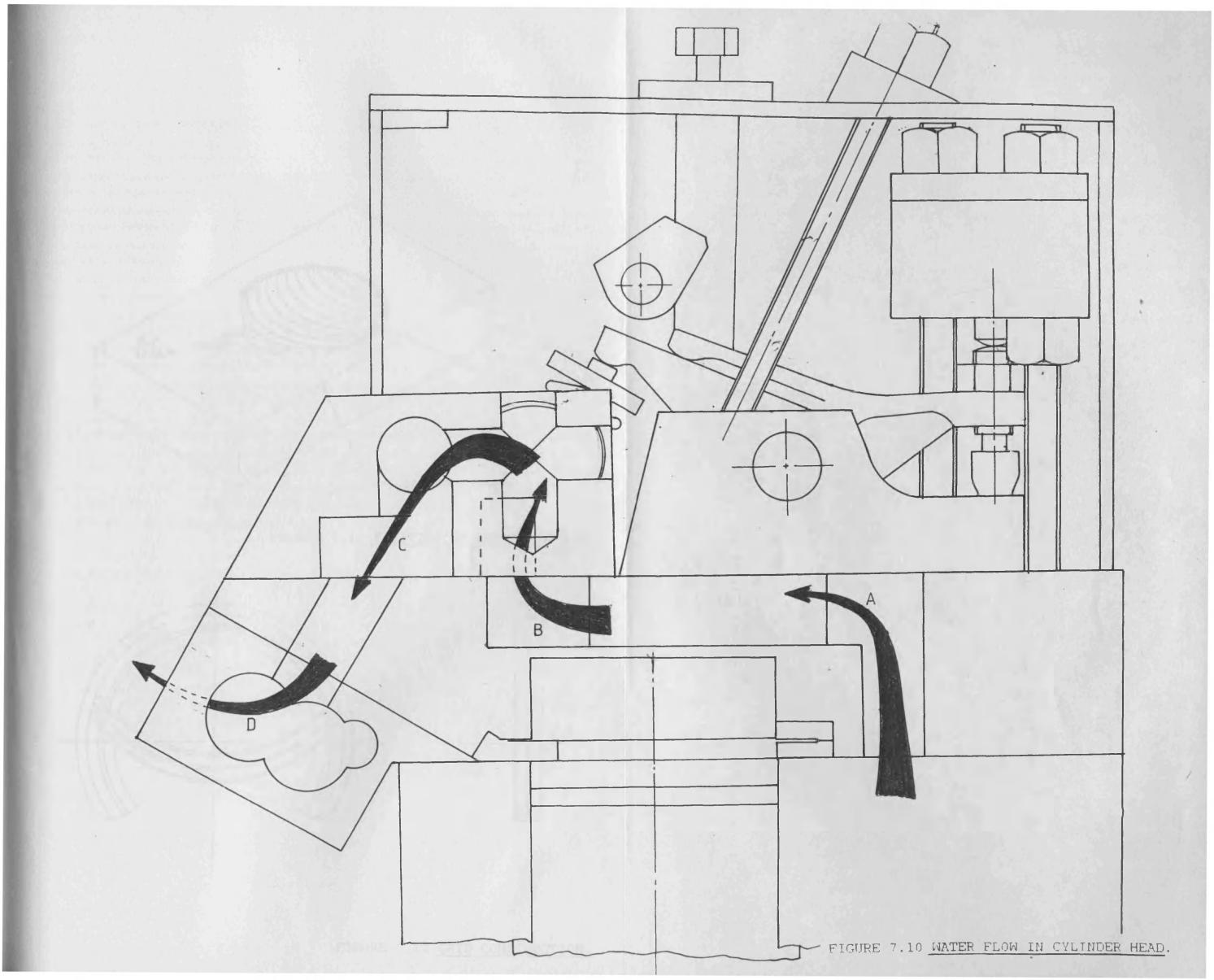

FIGURE 7.10 WATER FLOW IN CYLINDER HEAD.

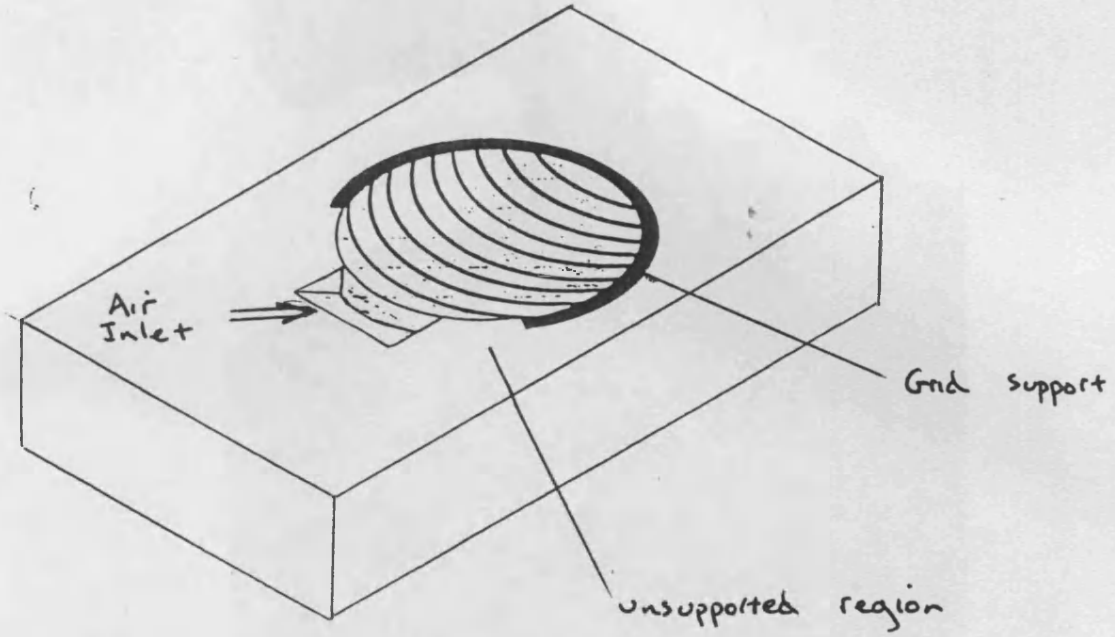

FIGURE 7.11 POSITION OF RETAINING RIG.

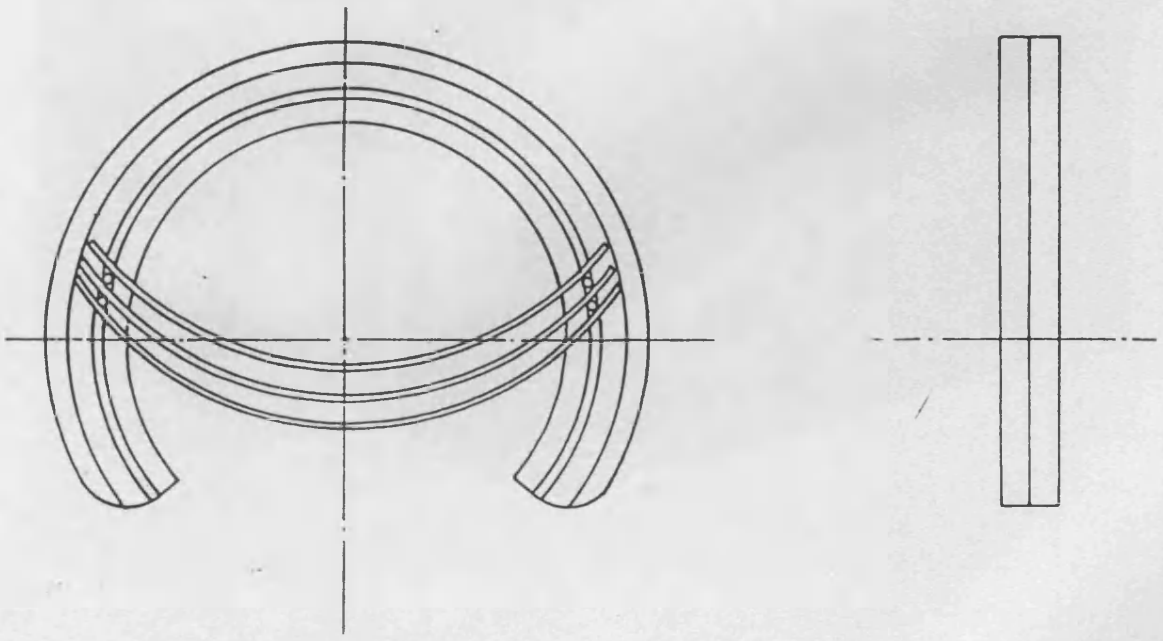

FIGURE 7.12 GRID CONSTRUCTION.

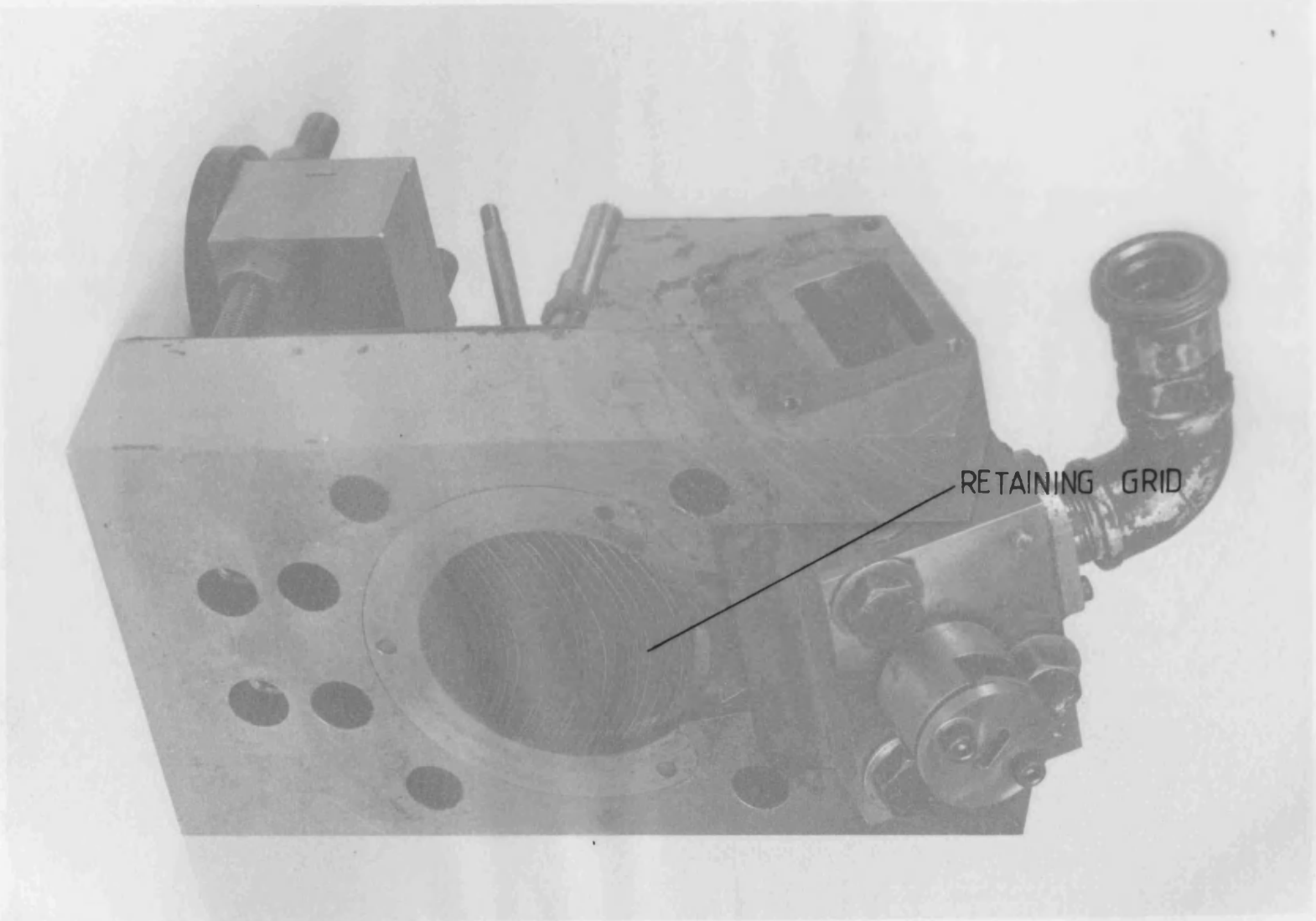

FIGURE 7.13 UNDERSIDE OF CYLINDER HEAD

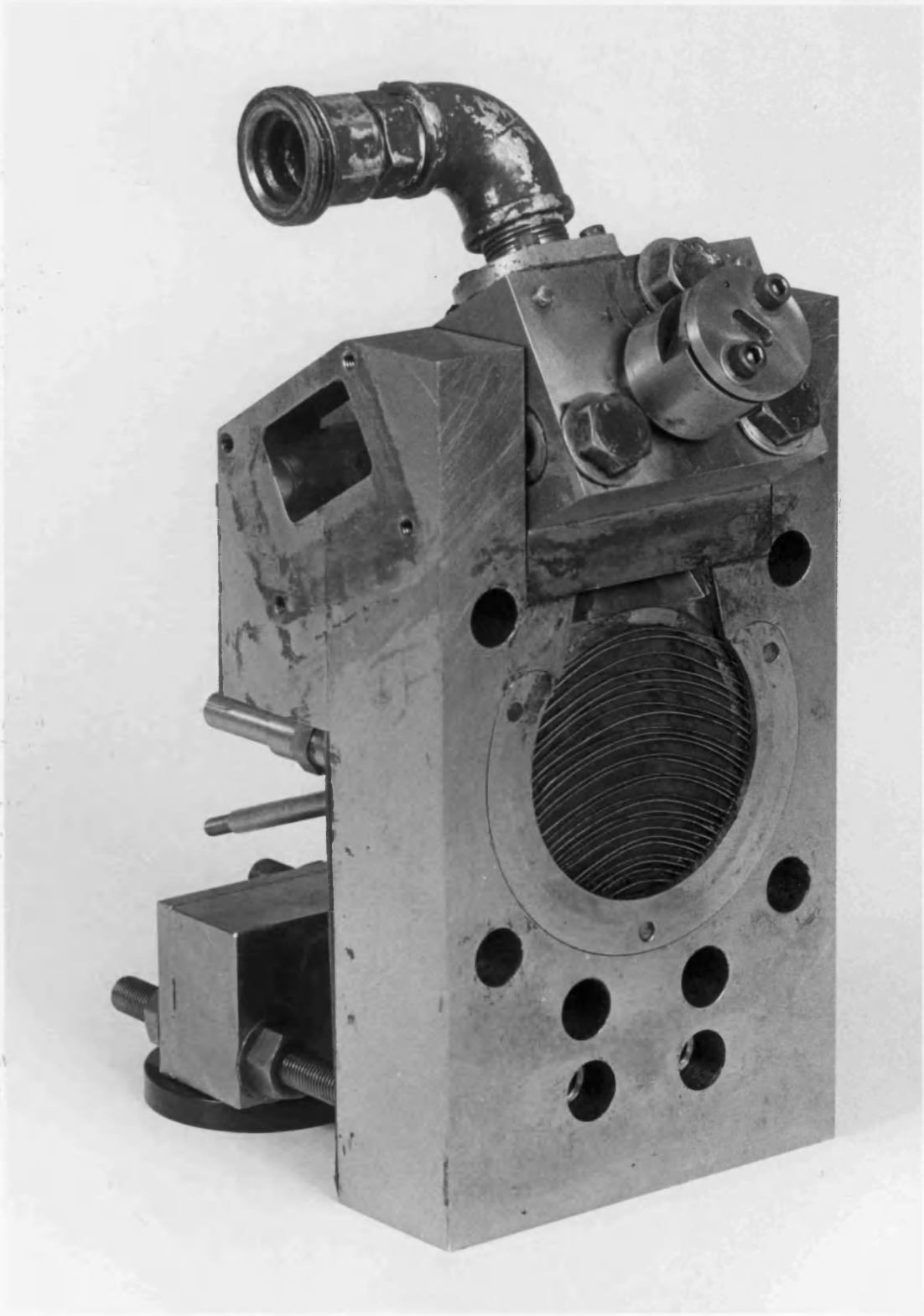

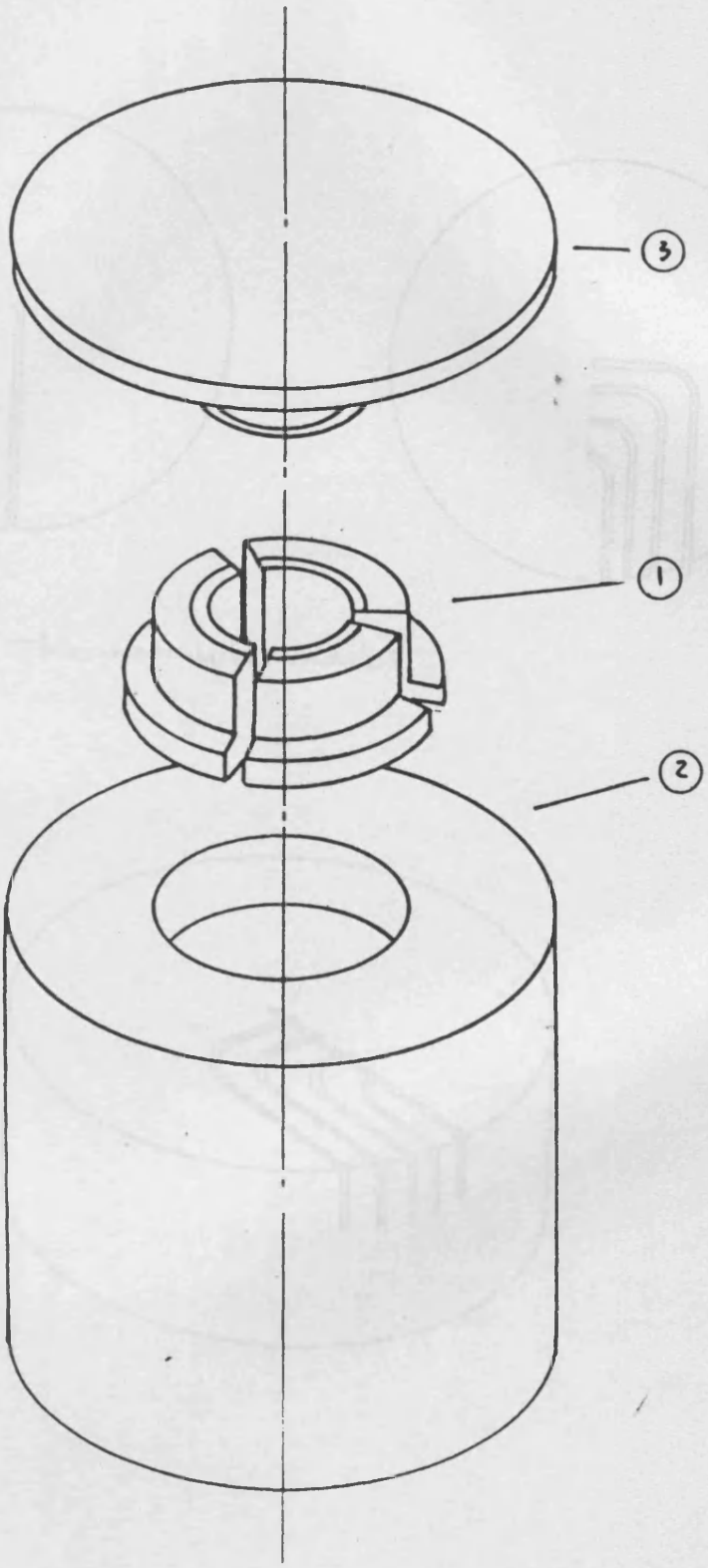

FIGURE 7.14 EXPLODED DIAGRAM OF PISTON CROWN.

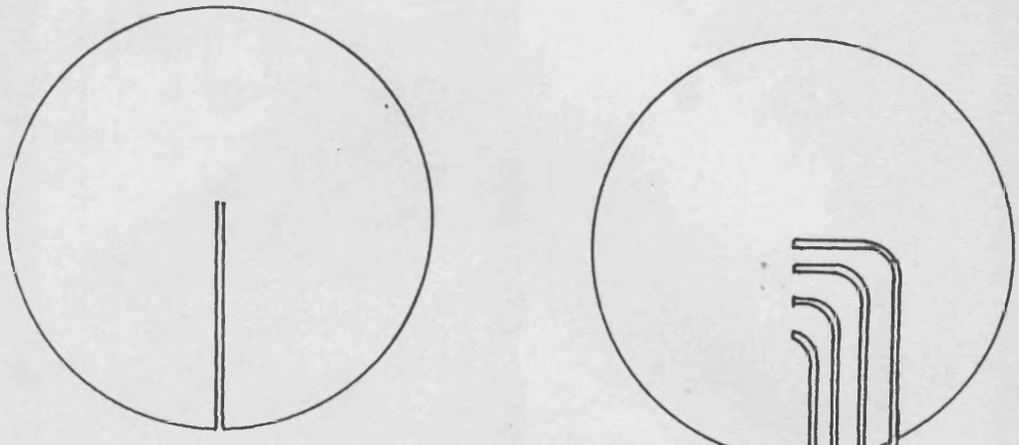

Thermocouple masks

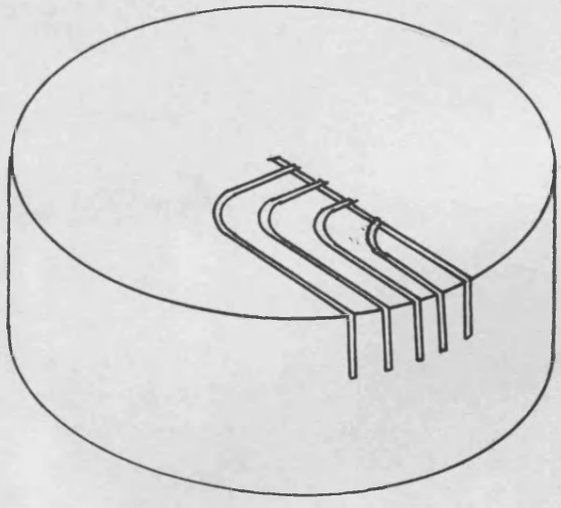

FIGURE 7.15 FORMATION OF THERMOCOUPLES.

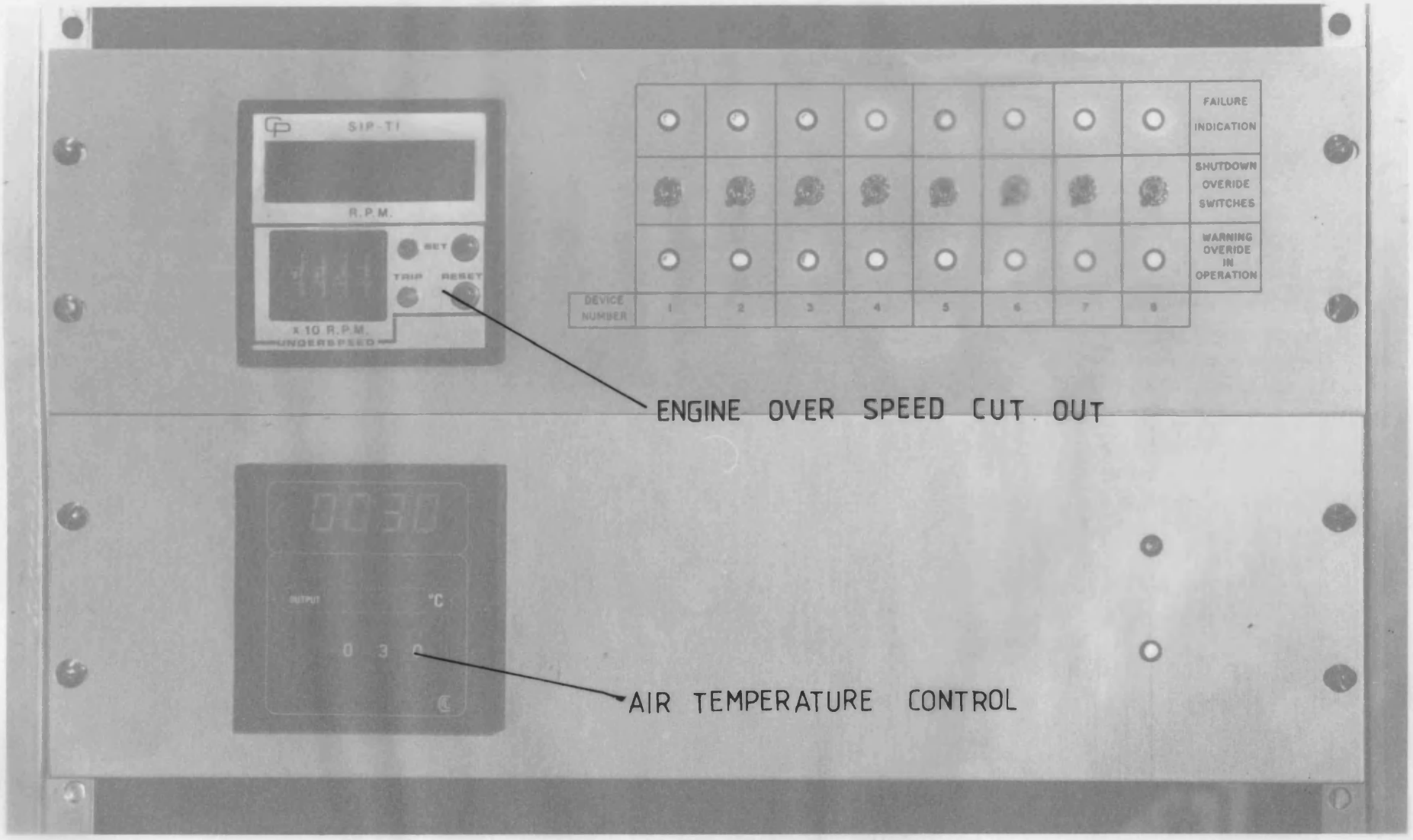

FIGURE 7.16 FAILURE DETECTION PANEL

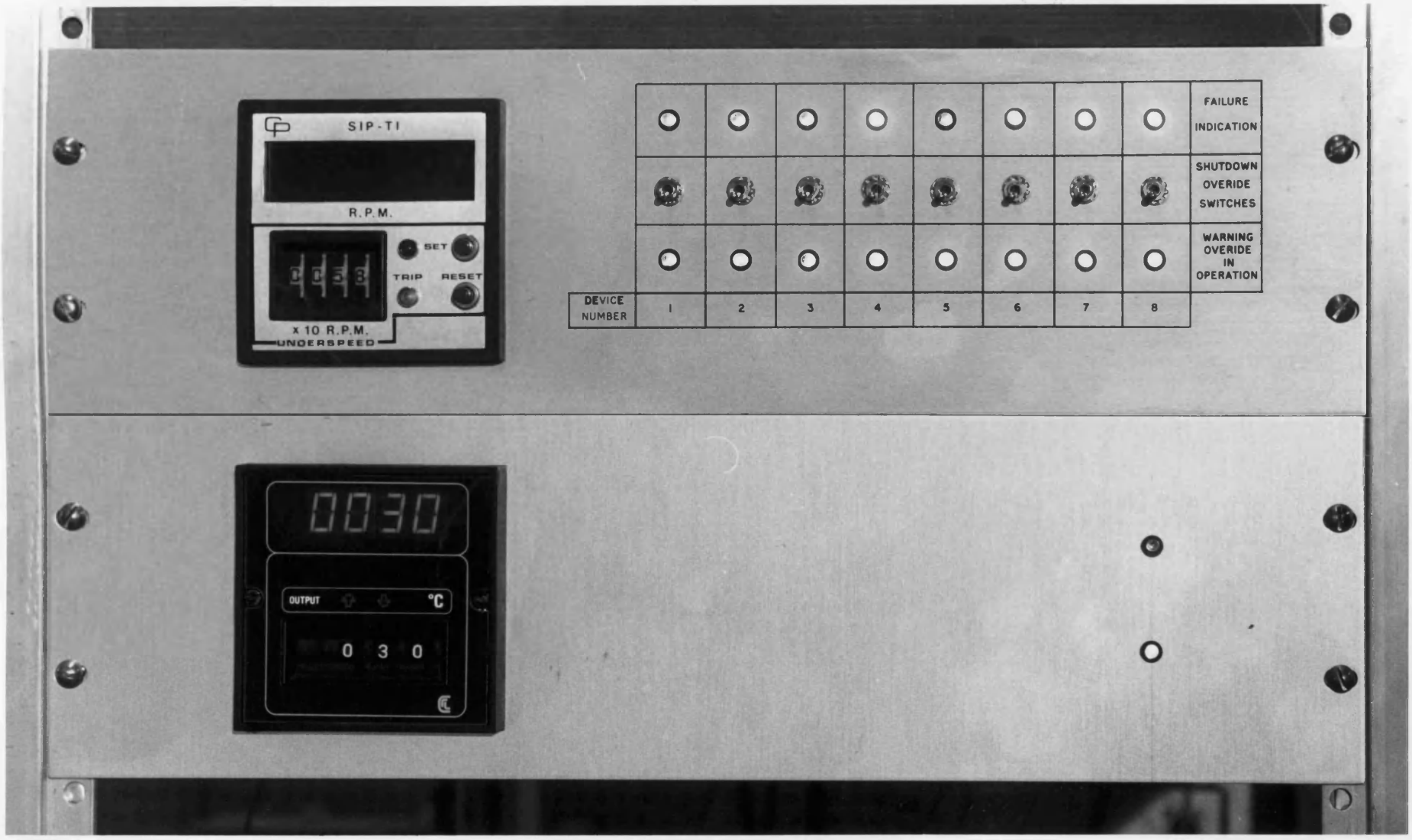
SIP-TI
R.P.M.
SET
TRIP
RESET
x 10 R.P.M.
UNDERSPEED
FAILURE INDICATION
SHUTDOWN OVERIDE SWITCHES
WARNING OVERIDE IN OPERATION
DEVICE NUMBER
1
2
3
4
5
6
7
8
0030
OUTPUT
°C
0 3 0

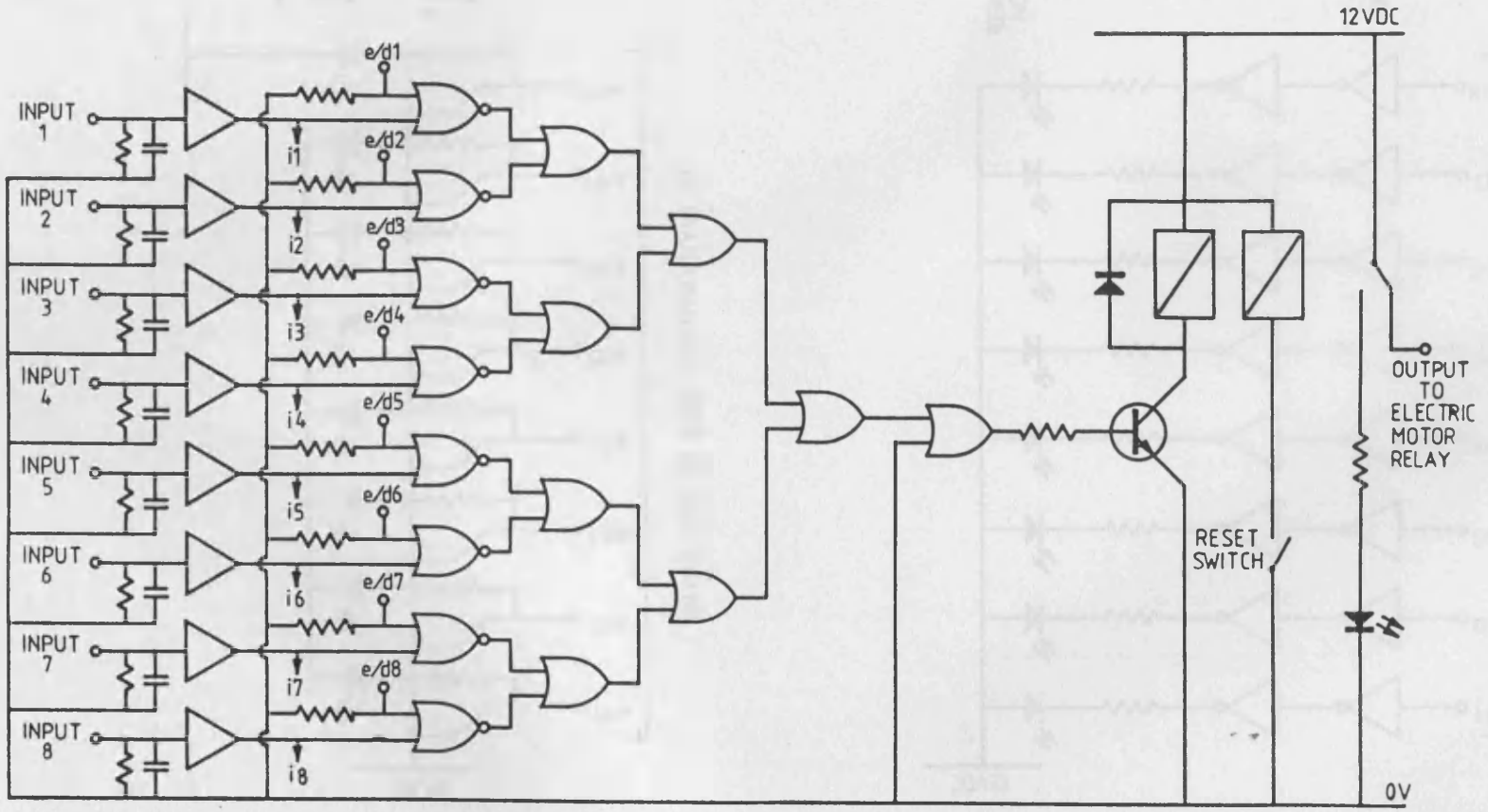

FIGURE 7.17 CERAMIC TEST RIG AUTOMATIC SHUTDOWN CIRCUIT DIAGRAM.

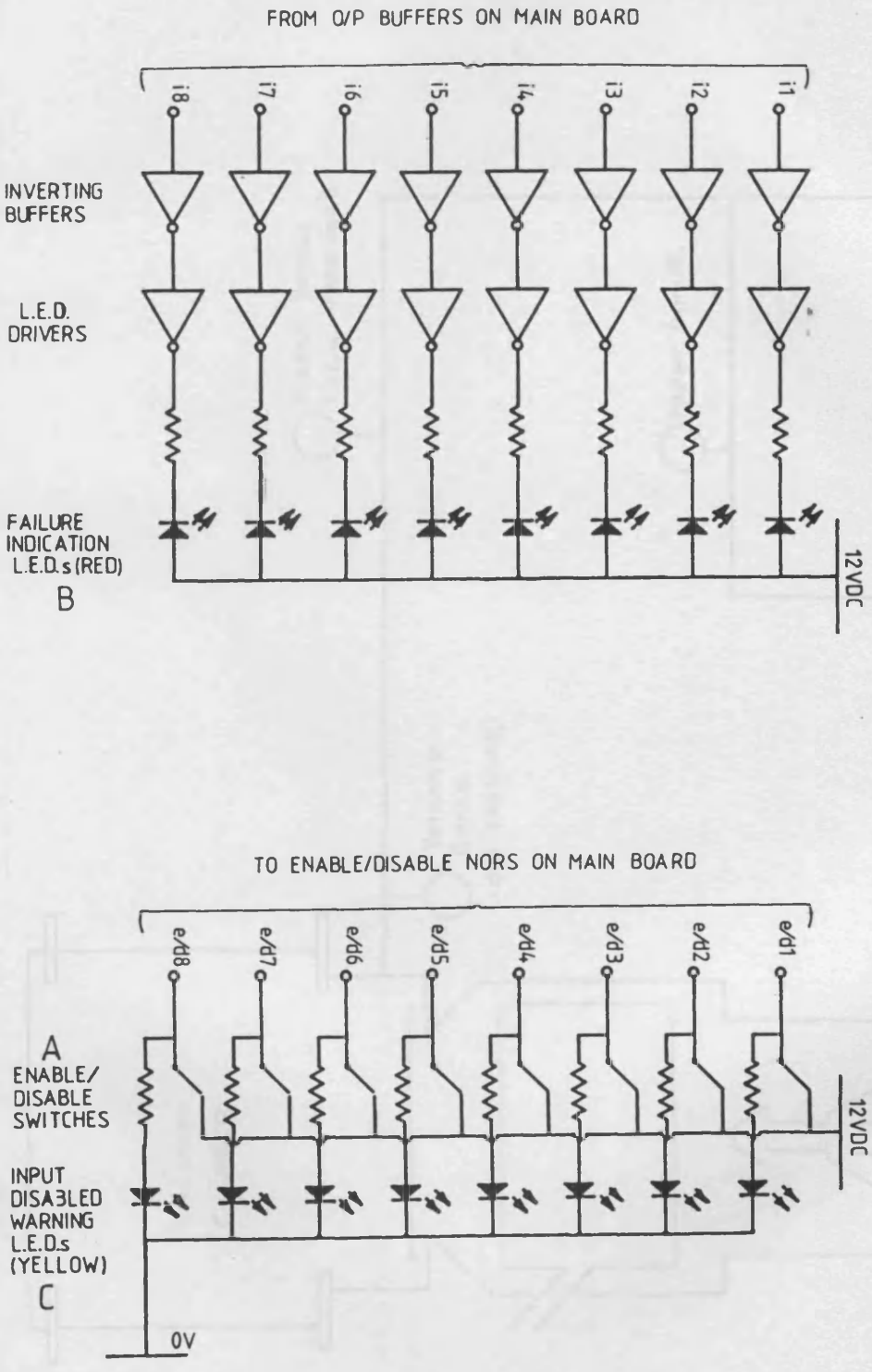

FIGURE 7.18 DETAILS OF AUTOMATIC SHUTDOWN SYSTEM DISPLAY CIRCUIT.

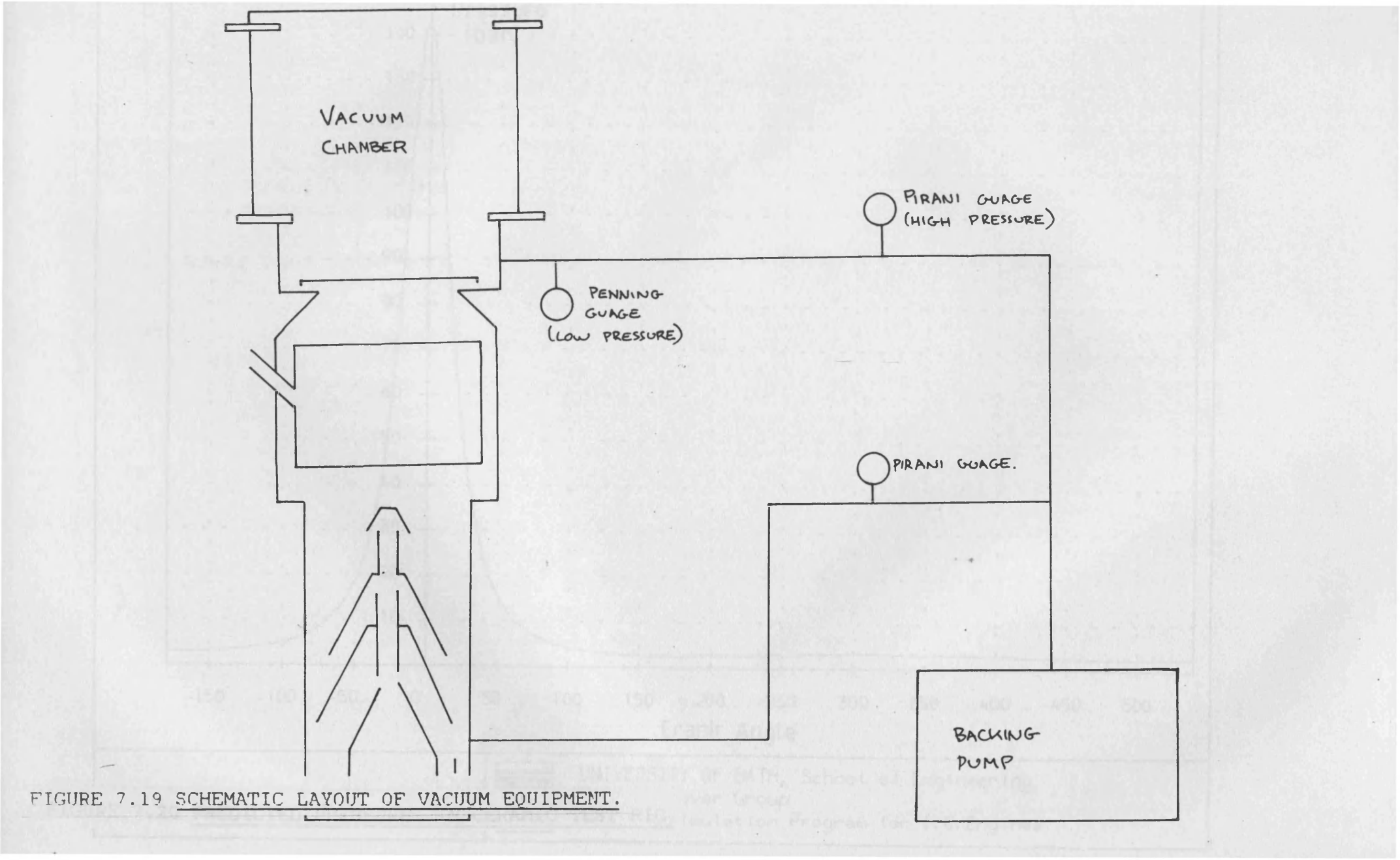

FIGURE 7.19 SCHEMATIC LAYOUT OF VACUUM EQUIPMENT.

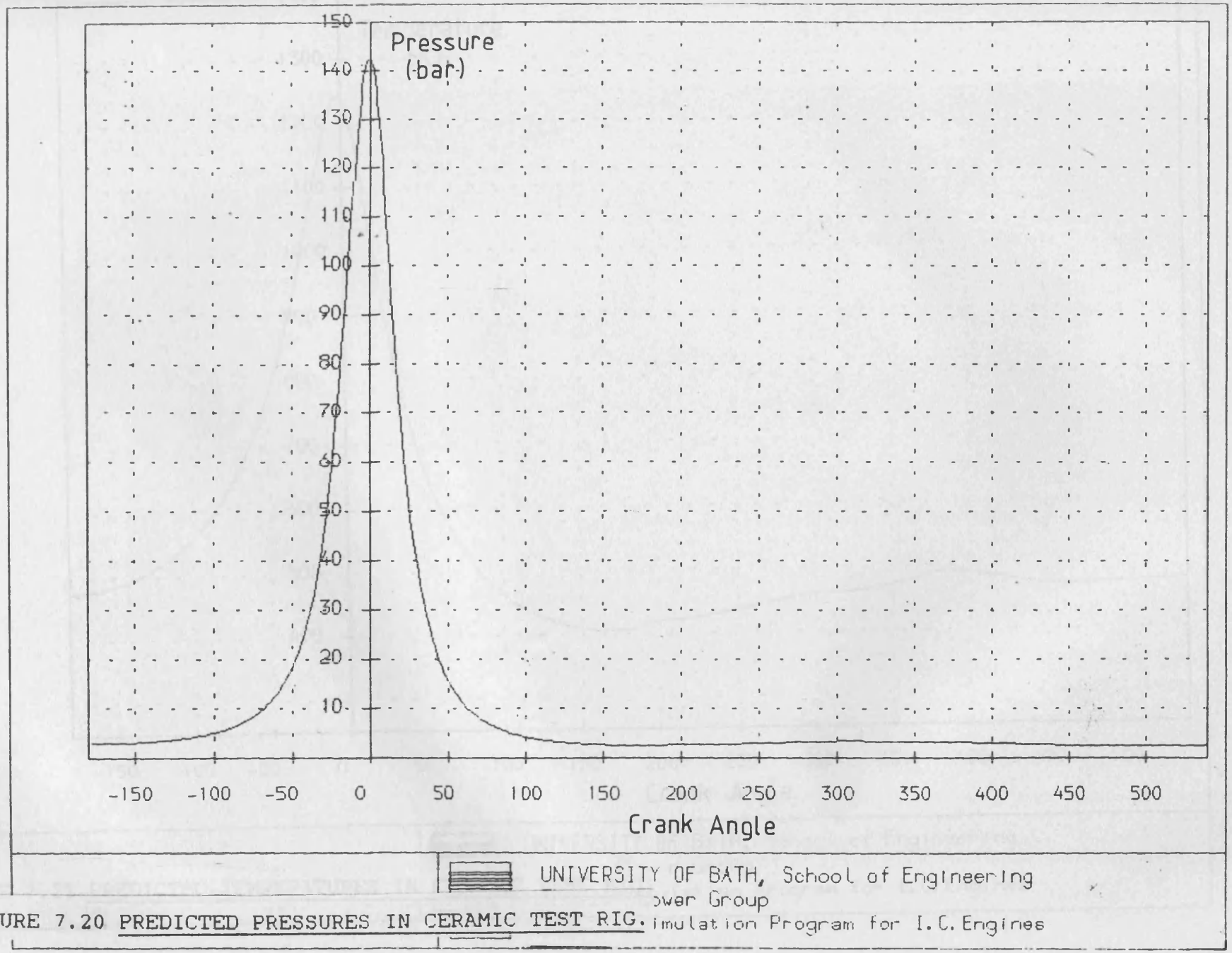

FIGURE 7.20 PREDICTED PRESSURES IN CERAMIC TEST RIG.

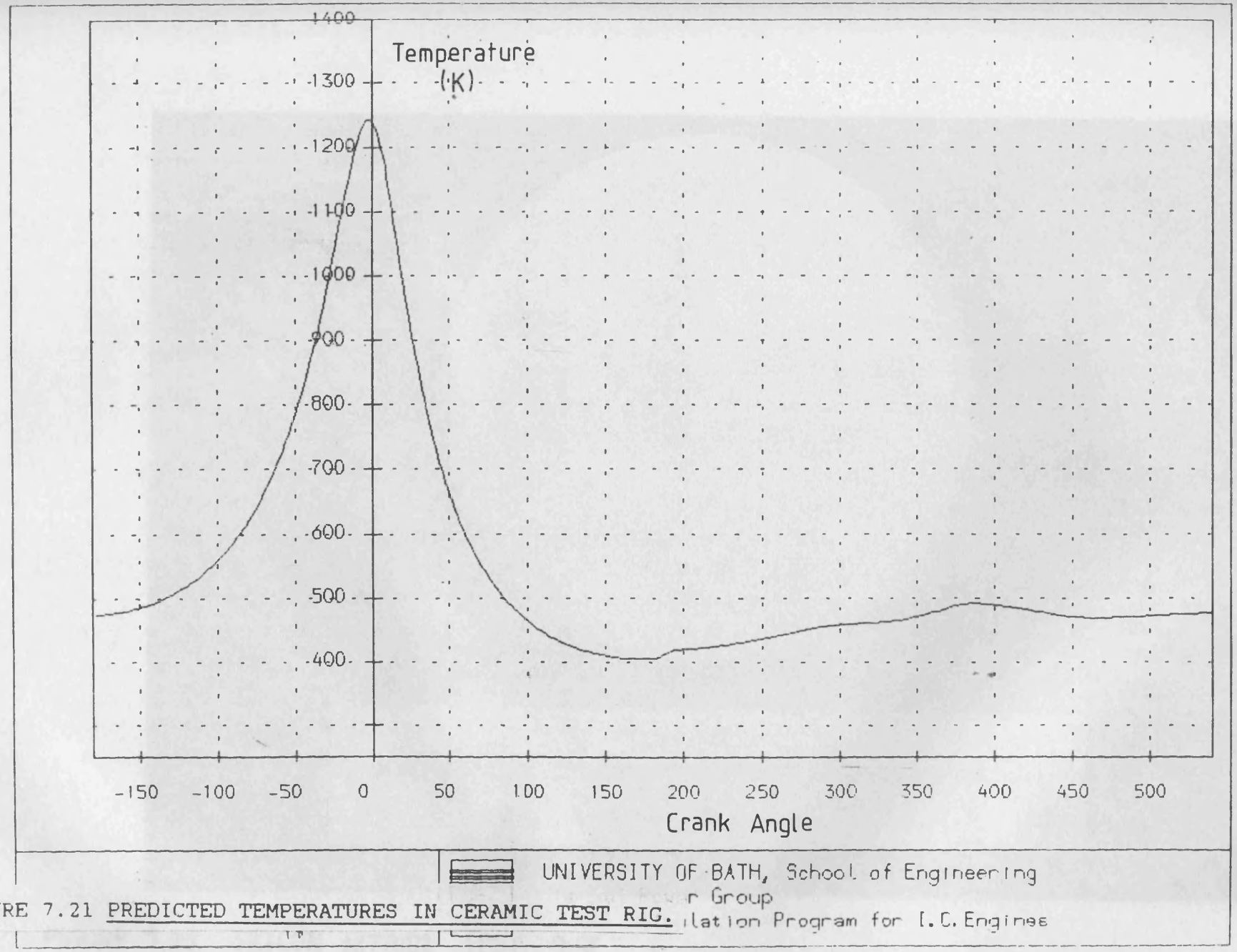

FIGURE 7.21 PREDICTED TEMPERATURES IN CERAMIC TEST RIG.

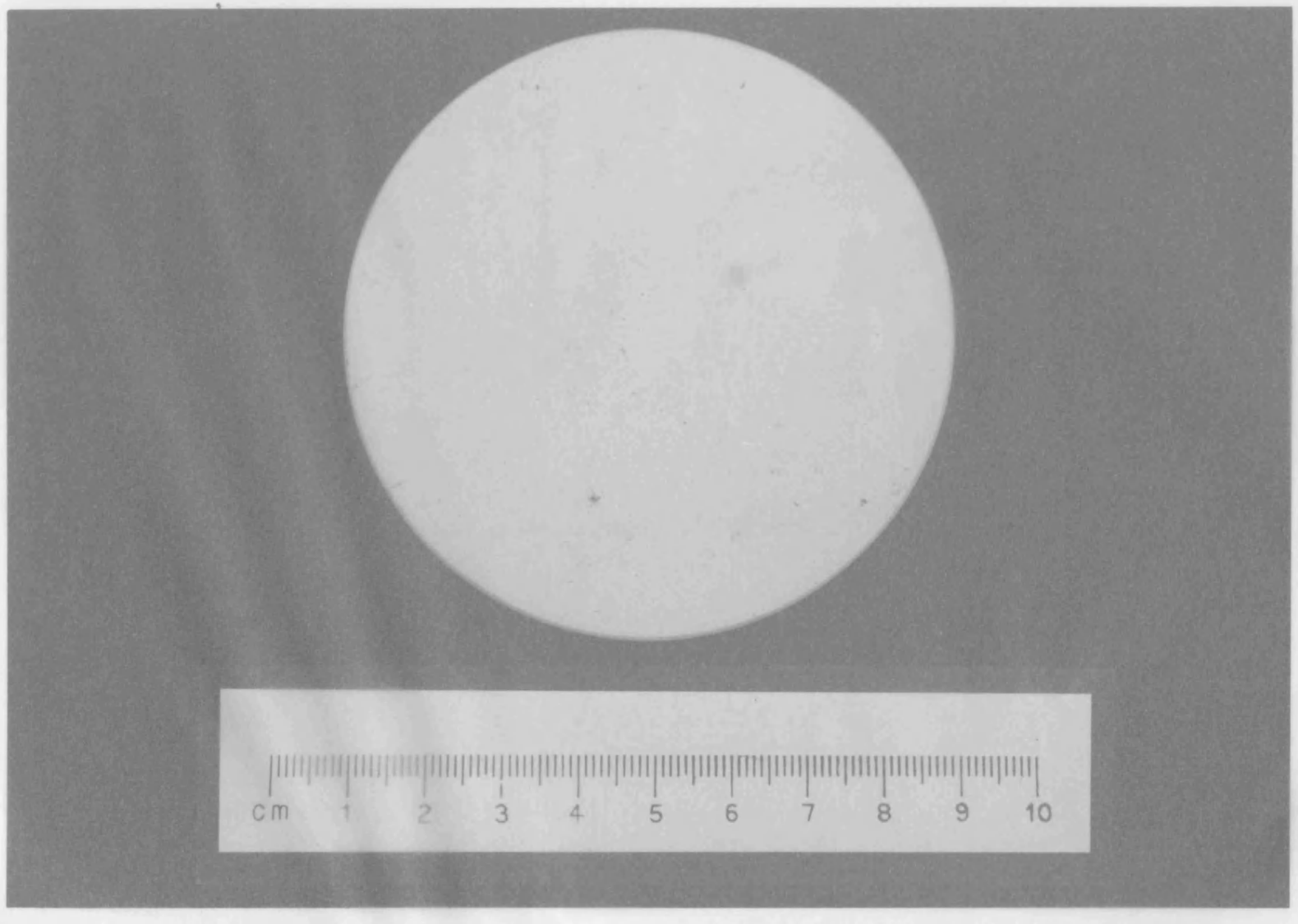

FIGURE 7.22 SILICON NITRIDE TEST DISC

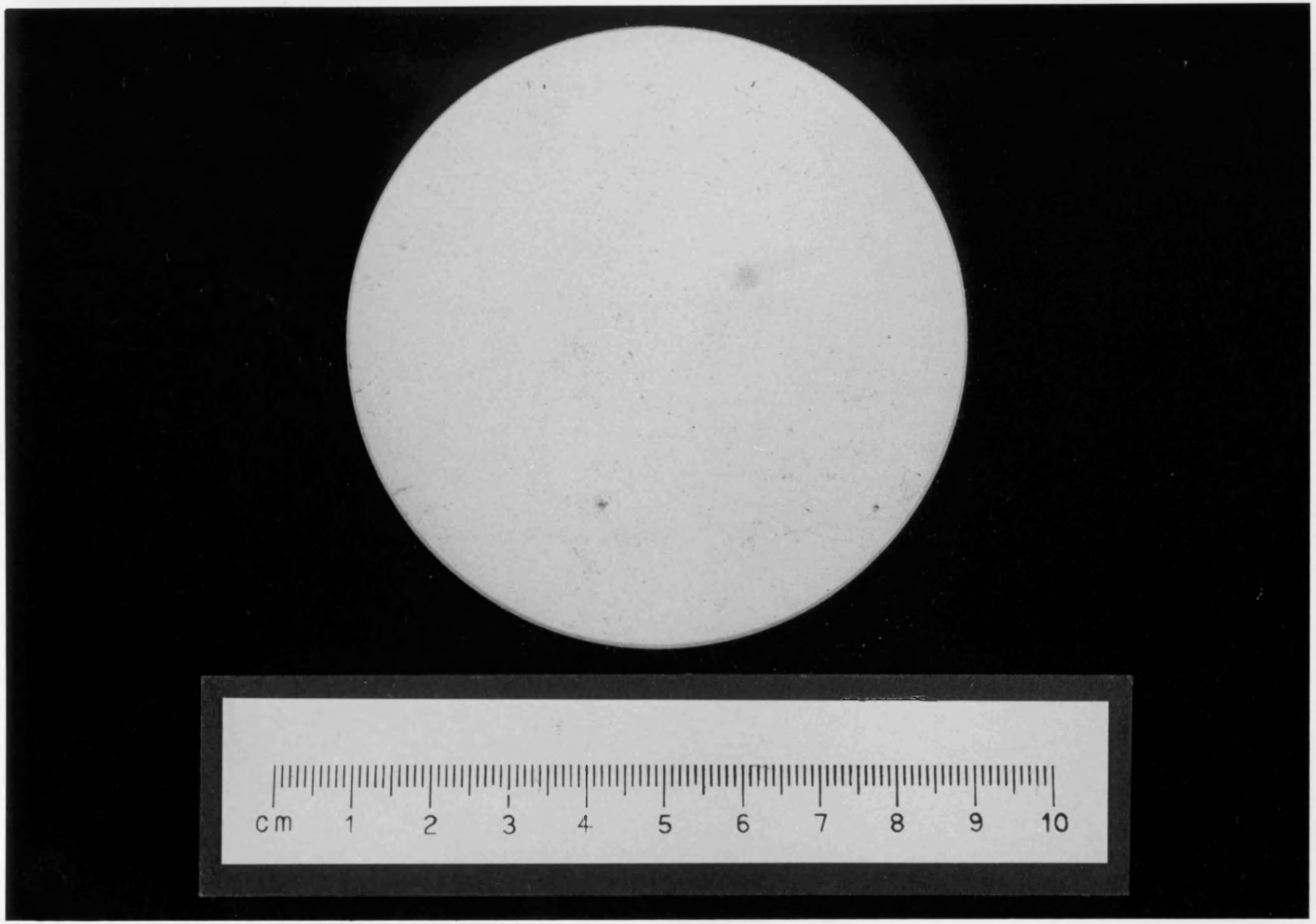
cm 1 2 3 4 5 6 7 8 9 10

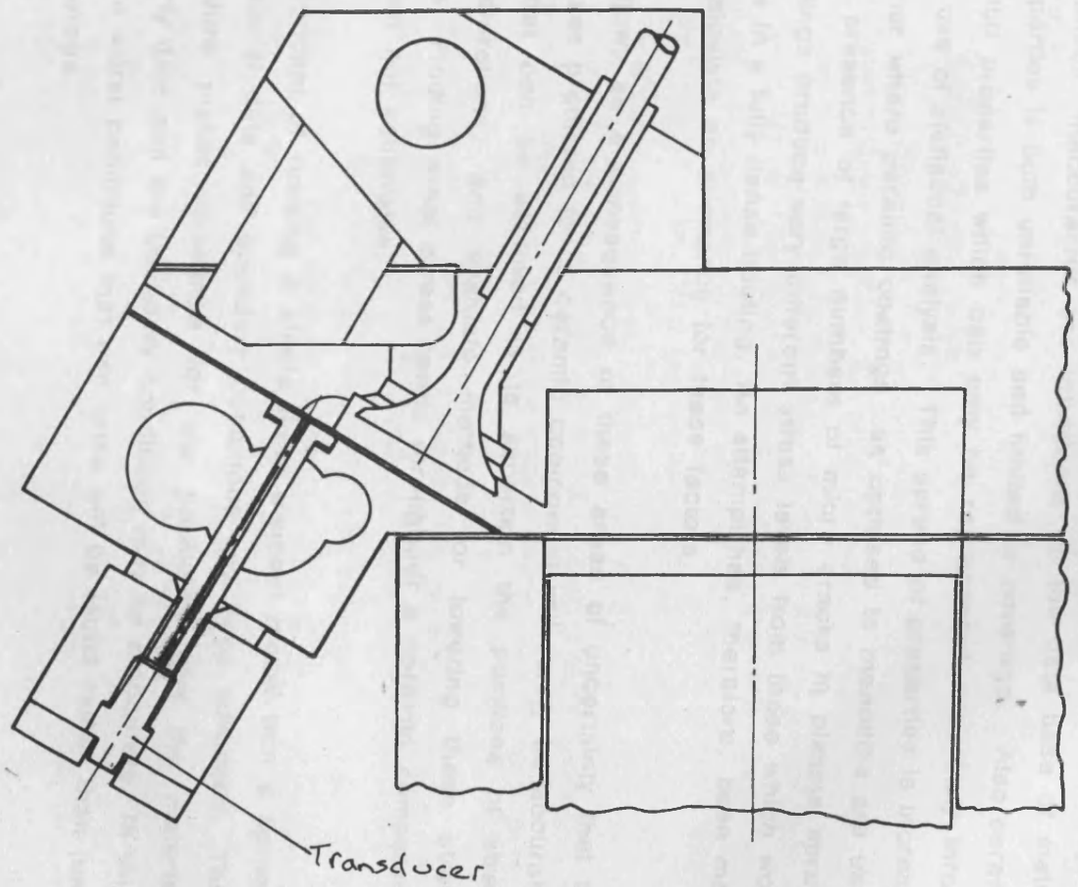

FIGURE 7.23 CROSS SECTION OF CYLINDER HEAD SHOWING TRANSDUCER MOUNTING.

8 CONCLUSIONS AND SUGGESTIONS FOR FUTURE WORK

8.1 THEORETICAL WORK

The theoretical work undertaken has revealed methods through which the stresses in coatings and monoliths can be minimised. However, it has also highlighted several problems peculiar to the analysis of ceramics. Inaccuracies are introduced as the data base of material properties is both unreliable and limited in coverage. Also ceramics exhibit properties which can only be represented accurately through the use of statistical analysis. This spread of properties is increased further where ceramic coatings as opposed to monoliths are used. The presence of large numbers of micro cracks in plasma sprayed coatings produce very different stress levels from those which would arise in a fully dense coating. An attempt has, therefore, been made to calculate an allowance for these factors.

It follows as a consequence of these areas of uncertainty that the stresses predicted for a ceramic component will rarely be accurate. All that can be achieved is to ascertain the positions of stress concentrations, and evaluate methods for lowering these stress peaks. Finding exact stress levels throughout a ceramic component is often not achievable.

The concept of running a single finite element model with a spread of material data and boundary conditions has been advanced. This procedure makes allowance for the possibility that the material property data and the boundary conditions may be inaccurate. In this way the worst conditions that can arise will be found rather than just the average.

The residual stresses in zirconia coatings is another area that was investigated. With the process of plasma spraying there are many parameters which can be varied, including zirconia feed rate, distance between substrate and spray head and spray head traverse rate. At present these variables are set to values which experience has demonstrated can produce satifactory coatings, without any real

appreciation of the reasons for success or failure. However, as coating thickness increases it has become necessary to gain a clearer understanding of how the variation of these parameters affects the coating. A simplified theoretical investigation was therefore made to predict the residual stresses in coatings. This work can only be regarded as a start into this field, but the model does indicate possible ways of maximising coating life. The theory used needs to be extended to allow for plastic deformation of the substrate, and to include the heating effect of the plasma on the substrate.

8.2 EXPERIMENTAL WORK

The environment within a firing diesel engine has extreme temperature and pressure peaks. In the initial stages of assessing the suitability of individual ceramic materials these conditions are likely to be too severe, the test pieces not lasting long enough to provide useful results. The test rig was therefore intended to provide a controllable environment, capable of being made progressively more severe as the tests proceed; from small pressure and temperature ratios, to the levels nearer those in a firing engine.

This apparatus is based on a Petter PH1W diesel engine with a replacement cylinder head. A variety of ceramic material types and configurations can be mounted within this replacement head. The area reserved for the ceramic inserts is directly above the cylinder, providing a site 88mm in diameter and 25mm deep.

The programme of experimental work initially envisaged has, unfortunately, not taken place. This has been partly due to the illness of workshop personnel. In addition a rebuild of the test cell where the apparatus was sited was undertaken part way through the commissioning, causing further delays.

Despite these delays the rig is now running satisfactorily and has completed 400hrs of tests, under both boosted and unboosted conditions, with and without air preheat.

The initial aim of providing peak incylinder conditions of about 1330K and 120bar has not been fully realised. Currently the maximum operating conditions are 1300K and 60bar. Leakage of air into the water cooling system under boosted conditions has prevented operation with air boost. With air boost off the appears to be highly reliable and capable of being left running unattended for long periods.

It was originally intended to monitor the temperature within the ceramic test pieces using thin film thermocouples. Unfortunately, the initial attempts at forming the metallic layers failed. A great deal of time was spent investigating leaks within the equipment used, unfortunately without improving the coating. Eventually the problem was traced to an electrical fault. This was repaired, but by this stage too much time had elapsed to develop the thermocouples for use in the insulation test rig. However it is intended that this work be continued, and these thermocouples installed at a later date.

(1) KAMO R. and BRYZIK W. : Adiabatic turbocompound engine performance prediction.
SAE 780068

(2) KAMO R. and BRAYZIK W. : Ceramics in heat engines.
U.S. Army Tank-Automotive reseach and development command, 1979

(3) YOSHIMITSU T. et al : Capabilities of heat insulated diesel engine.
Engine research Div. Komatsu ltd, 1982

(4) TIMONEY S.G. : No coolant diesel engine.
University College Dublin, 1979

(5) WALLACE F.J. et al : Thermally insulated diesel engines.
University of Bath, 1984

(6) WALLACE F.J., WAY R.J.B. and VOLLMERT H. : Effect of partial suppression of coolant on the high output diesel engine.
University of Bath, Dec 1978

(7) FAUD A. : Performance prediction for adiabatic compounded diesel engine.
MSc Thesis

(8) WALLACE F.J. and KAO T.K. : A new approach to the prediction of heat flow and temperature in engine pistons with special reference to thermal barriers.
Bath University

(9) VALLAD H. and WYSPIANSKI G.K. : A theoretical analysis of thermal barriers in diesel engine cylinders.
Norwegian Marine research, 1982

(10) COLE A. : PhD Thesis
Bath University 1986

(11) KAO T.K. : Prediction of heat flow and temperature distribution

in adiabatic engine components
Bath University 1980

(12) KAO T.K. : Prediction of heat flow, temperature and stress in diesel engine pistons incorperating thermal barriers.
PhD thesis, Bath University, 1982

(14) KAO T.K., HARDISTY H. and WALLACE F.J. : An energy balance approach to the finite element method applied to heat transfer analysis.
Int. Jou. Mech. Eng. Vol 11, No 1, 1982

(15) DAVIDGE R.W. : Mechanical behaviour of ceramics.
1979, 0-521-21915-9

(16) RICHERSON D.W. : Modern ceramic engineering.
0-8247-1843-7

(17) KIRCHNER H.P. : Strengthening of ceramics.
1979, 0-8247-6851-5

(18) GODFREY D.J. and PITMAN K.C. : Proof-testing of ceramics and its application to a defective large ceramic component.
ARE HH 84220

(19) GORDON J.E. : The new science of strong materials.
0-1402-0920-4

(20) HOLMES K. : Course on engine ceramics.
University of Keele, 17th and 18th Sept 1984

(21) TORTI M., LUCEK J.W. and WEAVER G.Q. : Densified silicon carbide an interesting material for diesel application.
SAE 780071

(22) MARMACH M. et al : Toughened PSZ ceramics their role as advanced engine components.
SAE 830318

(23) KUNITOMO T., MATSUOKA K. and OGURI T. : Prediction of radiative heat flux in a diesel engine.
SAE 750786

(24) SIEGLA D.C. and AMANN C.A. : Exploratory study of the low-heat-rejection diesel for passenger-car application.
General Motors reseach laboratories, SAE 840435

(25) WOSHNI G. : A universally applicable equation for the instantaneous heat transfer coefficient in the internal combustion engine.
SAE 670931

(26) WATSON N. et al : The performance potential of limited cooled diesel engines.
Proc. Instn. Mech. Engrs. Vol. 197A Power industries, 1983

(27) KHAN I.M. et al : Prediction of soot and nitric oxide concentrations in diesel engine exhausts.
SAE 730169 1971

(28) WADE W.R. et al : Fuel economy with an uncooled D.I. diesel engine.
SAE 841286 Ford Motor Company, 1984

(29) VALLAND H. and WYSPIANSKI G.K. : An investigation of the effects of thermal barriers using the cycle simulation program PROCES.
Norwegan institute of technology

(30) GODFREY D.J. : The use of ceramics in diesel engines.
Admiralty Materials Laboratory, 1982

(31) FELTCHER-JONES D. et al : New piston features for truck off highway and idustrial diesel engines.
AE Symp. April 1982 Wellworthy ltd, 1982

(32) KAMO R. and BRYZIK W. : Cummins-TARADCOM adiabatic turbo-compound engine program.
Cummins Engine Company, SAE 810070

(33) GIBSON B.D. and STONE R.B. : The design and performance of ceramic piston.

(34) TIMONEY S. : A low friction, unlubricated SiC diesel engine. University College Dublin. SAE 830313

(35) HAMANO Y. : Ceramic parts for a diesel engine. Proc. Int. Sym. on Automotive propolsion Ceramic Co ltd. April 1980

(36) PARKER D.A. and SMART R.F. : An evaluation of silicon nitride diesel pistons. Proc. British Ceramic Society. 1978

(37) McLAUGHLIN D. : Ceramic applications in the diesel engine. Proc. British Ceramic Society. 1978

(38) WACKER E. and SANDER W. : Piston design for high combustion pressures and reduced heat rejection to coolant. Karl Schmidth GmbH. SAE 820505

(39) WOODS M.E. and ODA I. : PSZ ceramics for adiabatic engine components. Cummins Engine Company. SAE 820429

(40) MURRAY R.G. : Performance and Emission characteristics of a semi adiabatic engine. Oklahoma State University. ASME 80-DGP-44

(41) KAMO R. et al : Thermal barrier coating for diesel engine piston. Cummins Engine Company. ASME 80-DGP-14

(42) BRYZIK W. and KAMO R. : TACOM/Cummins adiabatic engine program. US Army Tank-Automotive Command. SAE 830314

(43) ASNANI M. and KUONEN F.L. : Ceramic valve and seat insert performance in a diesel engine. TRW Inc. SAE 850358

(44) RADOVANOVIC R.S. et al : Tribological investigations for an insulated diesel engine.
Cummins Engine Company. SAE 830319

(45) MOORHOUSE P. et al : Solid lubrication studies for adiabatic diesel engines.
SAE 850508

(46) SHIMAUCHI T. et al : Tribology at high temperature for uncooled heat insulated engines.
Komatsu ltd. SAE 840429

(47) KAMO R. et al : Thermal barrier coating for diesel engine pistons.
Cummins Engine Company

(48) COLE R.M. and ALKIDAS A.C. : Evaluation of an air gap insulated piston in a divided chamber diesel engine.
General Motors research laboratories. SAE 850359

(49) ELSBETT K. et al : The Ferrun piston for diesel engines - a two piece articulated piston design.
Elsbett Konstruktion (ELKO). SAE 850505

(50) TOYAMA K. : Heat insulated turbocompound engine.
Komatsu ltd. SAE 831345

(51) KVERNES I. and FARTUM P. : Corrosion resistant plasma sprayed coating in diesel engines.
Int. Conf. on Metallurgical coatings. 1978

(52) DAVIES A.J. : The finite element method. A first approach.
1973. 0-19-859631-6

(53) STRANG G. and FIX G.J. : An analysis of the finite element method.
1973. 0-13-032946-0

(54) SEGERLIND L.J. : An applied finite element analysis.
1976. 0-471-77440-5

(55) DESAI C.S. : Elementry finite element method.
1979, 0-13-256636-2

(56) CIARLET P.G. : The finite element method for elliptic problems.
1978, 0-444-85028-7

(57) TARABAD M. : Effect of the engine insulation on the performance parameters of a turbocharged diesel engine.
Bath University MT/CSP1/Feb82

(58) DILS R.R. and FOLLANSBEE P.S. : Superalloy sensors.
Metal and Manuf. proc. of int. symp., 1976

(59) EAUCHAIS P. et al : Plasmas and high temperature research applications
University of Limoges

(60) PAWLOSKI L. et al : A model of the temperature distribution in an alumina coating during plasma spraying
Thin solid film 307-319 (1982)

(61) HSUEH C.H. and EVANS A.G. : Residual stresses in Metal/Ceramic bonded strips
I. Am. Ceram. Soc. 1985

(62) MULLEN R.L. et al : Correlation of compressive and shear stress with spalling of plasma sprayed ceramic material
I. Am. Ceram. Soc. 1984

(63) LUMBY R.J. et al : Syalon ceramics for advanced engine components.
SAE 850521

APPENDIX 4.1 STRESS ANALYSIS OF DISC

Using the principle of superposition we split the strain into a number of individual component strains.

a) When the disc is subject to a temperature difference between faces, each elemental disc will try to expand to its free diameter. If constrained to its original diameter then effective change in radius is Δr_c

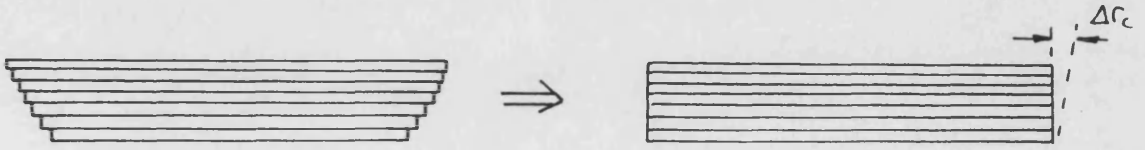

b) Δr_f is the change in radius required for radial equilibrium

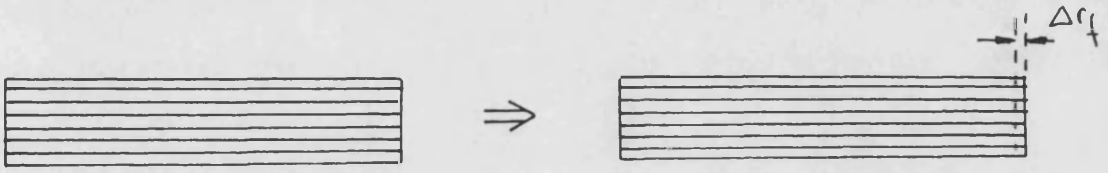

c) If disc is unrestrained then Δr_i is the change in radius of each elemental disc due to axial deformation.

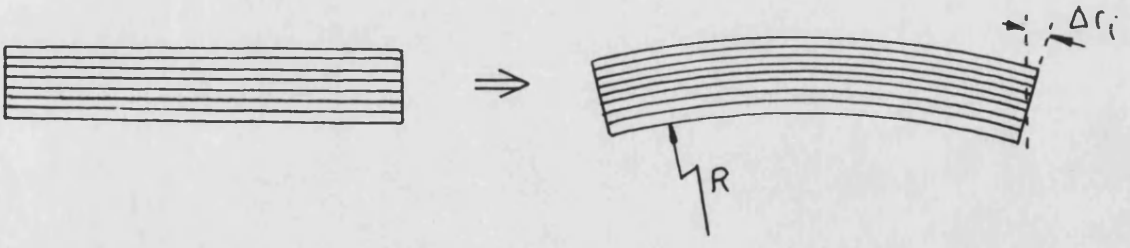

d) The introduction of an axial stress will also change the outer diameter.

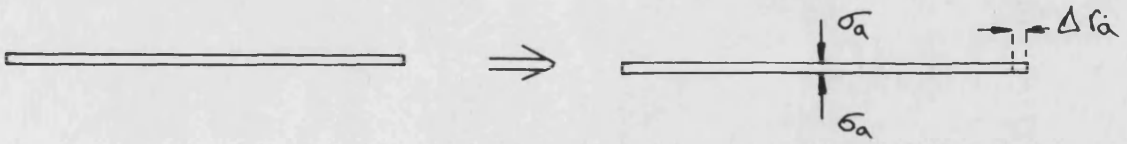

A disc will have three stress vectors,

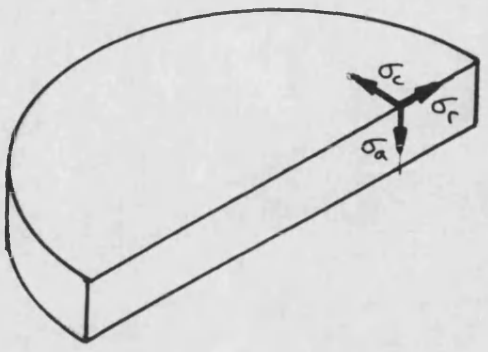

Taking element of disc,

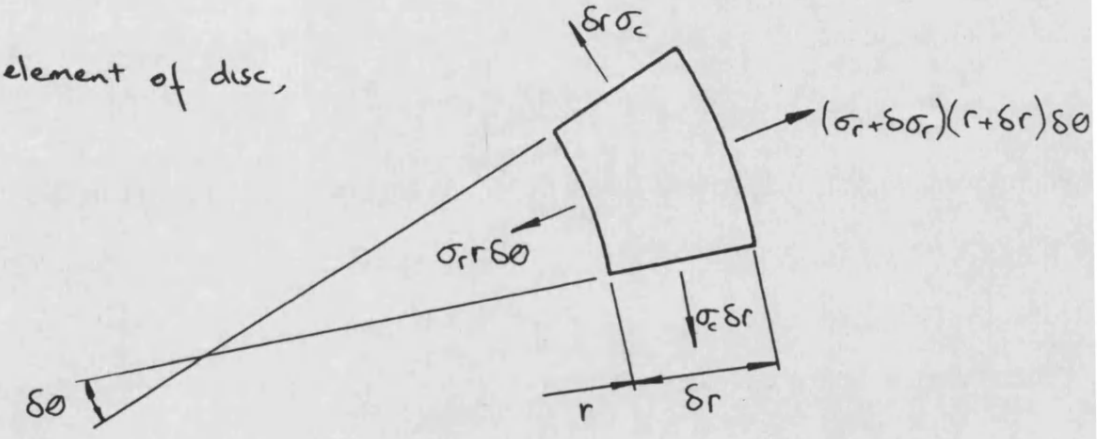

Equilibrium in radial direction,

$$2\sigma_c \delta r \sin\tfrac{1}{2}\delta\theta + \sigma_r r\delta\theta - (\sigma_r+\delta\sigma_r)(r+\delta r) = 0$$

In the limit

$$\sigma_c - \sigma_r - r\frac{d\sigma_r}{dr} = 0 \qquad (1)$$

Examining a concentric ring of the disc, subject to a radial load.

Let u be the radial shift at a radius r,

ie: r becomes $r+u$, after straining.

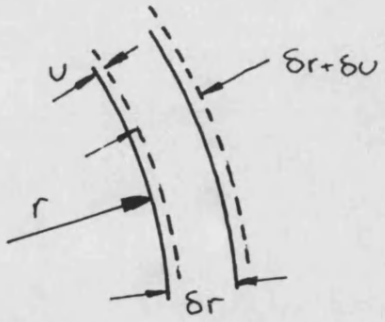

The circumferential, or hoop strain

$$\epsilon_c = \frac{\text{Increase of circumference}}{\text{Original circumference}}$$

$$= [2\pi(r+u) - 2\pi r]/2\pi r = u/r \qquad (2)$$

The radial displacement at the inner surface of the concentric ring is u, the outer displacement $u+\delta u$

$$\epsilon_r = (\text{Increase in } \delta r)/\delta r = \frac{du}{dr} \text{ in the limit} \qquad (3)$$

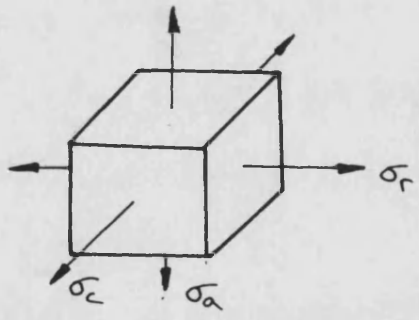

We know that;

$$\epsilon_c = \frac{1}{E}(\sigma_c - \nu\sigma_r - \nu\sigma_a)$$

so including a uniform temperature rise (ΔT)

$$E\epsilon_c = \sigma_c - \nu\sigma_r - \nu\sigma_a + \Delta T\gamma E \qquad (4)$$

using (2) $$E\frac{u}{r} = \sigma_c - \nu\sigma_r - \nu\sigma_a + \Delta T\gamma E \qquad (5)$$

also $E\epsilon_r = \sigma_r - \nu\sigma_c - \nu\sigma_a + \Delta T \gamma E$ (6)

using (3) $E\frac{du}{dr} = \sigma_r - \nu\sigma_c - \nu\sigma_a + \Delta T \gamma E$ (7) 4.3.1

Obtaining $E\frac{du}{dr}$ from (5), and equating with (7)

$$(\sigma_c - \sigma_r)(1+\nu) + r\frac{d\sigma_c}{dr} - \nu r\frac{d\sigma_c}{dr} = 0$$

substitute in (1)

$$r\frac{d\sigma_r}{dr}(1+\nu) + r\frac{d\sigma_c}{dr} - \nu r\frac{d\sigma_r}{dr} = 0$$

rearranging

$$\frac{d\sigma_c}{dr} = -\frac{d\sigma_r}{dr}$$

Integrating $\sigma_r + \sigma_c = A$

Substituting in (1)

$$r\frac{d\sigma_r}{dr} + 2\sigma_r = A$$

$$\therefore \sigma_r = \frac{A}{2} - \frac{B}{r^2}$$

Similarly $\sigma_c = \frac{A}{2} + \frac{B}{r^2}$

For a solid disc, then $B = 0$

$$\therefore \sigma_r = \sigma_c \quad (8)$$

from 1 $\sigma_c - \sigma_r = r\frac{d\sigma_r}{dr} = 0$

$$\therefore \frac{d\sigma_r}{dr} = 0 \quad (9)$$

Radial stress

Previously each elemental disc has been treated seperately and has been free to find its equilibrium condition. We must now examine the effect of applying boundary conditions to each elemental disc.

from (6)

$$\epsilon_r = \frac{1}{E}(\sigma_r - \nu\sigma_c - \nu\sigma_a) + \Delta T\gamma \qquad (10)$$

from (8) $\qquad \sigma_r = \sigma_c$

If each elemental disc is unrestrained then they will find their own equilibrium condition.
If we constrain the disc to a common diameter then some may be placed in tension, and some compression.

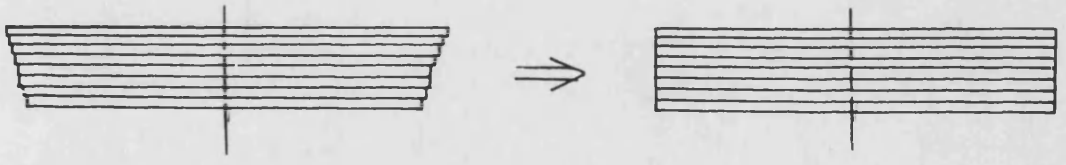

Under this condition there may be a tendency for the discs to deform.

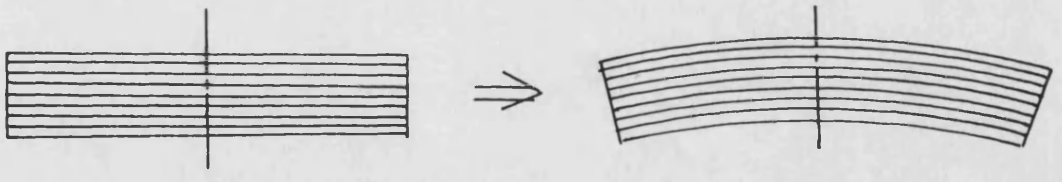

If no restraints are applied then equilibrium will be reached, and the net radial force and bending moment will be zero.

For each element,

$$\epsilon_r = \frac{2}{D}\left(\Delta r_c + \Delta r_f + \Delta r_i + \Delta r_a\right) + \Delta T\gamma$$

$$\therefore \frac{2}{D}\left(\Delta r_c + \Delta r_f + \Delta r_i + \Delta r_a\right) = \frac{1}{E}\left(\sigma_r - \nu\sigma_c - \nu\sigma_a\right) \quad \text{from } (10)$$

$$\sigma_r = \frac{2E\left(\Delta r_c + \Delta r_f + \Delta r_i + \Delta r_a\right)}{D(1-\nu)} + \frac{\nu\sigma_a}{(1-\nu)} \qquad (11) \quad 4.6.1$$

The radial force developed by each element, Fr

$$F_r = D\pi\omega\sigma_r$$

where ω is the element thickness.

$$F_r = \frac{\pi\omega E\left(\Delta r_c + \Delta r_f + \Delta r_i + \Delta r_a\right)}{(1-\nu)} + \frac{D\pi\omega\nu\sigma_a}{(1-\nu)} \qquad 4.6.2$$

Axial stress

The axial stress in each element is found from the radial stress in that element, and the axial stress in the previous element. The axial stress in the first element can be found from the gas pressure, the remaining stresses are calculated in sequence.

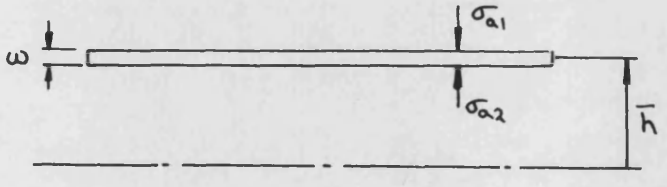

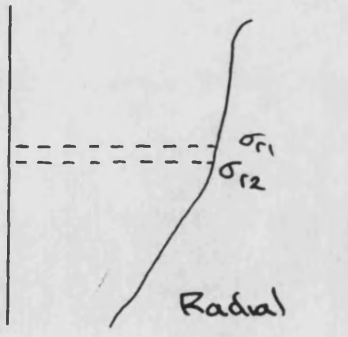

Radial stress distribution

Subscript 2, current element
1, last element

For each disc, B.M. due to radial stress

$$\text{B.M.} = (\pi D\omega_2\sigma_{r2})\bar{h} + \pi D\omega_2\left(\frac{\sigma_{r1}-\sigma_{r2}}{2}\right)\left(\bar{h} + \frac{2}{3}\omega_2\right) \qquad (12)$$

B.M. due to axial stresses,

$$= \frac{D}{6}(\sigma_{a2} - \sigma_{a1})\frac{\pi D^2}{4} \qquad (13)$$

12 = 13 , since Σ B.M. = 0

$$\sigma_{a2} = \sigma_{a1} + \frac{24\omega_2\sigma_{r2}\bar{h}}{D^2} + 12(\sigma_{r1} - \sigma_{r2})\frac{1}{D^2}\left(\bar{h} + \frac{2}{3}\omega_2\right)$$

From (11)

$$\sigma_{a2} = \sigma_{a1} + \left(\frac{2E(\Delta r_c + \Delta r_f + \Delta r_i + \Delta r_a)}{(1-\nu)D} + \frac{\nu\sigma_a}{(1-\nu)}\right)_2\left(\frac{24\omega_2\bar{h}}{D^2} - \frac{12}{D^2}\left(\bar{h} + \frac{2}{3}\omega_2\right)\right)$$

$$+ \left(\frac{2E(\Delta r_c + \Delta r_f + \Delta r_i + \Delta r_a)}{(1-\nu)D} + \frac{\nu\sigma_a}{(1-\nu)}\right)_1 \frac{12}{D^2}\left(\bar{h} + \frac{2}{3}\omega_2\right)$$

In general

$$\sigma_{ai} = \frac{\sigma_{ai-1}\left(1 \quad \frac{\nu_{i-1}}{1-\nu_{i-1}}\frac{12}{D^2}\left(\bar{h} + \frac{2}{3}\omega_i\right)\right) + B\left(\frac{\bar{h} + \frac{2}{3}\omega_{i-1}}{D^2}\right) + A.C.}{1 - \frac{\nu_i}{1-\nu_i}C} \qquad 4.6.3.$$

$$A = \left(\frac{2E(\Delta r_c + \Delta r_f + \Delta r_i - \Delta r_a)}{(1-\nu)D}\right)_i .12$$

$$B = \left(\frac{2E(\Delta r_c + \Delta r_f + \Delta r_i - \Delta r_a)}{(1-\nu)D}\right)_{i-1} .12$$

$$C = \frac{24\omega_i\bar{h}}{D^2} - \frac{12}{D^2}\left(\bar{h} + \frac{2}{3}\omega_2\right)$$

Change in axial stress across boundary between materials

Two materials A and B have common boundary, a sudden change in axial and radial stress at the boundary results.

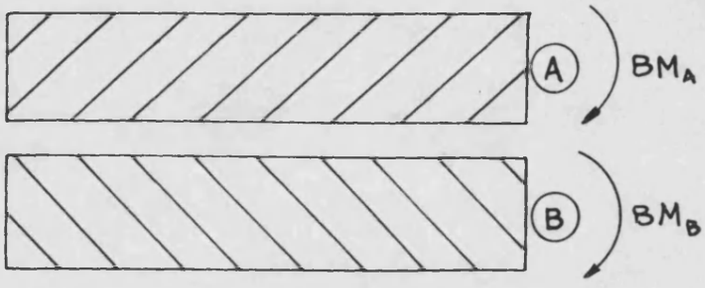

Each material piece is in equilibrium

ie: $\sum BM_A = \sum BM_B = 0$

If material A, is divided into n sections, then from (12) and (13)

$$\sum_{i=1}^{i=n} \left(\pi D w_{i+1} \sigma_{r(i+1)}\right)\bar{h} + \pi D w_{i+1}\left(\frac{\sigma_{ri} - \sigma_{r(i+1)}}{2}\right)\left(h + \frac{2}{3}w_{i+1}\right) + \frac{D}{6}\left(\sigma_{a(i+1)} - \sigma_{ai}\right)\frac{\pi D^2}{4} = 0$$

Similarly in material B, which is divided into m sections,

$$\sum_{i=n+1}^{n+m} \left(\pi D w_{i+1} \sigma_{r(i+1)}\right)\bar{h} + \pi D w_{i+1}\left(\frac{\sigma_{ri} - \sigma_{r(i+1)}}{2}\right)\left(h + \frac{2}{3}w_{i+1}\right) + \frac{D}{6}\left(\sigma_{a(i+1)} - \sigma_{ai}\right)\frac{\pi D^2}{4}$$

$$= 0.$$

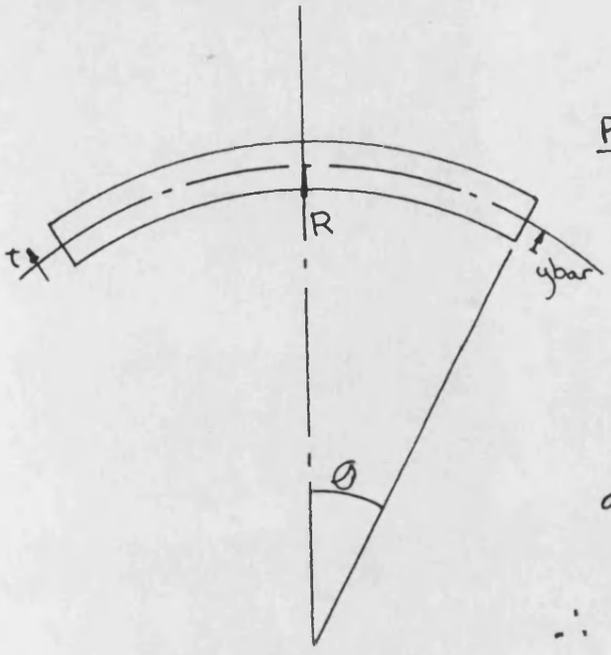

Position of Neutral Surface

Disc diameter = D

$$\theta = \frac{D}{2R}$$

and $$\theta = \frac{D + \Delta D}{2(R + t - ybar)}$$

$$\therefore \quad 2(t - ybar)\theta = \Delta D$$

$$\frac{\sigma_r - \nu\sigma_c - \nu\sigma_a}{E} = \frac{2(t - ybar)\theta}{D}$$

$$\frac{\sigma_r}{E} = \frac{t - ybar}{R(1-\nu)} \qquad (14)$$

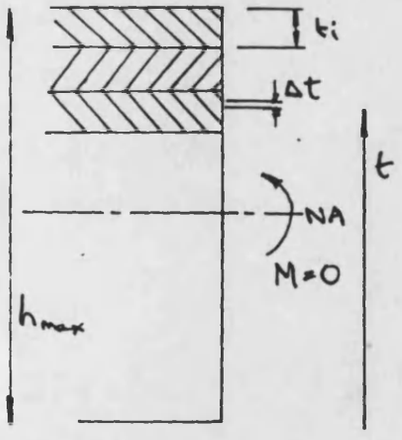

About N.A. $\quad \Sigma M = 0$

$$M = \sigma_r D.\Delta t.\pi.(t - ybar)$$

$$= \frac{D}{R}\frac{E}{(1-\nu)}(t - ybar)^2 \pi \Delta t$$

using (14)

$$\therefore \quad 0 = \frac{D\pi}{R}\sum_{0}^{h_{max}} \frac{E}{(1-\nu)}(t^2 - 2t\,ybar + ybar^2)\Delta t$$

$$0 = \frac{D\pi}{R}\left[\frac{Ei}{(1-\nu i)}\left(\frac{t^3}{3} - \frac{2t^2}{2}ybar + ybar^2 t\right)_{hi}^{hi+ti}\right.$$

$$\left. + \frac{Ei}{(1-\nu i)}\left(\frac{t^3}{3} - \frac{2t^2}{2}ybar + ybar^2 t\right)_{hi-1}^{hi-1+ti-1} + \ldots\ldots\right]$$

$$0 = \frac{D\pi}{R}\left[\frac{E_i}{(1-V_i)}\left(-h_i^3 + h_i^3 + 3h_i^2 t_i + 3h_i t_i^2 + t_i^3 - ybar\left(-h_i^2 + h_i^2 + t_i^2 + 2t_i h_i\right) + ybar^2 t_i\right) + \ldots\ldots\ldots\right]$$

$$0 = \frac{E_i}{(1-V_i)}\left(t_i\left(h_i^2 + h_i t_i + \frac{t_i^2}{3}\right) + t_i\left(ybar - 2(ybar.h_i) - ybar.t_i\right)\right) + \ldots$$

$$0 = \left(\left(h_i - ybar + \frac{t_i}{2}\right)^2 + \left(\frac{t_i}{12}\right)^2\right)\frac{E_i(1-V_n)}{E_n(1-V_i)}t_i + \ldots\ldots\ldots$$

APPENDIX 4.2 STRESS PROGRAM LISTING

```
c
c   This program has been modified to calculate the residual
c   stresses caused by plasma spraying
c     This program calculates the stress ( axial and circumferential ) in a circular disc that is subject
c     to a temperature drop across the faces.  The disc may be restrained in the axial direction, or
c     allowed to deform to its equilibrium position.  The program is structured to cope with either a disc
c     made of two materials or the disc may be divided up into not more than 195 layers each with its own
c     properties, so allowing for graded materials.
c
c     The program splits the disc into a number of thinner elements each with uniform properties.
c
c     In the case of a disc restrained axially, each disc is then allowed to expand freely in the radial direction
c     The force in each element is then found to restrain all the elemental discs to the same diameter.  This
c     diameter is then adjusted to the sum of all the radial forces is zero.  The stresses are then found in each
c     element.  Axial stresses in each element are found by further iteration involving a relationship between
c     the B.M. along the circumferance, temperature distribution , radius of curvature and the axial stress
c     When deformation is allowed the above is repeated with additional factors allowing stress changes
c     caused by the change in shape.  A further itteraiton is performed adjusting the radius until zero
c     net B.M. are found about the N.A.
c
c     Shooting methods are employed for convergence to the boundary conditons
c
c
c
c     set up arrays
c     t    thickness of each element     temp    temperature in S.S       temp2   transient temperature array
c     e    young's mod                   v       poisson's ratio          a       thermal expansion
c     cp   specific heat                 de      density
c
c
      dimension cp(300),de(300),nmat(20),temp2(50,200)
      dimension dtemp(100)
      dimension temp(200),force(200),fdis(200),bm(200),ford(200),forr(200),e(300),v(300),g(300),t(300),stresy(200),fory(200),n(100)
      real k1,k2,nfor,nbm,nbm2,haul,k(300),h
      integer type,ber,trans,props,bound,zfor,out,tempro,trtemp
      common k,e,v,g,t,cp,de
      pi=3.14159
c     set zfor to 1 when sufficient information is available to use shootin method to find rad. of curvature
      zfor=0
c     ntemp counts the number of transient calculations performed
      ipone=0
      ntemp=1
c     set net force to zero
      nfor=0.0
```

```
c     counter to stop restraint condition being entered for esch temperature transient
      alrdy=0
c
c     set input/output type
      write(6,800)
      read(5,835) type
c
c     read in number of calculations to be performed
      if(type.eq.2.or.type.eq.3) goto 100
      write(6,805)
  100 continue
      read(5,835)ber
c     write(6,801)
c     read(5,835) secon
      secon=0
  801 format(' if you wish to use only one convergence criteia enter a 1',
     &/,' for standard solution enter a 0',/)
c
c     if graded materials are used set trans=1
      if(type.eq.2.or.type.eq.3) goto 105
      write(6,810)
  105 continue
      read(5,835) trans
      props=0
      telast=1e6
c
c     if properties temperatures dependant set tempro=1
c     if(type.eq.2.or.type.eq.3) goto 106
      write(6,815)
  106 continue
      read(5,835) tempro
      if(tempro.eq.1) write(6,109)
  109 format(1x,' do you require help setting up the subroutine necessary',/,
     &' ans; "y" or "n"',/)
      if(tempro.eq.1) read(5,826) ans
      if(tempro.eq.1.and.ans.eq.'y') call help6
c
c     trtemp set to the number of transient cycles required
      if(type.eq.2.or.type.eq.3) goto 108
      write(6,820)
  108 continue
      read(5,835) trtemp
c
c     if residual stresses are to be calculated set iresid
      iresid=0
      write(6,1040)
 1040 format(1x,"enter 1 if residual stresses are to found from plasma spraying",/
     &" otherwise type a 0",/)
```

```
      read(5,835) iresid
      if(iresid.eq.1)write(6,847)
      if(iresid.eq.1) read(5,835) telast
  847 format(1x,' Enter temperature at which elastic properties start in the coating',/)
c
      if(trans.ne.1) goto 120
c
c
c------READ IN DATA FOR GRADED MATERIALS
c
c
c     if trans=1, props=number of layers
      write(6,825)
      props=200
      read(5,826) ans
  826 format(a1)
      if(ans.eq.'y') call help4
  110 read(5,835) e(props)
      if(e(props).lt.1.0e-5) goto 115
      read(5,835) k(props),v(props),g(props),t(props),nmat(props-199)
      props=props+1
      goto 110
  115 continue
      secon=1
      write(6,830)
      read(5,826) ans
      if(ans.eq.'y') call help5
      read(5,835) heat1,heat2,temp1,temp3,dia,dtemp(1)
c     set all of dtemp matrix if datum temperature is set
c
      do 1030 iuop=1,100
      dtemp(iuop)=-dtemp(1)
 1030 continue
c
      call section(n,tempro,temp(i),nmat)
c
      ncer=nmat(1)
      nmet=nmat(2)
      naste=2
      do 117 ic=1,20
      ntot=ntot+nmat(ic)
  117 continue
      eight=0
      do 118 ic=1,199
      eight=eight+t(ic)
  118 continue
      t1=t(1)
      t2=t(ncer+1)
```

```
 120 continue
c
c     start of loop for multiple runs
c
 125 ber=ber-1
     mfor=0
     zfor=0
     if(trans.gt.1.0e-5) goto 170
c
c
c------READ IN PROPERTIES FOR UNIFORM PROPERTIES
c
c
c     if trans not equal to 1
     if(type.eq.2.or.type.eq.3) goto 130
     write(6,840)
 130 continue
     read(5,836) ans
 836 format(a1)
     if(ans.eq.'y') call help1
     read(5,835)t1,t2,temp1,temp3,heat1,heat2,dia,ctemp,dpress
     ptemp1=temp1
     ptemp3=temp3
     if(type.eq.2.or.type.eq.3) goto 135
     if(tempro.ne.1) write(6,845)
 135 continue
     if(tempro.ne.1) read(5,846) ans
 846 format(a1)
     if(tempro.ne.1.and.ans.eq.'y') call help2
     if(tempro.ne.1) read(5,835)e1,e2,k1,k2,v1,v2,g1,g2,cp1,cp2,de1,de2
     if(type.eq.2.or.type.eq.3) goto 140
     write(6,850)
 140 continue
     read(5,835) ncer,nmet
     t1=t1/ncer
     t2=t2/nmet
     ntot=nmet+ncer
     if(iresid.eq.1) then
c    if residual stresses are being calculated then
c    find the stress free temperature of each layer
c
 266 if(iresid.lt.0.2.or.ipone.eq.1) goto 1005
     read(14,1010)(dtemp(ino),ino=1,ncer)
     ipone=1
1010 format(1x,1f10.3)
1005 continue
     endif
     if(tempro.eq.1) goto 155
```

```
c
c     for bi-material non temperature dependant properties set the property matrix
      do 145 i=1,ncer
      e(i)=e1
      k(i)=k1
      v(i)=v1
      g(i)=g1
      de(i)=de1
      cp(i)=cp1
      t(i)=t1
  145 continue
      do 150 i=(1+ncer),ntot
      e(i)=e2
      k(i)=k2
      v(i)=v2
      g(i)=g2
      de(i)=de2
      cp(i)=cp2
      t(i)=t2
  150 continue
      goto 170
  155 continue
c
c     for bi-material temperature dependant properties call subroutine properties to set property matrix
      do 260 iprof=1,3
      temp1=ptemp1
      temp3=ptemp3
      do 160 i=1,ncer
      matl=1
      t(i)=t1
c
c     set properties using user defined functions in 'properties'
c
      call properties(matl,temp(i),i)
c
  160 continue
      do 165 i=(ncer+1),ntot
      matl=2
      t(i)=t2
c
      call properties(matl,temp(i),i)
c
  165 continue
  170 continue
      uas=0.0
      if(tempro.eq.1.or.trans.eq.1) goto 175
      if(heat1.lt.1.0e-5.and.heat2.lt.1.0e-5) goto 190
c
```

```
c
c------FIND CHANGE IN SURFACE TEMPERATURES
c
c
      uas=0.0
      if(trans.ne.1) goto 185
c     find thermal resistance if graded structrue
  175 do 180 i=1,ntot
      uas=uas+(t(i)/k(i))
  180 continue
c     find thermal properties if uniform properties
  185 if(tempro.ne.1.and.trans.ne.1) uas=(t1*ncer/k1)+(t2*nmet/k2)
c     find overall thermal resistance
      if(heat1.gt.1.0e-5) uas=uas+(1.0/heat1)
      if(heat2.gt.1.0e-5) uas=uas+(1.0/heat2)
      uas=1.0/uas
      qhea=uas*(temp3-temp1)
c     record wall and gas temperatures
      if(heat1.gt.1.0e-5) gas1=temp1
      if(heat2.gt.1.0e-5) gas2=temp3
      if(heat1.gt.1.0e-5) temp1=(qhea/heat1)+temp1
      if(heat2.gt.1.0e-5) temp3=(qhea/heat2)+temp3
  190 continue
      temp1=temp1-ctemp
      temp3=temp3-ctemp
c
c
c------CALCULATE POSITION OF NA
c
c
c     first guess at position of NA
      ybar=(nmet*t2+ncer*t1)/2.0
      tot1=0.0
  195 h=nmet*t2+ncer*t1
      if(trans.eq.1) h=eight
c
      do 200 i=1,ncer
      h=h-t1
      sto=(((h-ybar+(t1/2.0))**2.0+(t1**2.0)/12.0)*(e(i)/e(1)))*t1
      if((h-ybar+(t1/2.0)).lt.0.0)sto=-sto
      tot=tot+sto
  200 continue
c
      do 205 i=(ncer+1),ntot
c     net second moment of area = 0
      h=h-t2
      sto=(((h-ybar+(t2/2.0))**2.0+(t2**2.0)/12.0)*(e(i)/e(1)))*t2
      if((h-ybar+(t2/2.0)).lt.0.0)sto=-sto
```

```
      tot=tot*sto
  205 continue
c
      if(abs(tot1).gt.1.0e-20) goto 210
      tot1=tot
      ybar1=ybar
      ybar=ybar*1.05
      tot=0.0
      goto 195
c
  210 tim1=ybar
      tim2=ybar1
      tim3=tot1
      tim4=tot
      if(abs(tot).lt.0.5e-10) goto 215
      if((tim1-tim2).eq.0) goto 215
      chayb=tim4*((tim2-tim1)/(tim3-tim4))
      if(abs(chayb).gt.(0.1*ybar)) chayb=0.1*ybar*chayb/abs(chayb)
      ybar=tim1-chayb
      if(abs(tim4).gt.abs(tim3)) ybar1=tim2
      if(abs(tim4).gt.abs(tim3)) tot1=tim3
      if(abs(tim4).lt.abs(tim3)) ybar1=tim1
      if(abs(tim4).lt.abs(tim3)) tot1=tim4
      tot=0.0
      goto 195
c
c
c------FIND TEMPERATURE AND FREE EXPANSION OF EACH ELEMENT
c
c
c     continue if transient conditions are required
  215 if(trtemp.lt.0.5) goto 235
      write(6,226)
  226 format(1x,' What uniform temperature is your disc starting at',/,
     &' you can use either degrees K or C, but keep to same throughout program',/)
      read(5,835)t12
      write(6,227)
  227 format(1x,' Is the temperature distribution already available in file70?',/,
     &' in which case type "y",',/,' or do you want the program to calculate the distribution for you,',/,
     &' in which case type "n"',/)
      read(5,826) ans
      if(ans.eq."n") write(6,228)
  228 format(1x,' To calculate transient temperature distribution, the user-written,',/,
     &' subroutine "tempbound" must be used, if you require help in preparing this',/,
     &' type "y"',/)
      jtrig=0
      if(ans.eq."y") jtrig=1
      if(ans.eq."n") read(5,826) ans2
```

```
      if(ans.eq."n".and.ans2.eq."y") call help3
      do 220 ibic=1,200
      temp(ibic)=t12
  220 continue
c
      if(jtrig.eq.1) goto 217
c     call transient temperature subroutine
      call temppro(temp,hf,tf,t12,temp2,ntot,time)
      goto 218
  217 do 216 itit=1,trtemp
      read(70,71) time,(temp2(itit,i),i=1,ntot)
   71 format(1x,/,f5.2,100f10.2)
  216 continue
  218 continue
c
      alrdy=0
c     start of transient loop
  225 continue
      zfor=0
      afor=0
      do 230 i=1,200
c     set temperature distribution to next time increment
      temp(i)=temp2(ntemp,i)
      fdis(i)=dia*g(i)*(temp(i)-dtemp(i))/2.0
  230 continue
      if(iprof.gt.0.5) goto 260
      goto 265
  235 continue
c     find temperature at internal boundary
      if(trans.eq.1) goto 237
      if(tempro.ne.1) goto 245
c     find temperature of each element in graded structure
  237 temp(1)=temp1
      fdis(1)=dia*g(1)*temp(1)/2.0
c
      do 240 i=2,ntot
c     find properties for element being considered
      temp(i)=temp(i-1)+(qhea*t(i)/k(i))
      fdis(i)=dia*g(i)*temp(i)/2.0
  240 continue
      if(iprof.gt.0.5) goto 260
      if(trans.eq.1) goto 265
      goto 260
c
c     find temperature distribution in uniform structure
  245 tempa=((temp1*(k1*t2*nmet/(k2*t1*ncer)))+temp3)*k2*t1*ncer/((k1*t2*nmet)+(k2*t1*ncer))
      qhea=k1*(temp1-tempa)/(t1*ncer)
c     find temperature of each element in coating
```

```
      if(iresid.ne.1) ddtemp=(temp1-tempa)/ncer
c     free expansion
      if(iresid.ne.1) temp(1)=temp1-(ddtemp/2.0)
      fdis(1)=dia*g1*(temp(1)-dtemp(1))/2.0
c
      do 250 i=2,ncer
      if(iresid.ne.1) temp(i)=temp(i-1)-ddtemp
      fdis(i)=dia*g1*(temp(i)-dtemp(i))/2.0
  250 continue
c     find temperature of each element in base
      ddtemp=(tempm-temp3)/nmet
c     free expansion
      if(iresid.ne.1) temp(ncer+1)=tempm-(ddtemp/2.0)
      fdis(ncer+1)=dia*g2*(temp(ncer+1)-dtemp(ncer+1))/2.0
c
      do 255 i=(ncer+2),ntot
      if(iresid.ne.1) temp(i)=temp(i-1)-ddtemp
      fdis(i)=dia*g2*(temp(i)-dtemp(i))/2.0
  255 continue
c
      goto 265
  260 continue
c
c
c------CALCULATE FORCE AND BM IN EACH ELEMENT
c
c
  265 haul=0.0
      if(type.eq.2.or.type.eq.3) goto 270
c     if transient conditions being calculated only ask restraining conditions for first cycle only
      if(alrdy.lt.0.5) write(6,855)
  270 continue
      crud=0
      spots=0
      if(alrdy.lt.0.5) read(5,835) rad
      if(alrdy.gt.0.5) rad=rady
      if(ber.lt.0.5) alrdy=1
      rady=rad
c     if fixed axially set haul= +1
      if(abs(rad).lt.1.0e-8) haul=1.0
c     if radius given set haul = -1
      if(rad.gt.1.0e-8)haul=-1.0
      if(abs(rad).gt.2.0) haul=-1.0
      if(abs(rad).gt.2.0) goto 275
c     if radius to be calculated take first estimate at r = 20
      if(rad.lt.-0.99) nuts=-1.0
      if(rad.lt.-0.99) crud=-1.0
      if(rad.lt.-0.99) rad=10
```

```
 275 continue
     if(tempro.eq.1) g1=g(1)
     if(tempro.eq.1) g2=g(ntot)
c    first guess at overall expansion rc
     rc1=0.25*(temp(1)*g(1)+temp(ntot)*g(ntot))*dia
c    for first iteration set value of 'last' iteration as -1
     rc2=-1.0
c    set dfor to previous value of net force
 280 continue
     sfor=0.0
c    find overall material height
     h=(nmet*t2+ncer*t1)+t1/2.0
     if(trans.eq.1) h=eight+t(i)/2.0
c
c    calculations in coating elements
c
     do 290 i=1,ncer
     curve=0.0
     h=h-t1
     if(crud.lt.-0.5.or.haul.lt.-0.5) curve=h*dia/(rad*2.0)
c    force in each element if expansion restrained
     force(i)=(pi*2.0*e(i)*t1*(fdis(i)))/(1.0-v(i))
c    force relaxation due to allowed expansion
     ford(i)=(pi*2.0*e(i)*t1*(rc1))/(1-v(i))
c    force relaxation due to curvature if any
     forr(i)=(pi*2.0*e(i)*t1*(curve))/(1-v(i))
c
c    calculate bending moments about NA
     if(i.lt.1.5) stresy(i)=dpress
     if(i.lt.1.5) fory(i)=stresy(i)*pi*dia*t1*v(i)/(1.0-v(i))
     if(i.lt.1.5) goto 285
c
c    calculate distance of N.A. to element centre
     hsub=(ncer*t1+nmet*t2)-ybar-(i*t1)+(t1/2.0)
     if(trans.eq.1) hsub=eight-ybar-(i*t1)+(t1/2.0)
c    calculate stress in axial direction
     asub=t1*(v(i-1)*(t(i)**2.0)/((1.0-v(i-1))*(dia**2.0)))
     asub=abs(asub)
     bsub=t1*(12.0*hsub-t1)/(dia**2.0)
     bsub=abs(bsub)
     str1=2.0*(fdis(i-1)-rc1-curve)/(dia*(1.0-v(i-1)))
     str2=2.0*(fdis(i)-rc1-curve)/(dia*(1.0-v(i)))
     if(str1.lt.str2) stresy(i)=(stresy(i-1)*(0.5-asub)+e(i)*(abs(str2)*bsub+abs(str1)*((t(i)/dia)**2.0)))/(0.5-bsub*((v(i)/(1.0-v(
i)))))
     if(str1.ge.str2) stresy(i)=(stresy(i-1)*(0.5-asub)-e(i)*(abs(str2)*bsub+abs(str1)*((t(i)/dia)**2.0)))/(0.5-bsub*((v(i)/(1.0-v(
1)))))
     fory(i)=stresy(i)*pi*dia*t1*v(i)/(1.0-v(i))
     ydir1=force(i-1)-ford(i-1)-forr(i-1)-fory(i-1)
```

```
      ydir2=force(i)-ford(i)-forr(i)-fory(i)
      if(ydir1.lt.ydir2) stresy(i)=(stresy(i-1)*(0.5-asub)+e(i)*(abs(str2)*bsub+abs(str1)*((t(i)/dia)**2.0)))/(0.5-bsub*((v(i)/(1.0-
v(i)))))
      if(ydir1.ge.ydir2) stresy(i)=(stresy(i-1)*(0.5-asub)-e(i)*(abs(str2)*bsub+abs(str2)*((t(i)/dia)**2.0)))/(0.5-bsub*((v(i)/(1.0-
v(i)))))
      fory(i)=stresy(i)*pi*dia*t1*v(i)/(1.0-v(i))
  285 continue
      bm(i)=(h-ybar)*(force(i)-forr(i)-ford(i)+fory(i))
  290 continue
c
c
      h=h-(t1/2.0)+(t2/2.0)
      out=0
      bound=1
      maste=2
c
c     calculations in base elements
c
  277 fro=ncer
      too=ntot
      if(trans.ne.1) goto 298
      fro=0
      do 276 i=1,(maste-1)
      fro=nmat(i)+fro
  276 continue
      too=fro+nmat(maste)
      maste=maste+1
  298 do 320 i=fro+1,too
      curve=0.0
      h=h-t2
      if(crud.lt.-0.5.or.haul.lt.-0.5) curve=h*dia/(rad*2.0)
      force(i)=pi*2.0*e(i)*t2*(fdis(i))/(1-v(i))
      ford(i)=pi*2.0*e(i)*t2*(rc1)/(1-v(i))
      forr(i)=pi*2.0*e(i)*t2*(curve)/(1-v(i))
c
c     if material boundary has been reached then continue, else goto 315
c
c     the slope of stress vs depth after the material boundary must be found so an accurate figure for the stress
c     at the boundary edges can be found.
c
c     when bound is set to zero then the do loop is set to its datum position and the calculations continue with dsta and dstb
c     containing the difference in radial stresses between the centre and the edge of the boundary elements.
      if(i.eq.(ncer+3).and.bound.lt.-0.5) bound=2
      if(bound.eq.2) h=h+3.0*t2
      if(bound.lt.0.5) goto 315
      if(zfor.lt.0.5) goto 430
      if(secon.lt.0.5) stresy(i)=chsty
      if(secon.lt.0.5) fory(i)=stresy(i)*pi*dia*t2*v(i)/(1.0-v(i))
```

```
      if(secon.lt.0.5) bound=0
      if(secon.lt.0.5) bm(i)=(h-ybar)*(force(i)-ford(i)-forr(i)+fory(i))
c
  310 continue
      bm(i)=(h-ybar)*(force(i)-ford(i)-forr(i)+fory(i))
      goto 320
c
c     the following calculations are performed for the main bulk of the material
  315 if(trans.ne.1) hsub=(ncer*t1+nmet*t2)-ybar-(ncer*t1)-(i-ncer)*t2+(t2/2.0)
      if(trans.ne.1) goto 317
      aight=0
      do 316 ci=1,i
      aight=aight+t(i)
  316 continue
  317 continue
      if(trans.eq.1)hsub=eight-aight+(t(i)/2.0)-ybar
      asub=t2*(v(i-1)*(t(i)**2.0)/((1.0-v(i-1))*(dia**2.0)))
      asub=abs(asub)
      bsub=t2*(12.0*hsub-t2)/(dia**2.0)
      bsub=abs(bsub)
      str1=2.0*(fdis(i-1)-rc1-curve)/(dia*(1.0-v(i-1)))
      str2=2.0*(fdis(i)-rc1-curve)/(dia*(1.0-v(i)))
       if(str1.lt.str2) stresy(i)=(stresy(i-1)*(0.5-asub)+e(i)*(abs(str2)*bsub+abs(str1)*((t(i)/dia)**2.0)))/(0.5-bsub*((v(i)/(1.0-v
(i)))))
      if(str1.ge.str2) stresy(i)=(stresy(i-1)*(0.5-asub)-e(i)*(abs(str2)*bsub+abs(str1)*((t(i)/dia)**2.0)))/(0.5-bsub*((v(i)/(1.0-v(
i)))))
      fory(i)=stresy(i)*pi*dia*t2*v(i)/(1.0-v(i))
      ydir1=force(i-1)-ford(i-1)-forr(i-1)+fory(i-1)
      ydir2=force(i)-ford(i)-forr(i)+fory(i)
      if(ydir1.lt.ydir2) stresy(i)=(stresy(i-1)*(0.5-asub)+e(i)*(abs(str2)*bsub+abs(str1)*((t(i)/dia)**2.0)))/(0.5-bsub*((v(i)/(1.0-
v(i)))))
      if(ydir1.ge.ydir2) stresy(i)=(stresy(i-1)*(0.5-asub)-e(i)*(abs(str2)*bsub+abs(str1)*((t(i)/dia)**2.0)))/(0.5-bsub*((v(i)/(1.0-
v(i)))))
      fory(i)=stresy(i)*pi*dia*t2*v(i)/(1.0-v(i))
      bm(i)=(h-ybar)*(force(i)-forr(i)-ford(i)+fory(i))
  320 continue
c
c
      if(trans.eq.1.and.nmat(maste).ne.0) goto 277
c     calculate net radial force and bending moments
      nbm=0.0
      do 325 i=1,ntot
      if(temp(i).gt.telast) then
      bm(i)=0
      force(i)=0
      ford(i)=0
      forr(i)=0
      fory(i)=0
```

```
      stresy(i)=0
      endif
      nfor=nfor+(force(i)-ford(i)-forr(i)+fory(i))
      nbm=nbm+bm(i)
  325 continue
c     if net radial force = 0, body in radial equilibrium
      if(abs(nfor).lt.0.1) goto 335
      if(abs(rc1-rc2).lt.2e-8) goto 335
c     if second or susequent iteration goto 330
      if(rc2.gt.-0.99.or.rc2.lt.-1.01) goto 330
      dfor=nfor
      rc2=rc1
c     set rc1=1.15*rc1 for second guess at rc1
      rc1=1.15*rc1
      goto 280
  330 tim1=rc1
      tim2=rc2
      tim3=dfor
      tim4=nfor
c
c
c------CONVERGENT CONDITIONS FOR ZERO NET FORCE
c
c
      rc1=tim1-tim4*((tim2-tim1)/(tim3-tim4))
      utopia=abs((rc1-tim1)/tim1)
      if(utopia.lt.5.0e-9) goto 335
      if(abs(tim4).gt.abs(tim3)) dfor=tim3
      if(abs(tim4).gt.abs(tim3)) rc2=tim2
      if(abs(tim4).lt.abs(tim3)) dfor=tim4
      if(abs(tim4).lt.abs(tim3)) rc2=tim1
      goto 280
c
c
c------CONVERGENT CONDITIONS FOR ZERO BM
c
c
c     if net bm = 0 goto 355
  335 if(haul.gt.0.5) goto 345
      if(abs(nbm).lt.0.5) goto 345
c     if radial restraint goto 335
c     if radius specified goto 335
      if(haul.lt.-0.99) goto 345
      if(nuts.gt.-0.99) goto 340
      rad2=rad
      nbm2=nbm
      rad=rad*1.1
      nuts=0
```

```
      goto 275
  340 tin1=rad
      tin2=rad2
      tin3=mbm2
      tin4=mbm
      rad=tin1-tin4*((tin2-tin1)/(tin3-tin4))
      if((tin1.lt.0.0.or.rad2.lt.0.0).and.rad.gt.0.0) rad=tin1/2
      if(abs(tin4).gt.abs(tin3)) mbm2=tin3
      if(rad.lt.0.0.and.spots.lt.0.5) rad=tin1/2.0
      if(abs(tin4).gt.abs(tin3)) rad2=tin2
      if(abs(tin4).lt.abs(tin3)) mbm2=tin4
      if(abs(tin4).lt.abs(tin3)) rad2=tin1
      if(rad.gt.1.0e3) muts=-1.0
      if(rad.gt.1.0e3) spots=1
      if(rad.gt.1.0e3) rad=-10.0
      goto 275
c
c
  345 bmsty=(stresy(mtot)-stresy(1))*(dia**3.0)*pi/24.0
      if(rad.gt.-1e-5.and.rad.lt.1e-5) goto 355
      if(crud.lt.-0.5.and.abs(bmsty).lt.5) goto 355
      if(abs((mbm+bmsty)/mbm).lt.5.0e-2) goto 355
      if(crud.lt.-0.5) muts=-1
      if(zfor.eq.2) goto 350
      cumbm2=mbm+bmsty
      chstr2=stresy(mcer+1)
      if(secon.gt.0.5) goto 355
      zfor=2
      chsty=(stresy(1)-stresy(mtot))-((mbm*24)/((dia**3.0)*pi))
      shsty=stresy(mcer+1)
      goto 275
  350 tin1=chsty
      tin2=chstr2
      tin3=cumbm2
      tin4=mbm+(stresy(mtot)-stresy(1))*(dia**3.0)*pi/24.0
      chsty=tin1-tin4*((tin2-tin1)/(tin3-tin4))
      if(abs(tin4).gt.abs(tin3)) cumbm2=tin3
      if(abs(tin4).gt.abs(tin3)) chstr2=tin2
      if(abs(tin4).lt.abs(tin3)) cumbm2=tin4
      if(abs(tin4).lt.abs(tin3)) chstr2=tin1
      goto 275
c
c
c------OUTPUT
c
c
c     set force matrix to stress levels
  355 do 360 i=1,mcer
```

```
      stresy(i)=stresy(i)/1.0e6
      force(i)=(force(i)-forr(i)-ford(i)+fory(i))/(pi*dia*t1*1.0e6)
  360 continue
      do 365 i=(ncer+1),ntot
      stresy(i)=stresy(i)/1.0e6
      force(i)=(force(i)-forr(i)-ford(i)+fory(i))/(pi*dia*t2*1.0e6)
  365 continue
      if(tempro.ne.1.and.trans.ne.1) write(6,860)
      if(tempro.eq.1.or.trans.eq.1) write(6,865)
      if(tempro.eq.1.or.trans.eq.1) goto 370
c     set units
      g1=g1*1.0e6
      g2=g2*1.0e6
      e1=e1/1.0e9
      e2=e2/1.0e9
      write(6,875)
      write(6,880)e1,e2
      write(6,895)k1,k2
      write(6,900)g1,g2
      write(6,905)v1,v2
      g1=g1/1.0e6
      g2=g2/1.0e6
      e1=e1*1.0e9
      e2=e2*1.0e9
  370 continue
      t1=t1*ncer
      t2=t2*nmet
      h=t1+t2
      ybar=h-ybar
      if(tempro.ne.1.and.trans.ne.1) write(6,910)t1,t2
      t1=t1/ncer
      t2=t2/nmet
      if(heat1.gt.1.0e-5.and.heat2.gt.1.0e-5) write(6,940) heat1,heat2,gas1,gas2
      if(heat1.gt.1.0e-5.and.heat2.lt.1.0e-5) write(6,950) heat1,gas1
      if(heat1.lt.1.0e-5.and.heat2.gt.1.0e-5) write(6,955) heat2,gas2
      disp=0.0
      if(rad.lt.0.05) goto 375
      disp=rad-(((rad**2.0)-((dia/2.0)**2.0))**0.5)
  375 continue
c     if long output is wanted goto 380
      if(type.eq.1.or.type.eq.3) goto 380
      goto 405
  380 mus=1
      mun=1
c     find max and min stress in coating
      do 385 i=2,ncer
      if(force(i).gt.force(mun)) mun=i
      if(force(i).lt.force(mus)) mus=i
```

```
385 continue
    nut=ncer+1
    nuo=ncer+1
c   find max and min stress in base
    do 390 i=(ncer+2),ntot
    if(force(i).gt.force(nut)) nut=i
    if(force(i).lt.force(nuo)) nuo=i
390 continue
    write(6,925) force(nun),force(nut)
    write(6,930) force(nus),force(nuo)
    nus=1
    nun=1
    do 395 i=2,ncer
    if(stresy(i).gt.stresy(nun)) nun=i
    if(stresy(i).lt.stresy(nus)) nus=i
395 continue
    nut=ncer+1
    nuo=ncer+1
    do 400 i=(ncer+2),ntot
    if(stresy(i).gt.stresy(nut)) nut=i
    if(stresy(i).lt.stresy(nuo)) nuo=i
400 continue
    write(6,960)stresy(nun),stresy(nut)
    write(6,965) stresy(nus),stresy(nuo)
    temp1=temp1+ctemp
    temp3=temp3+ctemp
    write(6,935) temp1,temp3
    write(6,915) rad
    if(abs(ctemp).gt.1.0e-5) write(6,945) ctemp
    disp=disp*1.0e3
    write(6,890) disp
    write(6,885) ybar
    qhea=qhea*(dia**2.0)*pi/4000
    if(trtemp.lt.0.5) write(6,990) qhea
    if(trtemp.gt.0.5) write(6,995) time
    if(tempro.ne.1.and.trans.ne.1) write(6,920)
    if(tempro.eq.1.or.trans.eq.1) write(6,870)
    if(ber.gt.0.5) goto 125
    ntemp=ntemp+1
    trtemp=trtemp-1
    if(trtemp.gt.0.5) goto 225
    stop
405 write(6,915) rad
    write(6,890) disp
    write(6,885) ybar
    qhea=qhea*(dia**2.0)*pi/4000
    if(trtemp.lt.0.5) write(6,990) qhea
    if(trtemp.gt.0.5) write(6,995) time
```

```
      if(tempro.ne.1.and.trans.ne.1) write(6,920)
      if(tempro.eq.1.or.trans.eq.1) write(6,870)
      bm(1)=t1/2.0
c     use bm matrix to record element depth
      do 410 i=2,mcer
      bm(i)=bm(i-1)+t1
  410 continue
      bm(mcer+1)=bm(mcer)+(t1+t2)/2.0
      do 415 i=(mcer+2),mtot
      bm(i)=bm(i-1)+t2
  415 continue
      if(tempro.ne.1.and.trans.ne.1) write(6,970)
      if(tempro.eq.1.or.trans.eq.1) write(6,975)
      do 420 i=1,mtot
      temp(i)=temp(i)+ctemp
      e(i)=e(i)/1.0e9
      g(i)=g(i)*1.0e6
  420 continue
      if(tempro.ne.1.and.trans.ne.1) write(6,980)(bm(i),temp(i),force(i),stresy(i),i=1,mtot)
      if(tempro.eq.1.or.trans.eq.1) write(6,985)(bm(i),temp(i),k(i),e(i),v(i),g(i),force(i),stresy(i),i=1,mtot)
      do 425 i=1,mtot
      e(i)=e(i)*1.0e9
      g(i)=g(i)/1.0e6
  425 continue
c     if performing multiple runs return to 1
      if(ber.gt.0.5) goto 125
      mtemp=mtemp+1
      trtemp=trtemp-1
c     if transient calculations being performed take next temperature profile
      if(trtemp.gt.0.5) goto 225
      stop
c
c
c-----------------------------------------------------------------------------------------------------------------
c
c
  800 format(' if you require a brief output enter 1, a brief input enter 2,'/
     &' both enter 3, for a conventional run enter 0.'/)
  805 format(' enter number of sets of calculations to be performed',/)
  810 format(1x,'if materials have graded structure or more than two materials are used',/
     &' enter a 1, otherwise enter a 0',/)
  815 format(1x,'if temperature dependant properties given on subroutine "properties"',/
     &' enter a 1, otherwise enter a 0',/)
  820 format(1x,'if transient solution is required enter number of cycles',/
     &' if a steady state solution is required enter a 0',/)
  825 format(1x,'enter youngs mod, thermal cond, poissons ratio, thermal exp,  depth properties extend, and number of elements each
section should be divided into',/,'when data complete enter a 0',/
     &' but first do you require more information; y or n.',/)
```

```
  830 format(1x,'for coating and base enter, heat transfer coeff, temperature, overall diameter and datum temperature',/
     &' but first do you require more information; "y" or "n"',/)
  835 format(v)
  840 format(' for coating and base enter, thickness, temperature, heat transfer coef',/,' overall diameter , datum temperature and
pressure - where appropriate',/
     &' but first, do you require more information; y or n',/)
  845 format(' enter youngs mod, thermal cond, poisson ratio, thermal exp, heat capacity, density for ceramic and metal',/
     &' but first, do you require more information; y or n.',/)
  850 format(' enter number of strips to be used in ceramic and metal layers',/
     &' ie: 35,35  : limit 150 strips',/)
  855 format(' if disc is axially restrained enter a 0',/,6x,
     &' if disc is free to deform enter -1',/,6x,
     &' for a forced displacement enter radius of curvature',/)
  860 format(1h,//,'------------------------------------------------------------')
  865 format(1h,//,'------------------------------------------------------------------------------------------------------------
-----')
  870 format(1x,///,'------------------------------------------------------------------------------------------------------------
------')
  875 format(1x,22x,'COATING',14x,'BASE',/)
  880 format(1x,'YOUNGS MOD',6x,f14.4,5x,f14.4,5x,'GPa')
  885 format(1x,'DEPTH TO NA',13x,f14.4)
  890 format(1x,'CENTRAL DISPLACEMENT',4x,f14.4)
  895 format(1x,'THERMAL COND',4x,f14.4,5x,f14.4,5x,'W/M2')
  900 format(1x,'THERMAL EXP',5x,f14.4,5x,f14.4,5x,'x10-6')
  905 format(1x,'POISSONS RATIO',2x,f14.4,5x,f14.4)
  910 format(1x,'DEPTH',11x,f14.4,5x,f14.4,5x,'M')
  915 format(1x,//,1x,'RADIUS OF CURVATURE   'f14.2)
  920 format(1x,//,'------------------------------------------------------------')
  925 format(1x,'MAX RAD STRESS',2x,f14.4,5x,f14.4,5x,'MPa')
  930 format(1x,'MIN RAD STRESS',2x,f14.4,5x,f14.4,5x,'MPa')
  935 format(1x,'MATL TEMP',7x,f14.4,5x,f14.4)
  940 format(1x,'HEAT TRANSF COEF',f14.4,5x,f14.4,5x,'W/M2K',/,1x,'GAS TEMP',8x,f14.4,5x,f14.4)
  945 format(1x,'DATUM TEMP',14x,f14.4)
  950 format(1x,'HEAT TRANSF COEF',f14.4,24x,'W/M2K',/,1x,'GAS TEMP',8x,f14.4)
  955 format(1x,'HEAT TRANSF COEF',19x,f14.4,5x,'W/M2K',/,1x,'GAS TEMP',17x,f14.4)
  960 format(1x,'MAX AXI STRESS',2x,f14.4,5x,f14.4,5x,'MPa')
  965 format(1x,'MIN AXI STRESS',2x,f14.4,5x,f14.4,5x,'MPa')
  970 format('    DEPTH        TEMPERATURE    STRESS (M)    STRESS (A)',/)
  975 format('    DEPTH      TEMPERATURE      K (W/M2)      E (GPa)          V        G (x10-6)    STRESS (A)     STRESS (R)',/)
  980 format(2x,f8.6,3f14.2)
  985 format(2x,f8.6,3f14.2,f13.3,3f14.2)
  990 format(1x,'HEAT TRANSFER',10x,f14.3,7x,'KW')
  995 format(1x,'TIME',15x,f14.4,5x,'S')
C
C
C-------------------------------------------------------------------------------------------------------
C-------------------------------------------------------------------------------------------------------
C
```

```
 430 continue
c
c     the slope of stress vs depth after the material boundary must be found so an aacurate figure for the stress
c     at the boundary edges can be found
c
c
c     when bound is set to zero then the loop is set to its datum position and the calculations continue with dsta and dstb
c     containing the difference in radial stresses between the centre and the edge of the boundary elements.
c
c     find axial stress by strain equilibrium
      stresy(i)=stresy(i-1)
      fory(i)=stresy(i)*pi*dia*t2*v(i)/(1.0-v(i))
      vserts=stresy(i)
      grot=0.0
c
c     to find sta and stb the values of radial stress in the centre of the two elements either side of the boundary
c     a value for radial stress must be known of the "new" material since this is derived from stb it is necessary
c     to converge onto the true solution this is done in the following do loop
      do 305 iop=1,10
      tim1=fory(i)
      temps=temp(i-1)-(temp(i-2)-temp(i-1))/2.0
      hbound=t2*ncer-ybar
      squib=-(stresy(i-1)*(v(i-1)*e(i)/(v(i)*e(i-1)))+temps*(g(i)*e(i)-g(i-1)*e(i))/v(i)
      if(i-1.5.lt.ncer) squib=(stresy(i-1)*(v(i-1)*e(i)/(v(i)*e(i-1)))+temps*(g(i)*e(i)-g(i-1)*e(i))/v(i)
      sta=-(force(i-1)-ford(i-1)-forr(i-1)+fory(i-1))/(pi*t1*dia)
      if(i-1.5.lt.ncer) sta=-(force(i-1)-ford(i-1)-forr(i-1)+fory(i-1))/(pi*t1*dia)
      stb=-(force(i)-ford(i)-forr(i)+fory(i))/(pi*t2*dia)
      stbs=-(force(i)-ford(i)-forr(i)+fory(i))/(pi*t2*dia)
c     for the first pass through the do  loop the value of dsta and dstb must be found this value is recorded and used
c     in subsequent calcualtions.
      if(bound.lt.1.5.and.grot.lt.0.5) goto 295
      grot=1.0
      ste=-(force(i-2)-ford(i-2)-forr(i-2)+fory(i-2))/(pi*t2*dia)
      stf=-(force(i-1)-ford(i-1)-forr(i-1)+fory(i-1))/(pi*t2*dia)
      stg=-(force(i-3)-ford(i-3)-forr(i-3)+fory(i-3))/(pi*t1*dia)
      if(i-3.5.lt.ncer) stg=-(force(i-3)-ford(i-3)-forr(i-3)+fory(i-3))/(pi*t1*dia)
      sth=-(force(i-4)-ford(i-4)-forr(i-4)+fory(i-4))/(pi*t1*dia)
       if(i-4.5.lt.ncer) sth=-(force(i-4)-ford(i-4)-forr(i-4)+fory(i-4))/(pi*t1*dia)
      dsta=(stg-sth)/2.0
      dstb=(ste-stf)/2.0
      dsaa=(fory(i-3)-fory(i-4))*(1-v(i-4))/(pi*dia*t(i-4)*v(i-4))
      dsab=-(fory(i-2)-fory(i-1))*(1-v(i-1))/(pi*dia*t(i-1)*v(i-1))
  295 continue
      if(crud.lt.-0.5.or.haul.lt.-0.5) thi3=dia/(2*rad)
      squab=squib-(sta+dsta)*e(i)*(1.0-v(i-1))/(v(i)*e(i-1))+(stb+dstb)*(1.0-v(i))/v(i)
      stresy(i)=squab
      thi1=((((1-v(i-1))*(-2*dsta)-v(i-1)*dsaa)/e(i-1))+g(i-1)*(temp(i-2)-temp(i-1)))*dia/(2*t(i-1))
      thi2=((((1-v(i))*2*dstb-v(i)*dsab)/e(i))+g(i)*(temp(i)-temp(i+1)))*dia/(2*t(i))
```

```
      stresy(i)=-fory(i)*(1-v(i))/(pi*dia*t2*v(i))
      tor=(e(i)/(2.0*(1.0+v(i))))*thi2-(e(i-1)/(2.0*(1.0+v(i-1))))*thi1
      strey2=((-tor)*hbound*6/dia)-stresy(i-1)
c     strey2 should equal stresy(i), adjust fory till they do
      if(abs(strey2-stresy(i)).lt.0.5) goto 306
      if(ireleas.eq.1) goto 300
      ireleas=1
      dstry2=strey2-stresy(i)
      dfory2=tim1
      fory(i)=tim1*1.05
      goto 305
  300 continue
      tim2=dfory2
      tim3=dstry2
      tim4=strey2-stresy(i)
      if(tim3.eq.tim4) goto306
      fory(i)=tim1-tim4*((tim2-tim1)/(tim3-tim4))
      if(abs(tim4).gt.abs(tim3)) dstry2=tim3
      if(abs(tim4).gt.abs(tim3)) dfory2=tim2
      if(abs(tim4).lt.abs(tim3)) dstry2=tim4
      if(abs(tim4).lt.abs(tim3)) dfory2=tim1
      tim1=fory(i)
  305 continue
  306 if(out.eq.1) bound=0
      ireleas=0
      stresy(i)=-stresy(i)
      fory(i)=pi*dia*t2*v(i)*stresy(i)/(1.0-v(i))
      if(bound.eq.1) bound=-1
      if(bound.lt.1.5) goto 310
      out=1
      bound=1
      stresy(i)=stresy(i+2)
      fory(i)=fory(i+2)
      i=i-3
      goto 320
      end
c
c
c-----------------------------------------------------------------------------------------------------------------------
c-----------------------------------------------------------------------------------------------------------------------
c
c
c     The following is used to set material properties if a graded structure is required
c
      subroutine section(n,tempro,temp,nmat)
      dimension e(300),v(300),g(300),m(100),temp(200),nmat(20),t(300)
      integer tempro
      real k(300)
```

```
      common k,e,v,g,t,cp,de
      if(tempro.eq.1) goto 100
      do 30 j=1,100
      do 10 i=1,nmat(j)
      iop=i
      if(j.lt.1.5) goto 60
      do 70 lo=1,(j-1)
      iop=iop+nmat(lo)
   70 continue
   60 continue
      t(iop)=t(j+199)/nmat(j)
      k(iop)=k(j+199)
      e(iop)=e(j+199)
      v(iop)=v(j+199)
      g(iop)=g(j+199)
   10 continue
      if(nmat(j+1).eq.0) return
   20 continue
   30 continue
      return
  100 continue
      matl=0
      do 50 j=1,100
      matl=matl+1
      do 40 i=1,nmat(j)
      if(j.lt.1.5) goto 80
      do 90 lo=1,(j-1)
      i=i+nmat(j-1)
   90 continue
   80 continue
      t(i)=t(j+200)/nmat(j)
      call properties(matl,temp(i),i)
   40 continue
      if(n(j+0).eq.0) return
   50 continue
      return
      end
c
c
      subroutine help1
c
      write(6,100)
      write(6,110)
  100 format(1x,' example input',/,' 1e-3,10e-3,100,200,0,0,86e-3,0,0',/,
     1' coating thickness 1e-3 metres, substrate thickness 10e-3 metres',/,
     1' surface of coating 100K, surface of substrate 200k,',/,
     1' heat transfer coefficients not needed if surface temperatures given',/,
     1' diameter 86e-3 meters, stress free temperature 0 k, pressure drop 0 bar',/)
```

```
  110 format(1x,' example input',/,' 1e-3,10e-3,1000,800,400,200,86e-3,280,1e5',/,
     &' as above except, gas conditions on top face 1000 k, 400w/mk',/,
     &' bottom face 600 k, 200w/mk',/,
     &' component is stress free at 280 k, and a 1e5 n/m2 pressure drop exists.',/)
      return
      end
c
c
      subroutine help2
c
      write(6,100)
      write(6,110)
  100 format(1x,' example input',/,' 300e9,200e9,1,30,0.23,0.3,3e-6,10e-6,0,0,0,0',/,
     &' ceramic properties e=300e9n/m2, k=1w/m2, poissons ratio=0.23,',/,
     &' thermal expansion=3e-6.',/,
     &' metals properties e=200e9N/m2, k=30w/m2, poissons ratio=0.3,',/,
     &' thermal expansion=10e-6.',/,
     & ' thermal capacity and density are not needed for S.S. calcualtions',/)
  110 format(1x,' example input',/,' 300e9,200e9,1,30,0.23,0.3,3e-6,10e-6,400,600,2000,5000',/,
     &' same as above but thermal capacity for the ceramic is 400 and density is 2000',/,
     &' for metal capacity is 600 and density is 5000',/)
      return
      end
      subroutine help3
c
c
      write(6,100)
      write(6,110)
      write(6,120)
  100 format(1x,' This subroutine must take the form',//,
     &' tempbound(tf,hf,time,delt,dangle,t11,temp)',//,
     &' not all of these variables need be used, in the simplest case only',/,
     &' "time" is passed to the subroutine, and "tf", "hf" and "t11" are returned',/,
     &' these are gas temperature and heat transfere coefficent on the gas side',/,
     &' and the rear face temperature - these can all be set as constants,',/,
     &' or varied with time, in which case the change in time "delt" will have',/,
     &' to be used, and example program follows, corresponding to the case',/,
     &' of the in-cylinder conditions in a firing engine',/)
  110 format(1x,' PROGRAM LISTING',//
     &'       subroutine tempbound(tf,hf,time,delt,dangle,t11,temp)',/,
     &' c     this subroutine can be used to set up desired thermal boundary conditions as a constant'
     &' c     or as a function of time.  This to be used if a transient solution is required.',/,
     &' c',/,
     &' c     set step for angle incrementation',/,
     &'       dangle=2',/,
     &' c    ',/,
     &'       pi=3.14159',/,
     &' c     set compression constant'./,
```

```
     &'       gamma=1.4',/,
     &' c     set engine operating speed',/,
     &'       frequency=20',/,
     &' c     set max volume ration',/,
     &'       vration=20',/,
     &' c     set inlet air temperature',/,
     &'       temp1=300',/,
     &' c     find effective compression ratio at the present time within the cylce',/,
     &'       comp=-vratio*cos(2.0*pi*time*frequency)',/,
     &'       comp=(vario/2.0)+(comp/2.0)',/,
     &'       comp=comp+1',/,
     &' c     calculate the time increment',/,
     &'       delt=dangle/(360.0*frequency)',/,
     &' c     find the instantaneous gas temperature',/,
     &'       tf=temp1*(comp**(gamma-1))',/,
     &'       tf=tf-273',/,
     &' c',/,
     &' c     set up heat transfer coefficient',/,
     &'       hf=1200',/,
     &' c',/,
     &' c     set up temperature of rear face',/,
     &'       t11=200',/,
     &'       if(t11.gt.200) t11=200',/,
     &'       return',/,
     &'       end',//)
  120 format(1x,' PROGRAM LISTING',/,
     &' c     alternatively the following structure can be used',/,
     &' c     which returns constant values with time',/,
     &'      subroutine tempbound(tf,hf,time,delt,dangle,t11,temp)',/,
     &'      dangle=2',/,
     &'      hf=1100',/,
     &'      tf=1200',/,
     &'      delt=0.0150',/,
     &'      t11=200',/,
     &'      return',/,
     &'      end',//)
      return
      end
C
C
      subroutine help4
C
C
      write(6,100)
      write(6,110)
  100 format(1x,' example input',/,' 300e9',/,' 30,0.23,10e-6,1e-3,20',/,
     &' 320e9',/,' 31,0.23,10e-3,1e-3,20',/,' 200e9',/,' 160,0.3,24e-6,10e-3,40',/,
     &' 0',/)
```

```
 110 format(1x,' The data given is for three layers each of a different material',/,
     &' The first has a Youngs modulas of 300e9',/,
     &'                Thermal conductivity 30',/,
     &'                Poissons ratio 0.23',/,
     &'                Thermal expansion 10e-6',/,
     &' These properties extend through a depth of 1e-3m',/,
     &' and this layer is divided into 20 strips',/,
     &' The units must be consistant.',/,
     &' The data is concluded with a 0',/)
     return
     end
C
C
     subroutine help5
C
C
     write(6,100)
     write(6,110)
  100 format(1x,' example input',/,' 0,0,400,200,86e-3,0',/,
     &' With this set of data the top of the disc is at 400K the bottom at 200k',/,
     &' The disc is 86 mm in diameter.',/)
  110 format(1x,/,' 1000,800,400,200,86e-3,0',/,
     &' With this set of data the top of the disc see a gas 1000W/m2K,400K',/,
     &' the bottom 800W/m2K,200K',/)
      return
      end
      subroutine help6
C
C
      write(6,100)
      write(6,110)
  100 format(1x,' It is necessary to set up a subroutine called properties',/,
     &' The temperature of each element is sent into this subroutine',/,
     &' and the properties Youngs Modulas, poisson ratio, thermal expansion',/,
     &' and conductivity are returned, these are held in the matrices e,v,g,k',/)
  110 format(1x,' The following is an example of such a subroutine',//,
     &'       subroutine properties(matl,temp,i)',/,
     &' c     This subroutine is called once for each disc element',/,
     &' c     The temperatue is automatically fed across as "temp"',/,
     &' c     i is the element number',/,
     &' c     matl is the material number',/,
     &' c     as the program stands only two material can be studied',/,
     &' c     ie matl=1 for ceramic layer',/,
     &' c        and matl=2 for metal layer',/,
     &'       dimension e(300),v(300),g(300),t(300),cp(300),de(300)',/,
     &'       real k(300)',/,
     &'       common k,e,v,g,t,cp,de',/,
     &'       if(matl.gt.1.5) goto 10',/,
```

```
      &' c    The following equations apply to the ceramic',/,
      &'        k(i)=25.625736-(1.15623e-2*temp)+(1.24994e-6*(temp**2.0))',/,
      &'        e(i)=290e9-(0.025e9*temp)',/,
      &'        v(i)=0.208-(5.7904e-5*temp)+(4.5621e-8*(temp**2.0))',/,
      &'        g(i)=1.21307e-6+(5.44759e-9*temp)-(2.8528e-12*(temp**2.0))',/,
      &'        return',/,
      &'     10 if(matl.gt.2.5) goto 20',/,
      &' c    The following equation apply to the metal',/,
      &'        k(i)=30',/,
      &'        e(i)=200e9',/,
      &'        v(i)=0.3',/,
      &'        g(i)=14e-6',/,
      &'        return',/,
      &'     20 continue',/,
      &'        end',/)
       return
       end

r 19:12 2.317 11
```

APPENDIX 4.3 COMPARISON OF STRESS ANALYSIS

Silicon Nitride disc, 20mm thick, 86mm diameter
Subject to a temperature drop of 90^{o} between faces.

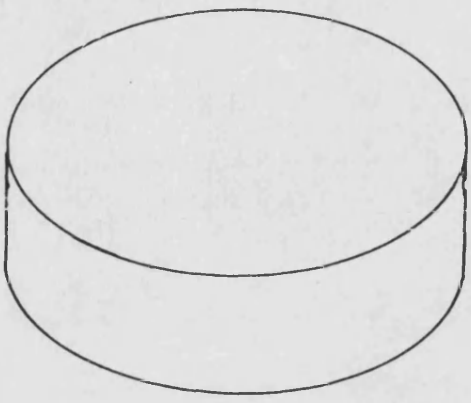

No external constraints are applied, the body is free to expand radially, and deform axially.

	Model	Theory	
Radius of curvature	67.34	67.34	M
All stresses	0.00	0.00	MPa

EXAMPLE 4.8.1.

	COATING	BASE	
YOUNGS MOD	300.0000	300.0000	GPa
THERMAL COND	3.0000	3.0000	W/K?
THERMAL EXP	3.3000	3.3000	x10-6
POISSONS RATIO	0.2300	0.2300	
DEPTH	0.0100	0.0100	M

RADIUS OF CURVATURE	67.34
CENTRAL DISPLACEMENT	0.0000
DEPTH TO NA	0.0100

DEPTH	TEMPERATURE	STRESS (R)	STRESS (A)
0.000143	199.36	-0.00	0.00
0.000429	198.07	-0.00	0.00
0.000714	196.79	-0.00	0.00
0.001000	195.50	-0.00	0.00
0.001286	194.21	-0.00	0.00
0.001571	192.93	-0.00	0.00
0.001857	191.64	-0.00	0.00
0.002143	190.36	-0.00	0.00
0.002429	189.07	-0.00	0.00
0.002714	187.79	-0.00	0.00
0.003000	186.50	-0.00	0.00
0.003286	185.21	-0.00	0.00
0.003571	183.93	-0.00	0.00
0.003857	182.64	-0.00	0.00
0.004143	181.36	-0.00	0.00
0.004429	180.07	-0.00	0.00
0.004714	178.79	-0.00	0.00
0.005000	177.50	-0.00	0.00
0.005286	176.21	-0.00	0.00
0.005571	174.93	-0.00	0.00
0.005857	173.64	-0.00	0.00
0.006143	172.36	-0.00	0.00
0.006429	171.07	-0.00	0.00
0.006714	169.79	-0.00	0.00
0.007000	168.50	-0.00	0.00
0.007286	167.21	-0.00	0.00
0.007571	165.93	-0.00	0.00
0.007857	164.64	-0.00	0.00
0.008143	163.36	-0.00	0.00
0.008429	162.07	-0.00	0.00
0.008714	160.79	-0.00	0.00
0.009000	159.50	-0.00	0.00
0.009286	158.21	-0.00	0.00
0.009571	156.93	-0.00	0.00
0.009857	155.64	-0.00	0.00
0.010143	154.36	0.00	0.00
0.010429	153.07	0.00	0.00
0.010714	151.79	0.00	0.00
0.011000	150.50	0.00	0.00
0.011286	149.21	0.00	0.00
0.011571	147.93	0.00	0.00
0.011857	146.64	0.00	0.00
0.012143	145.36	0.00	0.00
0.012429	144.07	0.00	0.00
0.012714	142.79	0.00	0.00
0.013000	141.50	0.00	0.00
0.013286	140.21	0.00	0.00
0.013571	138.93	0.00	0.00
0.013857	137.64	0.00	0.00
0.014143	136.36	0.00	0.00
0.014429	135.07	0.00	0.00
0.014714	133.79	0.00	0.00
0.015000	132.50	0.00	0.00
0.015286	131.21	0.00	0.00
0.015571	129.93	0.00	0.00
0.015857	128.64	0.00	0.00
0.016143	127.36	0.00	0.00
0.016429	126.07	0.00	0.00
0.016714	124.79	0.00	0.00
0.017000	123.50	0.00	0.00
0.017286	122.21	0.00	0.00
0.017571	120.93	0.00	0.00
0.017857	119.64	0.00	0.00
0.018143	118.36	0.00	0.00
0.018429	117.07	0.00	0.00
0.018714	115.79	0.00	0.00
0.019000	114.50	0.00	0.00
0.019286	113.21	0.00	0.00
0.019571	111.93	0.00	0.00
0.019857	110.64	0.00	0.00

2mm layer of Silicon Nitride
on 21mm base of steel.

Subject to a uniform temperature rise of 200^{o} from a zero stress level.

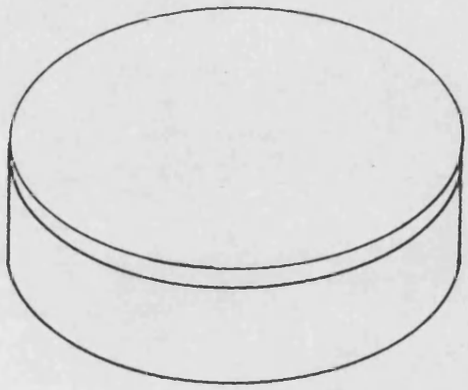

No external constraints are applied, body is free to expand radially, and deform axially.

	Model	Theory	
Radius of curvature	-17.51	-17.51	m
Top radial stress	-535.76	-527.8	MPa
Bottom radial stress	-119.26	-119.4	MPa
Top axial stress	0.00	0.00	MPa
Bottom axial stress	0.03	0.00	MPa

EXAMPLE 4.8.2.

	COATING	BASE	
YOUNGS MOD	290.0000	200.0000	GPa
THERMAL COND	20.0000	30.0000	W/M2
THERMAL EXP	2.5000	14.0000	x10-6
POISSONS RATIO	0.2300	0.3000	
DEPTH	0.0020	0.0210	M

RADIUS OF CURVATURE	-17.51
CENTRAL DISPLACEMENT	0.0000
DEPTH TO NA	0.0111

DEPTH	TEMPERATURE	STRESS (R)	STRESS (A)
0.000029	200.00	-535.76	0.00
0.000086	200.00	-537.32	-1.10
0.000143	200.00	-538.88	-2.20
0.000200	200.00	-540.44	-3.30
0.000257	200.00	-541.99	-4.39
0.000314	200.00	-543.55	-5.49
0.000371	200.00	-545.10	-6.57
0.000429	200.00	-546.66	-7.66
0.000486	200.00	-548.21	-8.75
0.000543	200.00	-549.76	-9.83
0.000600	200.00	-551.31	-10.90
0.000657	200.00	-552.86	-11.98
0.000714	200.00	-554.41	-13.05
0.000771	200.00	-555.96	-14.12
0.000829	200.00	-557.51	-15.19
0.000886	200.00	-559.06	-16.25
0.000943	200.00	-560.60	-17.31
0.001000	200.00	-562.15	-18.37
0.001057	200.00	-563.69	-19.43
0.001114	200.00	-565.24	-20.48
0.001171	200.00	-566.78	-21.53
0.001229	200.00	-568.32	-22.57
0.001286	200.00	-569.86	-23.61
0.001343	200.00	-571.40	-24.65
0.001400	200.00	-572.94	-25.69
0.001457	200.00	-574.48	-26.72
0.001514	200.00	-576.01	-27.75
0.001571	200.00	-577.55	-28.78
0.001629	200.00	-579.08	-29.80
0.001686	200.00	-580.62	-30.82
0.001743	200.00	-582.15	-31.83
0.001800	200.00	-583.68	-32.84
0.001857	200.00	-585.21	-33.85
0.001914	200.00	-586.74	-34.86
0.001971	200.00	-588.27	-35.86
0.002300	200.00	227.53	32.42
0.002900	200.00	216.42	29.35
0.003500	200.00	205.46	26.63
0.004100	200.00	194.65	24.24
0.004700	200.00	183.97	22.17
0.005300	200.00	173.42	20.39
0.005900	200.00	162.98	18.89
0.006500	200.00	152.66	17.65
0.007100	200.00	142.43	16.64
0.007700	200.00	132.30	15.84
0.008300	200.00	122.25	15.23
0.008900	200.00	112.27	14.79
0.009500	200.00	102.35	14.51
0.010100	200.00	92.49	14.34
0.010700	200.00	82.67	14.28
0.011300	200.00	72.87	14.25
0.011900	200.00	63.04	14.16
0.012500	200.00	53.20	14.05
0.013100	200.00	43.35	13.92
0.013700	200.00	33.51	13.81
0.014300	200.00	23.69	13.73
0.014900	200.00	13.89	13.72
0.015500	200.00	4.12	13.75
0.016100	200.00	-5.70	13.69
0.016700	200.00	-15.56	13.52
0.017300	200.00	-25.49	13.21
0.017900	200.00	-35.48	12.74
0.018500	200.00	-45.56	12.08
0.019100	200.00	-55.73	11.20
0.019700	200.00	-65.99	10.09
0.020300	200.00	-76.37	8.71
0.020900	200.00	-86.88	7.05
0.021500	200.00	-97.52	5.06
0.022100	200.00	-108.31	2.73
0.022700	200.00	-119.26	0.03

STOP
: 16:23 3.100 134

Silicon Nitride disc, 20mm thick, 86mm diameter
Subject to a uniform temperature rise of 200° from a zero stress level.

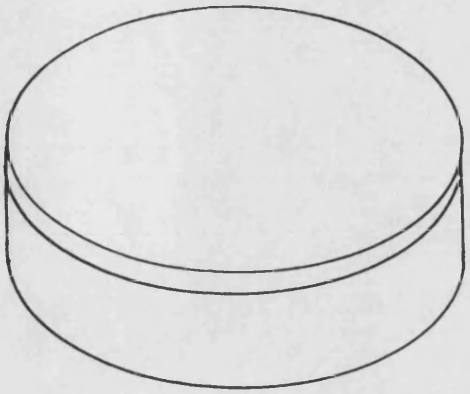

Body is free to expand radially, forced axial deformation about a radius of curvature of 4m.

	Model		Theory	
	Using '2 material' input	Using '4 material' input		
Top axial stress	0.00	0.00	0.00	MPa
Bottom axial stress	212.49	214.88	214.88	MPa

EXAMPLE 4.8.3.

	COATING	BASE	
YOUNGS MOD	300.0000	300.0000	GPa
THERMAL COND	3.0000	3.0000	W/M2
THERMAL EXP	3.3000	3.3000	x10-6
POISSONS RATIO	0.2300	0.2300	
DEPTH	0.0100	0.0100	M

RADIUS OF CURVATURE	4.00
CENTRAL DISPLACEMENT	0.0002
DEPTH TO NA	0.0100

DEPTH	TEMPERATURE	STRESS (R)	STRESS (A)
0.000143	200.00	-991.36	0.00
0.000429	200.00	-960.97	8.57
0.000714	200.00	-930.72	16.67
0.001000	200.00	-900.61	24.31
0.001286	200.00	-870.64	31.49
0.001571	200.00	-840.79	38.24
0.001857	200.00	-811.07	44.57
0.002143	200.00	-781.48	50.48
0.002429	200.00	-752.00	55.99
0.002714	200.00	-722.64	61.12
0.003000	200.00	-693.39	65.87
0.003286	200.00	-664.25	70.27
0.003571	200.00	-635.21	74.32
0.003857	200.00	-606.27	78.04
0.004143	200.00	-577.43	81.44
0.004429	200.00	-548.67	84.53
0.004714	200.00	-520.01	87.34
0.005000	200.00	-491.42	89.86
0.005286	200.00	-462.92	92.13
0.005571	200.00	-434.49	94.14
0.005857	200.00	-406.12	95.92
0.006143	200.00	-377.83	97.48
0.006429	200.00	-349.60	98.83
0.006714	200.00	-321.42	99.99
0.007000	200.00	-293.30	100.97
0.007286	200.00	-265.22	101.79
0.007571	200.00	-237.19	102.46
0.007857	200.00	-209.20	103.00
0.008143	200.00	-181.25	103.42
0.008429	200.00	-153.33	103.73
0.008714	200.00	-125.43	103.96
0.009000	200.00	-97.56	104.10
0.009286	200.00	-69.70	104.19
0.009571	200.00	-41.86	104.23
0.009857	200.00	-14.03	104.24
0.010143	200.00	13.80	104.24
0.010429	200.00	41.63	104.26
0.010714	200.00	69.48	104.31
0.011000	200.00	97.34	104.40
0.011286	200.00	125.21	104.55
0.011571	200.00	153.11	104.78
0.011857	200.00	181.03	105.10
0.012143	200.00	208.99	105.53
0.012429	200.00	236.98	106.07
0.012714	200.00	265.01	106.75
0.013000	200.00	293.09	107.57
0.013286	200.00	321.22	108.57
0.013571	200.00	349.39	109.74
0.013857	200.00	377.63	111.10
0.014143	200.00	405.93	112.68
0.014429	200.00	434.30	114.48
0.014714	200.00	462.74	116.52
0.015000	200.00	491.25	118.82
0.015286	200.00	519.85	121.39
0.015571	200.00	548.53	124.25
0.015857	200.00	577.31	127.41
0.016143	200.00	606.18	130.89
0.016429	200.00	635.14	134.70
0.016714	200.00	664.22	138.86
0.017000	200.00	693.40	143.39
0.017286	200.00	722.70	148.31
0.017571	200.00	752.11	153.62
0.017857	200.00	781.65	159.34
0.018143	200.00	811.32	165.50
0.018429	200.00	841.12	172.11
0.018714	200.00	871.07	179.19
0.019000	200.00	901.15	186.75
0.019286	200.00	931.39	194.80
0.019571	200.00	961.78	203.38
0.019857	200.00	992.33	212.49

RADIUS OF CURVATURE 4.00
CENTRAL DISPLACEMENT 0.0002
DEPTH TO NA 0.0000

DEPTH	TEMPERATURE	K (W/M2)	E (GPa)	V	G (x10-6)	STRESS (@)	STRESS (A)
0.000147	200.00	3.00	300.00	0.230	3.30	-990.31	0.00
0.000441	200.00	3.00	300.00	0.230	3.30	-959.03	8.80
0.000735	200.00	3.00	300.00	0.230	3.30	-927.91	17.09
0.001029	200.00	3.00	300.00	0.230	3.30	-896.93	24.90
0.001324	200.00	3.00	300.00	0.230	3.30	-866.09	32.23
0.001618	200.00	3.00	300.00	0.230	3.30	-835.39	39.10
0.001912	200.00	3.00	300.00	0.230	3.30	-804.82	45.52
0.002206	200.00	3.00	300.00	0.230	3.30	-774.39	51.51
0.002500	200.00	3.00	300.00	0.230	3.30	-744.07	57.08
0.002794	200.00	3.00	300.00	0.230	3.30	-713.88	62.25
0.003088	200.00	3.00	300.00	0.230	3.30	-683.81	67.02
0.003382	200.00	3.00	300.00	0.230	3.30	-653.85	71.42
0.003676	200.00	3.00	300.00	0.230	3.30	-623.99	75.46
0.003971	200.00	3.00	300.00	0.230	3.30	-594.24	79.15
0.004265	200.00	3.00	300.00	0.230	3.30	-564.59	82.51
0.004559	200.00	3.00	300.00	0.230	3.30	-535.04	85.55
0.004853	200.00	3.00	300.00	0.230	3.30	-505.57	88.29
0.005147	200.00	3.00	300.00	0.230	3.30	-476.92	88.29
0.005441	200.00	3.00	300.00	0.230	3.30	-447.62	90.47
0.005735	200.00	3.00	300.00	0.230	3.30	-418.40	92.40
0.006029	200.00	3.00	300.00	0.230	3.30	-389.25	94.09
0.006324	200.00	3.00	300.00	0.230	3.30	-360.16	95.55
0.006618	200.00	3.00	300.00	0.230	3.30	-331.14	96.81
0.006912	200.00	3.00	300.00	0.230	3.30	-302.17	97.87
0.007206	200.00	3.00	300.00	0.230	3.30	-273.26	98.74
0.007500	200.00	3.00	300.00	0.230	3.30	-244.40	99.48
0.007794	200.00	3.00	300.00	0.230	3.30	-215.58	100.04
0.008088	200.00	3.00	300.00	0.230	3.30	-186.79	100.51
0.008382	200.00	3.00	300.00	0.230	3.30	-158.05	100.84
0.008676	200.00	3.00	300.00	0.230	3.30	-129.33	101.08
0.008971	200.00	3.00	300.00	0.230	3.30	-100.63	101.24
0.009265	200.00	3.00	300.00	0.230	3.30	-71.96	101.33
0.009559	200.00	3.00	300.00	0.230	3.30	-43.30	101.38
0.009853	200.00	3.00	300.00	0.230	3.30	-14.64	101.39
0.010147	200.00	3.00	300.00	0.230	3.30	14.01	101.39
0.010441	200.00	3.00	300.00	0.230	3.30	42.66	101.41
0.010735	200.00	3.00	300.00	0.230	3.30	71.32	101.47
0.011029	200.00	3.00	300.00	0.230	3.30	100.00	101.57
0.011324	200.00	3.00	300.00	0.230	3.30	128.70	101.74
0.011618	200.00	3.00	300.00	0.230	3.30	157.42	101.99
0.011912	200.00	3.00	300.00	0.230	3.30	186.17	102.33
0.012206	200.00	3.00	300.00	0.230	3.30	214.96	102.80
0.012500	200.00	3.00	300.00	0.230	3.30	243.78	103.39
0.012794	200.00	3.00	300.00	0.230	3.30	272.65	104.13
0.013088	200.00	3.00	300.00	0.230	3.30	301.57	105.03
0.013382	200.00	3.00	300.00	0.230	3.30	330.54	106.11
0.013676	200.00	3.00	300.00	0.230	3.30	359.57	107.39
0.013971	200.00	3.00	300.00	0.230	3.30	388.66	108.88
0.014265	200.00	3.00	300.00	0.230	3.30	417.82	110.60
0.014559	200.00	3.00	300.00	0.230	3.30	447.06	112.56
0.014853	200.00	3.00	300.00	0.230	3.30	476.37	114.79
0.015147	200.00	3.00	300.00	0.230	3.30	505.77	117.30
0.015441	200.00	3.00	300.00	0.230	3.30	535.25	120.10
0.015735	200.00	3.00	300.00	0.230	3.30	564.83	123.22
0.016029	200.00	3.00	300.00	0.230	3.30	594.51	126.67
0.016324	200.00	3.00	300.00	0.230	3.30	624.29	130.46
0.016618	200.00	3.00	300.00	0.230	3.30	654.18	134.63
0.016912	200.00	3.00	300.00	0.230	3.30	684.19	139.17
0.017206	200.00	3.00	300.00	0.230	3.30	714.31	144.11
0.017500	200.00	3.00	300.00	0.230	3.30	744.56	149.48
0.017794	200.00	3.00	300.00	0.230	3.30	774.94	155.28
0.018088	200.00	3.00	300.00	0.230	3.30	805.46	161.53
0.018382	200.00	3.00	300.00	0.230	3.30	836.12	168.26
0.018676	200.00	3.00	300.00	0.230	3.30	866.92	175.48
0.018971	200.00	3.00	300.00	0.230	3.30	897.88	183.21
0.019265	200.00	3.00	300.00	0.230	3.30	928.99	191.46
0.019559	200.00	3.00	300.00	0.230	3.30	960.27	200.27
0.019853	200.00	3.00	300.00	0.230	3.30	991.72	209.64

	COATING	BASE	
YOUNGS MOD	200.0000	200.0000	GPa
THERMAL COND	3.0000	30.0000	W/M2
THERMAL EXP	11.0000	14.0000	x10-6
POISSONS RATIO	0.2700	0.3000	
DEPTH	0.0020	0.0210	M

RADIUS OF CURVATURE	4.92	
CENTRAL DISPLACEMENT	0.0002	
DEPTH TO NA	0.0115	
HEAT TRANSFER	2.550	KW

DEPTH	TEMPERATURE	STRESS (M)	STRESS (A)
0.000029	795.82	349.57	0.00
0.000086	787.46	327.29	-0.69
0.000143	779.09	305.04	-1.34
0.000200	770.73	282.80	-1.93
0.000257	762.37	260.58	-2.46
0.000314	754.01	238.37	-2.98
0.000371	745.64	216.19	-3.43
0.000429	737.28	194.02	-3.84
0.000486	728.92	171.87	-4.19
0.000543	720.56	149.73	-4.50
0.000600	712.20	127.62	-4.77
0.000657	703.83	105.52	-4.99
0.000714	695.47	83.43	-5.16
0.000771	687.11	61.36	-5.29
0.000829	678.75	39.31	-5.36
0.000886	670.38	17.28	-5.42
0.000943	662.02	-4.74	-5.43
0.001000	653.66	-26.78	-5.48
0.001057	645.30	-48.84	-5.58
0.001114	636.93	-70.90	-5.71
0.001171	628.57	-92.99	-5.89
0.001229	620.21	-115.09	-6.11
0.001286	611.85	-137.20	-6.37
0.001343	603.48	-159.33	-6.67
0.001400	595.12	-181.48	-7.01
0.001457	586.76	-203.64	-7.39
0.001514	578.40	-225.81	-7.81
0.001571	570.03	-248.00	-8.26
0.001629	561.67	-270.20	-8.76
0.001686	553.31	-292.42	-9.29
0.001743	544.95	-314.65	-9.86
0.001800	536.59	-336.89	-10.47
0.001857	528.22	-359.15	-11.11
0.001914	519.86	-381.42	-11.79
0.001971	511.50	-403.70	-12.50
0.002300	502.93	7.49	1.03
0.002900	494.15	7.17	0.92
0.003500	485.37	6.85	0.82
0.004100	476.59	6.54	0.73
0.004700	467.80	6.24	0.65
0.005300	459.02	5.93	0.59
0.005900	450.24	5.64	0.53
0.006500	441.46	5.34	0.47
0.007100	432.68	5.05	0.43
0.007700	423.90	4.76	0.39
0.008300	415.12	4.48	0.36
0.008900	406.34	4.20	0.34
0.009500	397.56	3.92	0.32
0.010100	388.78	3.64	0.31
0.010700	380.00	3.36	0.30
0.011300	371.22	3.09	0.30
0.011900	362.44	2.82	0.29
0.012500	353.66	2.54	0.28
0.013100	344.88	2.26	0.27
0.013700	336.10	1.99	0.26
0.014300	327.32	1.71	0.25
0.014900	318.54	1.43	0.24
0.015500	309.76	1.15	0.23
0.016100	300.98	0.88	0.22
0.016700	292.20	0.60	0.21
0.017300	283.41	0.33	0.20
0.017900	274.63	0.06	0.20
0.018500	265.85	-0.22	0.20
0.019100	257.07	-0.50	0.19
0.019700	248.29	-0.78	0.17
0.020300	239.51	-1.06	0.15
0.020900	230.73	-1.34	0.12
0.021500	221.95	-1.63	0.08
0.022100	213.17	-1.92	0.04
0.022700	204.39	-2.21	-0.01

STOP

EXAMPLE 4.8.4.

	COATING	BASE	
YOUNGS MOD	270.0000	200.0000	GPa
THERMAL COND	20.0000	30.0000	W/MK
THERMAL EXP	3.5000	14.0000	x10-6
POISSONS RATIO	0.2300	0.3000	
DEPTH	0.0020	0.0210	M

RADIUS OF CURVATURE	7.20	
CENTRAL DISPLACEMENT	0.0001	
DEPTH TO NA	0.0111	
HEAT TRANSFER	4.357	KW

DEPTH	TEMPERATURE	STRESS (M)	STRESS (A)
0.000029	798.93	-2109.59	0.00
0.000086	796.79	-2107.33	4.33
0.000143	794.64	-2105.07	8.63
0.000200	792.50	-2102.82	12.92
0.000257	790.36	-2100.57	17.18
0.000314	788.21	-2098.33	21.42
0.000371	786.07	-2096.10	25.64
0.000429	783.93	-2093.88	29.84
0.000486	781.79	-2091.66	34.02
0.000543	779.64	-2089.44	38.17
0.000600	777.50	-2087.24	42.30
0.000657	775.36	-2085.04	46.41
0.000714	773.21	-2082.85	50.50
0.000771	771.07	-2080.66	54.57
0.000829	768.93	-2078.48	58.61
0.000886	766.79	-2076.31	62.63
0.000943	764.64	-2074.14	66.63
0.001000	762.50	-2071.98	70.61
0.001057	760.36	-2069.83	74.57
0.001114	758.21	-2067.68	78.50
0.001171	756.07	-2065.54	82.42
0.001229	753.93	-2063.41	86.31
0.001286	751.79	-2061.28	90.17
0.001343	749.64	-2059.16	94.02
0.001400	747.50	-2057.04	97.84
0.001457	745.36	-2054.94	101.65
0.001514	743.21	-2052.84	105.43
0.001571	741.07	-2050.74	109.18
0.001629	738.93	-2048.65	112.92
0.001686	736.79	-2046.57	116.63
0.001743	734.64	-2044.50	120.32
0.001800	732.50	-2042.43	123.99
0.001857	730.36	-2040.37	127.64
0.001914	728.21	-2038.32	131.26
0.001971	726.07	-2036.27	134.87
0.002300	717.50	840.46	119.83
0.002900	702.50	799.40	108.47
0.003500	687.50	758.90	98.42
0.004100	672.50	718.93	89.60
0.004700	657.50	679.46	81.94
0.005300	642.50	640.46	75.37
0.005900	627.50	601.90	69.82
0.006500	612.50	563.73	65.22
0.007100	597.50	525.94	61.48
0.007700	582.50	488.49	58.53
0.008300	567.50	451.34	56.28
0.008900	552.50	414.46	54.67
0.009500	537.50	377.81	53.59
0.010100	522.50	341.36	52.98
0.010700	507.50	305.07	52.75
0.011300	492.50	268.83	52.63
0.011900	477.50	232.51	52.31
0.012500	462.50	196.13	51.87
0.013100	447.50	159.74	51.40
0.013700	432.50	123.37	50.98
0.014300	417.50	87.06	50.70
0.014900	402.50	50.85	50.64
0.015500	387.50	14.71	50.76
0.016100	372.50	-21.37	50.35
0.016700	357.50	-58.03	49.91
0.017300	342.50	-94.71	48.76
0.017900	327.50	-131.65	47.01
0.018500	312.50	-168.89	44.36
0.019100	297.50	-206.46	41.33
0.019700	282.50	-244.41	37.22
0.020300	267.50	-282.78	32.13
0.020900	252.50	-321.61	25.96
0.021500	237.50	-360.93	18.62
0.022100	222.50	-400.83	10.01
0.022700	207.50	-441.30	0.00

TOP

APPENDIX 4.4 TRANSIENT THERMAL ANALYSIS

The general form of the equation of conductance is;

$$\alpha\left(\frac{\partial^2 T}{\partial x^2} + \frac{\partial^2 T}{\partial y^2} + \frac{\partial^2 T}{\partial z^2}\right) + \frac{q_{INT}}{\rho C_p} = \frac{\partial T}{\partial t}$$

In this case we are considering a one dimensional problem only, so:

$$\frac{\partial T}{\partial t} = \alpha \frac{\partial^2 T}{\partial x^2} \qquad (1)$$

Taylors series

Examining the function of temperature through width x

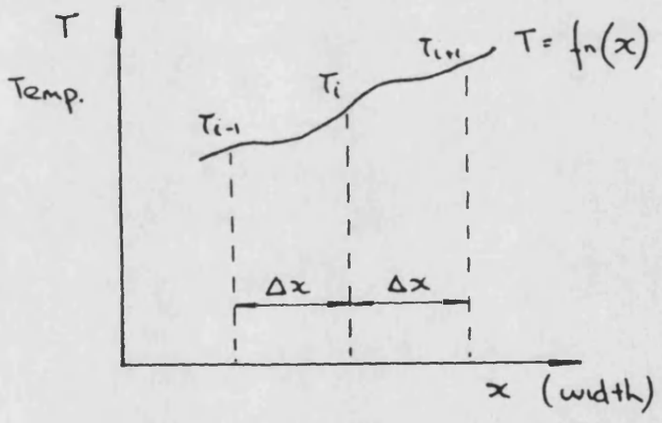

$$T_{i+1} = T_i + \Delta x\left(\frac{\partial T}{\partial x}\right) + \frac{\Delta x^2}{2!}\left(\frac{\partial^2 T}{\partial x^2}\right) + \ldots\ldots\ldots \qquad (2)$$

$$T_{i-1} = T_i - \Delta x\left(\frac{\partial T}{\partial x}\right) + \frac{\Delta x^2}{2!}\left(\frac{\partial^2 T}{\partial x^2}\right) + \ldots\ldots\ldots \qquad (3)$$

(2) + (3)

$$T_{i+1} - T_{i-1} = 2T_i + \Delta x^2\left(\frac{\partial^2 T}{\partial x^2}\right) + \ldots\ldots\ldots$$

Truncating after second term,

$$\frac{\partial^2 T}{\partial x^2} = \left[\frac{T_{i+1} - 2T_i + T_{i-1}}{\Delta x^2}\right] + fn(\Delta x^2)$$

This applies at any given time, so denoting subscript j to represent the present condition.

$$\frac{\partial^2 T}{\partial x^2} = \left[\frac{T_{i+1,j} - 2T_{i,j} + T_{i-1,j}}{\Delta x^2}\right] + fn(\Delta x^2)$$

The taylor's series for the first derivative with time

$$T_{i,j+1} = T_{i,j} + \Delta t\left(\frac{\partial T}{\partial t}\right) + \frac{\Delta t^2}{2!}\left(\frac{\partial^2 T}{\partial t^2}\right) + \cdots\cdots$$

Truncate after second term.

$$\frac{\partial T}{\partial t} = \left(\frac{T_{i,j+1} - T_{i,j}}{\Delta t}\right) + fn(\Delta t)$$

Substitute back in (1)

$$\frac{T_{i,j+1} - T_{i,j}}{\Delta t} = \alpha\left(\frac{T_{i+1,j} - 2T_{i,j+1} + T_{i-1,j}}{\Delta x^2}\right)$$

$$T_{i,j+1} = T_{i,j} + \alpha\left(\frac{\Delta t}{\Delta x^2}\right)\left(T_{i+1,j} - 2T_{i,j} + T_{i-1,j}\right)$$

Since $Fo = \frac{\alpha \Delta t}{\Delta x^2}$

then $T_{i,j+1} = Fo\left[T_{i+1,j} + T_{i-1,j} + \left(\frac{1}{Fo} - 2\right)T_{i,j}\right]$

Since this solution is unstable for $Fo < 1/2$ we require some average of the temperature gradient at the beginning and end of the time step.

Temperature gradient at j.

$$\left(\frac{\Delta T}{\Delta t}\right)_j = \alpha\left(\frac{T_{i+1,j} - 2T_{i,j} + T_{i+1,j}}{\Delta x^2}\right)$$

At end of time step, j+1

$$\left(\frac{\Delta T}{\Delta t}\right)_{j+1} = \alpha\left(\frac{T_{i+1,j+1} - 2T_{i,j+1} + T_{i-1,j+1}}{\Delta x^2}\right)$$

For Crank - Nicholson take arithmetic mean

$$\frac{T_{i,j+1} - T_{ij}}{\Delta t} = \alpha\left[\left(\frac{T_{i+1,j+1} - 2T_{i,j+1} + T_{i-1,j+1}}{2\Delta x^2}\right) + \left(\frac{T_{i+1,j} - 2T_{ij} + T_{i-1,j}}{2\Delta x^2}\right)\right]$$

Simplifies to,

$$-F_o T_{i-1,j+1} + (2+2F_o)T_{i,j+1} - F_o T_{i+1,j+1} = F_o T_{i-1,j} + (2-2F_o)T_{ij} + F_o T_{i+1,j}$$

or in matrix form;

$$\begin{bmatrix} (2+2F_o) & +F_o & 0 & 0 & \cdots \\ -F_o & (2+2F_o) & +F_o & 0 & \cdots \\ 0 & +F_o & (2+2F_o) & -F_o & \cdots \\ 0 & 0 & F_o & \cdots & \\ \cdots & & & & \end{bmatrix} \begin{bmatrix} T_{2,j+1} \\ T_{1,j+1} \\ T_{3,j+1} \\ \vdots \end{bmatrix} = \begin{bmatrix} (2-2F_o) & F_o & 0 & 0 & \cdots \\ F_o & (2-2F_o) & F_o & 0 & \cdots \\ 0 & F_o & (2-2F_o) & F_o & \cdots \\ 0 & 0 & \cdots & & \\ \cdots & & & & \end{bmatrix} \begin{bmatrix} T_{2,j} \\ T_{1,j} \\ T_{3,j} \\ \vdots \end{bmatrix}$$

Crank - Nicholson Convective boundary condition

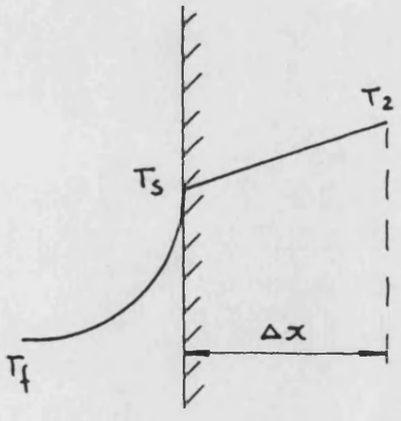

For constant fluid temperature

T_s ... Surface temperature

T_f ... Fluid temperature

take unit area $\Delta y \Delta z = 1$

From energy balance

$$-h(T_{sj} - T_{fj}) - k\left(\frac{T_{sj} - T_{2j}}{\Delta x}\right) = \frac{\Delta x \rho C_p}{2}\left(\frac{T_{sj+1} - T_{sj}}{\Delta t}\right)$$

Since $Bi = \frac{h\Delta x}{k}$

$$-Bi\left(T_{s,j} - T_{f,j}\right) - T_{s,j} + T_{2,j} = \frac{1}{2Fo}\left(T_{s,j+1} - T_{s,j}\right)$$

$$T_{s,j+1} - T_{s,j} = 2Fo\left[Bi\,T_{f,j} - (Bi+1)T_{s,j} + T_{2,j}\right]$$

Crank-Nicholson form

$$T_{s,j+1} - T_{s,j} = \frac{2Fo}{2}\left(Bi\,T_{f,j+1} - (Bi+1)T_{s,j+1} + T_{2,j+1} + (Bi+1)T_{s,j} + T_{2,j}\right)$$

$$\therefore -Bi\,Fo\,T_{f,j+1} + (Bi\,Fo + Fo + 1)T_{s,j+1} - Fo\,T_{2,j+1} = Bi\,Fo\,T_{f,j} - (Bi\,Fo + Fo - 1)T_{s,j} + Fo\,T_{2,j}$$

Interface between two solids

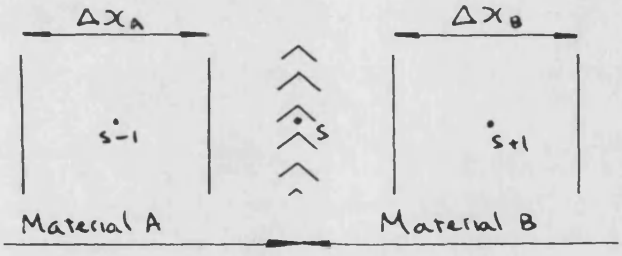

from energy balance

$$-\frac{k_A\left(T_{s,j} - T_{s-1,j}\right)}{\Delta x_A} - \frac{k_B\left(T_{s,j} - T_{s+1,j}\right)}{\Delta x_B} = \frac{(\Delta x_A + \Delta x_B)}{2}\frac{\left(T_{s,j+1} - T_{s,j}\right)}{\Delta t}\overline{\rho C_p} \quad (4)$$

take $\overline{\rho C_p} = \left(\frac{\rho_A C_{pA}\Delta x_A + \rho_A C_{pB}\Delta x_B}{\Delta x_A + \Delta x_B}\right)$

also $\alpha = \frac{k}{\rho C_p}$

$$\therefore \overline{\rho C_p} = \left(\frac{k}{\alpha}\right)_A \frac{\Delta x_A}{\Delta x_A + \Delta x_B} + \left(\frac{k}{\alpha}\right)_B \frac{\Delta x_B}{\Delta x_A + \Delta x_B}$$

from (4)

$$T_{s,j+1} - T_{s,j} = \frac{-2k_A\Delta t\left(T_{s,j} - T_{s-1,j}\right)}{\Delta x_A(\Delta x_A + \Delta x_B)\overline{\rho C_p}} - \frac{2k_B\Delta t\left(T_{s,j} - T_{s+1,j}\right)}{\Delta x_B(\Delta x_A + \Delta x_B)\overline{\rho C_p}}$$

$$T_{s,j+1} - T_{s,j} = \frac{-2k_A \Delta t \left(T_{s,j} - T_{s-1,j}\right)}{\left(\frac{k}{\alpha}\right)_A \Delta x_A^2 \left(1 + \frac{\Delta x_B}{\Delta x_A}\left(\frac{k}{\alpha}\right)_B \left(\frac{\alpha}{k}\right)_A\right)} - \frac{2k_B \Delta t \left(T_{s,j} - T_{s+1,j}\right)}{\left(\frac{k}{\alpha}\right)_B \Delta x_B^2 \left(1 + \frac{\Delta x_A}{\Delta x_B}\left(\frac{\alpha}{k}\right)_B \left(\frac{k}{\alpha}\right)_A\right)}$$

Let $K = \frac{k_B}{k_A}$ $\quad F_o = \frac{\alpha \Delta t}{\Delta x^2}$ and $C = \frac{\Delta x_A}{\Delta x_B}$

$$T_{s,j+1} - T_{s,j} = \left(\frac{-2 F_{oA} F_{oB}}{F_{oB} + CK F_{oA}}\right)\left(T_{s,j} - T_{s-1,j}\right) - \left(\frac{2K.C.F_{oA} F_{oB}}{F_{oB} + CR F_{oA}}\right)\left(T_{s,j} - T_{s+1,j}\right)$$

$$T_{s,j+1} = \left(\frac{F_{oA} F_{oB}}{F_{oB} + CK F_{oA}}\right)\left(2KC\, T_{s+1,j} + 2T_{s-1,j} + T_{s,j}\left(-2 - 2KC + \frac{F_{oB} + CK F_{oA}}{F_{oA} F_{oB}}\right)\right)$$

Crank-Nicholson form

$$T_{s,j+1} - T_{s,j} = \left(\frac{F_{oA} F_{oB}}{F_{oB} + CK F_{oA}}\right)\left[T_{s,j}\left(-1-KC\right) + T_{s-1,j} + KC\, T_{s+1,j} + T_{s,j+1}\left(-1-KC\right) + T_{s-1,j+1} + KC\, T_{s+1,j+1}\right]$$

taking $\quad \bar{F}_o = \frac{F_{oA} F_{oB}}{F_{oB} + CK F_{oA}}$

$$-\bar{F}_o T_{s-1,j+1} + \left(1 + (KC+1)\bar{F}_o\right) T_{s,j+1} - KC\bar{F}_o T_{s+1,j+1} = \bar{F}_o T_{s-1,j} + \left(1 + (1+KC)\bar{F}_o\right) T_{s,j+1} + KC\bar{F} T_{s+1,j}$$

In matrix form;

$$\begin{bmatrix} 1+(1+KC)\bar{F}_o & -2KC\bar{F}_o & 0 & \cdots \\ -\bar{F}_o & 1+(1+KC)\bar{F}_o & -KC\bar{F}_o & \cdots \\ 0 & -\bar{F}_o & 1+(1+KC)\bar{F}_o & \cdots \\ 0 & 0 & -\bar{F}_o & \cdots \\ \cdots & \cdots & \cdots & \cdots \end{bmatrix} \begin{bmatrix} T_{1,j+1} \\ T_{2,j+1} \\ T_{3,j+1} \\ \vdots \\ \end{bmatrix} = \begin{bmatrix} 1-(1+KC)\bar{F}_o & 2C\bar{F}_o K & 0 & \cdots \\ \bar{F}_o & 1-(1+KC)\bar{F}_o & KC\bar{F}_o & \cdots \\ 0 & \bar{F}_o & 1-(1+KC)\bar{F}_o & \cdots \\ 0 & 0 & \bar{F}_o & \cdots \\ \cdots & \cdots & \cdots & \cdots \end{bmatrix} \begin{bmatrix} T_{1,j} \\ T_{2,j} \\ T_{3,j} \\ \vdots \\ \end{bmatrix}$$

APPENDIX 4.5 SIMULTANEOUS EQUATION ALGORITHM

Each of the simultaneous equations assembled into the tri-diagonal matrix have the form;

$$a_i T_{i-1} + b_i T_i + c_i T_{i+1} = d_i \qquad (1)$$

We seek a general equation of the form

$$T_i = \gamma_i - \frac{c_i}{\beta_i} T_{i+1} \qquad (2)$$

where γ_i and β_i are constants

If this is true then

$$T_{i-1} = \gamma_{i-1} - \frac{c_{i-1}}{\beta_{i-1}} T_i \qquad (3)$$

substitute (3) in (1)

$$T_i = \left(\frac{d_i - a_i \gamma_{i-1}}{\beta_i}\right) - \frac{c_i}{\beta_i} T_{i-1}$$

thus $$\gamma_i = \frac{d_i - a_i \gamma_{i-1}}{\beta_i}$$

and $$\beta_i = b_i - \frac{a_i c_{i-1}}{\beta_{i-1}}$$

If there are n equations the above is used for $i = 2 \ldots n-1$

Similarly when $i=1$ the equation has the form

$$b_1 T_1 + c_1 T_2 = d_1$$

$$T_1 = \frac{d_1}{b_1} - \left(\frac{c_1}{b_1}\right) T_2$$

hence $\gamma_1 = \frac{d_1}{\beta_1}$ and $\beta_1 = b_1$

also when $i = n$

$$a_n T_{n-1} + b_n T_n = d_n$$

$$T_n = \frac{d_n}{b_n} - \left(\frac{a_n}{b_n}\right) T_{n-1}$$

$$\therefore \quad T_n = \frac{d_n - a_n \gamma_{n-1}}{\left[b_n - a_n\left(\frac{C_{n-1}}{B_{n-1}}\right)\right]}$$

APPENDIX 4.6 LISTING OF TRANSIENT PROGRAM

```
teppro.fortran  07/06/86  1848.8 bst Sun

      subroutine tempro(temp,hf,tf,t12,temp2,ntot,time)
c         program to calculate the temperature distribution in a multi layer disc
c         Implicit method (Crank-Nicolson) version
c
c         The time step is 0.0001 sec.
c
      real k(300)
      integer tt
      common k,e,v,g,t,cp,de
      dimension e(300),v(300),g(300),t(300),temp2(50,200),de(300),cp(300),temp(200)
      dimension a(200),b(200),c(200),d(200)
c
c
      do 201 iuy=1,199
      temp(iuy)=t12
  201 continue
c                               Fourier number
      Fo=delt*k(1)/(de(1)*cp(1)*t(1)*t(1))
c                               print out counter
      x=0.
      tt=1
c
c main time step loop 'j'
c
      write(6,101)
  101 format(1x,' How many time steps do you require,',/,
     &' how long should each time step be,',/,
     &' and after how many time steps should the data be printed out',/,
     &' example 500,0.1,25',/,' time is in seconds',/)
     read(5,102) isteps,delt,ipr
  102 format(v)
      do 10 j=1,isteps
c
c set up tri-diagonal coefficients
c
c note a(1) and c(10) are not used
c
      ten=temp(ntot)
      call tempbound(tf,hf,time,delt,dangle,t11,ten)
      time=j*delt
      Bi=hf*t(1)/k(1)
      Fo=delt*k(1)/(de(1)*cp(1)*t(1)*t(1))
      b(1)=Bi*Fo+Fo+1
      c(1)=-Fo
      d(1)=2*Bi*Fo*tf-(Bi*Fo+Fo-1)*temp(1)+Fo*temp(2)
```

```
C
C general values loop 'i'
C
      do 20 i=2,ntot
      Fa=delt*k(i-1)/(de(i-1)*cp(i-1)*t(i-1)*t(i-1))
      Fb=delt*k(i)/(de(i)*cp(i)*t(i)*t(i))
      con=t(i-1)/t(i)
      ron=k(i)/k(i-1)
      Fbar=(Fa*Fb)/(Fb+(con*ron*Fa))
      a(i)=-Fbar
      b(i)=1.0+((1.0+ron*con)*Fbar)
      c(i)=-ron*con*Fbar
C                              jump equation for i=10
      if(i.ne.ntot) goto 1000
      c(i)=0
      d(i)=Fbar*temp(i-1)+(1.0-((1.0+ron*con)*Fbar))*temp(i)+ron*con*Fbar*t11*2.0
      goto 20
C
 1000 d(i)=Fbar*temp(i-1)+(1.0-((1.0+ron*con)*Fbar))*temp(i)+ron*con*Fbar*temp(i+1)
   20 continue
C
C solve tri-diagonal matrix
C
      n=ntot
      call tridig(a,b,c,d,n,temp,j)
C
C write out results
C
      x=x+1.
      if(abs(x-ipr).gt.0.00001) goto 10
      angle=dangle*j
   40 format(1x,f5.1,f6.0)
      write(70,70) time,(temp(i),i=1,ntot)
      do 45 i=1,ntot
      temp2(tt,i)=temp(i)
   45 continue
   70 format(1x,/,f5.2,100f10.2)
      tt=tt+1
      x=0
C
   10 continue
C
      return
      end
      subroutine tridig(a,b,c,d,n,temp,j)
C program to solve a tridiagonal matrix with leading diagonal
C coefficients 'b',sub-diagonals 'a', super-diagonals 'c' and
C right hand sides 'd'.
```

```
c
c solution is returned in 'temp'
      dimension a(200),b(200),c(200),d(200),gamma(200),temp2(50,200),beta(200),temp(200)
c
c initialisation
c
      gamma(1)=d(1)/b(1)
      beta(1)=b(1)
c
c first loop for gammas and betas
c
      do 100 i=2,n-1
      beta(i)=b(i)-a(i)*c(i-1)/beta(i-1)
  100 gamma(i)=(d(i)-a(i)*gamma(i-1))/beta(i)
c
c second loop initialisation
c
      temp(n)=(d(n)-a(n)*gamma(n-1))/(b(n)-a(n)*(c(n-1)/beta(n-1)))
      l=n+1
c
c second loop for solution
c
      do 200 i=1,n-1
  200 temp(n-i)=gamma(n-i)-c(n-i)*temp(l-i)/beta(n-i)
      return
      end


r 18:48 0.278 1
```

APPENDIX 4.7 COMPARISON OF TRANSIENT ANALYSIS

TEMPERATURES IN THE SLAB :IMPLICIT METHOD

time	gas T	1	2	3	4	5	6	7	8	9	10	boundary
2.7	1200.	376.91	322.15	281.70	251.93	231.37	217.73	209.31	204.30	201.35	199.54	200.00
5.4	1200.	434.25	381.50	339.26	304.12	275.69	253.30	236.06	222.98	213.01	205.08	200.00
8.1	1200.	472.68	421.80	379.83	343.11	311.47	284.57	261.88	242.72	226.29	211.73	200.00
10.8	1200.	501.16	451.80	410.35	372.89	339.34	309.47	282.89	259.10	237.50	217.40	200.00
13.5	1200.	522.94	474.72	433.73	395.82	360.92	328.85	299.34	272.00	246.36	221.89	200.00
16.2	1200.	539.69	492.37	451.75	413.50	377.58	343.85	312.09	282.01	253.24	225.39	200.00
18.9	1200.	552.61	505.99	465.66	427.15	390.45	355.43	321.94	289.74	258.56	228.09	200.00
21.6	1200.	562.59	516.50	476.39	437.69	400.38	364.37	329.54	295.72	262.67	230.17	200.00
24.3	1200.	570.28	524.61	484.67	445.83	408.05	371.28	335.42	300.33	265.85	231.78	200.00
27.0	1200.	576.23	530.87	491.07	452.11	413.97	376.61	339.95	303.89	268.30	233.03	200.00
29.7	1200.	580.81	535.71	496.01	456.95	418.54	380.72	343.45	306.64	270.19	233.99	200.00
32.4	1200.	584.36	539.44	499.82	460.70	422.07	383.90	346.15	308.76	271.65	234.73	200.00
35.1	1200.	587.09	542.32	502.76	463.59	424.79	386.35	348.24	310.40	272.78	235.30	200.00
37.8	1200.	589.20	544.55	505.03	465.82	426.89	388.25	349.85	311.67	273.65	235.74	200.00
40.5	1200.	590.83	546.27	506.79	467.54	428.52	389.71	351.09	312.64	274.32	236.08	200.00
43.2	1200.	592.09	547.59	508.14	468.87	429.77	390.84	352.05	313.40	274.84	236.35	200.00
45.9	1200.	593.06	548.61	509.19	469.89	430.74	391.71	352.80	313.98	275.24	236.55	200.00
48.6	1200.	593.81	549.40	509.99	470.69	431.49	392.38	353.37	314.43	275.55	236.71	200.00
51.3	1200.	594.39	550.01	510.62	471.30	432.06	392.90	353.81	314.77	275.79	236.83	200.00
54.0	1200.	594.84	550.49	511.10	471.77	432.51	393.30	354.15	315.04	275.97	236.92	200.00
56.7	1200.	595.18	550.85	511.47	472.14	432.85	393.61	354.41	315.25	276.11	236.99	200.00
59.4	1200.	595.45	551.13	511.75	472.42	433.12	393.85	354.62	315.41	276.22	237.05	200.00
62.1	1200.	595.65	551.35	511.98	472.63	433.32	394.04	354.77	315.53	276.31	237.09	200.00
64.8	1200.	595.81	551.51	512.15	472.80	433.48	394.18	354.89	315.63	276.37	237.13	200.00
67.5	1200.	595.93	551.64	512.28	472.93	433.60	394.29	354.99	315.70	276.42	237.15	200.00
70.2	1200.	596.03	551.74	512.38	473.03	433.70	394.37	355.06	315.76	276.46	237.17	200.00
72.9	1200.	596.10	551.82	512.46	473.11	433.77	394.44	355.12	315.80	276.49	237.19	200.00
75.6	1200.	596.16	551.88	512.52	473.17	433.82	394.49	355.16	315.83	276.51	237.20	200.00
78.3	1200.	596.20	551.93	512.57	473.21	433.87	394.53	355.19	315.86	276.53	237.21	200.00
81.0	1200.	596.23	551.96	512.60	473.25	433.90	394.56	355.22	315.88	276.55	237.21	200.00
83.7	1200.	596.26	551.99	512.63	473.28	433.93	394.58	355.24	315.90	276.56	237.22	200.00
86.4	1200.	596.28	552.01	512.65	473.30	433.95	394.60	355.25	315.91	276.57	237.22	200.00
89.1	1200.	596.30	552.03	512.67	473.31	433.96	394.61	355.26	315.92	276.57	237.23	200.00
91.8	1200.	596.31	552.04	512.68	473.33	433.97	394.62	355.27	315.92	276.58	237.23	200.00
94.5	1200.	596.32	552.05	512.69	473.34	433.98	394.63	355.28	315.93	276.58	237.23	200.00
97.2	1200.	596.32	552.06	512.70	473.34	433.99	394.64	355.29	315.93	276.58	237.23	200.00
99.9	1200.	596.33	552.06	512.71	473.35	434.00	394.64	355.29	315.94	276.59	237.23	200.00
102.6	1200.	596.33	552.07	512.71	473.35	434.00	394.65	355.29	315.94	276.59	237.24	200.00
105.3	1200.	596.34	552.07	512.71	473.36	434.00	394.65	355.30	315.94	276.59	237.24	200.00
108.0	1200.	596.34	552.07	512.72	473.36	434.01	394.65	355.30	315.94	276.59	237.24	200.00
110.7	1200.	596.34	552.07	512.72	473.36	434.01	394.65	355.30	315.94	276.59	237.24	200.00
113.4	1200.	596.34	552.07	512.72	473.36	434.01	394.65	355.30	315.95	276.59	237.24	200.00

Explicit method

Time	T_w	T_1	T_2	T_3	T_4	T_5	T_6
0.5	1200	296.46	200	200	200	200	200
1.0	1200	328.69	229.75	200	200	200	200
1.5	1200	343.56	255.67	209.17	200	200	200
2.0	1200	366.82	268.63	220.68	206.83	200	200
2.5	1200	381.50	284.06	229.90	207.46	200.67	200
3.0	1200	395.46	297.41	239.68	212.34	202.63	200
3.5	1200	407.76	303.84	249.05	217.78	204.87	200
4.0	1200	419.03	321.29	258.15	223.42	207.33	200
4.5	1200	429.39	331.96	266.91	229.17	210.03	200
5.0	1200	439.01	341.95	275.35	234.41	212.84	200
5.5	1200	448.26	351.34	283.48	240.59	215.69	200
6.0	1200	456.58	360.28	291.32	246.11	218.52	200
6.5	1200	464.43	368.69	298.61	252.44	221.32	200
7.0	1200	471.92	376.60	305.98	257.08	224.38	200
7.5	1200	478.99	384.20	312.68	262.06	226.93	200
8.0	1200	486.04	391.38	319.43	266.84	229.46	200

Implicit method (computer Output)

2.7	1200	376.51	281.70	231.27	209.31	201.35	200
5.4	1200	434.25	339.26	275.69	236.06	213.01	200
8.1	1200	472.68	379.83	311.47	261.88	226.29	200

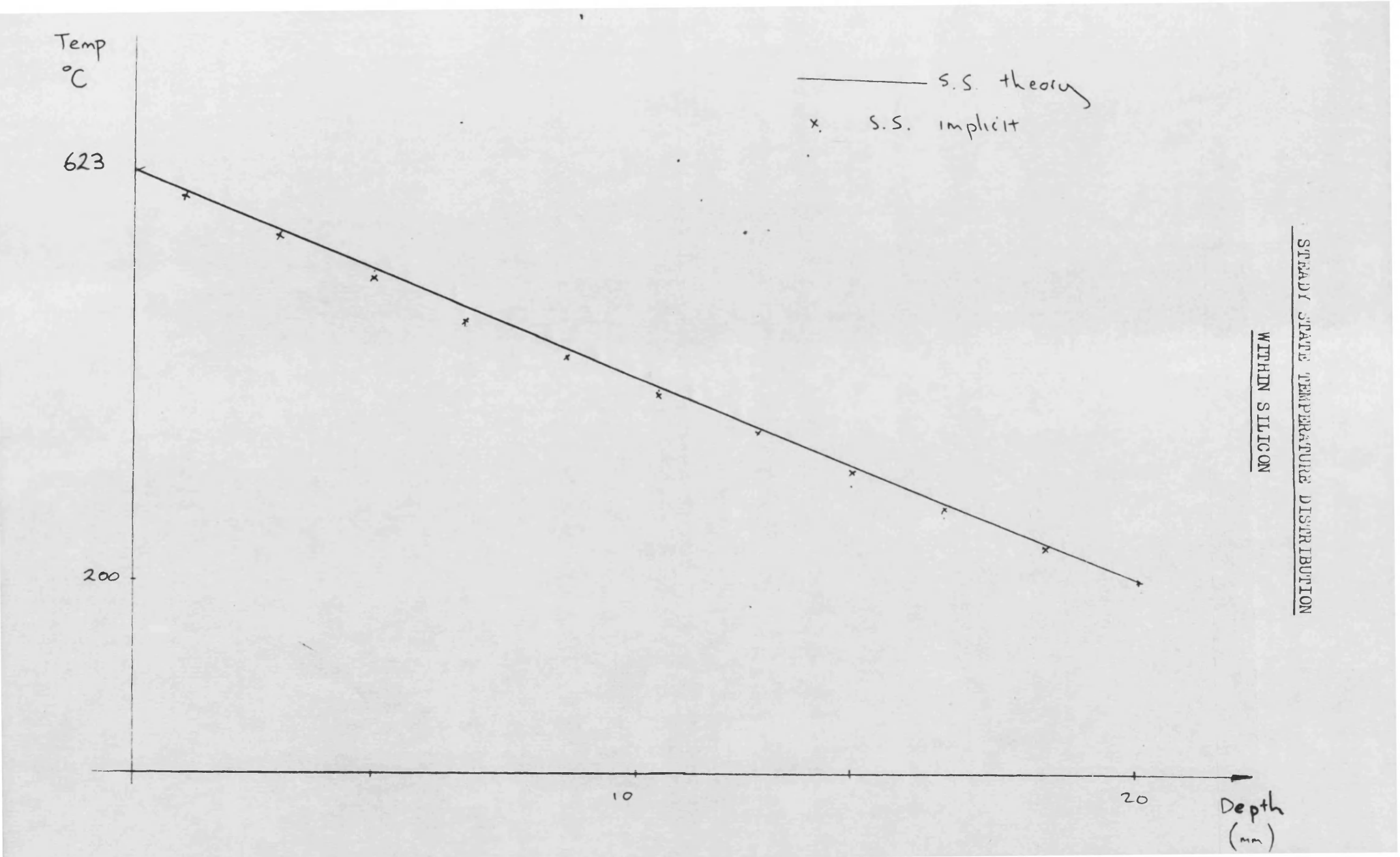

STEADY STATE TEMPERATURE DISTRIBUTION

WITHIN SILICON

APPENDIX 4.2 LISTING OF GRAPHICS PROGRAM

grap.fortran 07/07/86 1142.4 bst Mon

```
      dimension x(20,200),y(20,200),z(20,200),q(20,200),a(200),b(200)
      external plot_$setup(descriptors)
      external plot_(descriptors)
      external plot_$scale(descriptors)
      ls=1h-
      write(6,120)
      read(5,130) num
      i=0
   30 plop=0
      if(num.lt.0.5) goto 50
      j=1
      num=num-1
      i=i+1
   20 read(16,100) line
      if(line.eq.ls.and.plop.gt.0.5) goto 10
      if(line.eq.ls.and.plop.lt.0.5) plop=plop+1
      goto 20
   10 read(16,100) line
      read(16,100) line
      read(16,100) line
      read(16,100) line
   40 read(16,110) x(i,j),y(i,j),z(i,j),q(i,j)
      if(x(i,j).eq.0.0) goto 30
      j=j+1
      goto 40
   50 continue
      j=j-1
      xmax=x(1,1)
      xmin=x(1,1)
      ymin=z(1,1)
      ymax=z(1,1)
      ymax3=y(1,1)
      ymin3=y(1,1)
      ymax2=q(1,1)
      ymin2=q(1,1)
      do 51 ir=1,j
      do 52 is=1,i
      if(xmax.lt.x(is,ir)) xmax=x(is,ir)
      if(xmin.gt.x(is,ir)) xmin=x(is,ir)
      if(ymax.lt.z(is,ir)) ymax=z(is,ir)
      if(ymin.gt.z(is,ir)) ymin=z(is,ir)
      if(ymax3.lt.y(is,ir)) ymax3=y(is,ir)
      if(ymin3.gt.y(is,ir)) ymin3=y(is,ir)
      if(ymax2.lt.q(is,ir)) ymax2=q(is,ir)
```

```
      if(ymin2.gt.q(is,ir)) ymin2=q(is,ir)
   52 continue
   51 continue
      irept=i
      call plot_$setup("radial stress distribution","depth","stress",1,0e0,2,0)
      call plot_$scale(xmin,xmax,ymin,ymax)
   55 do 60 ir=1,j
      a(ir)=x(i,ir)
      b(ir)=z(i,ir)
   60 continue
      call plot_(a,b,j,1," ")
      i=i-1
      if(i.gt.0.5) goto 55
      i=irept
      call plot_$setup("axial stress distribution","depth","stress",1,0e0,2,0)
      call plot_$scale(xmin,xmax,ymin2,ymax2)
   56 do 61 ir=1,j
      a(ir)=x(i,ir)
      b(ir)=q(i,ir)
   61 continue
      call plot_(a,b,j,1," ")
      i=i-1
      if(i.gt.0.5) goto 56
      i=irept
      call plot_$setup("temperature distribution","depth","temperature",1,0e0,2,0)
      call plot_$scale(xmin,xmax,ymin3,ymax3)
   57 do 62 ir=1,j
      a(ir)=x(i,ir)
      b(ir)=y(i,ir)
   62 continue
      call plot_(a,b,j,1," ")
      i=i-1
      if(i.gt.0.5) goto 57
  100 format(a1)
  110 format(2x,f8.6,3f14.2)
  120 format("enter number of outputs")
  130 format(i3)
      stop
      end


r 11:42 0.400 3
```

APPENDIX 4.9 EXAMPLE COMPUTER RUNS

EXAMPLE 1

1mm THICK COATING

10mm THICK SUBSTRATE

FIXED TEMPERATURE DROP BETWEEN FACES

NO AXIAL MOVEMENT

— Program called trans

trans
if you require a brief output enter 1, a brief input enter 2,
both enter 3, for a conventional run enter 0.

0 — Full length output
enter number of sets of calculations to be performed

1 — One Calculation
if materials have graded structure or more than two materials are used
enter a 1, otherwise enter a 0

0 — Two material disc studied
if temperature dependant properties given on subroutine "properties"
enter a 1, otherwise enter a 0

0
if transient solution is required enter number of cycles
if a steady state solution is required enter a 0

0 — Steady State Solution
enter 1 if residual stresses are to found from plasma spraying
otherwise type a 0

0 — Not interested in residual stresses
for coating and base enter, thickness, temperature, heat transfer coef
overall diameter , datum temperature and pressure - where appropriate
but first, do you require more information; y or n

y
example input
1e-3,10e-3,100,200,0,0,86e-3,0,0
coating thickness 1e-3 metres, substrate thickness 10e-3 metres
surface of coating 100K, surface of substrate 200k,
heat transfer coefficients not needed if surface temperatures given
diameter 86e-3 meters, stress free temperature 0 k, pressure drop 0 bar

example input
1e-3,10e-3,1000,600,400,200,86e-3,280,1e5
as above except, gas conditions on top face 1000 k, 400w/mk
bottom face 600 k, 200w/mk
component is stress free at 280 k, and a 1e5 n/m2 pressure drop exists.

- 1 mm coating, 10 mm Substrate thicknesses
- ceramic surface at 800°, bottom of disc 200°
- Disc diameter 86mm

1e-3,22e-3,800,200,0,0.86e-3,0,0
enter youngs mod, thermal cond, poisson ratio, thermal exp, heat capacity, density for ceramic and metal
but first, do you require more information; y or n.

?

example input
300e9,200e9,1,30,0.23,0.3,3e-6,10e-6,0,0,0,0
ceramic properties e=300e9n/m2, k=1w/m2, poissons ratio=0.23,
thermal expansion=3e-6.
metals properties e=200e9N/m2, k=30w/m2, poissons ratio=0.3,
thermal expansion=10e-6.
thermal capacity and density are not needed for S.S. calcualtions

example input
300e9,200e9,1,30,0.23,0.3,3e-6,10e-6,400,600,2000,5000
same as above but thermal capacity for the ceramic is 400 and density is 2000
for metal capacity is 600 and density is 5000

300e9,200e9,1,30,0.23,0.3,10e-6,23e-6,0,0,0,0
enter number of strips to be used in ceramic and metal layers
ie: 35,35 : limit 150 strips

35,35
if disc is axially restrained enter a 0
if disc is free to deform enter -1
for a forced displacement enter radius of curvature

0

	COATING	BASE	
YOUNGS MOD	300.0000	200.0000	GPa
THERMAL COND	1.0000	30.0000	W/M2
THERMAL EXP	10.0000	23.0000	x10-6
POISSONS RATIO	0.2300	0.3000	
DEPTH	0.0010	0.0220	M

RADIUS OF CURVATURE	0.00	
CENTRAL DISPLACEMENT	0.0000	
DEPTH TO NA	0.0113	
HEAT TRANSFER	2.011	KW

DEPTH	TEMPERATURE	STRESS (R)	STRESS (A)
0.000014	795.05	260.70	0.00
0.000043	785.16	222.10	-0.23

Property	Ceramic	Metal
E	300 GPa	200 GPa
K	1w/mK	30 w/mK
V	0.23	0.3
γ	10×10^{-6}	23×10^{-6}

— 35 elements in coating, 35 in substrate

— Axially restrained

0.000071	775.27	183.51	-0.42
0.000100	765.38	144.93	-0.57
0.000129	755.49	106.36	-0.68
0.000157	745.60	67.81	-0.75
0.000186	735.71	29.27	-0.78
0.000214	725.82	-9.27	-0.79
0.000243	715.93	-47.82	-0.84
0.000271	706.04	-86.38	-0.93
0.000300	696.15	-124.95	-1.06
0.000329	686.26	-163.53	-1.22
0.000357	676.37	-202.12	-1.43
0.000386	666.48	-240.73	-1.67
0.000414	656.59	-279.35	-1.95
0.000443	646.70	-317.97	-2.27
0.000471	636.81	-356.61	-2.63
0.000500	626.92	-395.27	-3.03
0.000529	617.03	-433.93	-3.46
0.000557	607.14	-472.60	-3.93
0.000586	597.25	-511.28	-4.43
0.000614	587.36	-549.98	-4.98
0.000643	577.47	-588.69	-5.56
0.000671	567.58	-627.40	-6.18
0.000700	557.69	-666.13	-6.83
0.000729	547.80	-704.87	-7.52
0.000757	537.91	-743.62	-8.24
0.000786	528.02	-782.38	-9.01
0.000814	518.13	-821.15	-9.80
0.000843	508.24	-859.93	-10.64
0.000871	498.35	-898.72	-11.50
0.000900	488.46	-937.53	-12.40
0.000929	478.57	-976.34	-13.34
0.000957	468.68	-1015.16	-14.31
0.000986	458.79	-1054.00	-15.32
0.001314	450.22	871.61	-15.32
0.001943	442.97	817.06	-31.40
0.002571	435.71	763.29	-45.65
0.003200	428.46	710.26	-58.18
0.003829	421.21	657.93	-69.09
0.004457	413.96	606.25	-78.46
0.005086	406.70	555.18	-86.41
0.005714	399.45	504.68	-93.05
0.006343	392.20	454.69	-98.48
0.006971	384.95	405.17	-102.81
0.007600	377.69	356.07	-106.17
0.008229	370.44	307.34	-108.66
0.008857	363.19	258.93	-110.41
0.009486	355.93	210.79	-111.53
0.010114	348.68	162.86	-112.15

0.010743	341.43	115.10	-112.38
0.011371	334.18	67.41	-112.44
0.012000	326.92	19.67	-112.64
0.012629	319.67	-28.08	-112.84
0.013257	312.42	-75.87	-113.16
0.013886	305.16	-123.82	-113.83
0.014514	297.91	-171.98	-114.99
0.015143	290.66	-220.40	-116.77
0.015771	283.41	-269.14	-119.28
0.016400	276.15	-318.25	-122.66
0.017029	268.90	-367.79	-127.04
0.017657	261.65	-417.81	-132.55
0.018286	254.40	-468.38	-139.33
0.018914	247.14	-519.55	-147.52
0.019543	239.89	-571.39	-157.26
0.020171	232.64	-623.95	-168.70
0.020800	225.38	-677.30	-181.98
0.021429	218.13	-731.51	-197.27
0.022057	210.88	-786.65	-214.71
0.022686	203.63	-842.78	-234.48

STOP
r 15:03 1.956 23

EXAMPLE 2

1mm THICK COATING

10mm THICK SUBSTRATE

FIXED TEMPERATURE DROP BETWEEN FACES

AXIALLY FREE TO DEFORM

trans
if you require a brief output enter 1, a brief input enter 2,
both enter 3, for a conventional run enter 0.

0
enter number of sets of calculations to be performed

1
if materials have graded structure or more than two materials are used
enter a 1, otherwise enter a 0

0
if temperature dependant properties given on subroutine "properties"
enter a 1, otherwise enter a 0

0
if transient solution is required enter number of cycles
if a steady state solution is required enter a 0

0
enter 1 if residual stresses are to found from plasma spraying
otherwise type a 0

0
for coating and base enter, thickness, temperature, heat transfer coef
overall diameter , datum temperature and pressure - where appropriate
but first, do you require more information; y or n

n
1e-3,22e-3,800,200,0,0,86e-3,0,0
enter youngs mod, thermal cond, poisson ratio, thermal exp, heat capacity, density for ceramic and metal
but first, do you require more information; y or n.

n
300e9,200e9,1,30,0.23,0.3,10e-6,23e-6,0,0,0,0
enter number of strips to be used in ceramic and metal layers
ie: 35,35 : limit 150 strips

35,35
if disc is axially restrained enter a 0
      if disc is free to deform enter -1
      for a forced displacement enter radius of curvature

-1

— Axially free to deform

	COATING	BASE	
YOUNGS MOD	300.0000	200.0000	GPa
THERMAL COND	1.0000	30.0000	W/M2
THERMAL EXP	10.0000	23.0000	x10-6
POISSONS RATIO	0.2300	0.3000	
DEPTH	0.0010	0.0220	M

RADIUS OF CURVATURE	4.84	
CENTRAL DISPLACEMENT	0.0002	
DEPTH TO NA	0.0113	
HEAT TRANSFER	2.011	KW

DEPTH	TEMPERATURE	STRESS (M)	STRESS (A)
0.000014	795.05	-722.57	0.00
0.000043	785.16	-759.04	-0.79
0.000071	775.27	-795.52	-1.62
0.000100	765.38	-832.01	-2.48
0.000129	755.49	-868.52	-3.38
0.000157	745.60	-905.03	-4.31
0.000186	735.71	-941.55	-5.28
0.000214	725.82	-978.09	-6.28
0.000243	715.93	-1014.63	-7.32
0.000271	706.04	-1051.19	-8.39
0.000300	696.15	-1087.75	-9.50
0.000329	686.26	-1124.33	-10.64
0.000357	676.37	-1160.91	-11.82
0.000386	666.48	-1197.51	-13.03
0.000414	656.59	-1234.11	-14.27
0.000443	646.70	-1270.73	-15.55
0.000471	636.81	-1307.35	-16.86
0.000500	626.92	-1343.99	-18.20
0.000529	617.03	-1380.64	-19.58
0.000557	607.14	-1417.29	-20.99
0.000586	597.25	-1453.96	-22.43
0.000614	587.36	-1490.63	-23.90
0.000643	577.47	-1527.31	-25.41
0.000671	567.58	-1564.01	-26.95
0.000700	557.69	-1600.71	-28.52
0.000729	547.80	-1637.42	-30.12
0.000757	537.91	-1674.15	-31.75
0.000786	528.02	-1710.88	-33.42
0.000814	518.13	-1747.62	-35.11

0.000843	508.24	-1784.37	-36.84
0.000871	498.35	-1821.13	-38.60
0.000900	488.46	-1857.90	-40.39
0.000929	478.57	-1894.67	-42.20
0.000957	468.68	-1931.46	-44.05
0.000986	458.79	-1968.25	-45.93
0.001314	450.22	250.85	39.76
0.001943	442.97	238.58	35.79
0.002571	435.71	226.49	32.25
0.003200	428.46	214.57	29.12
0.003829	421.21	202.81	26.38
0.004457	413.96	191.22	23.99
0.005086	406.70	179.77	21.96
0.005714	399.45	168.45	20.23
0.006343	392.20	157.27	18.81
0.006971	384.95	146.19	17.65
0.007600	377.69	135.23	16.74
0.008229	370.44	124.35	16.04
0.008857	363.19	113.56	15.54
0.009486	355.93	102.84	15.21
0.010114	348.68	92.18	15.01
0.010743	341.43	81.57	14.93
0.011371	334.18	70.99	14.90
0.012000	326.92	60.37	14.81
0.012629	319.67	49.75	14.70
0.013257	312.42	39.12	14.58
0.013886	305.16	28.50	14.49
0.014514	297.91	17.91	14.44
0.015143	290.66	7.35	14.48
0.015771	283.41	-3.24	14.44
0.016400	276.15	-13.88	14.29
0.017029	268.90	-24.58	14.00
0.017657	261.65	-35.36	13.54
0.018286	254.40	-46.22	12.87
0.018914	247.14	-57.18	11.97
0.019543	239.89	-68.25	10.81
0.020171	232.64	-79.45	9.36
0.020800	225.38	-90.79	7.58
0.021429	218.13	-102.28	5.45
0.022057	210.88	-113.94	2.92
0.022686	203.63	-125.78	-0.02

STOP
r 15:09 11.002 0

EXAMPLE 3

1mm THICK COATING

BONDCOAT

10mm THICK SUSTRATE

FIXED TEMPERATURE DROP BETWEEN FACES

NO AXIAL MOVEMENT

```
trans
if you require a brief output enter 1, a brief input enter 2,
both enter 3, for a conventional run enter 0.

0
enter number of sets of calculations to be performed

1
if materials have graded structure or more than two materials are used
enter a 1, otherwise enter a 0

1                                                    — Three material disc is wanted
if temperature dependant properties given on subroutine "properties"
enter a 1, otherwise enter a 0

0
if transient solution is required enter number of cycles
if a steady state solution is required enter a 0

0
enter 1 if residual stresses are to found from plasma spraying
otherwise type a 0

0
enter youngs mod, thermal cond, poissons ratio, thermal exp,  depth properties extend, and number of elements each section should be
 divided into
hen data complete enter a 0
but first do you require more information; y or n.

y
 example input
300e9
30,0.23,10e-6,1e-3,20
320e9
31,0.23,10e-3,1e-3,20
200e9
160,0.3,24e-6,10e-3,40
0

 The data given is for three layers each of a different material
The first has a Youngs modulas of 300e9
               Thermal conductivity 30
               Poissons ratio 0.23
               Thermal expansion 10e-6
These properties extend through a depth of 1e-3m
and this layer is divided into 20 strips
The units must be consistant.
```

The data is concluded with a 0

300e9
1,0.23,10e-6,1e-3,20
220e9
30,0.23,20e-6,0.1e-5,10
200e9
160,0.3,24e-6,10e-3,30
0

	E	K	V	thickness	No. elements
Top layer	300 GPa	1 w/mK	0.23	1mm	20
Bond coat	220 GPa	30 w/mK	0.23	1μm	10
substrate	200 GPa	160 w/mK	0.3	10mm	30

for coating and base enter, heat transfer coeff, temperature, overall diameter and datum temperature
but first do you require more information; "y" or "n"

y
example input
0,0,400,200,86e-3,0
With this set of data the top of the disc is at 400K the bottom at 200k
The disc is 86 mm in diameter.

1000,800,400,200,86e-3,0
With this set of data the top of the disc see a gas 1000W/m2K,400K
the bottom 800W/m2K,200K

0,0,600,20,86e-3,0

- Ceramic surface 600°
- Substrate surface 20°
- Diameter 86mm

if disc is axially restrained enter a 0
if disc is free to deform enter -1
for a forced displacement enter radius of curvature

0

RADIUS OF CURVATURE 0.00
CENTRAL DISPLACEMENT 0.0000
DEPTH TO NA -0.0094
HEAT TRANSFER -3.171 KW

DEPTH	TEMPERATURE	K (W/M2)	E (GPa)	V	G (x10-6)	STRESS (A)	STRESS (R)

0.000025	600.00	1.00	300.00	0.230	10.00	1012.39	0.00
0.000075	572.71	1.00	300.00	0.230	10.00	906.03	-0.07
0.000125	545.41	1.00	300.00	0.230	10.00	799.68	-0.13
0.000175	518.12	1.00	300.00	0.230	10.00	693.33	-0.17
0.000225	490.83	1.00	300.00	0.230	10.00	586.98	-0.21
0.000275	463.53	1.00	300.00	0.230	10.00	480.64	-0.23
0.000325	436.24	1.00	300.00	0.230	10.00	374.30	-0.24
0.000375	408.95	1.00	300.00	0.230	10.00	267.96	-0.25
0.000425	381.65	1.00	300.00	0.230	10.00	161.62	-0.25
0.000475	354.36	1.00	300.00	0.230	10.00	55.28	-0.26
0.000525	327.07	1.00	300.00	0.230	10.00	-51.06	-0.26
0.000575	299.77	1.00	300.00	0.230	10.00	-157.40	-0.26
0.000625	272.48	1.00	300.00	0.230	10.00	-263.73	-0.26
0.000675	245.19	1.00	300.00	0.230	10.00	-370.07	-0.27
0.000725	217.89	1.00	300.00	0.230	10.00	-476.41	-0.28
0.000775	190.60	1.00	300.00	0.230	10.00	-582.76	-0.30
0.000825	163.31	1.00	300.00	0.230	10.00	-689.10	-0.33
0.000875	136.01	1.00	300.00	0.230	10.00	-795.45	-0.37
0.000925	108.72	1.00	300.00	0.230	10.00	-901.81	-0.42
0.000975	81.43	1.00	300.00	0.230	10.00	-1008.16	-0.49
0.001000	81.43	30.00	220.00	0.230	20.00	-506.99	-1.42
0.001000	81.42	30.00	220.00	0.230	20.00	-507.01	-1.42
0.001000	81.42	30.00	220.00	0.230	20.00	-507.02	-1.42
0.001000	81.42	30.00	220.00	0.230	20.00	-507.03	-1.42
0.001000	81.42	30.00	220.00	0.230	20.00	-507.04	-1.42
0.001001	81.42	30.00	220.00	0.230	20.00	-507.05	-1.42
0.001001	81.42	30.00	220.00	0.230	20.00	-507.06	-1.42
0.001001	81.41	30.00	220.00	0.230	20.00	-507.07	-1.42
0.001001	81.41	30.00	220.00	0.230	20.00	-507.08	-1.42
0.001001	81.41	30.00	220.00	0.230	20.00	-507.09	-1.42
0.001001	80.27	160.00	200.00	0.300	24.00	-422.02	-1.40
0.001001	79.14	160.00	200.00	0.300	24.00	-429.83	-1.42
0.001001	78.00	160.00	200.00	0.300	24.00	-437.63	-1.43
0.001001	76.86	160.00	200.00	0.300	24.00	-445.44	-1.45
0.001001	75.72	160.00	200.00	0.300	24.00	-453.24	-1.46
0.001002	74.59	160.00	200.00	0.300	24.00	-461.05	-1.48
0.001002	73.45	160.00	200.00	0.300	24.00	-468.85	-1.49
0.001002	72.31	160.00	200.00	0.300	24.00	-476.66	-1.51
0.001002	71.17	160.00	200.00	0.300	24.00	-484.46	-1.52
0.001002	70.04	160.00	200.00	0.300	24.00	-492.27	-1.54
0.001002	68.90	160.00	200.00	0.300	24.00	-500.07	-1.56
0.001002	67.76	160.00	200.00	0.300	24.00	-507.88	-1.57
0.001002	66.63	160.00	200.00	0.300	24.00	-515.68	-1.59
0.001002	65.49	160.00	200.00	0.300	24.00	-523.49	-1.61
0.001002	64.35	160.00	200.00	0.300	24.00	-531.29	-1.63
0.001003	63.21	160.00	200.00	0.300	24.00	-539.10	-1.65
0.001003	62.08	160.00	200.00	0.300	24.00	-546.91	-1.66
0.001003	60.94	160.00	200.00	0.300	24.00	-554.71	-1.68

0.001003	59.80	160.00	200.00	0.300	24.00	-562.52	-1.70
0.001003	58.67	160.00	200.00	0.300	24.00	-570.33	-1.72
0.001003	57.53	160.00	200.00	0.300	24.00	-578.13	-1.74
0.001003	56.39	160.00	200.00	0.300	24.00	-585.94	-1.76
0.001003	55.25	160.00	200.00	0.300	24.00	-593.75	-1.78
0.001003	54.12	160.00	200.00	0.300	24.00	-601.55	-1.81
0.001003	52.98	160.00	200.00	0.300	24.00	-609.36	-1.83
0.001004	51.84	160.00	200.00	0.300	24.00	-617.17	-1.85
0.001004	50.71	160.00	200.00	0.300	24.00	-624.98	-1.87
0.001004	49.57	160.00	200.00	0.300	24.00	-632.78	-1.89
0.001004	48.43	160.00	200.00	0.300	24.00	-640.59	-1.92
0.001004	47.29	160.00	200.00	0.300	24.00	-648.40	-1.94

STOP
r 16:04 3.575 49

EXAMPLE 4

1mm THICK COATING WITH TEMPERATURE DEPENDANT PROPERTIES

10mm THICK SUBSTRATE

FIXED TEMPERATURE DROP BETWEEN FACES

NO AXIAL MOVEMENT

```
trans
if you require a brief output enter 1, a brief input enter 2,
both enter 3, for a conventional run enter 0.

0
enter number of sets of calculations to be performed

1
if materials have graded structure or more than two materials are used
enter a 1, otherwise enter a 0

0
if temperature dependant properties given on subroutine "properties"
enter a 1, otherwise enter a 0

1
 do you require help setting up the subroutine necessary
ans; "y" or "n"

y
 It is necessary to set up a subroutine called properties
The temperature of each element is sent into this subroutine
and the properties Youngs Modulas, poisson ratio, thermal expansion
and conductivity are returned, these are held in the matrices e,v,g,k

 The following is an example of such a subroutine

      subroutine properties(matl,temp,i)
c     This subroutine is called once for each disc element
c     The temperatue is automatically fed across as "temp"
c     i is the element number
c     matl is the material number
c     as the program stands only two material can be studied
c     ie matl=1 for ceramic layer
c        and matl=2 for metal layer
      dimension e(300),v(300),g(300),t(300),cp(300),de(300)
      real k(300)
      common k,e,v,g,t,cp,de
      if(matl.gt.1.5) goto 10
c     The following equations apply to the ceramic
      k(i)=25.625736-(1.15623e-2*temp)+(1.24994e-6*(temp**2.0))
      e(i)=290e9-(0.025e9*temp)
      v(i)=0.208-(5.7904e-5*temp)+(4.5621e-8*(temp**2.0))
      g(i)=1.21307e-6+(5.44759e-9*temp)-(2.8528e-12*(temp**2.0))
      return
   10 if(matl.gt.2.5) goto 20
c     The following equation apply to the metal
```

— Temperature dependent properties.

This subroutine is used for this example it is called once with matl = 1 when the ceramics properties are found, and again when matl = 2 when the metals properties are found.

```
      k(i)=30
      e(i)=200e9
      v(i)=0.3
      g(i)=14e-6
      return
   20 continue
      end

if transient solution is required enter number of cycles
if a steady state solution is required enter a 0

0
enter 1 if residual stresses are to found from plasma spraying
otherwise type a 0

0
for coating and base enter, thickness, temperature, heat transfer coef
overall diameter , datum temperature and pressure - where appropriate
but first, do you require more information; y or n

y
 example input
1e-3,10e-3,100,200,0,0,86e-3,0,0
coating thickness 1e-3 metres, substrate thickness 10e-3 metres
surface of coating 100K, surface of substrate 200k,
heat transfer coefficients not needed if surface temperatures given
diameter 86e-3 meters, stress free temperature 0 k, pressure drop 0 bar

 example input
1e-3,10e-3,1000,600,400,200,86e-3,280,1e5
as above except, gas conditions on top face 1000 k, 400w/mk
bottom face 600 k, 200w/mk
component is stress free at 280 k, and a 1e5 n/m2 pressure drop exists.

1e-3,10e-3,1000,400,0,0,86e-3,0,0
enter number of strips to be used in ceramic and metal layers
ie: 35,35  : limit 150 strips

25,25
if disc is axially restrained enter a 0
      if disc is free to deform enter -1
      for a forced displacement enter radius of curvature

0
```

RADIUS OF CURVATURE	0.00	
CENTRAL DISPLACEMENT	0.0000	
DEPTH TO NA	0.0054	
HEAT TRANSFER	-8.782	KW

DEPTH	TEMPERATURE	K (W/M2)	E (GPa)	V	G (x10-6)	STRESS (A)	STRESS (R)
0.000020	1000.00	15.31	265.00	0.196	3.81	-1553.60	0.00
0.000060	996.06	15.35	265.10	0.196	3.81	-1558.81	-1.07
0.000100	992.13	15.38	265.20	0.195	3.81	-1564.05	-2.14
0.000140	988.21	15.42	265.29	0.195	3.81	-1569.30	-3.21
0.000180	984.30	15.46	265.39	0.195	3.81	-1574.58	-4.27
0.000220	980.39	15.49	265.49	0.195	3.81	-1579.88	-5.33
0.000260	976.50	15.53	265.59	0.195	3.81	-1585.20	-6.38
0.000300	972.61	15.56	265.69	0.195	3.81	-1590.55	-7.42
0.000340	968.74	15.60	265.78	0.195	3.81	-1595.91	-8.47
0.000380	964.87	15.63	265.88	0.195	3.81	-1601.29	-9.50
0.000420	961.01	15.67	265.98	0.194	3.81	-1606.70	-10.54
0.000460	957.16	15.71	266.07	0.194	3.81	-1612.12	-11.56
0.000500	953.32	15.74	266.17	0.194	3.81	-1617.56	-12.59
0.000540	949.48	15.78	266.27	0.194	3.81	-1623.02	-13.60
0.000580	945.66	15.81	266.36	0.194	3.81	-1628.50	-14.62
0.000620	941.84	15.85	266.46	0.194	3.81	-1634.00	-15.62
0.000660	938.04	15.88	266.56	0.194	3.81	-1639.51	-16.63
0.000700	934.24	15.92	266.65	0.194	3.81	-1645.04	-17.62
0.000740	930.45	15.95	266.75	0.194	3.81	-1650.59	-18.61
0.000780	926.66	15.99	266.85	0.194	3.81	-1656.15	-19.60
0.000820	922.89	16.02	266.94	0.193	3.81	-1661.74	-20.58
0.000860	919.13	16.06	267.04	0.193	3.81	-1667.33	-21.56
0.000900	915.37	16.10	267.13	0.193	3.81	-1672.94	-22.53
0.000940	911.62	16.13	267.23	0.193	3.81	-1678.57	-23.49
0.000980	907.88	16.17	267.32	0.193	3.81	-1684.21	-24.45
0.001200	887.72	30.00	200.00	0.300	14.00	1138.42	52.96
0.001600	867.56	30.00	200.00	0.300	14.00	1055.66	47.99
0.002000	847.41	30.00	200.00	0.300	14.00	973.27	43.90
0.002400	827.25	30.00	200.00	0.300	14.00	891.23	40.59
0.002800	807.09	30.00	200.00	0.300	14.00	809.49	37.99
0.003200	786.94	30.00	200.00	0.300	14.00	728.01	36.03
0.003600	766.78	30.00	200.00	0.300	14.00	646.78	34.60
0.004000	746.62	30.00	200.00	0.300	14.00	565.74	33.65
0.004400	726.46	30.00	200.00	0.300	14.00	484.86	33.07
0.004800	706.31	30.00	200.00	0.300	14.00	404.11	32.78
0.005200	686.15	30.00	200.00	0.300	14.00	323.48	32.74

0.005600	665.99	30.00	200.00	0.300	14.00	242.79	32.63
0.006000	645.84	30.00	200.00	0.300	14.00	162.10	32.50
0.006400	625.68	30.00	200.00	0.300	14.00	81.44	32.42
0.006800	605.52	30.00	200.00	0.300	14.00	0.81	32.42
0.007200	585.36	30.00	200.00	0.300	14.00	-79.90	32.23
0.007600	565.21	30.00	200.00	0.300	14.00	-160.73	31.75
0.008000	545.05	30.00	200.00	0.300	14.00	-241.72	30.91
0.008400	524.89	30.00	200.00	0.300	14.00	-322.91	29.61
0.008800	504.73	30.00	200.00	0.300	14.00	-404.32	27.78
0.009200	484.58	30.00	200.00	0.300	14.00	-486.00	25.33
0.009600	464.42	30.00	200.00	0.300	14.00	-567.99	22.16
0.010000	444.26	30.00	200.00	0.300	14.00	-650.31	18.20
0.010400	424.11	30.00	200.00	0.300	14.00	-733.02	13.35
0.010800	403.95	30.00	200.00	0.300	14.00	-816.14	7.53

STOP
r 17:50 2.245 23

EXAMPLE 5

TRANSIENT ANALYSIS

1mm THICK COATING

10mm THICK SUBSTRATE

FIXED GAS TEMPERATURE AND HEAT TRANSFER COEFFICIENT ON THE COATING SURFACE. REAR OF DISC IS IN CONTACT WITH A SURFACE AT A FIXED TEMPERATURE.

trans
if you require a brief output enter 1, a brief input enter 2,
both enter 3, for a conventional run enter 0.

0
enter number of sets of calculations to be performed

1
if materials have graded structure or more than two materials are used
enter a 1, otherwise enter a 0

0
if temperature dependant properties given on subroutine "properties"
enter a 1, otherwise enter a 0

0
if transient solution is required enter number of cycles
if a steady state solution is required enter a 0

4 — Four transient stress outputs wanted
enter 1 if residual stresses are to found from plasma spraying
otherwise type a 0

0
for coating and base enter, thickness, temperature, heat transfer coef
overall diameter , datum temperature and pressure - where appropriate
but first, do you require more information; y or n

n
1e-3,10e-3,0,0,0,0,86e-3,0,0
enter youngs mod, thermal cond, poisson ratio, thermal exp, heat capacity, density for ceramic and metal
but first, do you require more information; y or n.

n
300e9,200e9,1,30,0.23,0.3,10e-6,24e-6,400,600,3000,6000
enter number of strips to be used in ceramic and metal layers
ie: 35,35 : limit 150 strips

20,20
What uniform temperature is your disc starting at
you can use either degrees K or C, but keep to same throughout program

0
Is the temperature distribution already available in file70?
in which case type "y",
or do you want the program to calculate the distribution for you,
in which case type "n"

n
To calculate transient temperature distribution, the user-written, subroutine "tempbound" must be used, if you require help in preparing this type "y"

y
This subroutine must take the form

```
tempbound(tf,hf,time,delt,dangle,t11,temp)
```

not all of these variables need be used, in the simplest case only "time" is passed to the subroutine, and "tf", "hf" and "t11" are returned these are gas temperature and heat transfere coefficent on the gas side and the rear face temperature - these can all be set as constants, or varied with time, in which case the change in time "delt" will have to be used, and example program follows, corresponding to the case of the in-cylinder conditions in a firing engine

PROGRAM LISTING

```
      subroutine tempbound(tf,hf,time,delt,dangle,t11,temp)
c     this subroutine can be used to set up desired thermal boundary conditions as a constant c     or as a function of time.  This
 to be used if a transient solution is required.
c
c     set step for angle incrementation
      dangle=2
c
      pi=3.14159
c     set compression constant
      gamma=1.4
c     set engine operating speed
      frequency=20
c     set max volume ration
      vration=20
c     set inlet air temperature
      temp1=300
c     find effective compression ratio at the present time within the cylce
      comp=-vratio*cos(2.0*pi*time*frequency)
      comp=(vario/2.0)+(comp/2.0)
      comp=comp+1
c     calculate the time increment
      delt=dangle/(360.0*frequency)
c     find the instantaneous gas temperature
      tf=temp1*(comp**(gamma-1))
      tf=tf-273
c
c     set up heat transfer coefficient
```

This program simulates the temperature changes in a cycled diesel engine.

From the time it calculates the compression ratio and hence gas temperature

$T_{start} = 300K$

Vol. ratio = 20

$h_f = 1200.$

Temp at rear of test piece $t_{11} = 200$

```
      hf=1200
c
c     set up temperature of rear face
      t11=200

      return
      end


 PROGRAM LISTING
c     alternatively the following structure can be used
c     which returns constant values with time
      subroutine tempbound(tf,hf,time,delt,dangle,t11,temp)
      dangle=2
      hf=1100
      tf=1200
      delt=0.0150
      t11=200
      return
      end


 How many time steps do you require,
how long should each time step be,
and after how many time steps should the data be printed out
example 500,0.1,25
time is in seconds


500,0.1,50
if disc is axially restrained enter a 0
      if disc is free to deform enter -1
      for a forced displacement enter radius of curvature

0
```

500 Temperature calculations performed, at a spacing of 0.1 seconds, every 50th calculation recorded i.e. every 5 seconds

---

	COATING	BASE	
YOUNGS MOD	300.0000	200.0000	GPa
THERMAL COND	1.0000	30.0000	W/M2
THERMAL EXP	10.0000	24.0000	x10-6
POISSONS RATIO	0.2300	0.3000	
DEPTH	0.0010	0.0100	M

RADIUS OF CURVATURE 0.00

CENTRAL DISPLACEMENT 0.0000
DEPTH TO NA 0.0053
TIME 7.5000 S

DEPTH	TEMPERATURE	STRESS (M)	STRESS (A)
0.000025	608.03	1741.74	0.00
0.000075	575.66	1615.21	-1.37
0.000125	543.68	1490.23	-2.63
0.000175	512.11	1366.88	-3.77
0.000225	480.96	1245.20	-4.80
0.000275	450.23	1125.22	-5.72
0.000325	419.94	1006.97	-6.54
0.000375	390.09	890.45	-7.25
0.000425	360.67	775.65	-7.87
0.000475	331.69	662.57	-8.39
0.000525	303.13	551.16	-8.83
0.000575	274.98	441.38	-9.17
0.000625	247.23	333.19	-9.43
0.000675	219.86	226.50	-9.60
0.000725	192.85	121.25	-9.70
0.000775	166.19	17.36	-9.71
0.000825	139.84	-85.32	-9.77
0.000875	113.78	-186.87	-9.91
0.000925	87.99	-287.42	-10.11
0.000975	62.44	-387.06	-10.39
0.001250	37.09	-210.05	-10.38
0.001750	29.58	-262.25	-11.90
0.002250	23.76	-302.78	-13.39
0.002750	19.55	-332.22	-14.77
0.003250	16.88	-351.04	-15.94
0.003750	15.70	-359.53	-16.85
0.004250	16.00	-357.23	-16.26
0.004750	17.80	-344.73	-15.96
0.005250	21.17	-321.61	-15.93
0.005750	26.20	-287.05	-15.69
0.006250	32.98	-240.37	-15.31
0.006750	41.63	-180.88	-14.89
0.007250	52.23	-108.04	-14.57
0.007750	64.85	-21.54	-14.53
0.008250	79.47	78.88	-14.14
0.008750	96.03	192.90	-13.05
0.009250	114.38	319.64	-10.97
0.009750	134.29	457.63	-7.62
0.010250	155.46	604.89	-2.70

0.010750	177.50	758.96	4.10

	COATING	BASE	
YOUNGS MOD	300.0000	200.0000	GPa
THERMAL COND	1.0000	30.0000	W/M2
THERMAL EXP	10.0000	24.0000	x10-6
POISSONS RATIO	0.2300	0.3000	
DEPTH	0.0010	0.0100	M

RADIUS OF CURVATURE	0.00	
CENTRAL DISPLACEMENT	0.0000	
DEPTH TO NA	0.0057	
TIME	7.5000	S

DEPTH	TEMPERATURE	STRESS (M)	STRESS (A)
0.000025	654.43	1606.85	0.00
0.000075	624.48	1489.74	-1.36
0.000125	594.63	1373.09	-2.60
0.000175	564.90	1256.92	-3.73
0.000225	535.29	1141.25	-4.74
0.000275	505.80	1026.10	-5.65
0.000325	476.45	911.48	-6.44
0.000375	447.22	797.42	-7.13
0.000425	418.14	683.92	-7.72
0.000475	389.19	571.00	-8.21
0.000525	360.39	458.68	-8.60
0.000575	331.74	346.96	-8.89
0.000625	303.24	235.85	-9.09
0.000675	274.89	125.38	-9.20
0.000725	246.70	15.54	-9.21
0.000775	218.67	-93.70	-9.29
0.000825	190.80	-202.34	-9.45
0.000875	163.09	-310.36	-9.69
0.000925	135.55	-417.77	-10.01
0.000975	108.17	-524.55	-10.42
0.001250	80.96	-140.75	-10.42
0.001750	72.77	-197.46	-11.67
0.002250	66.28	-242.55	-13.03
0.002750	61.48	-275.98	-14.34
0.003250	58.38	-297.78	-15.52

0.003750	56.95	-308.00	-18.49
0.004250	57.18	-306.16	-15.80
0.004750	59.03	-293.25	-15.37
0.005250	62.48	-269.49	-15.19
0.005750	67.49	-235.13	-15.13
0.006250	74.00	-190.41	-14.94
0.006750	81.95	-135.82	-14.71
0.007250	91.25	-71.95	-14.55
0.007750	101.82	0.52	-14.54
0.008250	113.54	81.05	-14.20
0.008750	126.29	168.84	-13.35
0.009250	139.93	263.00	-11.80
0.009750	154.29	362.52	-9.37
0.010250	169.21	466.34	-5.86
0.010750	184.51	573.30	-1.09

	COATING	BASE	
YOUNGS MOD	300.0000	200.0000	GPa
THERMAL COND	1.0000	30.0000	W/M2
THERMAL EXP	10.0000	24.0000	x10-6
POISSONS RATIO	0.2300	0.3000	
DEPTH	0.0010	0.0100	M

RADIUS OF CURVATURE	0.00	
CENTRAL DISPLACEMENT	0.0000	
DEPTH TO NA	0.0053	
TIME	7.5000	S

DEPTH	TEMPERATURE	STRESS (M)	STRESS (A)
0.000025	676.31	1437.88	0.00
0.000075	647.54	1325.48	-1.13
0.000125	618.86	1213.42	-2.15
0.000175	590.27	1101.74	-3.07
0.000225	561.76	990.44	-3.89
0.000275	533.35	879.53	-4.61
0.000325	505.04	769.04	-5.23
0.000375	476.83	658.98	-5.76
0.000425	448.73	549.36	-6.20
0.000475	420.74	440.20	-6.55
0.000525	392.86	331.51	-6.81

0.000575	365.10	223.31	-6.98
0.000625	337.47	115.60	-7.07
0.000675	309.95	8.40	-7.08
0.000725	282.57	-98.31	-7.16
0.000775	255.32	-204.53	-7.31
0.000825	228.20	-310.25	-7.53
0.000875	201.22	-415.45	-7.83
0.000925	174.38	-520.12	-8.20
0.000975	147.69	-624.25	-8.64
0.001250	121.15	-50.84	-8.64
0.001750	113.08	-106.44	-9.25
0.002250	106.52	-151.73	-10.00
0.002750	101.47	-186.70	-10.77
0.003250	97.91	-211.37	-11.48
0.003750	95.83	-225.87	-12.04
0.004250	95.20	-230.39	-12.44
0.004750	95.97	-225.02	-12.24
0.005250	98.10	-210.40	-12.22
0.005750	101.53	-186.80	-12.07
0.006250	106.20	-154.70	-11.83
0.006750	112.03	-114.65	-11.57
0.007250	118.93	-67.25	-11.37
0.007750	126.81	-13.21	-11.36
0.008250	135.56	46.95	-11.13
0.008750	145.09	112.56	-10.49
0.009250	155.27	182.88	-9.30
0.009750	165.98	257.13	-7.42
0.010250	177.10	334.50	-4.69
0.010750	188.48	414.15	-0.99

	COATING	BASE	
YOUNGS MOD	300.0000	200.0000	GPa
THERMAL COND	1.0000	30.0000	W/M2
THERMAL EXP	10.0000	24.0000	x10-6
POISSONS RATIO	0.2300	0.3000	
DEPTH	0.0010	0.0100	M

RADIUS OF CURVATURE	0.00	
CENTRAL DISPLACEMENT	0.0000	
DEPTH TO NA	0.0057	
TIME	7.5000	S

DEPTH	TEMPERATURE	STRESS (M)	STRESS (A)
0.000025	694.37	1296.51	0.00
0.000075	666.60	1187.97	-1.08
0.000125	638.89	1079.73	-2.06
0.000175	611.26	971.82	-2.93
0.000225	583.71	864.24	-3.70
0.000275	556.23	757.00	-4.37
0.000325	528.85	650.13	-4.94
0.000375	501.55	543.62	-5.41
0.000425	474.34	437.50	-5.78
0.000475	447.22	331.78	-6.07
0.000525	420.21	226.47	-6.26
0.000575	393.29	121.58	-6.37
0.000625	366.48	17.12	-6.38
0.000675	339.78	-86.94	-6.45
0.000725	313.19	-190.59	-6.61
0.000775	286.71	-293.82	-6.84
0.000825	260.35	-396.63	-7.15
0.000875	234.10	-498.99	-7.54
0.000925	207.98	-600.91	-8.01
0.000975	181.98	-702.36	-8.55
0.001250	156.11	33.68	-8.55
0.001750	148.16	-20.93	-8.68
0.002250	141.50	-66.76	-9.05
0.002750	136.13	-103.78	-9.54
0.003250	132.04	-132.04	-10.06
0.003750	129.21	-151.65	-10.54
0.004250	127.61	-162.80	-10.92
0.004750	127.20	-165.72	-11.17
0.005250	127.93	-160.64	-11.06
0.005750	129.76	-148.09	-11.03
0.006250	132.62	-128.44	-10.91
0.006750	136.44	-102.15	-10.73
0.007250	141.15	-69.78	-10.57
0.007750	146.67	-31.90	-10.48
0.008250	152.91	10.90	-10.44
0.008750	159.78	58.11	-10.14
0.009250	167.17	109.11	-9.50
0.009750	175.00	163.25	-8.41
0.010250	183.15	219.85	-6.76
0.010750	191.52	278.24	-4.44

STOP
r 18:03 10.022 8

THE SUBROUTINE TEMPBOUND USED IN THIS CASE WAS

```
pr tempbound.fortran

                tempbound.fortran   07/06/86  1805.3 bst Sun

      subroutine tempbound(tf,hf,time,delt,dangle,t11,temp)
      dangle=2
      hf=1100
      tf=1200
      t11=200
      delt=0.0150
      return
      end

r 18:05 0.213 1

THE OUTPUT FILE CREATED IS FILE  70

pr file70

                file70    07/06/86  1806.1 bst Sun


 0.75    608.03    575.66    543.68    512.11    480.96    450.23    419.94    390.09    360.67    331.69    303.13    274.98    247
.23    219.86    192.85    166.19    139.84    113.78     87.99     62.44     37.09     29.58     23.76     19.55     16.88     15.7
0     16.00     17.80     21.17     26.20     32.98     41.63     52.23     64.85     79.47     96.03    114.38    134.29    155.46
   177.50

 1.50    654.43    624.48    594.63    564.90    535.29    505.80    476.45    447.22    418.14    389.19    360.39    331.74    303
.24    274.89    246.70    218.67    190.80    163.09    135.55    108.17     80.96     72.77     66.28     61.48     58.38     56.9
5     57.18     59.03     62.48     67.49     74.00     81.95     91.25    101.82    113.54    126.29    139.93    154.29    169.21
   184.51

 2.25    676.31    647.54    618.86    590.27    561.76    533.35    505.04    476.83    448.73    420.74    392.86    365.10    337
.47    309.95    282.57    255.32    228.20    201.22    174.38    147.69    121.15    113.08    106.52    101.47     97.91     95.8
3     95.20     95.97     98.10    101.53    106.20    112.03    118.93    126.81    135.56    145.09    155.27    165.98    177.10
   188.48

 3.00    694.37    666.60    638.89    611.26    583.71    556.23    528.85    501.55    474.34    447.22    420.21    393.29    366
.48    339.78    313.19    286.71    260.35    234.10    207.98    181.98    156.11    148.16    141.50    136.13    132.04    129.2
1    127.61    127.20    127.93    129.76    132.62    136.44    141.15    146.67    152.91    159.78    167.17    175.00    183.15
   191.52

 3.75    709.84    682.91    656.04    629.23    602.49    575.82    549.22    522.69    496.24    469.88    443.60    417.40    391
.29    365.28    339.36    313.53    287.80    262.18    236.65    211.24    185.93    176.06    171.29    165.62    161.03    157.5
```

```
σ   155.02   153.54   153.03   153.44   154.72   156.81   159.64   163.15   167.26   171.90   176.98   182.42   188.13
   194.02

 4.50   722.98   696.76   670.60   644.49   618.44   592.45   566.52   540.65   514.85   489.12   463.45   437.86   412
.35   386.91   361.55   336.28   311.08   285.98   260.96   236.03   211.19   203.39   196.52   190.57   185.55   181.4
2   178.18   175.78   174.20   173.40   173.33   173.94   175.18   176.99   179.31   182.07   185.20   188.63   192.29
   196.11

 5.25   734.10   708.49   682.93   657.42   631.95   606.53   581.16   555.85   530.59   505.39   480.25   455.17   430
.16   405.21   380.33   355.51   330.77   306.10   281.51   256.98   232.54   224.80   217.84   211.67   206.27   201.6
3   197.74   194.56   192.07   190.24   189.03   188.39   188.28   188.66   189.46   190.64   192.13   193.87   195.81
   197.87

 6.00   743.50   718.41   693.35   668.34   643.36   618.43   593.54   568.69   543.89   519.14   494.45   469.80   445
.21   420.67   396.19   371.77   347.41   323.11   298.87   274.69   250.58   242.89   235.86   229.49   223.77   218.7
0   214.26   210.42   207.16   204.46   202.28   200.59   199.35   198.51   198.03   197.87   197.97   198.29   198.77
   199.36

 6.75   751.44   726.78   702.15   677.56   653.00   628.48   603.99   579.54   555.13   530.76   506.44   482.16   457
.92   433.73   409.59   385.50   361.46   337.47   313.53   289.65   265.82   258.17   251.07   244.54   238.56   233.1
2   228.21   223.82   219.91   216.47   213.48   210.89   208.69   206.82   205.27   203.97   202.91   202.02   201.27
   200.61

 7.50   758.14   733.85   709.59   685.35   661.14   636.97   612.82   588.70   564.62   540.58   516.57   492.60   468
.66   444.77   420.91   397.10   373.33   349.60   325.92   302.28   278.69   271.07   263.93   257.25   251.05   245.3
0   240.00   235.13   230.68   226.62   222.93   219.60   216.58   213.85   211.38   209.13   207.07   205.17   203.38
   201.67


r 18:06 0.474 0
```

EXAMPLE 6

RESIDUAL STRESSES IN COATING

0.1mm THICK APPLIED LAYER

10mm THICK SUBSTRATE

COATING INITIALLY AT A UNIFORM TEMPERATURE WHICH DECAYS WITH TIME. ADIABATIC FACES ASSUMED.

resid
Enter the latent heat of fusion for Zirconia,
temperature of Zirconia at arrival at the substrate surface,
melting point of zirconia,
temperatue at which elastic properties can be assumed for the coating.
Units must be consistant.
ie:680000,3000,2700,2000

680000,3000,2700,2000
Enter the number of layers to be sprayed, 1 or 2

1
Enter number of elements layer should be divided into,
the thickness of the layer,
the time step to be used for calculation,
time interval you wish to use between stored data,
and time span for calculations.
ie:32,1e-4,1e-6,1e-5,1e-4

32,1e-4,1e-6,1e-5,1e-4
Enter for both Zirconia and the substrate, the thermal conductivity,
density and specific heat capacity
ie:1,30,3800,7850,800,460
This data set gives the Zirconia a conductivity of 1W/mK, density of 3000kg/m3
and a heat capacity of 800J/KgK. The substrat has a conductivity of 30W/mK,
density of 7850Kg/m3 and a heat capacity of 460J/KgK.

1,30,3800,7850,800,460
Enter the substrate thickness, number of elements in substrate,
and the initial temperatue of the substrate.
ie: 10e-3,20,300

10e-3,20,300
next layer

STOP
r 18:11 2.747 9

cf -a
r 18:11 0.044 0

rl -a
r 18:11 0.035 0

THE OUPUT FILES CREATED ARE@

ps file70

To calculate residual stresses the program resid must be run before trans. This writes the temperature distribution to file70 and file14

— Only one layer to be sprayed at this time

Ceramic layer is 0.1mm thick, it is divided into 32 elements.
The temperature field is calculated once every 1μsecond, and printed every 10μseconds, Calculation is stopped

file70 07/06/86 1811.7 bst Sun

0.00 3000.00 3000.00 3000.00 3000.00 3000.00 3000.00 3000.00 3000.00 3000.00 3000.00 3000.00 3000.00 3000
.00 3000.00 3000.00 3000.00 3000.00 3000.00 3000.00 3000.00 3000.00 3000.00 3000.00 3000.00 3000.00 3000.0
0 3000.00 2999.95 2999.23 2991.32 2930.06 2664.78 308.56 300.00 300.00 300.00 300.00 300.00 300.00
300.00 300.00 300.00 300.00 300.00 300.00 300.00 300.00 300.00 300.00 300.00 300.00 300.00

0.00 3000.00 3000.00 3000.00 3000.00 3000.00 3000.00 3000.00 3000.00 3000.00 3000.00 3000.00 3000.00 3000
.00 3000.00 3000.00 3000.00 3000.00 3000.00 3000.00 3000.00 3000.00 3000.00 3000.00 3000.00 2999.9
9 2999.91 2999.23 2994.57 2969.93 2877.12 2664.06 316.85 300.01 300.00 300.00 300.00 300.00 300.00
300.00 300.00 300.00 300.00 300.00 300.00 300.00 300.00 300.00 300.00 300.00 300.00 300.00

0.00 3000.00 3000.00 3000.00 3000.00 3000.00 3000.00 3000.00 3000.00 3000.00 3000.00 3000.00 3000.00 3000
.00 3000.00 3000.00 3000.00 3000.00 3000.00 3000.00 3000.00 3000.00 3000.00 3000.00 2999.99 2999.9
3 2999.50 2997.14 2986.33 2947.43 2844.49 2663.66 325.09 300.01 300.00 300.00 300.00 300.00 300.00
300.00 300.00 300.00 300.00 300.00 300.00 300.00 300.00 300.00 300.00 300.00 300.00 300.00

0.00 3000.00 3000.00 3000.00 3000.00 3000.00 3000.00 3000.00 3000.00 3000.00 3000.00 3000.00 3000.00 3000
.00 3000.00 3000.00 3000.00 3000.00 3000.00 3000.00 3000.00 3000.00 3000.00 2999.99 2999.95 2999.7
2 2998.55 2993.59 2976.18 2927.21 2821.40 2592.70 333.29 300.02 300.00 300.00 300.00 300.00 300.00
300.00 300.00 300.00 300.00 300.00 300.00 300.00 300.00 300.00 300.00 300.00 300.00 300.00

0.00 3000.00 3000.00 3000.00 3000.00 3000.00 3000.00 3000.00 3000.00 3000.00 3000.00 3000.00 3000.00 3000
.00 3000.00 3000.00 3000.00 3000.00 3000.00 3000.00 3000.00 3000.00 2999.99 2999.97 2999.85 2999.2
7 2996.93 2988.80 2964.43 2898.98 2712.45 2083.09 340.24 300.03 300.00 300.00 300.00 300.00 300.00
300.00 300.00 300.00 300.00 300.00 300.00 300.00 300.00 300.00 300.00 300.00 300.00 300.00

0.00 3000.00 3000.00 3000.00 3000.00 3000.00 3000.00 3000.00 3000.00 3000.00 3000.00 3000.00 3000.00 3000
.00 3000.00 3000.00 3000.00 3000.00 3000.00 3000.00 3000.00 3000.00 2999.98 2999.92 2999.63 2998.5
1 2994.58 2982.37 2948.17 2861.93 2688.07 1805.67 345.80 300.05 300.00 300.00 300.00 300.00 300.00
300.00 300.00 300.00 300.00 300.00 300.00 300.00 300.00 300.00 300.00 300.00 300.00 300.00

0.00 3000.00 3000.00 3000.00 3000.00 3000.00 3000.00 3000.00 3000.00 3000.00 3000.00 3000.00 3000.00 3000
.00 3000.00 3000.00 3000.00 3000.00 3000.00 3000.00 3000.00 2999.99 2999.96 2999.81 2999.26 2997.3
5 2991.32 2974.18 2930.84 2837.67 2685.37 1664.37 350.63 300.07 300.00 300.00 300.00 300.00 300.00
300.00 300.00 300.00 300.00 300.00 300.00 300.00 300.00 300.00 300.00 300.00 300.00 300.00

0.00 3000.00 3000.00 3000.00 3000.00 3000.00 3000.00 3000.00 3000.00 3000.00 3000.00 3000.00 3000.00 3000
.00 3000.00 3000.00 3000.00 3000.00 3000.00 3000.00 3000.00 2999.99 2999.98 2999.91 2999.63 2998.69 2995.7
2 2987.14 2965.01 2914.97 2820.26 2653.03 1592.50 355.08 300.08 300.00 300.00 300.00 300.00 300.00
300.00 300.00 300.00 300.00 300.00 300.00 300.00 300.00 300.00 300.00 300.00 300.00 300.00

0.00 3000.00 3000.00 3000.00 3000.00 3000.00 3000.00 3000.00 3000.00 3000.00 3000.00 3000.00 3000.00 3000
.00 3000.00 3000.00 3000.00 3000.00 3000.00 3000.00 3000.00 2999.99 2999.95 2999.82 2999.35 2997.88 2993.5
8 2982.22 2955.15 2896.24 2765.84 2417.57 1515.42 359.27 300.10 300.00 300.00 300.00 300.00 300.00

```
   300.00   300.00   300.00   300.00   300.00   300.00   300.00   300.00   300.00   300.00   300.00   300.00   300.00

 0.00   3000.00   3000.00   3000.00   3000.00   3000.00   3000.00   3000.00   3000.00   3000.00   3000.00   3000.00   3000.00   3000
.00   3000.00   3000.00   3000.00   3000.00   3000.00   3000.00   2999.99   2999.98   2999.91   2999.68   2998.94   2996.79   2990.9
4   2976.41   2942.74   2866.58   2695.54   2259.69   1431.17   363.15   300.12   300.00   300.00   300.00   300.00   300.00
   300.00   300.00   300.00   300.00   300.00   300.00   300.00   300.00   300.00   300.00   300.00   300.00   300.00

r 18:13 0.565 0


TO CALCULATE THE STRESSES


trans
if you require a brief output enter 1, a brief input enter 2,
both enter 3, for a conventional run enter 0.

                                                    — Brief output

1
enter number of sets of calculations to be performed

1
if materials have graded structure or more than two materials are used
enter a 1, otherwise enter a 0

0
if temperature dependant properties given on subroutine "properties"
enter a 1, otherwise enter a 0

0
if transient solution is required enter number of cycles
if a steady state solution is required enter a 0

4
enter 1 if residual stresses are to found from plasma spraying
otherwise type a 0

1
 Enter temperature at which elastic properties start in the coating

2000
for coating and base enter, thickness, temperature, heat transfer coef
overall diameter , datum temperature and pressure - where appropriate
but first, do you require more information; y or n
```

```
n
1e-4,10e-3,0,0,0,0,86e-3,0,0
enter youngs mod, thermal cond, poisson ratio, thermal exp, heat capacity, density for ceramic and metal
but first, do you require more information; y or n.

n
300e9,200e9,1,30,0.23,0.3,10e-6,24e-6,0,0,0,0
enter number of strips to be used in ceramic and metal layers
ie: 35,35  : limit 150 strips

32,20
 What uniform temperature is your disc starting at
you can use either degrees K or C, but keep to same throughout program

0
 Is the temperature distribution already available in file70?
in which case type "y",
or do you want the program to calculate the distribution for you,
in which case type "n"

y
if disc is axially restrained enter a 0
     if disc is free to deform enter -1
     for a forced displacement enter radius of curvature

0

-------------------------------------------------

                    COATING              BASE

YOUNGS MOD          300.0000           200.0000     GPa
THERMAL COND          1.0000            30.0000     W/M2
THERMAL EXP          10.0000            24.0000     x10-6
POISSONS RATIO        0.2300             0.3000
DEPTH                 0.0001             0.0100     M
MAX RAD STRESS        0.0000            55.7444     MPa
MIN RAD STRESS        0.0000            -3.0528     MPa
MAX AXI STRESS        0.0000             9.8807     MPa
MIN AXI STRESS        0.0000             9.6472     MPa
MATL TEMP             0.0000             0.0000

RADIUS OF CURVATURE          0.00
CENTRAL DISPLACEMENT         0.0000
DEPTH TO NA                  0.0050
TIME                  0.0000     S
```

	COATING	BASE	
YOUNGS MOD	300.0000	200.0000	GPa
THERMAL COND	1.0000	30.0000	W/M2
THERMAL EXP	10.0000	24.0000	x10-6
POISSONS RATIO	0.2300	0.3000	
DEPTH	0.0001	0.0100	M
MAX RAD STRESS	0.0000	109.9148	MPa
MIN RAD STRESS	0.0000	-5.8163	MPa
MAX AXI STRESS	0.0000	8.4821	MPa
MIN AXI STRESS	0.0000	8.0428	MPa
MATL TEMP	0.0000	0.0000	

RADIUS OF CURVATURE	0.00
CENTRAL DISPLACEMENT	0.0000
DEPTH TO NA	0.0051
TIME	0.0000 S

	COATING	BASE	
YOUNGS MOD	300.0000	200.0000	GPa
THERMAL COND	1.0000	30.0000	W/M2
THERMAL EXP	10.0000	24.0000	x10-6
POISSONS RATIO	0.2300	0.3000	
DEPTH	0.0001	0.0100	M
MAX RAD STRESS	0.0000	163.3970	MPa
MIN RAD STRESS	0.0000	-8.9371	MPa
MAX AXI STRESS	0.0000	7.6463	MPa
MIN AXI STRESS	0.0000	6.9733	MPa
MATL TEMP	0.0000	0.0000	

RADIUS OF CURVATURE	0.00
CENTRAL DISPLACEMENT	0.0000
DEPTH TO NA	0.0050

TIME 0.0000 S

	COATING	BASE	
YOUNGS MOD	300.0000	200.0000	GPa
THERMAL COND	1.0000	30.0000	W/M2
THERMAL EXP	10.0000	24.0000	x10-6
POISSONS RATIO	0.2300	0.3000	
DEPTH	0.0001	0.0100	M
MAX RAD STRESS	0.0000	217.0306	MPa
MIN RAD STRESS	0.0000	-11.6175	MPa
MAX AXI STRESS	0.0000	6.8442	MPa
MIN AXI STRESS	0.0000	5.9719	MPa
MATL TEMP	0.0000	0.0000	

RADIUS OF CURVATURE 0.00
CENTRAL DISPLACEMENT 0.0000
DEPTH TO NA 0.0051
TIME 0.0000 S

STOP
r 18:23 2.808 3

EXAMPLE 7

RESIDUAL STRESSES IN COATING

0.1mm THICK APPLIED LAYER

0.1mm THICK COOL LAYER OF CERAMIC

10mm THICK SUBSTRATE.

COATING INITIALLY AT A UNIFORM TEMPERATURE WHICH DECAYS WITH TIME. ADIABATIC SURFACES ASSUMED

resid
Enter the latent heat of fusion for Zirconia,
temperature of Zirconia at arrival at the substrate surface,
melting point of zirconia,
temperatue at which elastic properties can be assumed for the coating.
Units must be consistant.
ie:680000,3000,2700,2000

680000,3000,2700,2000
Enter the number of layers to be sprayed, 1 or 2

— Second layer of ceramic applied

2
Enter number of elements layer should be divided into,
the thickness of the layer,
the time step to be used for calculation,
time interval you wish to use betweem stored data,
and time span for calculations.
ie:32,1e-4,1e-6,1e-5,1e-4

— Each ceramic layer 0.1mm thick

32,1e-4,1e-6,1e-5,1e-4
Enter for both Zirconia and the substrate, the thermal conductivity,
density and specific heat capacity
ie:1,30,3800,7850,800,460
This data set gives the Zirconia a conductivity of 1W/mK, density of 3000kg/m3
and a heat capacity of 800J/KgK. The substrat has a conductivity of 30W/mk,
density of 7850Kg/m3 and a heat capacity of 460J/KgK.

1,30,3800,7850,800,460
Enter the substrate thickness, number of elements in substrate,
and the initial temperatue of the substrate.
ie: 10e-3,20,300

10e-3,20,300
next layer
next layer

STOP
r 18:27 4.415 3

cf -a
r 18:27 0.045 0

rl -a
r 18:27 0.034 0

THE OUTPUT FILES CREATED ARE@

pr file70

file70 07/06/86 1828.1 bst Sun

0.00 3000.00 3000.00 3000.00 3000.00 3000.00 3000.00 3000.00 3000.00 3000.00 3000.00 3000.00 3000.00 3000
.00 2999.77 2991.66 2798.84 501.16 308.34 300.23 300.00 300.00 300.00 300.00 300.00 300.00 300.0
0 300.00 300.00 300.00 300.00 300.00 300.00 300.00 300.00 300.00 300.00 300.00 300.00 300.00
300.00 300.00 300.00 300.00 300.00 300.00 300.00 300.00 300.00 300.00 300.00 300.00 300.00

0.00 3000.00 3000.00 3000.00 3000.00 3000.00 3000.00 3000.00 3000.00 3000.00 3000.00 3000.00 3000.00 2999
.93 2998.39 2971.56 2692.61 659.31 329.22 301.61 300.07 300.00 300.00 300.00 300.00 300.00 300.0
0 300.00 300.00 300.00 300.00 300.00 300.00 300.00 300.00 300.00 300.00 300.00 300.00 300.00
300.00 300.00 300.00 300.00 300.00 300.00 300.00 300.00 300.00 300.00 300.00 300.00 300.00

0.00 3000.00 3000.00 3000.00 3000.00 3000.00 3000.00 3000.00 3000.00 3000.00 3000.00 3000.00 2999.99 2999
.72 2995.63 2951.94 2693.09 792.45 358.20 304.75 300.30 300.01 300.00 300.00 300.00 300.00 300.0
0 300.00 300.00 300.00 300.00 300.00 300.00 300.00 300.00 300.00 300.00 300.00 300.00 300.00
300.00 300.00 300.00 300.00 300.00 300.00 300.00 300.00 300.00 300.00 300.00 300.00 300.00

0.00 3000.00 3000.00 3000.00 3000.00 3000.00 3000.00 3000.00 3000.00 3000.00 3000.00 3000.00 2999.95 2999
.27 2991.85 2935.13 2693.50 907.46 392.59 309.91 300.81 300.05 300.00 300.00 300.00 300.00 300.0
0 300.00 300.00 300.00 300.00 300.00 300.00 300.00 300.00 300.00 300.00 300.00 300.00 300.00
300.00 300.00 300.00 300.00 300.00 300.00 300.00 300.00 300.00 300.00 300.00 300.00 300.00

0.00 3000.00 3000.00 3000.00 3000.00 3000.00 3000.00 3000.00 3000.00 3000.00 3000.00 2999.99 2999.88 2998
.58 2987.42 2920.64 2693.85 1007.48 430.43 317.14 301.74 300.14 300.01 300.00 300.00 300.00 300.0
0 300.00 300.00 300.00 300.00 300.00 300.00 300.00 300.00 300.00 300.00 300.00 300.00 300.00
300.00 300.00 300.00 300.00 300.00 300.00 300.00 300.00 300.00 300.00 300.00 300.00 300.00

0.00 3000.00 3000.00 3000.00 3000.00 3000.00 3000.00 3000.00 3000.00 3000.00 3000.00 2999.98 2999.75 2997
.62 2982.56 2908.06 2694.17 1095.05 470.29 326.36 303.17 300.31 300.03 300.00 300.00 300.00 300.0
0 300.00 300.00 300.00 300.00 300.00 300.00 300.00 300.00 300.00 300.00 300.00 300.00 300.00
300.00 300.00 300.00 300.00 300.00 300.00 300.00 300.00 300.00 300.00 300.00 300.00 300.00

0.00 3000.00 3000.00 3000.00 3000.00 3000.00 3000.00 3000.00 3000.00 3000.00 3000.00 2999.95 2999.55 2996
.40 2977.46 2897.07 2694.44 1172.20 511.12 337.41 305.18 300.59 300.06 300.00 300.00 300.00 300.0
0 300.00 300.00 300.00 300.00 300.00 300.00 300.00 300.00 300.00 300.00 300.00 300.00 300.00
300.00 300.00 300.00 300.00 300.00 300.00 300.00 300.00 300.00 300.00 300.00 300.00 300.00

0.00 3000.00 3000.00 3000.00 3000.00 3000.00 3000.00 3000.00 3000.00 3000.00 2999.99 2999.92 2999.28 2994
.96 2972.22 2885.86 2633.08 1239.05 552.14 350.12 307.84 301.01 300.11 300.01 300.00 300.00 300.0
0 300.00 300.00 300.00 300.00 300.00 300.00 300.00 300.00 300.00 300.00 300.00 300.00 300.00
300.00 300.00 300.00 300.00 300.00 300.00 300.00 300.00 300.00 300.00 300.00 300.00 300.00

```
 0.00   3000.00   3000.00   3000.00   3000.00   3000.00   3000.00   3000.00   3000.00   3000.00   2999.99   2999.86   2998.93   2993
.30   2966.59   2869.17   2546.19   1291.89    592.46    364.24    311.16    301.60    300.19    300.02    300.00    300.00    300.0
0    300.00    300.00    300.00    300.00    300.00    300.00    300.00    300.00    300.00    300.00    300.00    300.00    300.00
   300.00    300.00    300.00    300.00    300.00    300.00    300.00    300.00    300.00    300.00    300.00    300.00    300.00

 0.00   3000.00   3000.00   3000.00   3000.00   3000.00   3000.00   3000.00   3000.00   3000.00   2999.97   2999.78   2998.49   2991
.40   2960.24   2848.51   2474.92   1333.53    631.30    379.52    315.17    302.39    300.32    300.04    300.00    300.00    300.0
0    300.00    300.00    300.00    300.00    300.00    300.00    300.00    300.00    300.00    300.00    300.00    300.00    300.00
   300.00    300.00    300.00    300.00    300.00    300.00    300.00    300.00    300.00    300.00    300.00    300.00    300.00


r 18:29 0.565 0

pr file14

                file14    07/06/86  1831.2 bst Sun

      0.000
      0.000
      0.000
      0.000
      0.000
      0.000
      0.000
      0.000
      0.000
      0.000
      0.000
      0.000
      0.000
      0.000
      0.000
   1700.000
   1700.000
   1700.000
   1700.000
   1700.000
   1700.000
   1700.000
   1700.000
   1700.000
   1700.000
   1700.000
   1700.000
   1700.000
   1700.000
   1700.000
   1700.000
   1700.000
```

```
 1700.000
 1700.000
 1700.000
    0.000
    0.000
    0.000
    0.000
    0.000
    0.000
    0.000
    0.000
    0.000
    0.000
    0.000
    0.000
    0.000
    0.000
    0.000
    0.000
    0.000
    0.000

r 18:31 0.174 2

TO CALCULATE THE STRESSES?

trans
if you require a brief output enter 1, a brief input enter 2,
both enter 3, for a conventional run enter 0.

0
enter number of sets of calculations to be performed

1
if materials have graded structure or more than two materials are used
enter a 1, otherwise enter a 0

0
if temperature dependant properties given on subroutine "properties"
enter a 1, otherwise enter a 0

0
if transient solution is required enter number of cycles
if a steady state solution is required enter a 0
```

```
4
enter 1 if residual stresses are to found from plasma spraying
otherwise type a 0

1
 Enter temperature at which elastic properties start in the coating

2000
for coating and base enter, thickness, temperature, heat transfer coef
overall diameter , datum temperature and pressure - where appropriate
but first, do you require more information; y or n

n
2e-4,10e-3,0,0,0,0,86e-3,0,0
enter youngs mod, thermal cond, poisson ratio, thermal exp, heat capacity, density for ceramic and metal
but first, do you require more information; y or n.

n
300e9,200e9,1,30,0.23,0.3,10e-6,24e-6,0,0.0,0
enter number of strips to be used in ceramic and metal layers
ie: 35,35  : limit 150 strips

32,20
 What uniform temperature is your disc starting at
you can use either degrees K or C, but keep to same throughout program

0
 Is the temperature distribution already available in file70?
in which case type "y",
or do you want the program to calculate the distribution for you,
in which case type "n"

y
if disc is axially restrained enter a 0
     if disc is free to deform enter -1
     for a forced displacement enter radius of curvature

0
```

	COATING	BASE	
YOUNGS MOD	300.0000	200.0000	GPa
THERMAL COND	1.0000	30.0000	W/M2
THERMAL EXP	10.0000	24.0000	x10-6

POISSONS RATIO	0.2300	0.3000	
DEPTH	0.0002	0.0100	M

RADIUS OF CURVATURE	0.00	
CENTRAL DISPLACEMENT	0.0000	
DEPTH TO NA	0.0051	
TIME	0.0000	S

DEPTH	TEMPERATURE	STRESS (M)	STRESS (A)
0.000003	3000.00	0.00	0.00
0.000009	3000.00	0.00	0.00
0.000016	3000.00	0.00	0.00
0.000022	3000.00	0.00	0.00
0.000028	3000.00	0.00	0.00
0.000034	3000.00	0.00	0.00
0.000041	3000.00	0.00	0.00
0.000047	3000.00	0.00	0.00
0.000053	3000.00	0.00	0.00
0.000059	3000.00	0.00	0.00
0.000066	3000.00	0.00	0.00
0.000072	3000.00	0.00	0.00
0.000078	3000.00	0.00	0.00
0.000084	2999.77	0.00	0.00
0.000091	2991.66	0.00	0.00
0.000097	2798.84	0.00	0.00
0.000103	501.16	-7370.53	7.59
0.000109	308.34	-8122.02	6.77
0.000116	300.23	-8153.86	5.96
0.000122	300.00	-8155.00	5.14
0.000128	300.00	-8154.76	5.96
0.000134	300.00	-8154.52	6.77
0.000141	300.00	-8154.27	7.58
0.000147	300.00	-8154.03	8.39
0.000153	300.00	-8153.79	9.21
0.000159	300.00	-8153.55	10.01
0.000166	300.00	-8153.30	10.82
0.000172	300.00	-8153.06	11.63
0.000178	300.00	-8152.82	12.44
0.000184	300.00	-8152.58	13.24
0.000191	300.00	-8152.34	14.05
0.000197	300.00	-8152.10	14.85
0.000450	300.00	82.06	14.87
0.000950	300.00	81.86	14.41
0.001450	300.00	81.68	14.00

0.001950	300.00	81.53	13.85
0.002450	300.00	81.41	13.35
0.002950	300.00	81.30	13.12
0.003450	300.00	81.22	12.93
0.003950	300.00	81.17	12.81
0.004450	300.00	81.14	12.74
0.004950	300.00	81.14	12.73
0.005450	300.00	81.11	12.67
0.005950	300.00	81.06	12.56
0.006450	300.00	80.99	12.39
0.006950	300.00	80.89	12.16
0.007450	300.00	80.77	11.88
0.007950	300.00	80.63	11.53
0.008450	300.00	80.45	11.13
0.008950	300.00	80.26	10.67
0.009450	300.00	80.03	10.16
0.009950	300.00	79.79	9.58

	COATING	BASE	
YOUNGS MOD	300.0000	200.0000	GPa
THERMAL COND	1.0000	30.0000	W/M2
THERMAL EXP	10.0000	24.0000	x10-6
POISSONS RATIO	0.2300	0.3000	
DEPTH	0.0002	0.0100	M

RADIUS OF CURVATURE 0.00
CENTRAL DISPLACEMENT 0.0000
DEPTH TO NA 0.0051
TIME 0.0000 S

DEPTH	TEMPERATURE	STRESS (M)	STRESS (A)
0.000003	3000.00	0.00	0.00
0.000009	3000.00	0.00	0.00
0.000016	3000.00	0.00	0.00
0.000022	3000.00	0.00	0.00
0.000028	3000.00	0.00	0.00
0.000034	3000.00	0.00	0.00
0.000041	3000.00	0.00	0.00
0.000047	3000.00	0.00	0.00
0.000053	3000.00	0.00	0.00

0.000059	3000.00	0.00	0.00
0.000066	3000.00	0.00	0.00
0.000072	3000.00	0.00	0.00
0.000078	2999.93	0.00	0.00
0.000084	2998.39	0.00	0.00
0.000091	2971.56	0.00	0.00
0.000097	2692.61	0.00	0.00
0.000103	659.31	-6754.08	7.84
0.000109	329.22	-8040.39	7.02
0.000116	301.61	-8148.21	6.19
0.000122	300.07	-8154.46	5.36
0.000128	300.00	-8154.98	4.53
0.000134	300.00	-8154.74	5.36
0.000141	300.00	-8154.49	6.19
0.000147	300.00	-8154.24	7.01
0.000153	300.00	-8153.99	7.84
0.000159	300.00	-8153.75	8.67
0.000166	300.00	-8153.50	9.49
0.000172	300.00	-8153.26	10.31
0.000178	300.00	-8153.01	11.14
0.000184	300.00	-8152.76	11.96
0.000191	300.00	-8152.52	12.78
0.000197	300.00	-8152.27	13.60
0.000450	300.00	81.65	13.57
0.000950	300.00	81.44	13.09
0.001450	300.00	81.26	12.67
0.001950	300.00	81.10	12.31
0.002450	300.00	80.97	12.00
0.002950	300.00	80.86	11.74
0.003450	300.00	80.78	11.55
0.003950	300.00	80.72	11.41
0.004450	300.00	80.68	11.33
0.004950	300.00	80.67	11.31
0.005450	300.00	80.66	11.26
0.005950	300.00	80.61	11.16
0.006450	300.00	80.54	11.00
0.006950	300.00	80.45	10.78
0.007450	300.00	80.33	10.50
0.007950	300.00	80.19	10.17
0.008450	300.00	80.02	9.77
0.008950	300.00	79.82	9.32
0.009450	300.00	79.60	8.81
0.009950	300.00	79.36	8.23

COATING BASE

YOUNGS MOD	300.0000	200.0000	GPa
THERMAL COND	1.0000	30.0000	W/M2
THERMAL EXP	10.0000	24.0000	x10-6
POISSONS RATIO	0.2300	0.3000	
DEPTH	0.0002	0.0100	M

RADIUS OF CURVATURE	0.00
CENTRAL DISPLACEMENT	0.0000
DEPTH TO NA	0.0051
TIME	0.0000 S

DEPTH	TEMPERATURE	STRESS (M)	STRESS (A)
0.000003	3000.00	0.00	0.00
0.000009	3000.00	0.00	0.00
0.000016	3000.00	0.00	0.00
0.000022	3000.00	0.00	0.00
0.000028	3000.00	0.00	0.00
0.000034	3000.00	0.00	0.00
0.000041	3000.00	0.00	0.00
0.000047	3000.00	0.00	0.00
0.000053	3000.00	0.00	0.00
0.000059	3000.00	0.00	0.00
0.000066	3000.00	0.00	0.00
0.000072	2999.99	0.00	0.00
0.000078	2999.72	0.00	0.00
0.000084	2995.63	0.00	0.00
0.000091	2951.94	0.00	0.00
0.000097	2693.09	0.00	0.00
0.000103	792.45	-6235.35	5.95
0.000109	358.20	-7927.47	5.15
0.000116	304.75	-8135.96	4.34
0.000122	300.30	-8153.54	3.52
0.000128	300.01	-8154.91	2.71
0.000134	300.00	-8154.71	3.52
0.000141	300.00	-8154.46	4.33
0.000147	300.00	-8154.22	5.15
0.000153	300.00	-8153.98	5.96
0.000159	300.00	-8153.74	6.77
0.000166	300.00	-8153.50	7.57
0.000172	300.00	-8153.26	8.38
0.000178	300.00	-8153.01	9.19
0.000184	300.00	-8152.77	9.99
0.000191	300.00	-8152.53	10.80

0.000197	300.00	-8152.29	11.60
0.000450	300.00	81.24	11.64
0.000950	300.00	81.04	11.17
0.001450	300.00	80.86	10.75
0.001950	300.00	80.70	10.39
0.002450	300.00	80.57	10.08
0.002950	300.00	80.47	9.84
0.003450	300.00	80.39	9.65
0.003950	300.00	80.33	9.52
0.004450	300.00	80.30	9.45
0.004950	300.00	80.30	9.44
0.005450	300.00	80.27	9.38
0.005950	300.00	80.22	9.26
0.006450	300.00	80.15	9.09
0.006950	300.00	80.05	8.86
0.007450	300.00	79.92	8.56
0.007950	300.00	79.77	8.21
0.008450	300.00	79.60	7.80
0.008950	300.00	79.39	7.33
0.009450	300.00	79.16	6.80
0.009950	300.00	78.91	6.20

	COATING	BASE	
YOUNGS MOD	300.0000	200.0000	GPa
THERMAL COND	1.0000	30.0000	W/M2
THERMAL EXP	10.0000	24.0000	x10-6
POISSONS RATIO	0.2300	0.3000	
DEPTH	0.0002	0.0100	M

RADIUS OF CURVATURE	0.00	
CENTRAL DISPLACEMENT	0.0000	
DEPTH TO NA	0.0051	
TIME	0.0000	S

DEPTH	TEMPERATURE	STRESS (M)	STRESS (A)
0.000003	3000.00	0.00	0.00
0.000009	3000.00	0.00	0.00
0.000016	3000.00	0.00	0.00
0.000022	3000.00	0.00	0.00
0.000028	3000.00	0.00	0.00

0.000034	3000.00	0.00	0.00
0.000041	3000.00	0.00	0.00
0.000047	3000.00	0.00	0.00
0.000053	3000.00	0.00	0.00
0.000059	3000.00	0.00	0.00
0.000066	3000.00	0.00	0.00
0.000072	2999.95	0.00	0.00
0.000078	2999.27	0.00	0.00
0.000084	2991.85	0.00	0.00
0.000091	2935.13	0.00	0.00
0.000097	2693.50	0.00	0.00
0.000103	907.46	-5787.88	6.11
0.000109	392.59	-7794.10	5.32
0.000116	309.91	-8116.48	4.49
0.000122	300.81	-8152.18	3.66
0.000128	300.05	-8155.39	2.83
0.000134	300.00	-8155.34	3.66
0.000141	300.00	-8155.09	4.48
0.000147	300.00	-8154.85	5.31
0.000153	300.00	-8154.60	6.14
0.000159	300.00	-8154.35	6.96
0.000166	300.00	-8154.11	7.79
0.000172	300.00	-8153.86	8.61
0.000178	300.00	-8153.61	9.43
0.000184	300.00	-8153.37	10.25
0.000191	300.00	-8153.12	11.07
0.000197	300.00	-8152.88	11.89
0.000450	300.00	80.88	11.95
0.000950	300.00	80.68	11.47
0.001450	300.00	80.49	11.04
0.001950	300.00	80.33	10.68
0.002450	300.00	80.20	10.36
0.002950	300.00	80.09	10.11
0.003450	300.00	80.01	9.91
0.003950	300.00	79.95	9.77
0.004450	300.00	79.91	9.69
0.004950	300.00	79.90	9.67
0.005450	300.00	79.88	9.62
0.005950	300.00	79.84	9.52
0.006450	300.00	79.77	9.36
0.006950	300.00	79.68	9.14
0.007450	300.00	79.56	8.86
0.007950	300.00	79.41	8.52
0.008450	300.00	79.24	8.12
0.008950	300.00	79.04	7.67
0.009450	300.00	78.82	7.15
0.009950	300.00	78.57	6.57

EXAMPLE 8

GRAPHICAL OUTPUT

CREATE INPUT FILE

ie file: input

```
0
1
0
0
0
0
n
1e-3,10e-3,100,200,0,0,86e-3,0,0
n
300e9,200e9,1,30,0.23,0.3,10e-6,23e-6,0,0,0,0
35,35
0
```

Then

```
io attach file05 vfile_ input
io attach file06 vfile_ ouput
trans
io detach file06
io detach file07
```

output now written to file: output

must now add blank line to end of output file

to run graphics program type

```
io attach file16 vfile_ output
sg -of graph
grap
```

The program will then ask how many graphs you have to enter, type say

1

file graph.graphics now contains graph

if you are performing a transient analysis you enter the number of cycles.

APPENDIX 6.1 SIMPLIFIED ANALYSIS OF THE RESIDUAL STRESSES IN A COATED DISC

Simplified Analysis of the residual stresses in a coated disc

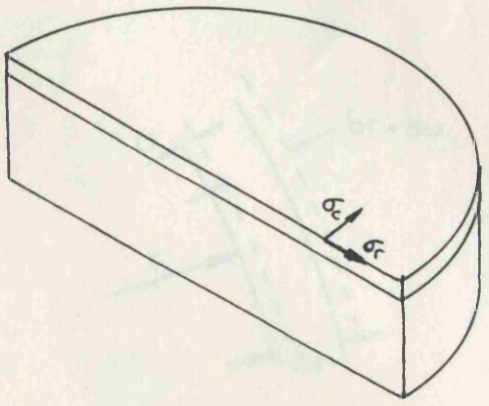

If we ignore axial stresses, and assume that the substrates dimensions are unchanged by plasma spraying, then examining an element of the zirconia coating.

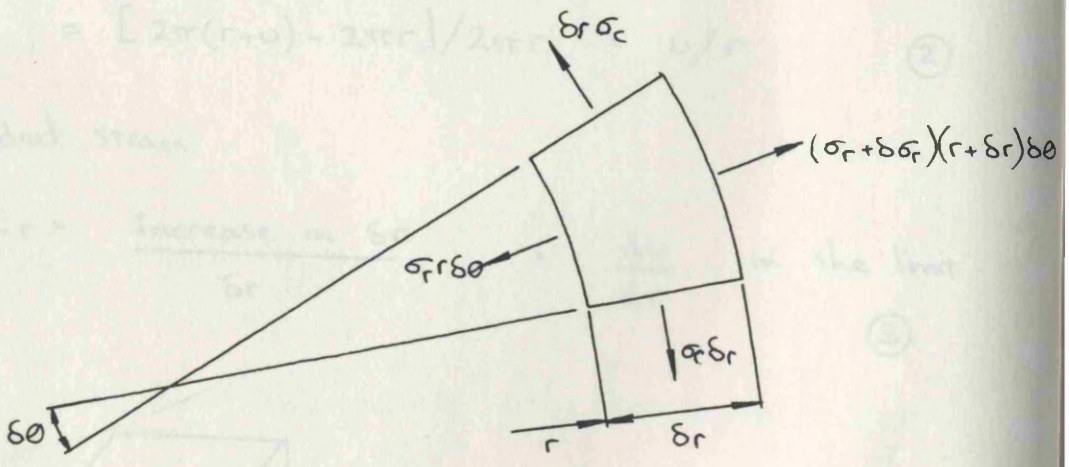

Taking equilibrium in the radial direction

$$2\sigma_c \delta r \sin\tfrac{1}{2}\delta\theta + \sigma_r r\delta\theta - (\sigma_r+\delta\sigma_r)(r+\delta r)\delta\theta = 0$$

In the limit this reduces to;

$$\sigma_c - \sigma_r - r\frac{d\sigma_r}{dr} = 0 \qquad (1)$$

Examining a concentric ring of the disc, subject to a radial load.

Let u be the radial shift at a radius r,

ie: r becomes $r+u$, after straining.

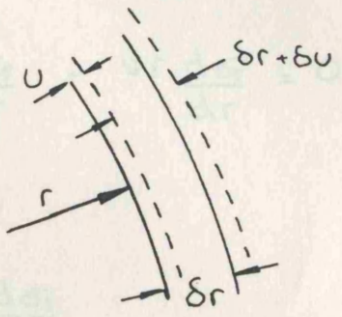

The circumferental, or hoop strain

$$\epsilon_c = \frac{\text{Increase of circumference}}{\text{Original circumference}}$$

$$= [2\pi(r+u) - 2\pi r]/2\pi r = u/r \qquad (2)$$

The radial strain

$$\epsilon_r = \frac{\text{Increase in } \delta r}{\delta r} = \frac{du}{dr} \quad \text{in the limit} \qquad (3)$$

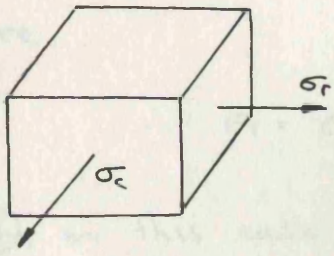

In a solid we know that

$\epsilon_c = \frac{1}{E}(\sigma_c - \nu\sigma_r)$ from (2) $\frac{u}{r}E = (\sigma_c - \nu\sigma_r)$ (4)

$\epsilon_r = \frac{1}{E}(\sigma_r - \nu\sigma_c)$ from (3) $\frac{du}{dr}E = (\sigma_r - \nu\sigma_c)$ (5)

Differentiating ④ and equating to ⑤

$$(\sigma_c - \sigma_r)(1-\nu) + r\frac{d\sigma_c}{dr} - \nu r\frac{d\sigma_c}{dr}$$

Sub. in ①

$$r\frac{d\sigma_r}{dr}(1+\nu) + r\frac{d\sigma_r}{dr} - \nu r\frac{d\sigma_r}{dr} = 0$$

rearranging

$$\frac{d\sigma_c}{dr} = -\frac{d\sigma_r}{dr}$$

Integrating $\sigma_r + \sigma_c = A$

Sub in ①

$$r\frac{d\sigma_r}{dr} + 2\sigma_r = A$$

$$\therefore \quad \sigma_r = \frac{A}{2} - \frac{B}{r^2}$$

Similarly $\sigma_c = \frac{A}{2} + \frac{B}{r^2}$

For a solid disc, then $B=0$, since stress not infinite at centre.

$$\therefore \quad \sigma_r = \sigma_c .$$

Taking ④, in this case the radial shift is caused by a temperature change.

ie: The shrinkage as the zirconia contracts to room temperature.

This shrinkage will be $\gamma \Delta T r$, (6)

where γ is the thermal expansion,

and ΔT is the difference between the substrates temperature and the temperature at which the zirconia can be assumed to behave elastically,

from (4) and (6)

$$E \gamma \Delta T = (1-\nu) \sigma_r$$

$$\therefore \sigma_r = \frac{E \gamma \Delta T}{(1-\nu)}$$

APPENDIX 6.2 PROGRAM TO PREDICT RESIDUAL STRESSES IN PSZ COATINGS

```
                resid.fortran       07/06/86  1842.7 bst Sun

c     This program produces transient temperatures derived
c     during the process of plasma spraying.
c
c
      dimension e(300),v(300),g(300),t(300),de(300),cp(300)
      dimension temp(100),tempm(100),solid(100),tempr(100)
      common ilay,layers,numt,solid,k,e,v,g,t,cp,de,temp,tempm,loop,itstep
      real k(300)
c
c
c     set up initial data
c
      write(6,201)
  201 format(1x,' Enter the latent heat of fusion for Zirconia,',/,
     &' temperature of Zirconia at arrival at the substrate surface,',/,
     &' melting point of zirconia,',/,
     &' temperatue at which elastic properties can be assumed for the coating.',/,
     &' Units must be consistant.',/,
     &' ie:680000,3000,2700,2000',/)
      read(5,102)lat,tplaz,tmelt,telast
      write(6,301)
  301 format(1x,' Enter the number of layers to be sprayed, 1 or 2',/)
      read(5,102) layers
      write(6,401)
  401 format(1x,' Enter number of elements layer should be divided into,',/,
     &' the thickness of the layer,',/,
     &' the time step to be used for calculation,',/,
     &' time interval you wish to use between stored data,',/,
     &' and time span for calculations.',/,
     &' ie:32,1e-4,1e-6,1e-5,1e-4',/)
      read(5,102) num,thick,delt,tstep,tspan
      itstep=(tstep/delt+0.1)
      thick=thick/num
      iloop=tspan/delt+0.01
c
  102 format(v)
c
      write(6,501)
  501 format(1x,' Enter for both Zirconia and the substrate, the thermal conductivity,',/,
     &' density and specific heat capacity',/,
     &' ie:1,30,3800,7850,800,460',/,
     &' This data set gives the Zirconia a conductivity of 1W/mK, density of 3000kg/m3',/,
     &' and a heat capacity of 800J/KgK.  The substrat has a conductivity of 30W/mk,',/,
     &' density of 7850Kg/m3 and a heat capacity of 460J/KgK.',/)
```

```
      read(5,102)cerK,metK,cerD,metD,cerC,metC
      write(6,601)
  601 format(1x,' Enter the substrate thickness, number of elements in substrate,',/,
     &' and the initial temperatue of the substrate.',/,
     &' ie: 10e-3,20,300',/)
c
      read(5,102) thick2,num2,startT
      numt=num
      t11=startT
      do 50 ilay=1,layers
c
c
c     set up initial temperature ddistribution
      loop=0
      do 10 i=1,100
      k(i)=metK
      temp(i)=startT
      de(i)=metD
      cp(i)=metC
      t(i)=thick2/num2
c
c     set up plasma spayed layers temperatures and properties
   10 continue
      do 30 it=1,num
      t(it)=thick
      k(it)=cerK
      de(it)=cerD
      cp(it)=cerC
   30 continue
      do 60 it=1,numt
      temp(it)=tplaz
   60 continue
      ntot=num+num2
c
c
c     the matrix solid contains the energy required
c     for each strip of liquid zirconia to solidify.
      do 61 irs=1,numt
      solid(irs)=de(irs)*t(irs)*lat
   61 continue
      do 62 irs=numt+1,ntot
      solid(irs)=0
   62 continue
c
c     call subroutine for calculating temperature distribution
      call temppro(hf,tf,t11,ntot,delt,time,tmelt,telast,num,iloop)
c
c     re set the number of layers of ceramic which will
```

```
c     be applied.
      numt=int(num/1.9999)
      thick=thick*2
c
      write(6,103)
  103 format(1x," next layer")
   50 continue
c
      if(layers.eq.2) goto 42
      do 41 iuy=1,100
      tempr(iuy)=0
   41 continue
      goto 46
   42 do 43 iuy=1,numt
      tempr(iuy)=0
   43 continue
      do 44 iuy=numt+1,num
      tempr(iuy)=telast-startT
   44 continue
      do 45 iuy=num+1,ntot
      tempr(iuy)=0
   45 continue
   46 continue
      write(14,40)(tempr(i),i=1,ntot)
   40 format(1x,1f10.3)
      stop
      end
c
c
c-----------------------------------------------------------------------
c-----------------------------------------------------------------------
c
c
      subroutine temppro(hf,tf,t11,ntot,delt,time,tmelt,telast,num,iloop)
c         program to calculate the temperature distribution in a multi layer disc
c         Implicit method (Crank-Nicolson) version
c
c         The time step is 0.0001 sec.
c
      dimension e(300),v(300),g(300),t(300),de(300),cp(300)
      dimension a(200),b(200),c(200),d(200)
      dimension solid(100),temp(100),tempa(100)
      real k(300)
      common ilay,layers,numt,solid,k,e,v,g,t,cp,de,temp,tempa,loop,itstep
      integer tt
      itran=0
c
c
```

```
c
c                              Fourier number
      tis=0
      Fo=delt*k(1)/(de(1)*cp(1)*t(1)*t(1))
c                              print out counter
      x=0.
      tt=1
c
c main time step loop 'j'
c
       do 10 j=1,iloop
c
c set up tri-diagonal coefficients
c
c note a(1) and c(10) are not used
c
      tem=temp(ntot)
      time=j*delt+tis
      Fo=delt*k(1)/(de(1)*cp(1)*t(1)*t(1))
      b(1)=(1+Fo)
      c(1)=-Fo
      d(1)=(1-Fo)*temp(1)+Fo*temp(2)
c
c general values loop 'i'
c
      do 20 i=2,ntot
      Fa=delt*k(i-1)/(de(i-1)*cp(i-1)*t(i-1)*t(i-1))
      Fb=delt*k(i)/(de(i)*cp(i)*t(i)*t(i))
      con=t(i-1)/t(i)
      ron=k(i)/k(i-1)
      Fbar=(Fa*Fb)/(Fb+(con*ron*Fa))
      a(i)=-Fbar
      b(i)=1.0+((1.0+ron*con)*Fbar)
      c(i)=-ron*con*Fbar
 c                             jump equation for i=10
      if(i.ne.ntot) goto 1000
      Fo=delt*k(i)/(de(i)*cp(i)*t(i)*t(i))
      a(i)=-Fo
      b(i)=(1+Fo)
      d(i)=Fo*temp(ntot-1)+(1-Fo)*temp(ntot)
      c(i)=0
      goto 20
c
 1000 d(i)=Fbar*temp(i-1)+(1.0-((1.0+ron*con)*Fbar))*temp(i)+ron*con*Fbar*temp(i+1)
c
c     if the element being considered is at the melting
c     point and the latent heat of solidification still
c     remains then the ceramic temperature will not drop.
```

```
      if((temp(i).lt.tmelt).and.(solid(i).gt.0.5)) then
      qlat=2*(temp(i)-temp(i+1))/((t(i)/k(i))+(t(i+1)/k(i+1)))
      if((qlat*delt).gt.solid(i)) qlat=solid(i)/delt
      d(i)=tmelt
      solid(i)=solid(i)-(qlat*delt)
      endif
   20 continue
c
c solve tri-diagonal matrix
c
      n=ntot
      call tridig(a,b,c,d,n,j,num)
c
c     check temperature of (10-itran)'th layer if less
c     than telast then elastic properties have started
c     Therefore find temperature of previous layer at
c     this same time, the temperature difference will
c     define the residual stress pattern.
c
      if(temp(ntot-10-itran).gt.telast) goto 110
      if(loop.gt.0.5) goto 110
      tempm(ntot-10-itran)=temp(ntot-10-itran)-temp(ntot-9-itran)
      itran=itran+1
      if(itran.gt.(ntot-10.5)) loop=1
  110 continue
c
c write out results
      x=x+1
      if(abs(x-itstep).gt.0.00001) goto 10
c
      if(layers.eq.2.and.ilay.eq.1) goto 10
      write(70,70) time,(temp(i),i=1,ntot)
   70 format(1x,/,f5.2,100f10.2)
      tt=tt+1
      x=0
c
   10 continue
      return
c
      end
c
c-----------------------------------------------------------------
c
      subroutine tridig(a,b,c,d,n,j,num)
c program to solve a tridiagonal matrix with leading diagonal
c coefficients 'b',sub-diagonals 'a', super-diagonals 'c' and
c right hand sides 'd'.
c
```

```
c solution is returned in 'tempm'
      dimension a(200),b(200),c(200),d(200),gamma(200),beta(200),temp(100)
      dimension solid(100),tempm(100)
      dimension v(300),e(300),g(300),t(300),cp(300),de(300)
      real k(300)
      common ilay,layers,numt,solid,k,e,v,g,t,cp,de,temp,tempm,loop,itstep
c
c initialisation
c
      gamma(1)=d(1)/b(1)
      beta(1)=b(1)
c
c first loop for gammas and betas
c
      do 100 i=2,n
      beta(i)=b(i)-a(i)*c(i-1)/beta(i-1)
  100 gamma(i)=(d(i)-a(i)*gamma(i-1))/beta(i)
c
c second loop initialisation
c
      temp(n)=d(n)-a(n)*gamma(n-1)
      temp(n)=temp(n)/(b(n)-a(n)*(c(n-1)/beta(n-1)))
      l=n+1
c
c second loop for solution
c
      do 200 i=1,n-1
  200 temp(n-i)=gamma(n-i)-c(n-i)*temp(l-i)/beta(n-i)
c
      return
      end


r 18:45 0.529 2
```